Author:
Morris, David T J

Title:
Dynamic Molecules with Switchable Hydrogen-Bond Directionality

School of Chemistry

Dynamic Molecules with Switchable Hydrogen-Bond Directionality

David Morris

2019

A thesis submitted to the University of Bristol for the degree of Doctor of Philosophy in the Faculty of Science

Project Supervisor – Professor Jonathan Clayden

Organic & Biological Chemistry

Abstract

Nowick and co-workers have reported that ethylene-bridged triureas can be synthesised with complete conformational control by judicious use of steric hindrance and hydrogen bonding.[1] The concept of complete but switchable conformational control of these structures has not been investigated and is of interest as it gains access to dynamic peptide mimics with switchable hydrogen-bond directionality.

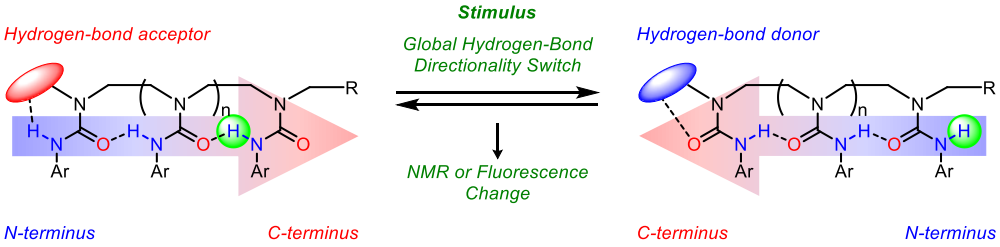

Figure 1 – Dynamic hydrogen-bond directionality-switchable oligoureas.

Previous work in the Clayden group has shown that achiral oligourea-derived foldamers can communicate stereochemical information by binding a chiral ligand and inducing a helical excess.[2] This served as the first example of reversible hydrogen-bond directionality in a synthetic foldamer. In our design, the global directionality of an ethylene-bridged oligourea foldamer can be controlled by applying an electronic bias at one terminus. When terminated with a hydrogen-bond acceptor (HBA), the global directionality of the foldamer is defined and controlled owing to the hydrogen bond between the HBA and the ureido proton of the adjacent urea, and the hydrogen bonding between the ureas in the foldamer. The orientation of the final urea can be inferred from variable-temperature ^{1}H NMR and NOE studies of the ureido protons and a benzylic methylene spectroscopic reporter. The opposite directionality can be accessed by using a terminal hydrogen-bond donor (HBD) instead of an HBA. The directionality of these foldamers can be switched by employing a terminal 2-pyridyl group, which can be switched between an HBD and an HBA by protonation/deprotonation. Upon protonation, the first urea reorients in order to hydrogen bond to the resultant pyridinium. This reorientation is communicated as binary information throughout the rest of the foldamer, resulting in a global directionality switch. Preliminary experiments on effecting the switching process with the light-induced photodissociation/association of a photoacid have been performed. Investigations into directionality-switchable foldamers with binding sites complementary to those of DNA nucleobases have been conducted. Different spectroscopic or chemical outputs at the reporting terminus have also been explored.

Ethylene-bridged oligoureas represent a new class of foldamers that can undergo a global directionality switch in response to pH change or exposure to light, and could be amenable to DNA ligand binding. The concept of switching hydrogen-bond directionality in foldamers is a significant simplification of how biological systems store and communicate information and could provide access to interesting and useful chemical and biomimetic functions.

Contents

Word Count – 84511

Declaration

I declare that the work in this dissertation was carried out in accordance with the requirements of the University's *Regulations and Code of Practice for Research Degree Programmes* and that it has not been submitted for any other academic award. Except where indicated by specific reference in the text, the work is the candidate's own work. Work done in collaboration with, or with the assistance of, others, is indicated as such. Any views expressed in the dissertation are those of the author.

SIGNED: …… DATE: / / ……

Acknowledgements

First and foremost – Jonathan, thank you so much for pitching this project to the CDT. It has been a fantastic journey for me, and I have learnt so much supramolecular, synthetic and physical organic chemistry from it. More than that, thank you for nurturing such a cohesive learning environment in your group, with such a large range of disciplines. It serves to make me and all other Clayden alumni exceptionally well-rounded chemists who are still eager to learn, and for that I am *incredibly* grateful.

John – thank you for your guidance throughout the project. You are a fantastic teacher, and I am very grateful that you taught me at the most crucial point of my career.

David – thank you too for your guidance and collaboration on the project, it has been excellent working with you, and I will be sure to leave a positive review on TripAdvisor.

Louise – You have been around for *everything*; thank you for the chats, chemistry talks and for the crazier nights out every now and again, but mainly for being a such a great person to know.

Mo – You are the craziest person I have ever met. This is the highest compliment I can give to anyone; your boundless positive energy truly has made every day in the group an adventure.

Jess – I feel so lucky to know you; you command a very positive presence and you are very good at making people feel good about themselves. Your height is very conducive to my hugs.

Romain – I am so pleased to have spent two years of my PhD with you; you are as fantastic a chemist as you are a person, and it was great working, drinking and board-gaming with you.

Mary – You are an amazing person to have around. You are always very positive, and you are always around to have a lovely chat with. I hope you keep up the guitar.

Quentin – What a mind. It has been inspiring to work with you, and you have been amazing to be around. It is a shame that I couldn't spend more of my PhD absorbing your massive brain.

Hossay – You epitomise peak Clayden. I am worlds better as a scientist and happier as a person for having you on the other side of the bay of dreams for half my PhD. Talking philosophy and having ChemByDesign sessions with you encapsulate some of the best days of my PhD.

Roman – My partner in crime; you're a great scientist, and excellent company. Thank you for being such good fun but crucially, thank you for teaching me photoredox catalysis.

Frank – You have always been brilliant company and your knowledge of retro video games has inspired great respect from me. You definitely own the being-a-total-legend skillcape.

Branca – You are such a good friend, and a great person to talk to about games and beyond. Your excitement when we discuss chemistry is one of my favourite things about the subject.

Matthew – Your myriad references to your ineffably immense etymological and chemical lexicon engenders my fervent desire to imbue you with the utmost gratitude.

Giulia – You are an excellent scientist and you host a great atmosphere. Thanks for working next to me and teaching me Italian. I can now ask for the toilet with the utmost confidence.

James, Jon and Lydia – Thank you for the good times in PACT and throughout the PhD.

Thank you to Elliot, David Bacos, Arron, Giulia and Aaron for all the work you have done on these projects, and for teaching me how to teach.

Thank you also to Johno, Josep, Matt, Jack, Laura, Dan, Alex Sandtorv, Rakesh, Makenzie, Jen, Alex Browning, Isabelle, Steve, Ellie, The Guardian and that table tennis table in the MVB for your guidance and/or company.

Thank you to Paul Lawrence and Tom Leman for your constant support and tolerance for my odd NMR experiments. Half of this thesis couldn't have been written without you.

Tom, Jon, Richard – *Thank* you.

Oli – You, your PS4 and your big TV have made living in Bristol so easy and so much fun and thank you for making such sweet Jambalaya with me. I hope you carry it on with those chonks.

The Celestial Owls of Malevolence – The intensity with which I appreciate you makes me want to take a belt sander to each of you. Thank you for the regression sessions.

Kawabata Group – Thank you all so much, particularly Sensei, for making me feel so welcome in Kyoto. I have many unforgettable memories from my placement that I will always cherish.

Vinegar – You have been a constant in my PhD. It has been amazing rocking with you, and I have loved jamming and performing with you, especially when science was misbehaving.

Mum – Thank you for your continuous and unwavering support. You have been a constant source of motivation for me.

Paul and Alice – You are tremendously important people to me. Thank you for your enthusiasm and for sustaining my excitement for chemistry by listening to me blabber on about my 'lines'.

Thanks to Dad, Katharine, Alan and other family members for support along the way.

Finally, thank you to Hossay, Frank, Dan, Matthew, Steve, Roman and Makenzie for proofreading this thesis.

Abbreviations

Ac	Acetyl	DMF	*N*,*N*-Dimethylformamide
ACHC	*trans*-2-Aminocyclohexanecarboxylic acid	DMP	Dess-Martin periodinane
ACPC	*trans*-2-Aminocyclopentanecarboxylic acid	DMSO	Dimethylsulfoxide
Aib	Aminoisobutyric acid	DNA	Deoxyribonucleic acid
Ar	Aryl	DTM	Dithiomaleimide
atm	Atmosphere (pressure)	e.e.	Enantiomeric excess
BINAP	2,2'-Bis(diphenylphosphino)-1,1'-binaphthyl	EDC	1-Ethyl-3-(3-dimethylaminopropyl)carbodiimide
Bn	Benzyl	EM	Effective molarity
Boc	*tert*-Butoxycarbonyl	ESI	Electrospray ionisation
Boc_2O	Di-*tert*-butyl dicarbonate	Et	Ethyl
Cbz	Carboxybenzyl	FTIR	Fourier transform infrared (spectroscopy)
CDI	1,1'-Carbonyldiimidazole	G	Gibbs free energy
COSY	(^{1}H-^{1}H) Correlation spectroscopy	GDP	Guanosine diphosphate
Cyclen	1,4,7,10-Tetraazacyclododecane	GPCR	G protein-coupled receptor
d	Doublet	GTP	Guanosine triphosphate
DBU	1,8-Diazabicyclo[5.4.0]undec-7-ene	H	Enthalpy
DCB	1,2-Dichlorobenzene	h	Planck's constant
DCE	1,2-Dichloroethane	HATU	1-[Bis(dimethylamino)methylene]-1*H*-1,2,3-triazolo[4,5-*b*]pyridinium 3-oxid hexafluorophosphate, *N*-[(Dimethylamino)-1*H*-1,2,3-triazolo-[4,5-*b*]pyridin-1-ylmethylene]-*N*-methylmethanaminium hexafluorophosphate *N*-oxide
DCM	Dichloromethane	HBA	Hydrogen-bond acceptor
DIPEA	*N*,*N*-Diisopropylethylamine	HBD	Hydrogen-bond donor

HBTU	*N,N,N′,N′*-Tetramethyl-*O*-(1*H*-benzotriazol-1-yl)uronium hexafluorophosphate, *O*-(Benzotriazol-1-yl)-*N,N,N′,N′*-tetramethyluronium hexafluorophosphate	^{n}Pr	*n*-Propyl
HCl	Hydrochloric acid	PCC	Pyridinium chlorochromate
Hexacyclen	1,4,7,10,13,16-Hexaazacyclooctadecane	PE	Petroleum ether (40-60)
HMBC	(^{1}H-^{13}C) Heteronuclear multiple bond correlation	Ph	Phenyl
HOBt	1-Hydroxybenzotriazole hydrate	PPY	4-Pyrrolidinopyridine
HOMO	Highest occupied molecular orbital	q	Quartet
HPLC	High-performance liquid chromatography	R	Molar gas constant
HR-MS	High-resolution mass spectrometry	R_f	Retention factor
HSQC	(^{1}H-^{13}C) Heteronuclear single quantum coherence	RT	Room temperature
^{i}Pr	Isopropyl	s	Singlet
k	Rate constant	S	Entropy
K	Equilibrium constant	SiO_2	Silica
k_B	Boltzmann constant	S_N2	Nucleophilic substitution (second order)
KHMDS	Potassium bis(trimethylsilyl)amide	S_NAr	Nucleophilic aromatic substitution
LDA	Lithium diisopropylamide	T	Temperature
LR-MS	Low-resolution mass spectrometry	t	Triplet
LUMO	Lowest unoccupied molecular orbital	TACN	1,4,7-Triazacyclononane
m	Multiplet	TBA	Tetrabutylammonium
M.P.	Melting point	^{t}Bu	*tert*-Butyl
MALDI	Matrix-assisted laser desorption ionisation	TCE	1,1,2,2-Tetrachloroethane
Me	Methyl	TEA	Triethylamine
mRNA	Messenger ribonucleic acid	Tf	Trifluoromethanesulfonyl
^{n}Bu	*n*-Butyl	TFA	Trifluoroacetic acid
NFSI	*N*-Fluorobenzenesulfonimide	TfOH	Trifluoromethanesulfonic acid
^{n}Hept	*n*-Heptyl	THF	Tetrahydrofuran
^{n}Hex	*n*-Hexyl	TLC	Thin layer chromatography
NMM	*N*-Methylmorpholine	tRNA	Transfer ribonucleic acid
NMR	Nuclear magnetic resonance (spectroscopy)	Ts	*p*-Toluenesulfonyl

NOE	Nuclear Overhauser effect		
$TsOH.H_2O$	*p*-Toluenesulfonic acid monohydrate	VTNMR	Variable-temperature NMR
v/v	Volume of solute / volume of solution	wt.	By weight
VSEPR	Valence Shell Electron Pair Theory		

1.0 Introduction

1.1 Informational Communication in Biological Systems

Hydrogen bonding is one of the most predominant and powerful interactions found in nature. It is responsible for myriad natural phenomena on a variety of scales. For example, it gives rise to the association of the nucleobases found in deoxyribonucleic acid (DNA) and to the highly selective binding of substrates in proteins.[3] It also results in the folding of proteins into their secondary and tertiary structures, which are vital to their function.[4,5] Hydrogen bonds vary greatly in strength (1-160 kJ mol^{-1}) but they are, relative to covalent and ionic bonds, weak interactions.[6] This lability confers a rich dynamic nature, which allows them to be switched on and off thermally at physiologically relevant temperatures. As a result, they can be exploited to modulate important properties, such as reactivity and binding affinity, with an immaculate level of spatial accuracy and precision.[7]

A hydrogen bond, as well as being an adhesive interaction, has an inherent directionality associated with it that can lend itself to more exotic functions.[8] It is this directionality of hydrogen bonds that is responsible for the storage, communication and processing of information in biological systems.[9,10] As a naturally ubiquitous example, codons are trinucleotides that use their specific pattern of hydrogen-bonding groups to code for a specific amino acid to be incorporated into a growing polypeptide chain by the ribosome.[11] In the 'CCC' codon, three units of cytidine are contiguously bound, which represents a detailed pattern of hydrogen-bond donors and acceptors to be templated by messenger RNA (mRNA) (Figure 2). This templating forms a new pattern of hydrogen bonds that exactly complements that of the codon. Transfer RNA (tRNA) then templates with the mRNA in the same fashion to form an adduct, which fits into the active site of aminoacyl tRNA synthetases. The tRNA synthetase then transfers a molecule of the amino acid, L-proline to the tRNA. This L-proline is then transferred to the ribosome by the tRNA for it to be incorporated into the growing polypeptide chain.

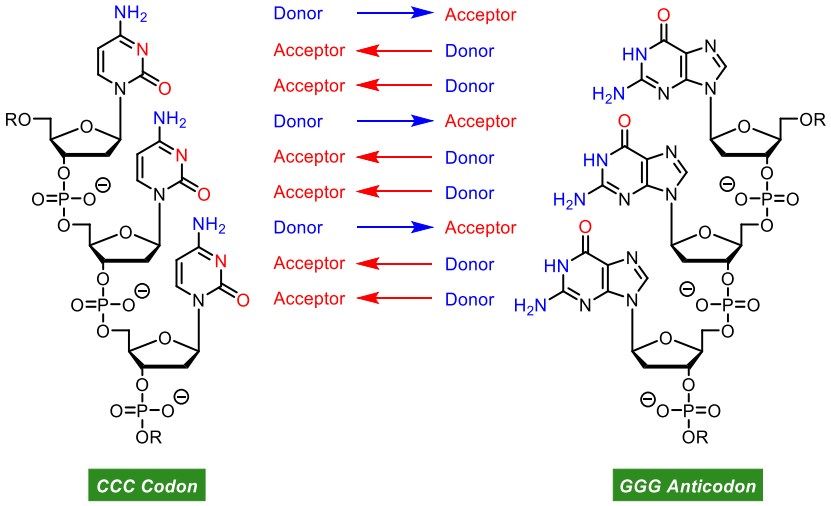

Figure 2 – Hydrogen-bond directionality in DNA templating.

There are four different nucleobases and therefore $4^3 = 64$ different permutations of how three nucleobases can be arranged in codons. These 64 codons code for the binding of tRNA to 21 different aminoacyl synthetases, each with a different amino acid bound to it for protein biosynthesis. Some codons are degenerate and therefore result in the incorporation of the same amino acid into the polypeptide chain, and some are known as 'stop' codons, which terminate protein biosynthesis and mark the end of the chain.[12] In this natural example, information in the form of hydrogen-bond directionality is stored in the codons, communicated through space by RNA, and results in the performance of a specific function by the resultant protein. Taking inspiration from nature, organic chemists have created many molecular machines that use hydrogen bonding to perform function.[13] However, there are few examples that exploit their inherent directionality to perform function despite its prominence in nature.[1]

1.2 Hydrogen-Bonding Theory

The theoretical consideration and treatment of the hydrogen bond has evolved enormously over the past two centuries. Although the study of chlorine decahydrate by Michael Faraday in 1823 alluded to such an interaction, it was almost a century later when hydrogen-bonding interactions became explicable following advances made in X-ray structural analysis and contemporary chemical bonding theory.[8] The term 'hydrogen bridge' was allegedly established by Maurice Huggins in his thesis in 1919 and was used to explain the tautomeric behaviour of acetoacetic acid. No records of the thesis exist, but the earliest extant citation of his work was by his colleagues, Latimer and Rodebush only a year later.[14] They described that a hydrogen nucleus may be held between two oxygen octets by forces which obey Hooke's law over great distances and that such a hydrogen would be capable of considerable displacement by an electric field. These postulates drawn from imagination and simple thermodynamic calculations served as the first appropriate recognition of what is today called a hydrogen bond. These early findings could account for empirical observations of the exotic properties of water, such as its unusual melting / boiling point, deviation from Raoult's Law, solubility properties, complex formation and viscosity.[8]

In 1925, the inception of X-ray analytical techniques incurred a significant advancement in bonding theory. Over the course of the following 5 years, scientists used these first crystal structures to provide evidence for covalent, ionic and metallic bonds, and to lend credence to Huggins' description of a hydrogen bridge. Linus Pauling published a seminal paper in 1931 describing the quantum mechanical nature of chemical bonds,[15] which later culminated in his celebrated book '*The Nature of the Chemical Bond*'.[16] Here, he described the bonding in $[H\text{-}F\text{-}H]^+$ and attributed the concept of what then became known as the hydrogen bond to Huggins. Rapidly, the hydrogen bond became recognised as a crucial element of structural chemistry. It not only began to explain previously unaccountable scientific findings such as the exotic properties of water, but informed future research which saw the discovery of the α-helix and the β-sheet – crucial elements of protein architecture, and culminated in the discovery of the DNA-double helix – the most significant scientific discovery of the 20th century.

The definition of a hydrogen bond has been subject to extensive refinement since its discovery. A modern interpretation, adapted from the theory of relative atom electronegativities from Pauling's '*The Nature of the Chemical Bond*', is that a hydrogen bond is an attractive interaction that forms when a hydrogen-bond donor (HBD), D-H donates a proton to a hydrogen-bond acceptor (HBA), A (Figure 3).[8] For the HBD to be able to donate a hydrogen bond, the electronegativity of D must be greater than H such that significant electron density can be withdrawn from the D-H σ-bond, leaving the proton partially deshielded. The HBA, A must have a lone pair of electrons or π electrons that can interact with the donor bond.

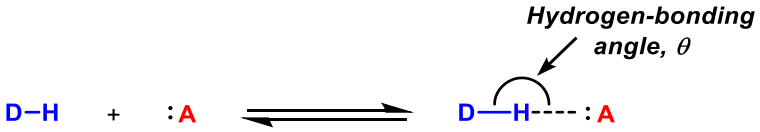

Figure 3 – The formation of a hydrogen bond.

There are five main components that affect the strength of a hydrogen bond: (a) electrostatic attraction, the attractive interaction between the negatively charged electrons in the HBA, and the positively charged proton of the HBD; (b) exchange repulsion, the repulsive interaction between two fermions which simultaneously occupy the same quantum state in the same quantum system, violating the Pauli exclusion principle; (c) polarisation, the attractive interaction between a charge cloud on the HBA and the permanent multipoles of the HBD; (d) charge transfer, the attractive quantum mechanical interaction arising from the construction of a new wavefunction for the hydrogen-bonded complex; and (e) dispersion, the attractive interaction arising from the fluctuating dipoles of the HBA and the HBD.[8] These five contributions to hydrogen-bond strength have different optimum hydrogen-bonding angles (the D-H-A angle, θ) and magnitudes depending on the chemical species. Nonempirical calculations performed by Duijneveldt have concluded that, in agreement with other independent semiempirical investigations, the electrostatic attraction, exchange repulsion, polarisation and charge transfer (a-d) contributions are all of the same order of magnitude as the total hydrogen-bond energy.[17] Exchange repulsion is insensitive to hydrogen-bonding angle and contributes only to hydrogen-bond length. This means that the dominant attractive contribution will depend on the specific hydrogen-bonded system, and that θ will be optimised in order to maximise that contribution.

For example, in hydrogen fluoride, the charge density map about the fluorine atom shows a near-spherically symmetrical electronic distribution about the lone pair hemisphere. This means that there would be no preferential hydrogen-bond trajectory from an electrostatic standpoint, provided it was above 90° to avoid proton-proton interactions. However, the maximum polarisation contribution to hydrogen-bond strength is at $\theta = 180°$, as this optimises interaction with each of the lone pairs of electrons about the sp^3-hybridised fluorine atom. Finally, the optimal charge transfer contribution would arise from direct overlap of the highest occupied molecular orbital (HOMO) of the hydrogen fluoride (the non-bonding π-orbitals of the fluorine atom, Figure 4) and the lowest unoccupied molecular orbital (LUMO) of the HBD (the σ* orbital of the D-H bond), which would correspond to $\theta = 102°$ according to valence shell electron pair repulsion theory (VSEPR). In the hydrogen fluoride dimer, the compromise of these factors culminates in a calculated minimum-energy angle of 140-160°. Interestingly, as the hydrogen fluoride oligomer gets longer, the charge transfer term becomes more dominant, resulting in a lowering of θ.

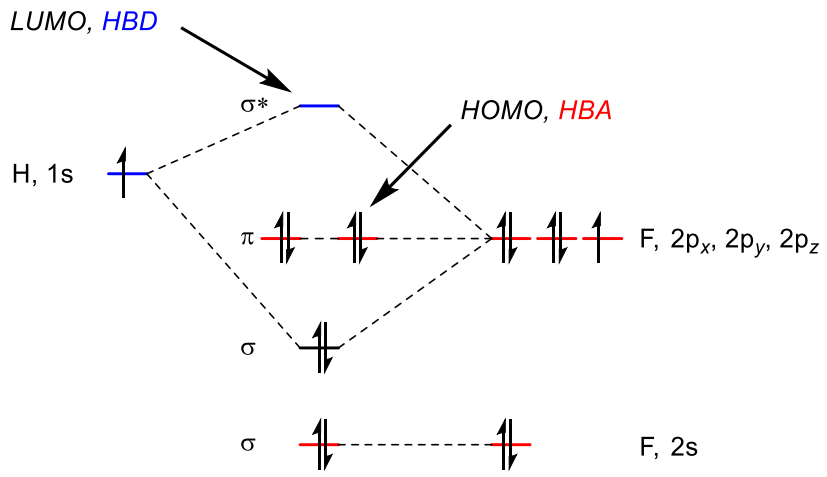

Figure 4 – Molecular orbital diagram for hydrogen fluoride.

When formaldehyde acts as an HBA, the HOMO is an n orbital of B_2 symmetry, where a nodal plane exists in the *xz* plane (if the *xy* plane is the molecular plane with the C=O bond in the *x* direction, Figure 5). The polarisation-favoured θ is 180° but transfer of electron density along this trajectory is symmetry-forbidden. Therefore, a charge transfer contribution to a hydrogen bond with formaldehyde must come from the lower energy A_1 σ orbital, where charge transfer is allowed. The A_1 σ orbital is substantially lower in energy than the B_2 n orbital, which means that there would only be a small charge transfer contribution to the hydrogen-bonding energy if the polarisation-favoured approach was followed. Therefore, in the case of formaldehyde, the polarisation-favoured trajectory is compromised in order to maximise charge transfer from the B_2 orbital, resulting in a θ of 116° when water is the HBD.[8]

Additionally, hydrogen bonds that deviate from the carbonyl plane can be bolstered by charge transfer occurring from the carbonyl π bond, which is of B_1 symmetry. This orbital is lower in energy than the B_2 orbitals and so the stabilisation from this effect is not as significant as charge transfer in the carbonyl plane.

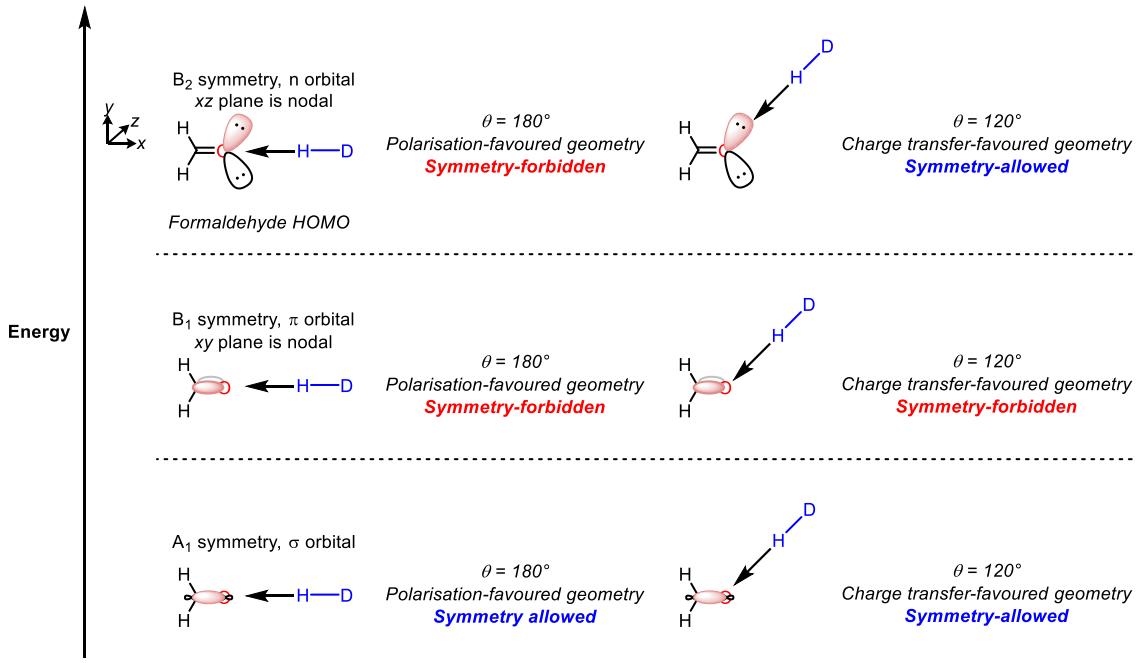

Figure 5 – Optimal geometries for hydrogen-bonding contributions in formaldehyde.

Dreyfus and Pullman extended this computational analysis and found that θ in the formamide dimer is near 120° and that the difference in energy between this conformer and that where θ = 180° is 6.3 kJ mol^{-1}, comparable to that of formaldehyde.[18] Similarly, the HOMO of formamide is an n orbital of B_2 symmetry, where the same orbital symmetry effects apply. These effects are sensitive to hydrogen-bonding distance – due to their quantum mechanical nature, the B_2 orbitals will transfer more charge to more proximate HBDs, such that the preference to follow the charge-transfer-favoured trajectory of 120° decays with distance and the hydrogen-bonding trajectory tends towards the polarisation-favoured direction of 180°. This is commensurate with observations from Coulson, Danielson and Michaelides that longer hydrogen bonds are more electrostatic in nature, whereas shorter hydrogen bonds have larger charge-transfer contributions and are more covalent in nature.[18,19] It is proposed that this concept can be extrapolated to trisubstituted ureas, in that the optimum θ for hydrogen-bonded urea oligomers is near 120°, and that the hydrogen bonding weakens significantly as it approaches 180°.[8,20]

Hydrogen bonds provide thermodynamic stabilisation to molecules, meaning that there are enthalpic and entropic contributions to their energy. The discussed phenomena have only applied to intermolecular hydrogen bonds, where hydrogen-bond strength can be optimised without geometric restriction. In an intermolecular hydrogen-bonding pair, dilution will increase the entropic cost to hydrogen bonding. The intramolecular analogy is that if a hydrogen bonding-pair must unite over a certain distance using a tether with many degrees of freedom, there is a high entropic cost to pay. As the distance between them increases, the entropic cost becomes greater. The enthalpic contribution may also differ from the intermolecular variant as geometric restriction may not allow optimal hydrogen bonding to take place.

Cockroft and co-workers investigated relative intramolecular hydrogen-bonding strength between *N*,*N*-dimethylamides and phenols by varying the number of rotatable bonds that separated them (Figure 6).[21] The strength of the intramolecular hydrogen bonds was extrapolated by measuring the propensity for external HBAs to interrupt the intramolecular hydrogen bonds.

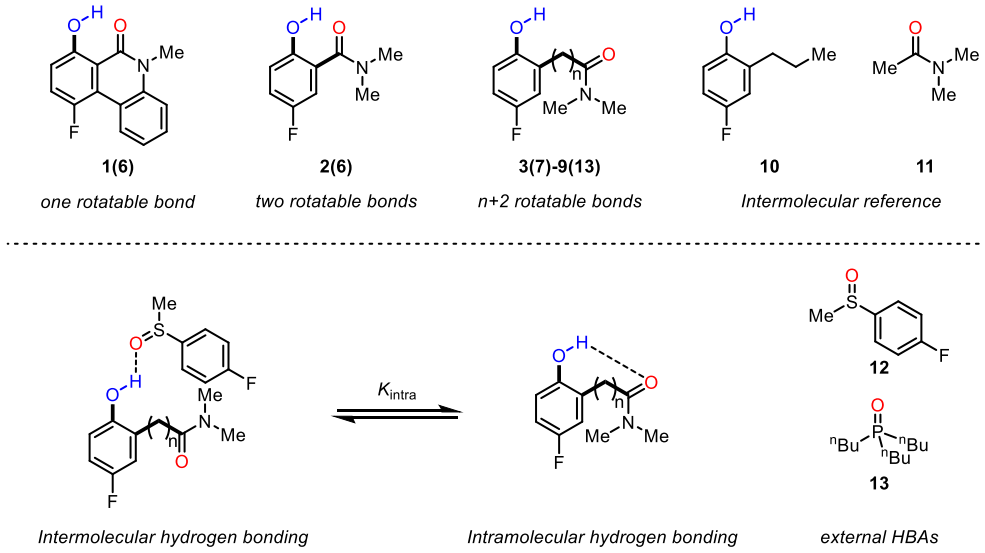

Figure 6 – Investigation of intramolecular hydrogen bonding by tether extension (the compound number denotes the number of rotatable bonds, and the number in brackets denotes the hydrogen-bonding ring size. Rotatable bonds are emboldened).[21]

Compounds **1(6)-9(13)** were analysed by ^{19}F NMR with equimolar quantities of external HBAs sulfoxide **12** and phosphine oxide **13**, and the difference in chemical shift of the aryl fluoride signal was monitored as the solutions were diluted. If a weak intramolecular hydrogen bond was present, it would be supplanted by an intermolecular hydrogen bond with the external HBA. Consequently, the aryl fluoride chemical shift would change with dilution due to the increased entropic penalty of intermolecular hydrogen bonding. If a strong intramolecular hydrogen bond was present, the aryl fluoride chemical shift would be insensitive to dilution as

there would be no contribution from intermolecular hydrogen bonding. For smaller hydrogen-bonding rings with fewer rotatable bonds, such as compounds **1(6)-5(9)**, sulfoxide **12** did not participate in any detectable intermolecular hydrogen bonding, representing strong intramolecular hydrogen bonding between the phenol and the amide (Figure 7a). Upon extending the alkyl amide tether to **6(10)**, intermolecular hydrogen bonding was detected, indicating a sharp decline in intramolecular hydrogen-bonding strength. The free energy change upon intermolecular binding, ΔG_{obs} was deduced by relation to the binding constant K_{obs} through the equation $\Delta G_{obs} = -RT\ln K_{obs}$, where K_{obs} was obtained by fitting the observed chemical shifts to a 1:1 binding model. Extension to **7(11)** saw a slight further attenuation of intramolecular hydrogen bonding which then stayed approximately constant upon further homologation. This plateau matched the observed free energy of hydrogen bonding for the intermolecular variant, phenol **10** with amide **11**. Phosphine oxide **13** is a much stronger HBA than sulfoxide **12** and therefore even with phenols **2(6)** and **3(7)**, partial intramolecular hydrogen-bond disruption was observed. Extension to **4(8)** mitigated the competitive intermolecular hydrogen bonding, bringing ΔG_{obs} near to zero. Above 4 rotatable bonds, phosphine oxide **13** exhibited the same behaviour as sulfoxide **12** (Figure 7a).

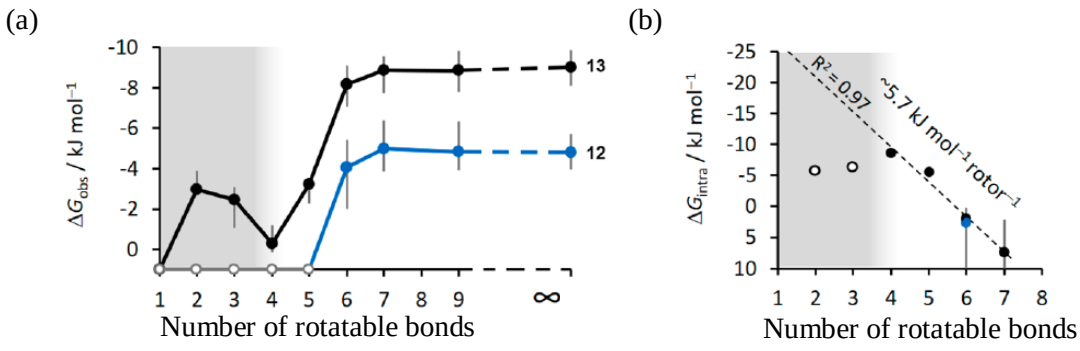

Figure 7 – The dependence of (a) experimental binding free energies, ΔG_{obs} and (b) dissected folding energies, ΔG_{intra} on the number of rotatable bonds in an alkyl tether.[21]

It can be inferred from this that structures with 5 or fewer rotatable bonds form very strong intramolecular hydrogen bonds that need remarkably strong HBAs to disrupt them. This shows that hydrogen-bonding rings with up to 9 members are among the most stable. However, it should be mentioned that the strong intramolecular hydrogen bonding in phenols **1(6)** and **2(6)** may be augmented by conjugation of the phenol with the amide. Additionally, dissected folding energies were deduced for compounds with 4 or more rotatable bonds by relating K_{obs} to the free energy change upon intramolecular hydrogen bonding, ΔG_{intra}. There was a steep and negative linear correlation between the number of rotatable bonds and ΔG_{intra} (Figure 7b). Inspection of this relationship revealed an entropic penalty to hydrogen bonding of 5.7 kJ mol^{-1} for each rotatable bond in this particular system at 20 °C. This hydrogen-bond weakening can also be

attributed to the transannular strain associated with the formation of the hydrogen-bonding ring. Finally, it is worth noting that the system described here only describes modification of the tether by extension with an sp^3-hybridised methylene group. Different atoms, hybridisations and substitutions within the tether are expected to have a large effect on intramolecular hydrogen bonding.

Effective molarity (EM) is a parameter that is commonly applied to intramolecular reactions. In the case of intramolecular hydrogen bonding, it is measured as the ratio between the intramolecular association constant and the corresponding intermolecular association constant.[22] Hunter and co-workers designed a method to deduce the dependence of the EM of hydrogen bonds on geometric and electronic factors. A broad range of zinc porphyrin complexes with pendent HBDs and pyridine ligands with pendent HBAs were synthesised.[23] The families of zinc porphyrin complexes and pyridine ligands were ligated and the contribution to the complexation by the resultant hydrogen-bonding interactions was determined by use of a double-mutant cycle (Figure 8).

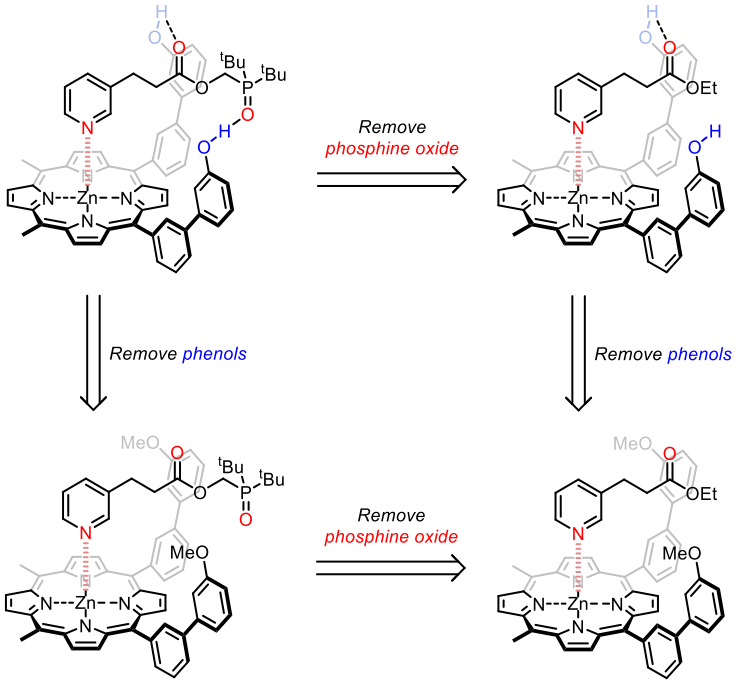

Figure 8 – Double-mutant cycle experiment for the determination of hydrogen-bond EM.[22]

The double-mutant cycle operated by using zinc porphyrin-pyridine complexes that were highly structurally analogous to the hydrogen-bonded system, except the HBDs and HBAs were sequentially removed. The free energy contributions upon ligand binding could then be deduced by using UV-Vis titrations and monitoring the fluorescence of the porphyrin. Comparison of ΔG_{obs} of these four complexes could be used to dissect out the contribution of secondary effects

of the ligand/complex to binding, leaving only the contribution of the hydrogen bond. This ΔΔG could then be used to deduce the association constant for hydrogen bonding, K_{assoc}, and by comparison to the analogous intermolecular complex, the EM of that particular hydrogen bond.

Double-mutant cycle experiments for 240 different zinc porphyrin-pyridine complexes revealed several correlations. First, different HBAs with similar geometries but different polarities were fused to the 3-(3-pyridyl)propionate ligand and contrasted. Comparison of complexes with pendent phosphine oxides, amides and esters showed that hydrogen-bond EM was insensitive to the polarity of the HBA and therefore the intrinsic strength of the hydrogen bond. Similarly, comparison of the complexes in toluene and 1,1,2,2-tetrachloroethane (TCE) revealed that hydrogen-bond EM was independent of the polarity of the medium. This means that the contribution of the solvent to hydrogen-bond strength is factored out by the double-mutant cycle experiment. However, phosphonate diesters and amides are HBAs with similar polarities, but different geometries. The two complexes formed of these groups exhibited different hydrogen-bond EMs, indicating a sensitivity to subtle changes in hydrogen-bond geometry. Finally, a wide range of pyridine linkers were synthesised to give an appropriate range of HBD-HBA distances, and it was found that hydrogen-bond EM differed greatly depending on the size of the linker. In these supramolecular architectures, hydrogen-bond EM can range between 3-240 mM, and its sensitivity derives only from hydrogen-bond geometry complementarity and length. The corollary of this is that, unless a more thermodynamically favourable alternative is available, a hydrogen bond will always form independent of hydrogen-bond strength and solvent polarity provided that the HBD and HBA are proximate and of the correct geometry to do so.

This work was extended by Hunter and co-workers to the hydrogen-bond-accepting solvent, cyclohexanone.[24] As discussed, EM is an intrinsic property of a complex, and so should be insensitive to the polarity of its medium. EMs determined in toluene and TCE were used to calculate expected complex stabilities in cyclohexanone. There was strong agreement between that of toluene and cyclohexanone, but there were significant discrepancies between TCE and cyclohexanone. Ligand coordination and hydrogen bonding were factored out using the double-mutant cycle experiments, and so these discrepancies were attributed to the stability of the solvent shell. It was further clarified that in the case of TCE, EMs of the hydrogen bonds were anomalously high due to steric desolvation of the phosphonate diesters upon pyridine coordination and hydrogen bonding. This means that hydrogen bonds may become more prone to formation if the bulk of the neighbouring groups do not accommodate for solvent molecules.

Hydrogen-bonding chains are highly prevalent in supramolecular and biological systems. Hydrogen-bond cooperativity – the theory that contiguously bound hydrogen-bonded units exhibit a synergistic effect on hydrogen-bond strength, has been widely accepted by the supramolecular community.[25] The use of this cooperativity to modulate hydrogen-bond strength remote from hydrogen-bonding sites is a very useful tool that both nature and supramolecular chemists have recognised and exploited to facilitate informational communication[26] and control macromolecular structure.[27,28] Although many properties are affected by hydrogen-bond cooperativity, it is very difficult to specifically measure the strength of the effect due to further contributions from intermolecular effects, entropy and modified electrostatic and polarisation parameters.[29]

To combat this issue, Cockroft and co-workers developed the use of *N*,*N*-diaryl formamides as molecular balances for the quantification of hydrogen-bond cooperativity.[29] One of the arenes bore varying numbers of amphoteric phenolic groups for the formation of contiguous hydrogen bonds (Figure 9). Due to the rotameric nature of the formamide, the equilibrium concentrations of the two rotamers could be quantified by ^{19}F NMR at 20 °C. The equilibrium distribution of rotamers was biased towards the s-*cis* conformation (with respect to the hydroxylated arene) due to the formation of a hydrogen bond between the formamide and the *ortho*-phenol. This approach eliminated effects arising from alternative hydrogen-bonding modes, intermolecular effects, and steric encumbrance.

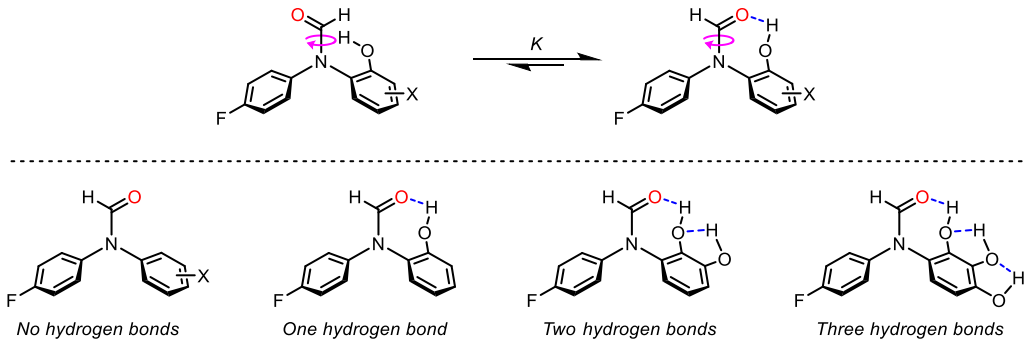

Figure 9 – *N*,*N*-diarylformamide balances for the quantification of hydrogen-bond cooperativity.[29]

The equilibrium distribution of rotamers was used to determine a value for the equilibrium constant, which was then used to determine the difference in free energy of the two rotamers, ΔG. ΔG was influenced by the electronic properties of the two arenes, but predominantly by the strength of the hydrogen bond that the formamide formed with the phenol. This meant that if cooperative hydrogen-bonding effects augmented the hydrogen-bond-donating ability of the *ortho*-phenol, then that effect would be represented by the change in equilibrium distribution of formamide rotamers, which could then be converted to ΔG. In the case of *ortho*-

phenol, **14**, where only one hydrogen bond was present, there was a strong preference for the hydrogen-bonded rotamer corresponding to $\Delta G = -4.2$ kJ mol^{-1} (Figure 10a). Interestingly, when a second hydrogen-bonding unit was added in the case of the 3-formamidocatechol, **15**, the free energy difference approximately doubled to $\Delta G = -8.1$ kJ mol^{-1}, suggesting that the terminal phenol became almost twice as good an HBD upon introduction of a second hydrogen bond. This effect was persistent even upon addition of 10% (v/v) acetonitrile as a competitive hydrogen-bond-accepting solvent. This change in hydrogen-bond-donating ability could have been attributed to the alteration of substituent effects, and so control experiments were performed by functionalising the hydrogen-bonding arene for Hammett analysis (Figure 10b).

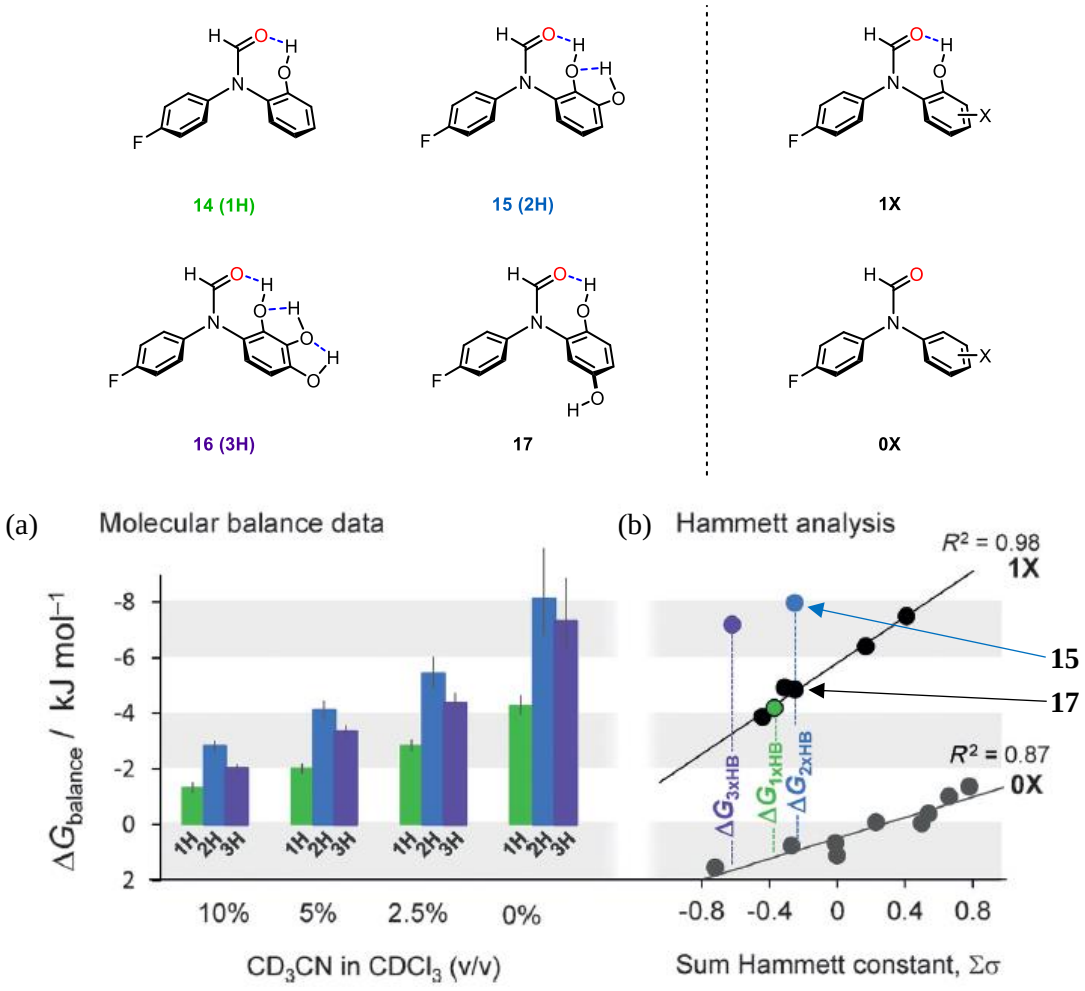

Figure 10 – Control experiments for *N*,*N*-diarylformamide balances. (a) ΔG values in the presence of CD_3CN (XH denotes how many intramolecular hydrogen bonds are present). (b) Hammett analyses of non-hydrogen-bonded arenes (0X) and singly hydrogen-bonded arenes (1X).[29]

Two Hammett plots were constructed by measuring ΔG for *N*,*N*-diaryl formamides with no hydrogen-bonding phenol (0X, Figure 10b) and with one hydrogen-bonding phenol (1X,

Figure 10b). The difference in ΔG for 0X and 1X at the certain ∑σ values represented the ΔG of hydrogen bonding with substituent effects that would arise from further hydroxylation removed. The most pertinent example is the comparison of catechol **15** and hydroquinone **17**, which are electronically similar as the second hydroxyl group is *meta* to the formamide in both cases. However, these molecules differ because a second hydrogen bond can form in catechol **15** but cannot in hydroquinone **17**. In this case, it was found that $\Delta G = -8.0$ kJ mol^{-1} for **15** and $\Delta G = -5.1$ kJ mol^{-1} for **17**, corresponding to a difference of -2.9 kJ mol^{-1} in hydrogen-bonding energy arising from hydrogen-bond cooperativity.

Upon extension to a third hydroxyl group in 4-formamidopyrogallol **16**, a minimal decrease in conformer ratio was observed, indicating a lack of cooperative effects with more than two hydrogen bonds. Unfortunately, the 2,3,4,5-tetrahydroxyanilide proved too unstable to be analysed, and so this example was substituted with B3LYP/6-311G* calculated conformational energies. These energies correlated very well with the experimental energy differences determined for the other balances. The simulated 2,3,4,5-tetrahydroxyanilide revealed no further improvement of hydrogen bonding at the *ortho*-phenol.

When phenols **14**, **15** and **16** were analysed with equimolar phenol as an intermolecular HBD to complement the hydrogen-bonding network, a cooperative effect was observed between phenol **14** and phenol, but upon extension to catechol **15** and pyrogallol **16**, no further benefit occurred. The rationalisation of these data is that addition of one hydrogen bond can substantially improve the strength of another by hydrogen-bond cooperativity, but further addition of hydrogen bonds has no effect. This phenomenon was accounted for by the fact that only the terminal hydrogen-bonding interaction was monitored. It was speculated that the other hydrogen bonds in the network thermodynamically benefitted from hydrogen-bond cooperativity upon introduction of more hydrogen bonds, but this could not be probed by the *N*,*N*-diarylformamide balances. This supposition was consistent with previous computations that suggested that polarisation changes are most prominent at the end of hydrogen-bonded chains.[28]

In conclusion, hydrogen bonds are interactions that nature has ubiquitously exploited and that chemists have recognised the potential of over the past two centuries. The sensitivity of their strength and geometry to a huge range of proximal and distal chemical effects render them highly valuable interactions for the design of chemical function such as chemical reaction,[30] highly specific guest binding[31] and informational communication.[26] Nature has evolved to rely on hydrogen bonds for the performance of each of these functions, and synthetic and supramolecular chemists are now harnessing their power to replicate and surpass those functions. Finally, concepts drawn from the increased understanding of hydrogen bonds have also allowed chemists to gain access to novel function that nature could not previously access.[2,32]

1.3 Conformational Change and Informational Communication in Dynamic Foldamers

The origin of life is a widely researched theme, where the most fundamental contribution to it is a subject of great controversy. However, it is widely accepted that the four prerequisites for life are compartmentalisation, metabolism, catalysis and informational processing.[33] Informational processing is the ability of a system to respond to a stimulus and communicate that response through space to a processing site remote from the informational source. Evolution has allowed nature to master this practice and has enabled it to communicate information reliably and with exquisite spatial and temporal precision.

Nature typically processes information by the induction of conformational change. A highly prevalent example of this is G protein-coupled receptors (GPCRs), which are responsible for processing physiological information and giving rise to the optical, olfactory and gustatory senses and maintenance of mood and the immune system.[34] GPCRs are membrane-bound receptors that differ by the host molecule(s) they can bind. There are nearly a thousand different GPCRs in humans, each endowed with a peptide sequence that allows highly specific binding of guest molecules found in their environment.[35] A G protein is a heterotrimeric protein that can bind either guanosine triphosphate (GTP) or guanosine diphosphate (GDP). When the GPCR is not bound to a guest, the G protein is bound to GDP and is closely associated with the GPCR. When the guest binds, a conformational change takes place in the GPCR, lowering the G protein's affinity to GDP, releasing it. This GDP is replaced by GTP, which changes the G protein's conformation, causing it to dissociate from the GPCR. The G protein then translates along the membrane and is free to interact with other membrane-bound proteins, which can stimulate a response. When the guest dissociates, the G protein releases the GTP and reassociates with GDP, resulting in turnover. In this biological example, the binding of a specific guest causes a conformational change, which is communicated through space from G protein movement and facilitates a response (from the stimulation of other membrane-bound proteins).

Chemists have taken inspiration from nature's informational communication mechanisms to make artificial molecules that can perform the same functions. These molecules form part of a family of synthetic molecules called *foldamers*. Coined by Gellman in 1996, foldamers are defined as polymers that have a strong tendency to adopt a specific compact conformation.[36] Many foldamers have been designed with the goal of making biologically orthogonal architectures that can exhibit the same spatially specific orientation of function as their natural counterparts. For example, Gellman and co-workers simulated and synthesised β-amino acid oligomers derived from *trans*-2-aminocyclohexanecarboxylic acid (ACHC) and *trans*-2-aminocyclopentanecarboxylic acid (ACPC). It was found that these oligomers formed particularly stable 14- and 12-helices (Figure 11).[37]

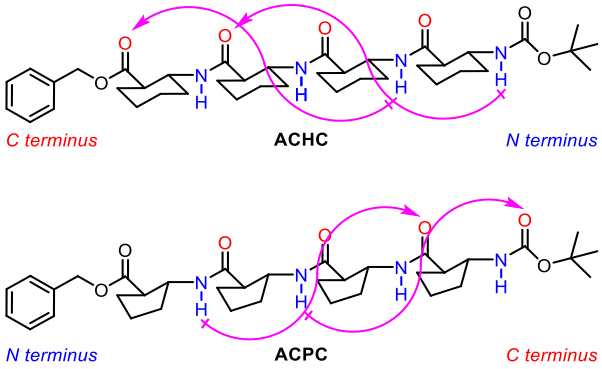

Figure 11 – ACHC- and ACPC-derived oligomers (arrows indicate the atoms between which hydrogen bonds form).

It was shown that the ACHC and ACPC helices were stable in methanol and pyridine solutions, and deuteration studies showed that the amido protons were involved in strong hydrogen bonds, as their rate of deuteration was slow relative to the exposed N-terminal amido protons. This and X-ray crystallographic studies confirmed the helical conformations that simulations had predicted. Interestingly, the ACHC and ACPC foldamers show hydrogen-bond donation in opposite directions. This shows that the conformation-dependent dipoles and hydrogen-bond directionality of the two helices also point in opposite directions. This switch in hydrogen-bond directionality is unknown in α-amino acid-based oligopeptides. Foldamers of this type and hybrid α/β-amino acid foldamers have been shown to bind to proteins such as Bcl-2 proteins, which act as apoptosis regulators.[38] The overexpression of some of these proteins, such as Bcl-x_L, can result in cancer, making helical foldamers a very promising area for the development of anti-cancer agents.[39] They are also known to inhibit other damaging protein-protein interactions, further bestowing them with medical application. Finally, they can also be used for enzyme biomimicry, such as the action of a designed aldolase foldamer.[40]

Whilst Gellman's definition implies the population of a single compact conformation, the definition has been extended to families of foldamers that can adopt more than one stable conformation. This conformational freedom deviates from the definition. However, if the different stable conformations can interconvert in response to a stimulus, they are rendered *dynamic foldamers*. For example, Huc and co-workers have developed aromatic oligoamide foldamers, which have been designed to either form β-sheet mimics or wide-diameter helices due to π-stacking interactions and the conformational preference of aryl amides.[41] These foldamers were combined with a metal-sensitive binding site to make a metal-mediated conformational switch which could turn the binding of a specific guest on and off (Figure 12).[42]

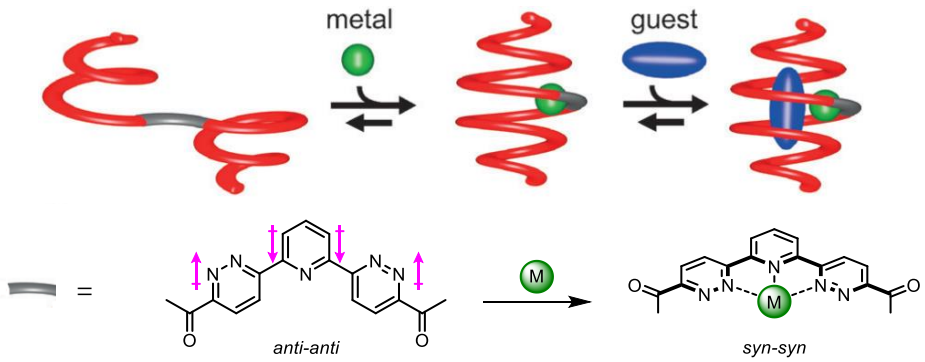

Figure 12 – Metal-mediated guest binding in aromatic oligoamide foldamers.

The 2,6-bis(3-pyridazyl)pyridines adopted an *anti-anti* relationship between the arenes to favour interdipolar interactions. In the presence of a metal cation such as copper or silver, the arenes reoriented to coordinate to the metal, adopting a *syn-syn* conformation. When this functional teraryl was connected to two of the helical aromatic oligoamide foldamers, the helices were separated from each other in the *anti-anti* form and did not have a preferred handedness relative to each other. Addition of copper or silver cations enforced a *syn-syn* conformation, which rotated the helices into proximity, making a new helix of one continual handedness. Numerous helices of this type were made with different diameters, and it was found that the metal-induced conformational change allowed acetonitrile and imidazole molecules to be captured by the cavity formed. Huc and co-workers have also used their work on β-sheet mimics and helices in aromatic oligoamides to synthesise other architectures. These architectures were designed with highly defined helical and sheet-like segments with specific geometries constructed with judicious employment of interdipolar interactions.[43]

Hamilton and co-workers have developed conformational switches that can respond to a variety of stimuli.[44–46] For example, it was shown that oligomers derived from 2,6-bis(*N*-imidazolidin-2-onyl)pyridines act as β-sheet-mimetic foldamers rigidified by interdipolar interactions.[47] This work was extended by using trifluoroacetic acid (TFA) and trifluoromethanesulfonic acid (TfOH) to protonate the pyridines in the oligomer (Figure 13).[48] When protonated, the imidazolidinones reoriented to hydrogen bond to the resultant protonated pyridinium cation. This changed the trajectory of the imidazolidinones and introduced curvature to the oligomer. In longer oligomers, this curvature and the enantioenrichment of the imidazolidinones gave rise to a right-handed helical conformation.

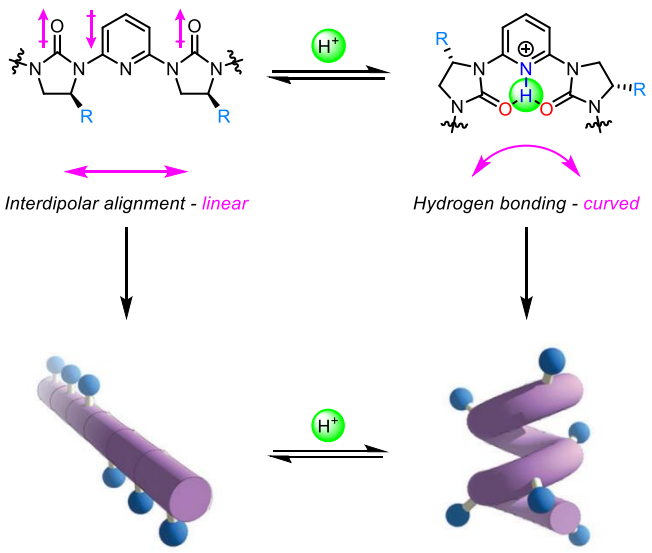

Figure 13 – pH-dependent topology in 2,6-bis(*N*-imidazolidin-2-onyl)pyridine oligomers.

Additionally, subtle changes to the electron-richness of different pyridines in the oligomer allowed site-selective protonation, bestowing spatial control of curvature. Finally, the basicities of the pyridines decreased with each subsequent protonation, allowing control of general curvature by addition of the correct acids in the correct stoichiometries.

These examples highlight macromolecular conformational change in response to a stimulus. This is very useful as it can confer very different function in different states, but informational processing does not necessitate this. For example, Hamilton and co-workers have also reported the use of diphenylacetylene balances appended with hydrogen-bonding groups that shift their conformational equilibrium in response to stimuli, such as the presence of halides (Scheme 1).[49]

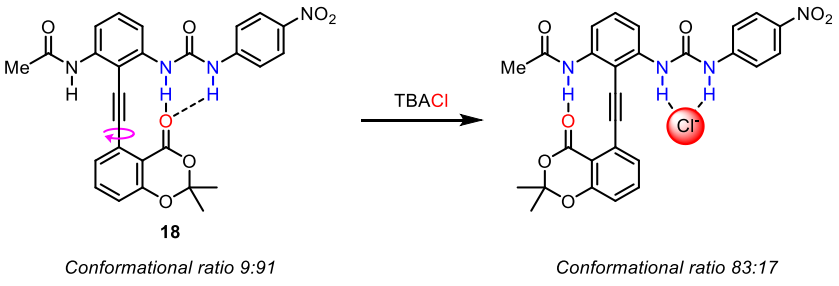

Scheme 1 – Hamilton's anion-dependent conformational switch.

The molecular balance, **18** exists as a mixture of two conformers in fast exchange on the NMR timescale at 25 °C. In these conformers, the benzodioxinone carbonyl hydrogen bonds either to the acetamide or to the urea, and the equilibrium constant represents the difference in hydrogen-bonding strength between the two groups. In the absence of salt, the conformer

distribution lies in favour of the hydrogen-bonded urea because the urea can donate two protons to the benzodioxinone. Halides are known to form strong complexes with *N*,*N'*-disubstituted ureas, and so upon addition of tetrabutylammonium chloride (TBACl), the chloride displaces the benzodioxinone. This forces the benzodioxinone to hydrogen bond to the acetamide instead and inverts the equilibrium. Similar balances were conceived from appending the diphenylacetylene scaffold with 4-(dimethylamino)benzamides, isonicotinamides and ferrocenecarboxamides and exploiting their basicities, Lewis acid affinities and redox sensitivities to effect conformational switching.[44–46] These balances constitute a versatile scaffold that can respond to subtle changes in hydrogen-bond-donating ability by changing conformation, and can respond to a wide range of stimuli. Whilst these examples have highlighted conformational changes in the response to information, they have not involved the relay of that information through a communicable scaffold.

Clayden and co-workers have devised several strategies for intramolecular informational communication. For example, xanthene-1,8-dicarboxamides are known to orient their amides antiparallel to each other and perpendicular to the plane of the xanthene owing to the conformational preference of tertiary benzamides and optimisation of interdipolar interactions.[50] This conformational preference could be intramolecularly communicated between xanthene units, meaning that the analogous tris(xanthene-1,8-dicarboxamide) exhibited an all-*anti* relationship of the amides (Scheme 2).

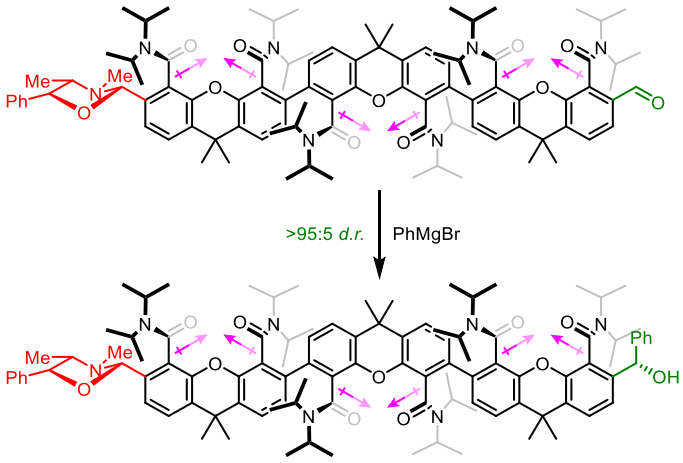

Scheme 2 – 1,23-stereoinduction in tris(xanthene-1,8-dicarboxamide)s.

When the tris(xanthene-1,8-dicarboxamide) was terminated with an ephedrine-derived chiral oxazolidine, the first amide was induced into a *P* conformation to minimise steric clashes. This conformational preference was communicated over the three xanthene units by alternating *P*,*P* and *M*,*M* xanthene configurations, meaning that an aldehyde incorporated at the opposite terminus would be influenced by the chirality of the oxazolidine 23 atoms away. This was

validated by treatment of the aldehyde with a Grignard nucleophile, which added to the aldehyde with complete diastereoselectivity. This example represents a long-range conformational relay where information in the form of chirality can be communicated throughout the scaffold and be processed in the form of asymmetric reaction.

Clayden and co-workers have published extensively in the area of foldamers, predominantly on the dynamics and functions of synthetic helices in the context of informational communication. For example, oligomers of the achiral quaternary amino acid aminoisobutyric acid (Aib) adopt 3_{10}-helical conformations.[26] By virtue of its conformation, a helix is a chiral object, which has diastereomeric screw-sense preferences when made up of chiral monomers and enantiomeric screw-sense preferences when made up of achiral monomers. When comprised of Aib monomers, the helix formed is configurationally achiral in solution as the screw sense of the helix interconverts rapidly at 20 °C. However, when terminated with a chiral quaternary amino acid, the equilibrium is biased towards one diastereomeric screw sense.

For example, a helical polypeptide was synthesised with two monomers of enantiomerically pure L-α-methylvaline at one terminus, with the rest of the helix being made up of iterations of four Aib units and a 1-aminocyclohexanecarboxylic acid unit (Figure 14). The two initial chiral monomers induced almost complete conformational preference for the structure to adopt a *P* helix, which became more pronounced with decreasing temperature.[26]

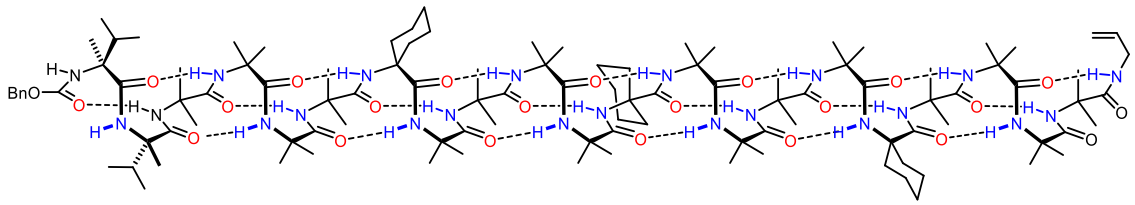

Figure 14 – Screw-sense preference of a 3_{10} helix induced by central chirality.

On the other end of the helix, stereoselective reactions were performed to determine the use of helical fidelity alone in asymmetric reaction (Scheme 3). Asymmetric hydrogenation of a *Z*-styrene in the helix to give the corresponding phenylalanine residue proceeded with excellent selectivity in favour of the L-phenylalanine diastereomer. Hydrogen-bonding solvents, such as methanol, were deleterious to the selectivity due to a lowering of the screw-sense preference of the helix, resulting from competitive hydrogen-bonding interactions with the solvent. Similar results were observed by terminating the helix with an acyliminium ion. An electron-rich arene was used to attack the acyliminium ion with high diastereoselectivity due to the chiral environment the helix imposed. This remote 1,61 asymmetric induction resulted in a diastereoselective reaction over 4 nm away from the nearest chiral centre.

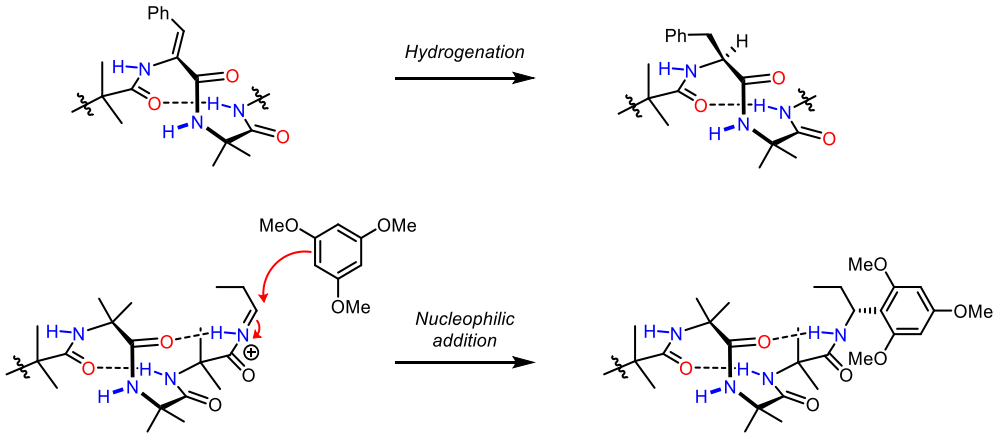

Scheme 3 – Helices in asymmetric reaction.

As exemplified by these studies, helices work as excellent communicators of binary information by maintaining a screw-sense preference that can be communicated from one terminus to the other. This can lend itself to a range of exotic functions and biomimicry, and thus methods for inducing screw-sense preference in achiral helices using external stimuli as opposed to inherent chirality were investigated.

Clayden and co-workers then extended this work by investigating a configurationally achiral Aib-derived helix whose screw-sense preference could be influenced by binding a chiral ligand. The system chosen used a basic pyridine unit to terminate the helix, and a variety of chiral Brønsted acids to interact with it (Figure 15).[51]

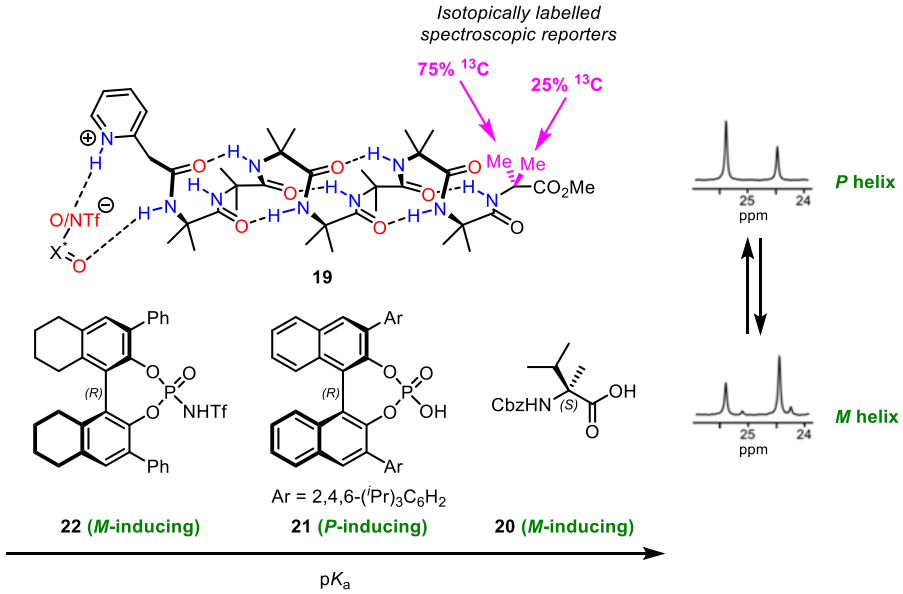

Figure 15 – Interaction of chiral Brønsted acids with a configurationally achiral Aib helix (*P* helix depicted).

To maximise the influence of the ligand's chirality on the helix, chiral carboxylic, phosphoric and phosphoramidic acids were used so that the conjugate bases could interact with the protonated helix. Isotopic labelling of the enantiotopic geminal methyl groups in the terminating Aib unit was used to determine terminal screw sense preference. One of the methyl groups was 25% enriched with ^{13}C, and the other was 75% enriched with ^{13}C. This meant that the terminal methyl groups, that were diastereotopic due to the chiral environment imposed by the helix, could be distinguished by relative integration. From this, it was inferred that pyridine protonation and binding of the acids could induce a high degree of helical excess with a defined screw sense that depended on which enantiomer of the acid was used. This system lent itself to the functioning of a complex four-component system whereby competitive acid-base interactions gave rise to a conformational switch that depended on what acids were available for binding in solution.

By itself, pyridine **19** rested as a rapidly racemising mixture of screw-sense preferences. Upon addition of enantioenriched carboxylic acid **20**, protonation of the pyridine and subsequent binding of the carboxylate formed an adduct with a screw-sense preference for an *M* helix. Addition of the opposite enantiomer of phosphoric acid **21** resulted in displacement of carboxylic acid **20** and reversed the screw-sense preference to a *P* helix due to the formation of a new, more favoured pyridine **19**/phosphoric acid **21** adduct. Next, the opposite enantiomer of phosphoramide **22** was added, which displaced phosphoric acid **21** and reversed the screw-sense preference of the helix back to *M* again. The path of screw-sense preference switches could then be completely reversed by addition of stoichiometric quantities of base. 1.5 equivalents of ammonia were added, forming the ammonium salt of the strongest acid, phosphoramide **22**. This left the next strongest acid, phosphoric acid **21**, to bind to the pyridine of the foldamer, so the screw-sense preference was reversed to *P* again. The same effect was observed upon addition of a further 1.5 equivalents of ammonia, whereby the ammonia formed the ammonium salt of phosphoric acid **21**, leaving carboxylic acid **20** to induce its screw-sense preference on the foldamer. Addition of a further 1.5 equivalents of ammonia resulted in full deprotonation of all the chiral acids, so the helical foldamer exhibited no screw-sense preference and thus was configurationally achiral. Finally, addition of 4.5 equivalents of HCl resulted in full protonation and liberation of all the chiral acids, where phosphoramide **22**, as the strongest acid, formed an adduct with the foldamer and induced an *M* helix once again. This represented a complex acid/base switch whereby different components of the mixture could form adducts with the foldamer and induce screw-sense preference depending on the degree to which free base was present. In this example, information was stored in the form of the chirality of the acids and was processed by the pyridyl terminus of the helix. Information was then propagated through space in the form of screw-sense preference, which was reported by an isotopically labelled spectroscopic reporter.

Clayden and co-workers also went on to design and construct a synthetic mimic of a GPCR which could also function in the membrane phase. The design comprised of a binding site for a cationic metal cofactor, an Aib oligomer for the communication of the chiral information through the membrane, and a chiral bis(pyrene) moiety at the opposite terminus (Figure 16).

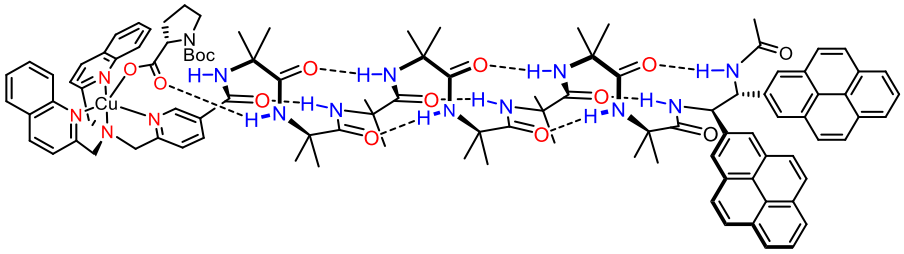

Figure 16 – Synthetic G protein-coupled receptor.

Upon binding of copper(II) and the enantioenriched carboxylate of Boc-L-proline, the hydrogen-bonding interactions between the proline and the Aib oligomer induced a screw-sense preference for a *P* helix in the membrane phase. Since the dipyrene spectroscopic reporter at the opposite terminus exhibits central chirality, binding of the two different enantiomers of Boc-proline carboxylate resulted in diastereomeric adducts whose anisochronicity was most pronounced at the bis(pyrene). This meant that, depending on which enantiomer of the Boc-proline was bound, different fluorescent responses could be elicited. This example represented a significant simplification of how GPCRs work and acted as a mimic that could perform its function in aqueous and biological media.

To summarise, foldamers have been used to gain access to conformational space that nature has not yet discovered, and they have been exploited as such for advances in biomimicry and medicine. More recently, *dynamic foldamers* have been used as sensors, which can respond to stimuli by changing macromolecular shape and binding affinity to certain guests. Similarly, other families of dynamic foldamers have been developed to communicate information in response to stimuli. In these cases, the informational input did not result in topological change, but in a subtle conformational change which was effectively communicated throughout the scaffold. From this, hydrogen-bonding networks can be influenced by a plethora of external stimuli and can be used to communicate binary information in solution and in the membrane phase to positions remote from the informational source. These biomimetic constructs have largely used diagnostic spectroscopic signals as their output, but they have also been able to perform function in the form of asymmetric reaction.

1.4 Light-Induced Conformational Changes in Foldamers

The presence or absence of light can also be considered as information, and it is a source of high information entropy according to information theory, due to the large range of wavelengths it can take.[52] Animals have evolved to harness light as a way to gain large amounts of information about their surroundings. This is typically done by using a type of GPCR called opsins, bound to a polyene chromophore called retinal.[53] The absorbance of retinal changes depending on the opsin it is bound to, bestowing an absorbance range of 400-700 nm light, and therefore a large amount of information that can be processed. Upon absorption of a photon of the correct wavelength, an olefin in retinal undergoes a *Z* to *E* isomerisation, which results in a conformational change of the opsin receptor. This conformational change then results in liberation of the G protein, which then interacts with other membrane-bound proteins and elicits a response.[54]

Inspired by nature, the vast utility and practicability of light has attracted a large amount of scientific research over the past two centuries, culminating in significant discoveries such as light-controlled memory devices, self-healing materials and light-triggered drug release.[55–57] In supramolecular chemistry, it has also been used for the development of unidirectional motors, molecular muscles and cargo transporters.[58–60]

Light has also found extensive use in dynamic foldamer chemistry. For example, Huc and co-workers reported a light-controlled conformational switch in an aromatic oligoamide foldamer based on the light-induced [4+4] cycloaddition of 1,8-diazaanthracenes (Scheme 4).[61]

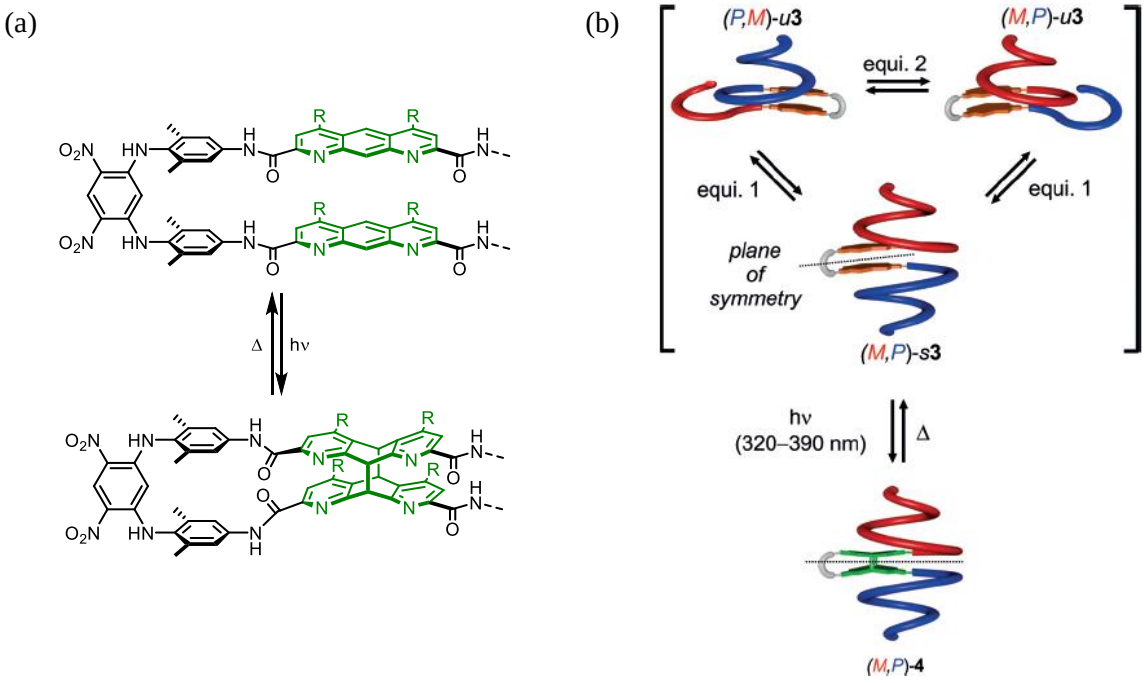

Scheme 4 – (a) Light-induced [4+4] cycloaddition of bis(diazaanthracene)s. (b) Conformational resolution in bis(diazaanthracene) aromatic oligoamide foldamers.

Due to the conformational restriction imposed by the 1,3-diaminobenzene linker, the diazaanthracenes aggregated in a parallel fashion, despite the repulsive interdipolar interactions. Before cycloaddition, the oligoamide helices were not well defined – they adopted three conformations in slow exchange on the NMR timescale in $CDCl_3$ at temperatures below 25 °C (Scheme 4b). Two of these conformers are enantiomeric and comprised of one helix of a particular handedness propagating away from the diazaanthracenes, and the other helix of the opposite handedness coiling around the first helix. The third conformer is a *meso* conformer, where the helices propagated away from the diazaanthracenes with opposite handedness. Upon quantitative photocycloaddition of the diazaanthracenes, the *meso* form was the only observable conformer. This represented a conformational resolution process that, due to the altered trajectory of the photoadduct, also resulted in foldamer elongation and cavity enlargement. The retro [4+4] reaction could be achieved quantitatively by heating for 48 h, showing that the diazaanthracene oligoamide foldamers can be quantitatively interconverted between morphologies. It was alluded to that these photoresponsive foldamers could be used for light-induced enantiospecific host-guest chemistry.

The bis(diazaanthracene) example is another of macromolecular conformational change in response to a stimulus, but light is also conducive to the modulation of function. For example, Hecht and co-workers have published extensively in the field of photoswitchable molecules, particularly focusing on the light-induced modulation of dithienylethenes. This motif has been used for light-induced modulation of organic semiconductors, photoswitchable polymerisation and in the storing of light energy.[62–64] More specifically, they have been designed to incorporate a hydrogen-bond acceptor-donor-acceptor (ADA) unit in the form of an imide and exploited it for its binding affinity to melamines, which have a complementary hydrogen-bonding pattern (DAD) (Scheme 5).[65]

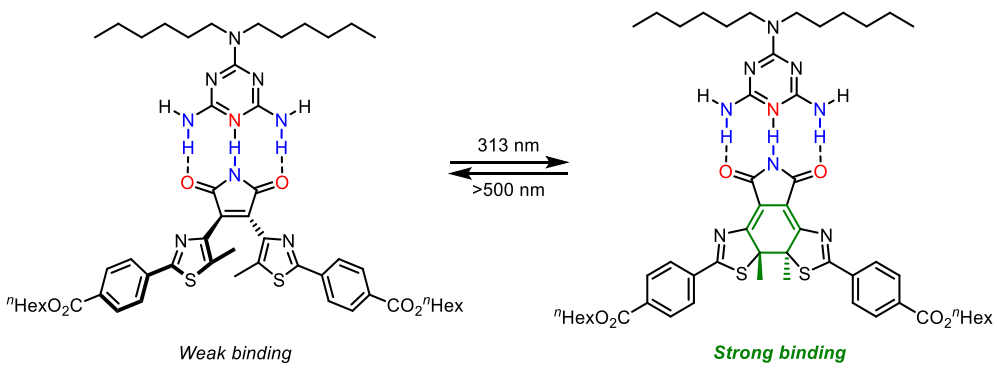

Scheme 5 – Photoswitchable binding of melamines to bis(thiazol-4-yl)maleimides.

In its ring-opened form, the thiazoles deviate from the maleimide plane in order to negate steric encumbrance of the 4-methyl groups. This deviation lowers electron density donation from the thiazoles to the imide, lowering its hydrogen-bond-accepting ability and giving rise to a melamine binding constant of 142 M^{-1}. Upon photocyclisation, the corresponding thiazolines increase their conjugation with the imide, promoting electron density donation and significantly strengthening melamine binding to 318 M^{-1}. This example represents the light-induced formation of a strong and specific triple hydrogen-bonding unit. This has been recognised as having potential utility in 'smart' materials, which can respond to light by increasing aggregation and changing its mechanical properties. Interestingly, property modulation by photoswitching usually takes the form of using a photoisomerisable bond to bring groups into and out of proximity, whereas this example uses light to change secondary electronic interactions.

Another example of light-induced modulation of function has been reported by Newhouse, where a bidirectionally quantitative photoswitch derived from hemithioindigo was developed (Scheme 6).[66]

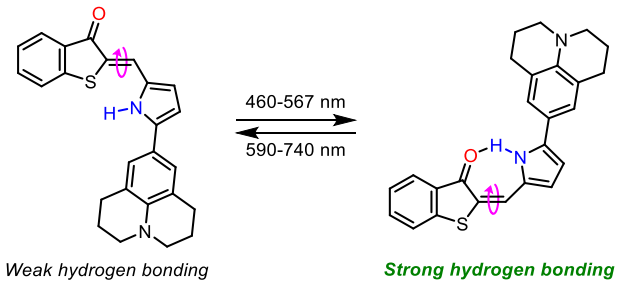

Scheme 6 – Light-induced formation/deletion of a hydrogen bond in hemithioindigos.

Nine photoswitches were synthesised with the hemithioindigo scaffold, where they could each be quantitatively interconverted between their *E* and *Z* forms by employing light of the appropriate wavelength. Generally, the absorption profile of the *Z* form was greatly blueshifted relative to the *E* form, owing to the modification of the electronic landscape by the hydrogen bond. Additionally, the absorption wavelengths were found to be highly sensitive to the substitution on the pyrrole moiety, where the absorption of the *E* form of the hemithioindigo was redshifted to 740 nm with a julolidinyl pyrrole substituent. This example represents a new family of photoswitches with highly tunable absorptions. Interestingly, in the *Z* form, the pyrrole is free to act as an HBD, which could be used to perform function. Upon photoisomerisation, the pyrrole would form a hydrogen bond with the hemithioindigo, precluding the function. Whilst there are many examples of photoswitches that can be used to modulate function, there have been few reports on the use of photoswitchable moieties for the *communication* of information.

Clayden and co-workers have reported a switch of screw-sense preference in a helical foldamer in the form of a fumaramide/maleamide photoswitch (Figure 17).[67] This was made by appending one side of a fumaramide (*E*) with a helix made up of Aib units. On the other side of the fumaramide, a chiral L-α-methylvaline unit was covalently bound. In the *E* geometry, the L-α-methylvaline was sufficiently separated from the Aib oligomer such that no transmission of stereochemical information over the fumaramide was observed, and thus there was no strong bias of screw-sense preference of the Aib oligomer. However, upon irradiation of the fumaramide, the olefin photoisomerised to form the corresponding maleamide (*Z*), bringing the L-α-methylvaline much closer to the Aib oligomer.

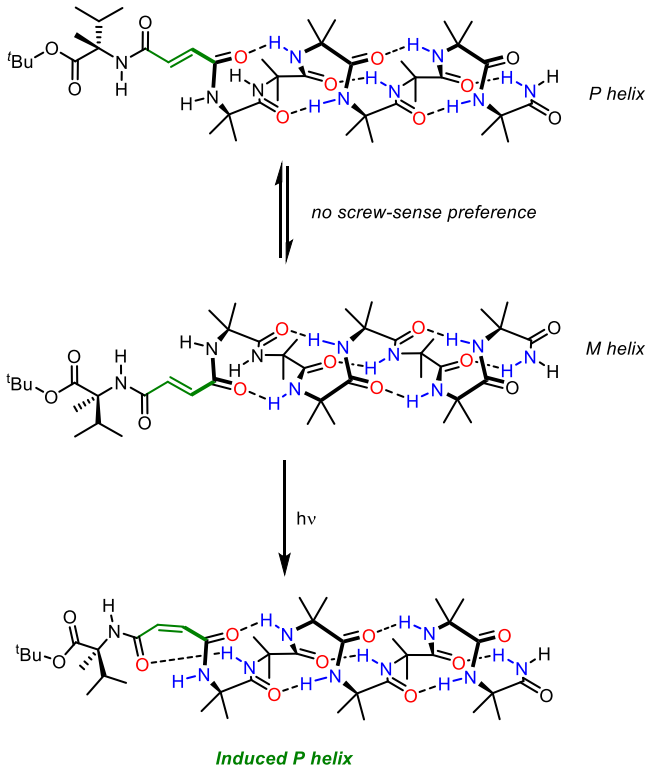

Figure 17 – Induction of screw-sense preference by photoisomerisation of a fumaramide.

In the *Z* orientation, the L-α-methylvaline was sufficiently proximate to the Aib oligomer to allow the chirality of the terminus to influence the screw-sense preference of the helix. By forming a reactive oxazolone on the opposite end of the helix, diastereoselective chain extension could be performed. In the fumaramide (*E*), where the L-α-methylvaline was too distant from the Aib oligomer to transmit stereochemical information, chain extension by the methyl ester of L-valine resulted in a 50:50 mixture of diastereomers. However, when photoisomerised to the maleamide (*Z*), where the L-α-methylvaline was brought close enough to the Aib oligomer to induce screw-sense preference, a diastereoselective reaction was observed, whose selectivity was augmented with decreasing temperature. Therefore, the use of a fumaramide/maleamide

photoswitch for induction of screw-sense preference of an otherwise configurationally achiral helical foldamer and its use in a diastereoselective reaction was demonstrated.

Helical foldamers derived from Aib have also shown to be sufficiently lipophilic to dissolve in the membrane phase. A similar Aib oligomer with a photoswitch derived from a diazobenzene moiety and a geminal di-(fluoromethyl) spectroscopic reporter has proven useful in transmitting stereochemical information by turning on and off the occupation of an L-valine unit in hydrogen bonding.[68] When the diazobenzene was in its *Z* orientation, the nitrogen of the diazo group hydrogen bonded weakly to the amido proton of the L-valine unit. This weak hydrogen bonding of the azobenzene allowed the L-valine to hydrogen bond strongly with the next Aib unit and propagate the stereochemical information along the length of the helix, as determined by solid state ^{19}F NMR in a phospholipid bilayer. Upon photoisomerisation of the diazobenzene to the *E* form, the phenyl groups deviated from coplanarity in order to accommodate for their steric encumbrance. This promoted the basicity of the diazo nitrogen, strengthening the hydrogen bond between it and the amide proton of the L-valine. As a result of this, the hydrogen bond between the L-valine and the next Aib unit was weakened, and therefore the influence of the chiral unit on the screw-sense preference of the otherwise achiral helical foldamer was greatly reduced. This effect was demonstrated in the membrane phase at lengths of up to 2 nm. As such, the diazobenzene moiety acted as an on/off switch for the transmission of stereochemical information by use of an Aib oligomer, whose helical fidelity was retained on the nanometre scale in the membrane phase. This system acted as a synthetic mimic of the photoswitchable vision protein, rhodopsin.

The highlighted examples represent advances in light-mediated conformational change. The host of photoswitchable moieties that chemists have developed have been harnessed by the supramolecular community to make on/off switches for different functions. These include biomimetic functions such as a macromolecular conformational change reminiscent of GPCRs, and the modulation of hydrogen bonding. Other examples have been highlighted where information has also been communicated through different media and then performed function, such as an asymmetric reaction.

1.5 Reversible Hydrogen-Bond Directionality in Synthetic Helices

An α-helix can adopt two different screw senses. Due to the chirality in natural α-amino acids, α-helices in nature ubiquitously form *P* helices.[37] Hydrogen-bonded helices also exhibit hydrogen-bond directionality, where the dipole of the helix orients from the N-terminus to the C-terminus (all the hydrogen bonds donate towards the N-terminus). Theoretically, these helices can adopt two conformations with opposite directionalities. Without exception, natural helices orient to universally adopt one directionality.[36]

Nature has failed to notice the function that can be conferred by reversible hydrogen-bond directionality.[37] The selection of the macromolecular dipole moment of a biological molecule and terminal hydrogen-bonding functionality could be used to orient other biological molecules in a desired fashion. These properties can be accessed by amino acid-derived foldamers whilst maintaining universal helical screw sense as alluded to by Gellman (Figure 11).[36] However, the use of a *dynamic* molecule that can switch between directionalities in response to a stimulus is an underexploited field in informational communication, and has not yet been observed in nature. Directionality-reversible dynamic foldamers represent a novel field in supramolecular chemistry, which can be used to gain access to informational communication mechanisms that nature has not harnessed.

The Guichard group have worked extensively on synthetic helices derived from ureas. These oligourea foldamers have been successfully employed for enantioselective catalysis, anion binding and as bactericides.[69–71] Oligoureas derived from *meso* cyclohexane-1,2-diamine that form $2.5_{12/14}$ helical conformations have been synthesised whereby two ureido protons hydrogen bond with the carbonyl of the urea two units preceding it (Figure 18).[2] This pattern propagated through the entire length of the helix and resulted in two pendent ureido protons at one terminus of the urea, and a ureido carbonyl at the other – defining the N- and C-termini. It is noteworthy that hydrogen-bond directionality reversal is accompanied by a helical inversion.

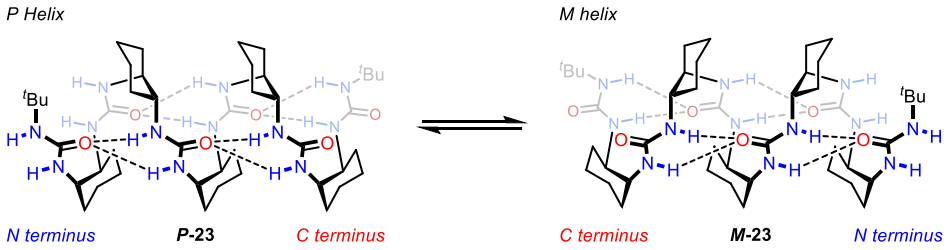

Figure 18 – Hydrogen-bond directionality-reversal in helical oligoureas.

By an iterative elongation method using orthogonally protected and enantioenriched cyclohexane-1,2-diamine derivatives, hexamer **23** was synthesised, giving a configurationally *meso* helix. Even in hydroxylic solvent, the two enantiotopic *tert*-butyl signals in the ^{1}H NMR spectrum gave rise to two different signals, indicating that the helix was in slow exchange between its two screw-sense preferences on the NMR timescale. Variable-temperature NMR (VTNMR) and Eyring analysis indicated that, depending on the solvent, the barrier to screw-sense inversion was around $\Delta G^{\ddagger}_{298\ K}$ = 70.0 kJ mol^{-1}. Due to the enantiotopicity of the two termini in the *meso* helix, a chiral ligand exclusively induced one *handedness* of the helix. Additionally, its hydrogen-bonding nature allowed it to bind to one *terminus* selectively, enforcing one directionality which was communicated through the length of the helix. In this system, the carboxylate of Boc-D-proline was formed by deprotonation of the corresponding acid using tetrabutylammonium hydroxide. The carboxylate and carbamate of the Boc-D-proline carboxylate acted as HBAs by each hydrogen bonding to a pair of ureido protons in the first two residues of the helix, forming a 1:1 adduct. This set the binding site at the N-terminus. While the central chirality in the ligand induced a screw-sense preference for a *P* helix in the oligourea, the Boc-D-proline carboxylate induced directionality in the oligourea by selectively binding at the N-terminus over the C-terminus. This example served as the first example of reversible hydrogen-bond directionality in oligourea foldamers.

This work was extended to the development of a molecular spring torsion balance by desymmetrisation of the helical oligourea (Figure 19).[32] Thioureas are much stronger HBDs and weaker HBAs than their analogous ureas due to the higher diffusivity of the orbitals on sulfur.[72] Therefore, when one of the enantiotopic ureas was replaced with a homologous thiourea, the helix equilibrium shifted to ensure the thiourea acted as an HBD, placing the thiourea at the C-terminus and enforcing a *P* helix.

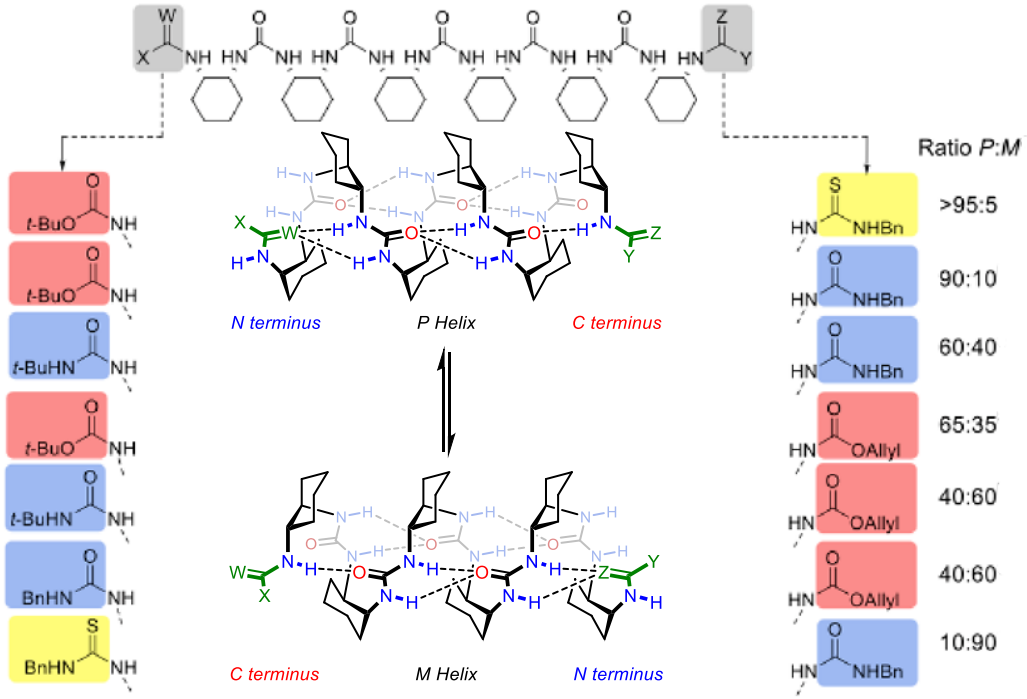

Figure 19 – Helical oligoureas as a molecular spring torsion balance.[32]

Carbamates can only act as single HBDs as there is only one nitrogen to have a pendent amido proton. Therefore, when a thiourea terminated the helix on one end, and a carbamate on the other, a *P* helix was formed exclusively. When a homologous urea was used, the preference was not as strong as ureas are weaker HBDs and stronger HBAs than thioureas. When termini of similar hydrogen-bond-donating/accepting ability were used, as is the case with *tert*-butyl and benzyl ureas, the helix approached being configurationally racemic. When the stronger/double HBDs were used on the opposite terminus, a directionality switch took place, swapping the N- and C-termini accompanied by a helical inversion. This scaffold acted as a molecular torsion balance which can compare the hydrogen-bond-donating/accepting abilities of terminating groups to see which biased the helical screw sense and therefore the directionality more strongly. These could be quantitatively compared by ascertaining free energy differences from the equilibrium constants.

1.6 Hydrogen-Bond Directionality Control in Ethylene-Bridged Oligoureas

Nowick and co-workers have investigated the conformational behaviour of oligoureas bridged with different lengths of aliphatic linkers and used them as molecular scaffolds for β-sheet mimicry. Using an iterative elongation method, Nowick synthesised di- and triureas derived from 1,3-diaminopropane and *N*-(3-aminopropyl)-1,3-diaminopropane (Figure 20).[73]

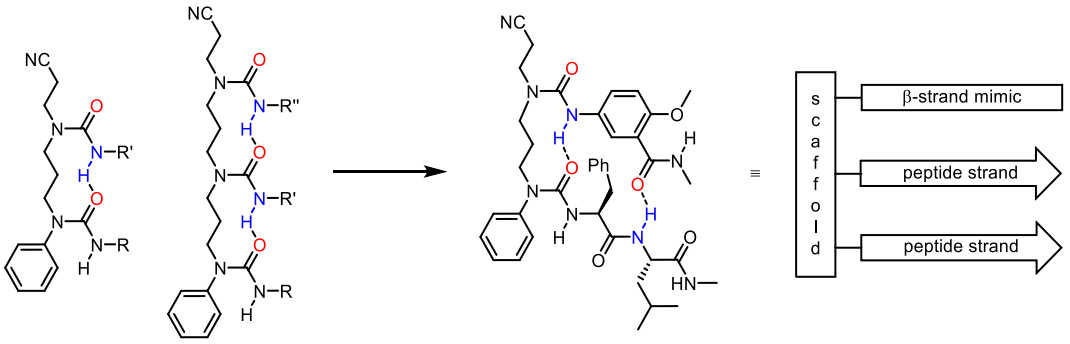

Figure 20 – Nowick oligoureas derived from 1,3-diaminopropane and *N*-(3-aminopropyl)-1,3-diaminopropane.

The oligoureas were synthesised with a variety of urea substituents and termini, using both bulky aromatic groups and smaller aliphatic groups, and their behaviour was studied using ^{1}H NMR and FTIR spectroscopy. When a phenyl group was used at one terminus, the adjacent urea was forced into a conformation whereby the aryl group and the carbonyl were *trans* to each other due to the electrostatic repulsion between the phenyl group and the ureido carbonyl.[74,75] This conformation induced the directionality of the first urea, which resulted in a pendent carbonyl being adjacent to the second urea. Due to this, the second urea hydrogen bonded to the first urea through its ureido proton, and thus the second urea had the same directionality as the first. This effect propagated through the oligourea, meaning that the phenyl group biased the global directionality in the ureas and exerted conformational control on the structure. The FTIR studies revealed an 85:15 ratio of conformers in $CHCl_3$, each with uniform directionality. In this example, the phenyl group set the phenyl urea at the N-terminus, and the dipole was communicated as binary information in the form of hydrogen-bond directionality from one terminus to the other.

Nowick conducted further studies on this hydrogen-bonding phenomenon by varying the length of the aliphatic linker between ureas. By comparison to analogous monoureas where no intramolecular hydrogen bonding could take place, the intramolecular hydrogen-bonding strength between the ureas with different aliphatic linkers could be quantified. Upon changing the linker from a 1,3-propane bridge to an ethylene bridge, a marked increase in hydrogen bonding was observed as shown by FTIR and ^{1}H NMR studies.[76] None of the directional conformer where the phenyl urea was at the C-terminus was observed, and this was further supported by molecular

mechanics calculations. Hence, 9-membered hydrogen-bonding rings (5 rotatable bonds) exhibit greater stability than that of 10-membered hydrogen-bonding rings (6 rotatable bonds) in these structures. This increased stability was attributed to the mitigated entropic contribution to hydrogen bonding, which was in agreement with analogous observations by Gellman in diamides.[5] This means that ethylene-bridged oligoureas prove to be better candidates for communicating directional information than 1,3-propane-bridged oligoureas due to their increased hydrogen-bonding fidelity.

Next, extensive conformational studies were conducted by ^{1}H NMR and molecular mechanics simulations (Figures 21-22). Initially, calculations were performed on diurea **24** using an AMBER* force field, which did not explicitly address the angular dependence of hydrogen bonding.[77] With these calculations, the four lowest energy conformers were identified, all of which were within 10 kJ mol^{-1} of the calculated ground state conformation.

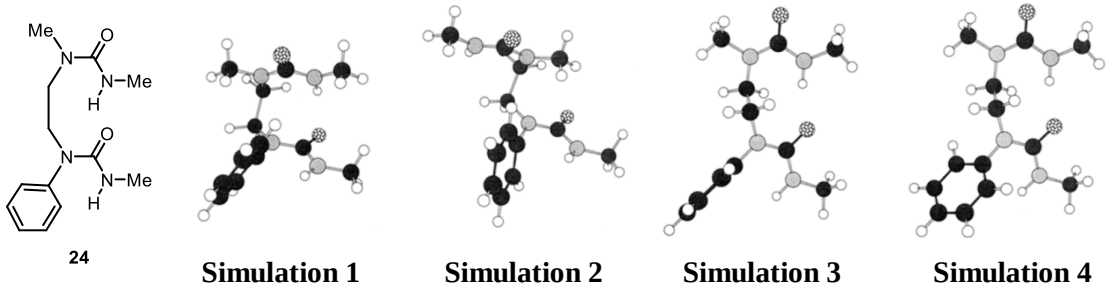

24

	Simulation 1	**Simulation 2**	**Simulation 3**	**Simulation 4**
Relative Energy	*Gauche* (hydrogen-bonded) 0 kJ mol^{-1}	Not hydrogen-bonded 6.2 kJ mol^{-1}	*Anti* (hydrogen-bonded) 8.9 kJ mol^{-1}	*Anti* (hydrogen-bonded) 9.7 kJ mol^{-1}

Figure 21 – Simulated conformations of 24.

The simulations revealed a *gauche* conformer, two *anti* conformers and a conformer with no hydrogen bond. The two *anti* conformers differed only by rotation of the N–Ph bond and so were treated as the same. Model inspection revealed that the hydrogen-bonded *gauche* and *anti* conformers had N–C–C–N torsion angles of 50° and 160°, respectively. The orientations of the ureas in the lower-energy *gauche* conformer were unusual as the hydrogen-bonded ureido proton seemed to hydrogen bond to the π cloud of the adjacent ureido carbonyl. In contrast, the hydrogen-bonded ureido proton in the *anti* conformation hydrogen bonded directly towards one of the sp^{2} lone pairs of electrons on the ureido carbonyl.

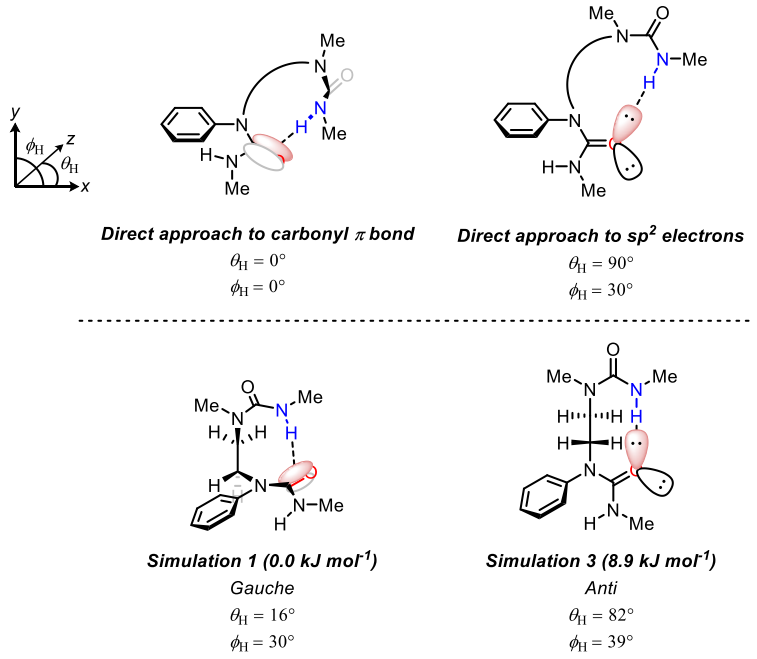

Figure 22 – Hydrogen bonding in *gauche* and *anti* conformers in ethylene-bridged diureas.

Taylor and co-workers have used the angles, θ_H and ϕ_H to quantify geometric relationships in carbonyls.[78] θ_H represents the deviation from the *z*-axis in the *xz* plane and ϕ_H represents the deviation from the *x*-axis in the *xy* plane (Figure 22). For example, a hydrogen bond donating directly to one of the carbonyl oxygen's sp^2 lone pairs would take $\theta_H = 90°$ and $\phi_H = 30°$. In the simulated *gauche* conformer, $\theta_H = 16°$ and $\phi_H = 30°$. This indicates that the ureido proton donates almost directly to the π bond, whereas the *anti* conformer, with $\theta_H = 82°$ and $\phi_H = 39°$, orients the ureido proton almost coplanar with the carbonyl and points directly towards an oxygen lone pair. When in the *gauche* conformation, the ureido carbonyl hydrogen bonds by donating electron density from its B_1-symmetrical π bond, and when in the *anti* conformation, it donates electron density from the higher-energy B_2-symmetrical oxygen lone pairs. As discussed (Section 1.2), hydrogen bonds formed from π bonds are weaker than those formed from lone pairs of electrons, as the lone pairs are higher in energy. The *gauche* conformation exhibits a hydrogen bond to the carbonyl π bond because the ureas are too close to allow efficient hydrogen bonding through the oxygen lone pairs. In contrast, the *anti* conformer involves a hydrogen bond through one of the oxygen lone pairs as the ureas are sufficiently separated. The force field used for the computational studies did not account for the angular dependence of hydrogen bonding, which rendered the simulations unreliable for the determination of the favourable hydrogen-bonded conformation. However, it did determine the specific hydrogen-bonding geometries of the *gauche* and *anti* conformers.

X-ray crystallographic analysis of **25** and related diureas showed a hydrogen-bonded *anti* relationship, which was in very strong agreement with the *anti* conformer that had been simulated. Additionally, the ^{1}H NMR signals of the methylenes connecting the ureas were analysed and found to exist as an AA'BB' system, with vicinal couplings of 5 and 10 Hz. The *gauche* and *anti* conformers were simulated, and the coupling constants were predicted to be 5 and 6 Hz for the *gauche* conformer, and 4 and 11 Hz for the *anti* conformer. This result indicated that **25** exists predominantly as two enantiomeric *anti* conformers that are in fast exchange on the NMR timescale, and that solid-state structures of the diureas are representative of that in solution. To further validate the notion that the diureas adopt an *anti* conformation, a diurea derived from *trans*-cyclohexane-1,2-diamine, **26** was synthesised and studied as an analogue with an imposed *gauche* conformation (Figure 23).

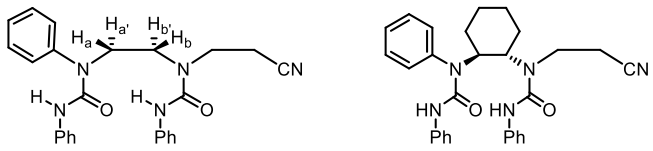

Figure 23 – Diureas for conformational analysis of the ethylene bridge.

^{1}H NMR analysis indicated that cyclohexyl diurea **26** existed as a 9:1 mixture of slowly interconverting conformers. Both ureas lay equatorial in both conformers and FTIR analysis revealed that the minor conformer was not hydrogen bonded. However, the relative wavenumbers and chemical shifts of the hydrogen-bonded ureido proton in the major conformer indicated that the hydrogen bonding was weaker in cyclohexyl diurea **26** than in acyclic diurea **25**. Finally, molecular mechanics simulations of **26** predicted an energy minimum which was superimposable on the *gauche* conformer simulated for **24**. This lent further credence to the notion that *gauche* relationships between the conformationally mobile diureas are not the true energy minimum corresponding to an optimised hydrogen bond. Next, the analogous triurea **27** was synthesised and studied by ^{1}H NMR and X-ray crystallography (Figure 24).[79]

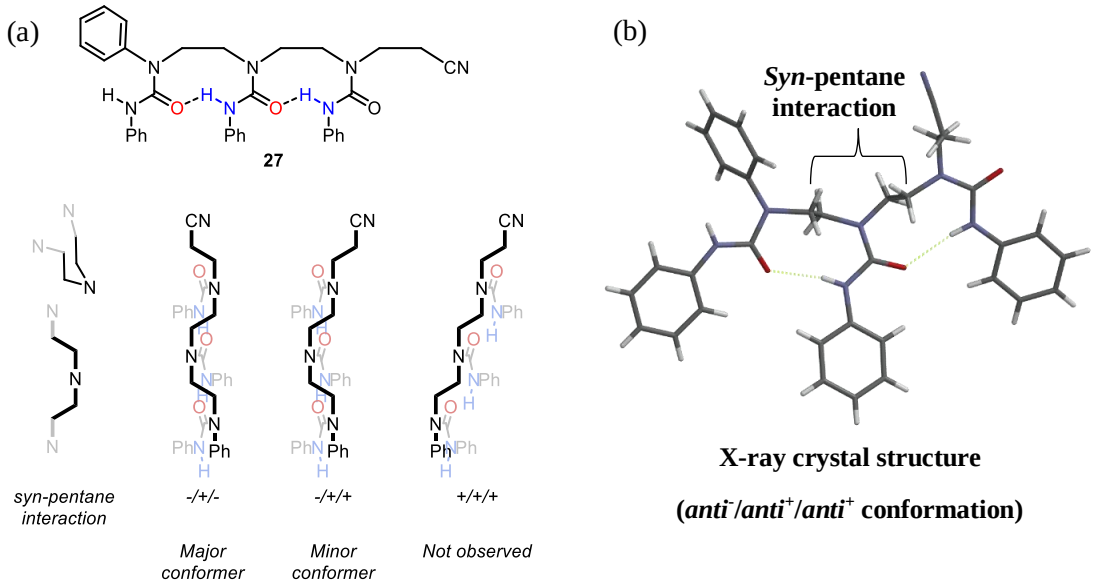

Figure 24 – (a) *Anti* relationships in ethylene-bridged triurea, 27. (b) X-ray crystal structure of 27.

Each of the ureas lay approximately coplanar, with *anti* relationships between each of the ureas. The N–Ph vectors were at an angle of 50°, displaying significant curvature in the diethylenetriamine scaffold. Analysis of the ^{1}H NMR resonances of the methylenes between the ureas show consistent 5 and 10 Hz vicinal couplings, indicative of all-*anti* relationships in $CDCl_3$ solution. Interestingly, when more than two ureas are present, the enantiomeric *anti* conformations become diastereomeric in relation to each other. It was envisaged that an *anti*$^{+}$/*anti*$^{+}$/*anti*$^{+}$ conformer would predominate to avoid repulsive *syn*-pentane interactions.[77] However, the alternating *anti*$^{-}$/*anti*$^{+}$/*anti*$^{-}$ conformation predominated with *anti*$^{-}$/*anti*$^{+}$/*anti*$^{+}$ minorly present, which was attributed to the appropriate alignment of the ureas for hydrogen bonding and to increase conjugation of the backbone nitrogen atoms.

By synthesising isocyanates from oligopeptides, the iterative synthesis of the scaffold allowed the installation of different oligopeptides onto the different ureas, whilst maintaining the rigid hydrogen-bonded conformation that the phenyl group imposed. Predictably, the order of these structures was well defined in chlorinated solvents, but was disrupted when studied in more polar solvents due to competitive hydrogen-bonding interactions.[80] The ureas were separated by 5 Å, which made them ideal scaffolds for the artificial introduction of β-turns and rendered them extremely effective in β-sheet mimicry.[76] β-turns are naturally constructed by incorporation of the amino acid, proline. This proline is incorporated into natural oligopeptides derived from α-amino acids, which have defined and irreversible hydrogen-bond directionality. The ethylene-bridged triurea scaffold studied by Nowick also has defined directionality due to the directional control imposed by the phenyl group. If the ureas were free to rotate, switching their N- and C-termini, the scaffold could be bestowed with directional reversibility. This directional reversibility could be controlled and give rise to a new family of dynamic foldamers with switchable hydrogen-bond directionality. The development of this property has been untouched by nature, where it has huge potential for the development of orthogonal communication mechanisms that could be conducive to biological systems. Control over this also confers selection of overall dipole moment and terminal foldamer functionality, which could be used to replace natural phenomena and even perform functions that nature could not previously access.

2.0 Project Aims

Studies performed by Clayden and co-workers have demonstrated that information in the form of *chirality* can be communicated through a configurationally achiral helix upon introduction of a chiral influence.[10,26,51,67] The aim of this project was to develop a novel class of foldamers that could communicate information in the form of hydrogen-bond directionality or *polarity*. Ethylene-bridged triureas terminated with phenyl groups have been shown to exhibit complete uniformity of hydrogen-bond directionality, where it has been used as a rigid scaffold for artificial parallel β-sheets.[77,79] The work in this project seeked to remove this conformational restriction and investigate if both directionalities could be accessed by the scaffold (Figure 25). The thermodynamic and kinetic factors affecting the prevalence of both directionalities were to be explored by variable-temperature NMR (VTNMR) experiments. With this information, directional control was to be implemented using covalently linked hydrogen-bonding groups, and the ability of the scaffold to communicate this directionality was to be determined.

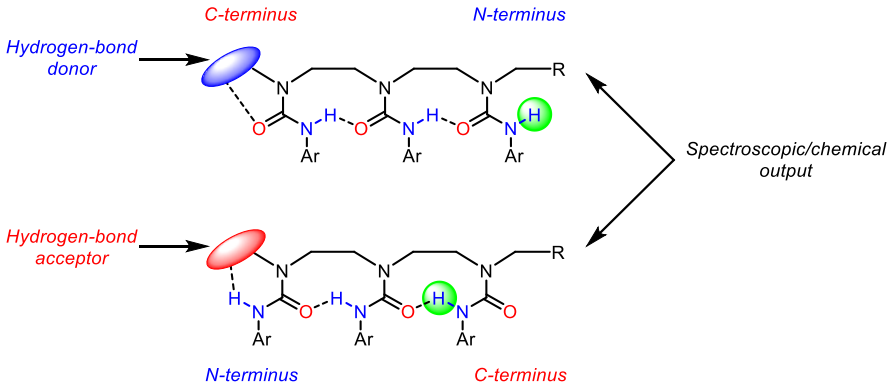

Figure 25 – Directionality control using hydrogen-bonding groups.

After directional reversal and control was established in these foldamers, these concepts were to be combined and manifested in directional switching (Figure 26). The directionalities were planned to be interconverted in response to a stimulus, and that switch to be propagated through the scaffold as binary information in the form of hydrogen-bond directionality and relayed by a remote spectroscopic or chemical reporter.

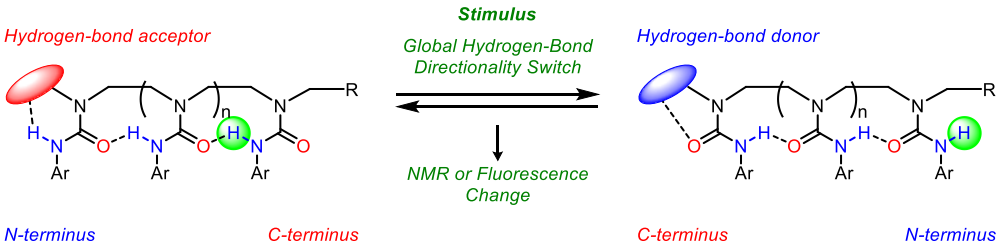

Figure 26 – Directionality switching using hydrogen-bonding groups that interconvert in response to a stimulus.

Investigation of hydrogen-bond directionality switching was envisaged by using acid and base, converting a basic site from an HBA in its neutral form to an HBD in its conjugate acid form. This process was then to be switched back using base. With the concept of hydrogen-bond directionality switchability having been successfully demonstrated, additional switching stimuli such as light and the presence of hydrogen-bonding additives like sulfoxides and anions was to be investigated. Initially, VTNMR would be used to ascertain the different directionalities and the degree to which they were present. After this method was used to study the scaffold, other responses would be used in local directionality detection remote from the informational source at millimolar concentrations, such as fluorescence change. Finally, this research aimed to develop ethylene-bridged oligoureas into robust conformational relays that can process information and communicate it through a barrier or into a compartment, where the information could be used to deliver interesting and novel biomimetic or nanomechanical functions.

3.0 Hydrogen-Bond Directionality in Ethylene-Bridged Oligoureas

3.1 Development of Conformationally Mobile Oligoureas

X-ray crystallographic, solution-state FTIR and ^{1}H NMR studies conducted by Nowick showed that ethylene-bridged triurea, **27** adopts a single conformation whereby the *N*,*N'*-diphenyl urea ureido proton is not hydrogen bonded, but the two other ureido protons are contiguously hydrogen bonded (Figure 27).[79] This conformational bias arises due to the strong preference for the *N*-phenyl group of the trisubstituted nitrogen atom to be oriented *trans* to the ureido carbonyl in order to avoid electrostatic repulsion of the groups.[74,75] This directionality is propagated to the next two ureas by formation of inter-urea hydrogen bonds, defining the diphenyl urea terminus as the N-terminus.

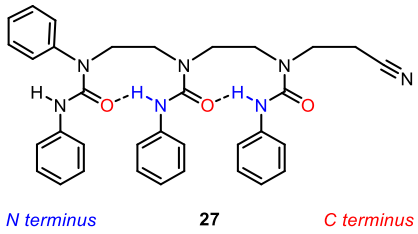

Figure 27 – Nowick's conformationally controlled ethylene-bridged triurea, 27.

Initial efforts on derivatising the oligoureas were focused on varying the ureido arenes to ensure they could be modified to confer desirable properties without damaging the fidelity of the intramolecular communication. The first change made was the conversion of the phenyl ureas to 4-methoxyphenyl ureas to show that alkoxy groups were conducive to the hydrogen-bonding network and could be used to aid characterisation of longer oligoureas. Triurea, **32** was synthesised by a method analogous to that of Nowick (Scheme 7).[79]

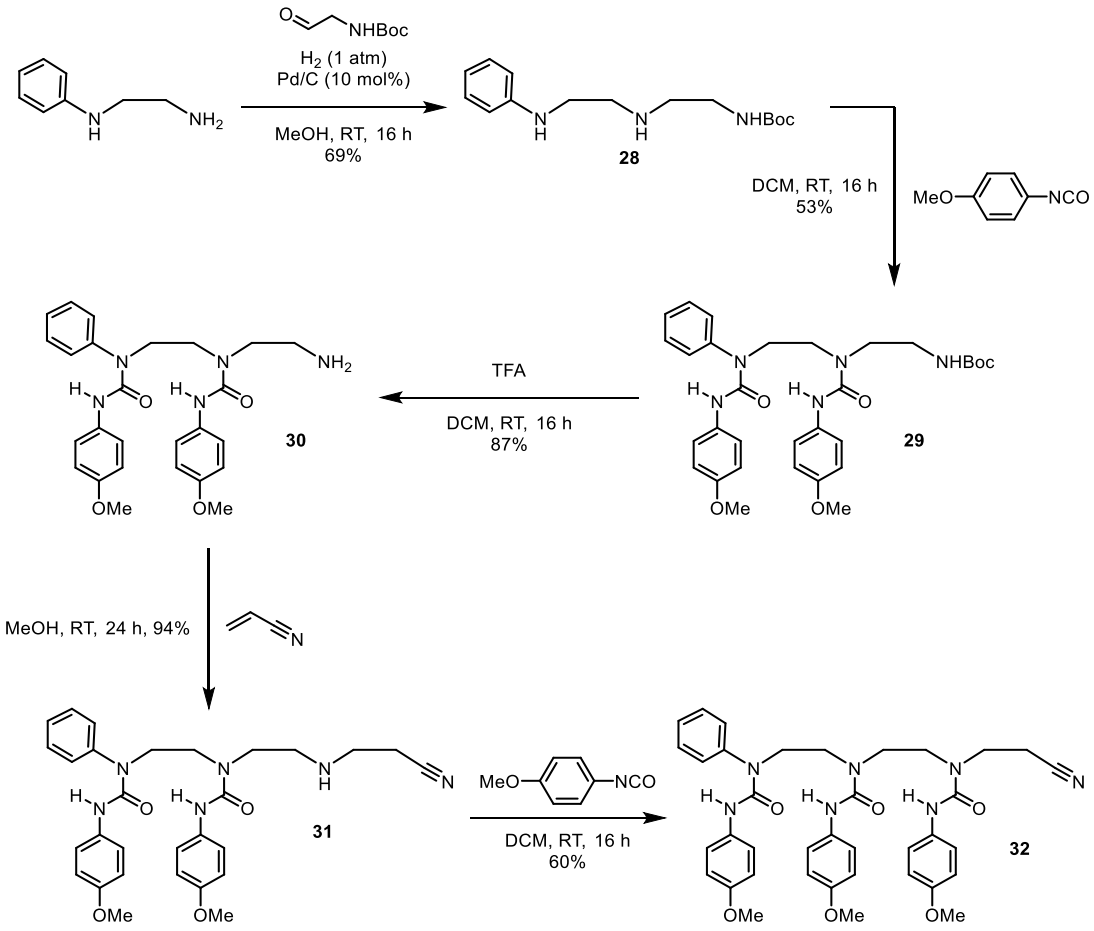

Scheme 7 – Synthesis of triurea 32.

N-Phenylethylenediamine underwent palladium-catalysed hydrogenative reductive alkylation with *N*-Boc-2-aminoacetaldehyde to afford carbamate **28** in good yield. Two 4-methoxyphenyl ureas were then installed on **28** using 4-methoxyphenyl isocyanate to give diurea **29** in moderate yield. The Boc group was then cleaved using TFA to give the corresponding primary amine, **30**, which then underwent a Michael addition to acrylonitrile, which proceeded in excellent yield. Carboxamidation of the corresponding secondary amine **31** gave the target triurea, **32**, in good yield.

If more than one conformation was appreciably populated upon derivatisation of Nowick's triurea **27**, then it would be difficult to identify them by Nowick's method of solution-state FTIR as this would only reveal the number of hydrogen-bonding and non-hydrogen-bonding environments. Instead, variable-temperature ^{1}H NMR (VTNMR) was used, where a sample of triurea **32** was prepared in CD_2Cl_2 and its ^{1}H NMR spectrum recorded at 25 °C. Spectra were then recorded at temperatures from 25 °C to −25 °C in increments of 10 °C (Figure 28).

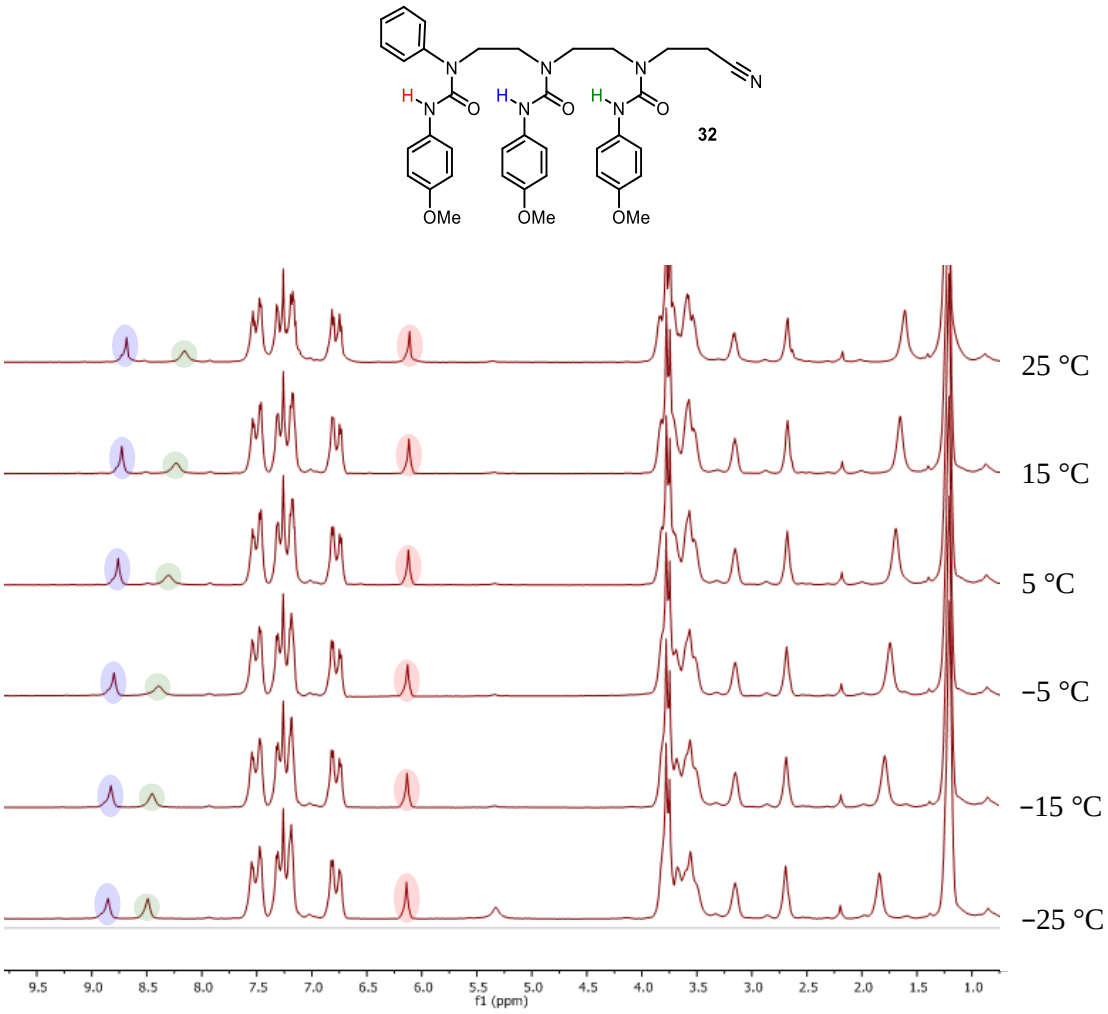

Figure 28 – VTNMR of 32 ($CDCl_3$, 500 MHz, 15 mM).

In triurea **32**, signals were observed at 6.11 (diaryl urea ureido proton), 8.16 (peripheral ureido proton) and 8.70 ppm (central ureido proton) at 25 °C. Upon cooling of the sample, the signal at 6.11 ppm remained at approximately the same chemical shift. The other two signals at 8.16 and 8.70 ppm, however, shifted markedly downfield. The other alkyl and aromatic signals remained approximately constant. These observations can be explained by the *N*,*N'*-diaryl urea adopting a conformation whereby the carbonyl and the phenyl group are oriented *trans* to each other, forcing the ureido proton away from the adjacent urea. In this orientation, this ureido proton would not be hydrogen bonded and would therefore correspond to a relatively upfield signal (6.11 ppm at 25 °C). The other two ureido protons signals are much more downfield because they are in hydrogen bonds with their adjacent ureas. As the sample is cooled, the entropic cost of intramolecular hydrogen bonding is mitigated and so the hydrogen bonds became stronger, hence the downfield shifting with decreasing temperature. Finally, if the directionalities were in slow exchange on the NMR timescale at one of the recorded temperatures, signal decoalescence would indicate the presence of two or more distinct, populated conformations. In this case, no such

decoalescence has occurred, showing either that slow exchange can only be reached at lower temperatures, or triurea **32** exists as one populated conformation, where the diaryl urea is at the N-terminus. In the latter case, this would indicate that conformation control is still established by the phenyl group and that 4-alkoxylphenyl ureas are conducive to the hydrogen-bonding network.

Next, it was desirable to design a more dynamic foldamer to show that both directionalities could be accessed by the same molecule and to more conclusively assign the dynamics observed in **32**. The proposed triurea, **37**, was analogous to Nowick's triurea, **27**, but the terminating phenyl group was replaced by an ethyl group in the hope that the ethyl group would not subject the oligourea to any directional bias. Triurea **37** was synthesised in an analogous manner to diaryl urea **32** to provide ethyl urea **37** in 36% total yield over five steps (Scheme 8).

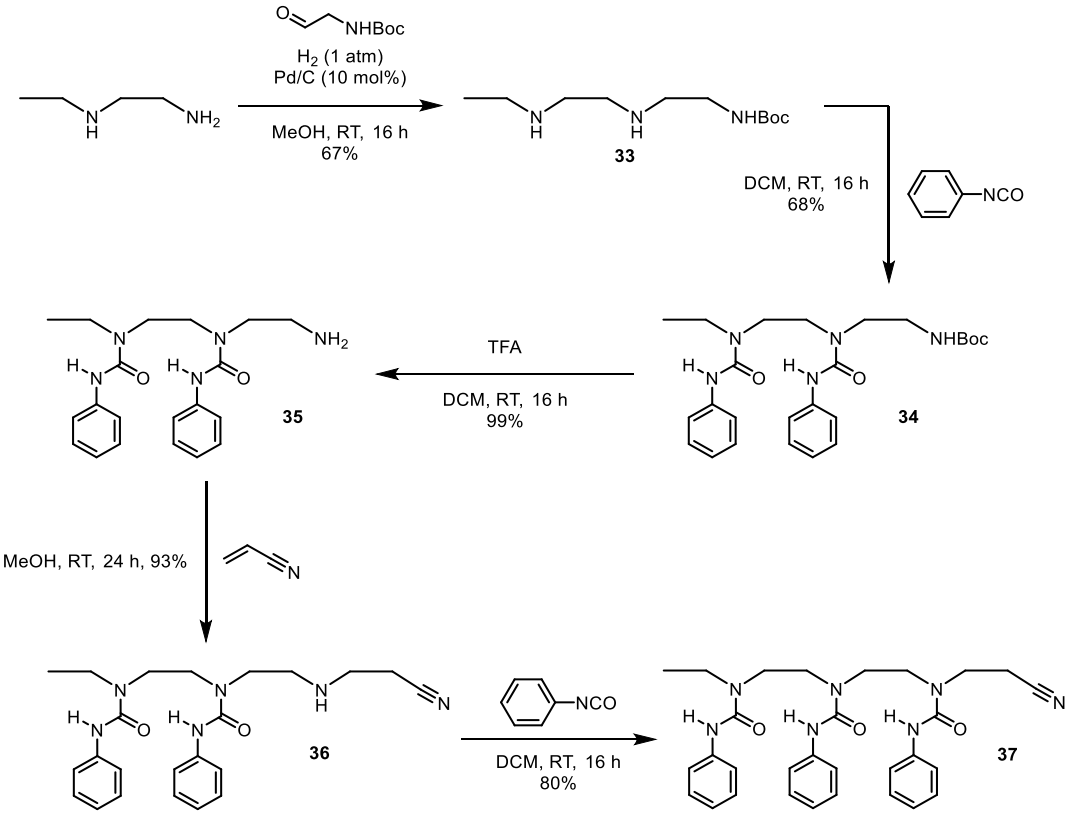

Scheme 8 – Synthesis of triurea 37.

Triurea **37** was then studied by VTNMR. To increase the likelihood that the triurea would reach slow exchange on the NMR timescale, spectra were recorded at temperatures from 20 °C to −80 °C in increments of 10 °C (Figure 29). CD_2Cl_2 was the solvent of choice because it does not participate in hydrogen bonding and it does not freeze at the analytical temperatures.

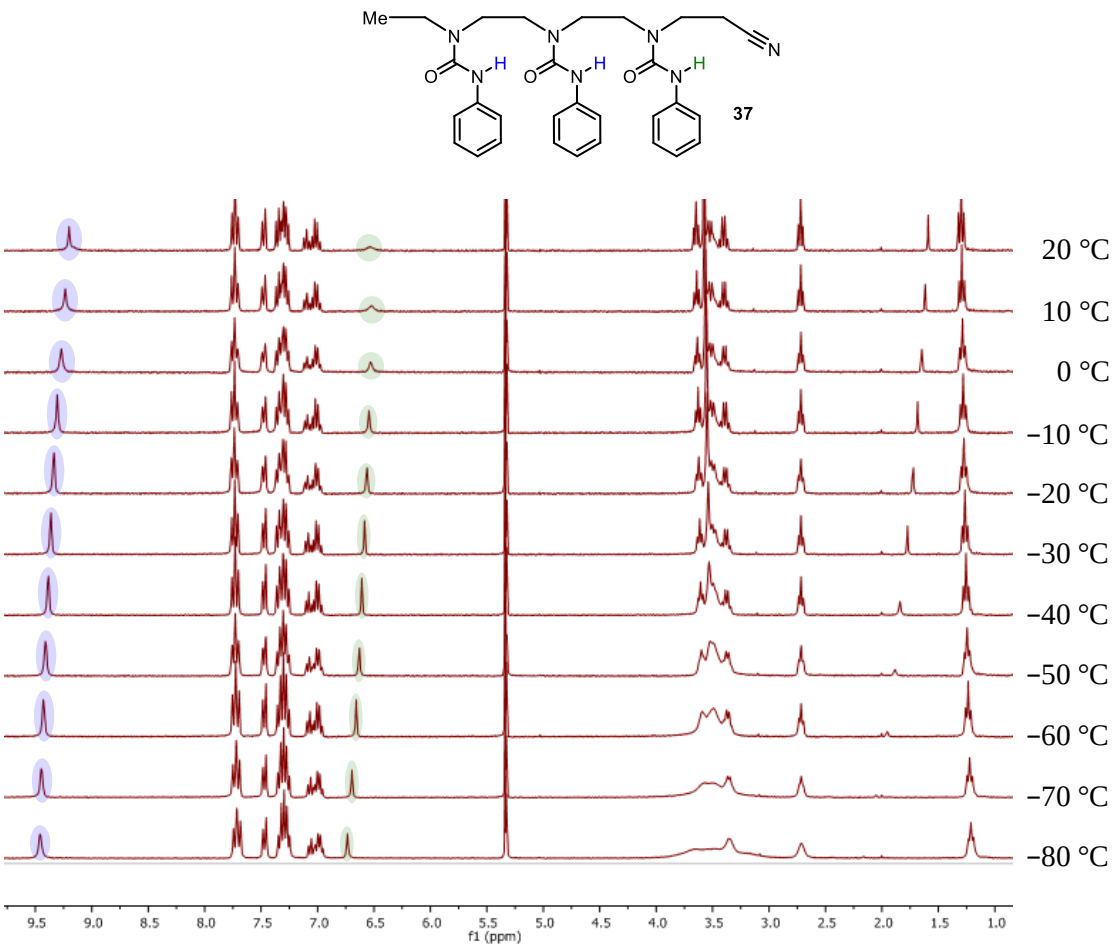

Figure 29 – VTNMR of 37 (CD_2Cl_2, 300 MHz, 18 mM).

Triurea **37** showed one broad signal at 6.53 ppm (cyanoethyl urea ureido proton) and two closely overlapping signals at 9.20 ppm (the two other ureido protons) at 20 °C. Upon cooling, the signals at 6.53 and 9.20 ppm sharpened and shifted downfield with decreasing temperature. The two signals at 9.20 ppm were not distinguishable at any temperature and they maintained an integration of two protons throughout the experiment. The remaining aromatic signals stayed approximately constant with decreasing temperature, whereas the alkyl signals broadened at −50 °C. Like triurea **32**, these data indicated either that slow exchange had not been reached, or **37** exists as one populated conformation. The downfield shifting of each of the ureido protons indicated that each ureido proton was involved in a hydrogen bond, one of which was significantly weaker than the other two. The two ureido protons in stronger hydrogen bonds were in the same hydrogen-bonding environment as they both have the same chemical shift-dependence on temperature. The broadening of signals in the alkyl region below −50 °C could be attributed to the slowing down of the interconversion between diastereotopic ± *gauche* and ± *anti* conformers of the ethylene bridges on the NMR timescale at these temperatures.[77]

These observations could be accounted for by orientation of the cyanoethyl urea so that its ureido proton protruded towards the nitrile. This would then form a complementary hydrogen-bonding pair where the ureido proton acts as an HBD, and the nitrile as an HBA, allowing the foldamer to homodimerise (Figure 30a). This would set the directionality of the cyanoethyl urea, which would be communicated to the other two ureas, making the cyanoethyl urea at the N-terminus. The C_{2h}-symmetry of the proposed dimer was consistent with exactly three different hydrogen-bonding environments, where two of the hydrogen-bonding environments are nearly identical. This would be consistent with reports by Nowick and co-workers that *N*-bis(cyanoethyl)-*N'*-phenyl ureas form homodimers of the this type.[82] To further validate the hypothesis that foldamer homodimerisation was occurring, a concentration-dependence study was performed whereby a solution of the foldamer was diluted and the ^{1}H NMR spectrum was recorded at each new concentration.

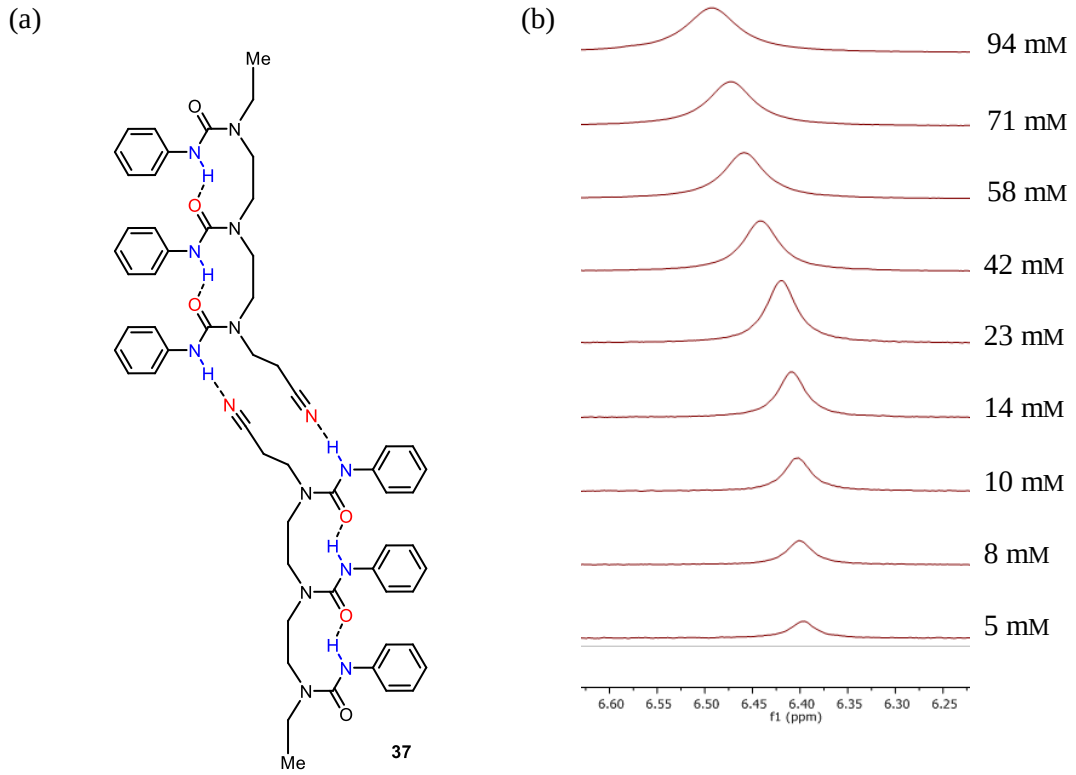

Figure 30 – (a) Proposed homodimer of 37. (b) Concentration-dependence study of 37 (CD_2Cl_2, 500 MHz).

Monitoring the signal corresponding to the ureido proton of the cyanoethyl urea, where intermolecular hydrogen bonding was suspected to be taking place, revealed a clear chemical shift dependence on concentration. Even though only one directionality was observable in **37**, it is noteworthy that the populated directionality places the cyanoethyl urea at the N-terminus. In the parent foldamer **32**, (Figure 28) the cyanoethyl urea was at the C-terminus. This indicated that

replacement of the directionality-controlling phenyl group with an alkyl group allowed conformational freedom such that it could be controlled by other factors, such as homodimerisation.

As the propionitrile terminus in **37** was giving rise to global directionality control, a new target compound was sought where the propionitrile was replaced with another group which would not subject the oligourea to directionality control. The target triurea, **41**, where a benzyl urea was used instead of a cyanoethyl urea, was synthesised in two steps from **39** (Scheme 9), which was synthesised analogously to **30** (Scheme 7) using *N*-ethylethylenediamine as the starting material.

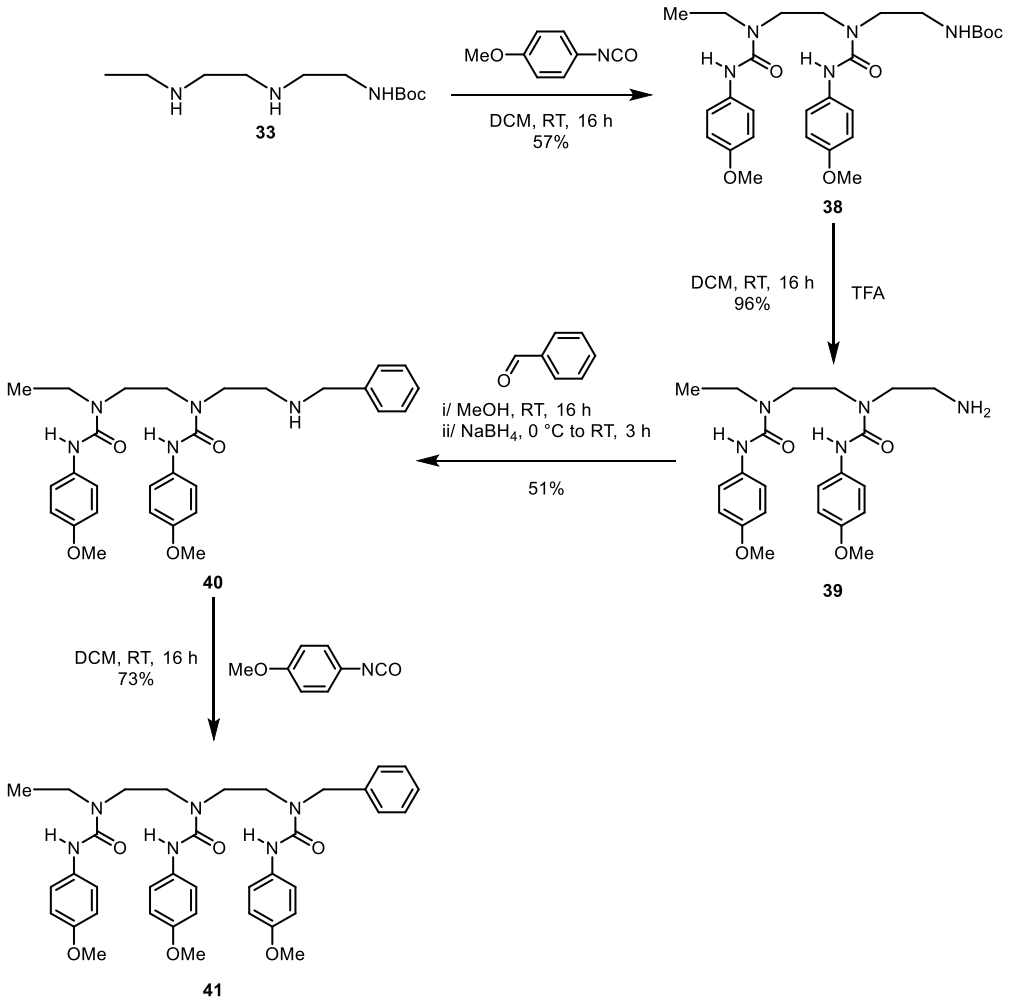

Scheme 9 – Synthesis of triurea 41.

Amine **39** underwent reductive alkylation with benzaldehyde by a one-pot condensation/reduction using sodium borohydride to give secondary amine **40** in moderate yield. Amine **40** then underwent carboxamidation using 4-methoxyphenyl isocyanate to give the target triurea **41** in good yield. **41** was then studied by VTNMR (Figure 31).

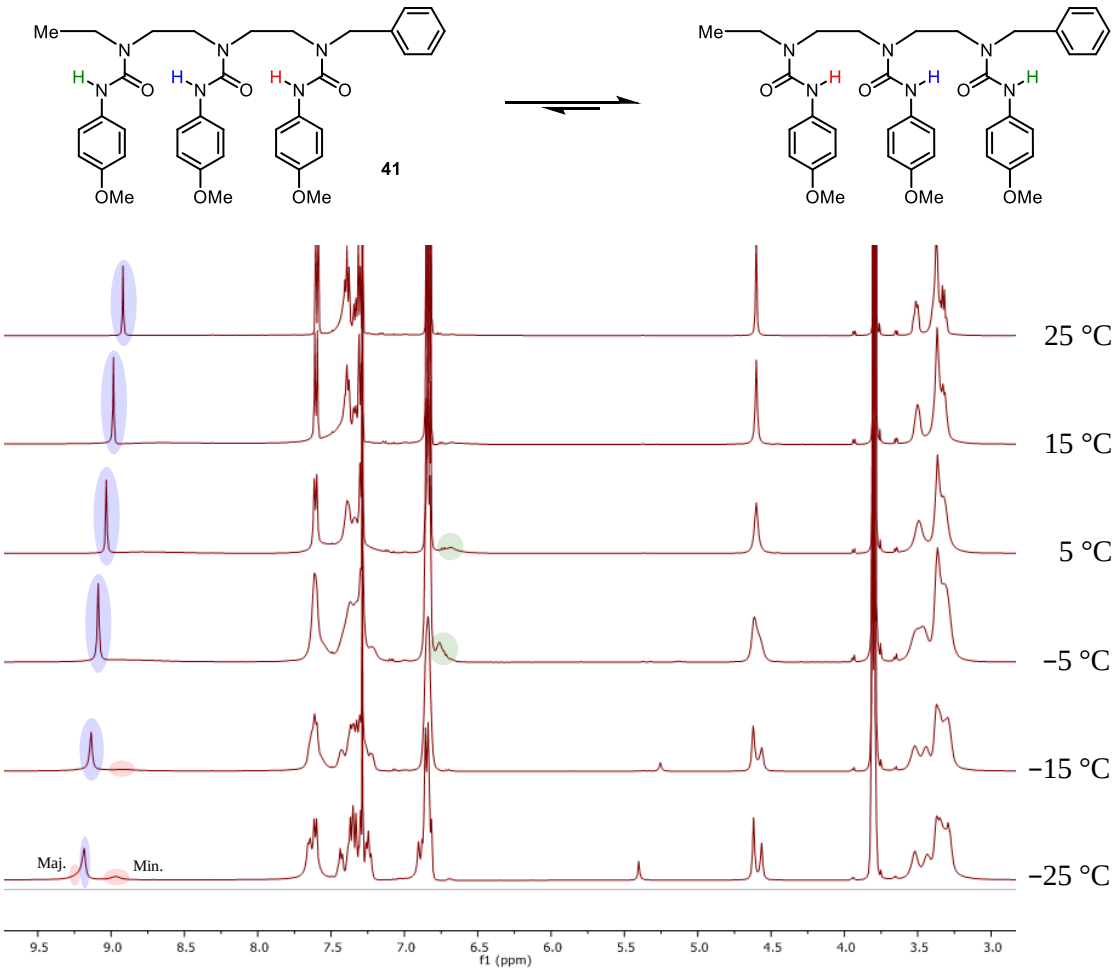

Figure 31 – VTNMR of 41 (CD_2Cl_2, 500 MHz, 15 mM).

In triurea **41**, signals were observed at 4.60 (benzylic methylene) and 8.92 ppm (central urea ureido proton) at 25 °C. Upon cooling, the signal at 4.60 ppm broadened and decoalesced into two distinct singlets at −15 °C. These decoalesced signals sharpened at −25 °C, where they were present in a ratio of 60:40. The signal at 8.92 ppm (1 H) shifted downfield with decreasing temperature to reach a value of 9.19 ppm at −25 °C. At 5 °C, a new signal appeared at 6.76 ppm (1 H), which sharpened and shifted downfield upon further decreasing the temperature. Similarly, new signals emerged at 8.90 (0.40 H) and 9.23 ppm (0.60 H, overlapping) at −15 °C, which behaved the same. These data showed that there were two conformations in fast exchange on the NMR timescale at 20 °C, which enter the slow-exchange region between −5 °C and −15 °C. These two conformations are the two different directionalities, populated in a 40:60 ratio at −25 °C. Each of the directionalities have two hydrogen-bonded ureido protons, and a non-hydrogen-bonded ureido proton. The signals at 6.76 and 9.19 ppm at −25 °C correspond to the non-hydrogen-bonded and central hydrogen-bonded ureido protons, respectively of both conformers. The signals at 8.90 (0.40 H) and 9.23 ppm (0.60 H) at −25 °C correspond to the peripheral hydrogen-bonded ureido protons in the minor and major conformers, respectively. It is proposed

that the major conformer is where the benzyl urea is at the N-terminus as the benzyl group can form an attractive N-H-π interaction with the proximate urea.[83]

This result confirmed the supposition that triureas **32** and **37** exist as one conformation due to the control imposed by their termini. It also indicated that foldamers terminated with alkyl groups confer conformational mobility in oligoureas such that both directionalities can be accessed by the same foldamer. The directionalities in the oligoureas are in fast exchange on the NMR timescale, and enter the slow-exchange region between −5 °C and −15 °C when using a 500 MHz spectrometer. It is notable that the peripheral ureido protons gave rise to very broad signals at 20 °C, indicating that directionality reversal is either much slower or much faster at the ends of the foldamer.

Now that it had been established that alkyl-terminated foldamers conferred conformational mobility in the oligoureas, the kinetics of the interconversion between the directionalities were investigated. A series of analogous compounds with different numbers of ureas was then synthesised (Scheme 10) and their dynamics analysed by VTNMR to determine the effect of the number of urea units on hydrogen-bonding dynamics.

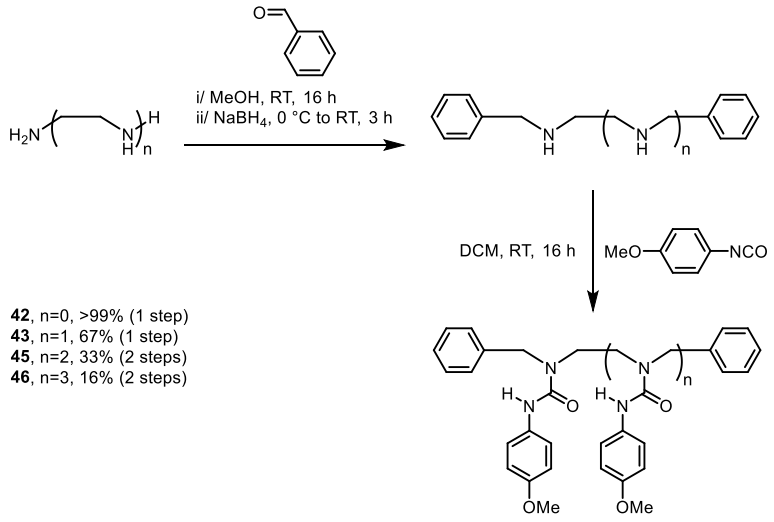

Scheme 10 – Synthesis of 42-46.

Monourea **42** and diurea **43** were synthesised by reacting the appropriate benzylated amines with 4-methoxyphenyl isocyanate. Triurea **45** and tetraurea **46** were synthesised by twofold reductive alkylation of the corresponding oligoethylenediamine with benzaldehyde followed by reaction with isocyanate. The synthesis of **45** proceeded in moderate yield over two steps. The crude product of the dibenzylated tetramine was reacted with isocyanate to afford tetraurea **46**. **46** was successfully isolated, albeit in poor yield due to the increased competitive formation of imidazolidines from the 1,2-diamines and benzaldehyde. Ureas **42**, **43**, **45** and **46** were then studied by VTNMR (Figures 32-33, Figures A2, A4).

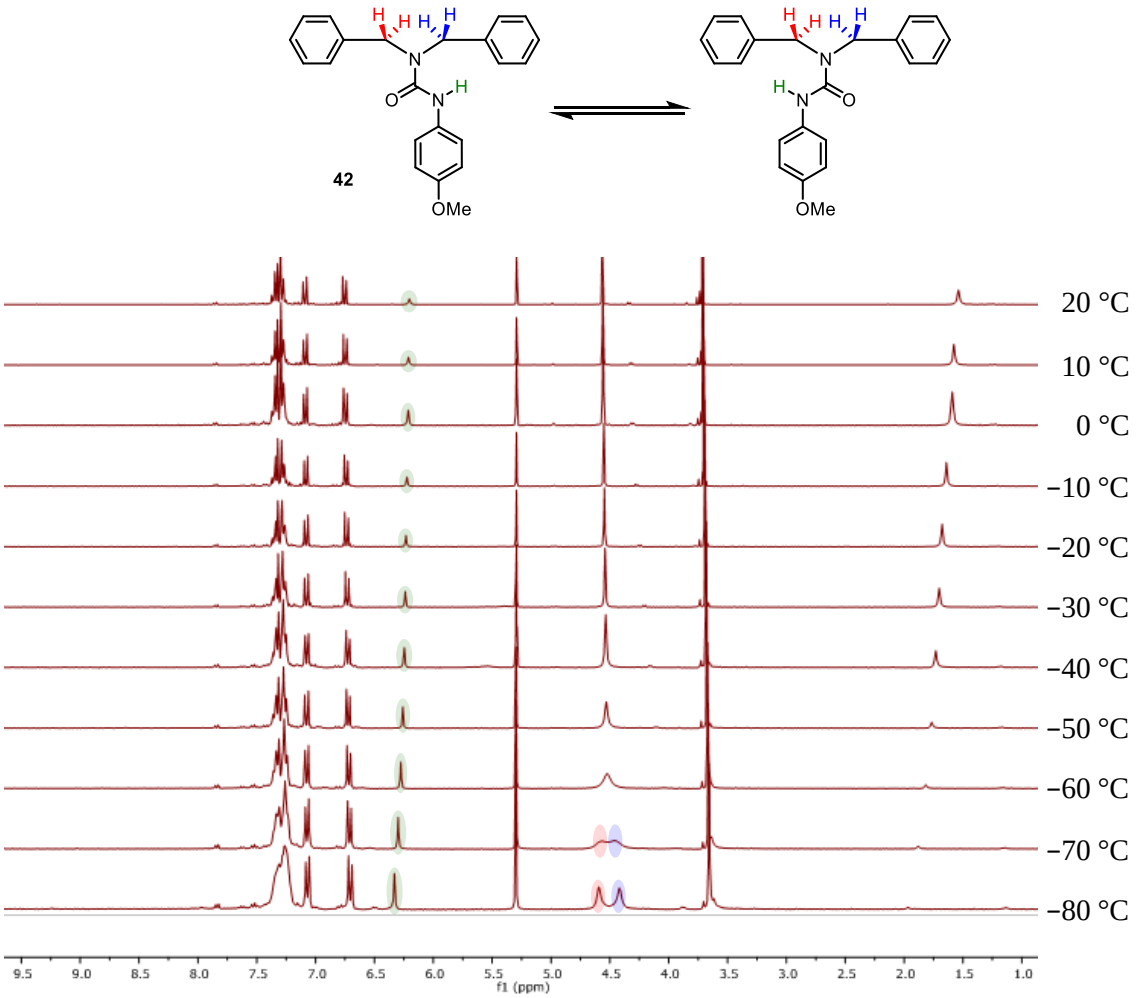

Figure 32 – VTNMR of 42 (CD_2Cl_2, 300 MHz, 29 mM).

Monourea **42** showed signals at 4.56 (benzylic methylenes) and 6.20 ppm (ureido proton) at 20 °C. The signal at 4.56 ppm was unaffected by decreasing temperature until −50 °C, where it broadened and eventually decoalesced into two singlets in a 50:50 ratio at −70 °C, which sharpened further at −80 °C. The signal at 6.20 ppm sharpened with decreasing temperature and moved steadily downfield. The design was been contrived so the two directionalities are identical to each other and are related by C_2 symmetry about the axis going through the Bn_2N–CO bond. These data were consistent with one populated conformation where rotation of the Bn_2N–CO bond is fast on the NMR timescale and becomes slow between −60 °C and −70 °C. The signals corresponding to the benzylic methylenes decoalesced because at slow exchange, one of the benzylic methylenes is proximate to a ureido proton, and the other is proximate to a ureido carbonyl, making them chemically inequivalent. Additionally, the downfield shift of the ureido proton with decreasing temperature is attributed to intermolecular hydrogen bonding. The assignment of the decoalesced benzylic methylene signals is arbitrary – it is unknown which methylene is proximate to the ureido carbonyl/proton.

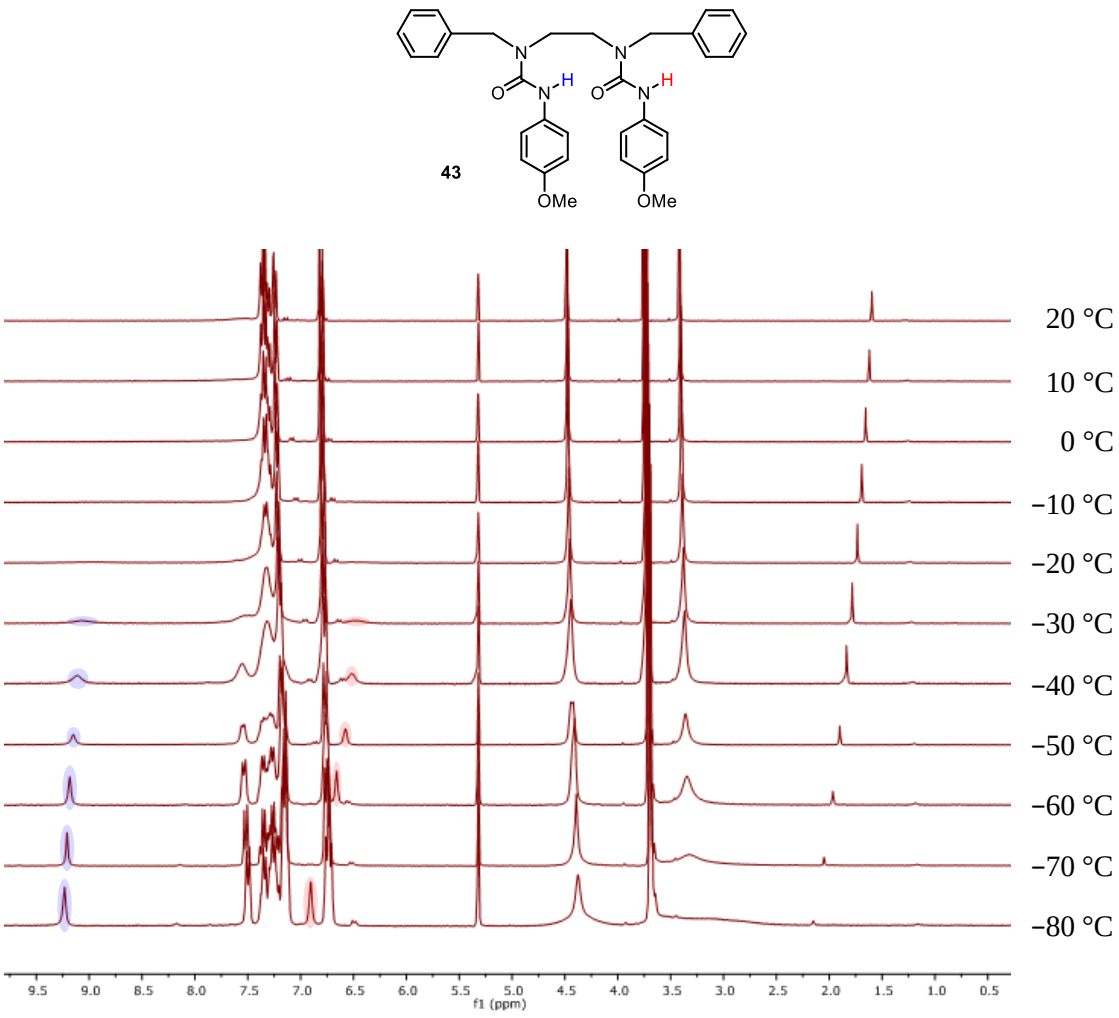

Figure 33 – VTNMR of 43 (CD_2Cl_2, 300 MHz, 19 mM).

Diurea **43** displayed a signal at 4.48 ppm (benzylic methylenes) at 20 °C. Upon cooling, this signal broadened and decoalesced at −50 °C. The decoalesced signals appeared to recombine at −70 °C. Signals appeared at 6.47 (1 H) and 9.06 ppm (1 H) at −30 °C, which sharpened and shifted downfield with decreasing temperature. These data were also consistent with one populated conformer of uniform directionality where the two benzylic methylenes are chemically inequivalent at slow exchange. At slow exchange, one ureido proton is in hydrogen bonding (9.06 ppm at −40 °C) and the other is not (6.47 ppm at −40 °C). Triurea **45** and tetraurea **46** were also analysed by VTNMR (Figures A2, A4), and they were found to behave analogously to diurea **43**, but with increasing numbers of hydrogen-bonding ureido protons.

There are numerous ways to examine the dynamics of interconverting mixtures of conformers in solution.[84] Such methods are useful for quantifying barriers to rotation in atropisomers, elucidating the mechanism of interconversion of conformers in dynamic structures, and quantifying the rates and activation barriers at/through which they happen. VTNMR is a powerful tool for examining dynamics in solution. It can be used to identify different conformers present in solution and quantify to what degree they are present at different temperatures. Using NMR simulation software, the rates of interconversion between the conformers, along with their enthalpy/entropy of activation and other useful parameters, can be determined.

In a dynamic system where two interconverting nuclei A and B are enantiotopic and necessarily isoenergetic, their rate of interconversion can be determined by use of the Eyring-Polanyi equation (Equation 1).[85]

$$k = \frac{k_B T}{h} e^{\frac{-\Delta G^{\ddagger}}{RT}}$$

k = Rate constant (s^{-1}) h = Planck's constant = 6.63×10^{-34} J s

k_B = Boltzmann constant = 1.38×10^{-23} J K^{-1} $\Delta G^{\ddagger}$ = Activation energy (J mol^{-1})

T = Temperature (K) R = Molar gas constant = 8.31 J K^{-1} mol^{-1}

Equation 1 – The Eyring-Polanyi equation.

By use of the Gibbs free energy equation (Equation 2), the Gibbs free energy can be separated into its enthalpic and entropic contributions.

$$\Delta G^{\ddagger} = \Delta H^{\ddagger} - T\Delta S^{\ddagger}$$

$\Delta H^{\ddagger}$ = Enthalpy of activation (J mol^{-1}) $\Delta S^{\ddagger}$ = Entropy of activation (J K^{-1} mol^{-1})

Equation 2 – The Gibbs free energy equation.

Substituting the Gibbs free energy equation into the Eyring-Polanyi equation, and subsequent rearrangement gives the Eyring-Polanyi equation in its linear form (Equation 3).

$$ln\frac{k}{T} = \frac{-\Delta H^{\ddagger}}{R}\frac{1}{T} + ln\frac{k_B}{h} + \frac{\Delta S^{\ddagger}}{R}$$

Equation 3 – The linear form of the Eyring-Polanyi equation.

From this, plotting ln(k/T) against (1/T) produces a straight line whose gradient is equal to ($-\Delta H^{\ddagger}/R$) and intercept is equal to ($\ln(k_B/h) + \Delta S^{\ddagger}/R$). In a dynamic system where two interconverting nuclei A and B are diastereotopic and therefore of different energy, the rate constants for the forward reaction and backward reaction will be different. If K and the rate are known, then the rate can be dissected into the different rate constants of the forward and backward reactions. If rate constants can be determined for different temperatures, then the $\Delta H^{\ddagger}$, $\Delta S^{\ddagger}$, and therefore $\Delta G^{\ddagger}$ can be determined for the dynamic process in question at any temperature. These data can be used to determine the values of other useful parameters in dynamic processes such as half-life and rate constants at unmeasured temperatures.

The signals corresponding to the benzylic methylenes of oligoureas **42** (monourea), **43** (diurea), **45** (triurea) and **46** (tetraurea) were modelled using SpinWorks 4 NMR processing and simulation software and the rate constants at different temperatures extracted. The rate constants were then plotted as a function of temperature to give an Eyring plot (see Appendix, section 8.2) whose gradient and intercept were used to deduce the free energy barrier of directionality reversal, $\Delta G^{\ddagger}$. Eyring analyses were then performed on ureas **42**, **43**, **45** and **46** to reveal $\Delta G^{\ddagger}_{298\,K}$ (CD_2Cl_2) to be 48.9, 59.4, 59.0 and 60.9 kJ mol^{-1}, respectively. This shows that, upon introduction of an intramolecular hydrogen bond (**42** to **43**), $\Delta G^{\ddagger}$ dramatically increases as directionality reversal is now associated with the breakage and reformation of a hydrogen bond. Upon addition of a third urea and a second hydrogen bond (**45**), there is no change in $\Delta G^{\ddagger}$. Finally, upon introduction of a fourth urea and a third hydrogen bond (**46**), there is an insignificant increase in $\Delta G^{\ddagger}$. These results appear to contradict hydrogen-bond cooperativity from a kinetic standpoint.[29] If hydrogen-bond cooperativity was operating in these foldamers, it is expected that $\Delta G^{\ddagger}$ would be greater in triurea **45** than in diurea **43**, as the cooperative effects would strengthen the intramolecular hydrogen bonds and confer additional kinetic stability. However, it is possible that the kinetic stability of the intramolecular hydrogen bonds is independent of hydrogen-bond cooperativity. The breakage and reformation of the hydrogen bonds could be occurring at the same rate, but the hydrogen bonds are more thermodynamically stable. Future work in this area will focus on addressing the possibility of hydrogen-bond cooperativity in these structures from a thermodynamic perspective.

Interestingly, $\Delta S^{\ddagger}$ was found to be universally negative, meaning that oligourea directionality reversal goes by an associative mechanism. $\Delta G^{\ddagger}_{298\,K}$ (CD_2Cl_2) of tetraurea **46** corresponded to a rate of directionality reversal of 130 s^{-1} at 298 K, showing that if an ethylene-bridged oligourea foldamer had controlled directionality, a perturbation of that directionality control would be communicated through the foldamer on the order of milliseconds. Eyring analysis was also performed on triurea **41** (Figure 31), where $\Delta G^{\ddagger}_{298\,K}$ (CD_2Cl_2) was found to be 58.1 kJ mol^{-1} for the minor to major conformer transition, and 59.2 kJ mol^{-1} for the major to minor conformer transition. Finally, due to the lack of discrepancy between the barriers of triureas **41**

and **45**, bis(ethyl) diurea, **47** was synthesised so its kinetic behaviour could be compared to that of the analogous bis(benzyl) diurea, **43**. Diurea **47** was synthesised by reaction of *N*,*N'*-diethylethylenediamine with 4-methoxyphenyl isocyanate, which proceeded in excellent yield. **47** was then studied by VTNMR (Figure 34).

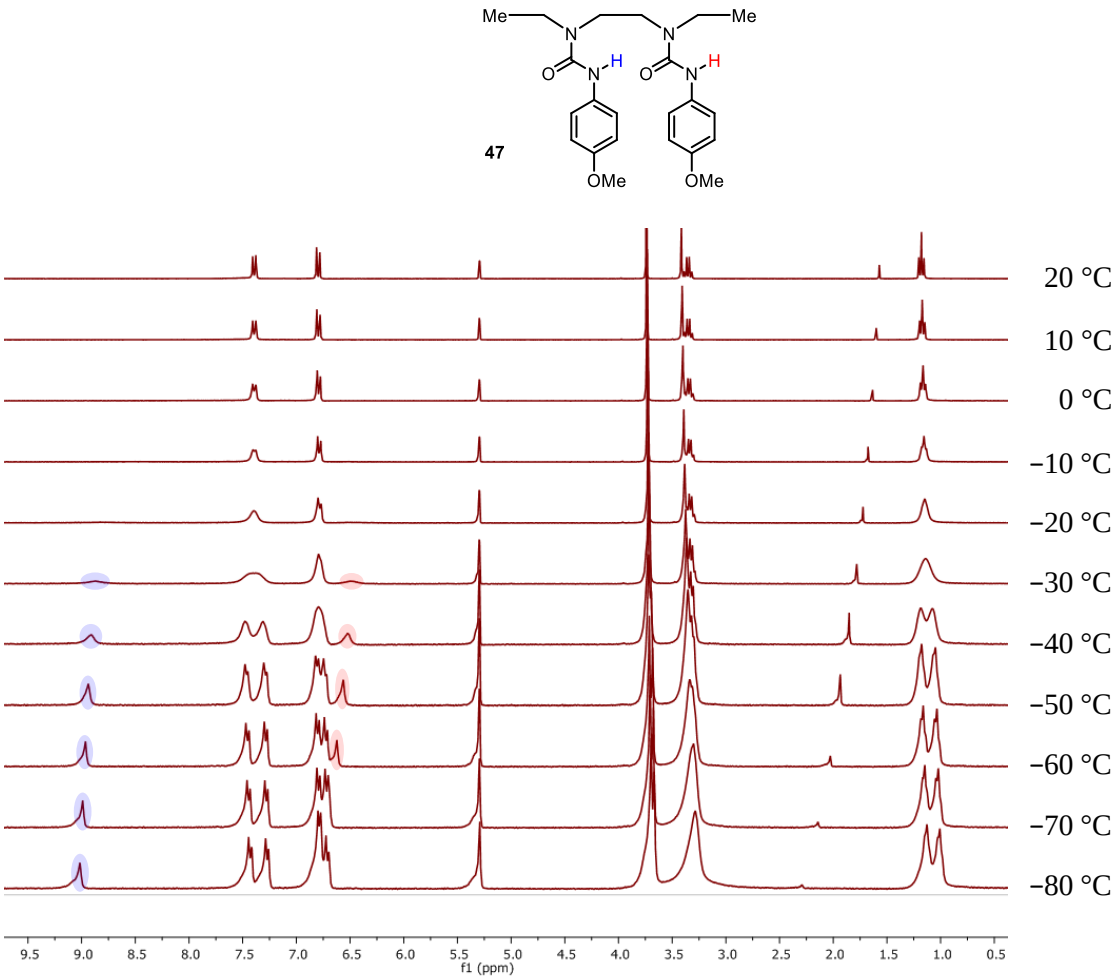

Figure 34 – VTNMR of 47 (CD_2Cl_2, 300 MHz, 24 mM).

Diurea **47** displayed a signal at 1.18 ppm (terminal methyl groups) at 20 °C. Upon cooling, the signal at 1.18 ppm lost its multiplicity and broadened until it decoalesced at −40 °C into two broad triplets. At −30 °C, signals appeared at 6.49 (1 H) and 8.86 ppm (1 H), which sharpened and shifted downfield upon further decreasing the temperature. These data showed that bis(ethyl) diurea **47** behaves analogously to bis(benzyl) diurea **43**, further validating the hypothesis that ethyl groups and benzyl groups can be used to terminate the oligoureas and permit conformational mobility. Eyring analysis of **47** revealed $\Delta G^{\ddagger}_{298\ K}$ (CD_2Cl_2) to be 51.5 kJ mol^{-1}, a value substantially lower than that of **43**, indicating that the barrier to and therefore the rate of directionality reversal is sensitive to the alkyl groups that terminate the foldamer.

Initial investigations into alternative terminations of ethylene-bridged oligoureas have shown that conformational mobility is conferred to the foldamer if they are terminated with alkyl groups. Access to these conformationally mobile oligoureas has allowed Eyring analyses, which have been used to determine $\Delta G^{\ddagger}$ in foldamers with a variety of lengths. Use of different termini had a significant effect on $\Delta G^{\ddagger}$, which will be considered when making foldamers with directional control. It was shown that intramolecular hydrogen bonding introduces kinetic stability to the foldamer, slowing down directionality reversal. This kinetic stability did not augment upon introduction of more hydrogen bonds to the network, suggesting a lack of hydrogen-bond cooperativity in these structures. The consistency of $\Delta G^{\ddagger}$ across oligoureas **43**, **45** and **46** indicates that further extension of the oligourea should not affect hydrogen-bonding dynamics, which could lend itself to function in long-distance informational communication.

3.2 Solvent Effects on Hydrogen-Bond Directionality

If these oligoureas were to be used in a biological setting, the communication of information would have to be feasible in the presence of biologically relevant molecules such as phospholipids, sugars, purine and pyrimidine-based nucleotides and most importantly, water. With oligoureas **42**, **43**, **45** and **46** in hand, it was desirable to further examine the effect of hydrogen-bonding additives on the fidelity of the hydrogen-bonding network. Firstly, monourea **42**, diurea **43** and triurea **45** were studied by VTNMR in CD_2Cl_2 with 40% v/v of CD_3OH as a competitive hydrogen-bonding solvent (Figures 35-36, Figure A3). The CD_2Cl_2/CD_3OH mixture was used to maintain solubility, and d_4-methanol was not used as proton-deuteron exchange would prohibit analysis of the ureido protons.

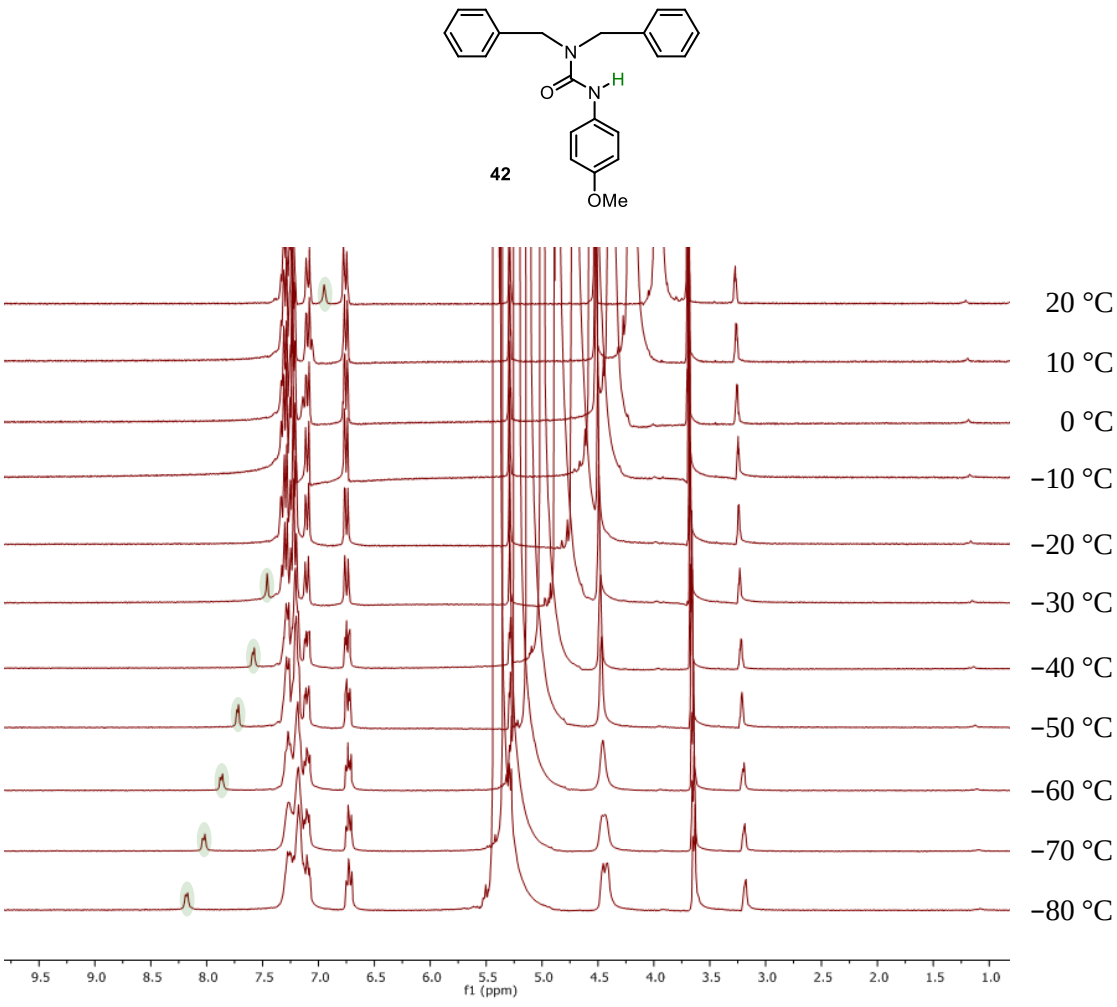

Figure 35 – VTNMR of 42 (40% v/v CD_3OH in CD_2Cl_2, 300 MHz, 29 mM).

In monourea **42**, signals were observed at 4.52 (benzylic methylenes) and 6.95 ppm (ureido proton) at 20 °C. Upon cooling, the signal at 4.52 ppm broadened until eventually decoalescing at −70 °C. The signal at 6.95 ppm shifted downfield with decreasing temperature.

At −40 °C, the peak at 7.58 ppm (ureido proton) decoalesced into two singlets in a 40:60 ratio which shifted downfield at the same rate upon further cooling. These results indicated that the ureido proton is in two different hydrogen-bonded chemical environments when in slow exchange. In the presence of CD_3OH, **42** either hydrogen bonds with itself or with CD_3OH, giving rise to the two different intermolecularly hydrogen-bonded environments. In comparison to that observed in neat CD_2Cl_2 (Figure 32), a decoalescence event was observed at the same temperature but the anisochronicity was much less pronounced in the presence of CD_3OH. The ureido proton signal was also much more downfield in the presence of CD_3OH due to intermolecular hydrogen bonding with the solvent.

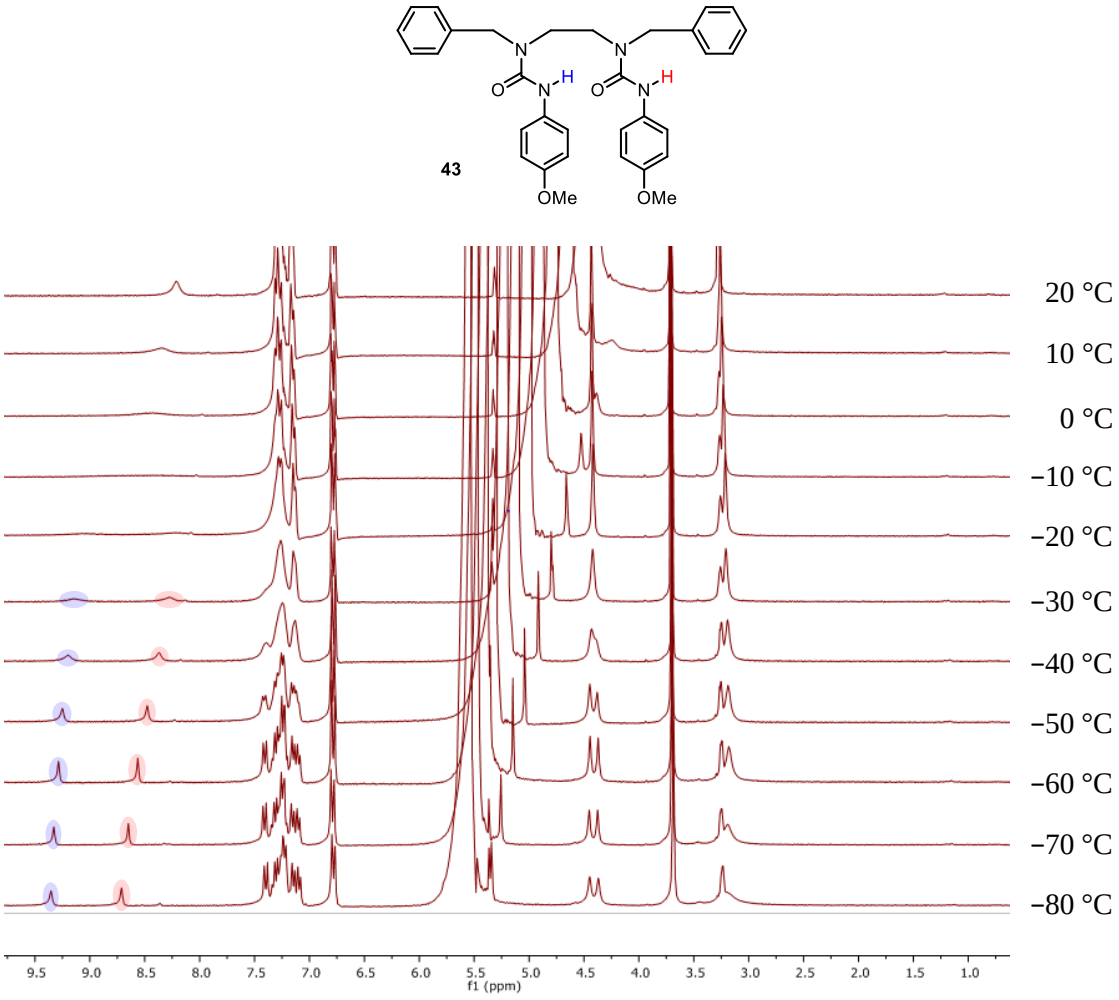

Figure 36 – VTNMR of 43 (40% v/v CD_3OH in CD_2Cl_2, 300 MHz, 19 mM).

In diurea **43**, signals were observed at 4.43 (benzylic methylenes) and 8.21 ppm (ureido protons) at 10 °C (the benzylic methylene signal was obscured by the alcohol peak at 20 °C). Upon cooling, the signal at 4.43 ppm broadened with decreasing temperature and decoalesced at −40 °C into two singlets in a 50:50 ratio, which sharpened upon further cooling. The signal at 8.21 ppm shifted downfield and broadened with decreasing temperature, until it decoalesced into

two broad singlets (1 H each) at −30 °C. These singlets sharpened and shifted further downfield with further cooling. If the CD_3OH interrupted the intramolecular hydrogen bonding, the resultant intermolecular hydrogen bond with CD_3OH would give rise to conformations where both ureas are chemically identical at slow exchange. However, decoalescence of the benzylic methylenes was still observed, indicating directional uniformity. The CD_3OH did not interrupt the intramolecular hydrogen bonding, it simply complemented it by hydrogen bonding to both ends; one through the hydroxyl oxygen and the other through the hydroxyl proton. This was further validated by the chemical shifts of the ureido protons at low temperature. At −60 °C, there is a signal at 9.29 ppm corresponding to an intramolecularly hydrogen-bonded ureido proton, which is very similar to **43** in CD_2Cl_2 (9.18 ppm). The other ureido proton shows a signal at 8.56 ppm, which is very different to that observed in CD_2Cl_2 (6.66 ppm) due to the formation of a hydrogen bond with CD_3OH (Figure 33). The anisochronicity of the benzylic methylenes in the presence of CD_3OH is much more pronounced than that in neat CD_2Cl_2 ($\Delta\Delta\delta_{298\,K}$ = 0.05 ppm). This is because at slow exchange, both benzylic methylenes are proximate to hydrogen-bonding CD_3OH, and the difference between these two environments is much more pronounced. Triurea **45** was also analysed by VTNMR (Figure A3), and was found to behave analogously to diurea **43**, but with two hydrogen-bonding ureido protons.

As methanol hydrogen bonds to the ends of these oligoureas, it was desirable to determine to what extent the central ureas interact with the solvent. To this end, triurea **45** was dissolved in CD_2Cl_2 and its ^{1}H NMR spectrum was recorded. Three equivalents of d_4-methanol were then added to the sample and its ^{1}H NMR spectrum recorded after specified times in order to see the rate at which the central ureido proton undergoes proton-deuteron exchange (Figure 37).

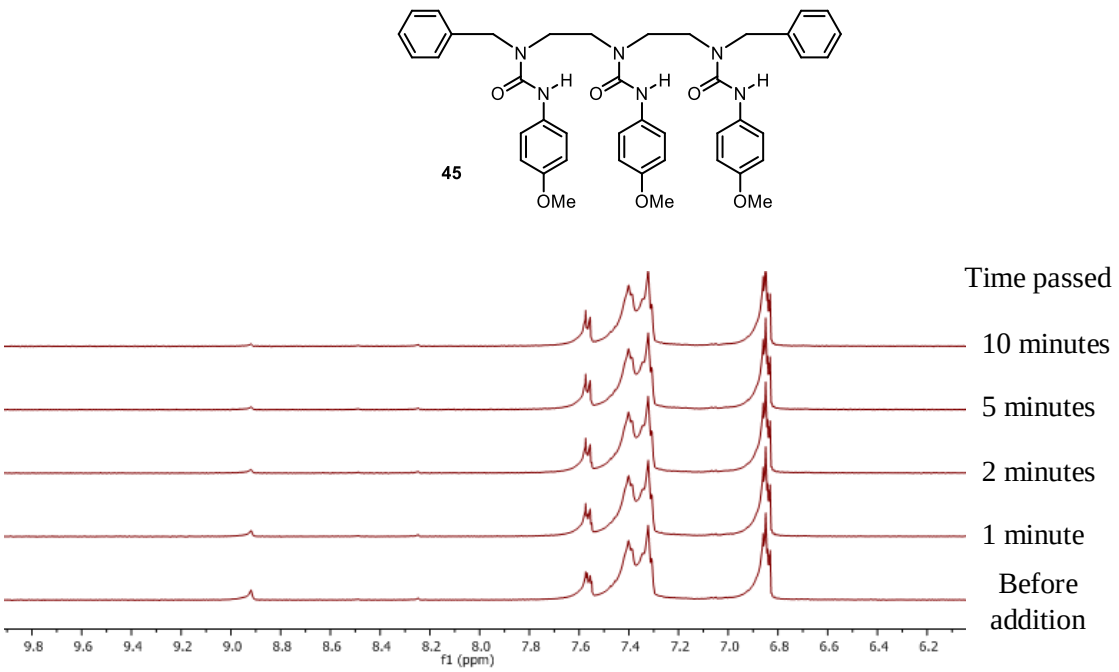

Figure 37 – ^{1}H NMR array upon addition of d_4-methanol to 45.

Unfortunately, the peripheral ureido protons could not be observed at 20 °C, so their rate of deuteration could not be determined. Upon addition of d_4-methanol, the central ureido proton signal (8.92 ppm) attenuated to 60% of its original integration. This attenuation continued until it stopped after 10 minutes. This result shows that the central ureas in these oligourea foldamers are protected from solvent to the extent that proton-deuteron exchange does not occur instantaneously. However, it is unknown whether deuteration of the central urea occurs directly from exchange with the d_4-methanol or by intramolecular exchange with adjacent ureas.

42, **43**, **45** and **46** were analysed by VTNMR with 10% v/v of d_6-DMSO as a competitive HBA (Figures 38-39, Figures A4, A6). The CD_2Cl_2/d_6-DMSO mixture was used instead of d_6-DMSO alone because d_6-DMSO freezes above the slow-exchange region of the oligoureas when using a 300 MHz spectrometer.

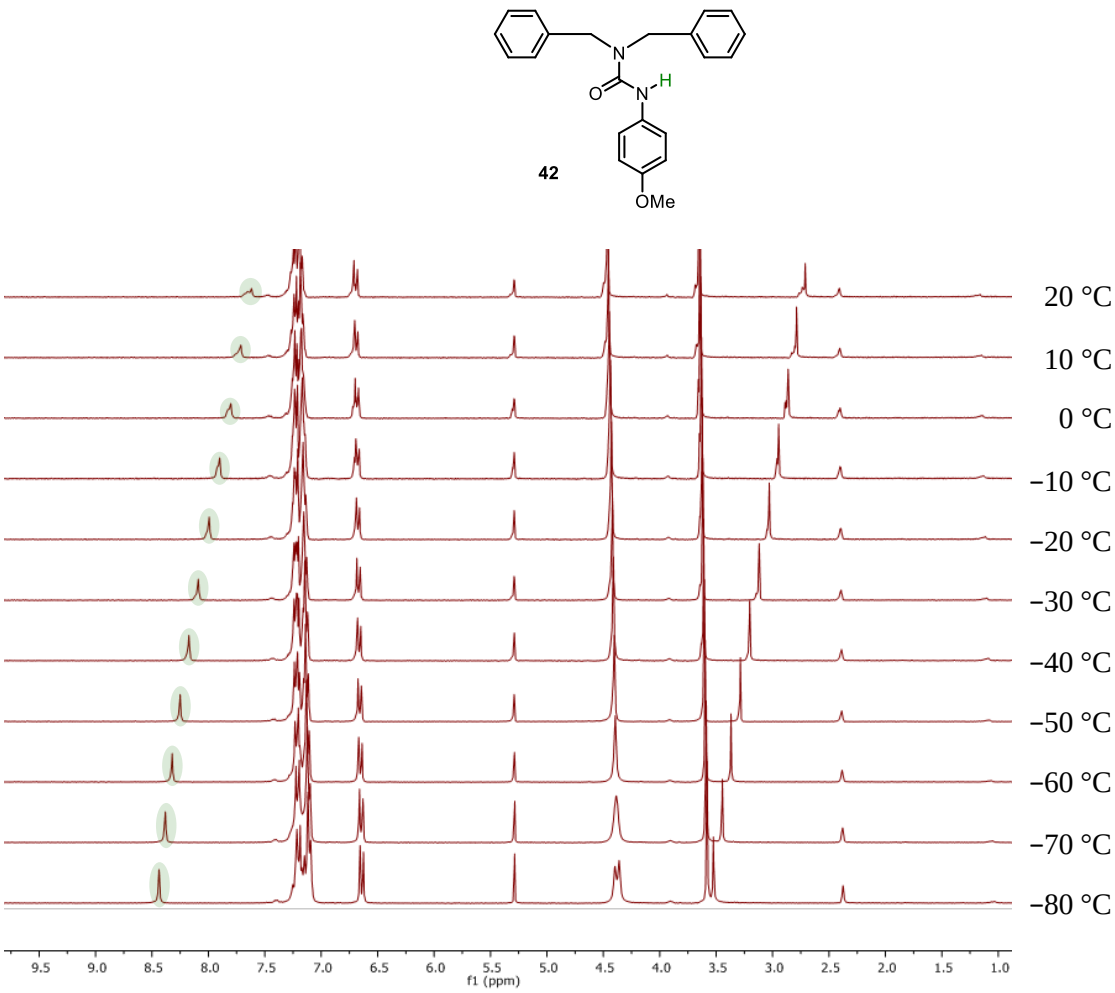

Figure 38 – VTNMR of 42 (10% v/v d_6-DMSO in CD_2Cl_2, 300 MHz, 29 mM).

In monourea **42**, signals were observed at 4.46 (benzylic methylenes) and 7.63 ppm (ureido proton) at 20 °C. The signal at 4.46 ppm broadened with decreasing temperature and eventually decoalesced at −80 °C. The signal at 7.63 ppm shifted downfield and sharpened upon cooling. These results showed that **42** exists as one conformation, and rotation about the Bn_2N–CO bond is slow on the NMR timescale below −80 °C. Additionally, d_6-DMSO hydrogen bonds to the ureido proton, as is demonstrated by its downfield shift with decreasing temperature.

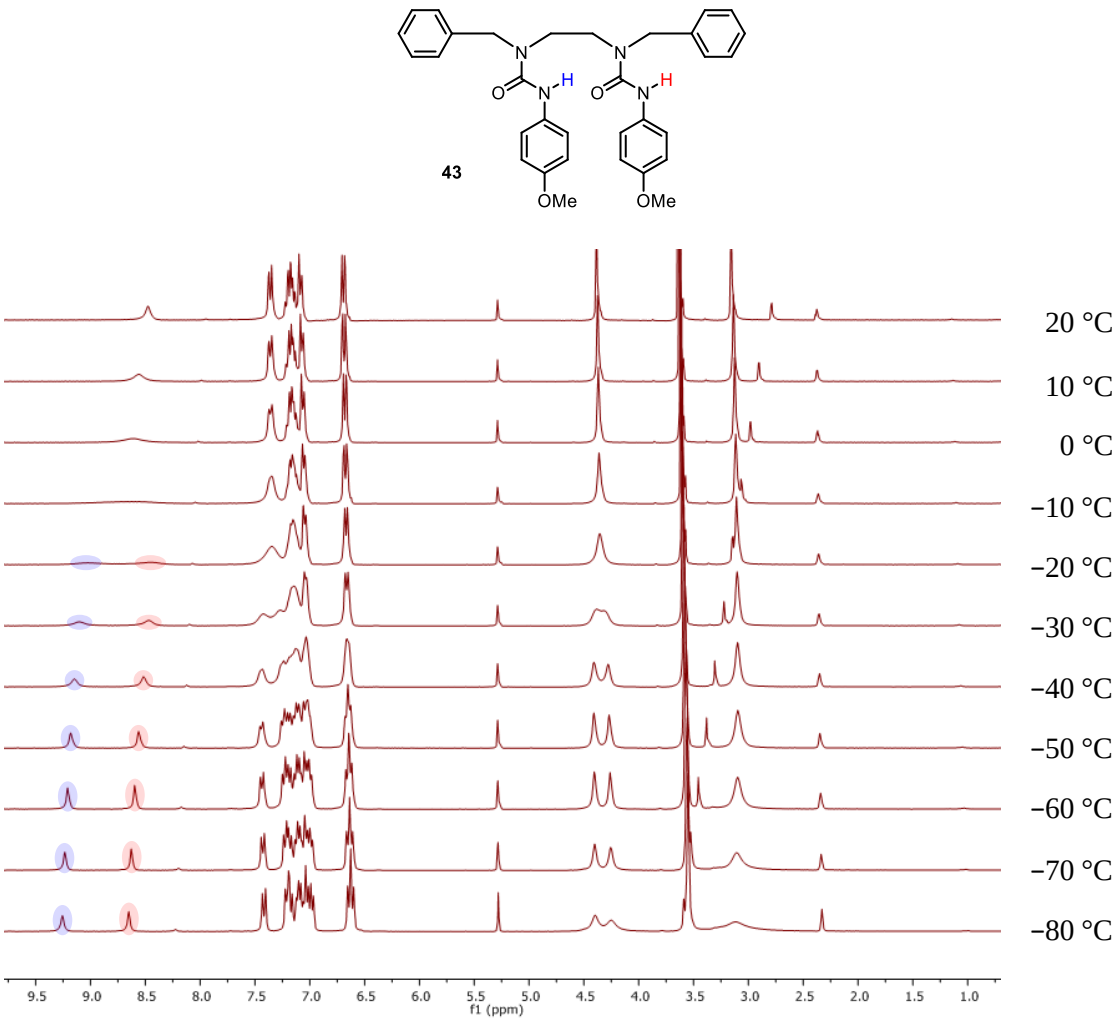

Figure 39 – VTNMR of 43 (10% v/v d_6-DMSO in CD_2Cl_2, 300 MHz, 19 mM).

In diurea **43**, signals were observed at 4.38 (benzylic methylenes) and 8.47 ppm (ureido protons) at 20 °C. The signal at 4.38 ppm broadened and decoalesced at −30 °C into two singlets in a 50:50 ratio, which sharpened further upon cooling. The signal at 8.47 ppm shifted downfield and broadened with decreasing temperature, until it decoalesced into two singlets (1 H each) at −20 °C, which then sharpen and shift further downfield with decreasing temperature. These data concluded that that d_6-DMSO also does not interrupt the intramolecular hydrogen bonding in **43**, it instead complements it by hydrogen bonding to the exposed terminal ureido proton. This is further validated by the chemical shifts of the ureido protons at low temperature. At −60 °C, there is a signal at 9.21 ppm corresponding to a ureido proton intramolecularly hydrogen bonded to the other urea. The other ureido proton shows a signal at 8.59 ppm, which is much more downfield than that observed in CD_2Cl_2 (6.66 ppm at −60 °C) as it is hydrogen bonding with d_6-DMSO. Triurea **45** and tetraurea **46** were also analysed by VTNMR (see Appendix, Figures A4, A6), and they were found to behave analogously to diurea **43**, but with increasing numbers of hydrogen-bonding ureido protons.

These results were then subject to Eyring analyses to reveal $\Delta G^{\ddagger}_{298\,K}$ values with varying numbers of ureas and in the presence of different hydrogen bonding cosolvents (Table 1).

Table 1 – $\Delta G^{\ddagger}_{298\,K}$ values (kJ mol^{-1}) for ureas 42, 43, 45 and 46 in the presence of hydrogen bonding cosolvents (the number in brackets denotes the number of intramolecular hydrogen bonds).

	$\Delta G^{\ddagger}_{298\,K}$ (kJ mol^{-1})		
Cosolvent	**None**	**40% v/v CD_3OH**	**10% v/v d_6-DMSO**
Monourea 42 (0)	48.9	59.9	54.5
Diurea 43 (1)	59.4	55.3	52.3
Triurea 45 (2)	59.0	58.6	54.9
Tetraurea 46 (3)	60.9	-	53.7

The Eyring analyses of **42**, **43**, **45** and **46** are explicable by considering intermolecular hydrogen bonding with cosolvent. Monourea **42** showed a significant increase in $\Delta G^{\ddagger}$ upon introduction of CD_3OH as directionality reversal is now being associated with breakage of two hydrogen bonds to CD_3OH or concurrent movement of CD_3OH with C–N bond rotation, resulting in inhibited directionality reversal. The $\Delta S^{\ddagger}$ term is still negative for **42**, **43** and **45**, suggesting the latter is the rate-determining step because the release of two molecules of CD_3OH is presumed to result in a positive $\Delta S^{\ddagger}$ term. CD_3OH forms two hydrogen bonds as it can act as an HBD through the hydroxyl proton and as an HBA through the oxygen lone pairs and hydrogen bond with the ureido carbonyl and proton, respectively. The $\Delta G^{\ddagger}$ for **43** decreases a small amount and is approximately the same in **45** when CD_3OH is present. This is also consistent with slowed C–N bond rotation in tertiary amides in polar media.[86] In the presence of d_6-DMSO, $\Delta G^{\ddagger}$ changes for **42**, **43**, **45** and **46** to approximately 54 kJ mol^{-1}. This is lower than that observed with CD_3OH because two urea-CD_3OH hydrogen bonds are weaker than one urea-d_6-DMSO hydrogen bond. Much like the case of CD_3OH, this is consistent with directionality reversal being associated with breakage and reformation of a hydrogen bond with DMSO. It is notable that $\Delta S^{\ddagger}$ is still negative in the presence of d_6-DMSO, suggesting that directionality reversal is associated with concurrent movement of d_6-DMSO with C–N bond rotation.

VTNMR and subsequent Eyring analyses have concluded that the intramolecular hydrogen bonding in the oligoureas is robust in the presence of hydrogen-bonding cosolvents CD_3OH and d_6-DMSO. In some cases, the kinetic parameters are significantly altered, but thermodynamically, the oligoureas are most stable when forming an intramolecular hydrogen-bonding network, which may or may not be complemented by HBDs and HBAs present in the bulk. This result indicates that this class of foldamers may be conducive to informational communication in the presence of other competitive hydrogen-bonding molecules that would be present in a biological setting.

With these encouraging results surrounding the robustness of the hydrogen-bonding network in these oligourea foldamers, it was interesting to find out how strong hydrogen-bonding competitors need to be in order to provide a better thermodynamic alternative to intramolecular hydrogen bonding. The VTNMR experiment of **45** was repeated with 50% v/v d_6-DMSO in CD_2Cl_2 (Figure 40). Spectra were not recorded below −60 °C as the solution began to freeze between −50 °C and −60 °C.

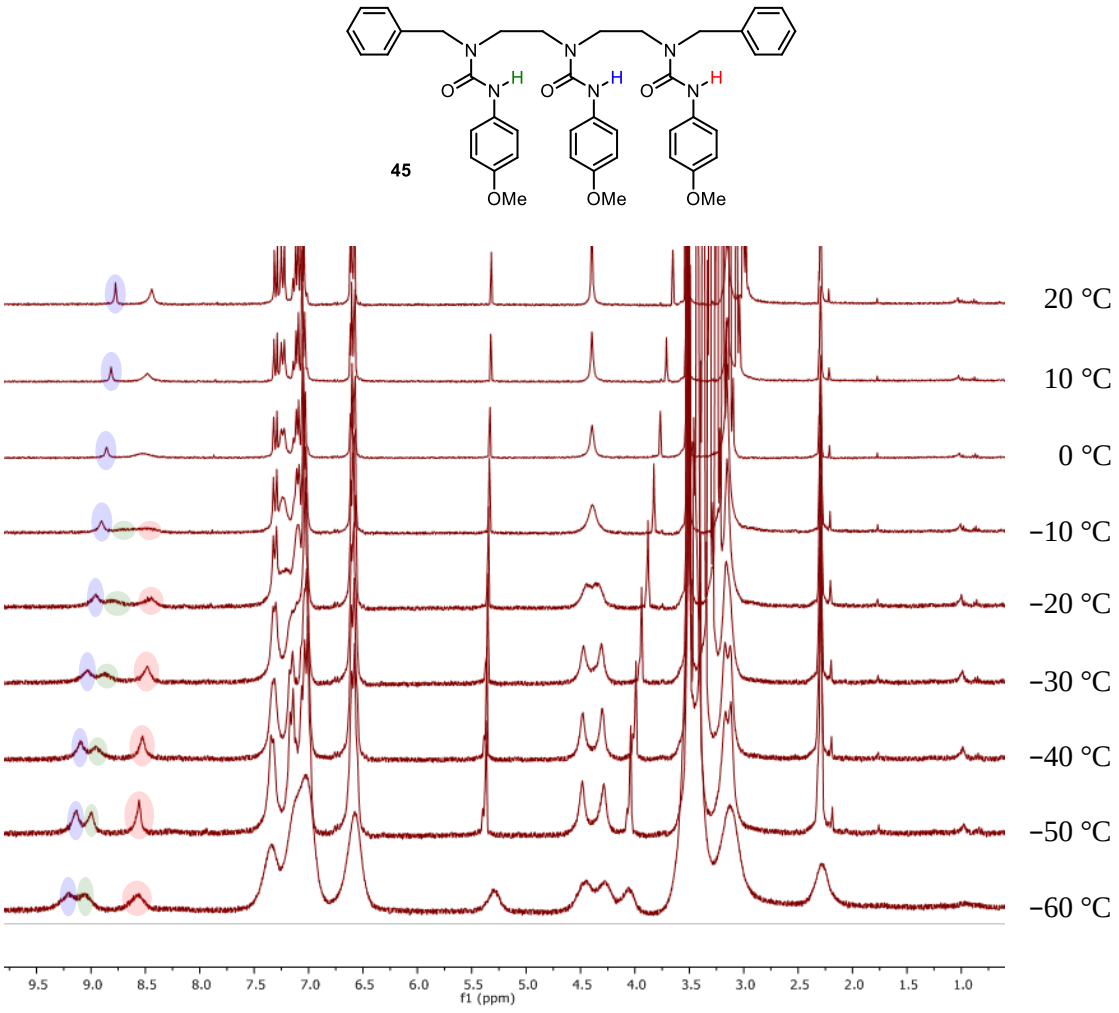

Figure 40 – VTNMR of 45 (50% v/v d_6-DMSO in CD_2Cl_2, 300 MHz, 14 mM).

Triurea **45** with 50% v/v d_6-DMSO in CD_2Cl_2 behaved in a highly analogous fashion to when it was in 10% v/v d_6-DMSO in CD_2Cl_2, showing that d_6-DMSO is not a strong enough HBA to disrupt the intramolecular hydrogen bonding in **45**. It may be that disruption of the hydrogen-bonding network could be achieved with stronger HBAs, such as phosphine oxides.

Schreiner's thiourea is a very strong double HBD which forms very stable complexes with carbonyl compounds (Figure 41).[87] It was suspected that this may have sufficient hydrogen-bond-donating power to disrupt the hydrogen-bonding network. 2.5 equivalents of Schreiner's

thiourea were added to **45** in CD_2Cl_2. More Schreiner's thiourea would have been used to help destroy the hydrogen-bonding network, but its solubility in CD_2Cl_2 was limiting. The same stoichiometry was maintained throughout the VTNMR experiment (Figure 41), but particulate precipitation resulted in a loss of resolution at lower temperatures.

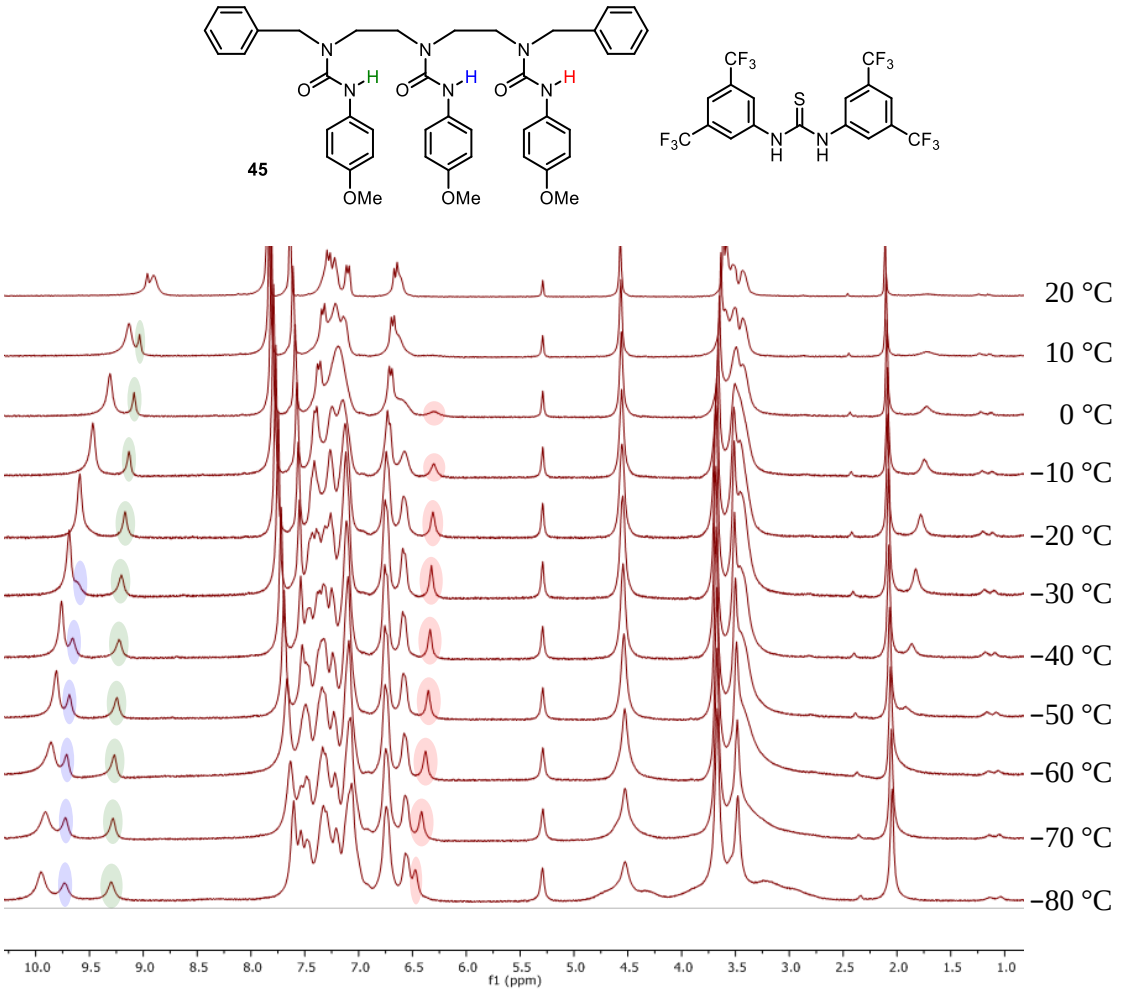

Figure 41 – VTNMR of 45 with 2.5 equivalents of Schreiner's thiourea (CD_2Cl_2, 300 MHz, 14 mM).

Triurea **45** showed signals at 4.57 (benzylic methylenes), 8.90 (Schreiner's thiourea thioureido protons) and 8.96 ppm (central ureido proton) at 20 °C. The signal at 4.57 ppm broadened with decreasing temperature but did not appear to decoalesce, and the signals at 8.90 and 8.96 ppm shifted downfield. At 0 °C, new signals appeared at 6.30 and 9.31 ppm (obscured by Schreiner's thiourea thioureido protons), which sharpened and shifted downfield with decreasing temperature. These results can be explained by the population of only one conformer with uniform directionality where, at slow exchange, there is one non-hydrogen-bonded ureido proton (6.38 ppm at −60 °C) and two intramolecularly hydrogen-bonded ureido protons (9.27 and 9.72 ppm at −60 °C). Schreiner's thiourea complements the directionality by hydrogen bonding to the terminal ureido carbonyl, hence the downfield shift of the thioureido protons with

decreasing temperature. It is proposed that a decoalescence of the benzylic methylene signal is not observed due to a loss of spectral resolution associated with particulate precipitation of Schreiner's thiourea.

Experiments with 50% v/v d_6-DMSO and Schreiner's thiourea showed that strong hydrogen-bonding additives, even when present to a high degree, are not powerful enough to impart any preferential thermodynamic alternative to these foldamers. This further supports the notion that these oligoureas could lend themselves to informational communication in biological settings without disruption from biological molecules. Unfortunately, these foldamers are not soluble in mixtures of DCM/methanol that would solubilise other biologically relevant potent hydrogen-bonding molecules. Further work in this area will involve derivatisation of the foldamers to confer water/methanol solubility, such that water/methanol mixtures can be used to study the oligoureas by VTNMR in the presence of sugars, phospholipids and nucleotides.

3.3 Electronic Control of Hydrogen-Bond Directionality

At this point, a host of conformationally mobile oligourea foldamers had been synthesised and used to demonstrate hydrogen-bonding fidelity within the ethylene-bridged oligourea scaffold. Next, research was focused on making oligourea foldamers terminated with groups that can control directionality electronically. The initial target selected was thiourea, **49** (Scheme 11) in the hope that it would control directionality in the opposite fashion to the phenyl groups established by Nowick (act as the C-terminus). Thioureas are much stronger HBDs and weaker HBAs than their homologous ureas due to the higher diffusivity of the orbitals on sulfur, so it was expected that they could impose directional control by hydrogen bonding through their thioureido protons.[87,88] The 4-nitrophenyl substitution on the thiourea was used to further augment the thiourea's hydrogen-bond-donating ability.

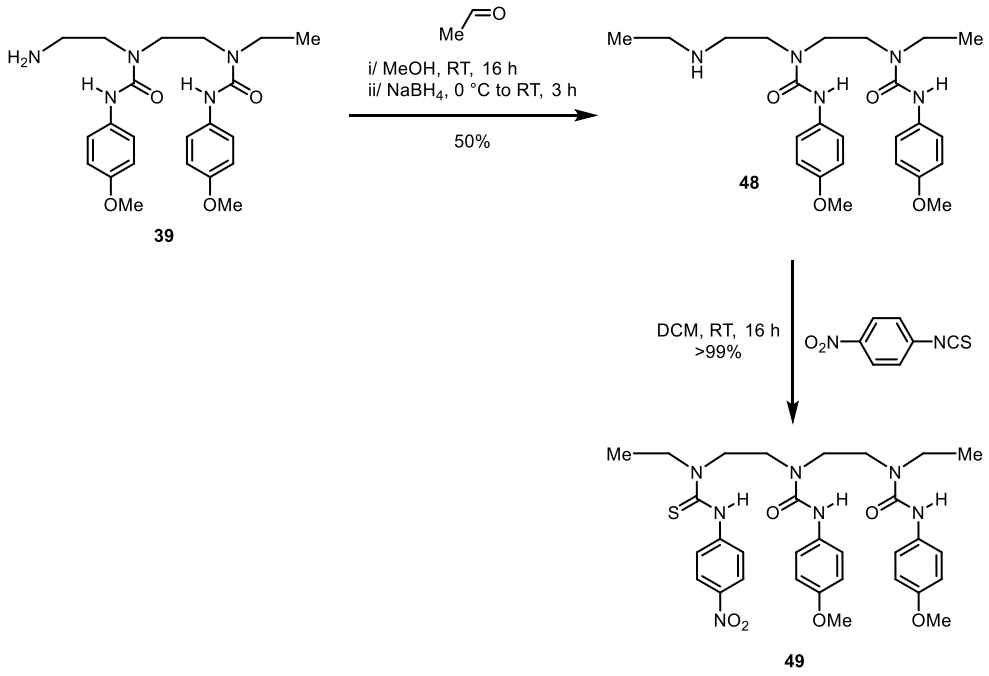

Scheme 11 – Synthesis of 49.

Amine **39** underwent reductive alkylation with acetaldehyde, and the corresponding secondary amine was reacted with 4-nitrophenyl isothiocyanate to give the target thiourea **49** in reasonable yield over two steps. **49** was then studied by VTNMR (Figure 42).

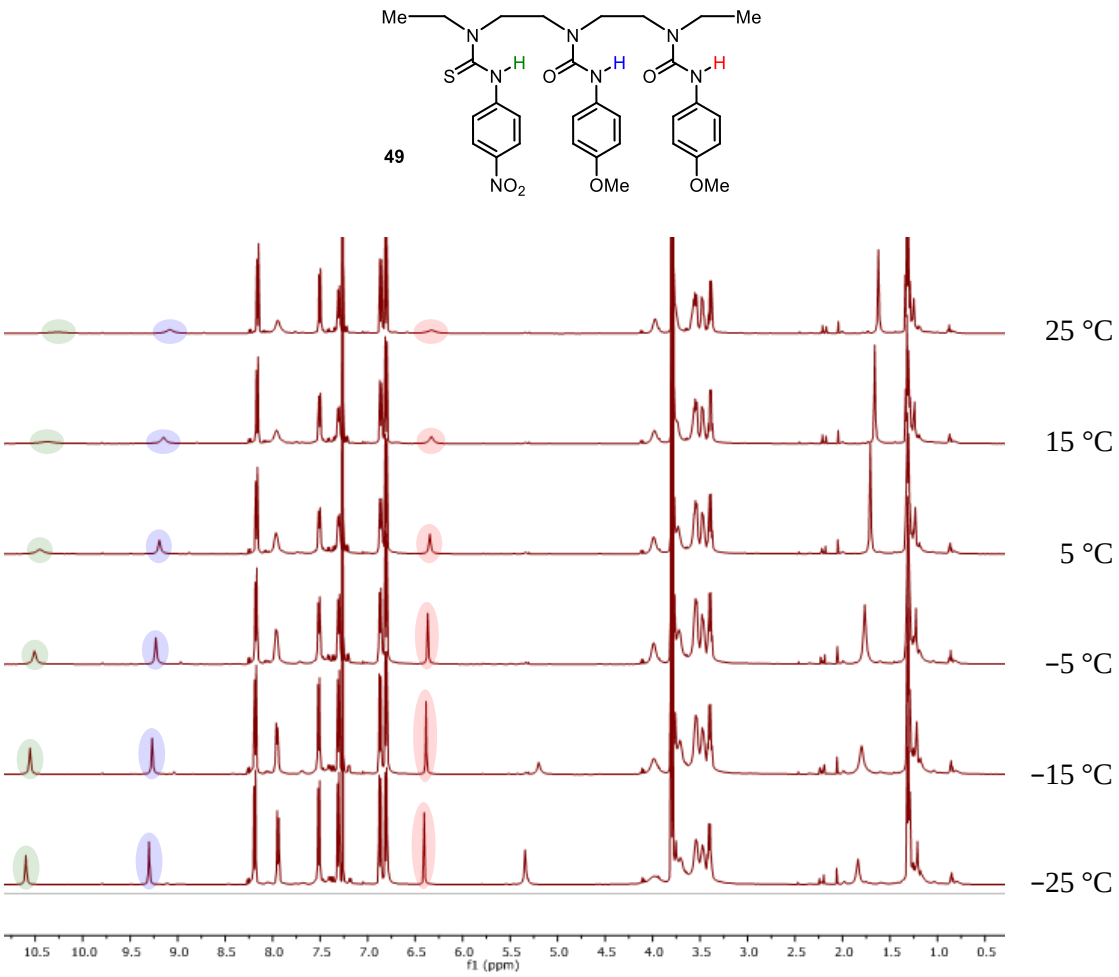

Figure 42 – VTNMR of 49 ($CDCl_3$, 500 MHz, 16 mM).

Thiourea **49** showed signals at 6.32 (peripheral ureido proton), 9.09 (central ureido proton) and 10.26 ppm (thioureido proton) at 25 °C. Each of these signals were broad at 25 °C, but all sharpened and shifted downfield upon cooling. There was no observable decoalescence of the alkyl or aromatic signals throughout the experiment. These data indicate that **49** exists as one conformation, where the thioureido proton (10.26 ppm at 25 °C) is in hydrogen bonding. The central ureido proton (9.09 ppm at 25 °C) is also in hydrogen bonding with another urea, but the peripheral ureido proton (6.32 ppm at 25 °C) is not hydrogen bonded. This shows that the thiourea establishes complete conformational control over the diurea by forcing the adjacent urea to hydrogen bond to it through its carbonyl. This directionality is communicated to the second urea, and so the ureido proton in the peripheral urea cannot form an intramolecular hydrogen bond, defining the thiourea terminus as the C-terminus.

These studies have shown that electron-deficient thioureas can impart total directional control in ethylene-bridged diureas. Next, the synthesis of longer oligoureas with terminal hydrogen-bonding groups was sought to show that directional control still operates with more ureas in the foldamer. Additionally, another hydrogen-bonding group that would act as an HBA (act as the N-terminus) was also desired. Imides do not contain acidic protons, and so it was expected that they could impose directional control by acting as an HBA through their imido carbonyls. Due to the slow, poorly yielding and wasteful nature of an iterative process, the synthesis of the new targets, thiourea **50** and phthalimide **51** (Figure 43) was to be achieved in a more modular process deriving from the corresponding oligoethylenediamine. Previous experiments had shown that the benzylic methylene would be remote from other signals in the ^{1}H NMR spectrum, meaning that it could be used as an effective spectroscopic reporter for conformer distribution. In thiourea **50**, phenyl groups are used at both ends in order to remove any steric effects that could be associated with directionality control.

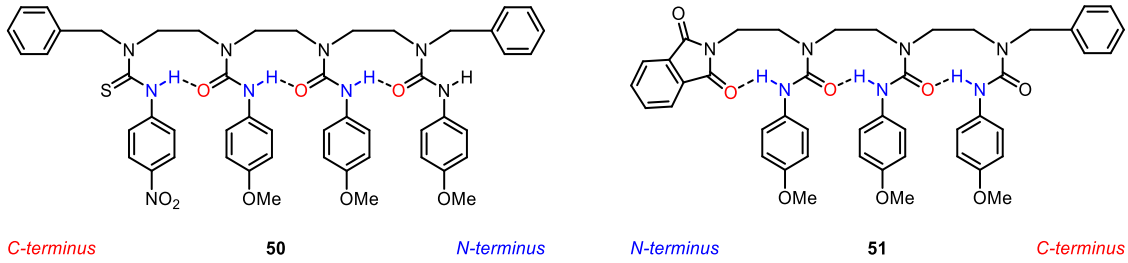

Figure 43 – Elongated directionality-controlled targets, 50 and 51.

The first attempted method was adapted from Leigh and co-workers by making a directionality-controlling fragment attached to an aldehyde, which could be coupled to the *N*-benzyl-substituted oligoethylenediamine by reductive amination (Scheme 12).[89] After coupling of these fragments, protecting group removal and subsequent installation of the ureas would give the target directionality controlled oligoureas, thiourea **50** and phthalimide **51**.

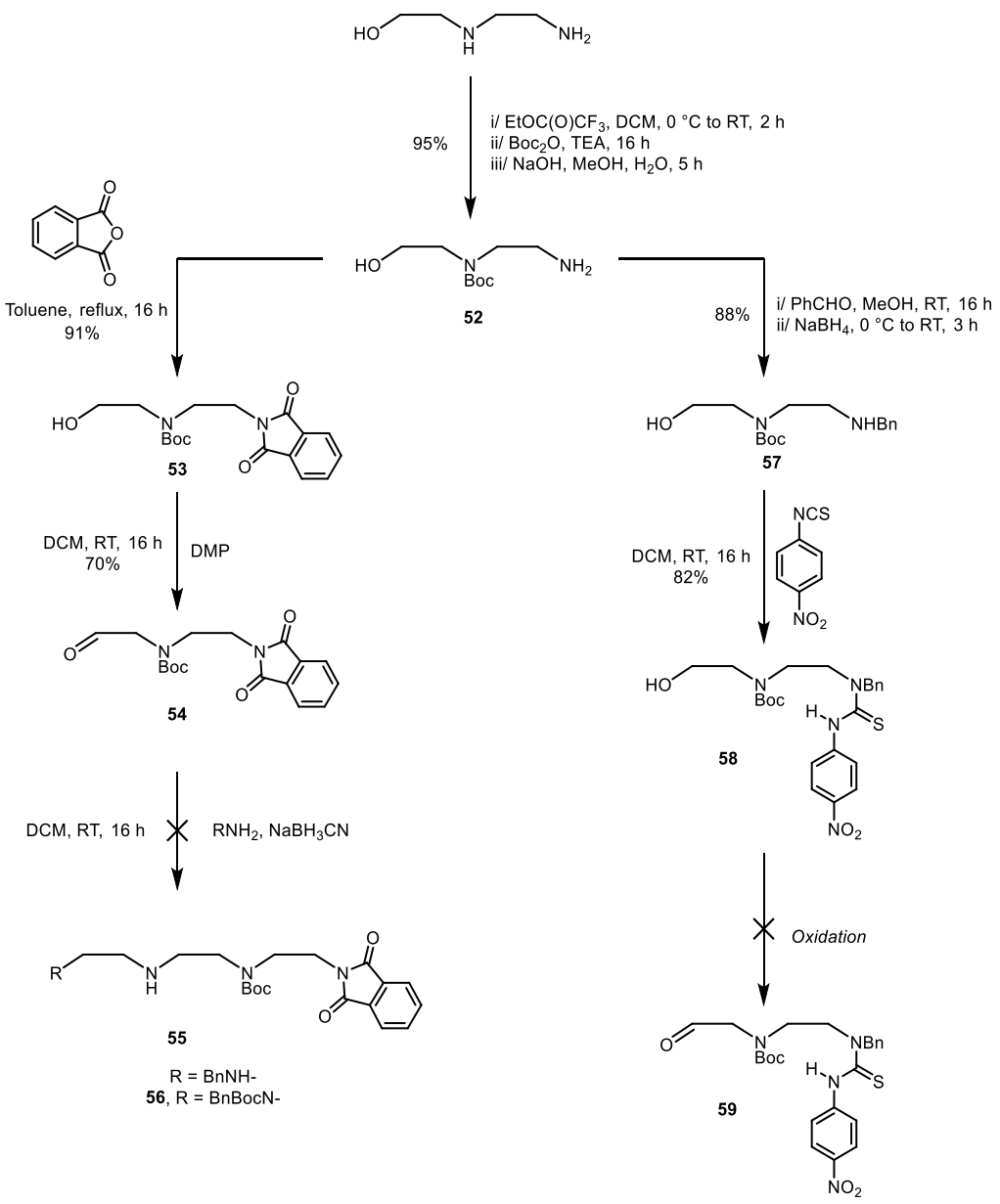

Scheme 12 – Synthesis of aldehyde fragments, 54 and 59.

N-(2-hydroxyethyl)ethylenediamine was protected selectively at the secondary amine by trifluoroacetylation of the primary amine, Boc-protection of the secondary amine and then hydrolysis of the corresponding trifluoroacetamide.[89] The synthetic scheme was then bifurcated to make the two different aldehyde fragments, **54** and **59**. Amine **52** was reacted with phthalic anhydride to give the corresponding amic acid, which was then activated to cyclisation using excess CDI (1,1'-carbonyldiimidazole) to give the corresponding phthalimide. This effected the desired cyclisation, but unfortunately, the alcohol also reacted with the CDI to give an imidazolyl carbamate. Attempts to hydrolyse the carbamate using aqueous sodium hydroxide resulted in hydrolysis of both the carbamate and the phthalimide. Instead, the cyclisation of the amic acid was triggered thermally by heating in toluene, giving phthalimide **53** in excellent yield. Oxidation

of the alcohol to the aldehyde using Dess-Martin periodinane (DMP) proceeded in good yield to give the target aldehyde fragment **54**. Next, reductive amination using *N*-benzylethylenediamine and sodium cyanoborohydride was attempted. This reducing agent was chosen to avoid potential overreduction of the phthalimide to the corresponding isoindolinone. However, decomposition was observed under these reductive amination conditions. The same was also observed when the imine was preformed in methanol and also when no reducing agent was present. Due to the known stability of the aldehyde, it was presumed that the imine was the unstable component that was decomposing before it could be reduced. It was speculated that the 1,2-diamine relationship in the nucleophile was causing the decomposition as the imine could react further intramolecularly to form an imidazolidinone. *N*-Boc-*N*-benzylethylenediamine was synthesised in an analogous way to amine **52** from *N*-benzylethylenediamine (Scheme 12) and used for imine formation, but unfortunately, decomposition of aldehyde **54** was still observed. Due to the instability of **54** to reductive amination conditions, an alternative method was sought.

The synthesis of thiourea fragment, **59** was then attempted. Reductive alkylation of **52** with benzaldehyde followed by reaction with 4-nitrophenyl isothiocyanate afforded **58** in excellent yield over two steps. Next, oxidation of the alcohol to the aldehyde using DMP yielded numerous products, none of which corresponded to the desired aldehyde. Other attempts to oxidise the alcohol included Swern oxidation, reaction with MnO_2 and with pyridinium chlorochromate (PCC), all with similar results. From this, the thiourea was deemed too reactive to be conducive to a fragment-based synthesis of the longer directionality-controlled oligoureas. It was speculated that the thiourea was reacting with the oxidising agents at the sulfur atom, resulting in decomposition. The fragment-based synthesis of the longer directionality-controlled oligoureas was consequently abandoned, and it was deduced that these controlling groups had to be installed near the end of the synthesis.

A new stratagem was devised for the synthesis of the longer directionality-controlled oligoureas based on a method from Leigh and co-workers.[89] The method involved the protection of the secondary amines of an oligoethylenediamine, followed by desymmetrising reductive alkylation and further functional group manipulation to afford the desired directionality-controlled oligoureas (Scheme 13).

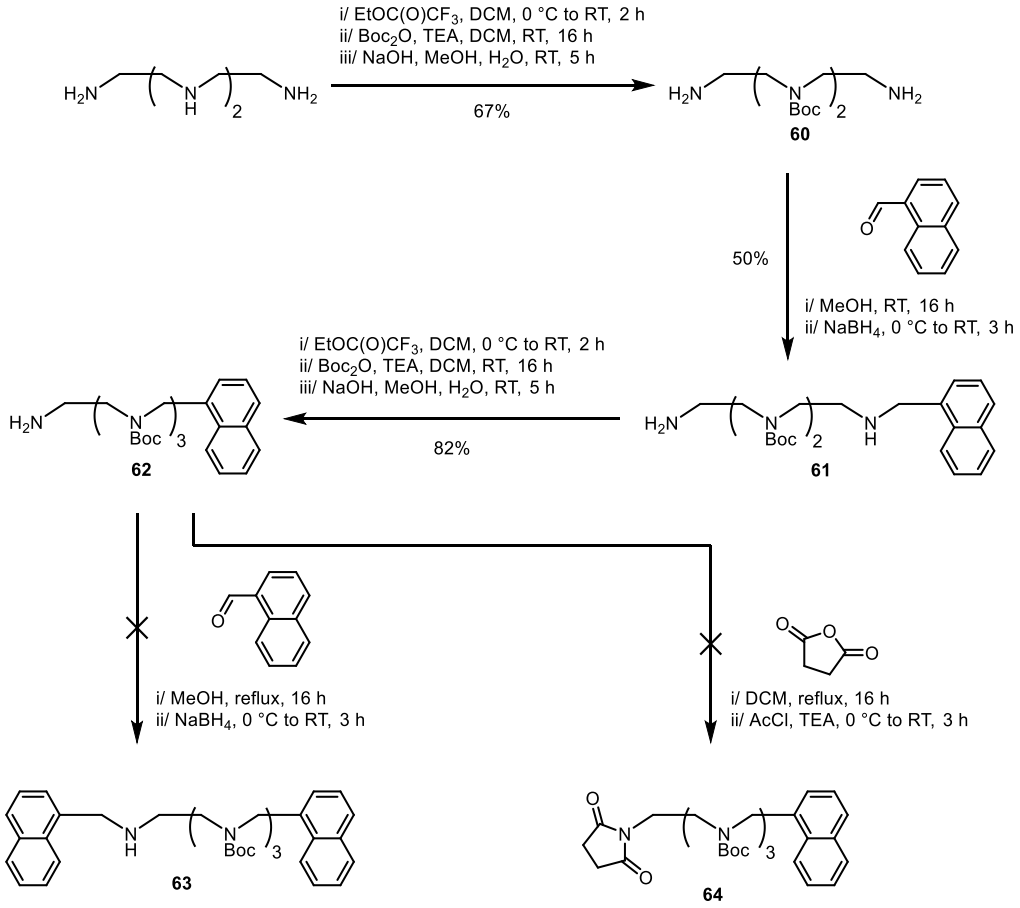

Scheme 13 – Synthesis of intermediates, 63 and 64.

Triethylenetetramine was protected at the secondary amines with Boc groups analogously to amine **52** (Scheme 12). Desymmetrising reductive alkylation was then attempted with diamine **60** and benzaldehyde but unfortunately, only the dibenzylated product could be isolated. As Leigh and co-workers have previously performed desymmetrising reductive alkylations using 1-naphthaldehyde, the desymmetrisation was attempted using 1-naphthaldehyde instead of benzaldehyde. This reaction proceeded in poor yield to give naphth-1-ylmethylamine **61**, but upon scale-up and dropwise addition of the aldehyde to a concentrated solution of the diamine, the yield was improved to 50%. As this method for desymmetrisation proved successful, the naphth-1-ylmethyl group was used to terminate the longer directionality-controlled triureas.

Next, trifluoroacetamide formation, Boc installation and trifluoroacetamide hydrolysis installed a final Boc group on the remaining secondary amine. This proceeded in excellent yield over the three steps to give the primary amine, **62**. **62** was then heated to reflux in toluene with succinic anhydride to form the imide. This saw no conversion of starting material and the same result was observed when **62** was heated with an excess of triethylamine and succinic anhydride. Similarly, when heated in ethanol with an excess of 1-naphthaldehyde and 1 mol% of acetic acid, no imine formation was observed. From this, it was concluded that upon formation of the third

Boc group on the tetramine, the Boc groups distorted the conformation of the oligoethylenediamine such that the reactivity of the primary amine was greatly inhibited. Due to this, the steps of the synthesis were rearranged so that the ureas were installed before formation of the directionality controller (Scheme 14).

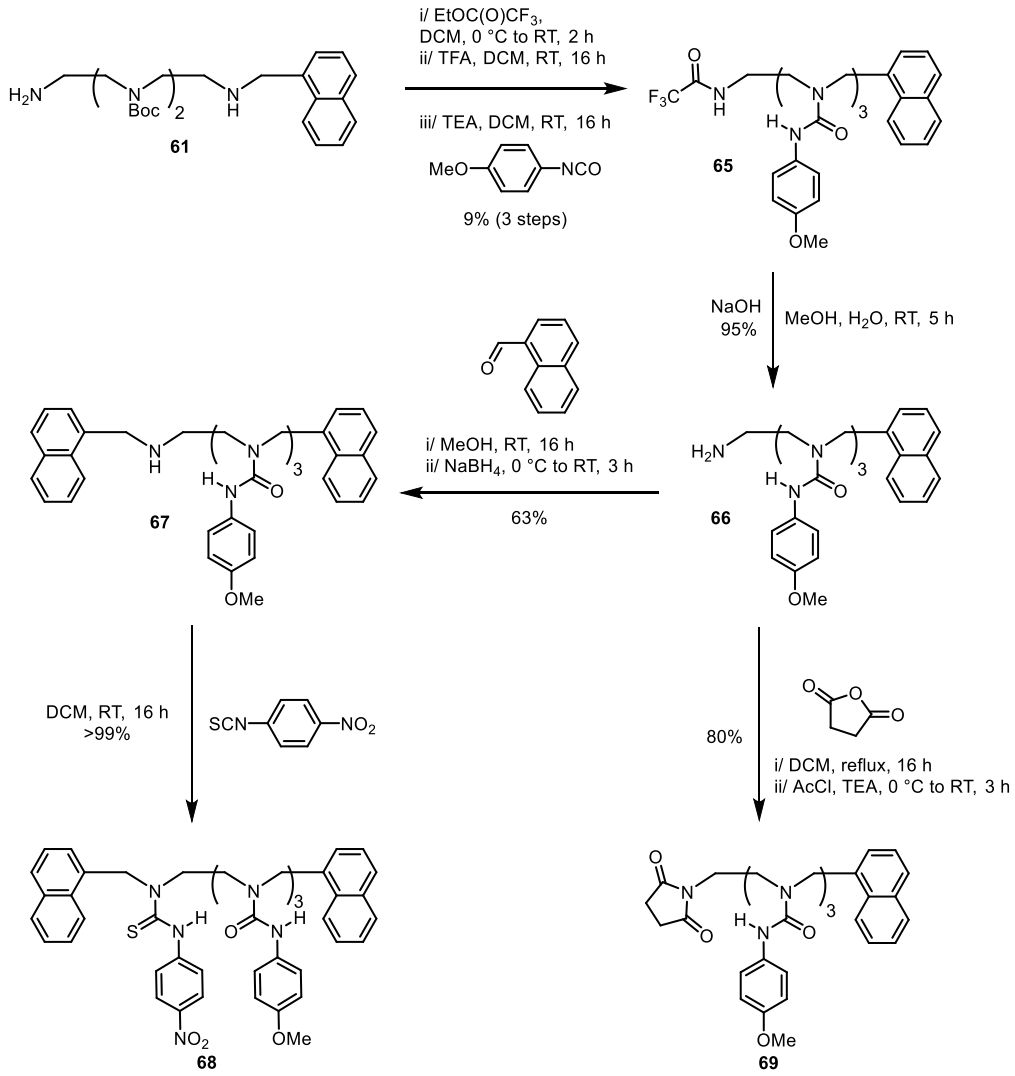

Scheme 14 – Synthesis of directionality-controlled oligoureas, 68 and 69.

In this method, the desymmetrised amine, **61** was deprotected using TFA to liberate the mono-naphth-1-ylmethylated tetramine. Unfortunately, during purification, this tetramine partitioned into the aqueous phase despite attempting different polar organic phases, including when the aqueous phase was strongly alkaline. The aqueous phase was concentrated and the residue triturated with ethyl acetate, but this did not furnish the desired tetramine. Hence, the synthetic steps were rearranged again to promote organic solubility. Primary amine **61** was trifluoroacetylated at the primary amine, and the Boc groups cleaved using TFA. Three ureas were then installed to give the desired triurea **65**, albeit in poor yield over the three steps. The

trifluoroacetamide was then hydrolysed using aqueous hydroxide to create the primary amine **66**, which was then used to install the two different directionality-controlling groups.

Primary amine **66** underwent reductive alkylation with 1-naphthaldehyde to give the corresponding naphth-1-ylmethylamine **67**, which was then reacted with 4-nitrophenyl isothiocyanate to form the target thiourea, **68**. Separately, **66** was reacted with succinic anhydride and acetyl chloride, giving the target succinimide, **69** in good yield. Thiourea **68** and succinimide **69** were then studied using VTNMR (Figures 44-45).

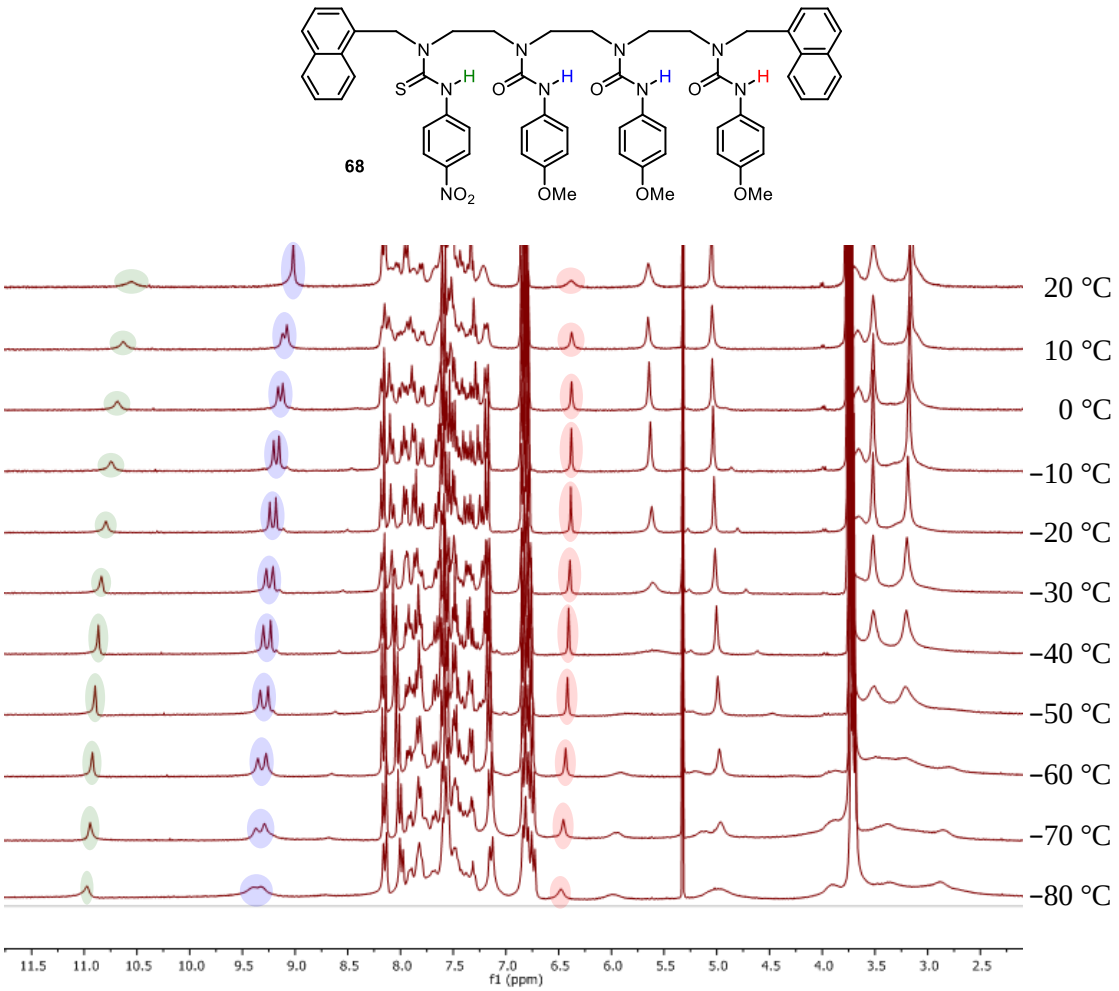

Figure 44 – VTNMR of 68 (CD_2Cl_2, 300 MHz, 19 mM).

In thiourea **68**, signals were observed at 5.05 (urea benzylic methylene), 5.65 (thiourea benzylic methylene), 6.38 (peripheral ureido proton), 9.01 (two central ureido protons) and 10.55 ppm (thioureido proton) at 20 °C. Upon cooling, the signal at 5.05 ppm remained approximately constant until broadening at −60 °C. The signal at 5.65 ppm broadened and decoalesced into two equal singlets (1 H each) at −60 °C. The signals at 6.38, 9.01 and 10.55 ppm sharpened and shifted downfield with decreasing temperature. A lack of decoalescence of the reporting terminal benzylic methylene and thio(ureido) protons shows that **68** exists as one conformation. This

conformation is the directionality where the thiourea is at the C-terminus, as the chemical shifts indicate that the thioureido proton and two ureido protons are in hydrogen bonding (10.55 and 9.01 ppm, respectively at 20 °C), and one ureido proton is not (6.38 ppm at 20 °C). It is worth noting that the thioureido benzylic methylene decoalesces into two equal singlets (1 H each) at very low temperature, which is attributed to diastereotopicity arising from the chiral *anti* conformations in the adjacent ethylene bridge.

A nuclear Overhauser effect (NOE) ^{1}H NMR experiment was then performed on thiourea **68**. NOE experiments are used as a method to determine how close two nuclei are in space, which makes it an excellent tool for the determination of conformation in solution.[90] An NOE experiment is performed by irradiating a specific nucleus according to the energy difference between its spin up and spin down state (chemical shift). That specific nucleus can then relax its spin state and reemit a photon of the same energy that irradiated it. However, proximate nuclei can also concurrently relax their spin states due to the interdipolar interactions of the nuclear spins, releasing a photon of different energy. This process is known as cross-relaxation. These released photons correspond to the energy difference of spin states of the proximate nucleus, meaning that an NOE correlation will be observed at their chemical shift. This cross-relaxation is highly sensitive to internuclear distance, and the decay of this effect correlates with r^6, where r is the internuclear distance. NOE analysis of **68** revealed a correlation between the terminal non-hydrogen-bonding ureido proton with the benzylic methylene (see Appendix, Figures A27-28), indicating they are close in space and further validating the proposed directionality.

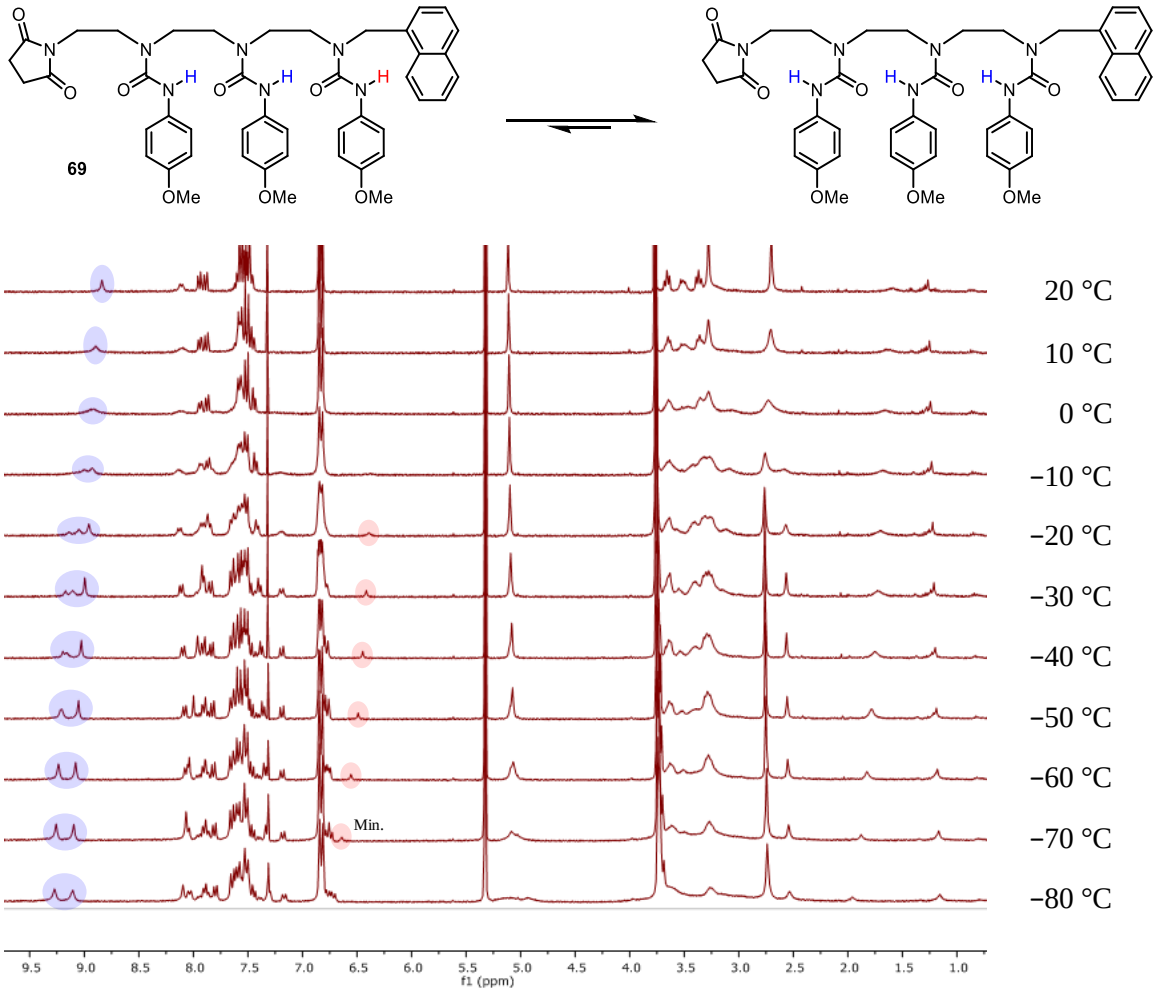

Figure 45 – VTNMR of 69 (CD_2Cl_2, 300 MHz, 12 mM).

In succinimide **69**, signals were observed at 2.70 (succinimidyl methylenes), 5.11 (benzylic methylene) and 8.84 ppm (one ureido proton) at 20 °C. Upon cooling, the signal at 2.70 ppm broadened and decoalesced at −10 °C into two singlets, which then sharpened upon further decreasing the temperature (2.87 H and 1.13 H at −60 °C). The signal at 5.11 ppm also broadened and decoalesced into two closely overlapping singlets at −40 °C. The signal at 8.84 ppm moved downfield with decreasing temperature before decoalescing into three signals at −20 °C, which then shifted further downfield. Additionally, a new signal appeared at 6.39 ppm (0.28 H) at −10 °C, which sharpened and moved downfield upon further decreasing the temperature. These data are consistent with the presence of two conformations populated in a 28:72 ratio at −60 °C, which are the two different directionalities. This is indicated by the two different environments of the succinimide at slow exchange – one where it is hydrogen bonding to the adjacent urea, and one where it is not. Finally, the two different conformations give rise to six different environments for ureido protons. Five of these ureido protons hydrogen bond either to other ureas or to the succinimide, but the sixth ureido proton is not hydrogen bonded, giving rise to a signal at 6.39 ppm at −10 °C. This signal also integrates for 0.28 H at −60 °C, and the other ureido proton

integrations account for the remaining 2.72 H, indicating that the conformer where the succinimide is at the C-terminus is the minor conformer.

Unfortunately, the VTNMR experiment on succinimide **69** revealed that succinimides are not powerful enough HBAs to impose total directionality control on ethylene-bridged triureas. This was attributed to the fact that **69** was terminated with a naphth-1-ylmethyl group, which can form an attractive N-H-π interaction, promoting the conformation where the succinimide was at the C-terminus.[83]

To combat the issues associated with the succinimide, a stronger HBA was sought. The proposed target was tetrasubstituted urea, **71** (Scheme 15), which is analogous to the other ureas in the foldamer except it has been methylated at nitrogen, removing its ability to donate hydrogen bonds and rendering it exclusively an HBA. Additionally, this meant that **71** could also be terminated with naphth-1-ylmethyl groups at both ends, so any directionality control could be attributed to the tetrasubstituted urea as opposed to the naphth-1-ylmethyl group at the reporting end of the foldamer.

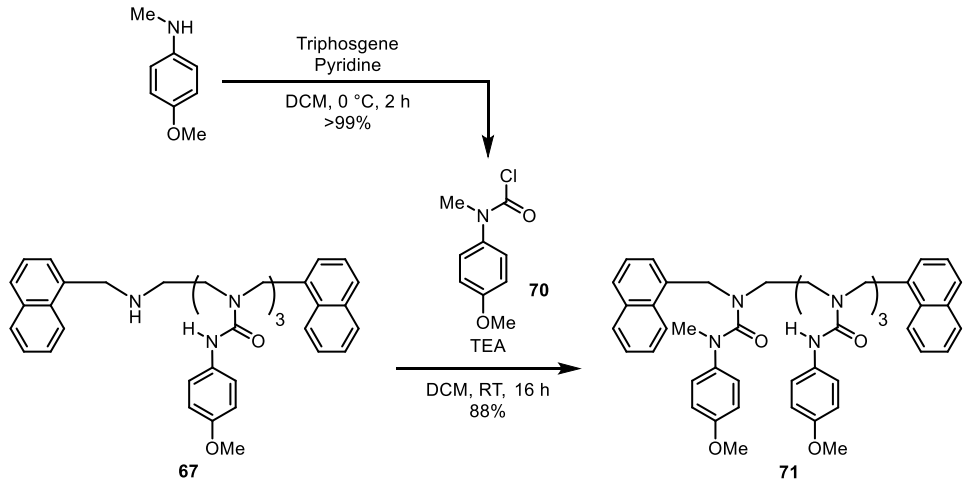

Scheme 15 – Synthesis of 71.

Chloroformylation of *N*-methyl-4-methoxyaniline gave carbamoyl chloride, **70** in quantitative yield. **70** was then reacted with secondary amine, **67** to give the new directionality-controlled oligourea, **71** in good yield. **71** was then studied by VTNMR (Figure 46).

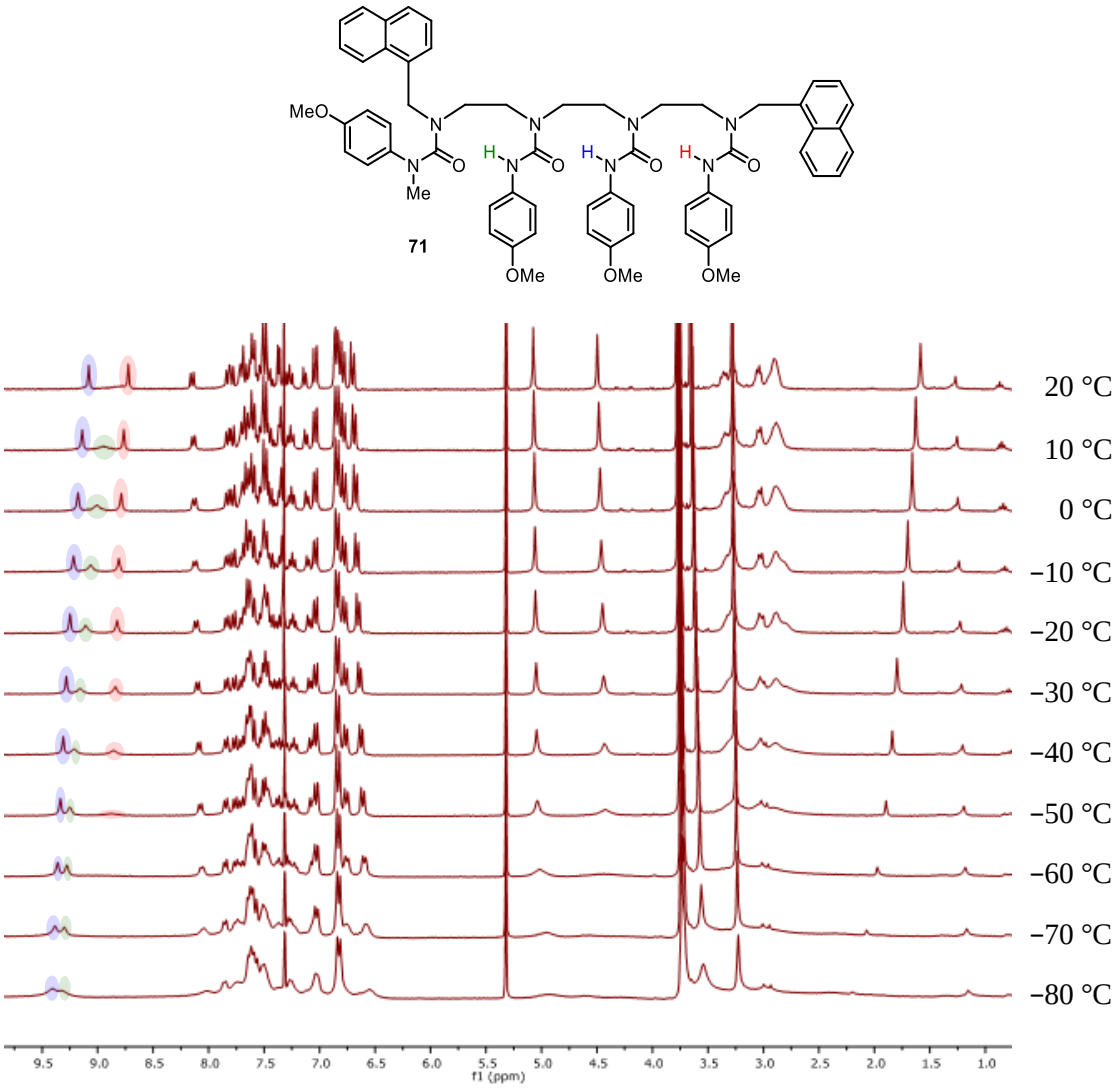

Figure 46 – VTNMR of 71 (CD_2Cl_2, 300 MHz, 13 mM).

Tetraurea **71** showed signals at 4.50 (tetrasubstituted urea benzylic methylene), 5.07 (trisubstituted urea benzylic methylene), 8.72, 8.79 (very broad) and 9.08 ppm (three ureido protons) at 20 °C. Upon cooling, the signals at 4.50 and 5.07 ppm remained approximately constant until broadening at −40 °C. The signals at 8.72, 8.79 and 9.08 ppm all shifted downfield and sharpened with decreasing temperature until they broadened at −40 °C. These results show that **71** exists as one conformer, which is the directionality where the tetrasubstituted urea is at the N-terminus. The chemical shifts of the ureido protons show that they are all in hydrogen bonding, and there is no observable signal for non-hydrogen-bonded ureido protons at around 6.40 ppm. In direct contrast to thiourea **68**, NOE analysis showed that the reporting benzylic methylene are not proximate to any ureido protons (see Appendix, Figure A29), further supporting the notion that the tetrasubstituted urea is at the N-terminus. Finally, it is notable that the 4-methoxyphenyl group in the tetrasubstituted urea is oriented s-*trans*.[75]

To conclude, electron-deficient thioureas and tetrasubstituted ureas can be used to attain complete directional control in ethylene-bridged triureas in opposite fashions. The non-iterative synthesis of triureas with different terminal functionalities has been developed, allowing the appendage of different functions to the termini of the foldamer in a convergent manner. Finally, terminating benzylic ureas have been shown to be effective reporters of local hydrogen-bond directionality, where NOEs can be observed with adjacent ureido protons in one directionality, and cannot be observed in the opposite directionality.

3.4 The Development of the Synthesis of Longer Oligoureas

It has been established that ethylene-bridged triureas with different directionality-controlling termini can be synthesised from triethylenetetramine. It was next desirable to determine if any decay in informational communication manifests in longer oligoureas. It was proposed that the corresponding pentaurea could be synthesised by an analogous method using the largest commercially available oligoethylenediamine, pentaethylenehexamine (Scheme 16).

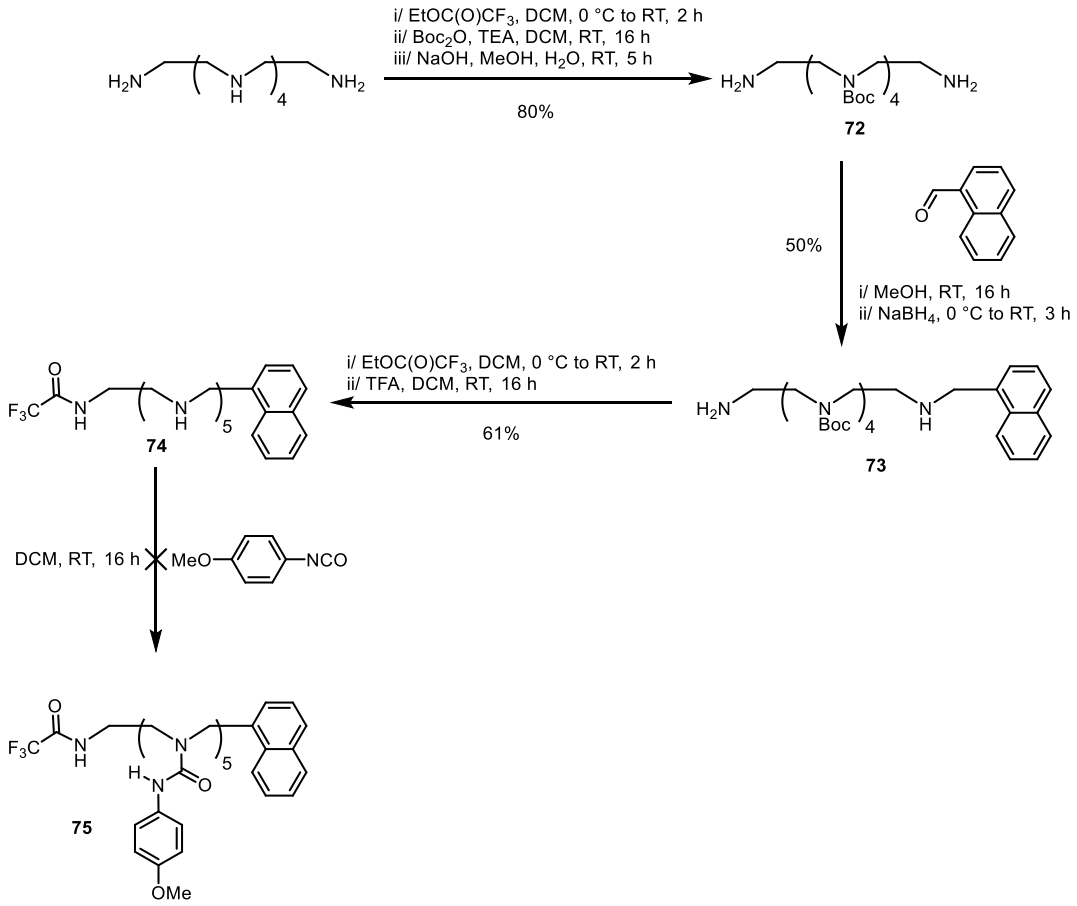

Scheme 16 – Synthesis of 75.

Pentaethylenehexamine underwent a twofold trifluoroacetylation and fourfold Boc-protection in one pot in good yield. The corresponding bis(trifluoroacetamide) was then hydrolysed to give diamine **72** in excellent yield over the three steps. **72** then underwent reductive alkylation with 1-naphthaldehyde to give naphth-1-ylmethylamine **73** in moderate yield. The four Boc groups were then cleaved using TFA to give the corresponding pentamine, which proceeded in only reasonable yield due to the loss of some product to the aqueous phase during purification. Finally, pentamine **74** was to undergo a fivefold carboxamidation using excess isocyanate, but unfortunately a complex mixture of products was observed corresponding to different permutations of missing ureas from the product.

Upon resubmission of the crude product to the reaction conditions with more isocyanate and heating, no further conversion was observed. From this, it was deduced that the installation of several ureas at once can prove difficult depending on the order in which the ureas are formed. It was envisaged that installation of the central ureas as early in the synthesis as possible would be conducive to a much more practical and convergent synthesis of longer oligourea foldamers.

To this end, pentaethylenehexamine was submitted to the same trifluoroacetylation procedure, but instead of adding Boc_2O, 4-methoxyphenyl isocyanate was added in the hope that the corresponding protected tetraurea would be formed (Scheme 17).

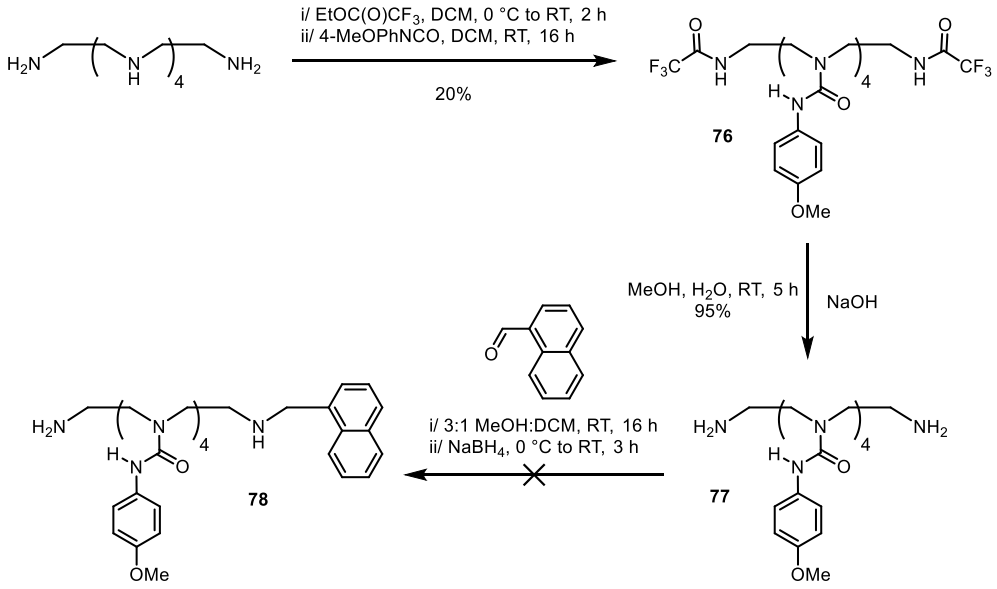

Scheme 17 – Synthesis of 78.

Gratifyingly, the desired product precipitated out of solution after stirring for 16-48 h, giving the desired protected tetraurea **76** in poor yield. This poor yield was tolerated due to the large amount of functionalisation the reaction involved and because the reaction was conducive to scale-up. More of the desired product was identified in the filtrate and could be isolated by recrystallisation from DCM:MeOH mixtures. A majority of the converted mass corresponded to products with different permutations of missing ureas but fortunately, these by-products could be easily removed by filtration. Tetraurea **76** could then be solubilised in the subsequent hydrolysis reaction mixture and after 3-5 h, the corresponding diamine precipitated out of the mixture and could be easily filtered to attain the desired diamine **77** in excellent yield. **77** was found to be insoluble in MeOH, so the subsequent reductive alkylation was performed after solubilising in a heated DCM:MeOH mixture. After the proposed monoimine formation, a precipitate was observed. Filtration and subsequent analysis revealed that the bis(imine) had formed and precipitated with remaining **77**. The reaction mixture was treated with sodium borohydride in the hope that reduction of any monoimine present would yield the desired product. Unfortunately,

the subsequent purification revealed that only the bis(naphth-1-ylmethyl)amine, and the starting material **77** could be isolated. In the reaction mixture, monoimine formed upon reaction of **77** with 1-naphthaldehyde, but undesirably reacted again to form the bis(imine). The bis(imine) was then insoluble in the reaction mixture and precipitated. This precipitation then greatly inhibited the reverse reaction to the monoimine, such that all of the 1-naphthaldehyde was consumed in forming the bis(imine). Reduction then converted the two imines irreversibly to the undesired bis(naphth-1-ylmethyl)amine. As there was a substoichiometric amount of 1-naphthaldehyde used for disubstitution, **77** was also left in the reaction mixture. Due to the concomitant precipitation of **77**, it was supposed that DCM:MeOH solutions of **77** are metastable, and precipitate given sufficient time. Subsequent reaction attempts corroborated this hypothesis.

Due to the solubility issues associated with the desymmetrisation of **77**, the oligourea intermediate was changed to the corresponding triurea to be derived from tetraethylenepentamine (Scheme 18). To supplement this shortened oligourea with additional amines, the reductive alkylation partner was chosen to be Boc-protected aminoacetaldehyde, **82**.

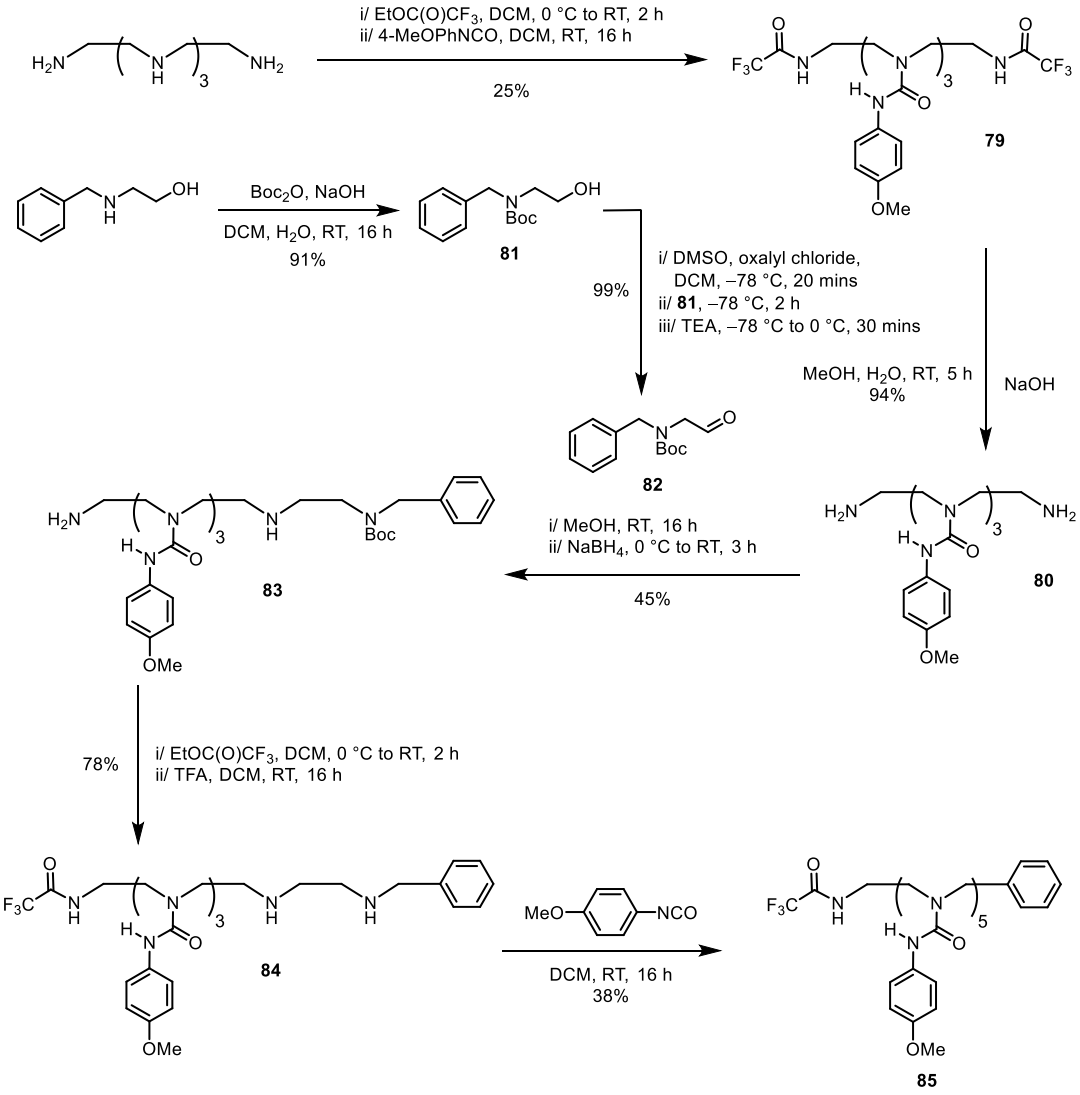

Scheme 18 – Synthesis of 85.

Tetraethylenepentamine was protected at the primary amines with ethyl trifluoroacetate and reacted at the secondary amines with 4-methoxyphenyl isocyanate to give the corresponding triurea, **79** in poor yield. Much like tetraurea **76**, triurea **79** precipitated out of the reaction mixture and was collected by filtration. Similarly, the trifluoroacetamides were then hydrolysed to give diamine **80**, which also precipitated in excellent yield. Separately, 2-(benzylamino)ethanol was Boc-protected and the alcohol oxidised by Swern oxidation to furnish the desired aldehyde fragment **82** in excellent yield over the two steps. **80** then underwent reductive alkylation with **82**, which saw no solubility issues and provided **83** in moderate yield, along with the undesired dialkylated product. Primary amine **83** was then protected at the primary amine as a trifluoroacetamide, and the Boc group removed with TFA to give the corresponding protected diamine **84** in good yield. Subsequent dicarboxamidation then furnished the corresponding pentaurea **85**, albeit in poor yield.

Next, the trifluoroacetamide protecting group was hydrolysed (Scheme 19), and the corresponding amine underwent reductive alkylation with **82** to give amine **87** in moderate yield. A sixth urea was formed, and the Boc group cleaved using TFA to give amine **89** in excellent yield over the two steps. Amine **89** was then reacted with 4-nitrophenyl isothiocyanate and carbamoyl chloride **70** to furnish the desired longer directionality-controlled oligoureas, thiourea **90** and tetrasubstituted urea **91**.

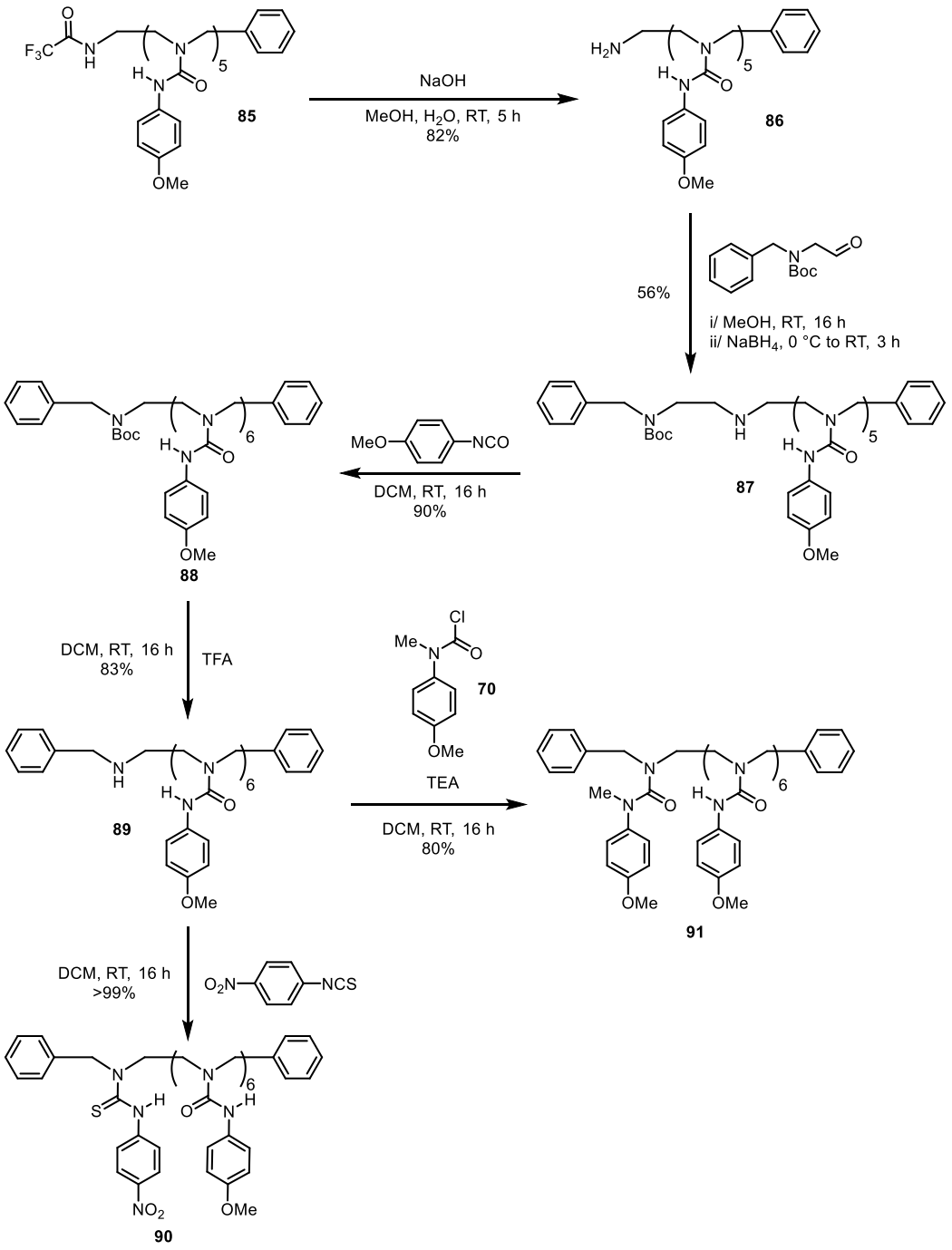

Scheme 19 – Synthesis of 90 and 91.

90 and **91** were then studied by VTNMR (Figures 47-48).

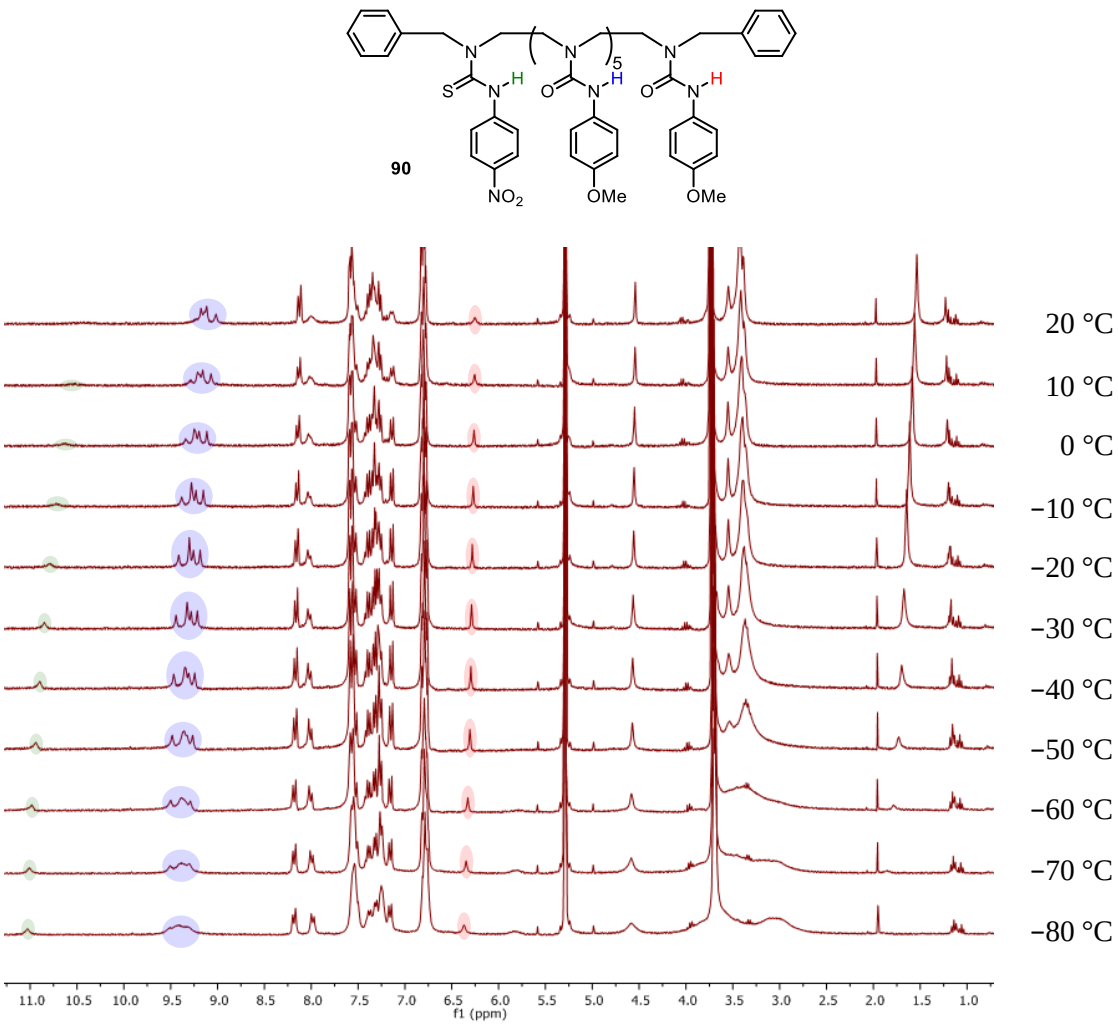

Figure 47 – VTNMR of 90 (CD_2Cl_2, 300 MHz, 30 mM).

Thiourea **90** showed signals at 4.54 (ureido benzylic methylene), 5.25 (thioureido benzylic methylene), 6.25 (peripheral ureido proton), from 9.02-9.23 (central ureido protons, 5 H) and 10.43 ppm (thioureido proton) at 20 °C. Upon cooling, the signal at 4.54 ppm remained approximately constant until broadening at −60 °C. The signal at 5.25 ppm (obscured by the residual $CDHCl_2$ peak) broadened and decoalesced into two singlets (1 H each) at −50 °C. The signals at 6.25, from 9.02-9.23 and at 10.43 ppm all sharpened and shifted downfield with decreasing temperature. The lack of the decoalescence of the reporting benzylic methylene indicated that **90** exists as one populated conformer, which is the directionality where the thiourea is at the C-terminus. The chemical shifts of the (thio)ureido protons indicate that one ureido proton is not hydrogen bonded, but the other five and the thioureido proton are. This hypothesis was further validated by NOE experiments, which showed the reporting benzylic methylene is proximate to the non-hydrogen-bonding ureido proton (see Appendix, Figure A30). Finally, it is worth noting that like thiourea **68**, the thioureido benzylic methylene decoalesces at very low

temperature as it enters the slow-exchange region of the chiral conformations of the adjacent ethylene bridge.

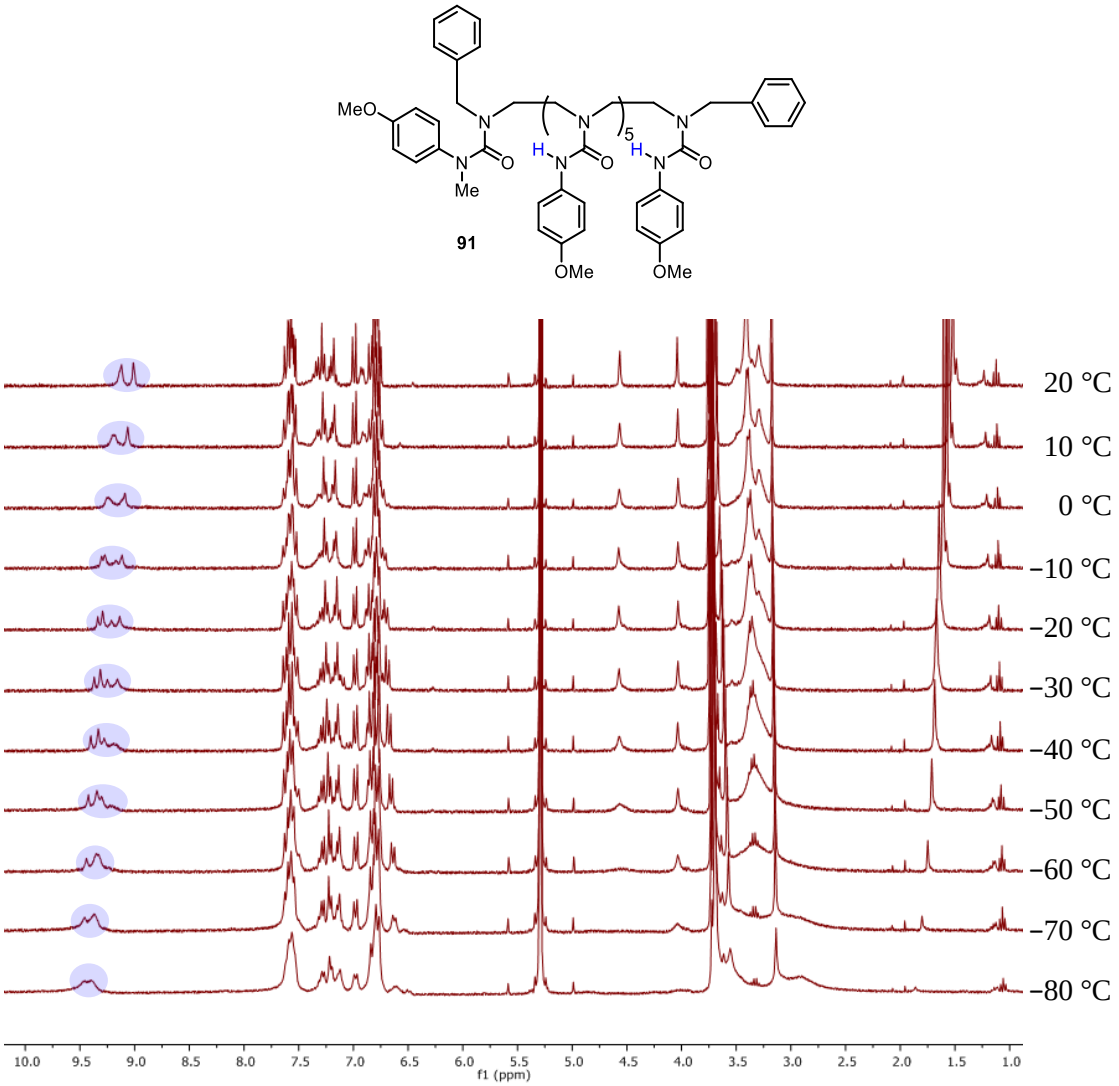

Figure 48 – VTNMR of 91 (CD_2Cl_2, 300 MHz, 24 mM).

In heptaurea **91**, signals were displayed at 4.04 (tetrasubstituted urea benzylic methylene), 4.56 (trisubstituted urea benzylic methylene) and from 9.00-9.15 ppm (ureido protons, 5 H) at 20 °C. Upon cooling, the signal at 4.04 ppm stayed approximately constant until it broadened at −60 °C. The signal at 4.56 ppm behaved similarly but broadened at −40 °C. The signals from 9.00-9.15 ppm (5 H) resolved, sharpened and shifted downfield with decreasing temperature. Finally, a broad signal appeared at 9.12 ppm at 0 °C, which also sharpened and shifted downfield with decreasing temperature. The lack of decoalescence of the reporting benzylic methylene indicated that one conformation is populated, which is the directionality where the tetrasubstituted urea is at the N-terminus. At 20 °C, it is shown that five ureido protons are in hydrogen bonding, but the peripheral ureido proton signal is too broad to be observed. Crucially, there is no signal around 6.25 ppm corresponding to any non-hydrogen-bonding ureido protons. However, at 0 °C, the final

ureido proton appears at 9.12 ppm and joins the other hydrogen-bonding ureido protons. This proposition was further validated by the lack of NOE correlations between the reporting benzylic methylene and any ureido protons (see Appendix, Figure A31).

These experiments have shown that electron-deficient thioureas and tetrasubstituted ureas can be utilised to impose directional control on adjacent ureas, and that bias can be communicated through six ureas with no sign of signal decay. The developed synthetic strategy also represents a facile method for the synthesis of heptameric structures, where the orthogonal protecting group strategy endows simple modification of foldamers at their termini. After coupling, the protected aldehyde fragments can be functionalised separately, allowing the diversification of foldamer targets at a late stage. Crucially, informational transfer can occur with no apparent loss of hydrogen-bonding fidelity over distances of up to six ureas, rendering the oligourea scaffold a very promising candidate for nanometre-scale transmission of binary information in the form of hydrogen-bond directionality.

3.5 Hydrogen-Bond Directionality Switching

Now that families of foldamers had been synthesised with the ability to enforce one directionality in ethylene-bridged oligourea foldamers, it was desirable to see whether one foldamer could be made to switch between both directionalities in response to a stimulus. The initial target was 2-pyridyl-terminated foldamer **97** with the proposal that, under neutral conditions, the pyridine would act as an HBA, enforcing the directionality where the pyridine is at the N-terminus (Scheme 20). Upon treatment with acid, the resultant pyridinium would act as an HBD, and enforce the opposite directionality, where the pyridinium would be at the C-terminus.

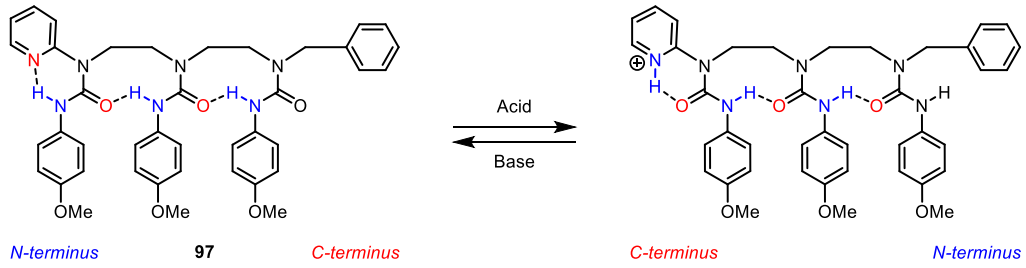

Scheme 20 – Initial target for an acid-mediated directionality switch, 97.

Ethylenediamine underwent nucleophilic aromatic substitution (S_NAr) with 2-fluoropyridine to give *N*-(2-pyridyl)ethylenediamine in excellent yield. This was then used as the starting material to synthesise pyridyl urea **97** in an analogous manner to triurea **41** (Scheme 7 and 9) to give the desired triurea in 4% total yield. **97** was then studied by VTNMR (Figure 49).

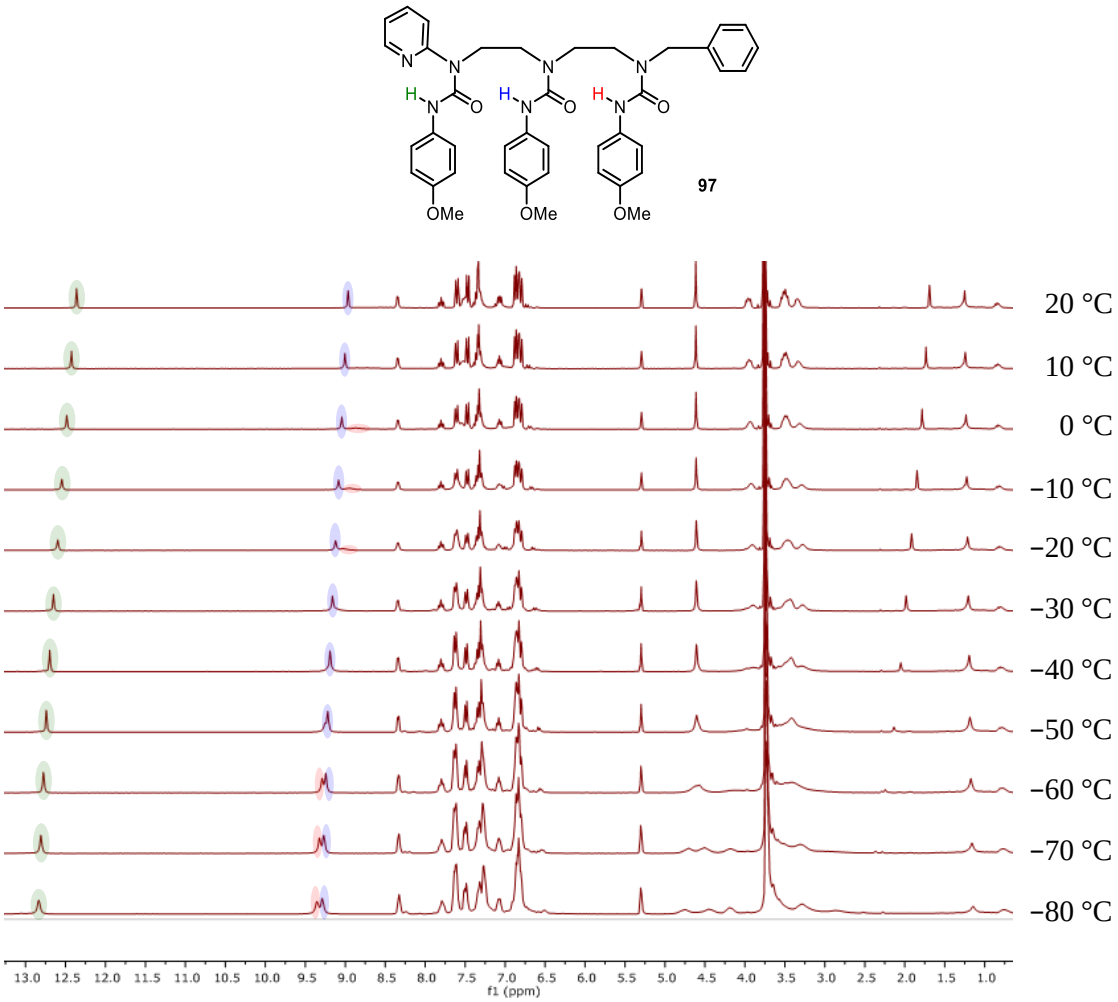

Figure 49 – VTNMR of 97 (CD_2Cl_2, 300 MHz, 14 mM).

Pyridyl urea **97** showed signals at 3.96 (pyridyl urea α-methylene) 4.61 (benzylic methylene), 8.97 (central ureido proton) and 12.36 ppm (pyridyl urea ureido proton) at 20 °C. Upon cooling, the signal at 3.96 ppm broadened, losing its multiplicity, until decoalescing into two singlets (1 H each) at −60 °C. Similarly, the signal at 4.61 ppm stayed approximately constant until it broadened at −50 °C and decoalesced at into two singlets (1 H each) at −70 °C. The signals at 8.97 and 12.36 ppm sharpened and shifted downfield with decreasing temperature. At 0 °C, a signal appeared at 8.86 ppm (1 H), which sharpened and shifted downfield upon further cooling. The lack of the decoalescence of the benzylic methylene signal until very low temperature indicated the population of one conformation. This conformation is the directionality where the pyridine is at the N-terminus. This is further validated by the chemical shifts of the ureido protons, where two of them are hydrogen bonding with other ureas (9.25 and 9.29 ppm at −60 °C) and the third is in a very strong hydrogen bond with the pyridine (12.77 ppm at −60 °C). Similar to **68** and **91**, the decoalescence of the pyridyl urea α-methylene and the benzylic methylene into two equal signals is attributed to diastereotopicity arising from the chiral conformations in the ethylene

bridges. Additionally, NOE analysis revealed no correlation between the benzylic methylene and any ureido protons (see Appendix, Figure A32).

Now that it had been proven that the pyridyl urea of **97** controls directionality in the desired fashion, directionality switching with acid was attempted. Five equivalents of acetic acid were added to the sample, which unfortunately saw no change in the signals of **97**. As the protonation site is a 2-pyridyl urea, with the pyridyl nitrogen engaged in a strong 6-membered hydrogen-bonding ring, it was supposed that acetic acid was not a strong enough acid in DCM to protonate the pyridine to an appreciable level. Instead, TFA was titrated into the sample of **97** (Figure 50).

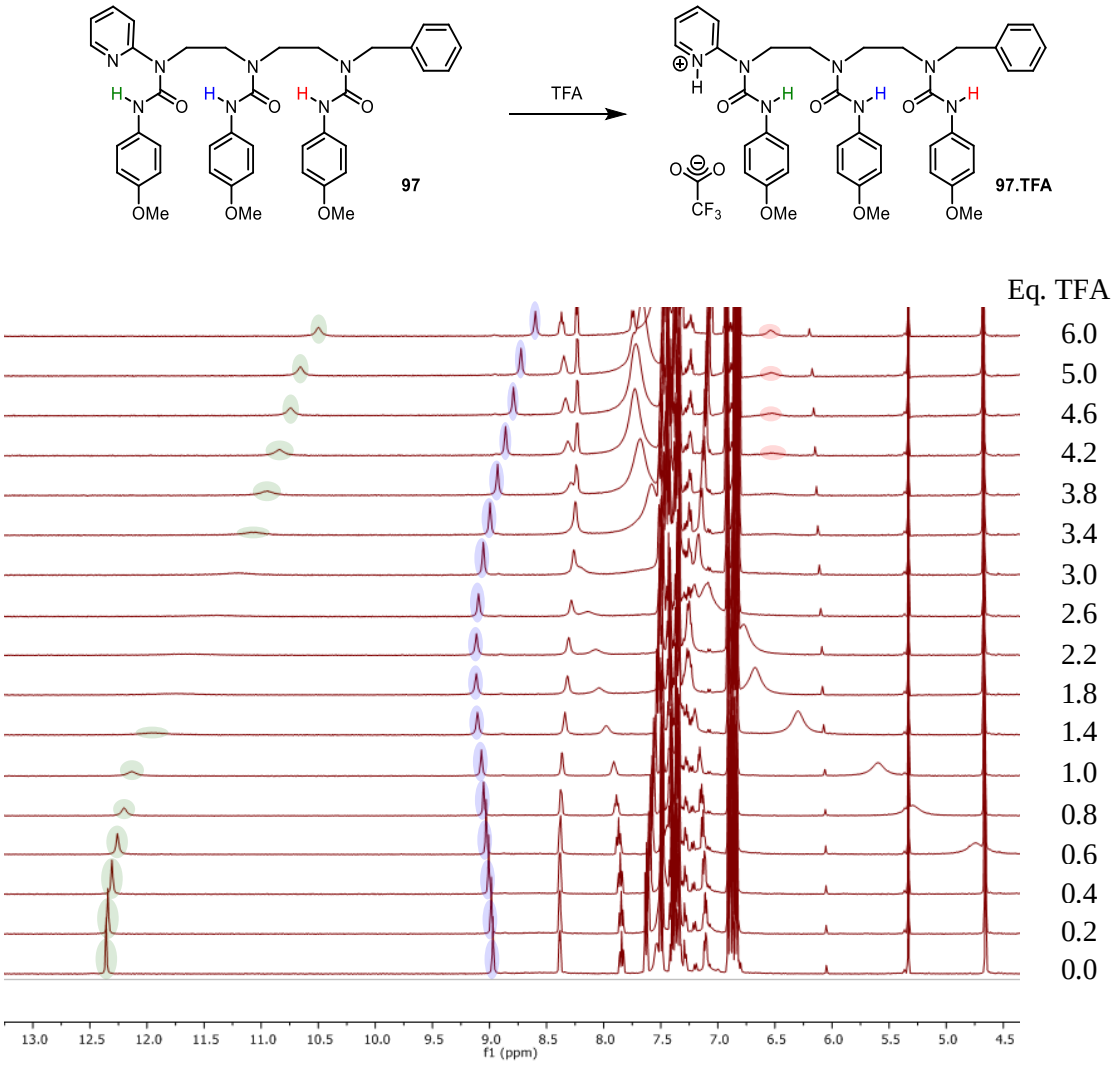

Figure 50 – Titration of TFA into 97 (4.50-13.00 ppm region, CD_2Cl_2, 500 MHz, 14 mM).

Before addition, signals were observed for pyridyl urea **97** at 7.84 (pyridyl *para* methine), 8.38 (pyridyl *ortho* methine), 8.97 (central ureido proton) and 12.36 ppm (pyridyl urea ureido proton). Upon addition of TFA, the signal at 7.84 ppm shifted downfield and broadened with a

concomitant upfield shift and broadening of the signal at 8.38 ppm. These two signals then sharpened again above 3.8 equivalents of TFA. The signal at 8.97 ppm shifted downfield with TFA addition, and then moved upfield again after 2.2 equivalents. The signal at 12.36 ppm broadened and shifted upfield, before sharpening again after the addition of 3.4 equivalents of TFA. A broad signal (2.6 H) was observed at 4.75 ppm, which shifted downfield with increasing TFA and grew in relative integration before arriving at 7.71 ppm at 4.0 equivalents. Finally, at 4.2 equivalents, a new signal appeared at 6.54 ppm (1 H), which then sharpened with further addition. The relative shifting of the *ortho* and *para* pyridyl methines is characteristic of protonation taking place at pyridine. If a directionality switch took place, the central ureido proton would not be expected to change markedly in its chemical shift as it is shifting between two 9-membered hydrogen-bonding rings with ureas. Hence this signal did not displace significantly from its starting position. The reason for the downfield and then upfield shifting is unknown. The pyridyl urea ureido proton shifted significantly upfield ($\Delta\delta$ = 1.86 ppm) with TFA, indicating that it moved out of a very strong 6-membered hydrogen bond with a pyridine into a relatively weaker 9-membered hydrogen-bonding ring with a urea. The signal that appeared at 4.75 ppm at 0.6 equivalents of TFA corresponds to the TFA, which was in fast exchange with the present water and the pyridinium. This equilibrium shifted towards the pyridinium trifluoroacetate with increasing TFA before arriving at 7.71 ppm when the pyridine was completely protonated. The appearance of a signal at 6.54 ppm signified the presence of a non-hydrogen bonded ureido proton. Finally, superstoichiometric quantities of TFA were required to promote pyridine protonation, presumably due to the comparable acidities of the pyridinium and TFA in DCM. These data indicated that protonation of the pyridine had taken place and that it resulted in a global directionality switch, making the pyridinium at the C-terminus. To further corroborate this finding, **97**.TFA was analysed by VTNMR (Figure 51).

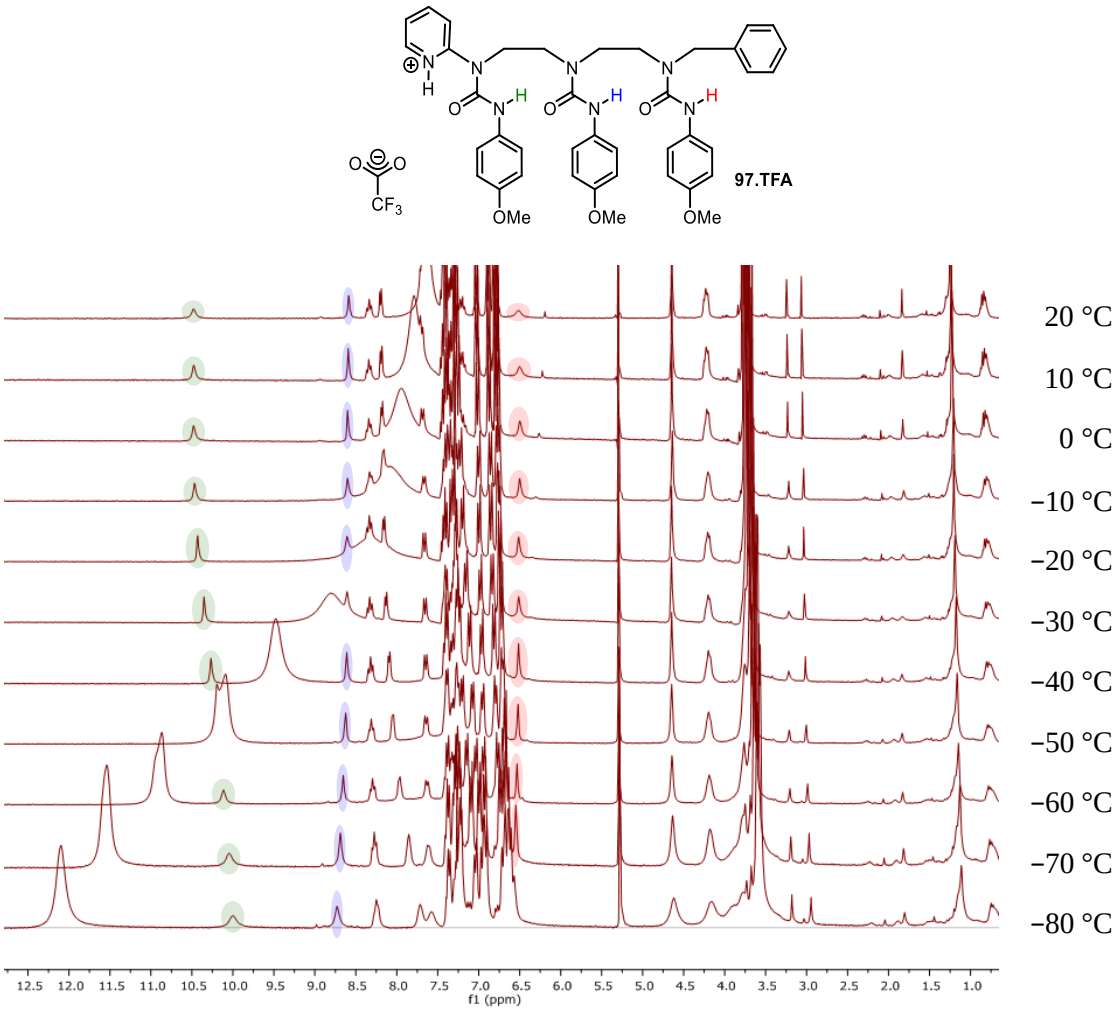

Figure 51 – VTNMR of 97.TFA (CD_2Cl_2, 300 MHz, 14 mM).

Pyridinium trifluoroacetate **97**.TFA displayed signals at 4.64 (benzylic methylene), 6.54 (peripheral ureido proton), 8.59 (central ureido proton) and 10.48 ppm (pyridyl urea ureido proton) at 20 °C. Upon cooling, the signal at 4.64 ppm remained approximately constant until broadening at −80 °C. The signals at 6.54 and 8.59 ppm sharpened and shifted downfield with decreasing temperature, whereas the signal at 10.48 ppm shifted upfield. The lack of decoalescence of the benzylic methylene signal indicated one populated conformer, which is the directionality-switched structure, where the pyridinium is at the C-terminus. This was also alluded to by the chemical shifts of the ureido protons, where there are two hydrogen-bonded ureido protons (8.65 and 10.12 ppm at −60 °C) and one non-hydrogen-bonded ureido proton (6.53 ppm at −60 °C). The upfield shifting of the pyridyl urea ureido proton signal is peculiar, and its reasoning is unknown. Finally, the conformation of **97**.TFA was confirmed by the observed NOE correlations between the reporting benzylic methylene and the non-hydrogen-bonded ureido proton, where no such correlation existed before the switch (see Appendix, Figure A33). To further validate the proposition that TFA was not acidic enough in DCM to effect a stoichiometric

switch, **97** was protonated with 1.5 equivalents of a stronger acid, *p*-toluenesulfonic acid monohydrate ($TsOH.H_2O$), which resulted in the same degree of protonation as 4.6 equivalents of TFA (see Appendix, Figure A1).

It was shown that treatment of pyridyl urea **97** with TFA resulted in a global directionality switch. To be sure that this switch could be attributed to protonation of the pyridine and subsequent urea reorientation and not from coordination of the trifluoroacetate anion or protonation at other atoms in the molecule, a control experiment was designed. Phenyl-terminated triurea **99** was used as an analogue of pyridyl urea **97** without its basic functionality. Conveniently, the phenyl group would control directionality analogously to the pyridine in **97** but cannot be protonated and therefore would not switch directionality upon treatment with TFA. **99** was synthesised analogously to triurea **97** using amine **30** as the starting amine (Scheme 21).

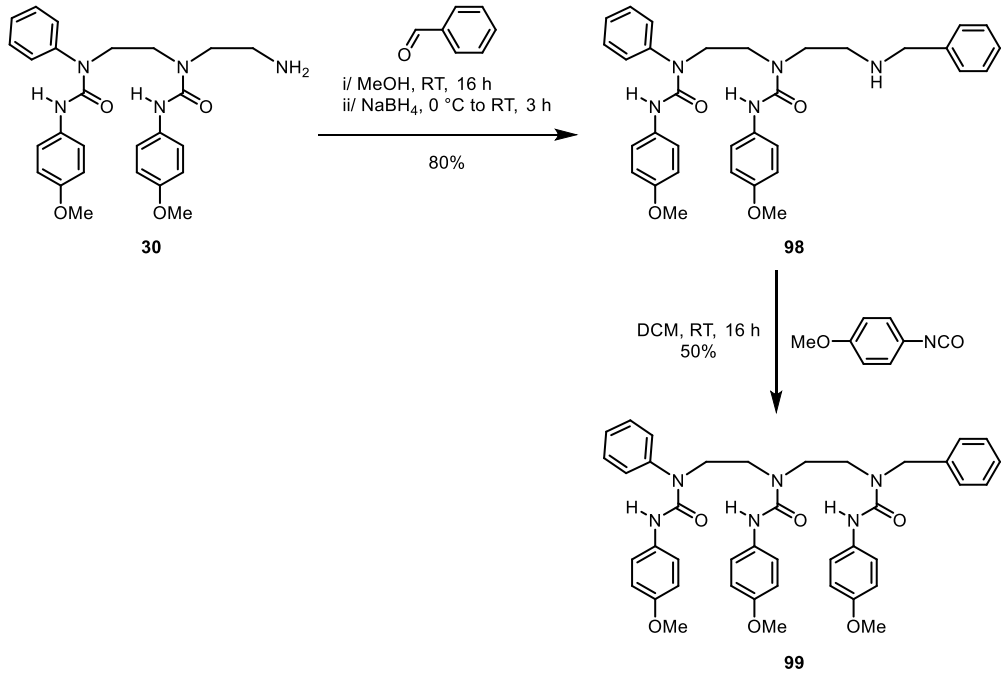

Scheme 21 – Synthesis of 99.

To appropriately simulate the TFA-mediated switch conditions with **99**, pyridinium cations and trifluoroacetate anions had to be present. To attain this, triurea **99** was combined with an equivalent of pyridine, and TFA was titrated into the sample (Figure 52).

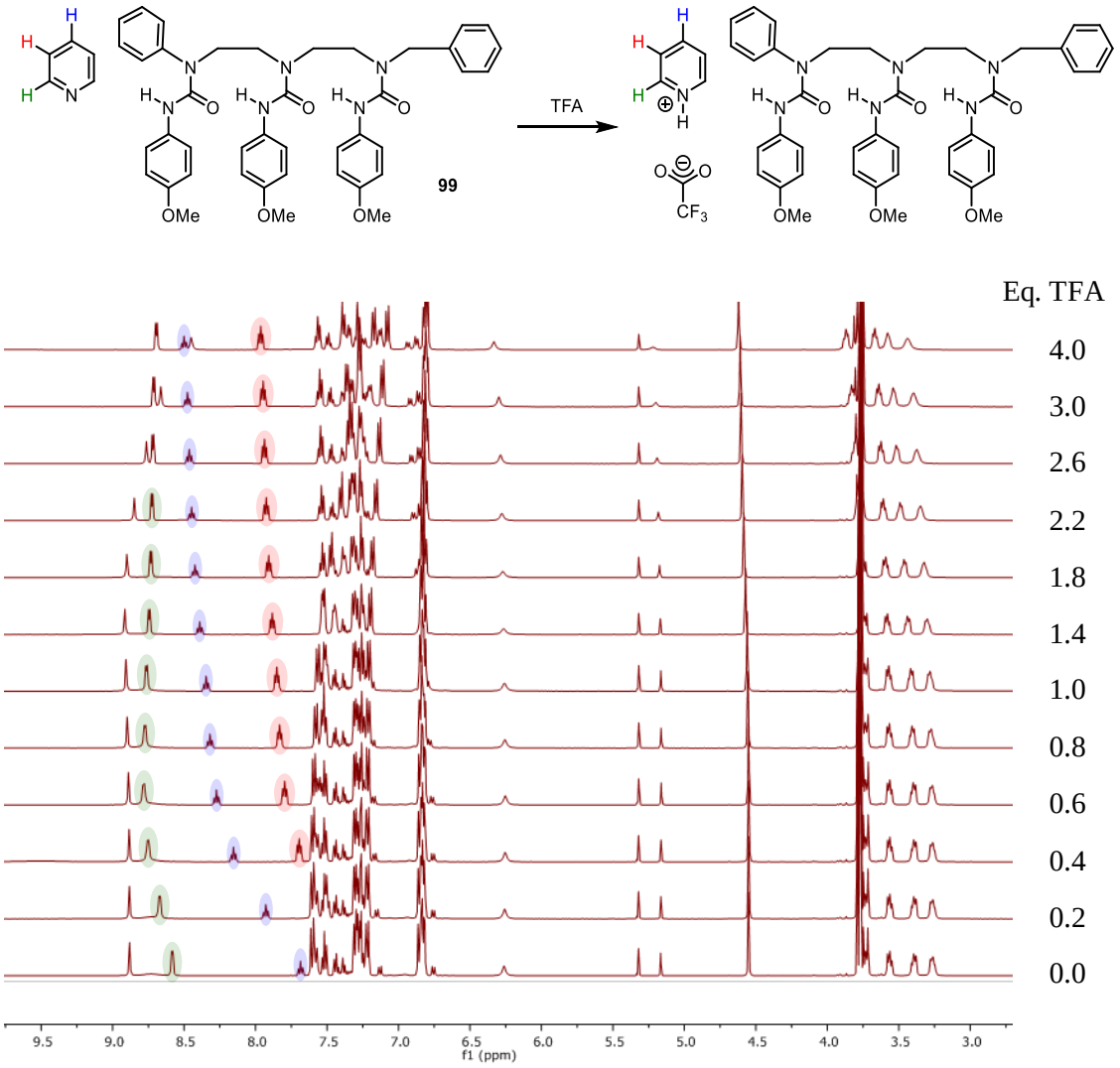

Figure 52 – Titration of TFA into 99.pyridine (CD_2Cl_2, 500 MHz, 14 mM).

The triurea **99**/pyridine mixture showed signals at 6.26 (phenyl urea ureido proton), 7.50 (pyridine *meta* protons), 7.69 (pyridine *para* proton), 8.58 (pyridine *ortho* protons), 8.73 (peripheral ureido proton) and 8.88 ppm (central ureido proton) with no TFA present. Upon TFA addition, the signal at 6.26 ppm remained approximately constant until it shifted downfield at 2.6 equivalents. The signals at 7.50, 7.69 and 8.58 ppm all shifted significantly downfield after addition of 0.2 equivalents of TFA and continued to do so upon further addition. The signal at 8.73 ppm broadened upon addition and could not be observed at 0.6 equivalents. Finally, the signal at 8.88 ppm stayed approximately constant with increasing TFA, until it moved quickly upfield at 2.2 equivalents. The immediate and significant alteration of the pyridine signals indicated that it had protonated. The pyridine signal shifting continued (indicating equilibrium shifting to pyridinium trifluoroacetate) upon further addition of TFA until it became approximately constant after 1.8 equivalents. At this point, it is worth noting that pyridine signal shifting is greater for pyridine than for **97** due to the much greater basicity of pyridine. The signals

corresponding to **99** were unaffected by TFA until 2.2 equivalents, at which time they did not shift according to a directionality switch. These results indicated that **99** is unaffected by the presence of pyridinium cations and trifluoroacetate anions in solution, further proving that the directionality switch observed in **97** can be fully attributed to protonation of the pyridine instead of any ionic effects. However, it is worth noting that excess TFA could potentially affect the foldamer, presumably by partial protonation of the ureas.

Gratifyingly, washing of the sample with aqueous $NaHCO_3$ quantitatively recovered **97** and restored all original signals of the neutral form. These experiments have shown that 2-pyridyl ureas can be used to terminate ethylene-bridged triureas, which confers the property of hydrogen-bond directionality-switchability. The alternate directionalities can be selected by use of acid and base and can be quantitatively switched between the two. In both forms, the directionality enforced by the pyridine/pyridinium is communicated throughout the foldamer. This serves as the first ethylene-bridged oligourea foldamer that can communicate binary information in the form of hydrogen-bond directionality in the response to a stimulus – the presence or absence of acid.

Now that pyridyl ureas had been used for directionality switching, it was desirable to append pyridyl ureas to longer oligoureas by using the methodology applied to the synthesis of **90** and **91**. To achieve this, the development of an electrophilic source of *N*-(2-pyridyl)ethylamine was required, preferably in the aldehyde oxidation state to allow the established coupling by reductive amination. The first proposed electrophile was **102**, where the 2-aminopyridine was protected with a Boc group, as it was suspected that the unprotected aminoacetaldehyde would decompose by polymerisation (Scheme 22).

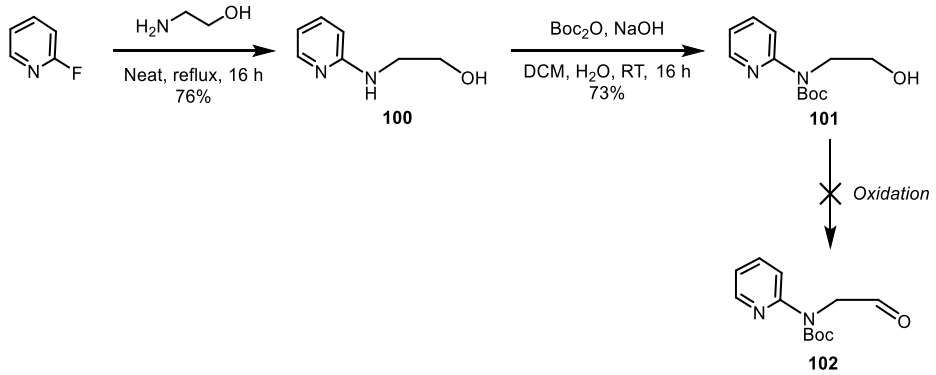

Scheme 22 – Synthesis of 102.

2-Fluoropyridine underwent S_NAr by heating in neat ethanolamine to provide **100** in good yield. The amine was then protected with a Boc group to give carbamate, **101** in good yield. **101** was then oxidised by Swern oxidation, which led to decomposition, presumably by polymerisation. It was hoped that the aldehyde was metastable and was simply sensitive to the

oxidation conditions, so other attempts to oxidation involved the use of DMP, PCC and MnO_2, each with the same result. Due to this, the synthesis of aldehyde **102** by alcohol oxidation was abandoned. Due to the stability of Boc-protected aminoacetaldehyde **82**, it was presumed that the instability of **102** could be attributed to the proximate *N*-pyridyl carbamate. To circumvent this issue, the pyridine was distanced by introduction of an additional Boc-protected amine (Scheme 23).

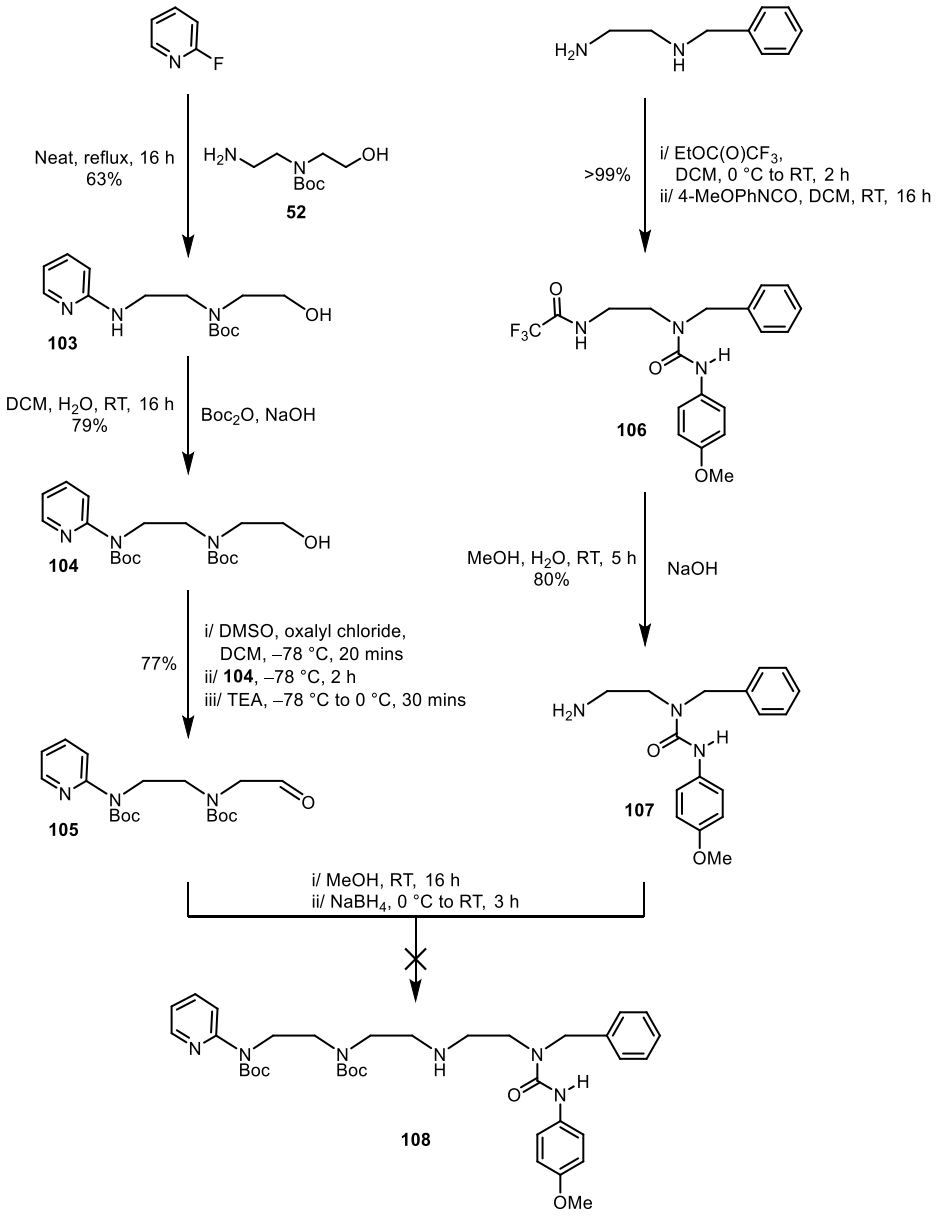

Scheme 23 – Synthesis of 108.

2-Fluoropyridine underwent S_NAr with amine **52** to give pyridyl amine **103** in reasonable yield. The remaining amine of **103** was then protected with a Boc group using Boc_2O to give bis(carbamate) **104** in good yield. **104** was then subjected to Swern oxidation conditions, which furnished the desired aldehyde in good yield. Now that an electrophilic source of *N*-(2-

pyridyl)ethylamine had been accessed, it was trialled in a model reductive amination to save the unnecessary consumption of amine **86**. Model monourea **107** was synthesised by trifluoroacetylation and urea formation on *N*-benzylethylenediamine, affording **106** quantitatively. **106** then underwent hydrolysis to give **107** in good yield. **107** and **105** were then subject to a trial reductive amination. The trial reaction resulted in total conversion of **105** back to **104** by aldehyde reduction, indicating that imine formation did not take place. This was corroborated by monitoring the ^{1}H NMR of aliquots of the reaction as it progressed. It was suspected that the two Boc groups were providing such steric encumbrance that they were forced into a conformation which inhibited nucleophilic addition to the aldehyde. Attempts to circumvent this issue were imine formation by heating in methanol, and heating in toluene with an attached Dean-Stark apparatus, but neither saw any conversion of the aldehyde to the desired imine. Due to this, **105** was deemed too unreactive to be used as a reductive alkylation partner as a result of steric encumbrance.

To mitigate the steric hindrance in bis(carbamate) **105**, an analogous compound was made with the ureas already installed instead of the Boc groups (Scheme 24). Decomposition of diurea **111** was foreseen by cyclisation of the central urea onto the aldehyde. However, it was hoped that the directional control that the pyridine provides would bestow kinetic stability on the aldehyde, as the ureido nitrogen would be locked in a hydrogen bond with the adjacent urea.

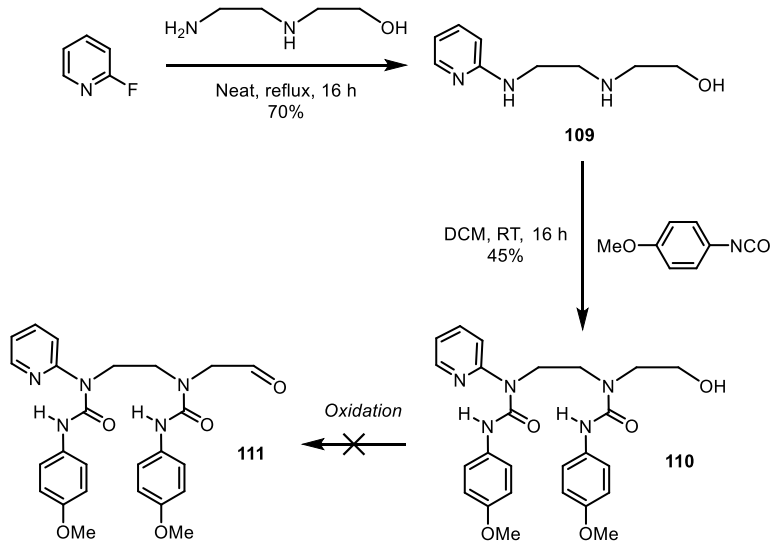

Scheme 24 – Synthesis of 111.

Diurea **110** was synthesised by S_NAr of *N*-(2-hydroxyethyl)ethylenediamine with 2-fluoropyridine, which proceeded in good yield. Dicarboxamidation using 4-methoxyphenyl isocyanate then afforded diurea **110** in moderate yield. Unfortunately, oxidation of this substrate resulted in decomposition upon treatment with DMP, PCC, MnO_2 and under Swern oxidation conditions, so this route was abandoned as a reductive amination candidate.

It was hoped that the need to isolate an electrophilic source of *N*-(2-pyridyl)ethylamine could be circumvented by using an electrophilic source of pyridine and using S_NAr or Buchwald-Hartwig chemistry. Hence, reaction of amine **107** with 2-fluoropyridine was attempted, but this unfortunately resulted in thermal deureation. Buchwald-Hartwig amination of 2-bromopyridine and **107** was also attempted, but this also decomposed **107**.

At this point, alcohols **100**, **101**, **104** and **110** did not provide viable aldehydes for reductive alkylation. Instead, each was converted into its corresponding alkyl chloride and tosylate to see if these compounds could be used for monoalkylation of amine **106** instead. Unfortunately, treatment of **100**, **101**, **104** and **110** with tosyl chloride and TEA resulted in decomposition, possibly by elimination and polymerisation. Treatment of **101**, **104** and **110** with thionyl chloride and TEA saw the same result. Interestingly, reaction of alcohol **100** with thionyl chloride alone provided the corresponding alkyl chloride **112** in reasonable yield (Scheme 25). However, reaction with amine **107** saw no conversion of **107**, but decomposed the alkyl chloride by what was presumed to be polymerisation.

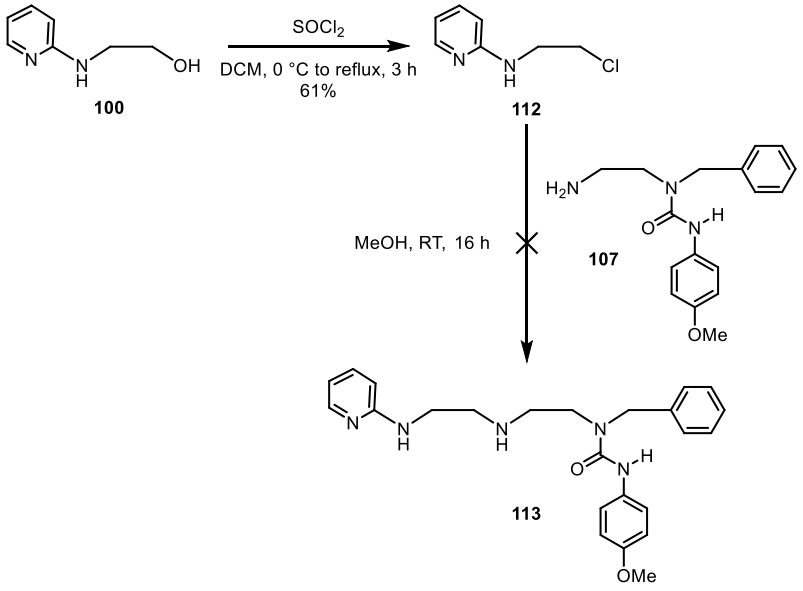

Scheme 25 – Synthesis of 113.

Alcohol oxidation and the formation of alkyl tosylates and alkyl chlorides had failed to furnish an electrophilic source of *N*-(2-pyridyl)ethylamine. Next, acquisition of pyridyl aldehydes by Johnson-Lemieux oxidation of the corresponding allyl amines was investigated (Scheme 26).

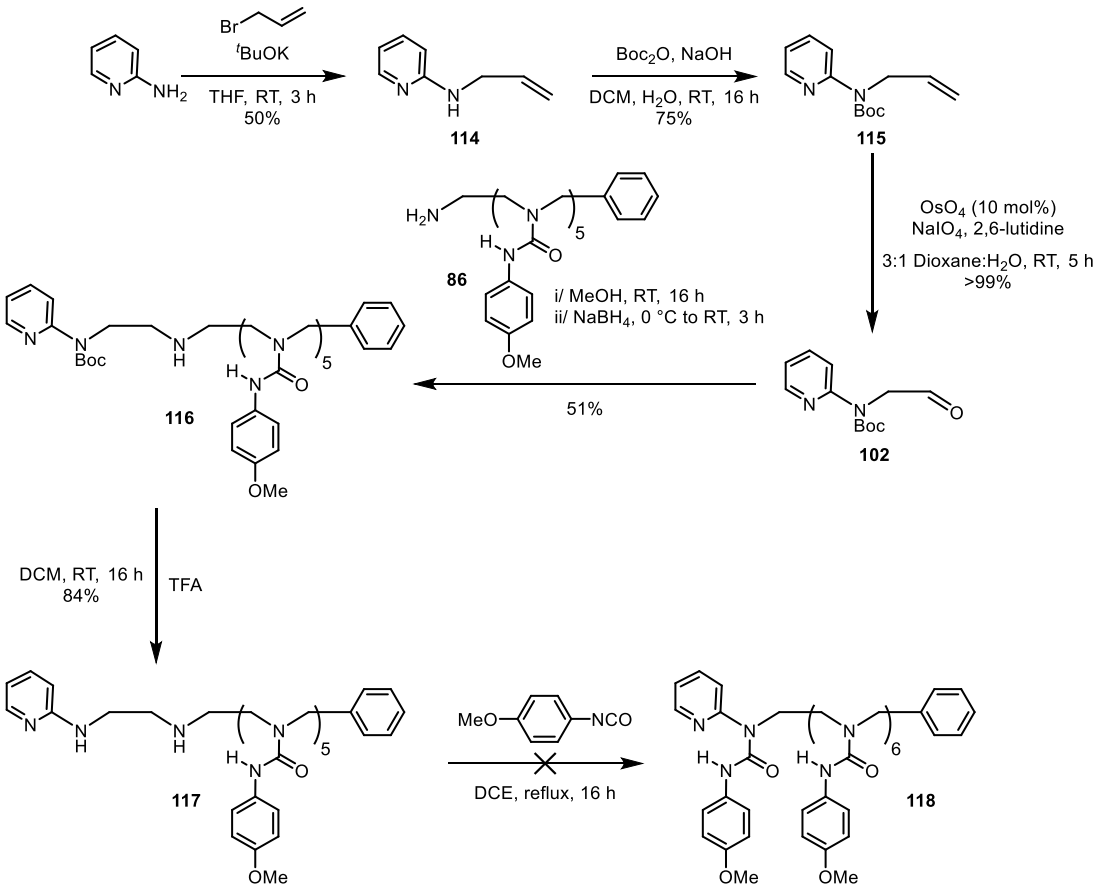

Scheme 26 – Synthesis of 118.

2-Aminopyridine underwent a nucleophilic substitution (S_N2) reaction with allyl bromide to yield allylamine **114**, which was then Boc-protected to give the corresponding carbamate **115** in reasonable yield over the two steps. **115** was then subjected to Lemieux-Johnson oxidation conditions, which furnished the desired aldehyde quantitatively. Aldehyde **102** was then used for a successful reductive alkylation with amine **86** to give the coupled product **116** in moderate yield. The Boc group was removed with TFA and then the corresponding diamine, **117**, was reacted with 4-methoxyphenyl isocyanate in DCM at room temperature. A urea was successfully installed on the dialkylamine, but the 2-aminopyridine was inert to the reaction conditions. The reaction was further encouraged by heating with an excess of 4-methoxyphenyl isocyanate in 1,2-dichloroethane (DCE). A new product formed, which was studied by ^{1}H NMR (Figure 53).

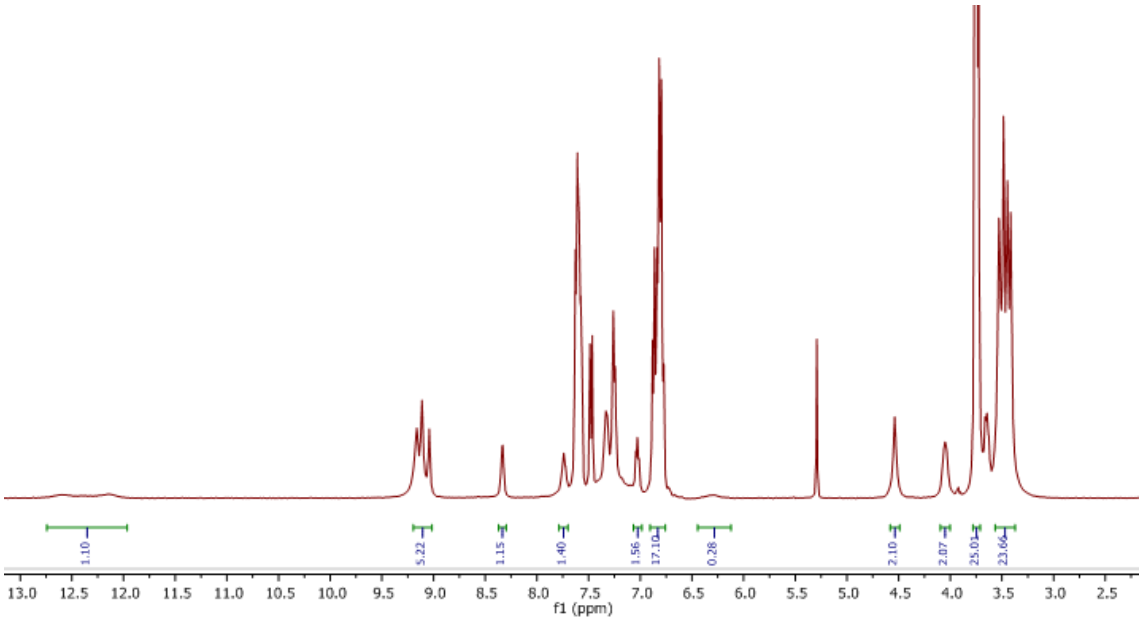

Figure 53 – ^{1}H NMR of the product of reaction of 117 with 4-methoxyphenyl isocyanate (CD_2Cl_2, 500 MHz).

The signals at 4.04 (2-pyridyl urea α-methylene), 7.03 (pyridyl *meta* methine), 7.73 (pyridyl *para* methine) and 8.33 ppm (pyridyl *ortho* methine) were all consistent with carboxamidation having taken place at the 2-aminopyridine. Signals between 9.02 and 9.23 ppm (ureido protons, 5 H) were consistent with 5 ureido protons in hydrogen bonding. However, two broad signals were observed at 12.14 (0.46 H) and 12.59 ppm (0.43 H), where it was expected that only one 2-pyridyl urea ureido proton signal would be observed. Additionally, the signals at 3.78 (methoxy groups) and 6.81 ppm (4-methoxyphenyl *ortho* methines) integrated much more highly than was expected, and a signal was observed at 6.30 ppm (0.28 H). It was deduced that some of the isocyanate had decomposed into a *N*,*N'*-disubstituted urea from the presence of water (Scheme 27).[91]

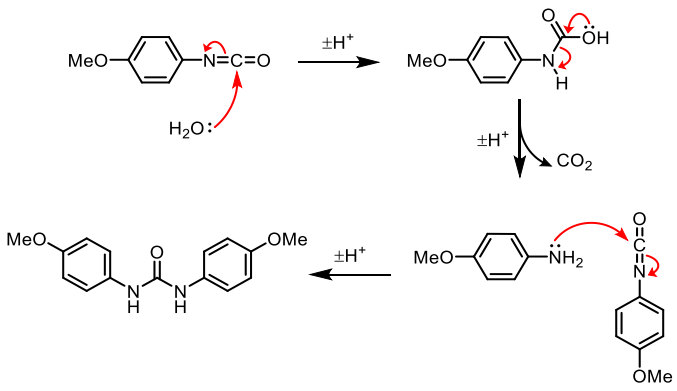

Scheme 27 – Mechanism for isocyanate decomposition into a *N*,*N*'-disubstituted urea.

The presence of this decomposition product accounted for additional signals in the 4-methoxyphenyl regions and the ureido protons at 6.30 ppm. However, the additional signal in the 2-pyridyl urea ureido proton region was not accounted for. Mass spectrometric analysis revealed that the desired mass ion for heptaurea **118** was observed, so it was suspected that the isocyanate decomposition product was tightly binding to **118** and giving rise to two environments for the pyridyl urea ureido proton. This was further corroborated by COSY and HMBC NMR techniques, which showed that the additional signals did not correlate with that of **118**. The decomposition product is a *N*,*N'*-disubstituted urea, and so its removal was attempted by washing it into an aqueous phase with acid, base, LiCl and urea, to no avail. Trituration using DCM/Et_2O, acetone/Et_2O and DMSO/Et_2O gave similar results. Due to this, it was proposed that heptaurea **118** could be synthesised effectively from amine **117** if the isocyanate decomposition product was not able to form. This could be ensured if the final urea was formed from an isocyanate surrogate, such as an aryl or *N*-hydroxysuccinimidyl carbamate, or a *N*'-imidazolyl urea.[92]

Alternatively, the difficulties associated with installing the final urea at such a late stage could be avoided if the 2-pyridyl urea was incorporated into the aldehyde fragment, **102**. This was preliminarily investigated by the synthesis of aldehyde **120**, which was achieved in an analogous manner to aldehyde **102** (Scheme 28), with the hope that the directional control imposed by the pyridine would confer kinetic stability to the aldehyde.

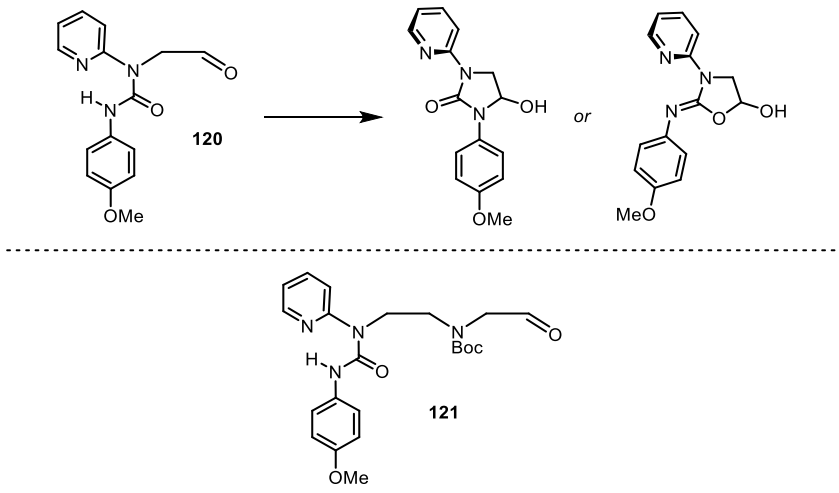

Scheme 28 – Decomposition of 120.

Unfortunately, upon formation, the urea cyclised onto the aldehyde to give the corresponding 5-membered heterocycle. It is unknown whether the corresponding 4-hydroxyimidazolidin-2-one or 4-hydroxy-2-iminooxazolidinone formed, but the product was inert to any subsequent reductive amination conditions attempted. To use this strategy to make a viable reductive amination partner, the aldehyde would have to be removed from the pyridyl urea by another amine, as is proposed in pyridyl urea **121** (Scheme 28). It is hoped that due to the

removal of the aldehyde from the pyridyl urea, cyclisation will not occur and the aldehyde will be stable enough for reductive amination. Having a pyridyl urea as opposed to the pyridyl *tert*-butyl carbamate in **104** will also mitigate the steric bulk about the aldehyde, allowing reductive amination to proceed.

All of the proposed switches discussed so far have involved the protonation of a basic site to provide an HBD. In theory, the opposite can also be exploited – an acidic site that acts as an HBD could be deprotonated to form an anion, which would then act as an HBA. To test this concept, 1,8-diazabicyclo[5.4.0]undec-7-ene (DBU) was titrated into a sample of thiourea **68**, which had already been established to control directionality by acting as an HBD (Figure 54). It was proposed that the thiourea was the most acidic function in **68**, meaning that a base would deprotonate it first, giving the corresponding anion, which would then switch the directionality.

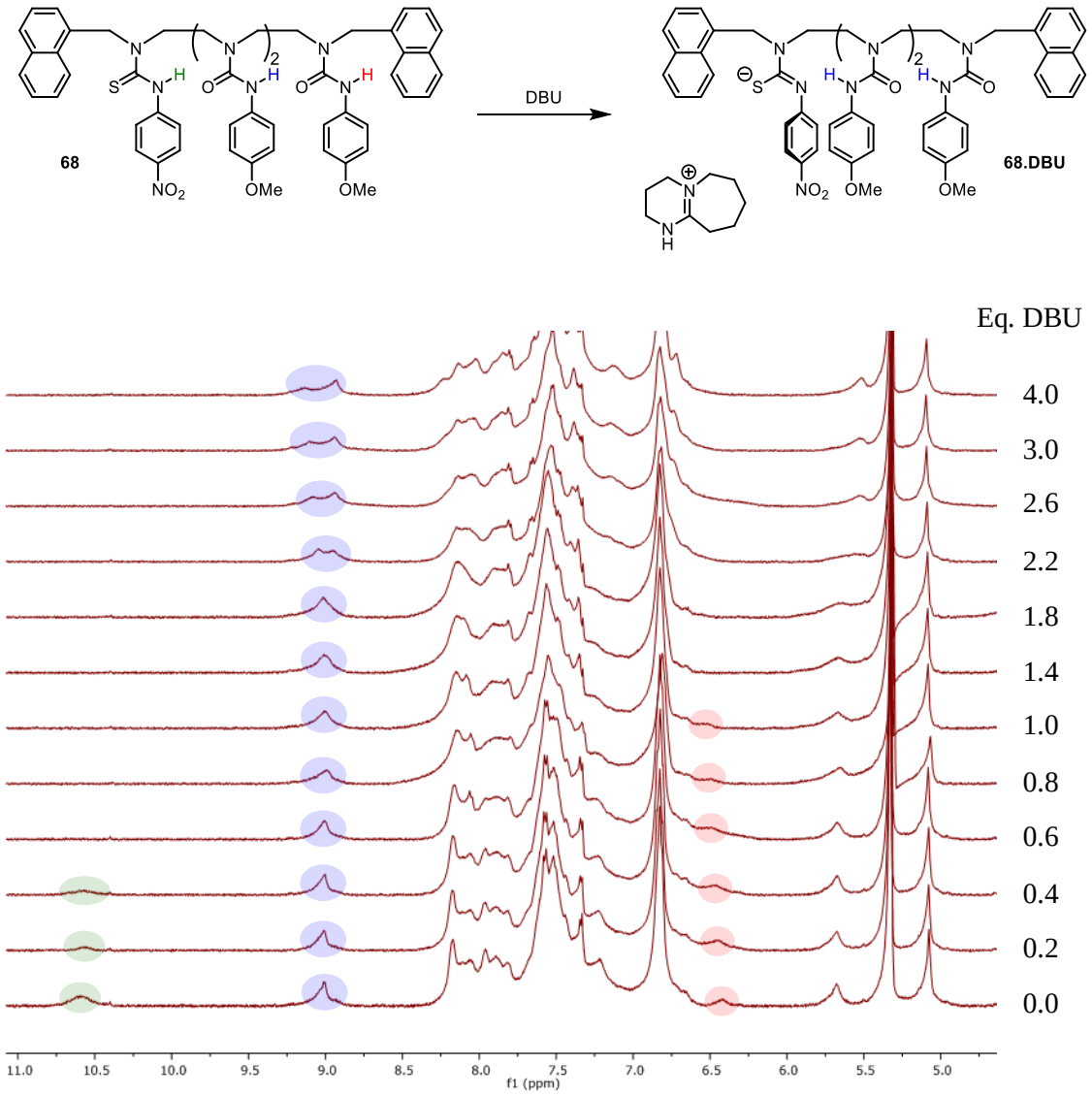

Figure 54 – Titration of DBU into 68 (4.50-11.00 ppm region, CD_2Cl_2, 500 MHz, 19 mM).

In thiourea **68**, signals were observed at 6.42 (peripheral ureido proton), 9.00 (central ureido protons, 2 H) and 10.58 ppm (thioureido proton). Upon addition of 0.2 equivalents of DBU, the signal at 6.42 ppm attenuated, broadened and shifted downfield. The signals at 9.00 ppm stayed approximately constant throughout the experiment. The signal at 10.58 ppm attenuated immediately upon addition of DBU and continued to attenuate until it was no longer observable at 0.8 equivalents. A new signal appeared at 9.04 ppm at 2.2 equivalents and shifted downfield thereafter. These results are consistent with deprotonation of the thiourea, where the equilibrium had shifted to total deprotonation by 1.0 equivalents of DBU. The central ureido protons would be switching between two 9-membered hydrogen-bonding rings, so it is not expected that they would change appreciably in chemical shift. It is notable that one central ureido proton would switch out of hydrogen bonding with another urea and into hydrogen bonding with a thioureido anion. It is suspected that the hydrogen-bond-accepting nature of this would be comparable to an amidine, as the negative charge would presumably be localised on the sulfur atom.[72] The peripheral ureido proton, shifted downfield with increasing DBU, until joining the other ureido protons at 1.8 equivalents, indicating that it had entered hydrogen bonding. DBU did not further deprotonate **68** as all of the other ureido protons were accounted for, even at superstoichiometric quantities of DBU. These data indicated that thiourea **68** underwent a base-induced directionality switch, which was further validated by the absence of any NOE correlation between the ureido benzylic methylene and any ureido protons. The same experiment was performed using thiourea **90** to see if this long-range directional change could be communicated by the thioureido anion (Figure 55).

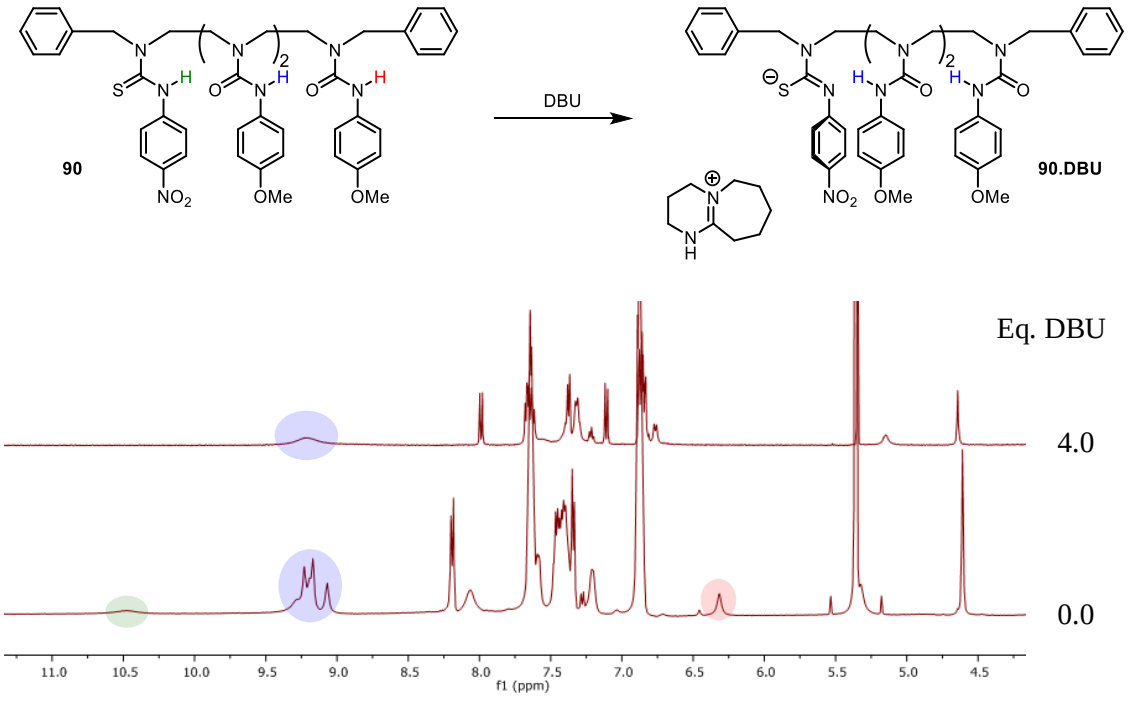

Figure 55 – Addition of DBU to 90 (4.50-11.00 ppm region, CD_2Cl_2, 500 MHz, 30 mM).

Thiourea **90** showed signals at 6.31 (peripheral ureido proton), 9.03-9.30 (central ureido protons, 5 H) and 10.47 ppm (thioureido proton). Upon addition of DBU, the signal at 6.31 ppm attenuated and the signals at 9.03-9.30 ppm broadened to make an apparent singlet (6 H). The signal at 10.47 ppm completely attenuated with addition of DBU. These data show that the directional switch occurred due to the disappearance of the thioureido proton signal and the shifting of the peripheral ureido proton signal to the urea-urea hydrogen-bonding region. This was further validated by the absence of an NOE between the ureido benzylic methylene and any ureido protons, where one originally existed.

These experiments have shown that thioureas can also be used for directionality switching by exploiting their relative acidity. Deprotonation of the thiourea using an organic base liberates an anion which acts as an HBA and switches the directionality of the entire foldamer. This is particularly significant in the case of thiourea **90**, as the directionality switch is communicated through six ureas. Gratifyingly, the signals of the neutral form are restored upon washing with hydrochloric acid, meaning that the directionality reversal can be switched between the forms selectively without the expense of hydrogen-bonding fidelity with each iteration.

In each of the switches discussed, the exact numbers of hydrogen bonds between the two forms are the same. Tetrasubstituted urea **71** exhibits three hydrogen bonds between each of the ureas. It was suspected that if the foldamer was provided a better alternative hydrogen-bond-accepting additive to the tetrasubstituted urea, then **71** would also undergo a global directionality switch. The HBA could coordinate in two places – at the N-terminus, where there would be no directionality switch as the tetrasubstituted urea would be simply replaced by the HBA, and the C-terminus, where there would be a directionality switch. To investigate this, **71** was studied by VTNMR with 10% v/v of competitive HBA, d_6-DMSO (Figure 56).

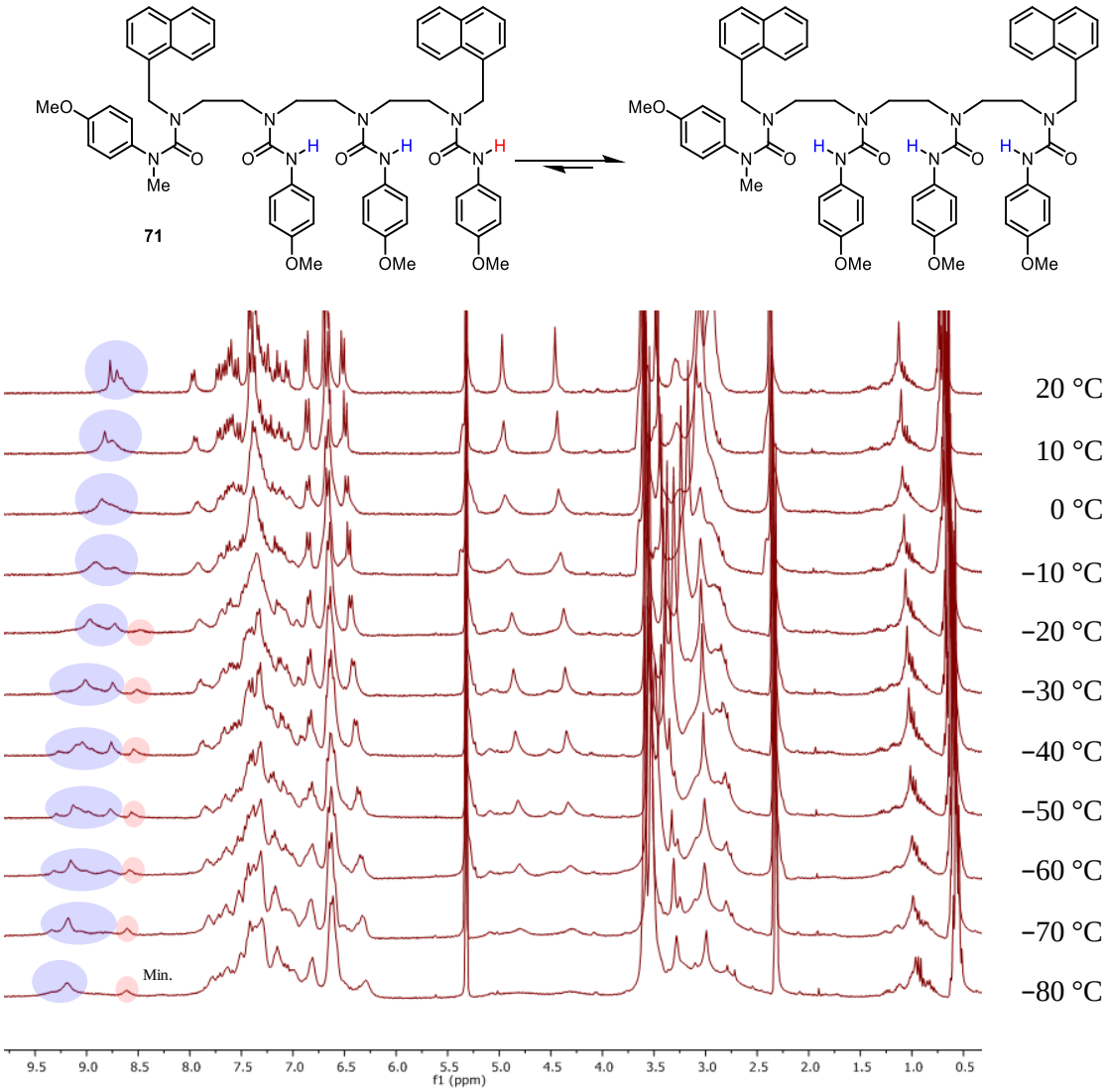

Figure 56 – VTNMR of 71 (10% v/v d_6-DMSO in CD_2Cl_2, 300 MHz, 13 mM).

Tetrasubstituted urea **71** displayed signals at 4.46 (tetrasubstituted urea benzylic methylene), 4.97 (trisubstituted urea benzylic methylene) and at 8.66-8.77 ppm (ureido protons, 3 H) at 20 °C. Upon cooling, the signals at 4.46 and 4.97 ppm broadened and each decoalesced into two singlets (0.64 and 1.36 H) at −30 °C. The signals broadened further with decreasing temperature. The signals at 8.66-8.77 ppm broadened and shifted downfield with decreasing temperature, before decoalescing at −30 °C, where a signal appeared at 8.51 ppm (0.32 H). The decoalesced signals broadened further with further cooling. These data revealed that, in the presence of d_6-DMSO, **71** exists as a mixture of two conformations in a ratio of 32:68 at −30 °C. These conformations are the two directionalities – one where the tetrasubstituted urea is at the N-terminus, and the other where d_6-DMSO hydrogen bonds to the opposite end of the foldamer, making the tetrasubstituted urea at the C-terminus. The signal at 8.51 ppm (0.32 H) at −30 °C

corresponds to a terminal ureido proton hydrogen bonding to d_6-DMSO. This attributed the minor conformer to the directionality where the tetrasubstituted urea is at the C-terminus. It is suspected that the d_6-DMSO facilitates a directionality switch by hydrogen bonding to the opposite end of the foldamer to the tetrasubstituted urea. This is because coordination next to the tetrasubstituted urea would transmit hydrogen-bonding information in the same way, such that a carbonyl would still be proximate to the reporting benzylic methylene. This would cause a negligible change in chemical environment and a lack of an observable decoalescence.

In summary, ethylene-bridged oligourea foldamers can undergo global hydrogen-bond directionality switching using acid and base when terminated with the appropriate basic and acidic functionality. Foldamers with directional control imposed by tetrasubstituted ureas can also undergo a partial additive-induced switch, and it is proposed that they could be switched more completely if a strong hydrogen-bond-accepting additive, such as a phosphine oxide, was employed. Foldamers can be switched between their directional forms by the appropriate addition of acid/base and subsequent washing with base/acid with no erosion of hydrogen-bonding fidelity. The switch can also be communicated over nanometre distances as demonstrated by **90**, where a base-induced switch culminated in directional reorientation over six ureas. The robustness of the hydrogen-bonding network over these distances and its amenability to directional switching bestow great applicability upon these foldamers, as they are now able to take hydrogen-bonding information and reliably communicate it to the opposite end of the foldamer over a relatively large distance.

3.6 Towards a Light-Induced Hydrogen-Bond Directionality Switch

It has been shown that ethylene-bridged oligourea foldamers can communicate hydrogen-bonding information over nanometre distances and with high fidelity. The directionality switches described previously necessitate the use of strong acids and bases. These stimuli are not compatible with biological environments, where there are stronger bases and acids than pyridyl ureas and thioureas such as lysine and aspartic acid residues.[93] Additionally, the stimulus may interact with the biomolecules in a negative way, such as disrupting the pH balance in a cell, which would result in its death.

A prevalent way to evade the issues associated with the use of chemical stimuli is light. Light is non-invasive – it does not require the insertion of a chemical into a system as it can travel through barriers. Also, a wide range of wavelengths are available for the selective irradiation of a certain bond or species, which lends itself to biological orthogonality with high spatial and temporal precision. Over the past decades, chemists have developed a plethora of photoswitchable moieties, which cover an excellent range of conformational space and irradiation wavelengths and have been exploited as such. Since the 1970s, a prominent category of photoswitchable molecules known as photoacids has been emerging. Photoacids are molecules that, upon irradiation, isomerise into a form that is more acidic (Figure 57). They have been used to facilitate many acid-catalysed processes reversibly by exposure to light of the appropriate wavelength.[94]

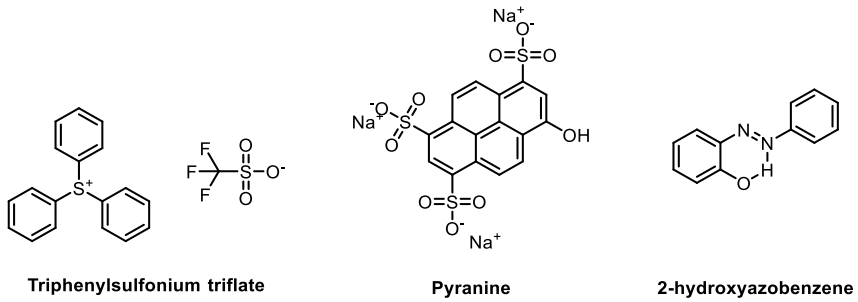

Figure 57 – Commonly employed photoacids.

Photoacids fall into two classes – photoacid generators and reversible photoacids. Photoacid generators are molecules that adopt their excited state, and irreversibly convert to a highly acidic species, such as the photochemical decomposition of triphenylsulfonium triflate into triflic acid. Reversible photoacids adopt an acidic photoexcited state but can revert back to the less acidic ground state. The reversibility property is highly desirable in photoacids as it allows the modulation of pH by altering the intensity of light, which can lend itself to the halting or reversal of a pH-sensitive process.

One of the most prevalent photoacid classes are the merocyanines (Scheme 29). Multiple research groups have derivatised the merocyanines to shift the pH ranges they can access, their absorbance wavelengths, kinetic parameters and organic solubility for specific applications.[95–97]

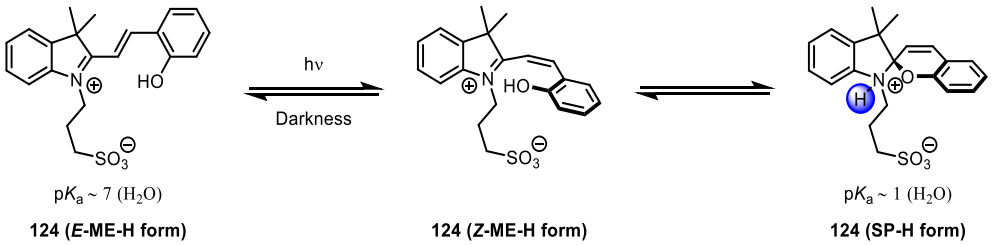

Scheme 29 – Isomerisation of merocyanine-derived photoacids.

Liao and co-workers have extensively studied merocyanine systems and the factors that affect their photophysics. Photoacid, **124** is stable in its zwitterionic indolium sulfonate (ME-H) form, and the proton is localised on the phenoxide.[98] Upon irradiation with visible light, the olefin photoisomerised to the *Z* form, where the phenol spirocyclised to give corresponding spiropyran (SP-H) form. The phenol then transfers its proton to the indoline to give an indolinium, which was much more acidic than the parent phenol. Electron-withdrawing groups on the phenol have often been used to enhance the acidity of the *E*-ME-H and *Z*-ME-H forms, but this also inhibits the spirocyclisation step relative to thermal isomerisation of *Z*-ME-H back to *E*-ME-H. Conversely, electron-donating groups have been used to speed up the spirocyclisation, but this also decreases the acidity of *E*-ME-H, *Z*-ME-H and SP-H. These modifications also affect the absorption wavelength of *E*-ME-H and the quantum yield of the transformation.

The kinetics of the reverse reaction have been studied in water, ethanol and DMSO.[98] The kinetic data fit well to a second order rate equation in each case, indicating that protonation was involved in the rate-determining step. This also meant that the reverse reaction was highly sensitive to concentration. These experiments determined rate constants of 73, 1.6, and 0.03 M^{-1} s^{-1} in water, ethanol and DMSO, respectively. These data were correlated with the solvents ability to donate hydrogen bonds, where the reverse reaction proceeded more quickly in solvents with a greater hydrogen-bond-donating capacity. This is because the developing negative charge on the phenoxide can be stabilised by HBDs during the reverse reaction.[94]

As an initial method for light-induced directionality switching, **124** was synthesised (Scheme 30) and combined with pyridyl urea **97** in the hope that the generated indolium sulfonate acid would be of sufficient acidity to protonate the foldamer in DCM. It was assumed that, because of DCM's inability to donate hydrogen bonds, reversion of the photostationary state to *E*-ME-H after irradiation had stopped would occur slowly enough to allow analysis by ^{1}H NMR in solutions of concentration ~ 10 mM.

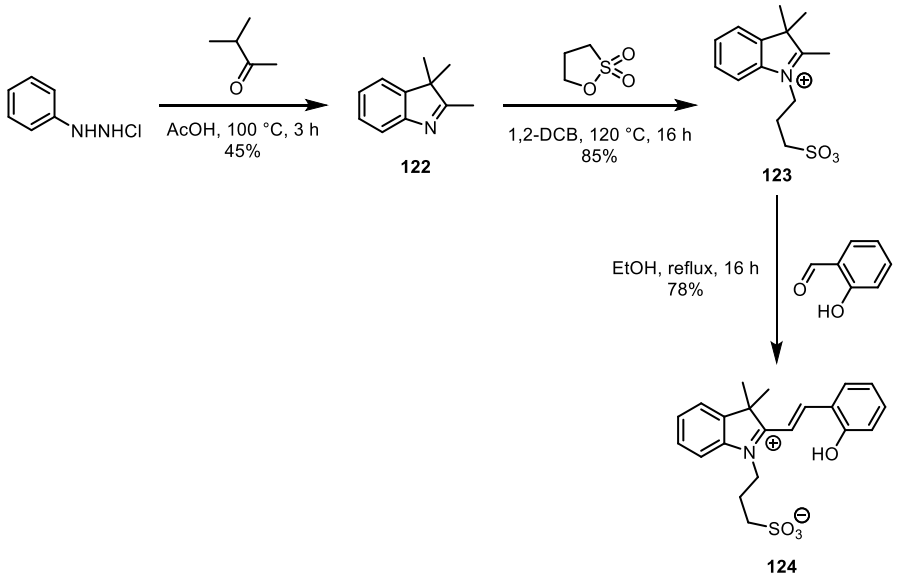

Scheme 30 – Synthesis of 124.[*]

Phenylhydrazine hydrochloride underwent a Fischer indole reaction with methyl isopropyl ketone to give the corresponding indolenine, **122**, which was then reacted with 1,3-propane sultone to give the zwitterion, **123** in moderate yield over two steps. **123** then underwent an aldol condensation with salicylaldehyde to give **124**, in good yield. **97** was then combined with an equivalent of **124**, irradiated at 485 nm for one hour in CD_2Cl_2 and studied by ^1H NMR (Figure 58). Unfortunately, **124** was found to be insoluble in CD_2Cl_2, but it was assumed that the SP-H form would be soluble, and the pyridinium sulfonate salt that would form from protonation of the foldamer would also be soluble.

[*] Work performed by Bryden Le Bailly.

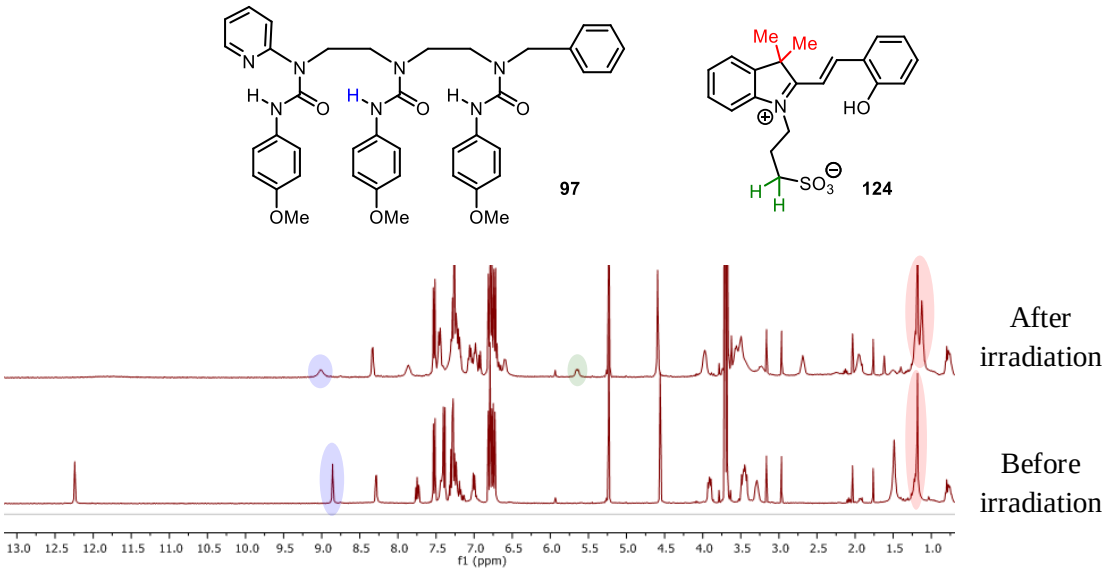

Figure 58 – Irradiation of 97.124 (500 MHz, CD_2Cl_2, 10 mM).

Signals were observed at 8.84 (central ureido proton) and 12.24 ppm (pyridyl urea ureido proton) before irradiation. Upon irradiation, the signal at 8.84 ppm broadened and moved downfield, whereas the signal at 12.24 ppm broadened and shifted significantly upfield. Additionally, several new alkyl and aromatic signals appeared, the most pertinent of which were the signals at 1.12 (one of the diastereotopic methyl groups in the SP form, 2.17 H) and 2.68 ppm (sulfonate α methylene, 1.35 H). These results show that after irradiation, approximately 0.67 equivalents (based on the sulfonate α methylene) of merocyanine **124** were present in solution. This resulted in partial protonation of the foldamer as indicated by the shifting of the ureido proton signals. However, it did not correspond to a full directionality switch as was seen with 5.0 equivalents of TFA or 1.5 equivalents of $TsOH.H_2O$. Due to the substoichiometric generation of the indolinium, an additional four equivalents of **124** were added to the sample and the experiment was repeated. This gave no further improvement on the switch and broadened the signals in the sample due to the amount of solid in the suspension. Mixing the sample with CD_3OH did not improve the solubility, but d_6-DMSO fully dissolved the **97**/**124** mixture. However, irradiation of this sample gave no change in the foldamer signals at all. It was hoped that a more hydrophobic analogue of **124** would solubilise the photoacid in CD_2Cl_2, where the acid-induced directionality switch was known to proceed. Merocyanine **127** was synthesised analogously to **124** using (4-*n*-hexylphenyl)hydrazine hydrochloride and 3-butyl-heptan-2-one in 12% total yield (Scheme 30). Gratifyingly, **127** was found to be fully soluble in CD_2Cl_2. However, it is notable that the alkyl substitution will raise the pK_a of the SP-H form, making it less favourable for the foldamer to deprotonate it. The behaviour of **127** upon irradiation at 485 nm was examined by ^{1}H NMR (Figure 59).

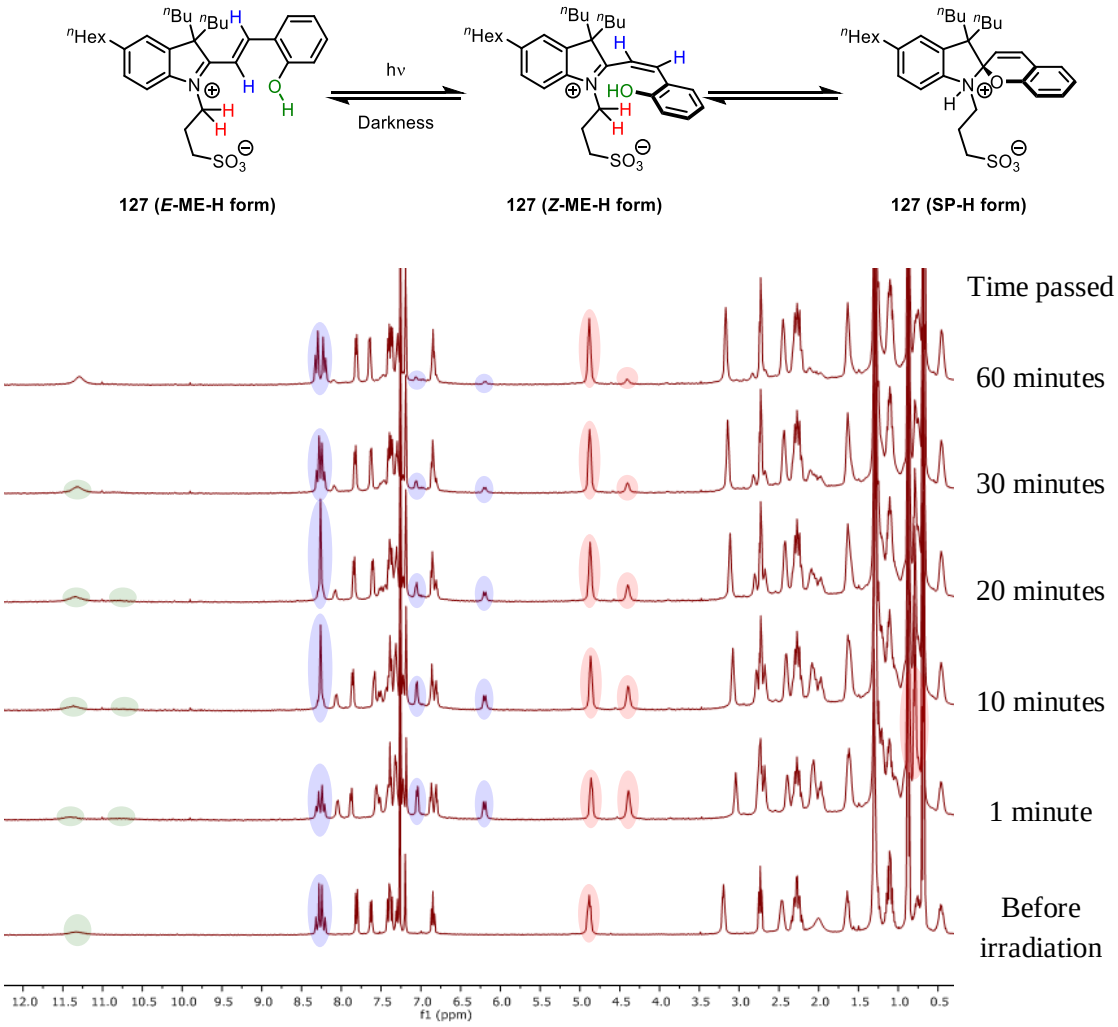

Figure 59 – Irradiation of 127 ($CDCl_3$, 500 MHz, 10 mM).

Merocyanine **127** displayed signals at 4.88 (indolium α methylene), 6.85 (phenol *para* methine), 8.22-8.30 (olefin protons) and 11.32 ppm (phenolic proton) before irradiation (in the *E*-ME-H form). After irradiation, all of the aforementioned signals attenuated and additional signals appeared at 4.39 (indolium α methylene, 1.0 H), 6.19 (olefin proton, 0.5 H), 7.04 (olefin proton, 0.5 H), 8.04 (phenol *meta* methine, 0.5 H) and 10.82 ppm (phenolic proton, 0.5 H). Over the course of one hour, each of the new peaks attenuate with concurrent restoration of the original peaks. These data show that, after irradiation, a new chemical species arose which was in a 50:50 ratio with the original *E*-ME-H form. The new olefinic signals corresponding to this species were consistent with a *Z* olefin, indicating that photoisomerisation had taken place. However, a phenolic resonance (10.82 ppm) was still present, and diastereotopicity was not revealed in the geminal methylenes (1.29 ppm), which would occur if spirocyclisation had taken place. These results indicated that, at the photostationary state, the *E*-ME-H and *Z*-ME-H forms were present in an equimolar ratio, but the phenol failed to spirocyclise onto the indolium. This meant that the

indolinium acid did not generate and therefore, combination of five equivalents of **127** with **97** and subsequent irradiation resulted in no change in the signals of **97**.

It was suspected that, as the geminal dimethyl group had been changed to a geminal di-*n*-butyl group, the steric bulk about the indolyl iminium was too great for the phenol to attack in the *Z*-ME-H form. To combat this issue, merocyanine **130** was synthesised as an analogous molecule to **127** (Scheme 30), with the *n*-hexyl group to promote organic solubility, but with geminal methyl groups to allow spirocyclisation to occur. **130** was synthesised in 30% total yield and then analysed by ^{1}H NMR upon irradiation (Figure 60). Unfortunately, **130** was contaminated with its zwitterionic precursor, **129**, but it was suspected that this would be insensitive to light as it does not contain a photosensitive olefin.

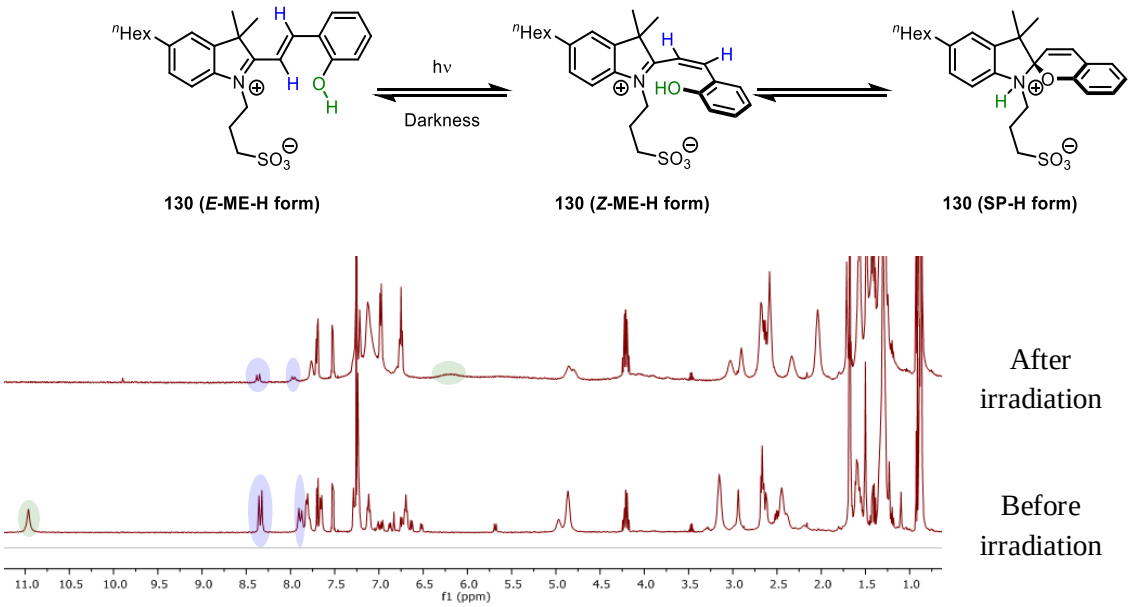

Figure 60 – Irradiation of 130 ($CDCl_3$, 500 MHz, 10 mM).

Before irradiation, merocyanine **130** showed signals at 4.86 (indolium α methylene), 7.89 (olefin proton), 8.34 (olefin proton) and 10.96 ppm (phenolic proton). After irradiation, the signal at 4.86 ppm stayed approximately the same, but signals at 7.89 and 8.34 ppm attenuated by 91%. Also, the signal at 10.96 ppm completely attenuated and a new signal appeared at 6.19 ppm. These data show that at the photostationary state, 91% of the *E*-ME-H form was consumed. All of the *E*-ME-H form converted to the SP-H form, since no phenolic resonance remained after irradiation and a new signal appeared at 6.19 ppm, which could correspond to the indolinium. Unfortunately, the olefin shifts in the *Z*-ME-H or the SP-H form were not observed and diastereotopicity in the geminal methyl groups was not evident in the ^{1}H NMR spectrum. Additionally, thermal relaxation did not quantitatively restore all of the signals of the *E*-ME-H form. Instead, a small amount of an unidentified decomposition product was observed.

Pyridyl urea **97** was then combined with five equivalents of merocyanine **130** and irradiated for one hour at 485 nm. Unfortunately, this gave rise to no change in the signals of **97**. As **124** can undergo facile spirocyclisation, the lack of interaction with **97** was not attributed to inhibited spirocyclisation. Instead, it was suspected that due to the alkyl substitution on the indole, the increased basicity of the indoline disfavoured deprotonation of the corresponding indolinium by pyridyl urea **97**. This could be counteracted by furnishing the pyridine of **97** with electron-donating groups, increasing its basicity and making it more favourable to be protonated by merocyanines **124** or **130**.

Zwitterionic merocyanine-derived photoacids were unable to give rise to effective directional switching in pyridyl urea-terminated oligoureas, so the photoacid scaffold was altered. Photoacids without a sulfonate tether, such as spiropyran **132** have also been successfully employed in acid-mediated processes (Scheme 31).[99,100]

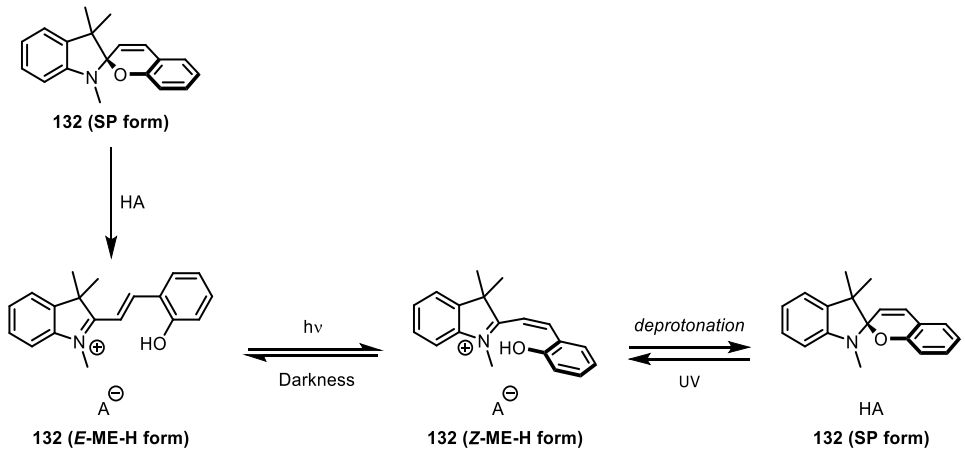

Scheme 31 – Isomerisation of merocyanine salt-derived photoacids.

Browne and co-workers have shown that spiropyran **132** is stable under neutral conditions, but upon exposure to a sufficiently strong acid, it undergoes ring opening and isomerisation to form **132** in its thermodynamically stable *E*-ME-H form.[97] Upon photoisomerisation, the *Z*-ME-H form was metastable and several pK_a units lower than the corresponding *E*-ME-H form (as deduced in MeCN). The phenol was not nucleophilic enough to attack the indolyl imine, but if the conjugate base A^- was sufficiently basic, the phenol could be deprotonated and facilitate an irreversible spirocyclisation to form the indoline, SP. The spiropyran could then only be reopened by exposure to ultraviolet (UV) light. Further studies have investigated this pH-gating phenomenon using NaH_2PO_4, where its pK_{aH} was sufficiently low so as to not deprotonate the *E*-ME-H form, but high enough to deprotonate the *Z*-ME-H form.[97] It is hoped that the pK_{aH} of pyridyl urea **97** is intermediate to the pK_as of the *E*-ME-H and

Z-ME-H forms of **132** to allow efficient pH-gated directionality switching. With this, **132** was synthesised by the procedure reported by Browne and co-workers (Scheme 32).[97]

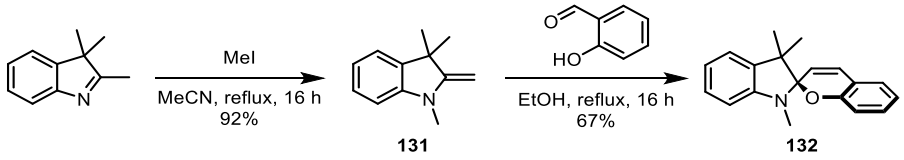

Scheme 32 – Synthesis of 132.

Spiropyran **132** was synthesised by methylation of 2,3,3-trimethyl-3*H*-indole to give **131**, which then underwent a pseudo-aldol condensation with salicylaldehyde to afford **132** in good yield over two steps. **132** was then to be reacted with TFA to generate its *E*-ME-H form (Scheme 33), where the trifluoroacetate anion is not basic enough to deprotonate either the *E*-ME-H or *Z*-ME-H forms of **132**, and so would be dormant in the photoswitching procedure. Pyridyl urea **97**, however, would act as the base in the procedure – upon photoisomerisation of **132** to the more acidic *Z*-ME-H form, **97** would deprotonate **132**, irreversibly facilitating spirocyclisation to the SP form. **97** would then retain the proton originally belonging to the phenol, resulting in the directionality switch.

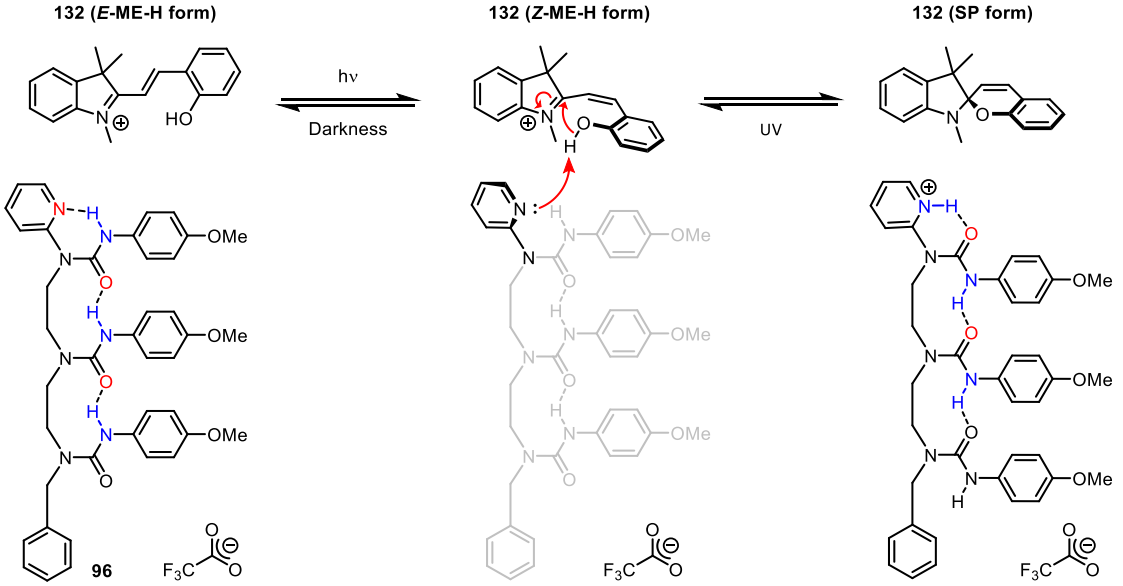

Scheme 33 – Proposed photoacid-induced directionality switching in 97.

As established, the trifluoroacetate anion was not basic enough to deprotonate the conjugate acid of pyridyl urea **97**, and it was also hoped that the same applied to the indolinyl moiety in the SP form of **132**. This would give rise to a pH-gated switch, where the SP form of **129** could only be reopened upon irradiation with UV light. This would convert **132** between the SP and *Z*-ME forms. The *Z*-ME form would not be basic enough to deprotonate the pyridinium

trifluoroacetate of **97**, but thermal isomerisation yields the *E*-ME form, which would be. The *E*-ME form of **132** would then deprotonate the pyridinium trifluoroacetate of **97**, returning the *E*-ME-H form and switching the directionality of **97** back again.

As a preliminary investigation into this, merocyanine **132** was combined with one equivalent of TFA. It took around 24 h for the SP-H form to convert to the *Z*-ME-H form and subsequently to the *E*-ME-H form. Samples of **132**.TFA were then irradiated for 1 h at 485 nm with and without an equivalent of pyridine (Figure 61).

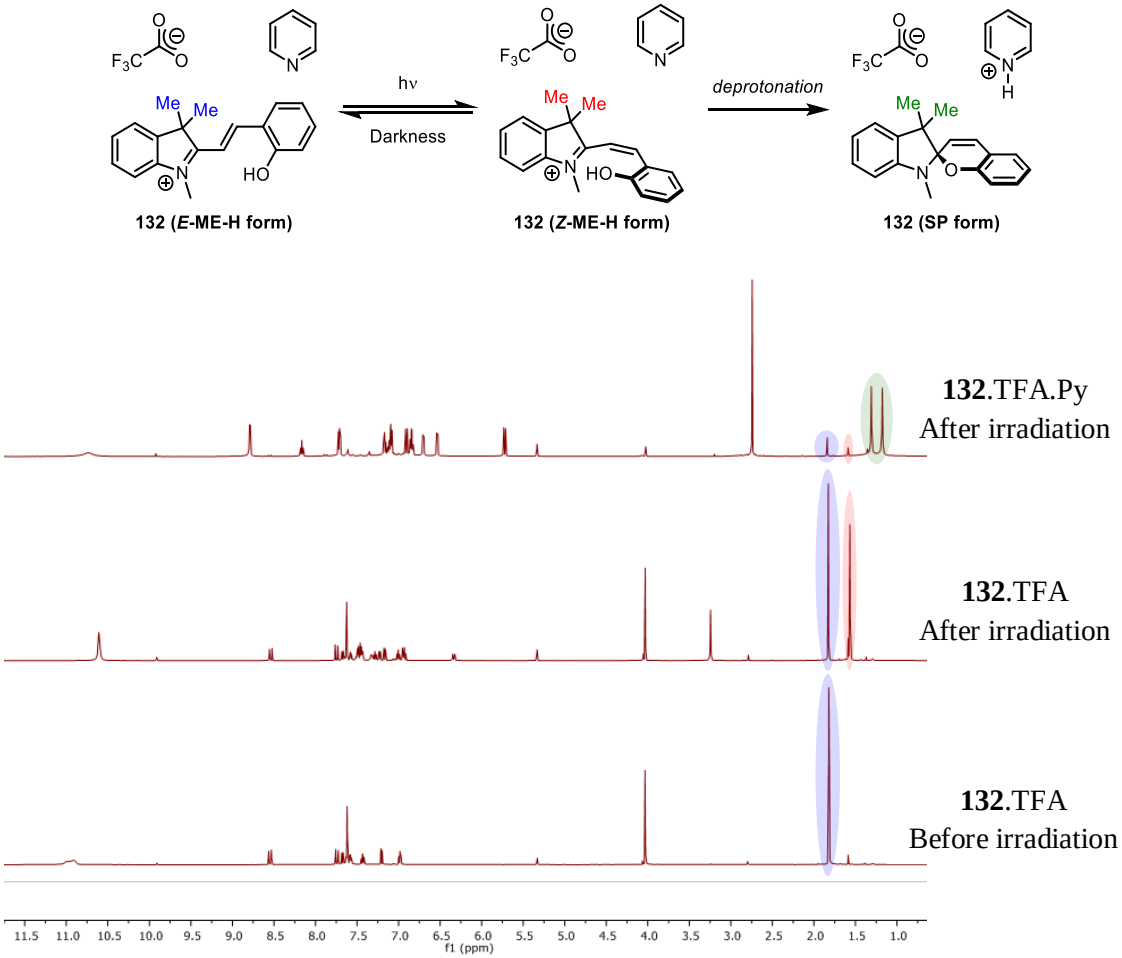

Figure 61 – Irradiation of 132 with 1 eq. of pyridine and/or TFA (CD_2Cl_2, 500 MHz, 10 mM).

Before irradiation, signals were observed at 1.82 (geminal methyls, *E*-ME-H form), 4.04 (*N*-methyl, *E*-ME-H form) and 8.54 ppm (olefin proton, *E*-ME-H form). Upon irradiation at 485 nm for one hour, these signals attenuated and new signals appeared at 1.59 (geminal methyls, *Z*-ME-H form, 1.74 H), 3.25 (*N*-methyl, *Z*-ME-H form, 3.49 H) and 6.35 ppm (olefin proton, *Z*-ME-H form, 0.61 H). The olefin coupling constants were consistent with the proposed geometries. The signals corresponding to *Z*-ME-H **132** attenuated to restore the original spectrum over 16 h. The signal ratios did not change upon further irradiation, indicating that the photostationary state

had been reached. These data showed that in the presence of one equivalent of TFA, the photostationary state shows a 42:58 ratio of *E*:*Z* forms of **132**. It is notable that when base is introduced, the equilibrium will dynamically resolve to the *Z*-ME-H form as any *Z*-ME-H will be deprotonated and converted irreversibly to the SP form.

To ensure that the *Z*-ME-H form could be deprotonated by pyridine bases in DCM, **132**.TFA was combined with an equivalent of pyridine and irradiated at 485 nm for one hour (Figure 61). Upon addition of pyridine, the signals at 1.82 (geminal methyls, *E*-ME-H form, 0.31 H), 4.04 (*N*-methyl, *E*-ME-H form) and 8.54 ppm (olefin proton, *E*-ME-H form) attenuated to 10% of their original size. The signals at 3.25 (*N*-methyl, *Z*-ME-H form), 4.04 (*N*-methyl, *E*-ME-H form) and 6.35 ppm (olefin proton, *Z*-ME-H form) also greatly attenuated. New signals appeared at 1.18 and 1.31 (diastereotopic geminal methyls, SP form, 3 H each), 2.74 (*N*-methyl, SP form) and 5.72 ppm (olefin proton, SP form). Notably, a signal at 8.16 ppm (pyridine *para* proton) also appeared. These results indicated that the pyridine deprotonated all of the **132** *Z*-ME-H to give *Z*-ME, which spirocyclised to give SP. This removed *Z*-ME-H from the *E*-ME-H/*Z*-ME-H equilibrium, and so *E*-ME-H attenuated to convert to more *Z*-ME-H and SP, leaving behind only 10% of the original *E*-ME-H. It was assumed that *E*-ME-H was present instead of the deprotonated *E*-ME as the signals corresponding to *E*-ME-H did not change. Additionally, the pyridine signals were markedly downfield shifted in comparison to its neutral form, indicating that protonation had taken place. Finally, the sample was left for 24 h, with no change in signals occurring, indicating that the spiropyran was stable in the presence of pyridinium trifluoroacetate. With this, ten equivalents of **132**.TFA were combined with an equivalent of **97**. The mixture was irradiated with 485 nm light for one hour and studied by ^{1}H NMR (Figure 62).

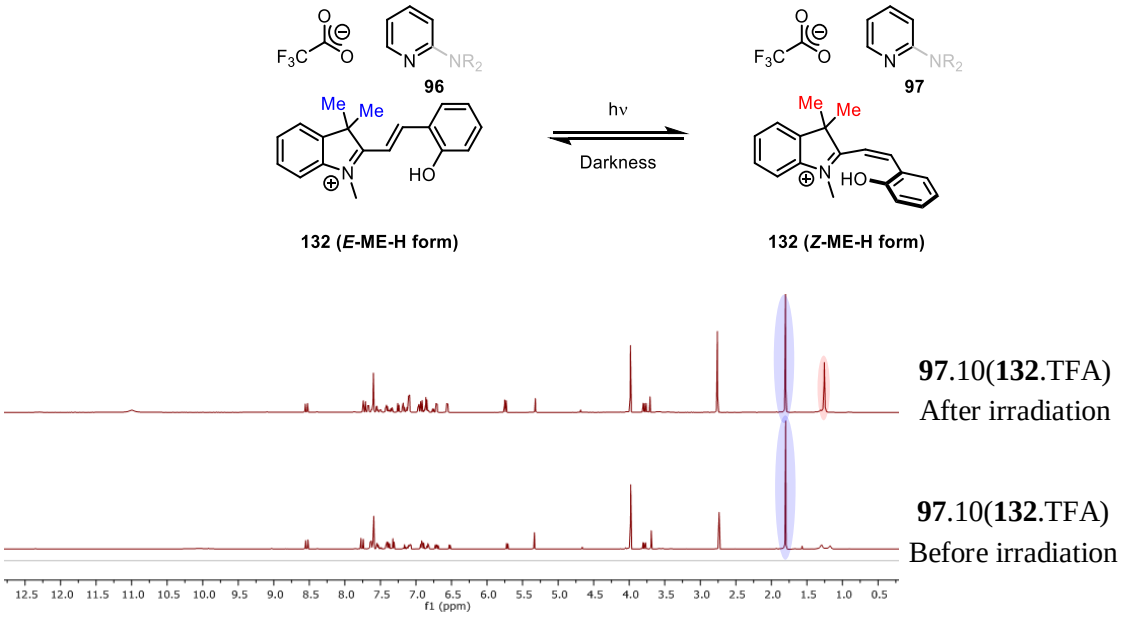

Figure 62 – Irradiation of 97.10(132.TFA) (CD_2Cl_2, 500 MHz, 10 mM).

Prior to irradiation, a signal was observed at 1.80 ppm (geminal methyls, *E*-ME-H form). After irradiation, this signal attenuated with concomitant appearance of a signal at 1.25 ppm (geminal methyls, *Z*-ME-H form). All of the signals corresponding to **97** remained the same.

These experiments showed that upon irradiation, **132** *E*-ME-H photoisomerised to *Z*-ME-H, but the foldamer was not basic enough to deprotonate either form. Pyridyl urea **97** remained unaffected, and the *Z*-ME-H form thermally reverted back to the *E*-ME-H form over 16 h. From this, it was inferred that acidification of **132**.TFA was required to shift the pK_a range down to the pK_{aH} of **97**. To this end, **133** was synthesised as an analogous photoacid with a *para*-nitro group on the salicylaldehyde fragment. **133** was synthesised from **131** using 4-nitrosalicylaldehyde (Scheme 32). **133** was then ring-opened with TFA to give the *E*-ME-H form. Five equivalents of this were added to **97** and the resulting mixture was studied by ^{1}H NMR (Figure 63).

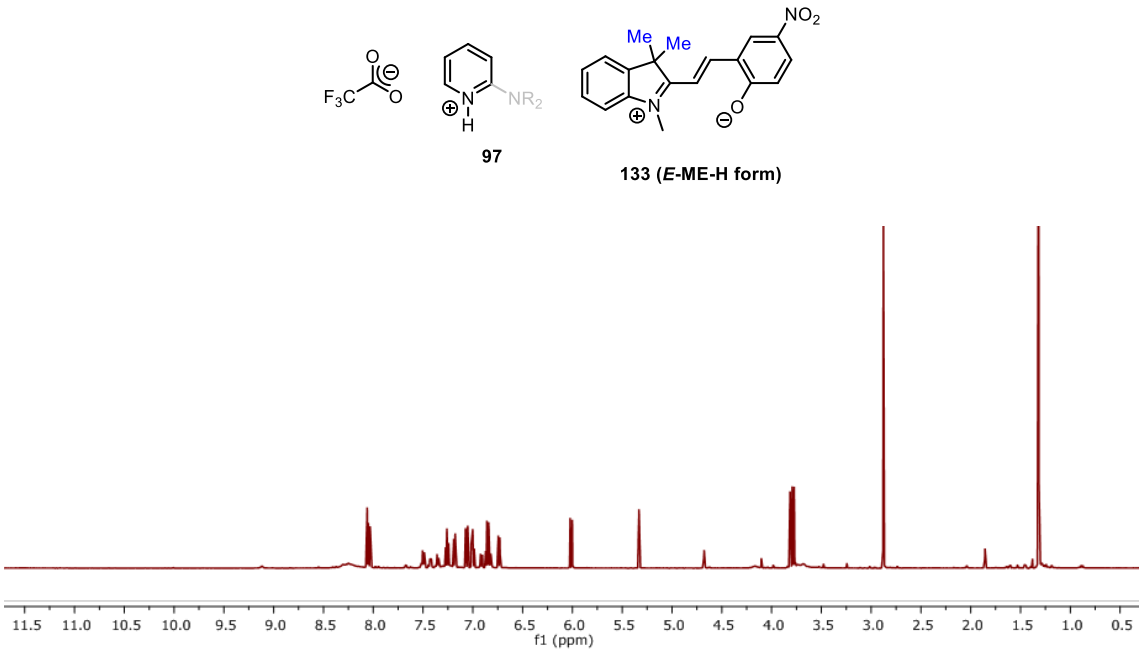

Figure 63 – 97.5(133.TFA) (CD_2Cl_2, 500 MHz, 10 mM).

Merocyanine **130** showed signals at 1.30 (geminal methyls, *E*-ME-H form) and 2.83 ppm (*N*-methyl, *E*-ME-H form). The central ureido proton of pyridyl urea **97** was observed at 9.12 ppm. Unfortunately, the signals of **97** indicated that the *E*-ME-H form of **133** was sufficiently acidic to protonate **97**. This meant that acidifying **132** with a *para* nitro group lowered the pK_as too much, to the point that both forms protonate **97**, rendering the photoswitching process redundant. In order to overcome this issue, another photoacid needs to be synthesised with an electron-withdrawing substituent on the salicylaldehyde fragment of intermediate electron-withdrawing ability such that the pK_{aH} of **97** lies between that of the *E*-ME-H and *Z*-ME-H forms. Alternatively, it was shown that in DCM, the pK_{aH} of pyridine lied in this region and allowed efficient pH-gating. Therefore, an alternative acid-sensitive directional switch could be made with

electron-donating groups on the pyridine. This would increase the basicity of the foldamer, and could raise the pK_{aH} to the appropriate region for pH-gating with **132**. This may also allow deprotonation of **130** upon irradiation, and allow directionality switching using weaker acids, which would make the switch more tolerable and feasible under physiological conditions.

The attempted light-induced directionality switches described still necessitate the use of acids, which may give rise to undesirable side-processes in biological settings. The photoacid also does not need to associate with the foldamer, and so the acid generated can protonate other basic moieties instead. A more functional alternative would be to have the photoswitchable moiety as a part of the foldamer, meaning that photoisomerisation could affect the foldamer directly from intramolecular interactions. The proposed method of doing this is to have an HBD and HBA as different substituents on a photosensitive bond (Scheme 34).

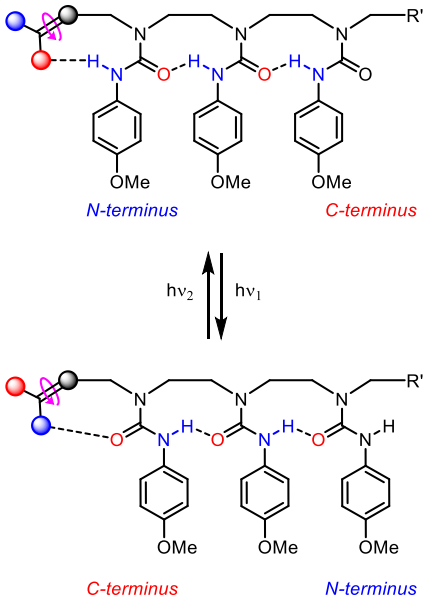

Scheme 34 – Schematic for light-induced conformational switching of oligourea foldamers.

Ideally, the *E* and *Z* forms of the photosensitive bond would have orthogonal light absorption, allowing the two forms to interconvert upon exposure to different wavelengths of light. In one form, an HBA would be proximate to the adjacent urea and the HBD on the other side of the olefin would not. The HBA would form a hydrogen bond with the adjacent ureido proton, and the directionality would be controlled as such. Photoisomerisation would switch the HBA out of hydrogen bonding and bring the HBD close to the adjacent urea. The directionality of the adjacent urea would then switch in order to form a new hydrogen bond with the HBD through the ureido carbonyl, and the new directionality would be communicated through the foldamer. Previous work by Clayden and co-workers has explored numerous candidates to satisfy this phenomenon, and it has been shown that fumaramides (*E*) can photoisomerise to form the

corresponding maleamides (*Z*) and hydrogen bond with adjacent ureas (Figure 64). The advantage of this scaffold is that HBDs and HBAs are already present in the form of amides.

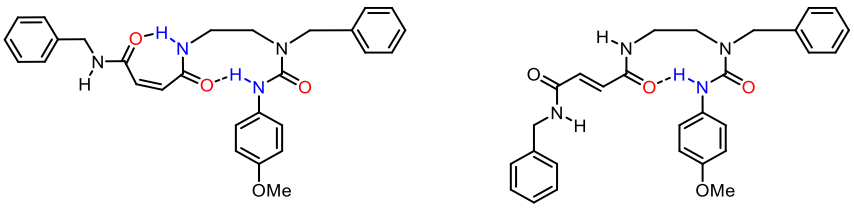

Figure 64 – Directionality control using fumaramides (*E*) and maleamides (*Z*).

Unfortunately, it was discovered that in both the *E* and *Z* forms of the diamide, the amido carbonyl acted as an HBA, imposing directional control on the proximate urea such that the diamide was at the N-terminus.* In order to attain a light-mediated directionality switch, one of the forms must act as an HBD instead. In the case of the fumaramide, the amido carbonyl acts as an HBA. This interaction can be changed by acidifying the amido proton or decreasing the hydrogen-bond-accepting ability of the amido carbonyl (Figure 65).

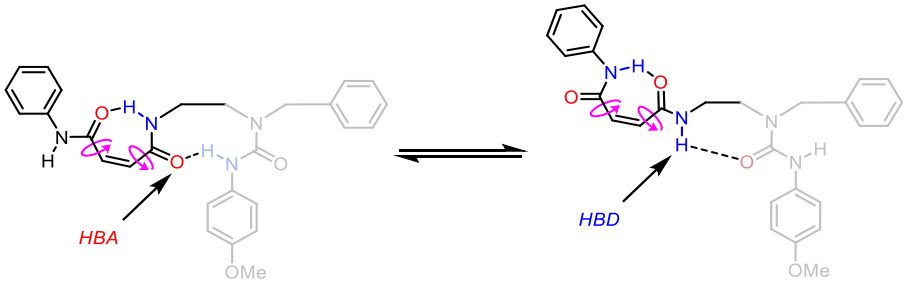

Figure 65 – Interconversion of the 7-membered hydrogen-bonding rings in maleamides.

The maleamide, however, can act as either an HBA or an HBD to the proximate urea by interconversion between two different 7-membered hydrogen-bonding rings. When the maleamide was terminated with a benzyl group, the leftmost hydrogen-bonding ring predominated (Figure 65), resulting in the maleamide acting as an HBA. It is proposed that if this terminal amide was acidified by an electron-withdrawing substituent, the rightmost 7-membered hydrogen-bonding ring would be more thermodynamically favoured. This would leave an amido proton proximate to the urea, setting the opposite directionality to the fumaramide. It was hoped that the hydrogen-bonding properties of the fumaramide would be unaffected by this modification. The initial target was phenyl-substituted maleamide, **135** (Scheme 35).

* Work performed by MSc student Arron Aatkar.

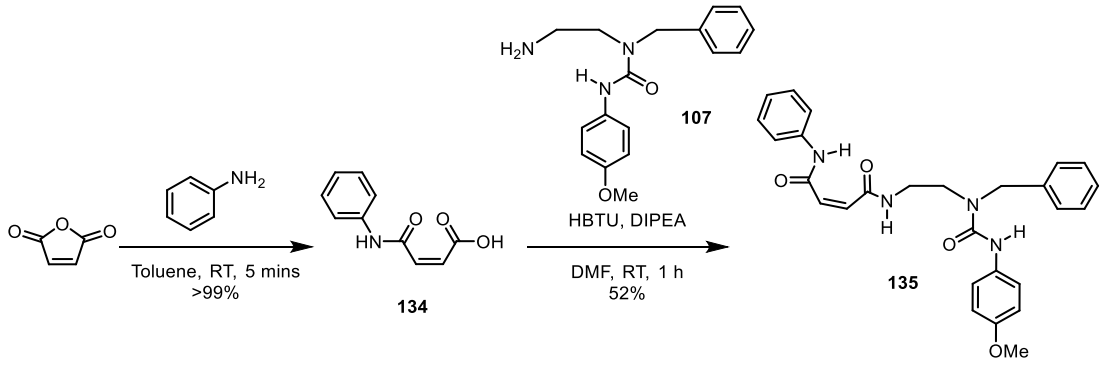

Scheme 35 – Synthesis of 135.

Maleamide **135** was synthesised by acylation of aniline using maleic anhydride followed by coupling of the corresponding amic acid with amine **107** using peptide coupling reagents, providing **135** in good yield over two steps. To ascertain the directionality that the *N*-phenyl maleamide imposed, **135** was then studied by VTNMR (Figure 66).

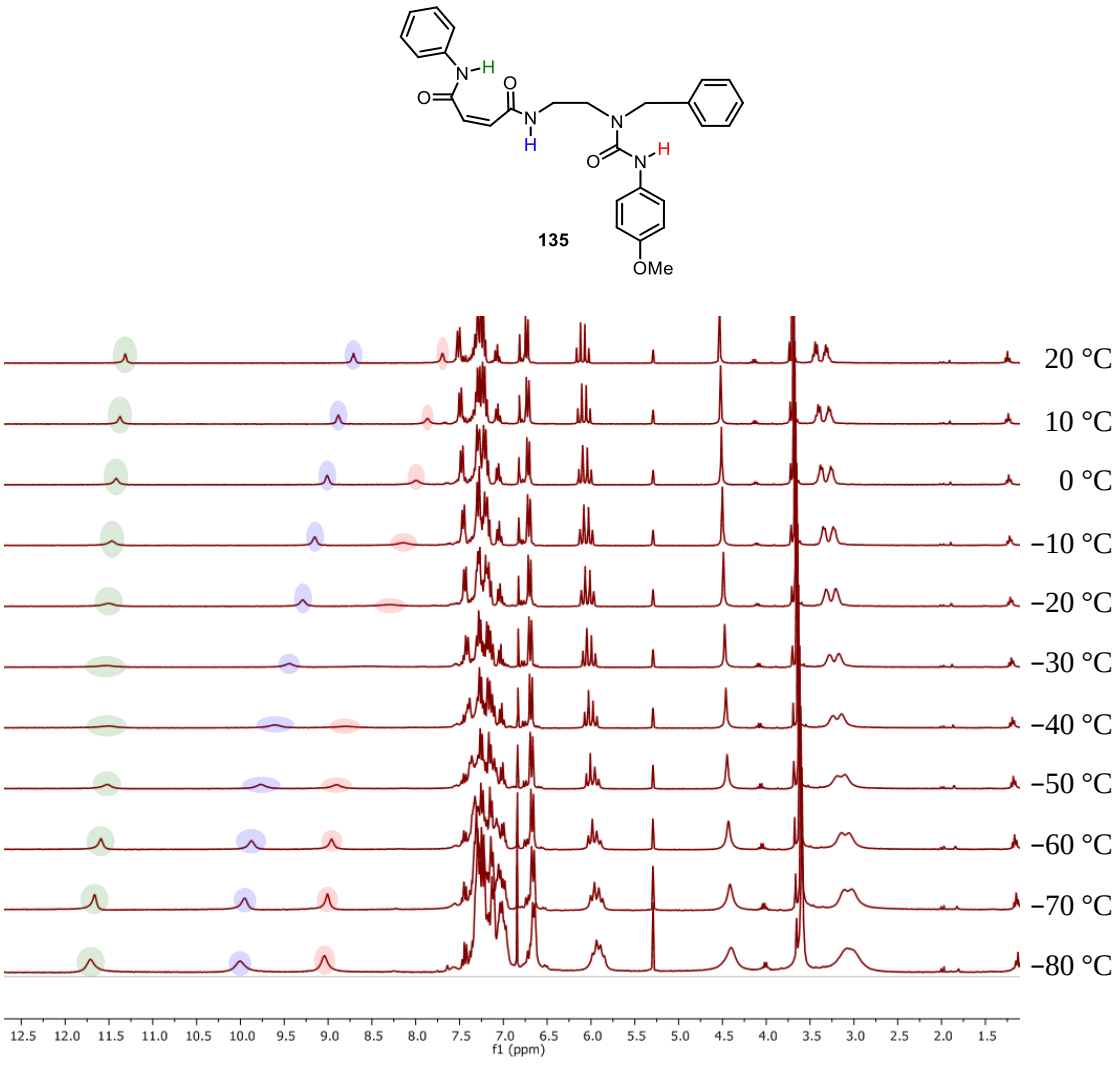

Figure 66 – VTNMR of 135 (CD_2Cl_2, 300 MHz, 21 mM).

Maleamide **135** showed signals at 4.53 (benzylic methylene), 6.05 and 6.14 (olefin protons), 7.69 (ureido proton), 8.71 (alkyl amido proton) and 11.31 ppm (phenyl amido proton) at 20 °C. Upon cooling, the signals at 4.53, 6.05 and 6.14 ppm stayed approximately constant until they broadened at −60 °C. The signals at 7.69, 8.71 and 11.31 ppm shifted downfield and broadened with decreasing temperature and then sharpened again at −50 °C. The lack of decoalescence of the benzylic methylene indicated that one conformation is populated. It is hoped that the maleamide is at the C-terminus, as is the case in thioureas **68** and **90**. By chemical shift inspection, it is difficult to assign the directionality of the adjacent urea. However, the ureido proton chemical shift is likely to be very different to that of **68** and **90**, as the urea is in a 7- or 9-membered hydrogen-bonding ring with an amide. NOE analyses were performed (see Appendix, Figures A34-35), and it was shown that the benzylic methylene was proximate to the ureido proton, but the other two methylenes in the ethylene bridge were not. This indicated that the urea directionality was set such that the maleamide was at the C-terminus, as desired.

Future work on this light-induced directionality switch will be to extend maleamide **135** by one urea, to ensure that the first urea can communicate its directionality to the second. By analogy with thiourea **90** and tetrasubstituted urea **91**, if the first and second urea can communicate, then the hydrogen-bonding information can be communicated throughout the rest of a larger foldamer. The analogous fumaramide will have to be synthesised to ensure that opposite directionality is retained upon phenyl substitution. Finally, the forms will be interconverted between each other by use of UV light. Additionally, it is noteworthy that maleamides can be chemically isomerised to fumaramides using amine catalysts, meaning that **135** could also undergo a mild chemical-induced directionality reversal.[101] However, the maleamide would have to be restored photochemically. Finally, fumaramides and maleamides photoisomerise under exposure to UV light. It would be useful if olefin modification redshifted the absorption wavelength of the photoswitch to allow photoisomerisation using light that is more conducive to biological systems.

To conclude, significant progress has been made towards attaining a light-induced directionality switch in ethylene-bridged oligourea foldamers, both in inter- and intramolecular fashions. The development of this kind of foldamer provides access to molecules that can communicate hydrogen-bonding information in response to a non-invasive stimulus with excellent spatial and temporal control. These foldamers could also be developed further to be controlled effectively by biologically benign light.

3.7 A Fluorescent Reporter for Local Hydrogen-Bond Directionality

Up to this point, local directionality in ethylene-bridged oligourea foldamers has been inferred from chemical shift and the presence or absence of an NOE correlation using an appropriate spectroscopic reporter. This has been used effectively to ascertain the kinetic and thermodynamic behaviour of the oligoureas, but as the oligoureas get larger, the relative size of the relevant signals gets smaller, making them more difficult to analyse. Additionally, larger molecules tumble more slowly in solution, which makes NOE analyses more problematic.[90] Finally, the ^{1}H NMR reporters have been used at concentrations above 10 mM, as obfuscation by spectroscopic noise renders them unreliable at higher dilution. This drawback is particularly pertinent in biological settings, where analysis must be carried out at sub-millimolar concentrations.

Fluorescence has been very well established as a method for the microscopic analysis of compounds. It occurs by photoexcitation of a fluorophore to a high energy state, which then undergoes a non-radiative relaxation process to adopt to a lower-energy state.[102] The fluorophore then emits a photon whose wavelength is redshifted relative to the absorption wavelength. This is very useful in biomedical applications, as fluorophores can typically be irradiated with biologically orthogonal light. The redshift of their emission also means that their presence can be detected precisely in biological systems. Hence it is very common for fluorophores to be ligated to biological molecules and later irradiated to monitor their position by fluorescence.

Due to the increased sensitivity and effectiveness of fluorophores in biomedical scenarios, a fluorescent reporter for local hydrogen-bond directionality in ethylene-bridged oligourea foldamers was highly desirable. The first design incorporating a fluorescent moiety was pyridyl urea **137** (Scheme 36), where the foldamer was terminated with a fluorescent pyrene group.

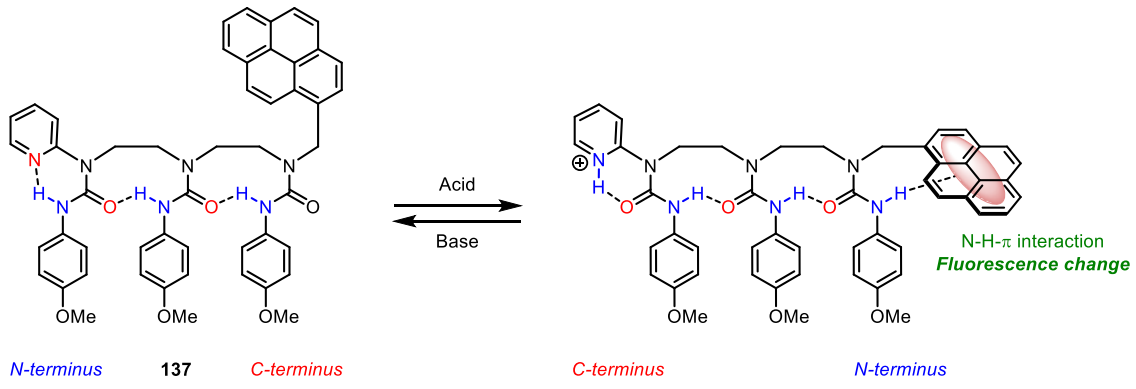

Scheme 36 – Local directionality-detection by pyrene fluorescence.

It was proposed that in the directionality where pyridine is at the N-terminus, the pyrene would not be involved in any intramolecular interactions and therefore give rise to a certain fluorescence. However, upon directional switching, a pendent ureido proton would form an N-H-π interaction with the pyrene, giving rise to a fluorescence change. Pyrene **137** was synthesised in an analogous manner to pyridyl urea **97**, but reductive alkylation was performed using 1-pyrenecarboxaldehyde in a DCM/MeOH mixture (Scheme 37).

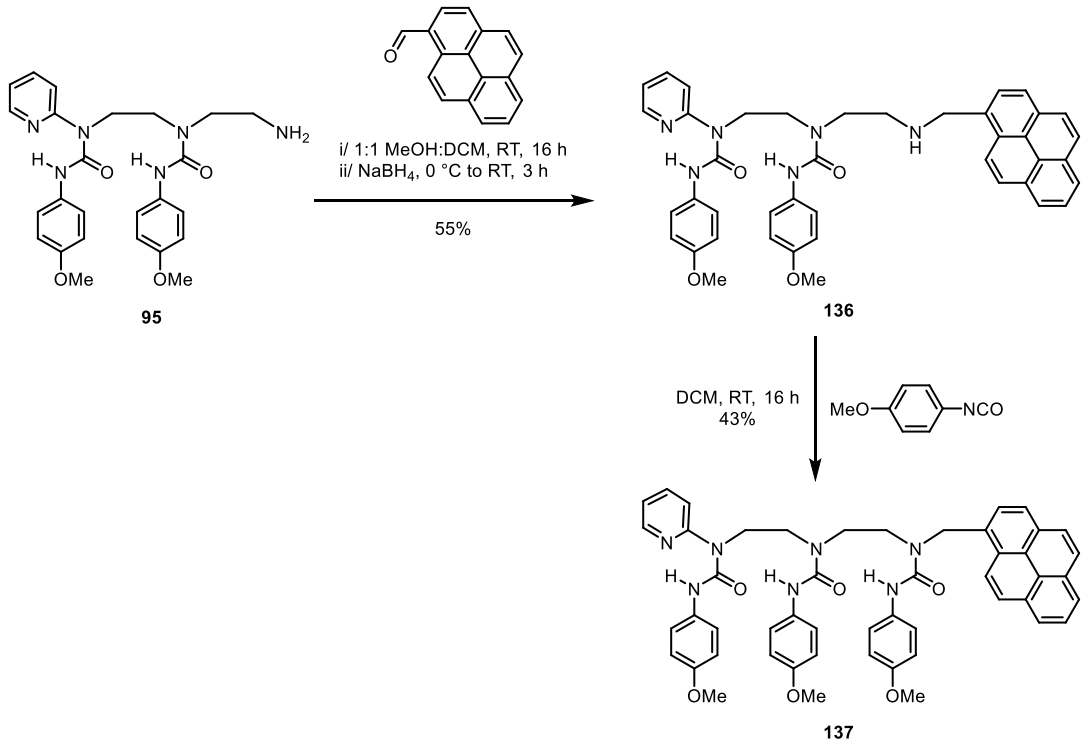

Scheme 37 – Synthesis of 137.

Five equivalents of TFA were then added to **137** and the resulting mixture was analysed by ^{1}H NMR. Unfortunately, it was evident that the acid had resulted in decomposition of the pyrene, yielding numerous products corresponding to the different permutations of pyrene oxidation.

An alternative fluorescent reporter proposed was bis(pyrene) **139** (Scheme 38), where in the directionality where the pyridine is at the N-terminus, the pyrene moieties would not associate with each other intramolecularly. Upon directional switching, the pyrenes would be brought closer together, allowing the formation of an excimer, which could be detected by fluorescence.[10]

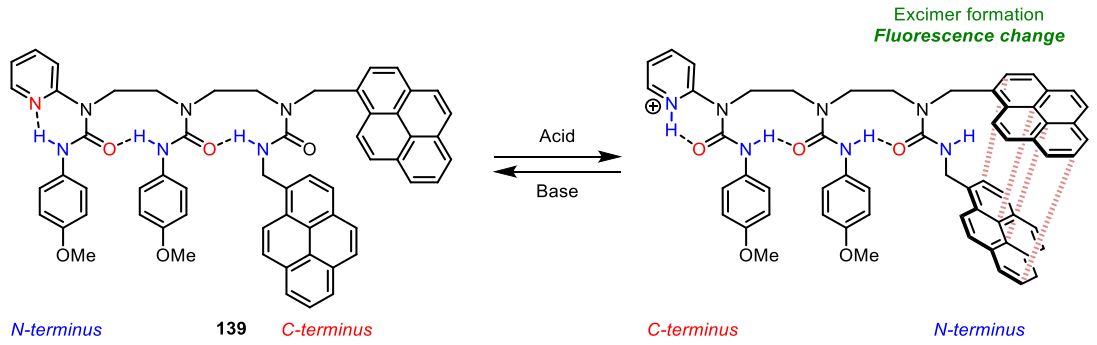

Scheme 38 – Local directionality-detection by bis(pyrene) fluorescence.

Bis(pyrene) **139** was synthesised from **136** and 1-(isocyanatomethyl)pyrene, which was made from 1-pyrenylmethylammonium chloride and triphosgene (Scheme 39).

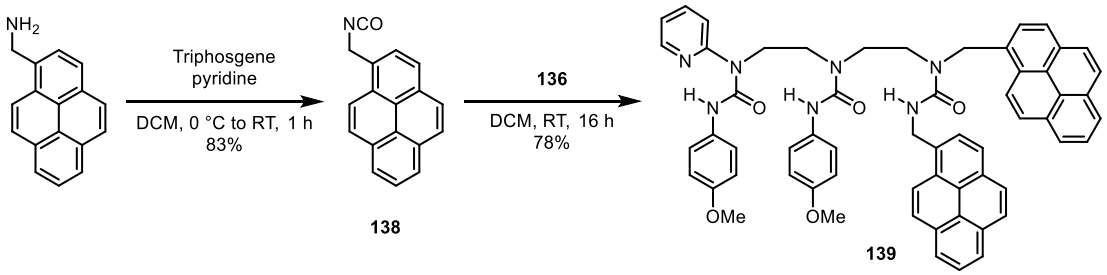

Scheme 39 – Synthesis of 139.

Bis(pyrene) **139** was successfully isolated, but unfortunately, oxidation of the pyrenes took place upon treatment with TFA. Due to the instability of the pyrenes in the presence of TFA, an alternative fluorescent scaffold was sought.

O'Reilly and co-workers reported the use of a dithiomaleimide (DTM) functional group as a highly emissive and sensitive fluorescent reporter for supramolecular architecture, such as the detection of self-assembled micelles.[103] The DTM is a maleimide, and so it was suspected that the imido carbonyls could be used as a weak HBA that, if presented with an HBD, would hydrogen bond and result in a fluorescence change. Similar to the succinimide in **69**, as maleimides are relatively weak HBAs, it was hoped they would not be able to strongly impose any directional preference. The pyridyl urea would still maintain complete conformational control and the DTM would only hydrogen bond if a pendent HBD was available (Scheme 40).

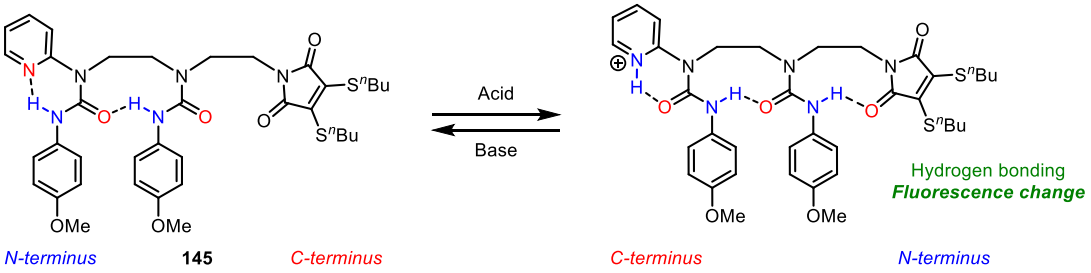

Scheme 40 – Local directionality-detection by DTM fluorescence.

Pyridyl urea **145** was synthesised by the development of an electrophilic source of the DTM in the aldehyde oxidation state (Scheme 41). This electrophilic source of the DTM was to be coupled to a *N*-(2-pyridyl)ethylenediamine by reductive amination.

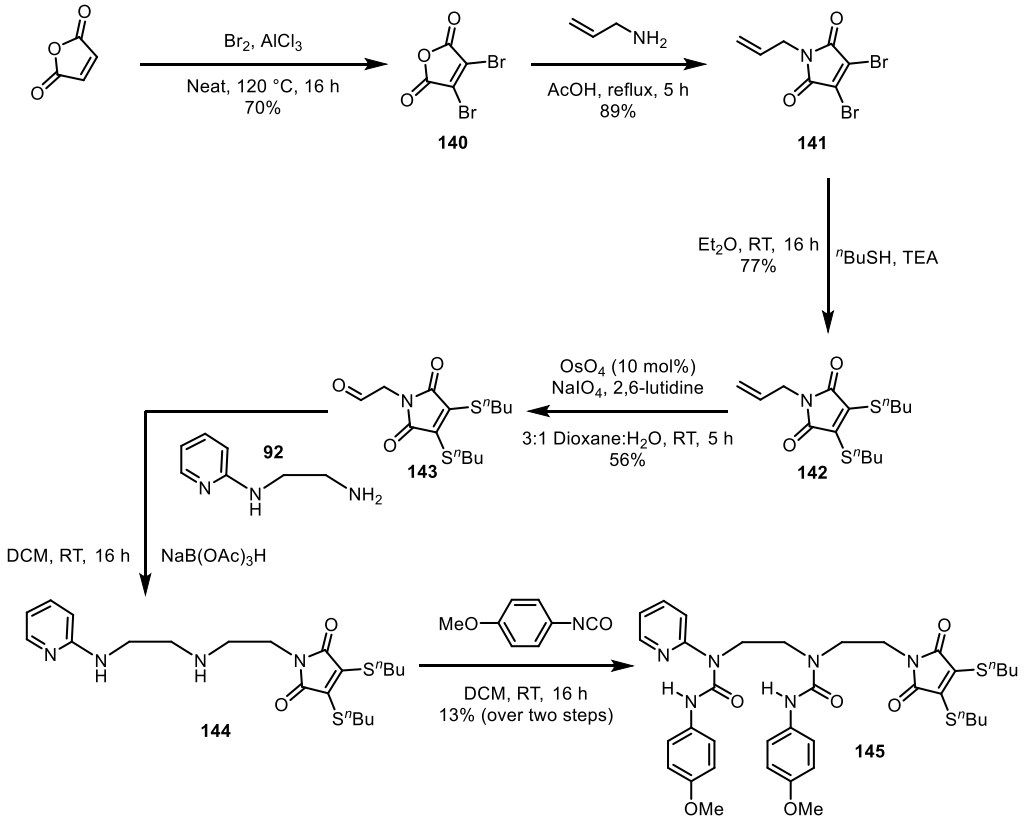

Scheme 41 – Synthesis of 145.

Maleic anhydride underwent a twofold dibromination/elimination cascade to give dibromomaleic anhydride **140** in good yield. The anhydride was then used to acylate allylamine and underwent a ring-closing condensation in acetic acid to give the corresponding allyl maleimide in excellent yield.[103] **141** then underwent twofold bromide substitution using *n*-butanethiol to provide **138**, and subsequent Lemieux-Johnson oxidation of **142** furnished aldehyde **143** in moderate yield over two steps. With an electrophilic source of the DTM acquired, **92** underwent a reductive alkylation with **143** and $NaB(OAc)_3H$ to prevent potential overreduction

of the imide, giving amine **144**. The crude product was then reacted with 4-methoxyphenyl isocyanate to give the desired diurea **145** in poor yield over two steps. To ensure that **145** behaved analogously to pyridyl urea **97** and did not decompose under acidic conditions, TFA was titrated into **145** (Figure 67).

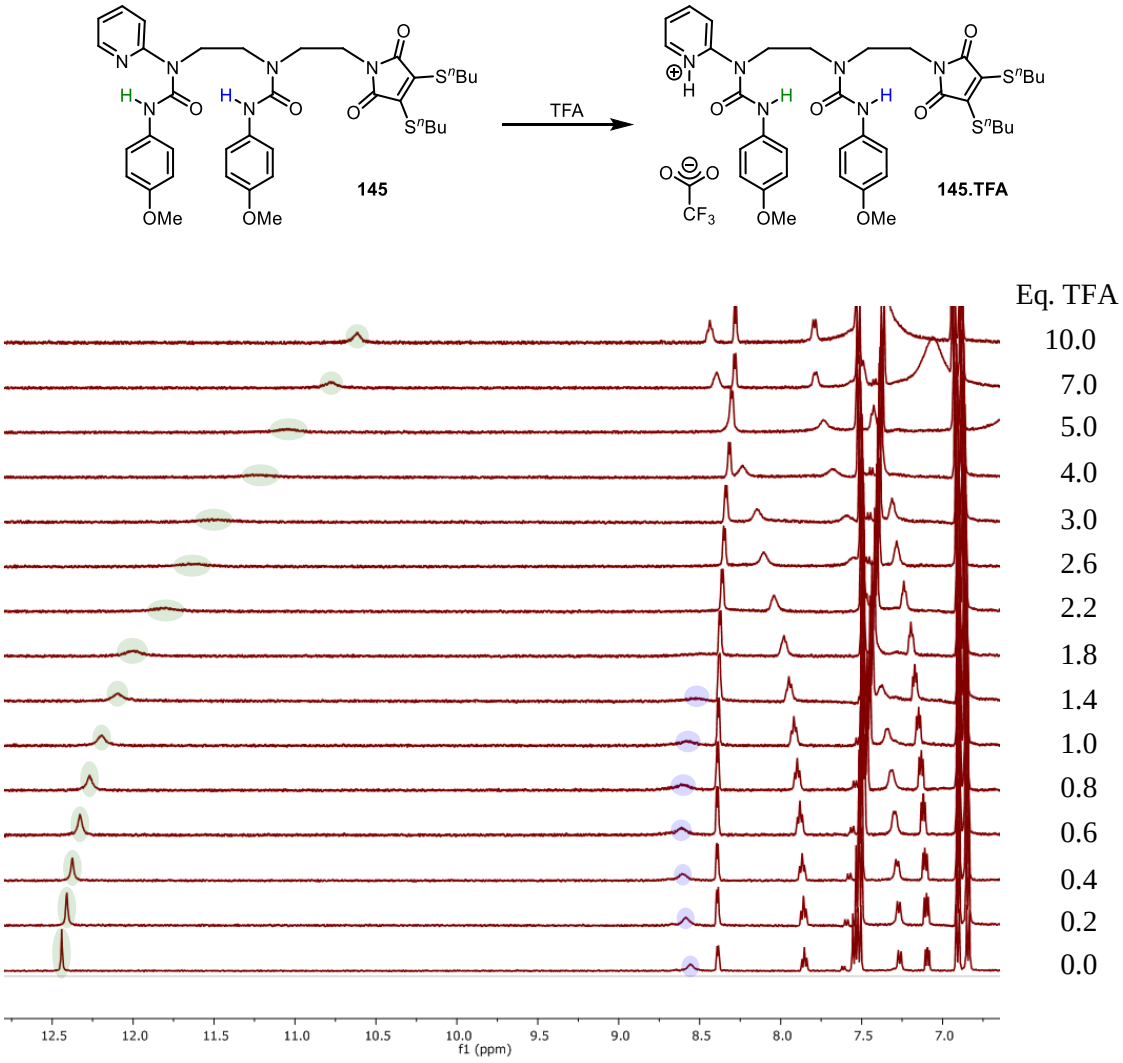

Figure 67 – Titration of TFA into 145 (6.50-13.00 ppm region, CD_2Cl_2, 500 MHz, 14 mM).

In its neutral form, pyridyl urea **145** displayed signals at 7.09 (pyridine *meta* methine), 7.26 (pyridine *meta* methine), 7.85 (pyridine *para* methine), 8.39 (pyridine *ortho* methine), 8.56 (rightmost ureido proton) and 12.44 ppm (pyridyl urea ureido proton). Upon addition of TFA, the signals at 7.09, 7.26 and 7.85 ppm all shifted downfield, broadened (losing their multiplicity) at 2.2 equivalents and sharpened at 10.0 equivalents. Conversely, the signal at 8.39 ppm shifted upfield with increasing TFA and maintained its multiplicity throughout. The signal at 8.56 ppm shifted downfield up to 0.6 equivalents of TFA, and then shifted downfield again, before broadening and becoming too broad to observe at 1.8 equivalents. Finally, the signal at 12.44 ppm shifted upfield as TFA was added. This signal also broadened but sharpened again at 5.0

equivalents. Fortunately, no signals corresponding to decomposition arose during the experiment. In its neutral form, the chemical shifts of the ureido protons agreed closely with that of **97**, indicating uniform directionality in the desired fashion. These data were consistent with protonation of the pyridine due to the relative shifting of their signals.

Much like the case of pyridyl urea **97**, the central ureido proton moved downfield and then upfield with increasing TFA. The pyridyl urea ureido proton shifted significantly upfield with increasing TFA, indicating directional switching taking place. These results were commensurate with that observed with triurea **97**, where superstoichiometric TFA was required to effect the directionality switch. This is explicable by the lack of basicity of the pyridyl ureas in triurea **97** and DTM **145** in DCM. A stoichiometric switch could be attained by using a more basic foldamer, a stronger acid such as TsOH.H_2O, or by using a solvent system where the pK_a of TFA is much lower than the pK_{aH} of pyridyl urea **145**.

At this point, analysis by ^{1}H NMR indicated that the DTM was stable in the presence of acid, and that protonation of pyridyl urea **145** resulted in a directionality switch. The ability of the DTM to detect this change was then investigated. A 1 mM solution of **145** was prepared in DCM, and its emission profile upon irradiation with 405 nm light was recorded (Figure 68).

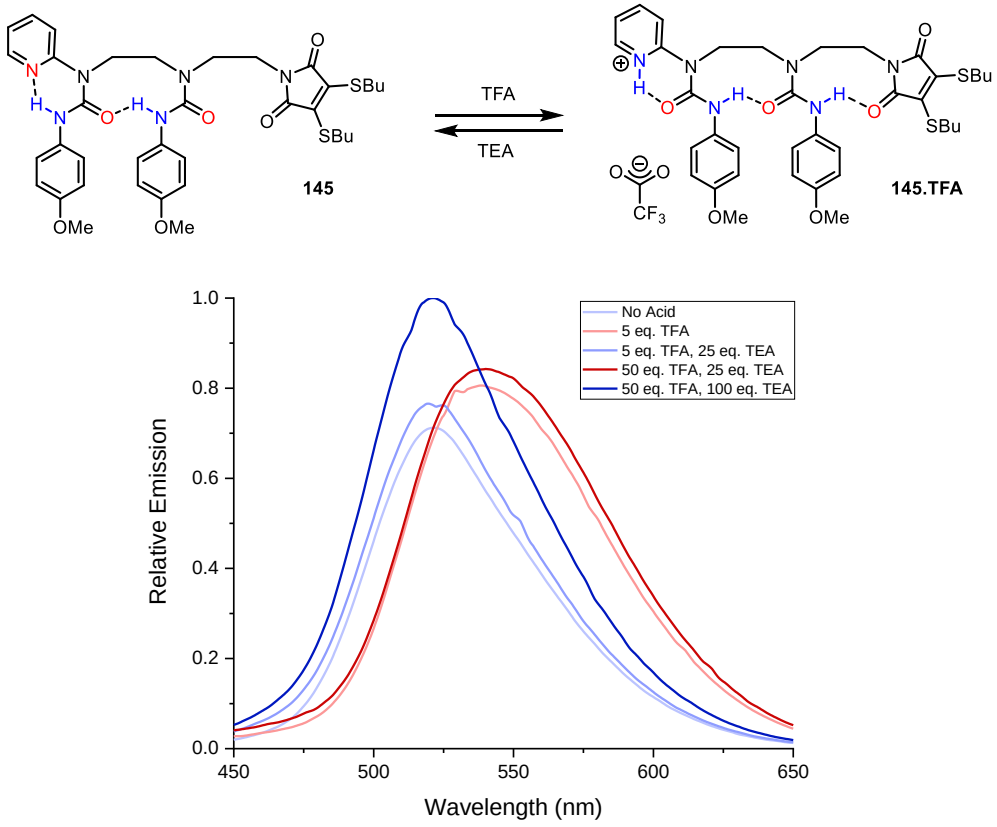

Figure 68 – Emission profile of 145 after addition of TFA/TEA (irradiation at 405 nm, ~1 mM).

In its neutral form, DTM **145** emitted with a nominal wavelength of 522 nm. After addition of 5.0 equivalents of TFA, this wavelength redshifted to 539 nm, accompanied by a hyperchromic shift. Addition of TEA returned the nominal wavelength to 522 nm and attenuated the signal. Excess addition of TFA relative to the TEA shifted the nominal wavelength to 539 nm and augmented the signal. Finally, addition of excess TEA relative to the TFA restored the nominal wavelength of 522 nm, associated with a large hyperchromic shift. It was presumed that the hyper- and hypochromic shifts were associated with sensitisation of the salts and differing quantum yields between the neutral and protonated species.[103] These results showed that upon protonation of the foldamer, the DTM formed a hydrogen bond with the proximate urea, resulting in a redshift of the emission wavelength. Deletion of this hydrogen bond upon treatment with base restored the original spectrum. This process was switched forwards and backwards twice, indicating robustness of the DTM in local directionality detection, and that directionality can be switched backwards and forwards in acid-sensitive oligoureas in the same pot without any detectable erosion of fidelity.

It was next desirable to ensure that the fluorescence change accompanying the directionality switch came from the formation of a hydrogen bond between the DTM and the adjacent urea. To this end, a 1 mM solution of DTM intermediate **142** was treated with TFA and the emission profile upon irradiation with 405 nm light was recorded (Figure 69).

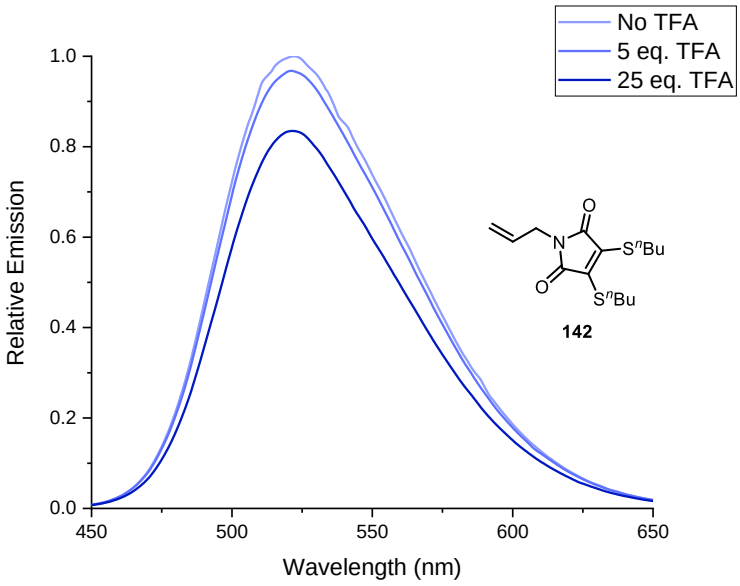

Figure 69 – Emission profile of 142 after addition of TFA (irradiation at 405 nm, ~1 mM).

In DTM **142**, the nominal wavelength observed upon irradiation with 405 nm light was at 522 nm. Interestingly, this was the same nominal wavelength as the neutral form of DTM **145**, where the DTM was not hydrogen bonded. Addition of TFA gave rise to no change in nominal wavelength of the DTM. Next, it was desirable to see if the presence of pyridinium cations and

trifluoroacetate anions, as would be present in **145**, gave rise to any fluorescence change in DTMs. A 1 mM solution of **142** was combined with an equivalent of pyridine and the emission profile upon irradiation with 405 nm light was recorded (Figure 70).

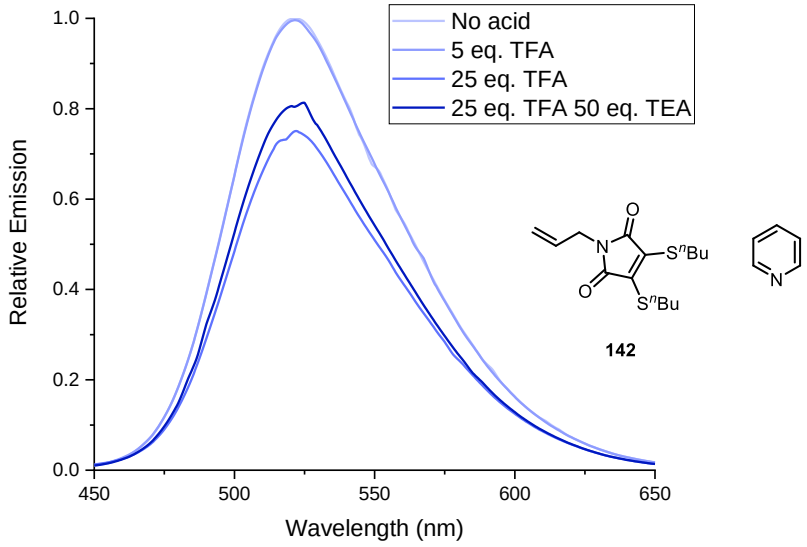

Figure 70 – Emission profile of 142/pyridine after addition of TFA (irradiation at 405 nm, ~1 mM).

Again, no change in nominal wavelength was observed in the **142**/pyridine mixture upon addition of TFA, nor when the TFA was neutralised with TFA. These experiments showed that the change in fluorescence of DTM **145** can be fully attributed to the formation of an intramolecular hydrogen bond between the DTM and its adjacent urea. The pyridine was cycled between protonated and neutral states twice, and each time the state was communicated through the oligourea scaffold effectively and the information was relayed to the DTM reporter.

To summarise, fluorimetry experiments have revealed that DTMs can be used as efficient reporters for local hydrogen-bond directionality in ethylene-bridged oligoureas without imparting any directionality bias. The DTM can be attached to the foldamer by coupling of an amine function with an electrophilic source of DTM, **142** under mild reductive alkylation conditions. The reporter is robust, and very sensitive to intramolecular effects as opposed to any intramolecular hydrogen bonding from HBDs such as TFA and triethylammonium trifluoroacetate at millimolar concentrations. It is notable that this phenomenon may be general, in that DTMs may be able to detect the presence of intramolecular HBDs in other systems as well. This development represents a significant advancement in the study of ethylene-bridged oligourea foldamers, as the hydrogen-bonding information can be relayed in a foldamer and be effectively reported at millimolar concentrations.

3.8 Hydrogen-Bond Directionality Switching by Anion Binding

Another desirable stimulus for informational communication is the binding of specific chemical species. Nature has recognised the utility of such an event and has evolved to utilise the spatially specific binding of certain ligands to communicate information and/or perform function. For example, porphyrins are highly prolific in biological systems due to their ability to bind transition metal cations. In the metalloprotein, haemoglobin, the exotic redox properties of iron porphyrins are harnessed to bind oxygen and carbon dioxide reversibly and transport them around the body.[104] When carbon dioxide is in high concentration, oxygenated haemoglobin undergoes a conformational change that lowers oxygen binding affinity, resulting in the release of oxygen from the haemoglobin. Conversely, in areas of high oxygen concentration, such as in the alveoli, the conformation of the haemoglobin shifts to increase oxygen binding affinity. Additionally, this initial oxygen binding results in further conformational change and renders oxygen binding cooperative. The haemoglobin can also be appended with specific amino acid residues meaning that they will capture and release carbon dioxide and oxygen at highly specific sites.

Previous work by Clayden and co-workers has shown that *N*-3,5-bis(trifluoromethyl)phenyl-*N*'-alkyl ureas are very strong HBDs, which can hydrogen bond favourably to alkyl ureas intramolecularly. Alkyl ureas are weaker HBDs than their analogous aryl ureas due to a lack of electron-density delocalisation into the arene. However, if the *N*-3,5-bis(trifluoromethyl)phenyl urea can form a stronger intermolecular hydrogen bond, then its directionality may switch and force the adjacent alkyl urea to act as an HBD (Scheme 42).* This effect did not translate to aryl ureas, as their hydrogen-bond-donating/accepting abilities were comparable to the *N*-3,5-bis(trifluoromethyl)phenyl urea such that directionality was not completely controlled by the *N*-3,5-bis(trifluoromethyl)phenyl urea.

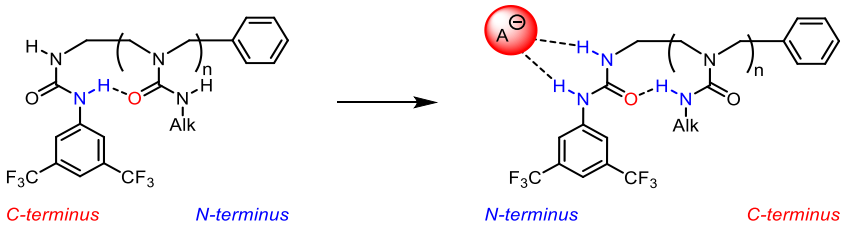

Scheme 42 – Directionality switching using anions.

As a continuation of the study of anion binding to ethylene-bridged oligourea, the aim of this work was to extend the concept to foldamers where the anion binding event would communicate through the foldamer and be read out by the previously designed DTM fluorescent

* Work performed by Dr David Tilly.

reporter. This was done to ensure that the DTM could read out hydrogen-bonding information in response to remote stimuli other than the presence of acid. Initially, it was desirable to ascertain if alkyl ureas were conducive to communication through the ethylene-bridged oligourea scaffold, and if they also exhibited uniform directionality. Triurea, **146** was made by reaction of **44** with *n*-butyl isocyanate (Scheme 43).

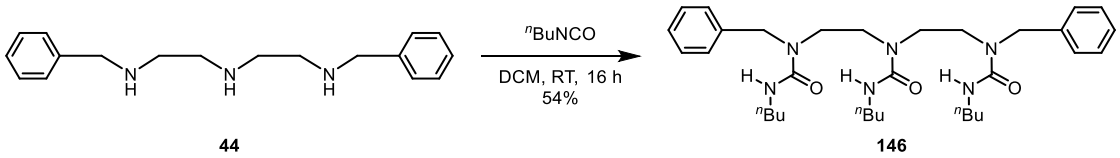

Scheme 43 – Synthesis of 146.

Triurea **146** was then studied by VTNMR (Figure 71).

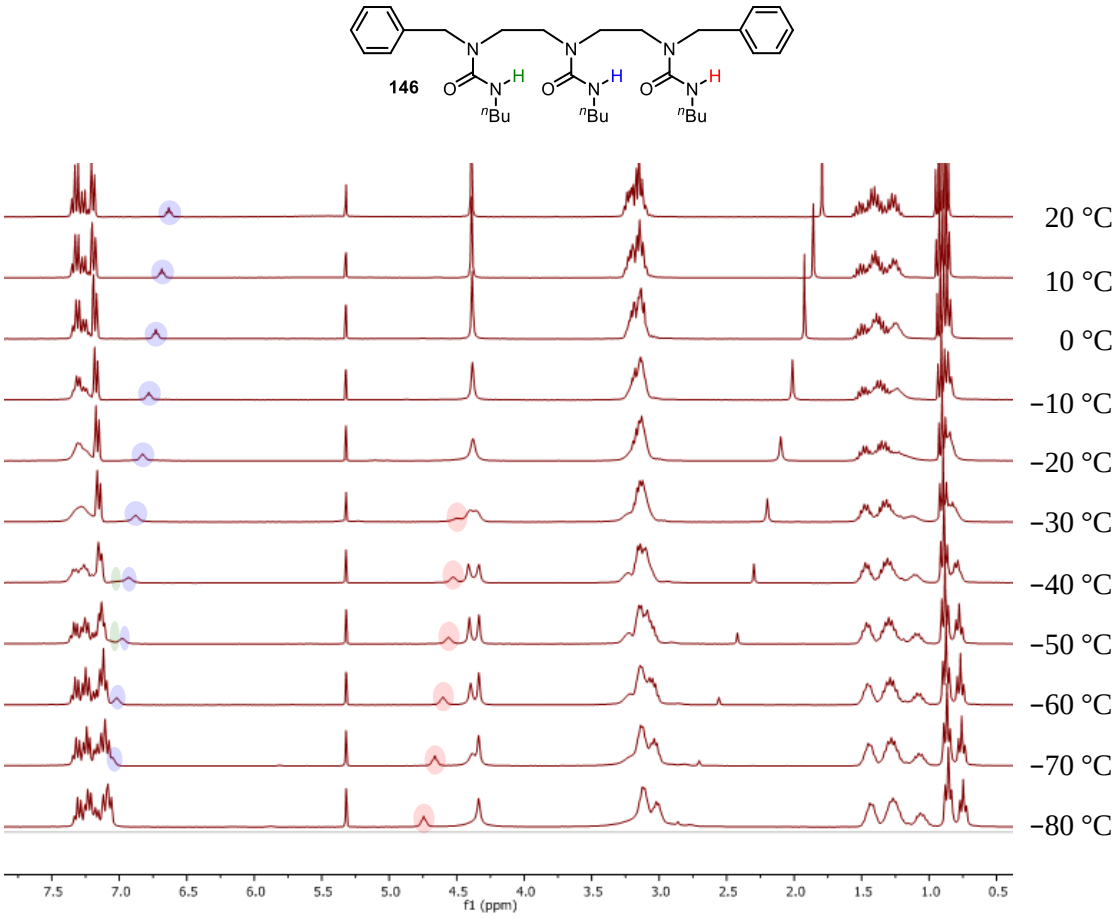

Figure 71 – VTNMR of 146 (CD_2Cl_2, 300 MHz, 17 mM).

Triurea **146** displayed signals at 4.39 (benzylic methylenes) and 6.63 ppm (central ureido proton) at 20 °C. Upon cooling, the signal at 4.39 ppm broadened and decoalesced into two singlets (2 H each) at −30 °C. The signal at 6.63 ppm shifted downfield with decreasing temperature. At −30 °C, additional signals appeared at 4.49 (1 H) and 6.92 ppm (1 H, broad and

overlapping) and shifted downfield upon further decreasing the temperature. These data indicated that **146** exists as one conformation of uniform directionality, where the directionalities interconvert between each other slowly on the NMR timescale below −30 °C. This is supported by the chemical shifts, where one ureido proton is not hydrogen bonded (4.49 ppm at −30 °C) and two of them are (6.88 and 6.92 ppm at −30 °C). It can be inferred from this that alkyl ureas are fully conducive to intramolecular hydrogen bonding in ethylene bridged oligoureas in apolar solvents. Eyring analysis of **146** revealed a $\Delta G^{\ddagger}_{298\ K}$ (CD_2Cl_2) of 57.9 kJ mol^{-1}, a value commensurate with that of the analogous tris(aryl urea), **45**. Alkyl ureas are weaker HBDs but stronger HBAs than their corresponding aryl ureas, so this result shows that these effects approximately cancel each other from a kinetic perspective.

Aryl ureas may also be present in the proposed anion-sensitive directional switch, so it was also desirable to investigate the effects on the thermodynamics of mixed alkyl/aryls ureas. To this end, triurea **151** was synthesised (Scheme 44).

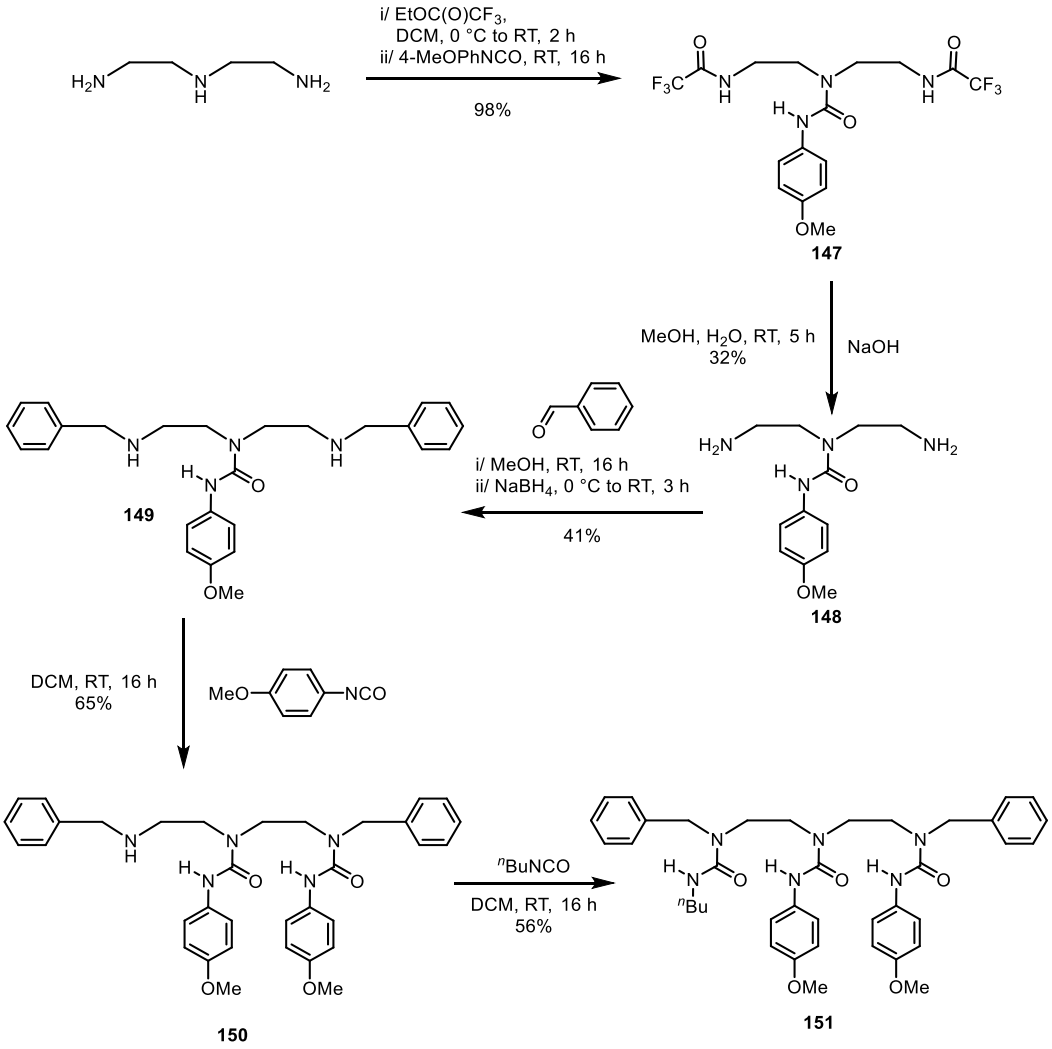

Scheme 44 – Synthesis of 151.

Diethylenetriamine underwent twofold trifluoroacetylation at the primary amines, and the secondary amine was reacted with 4-methoxyphenyl isocyanate to give the corresponding monourea, **147** in excellent yield. The trifluoroacetamides were hydrolysed and the diamine **148** was isolated in poor yield. Loss of product may have occurred due to water solubility of the product during purification. Twofold reductive alkylation using benzaldehyde gave diamine **149** in poor yield. Installation of one urea proceeded in good yield, and a final alkyl urea was formed using *n*-butyl isocyanate, affording the target triurea **151** in moderate yield. **151** was then analysed by VTNMR (Figure 72).

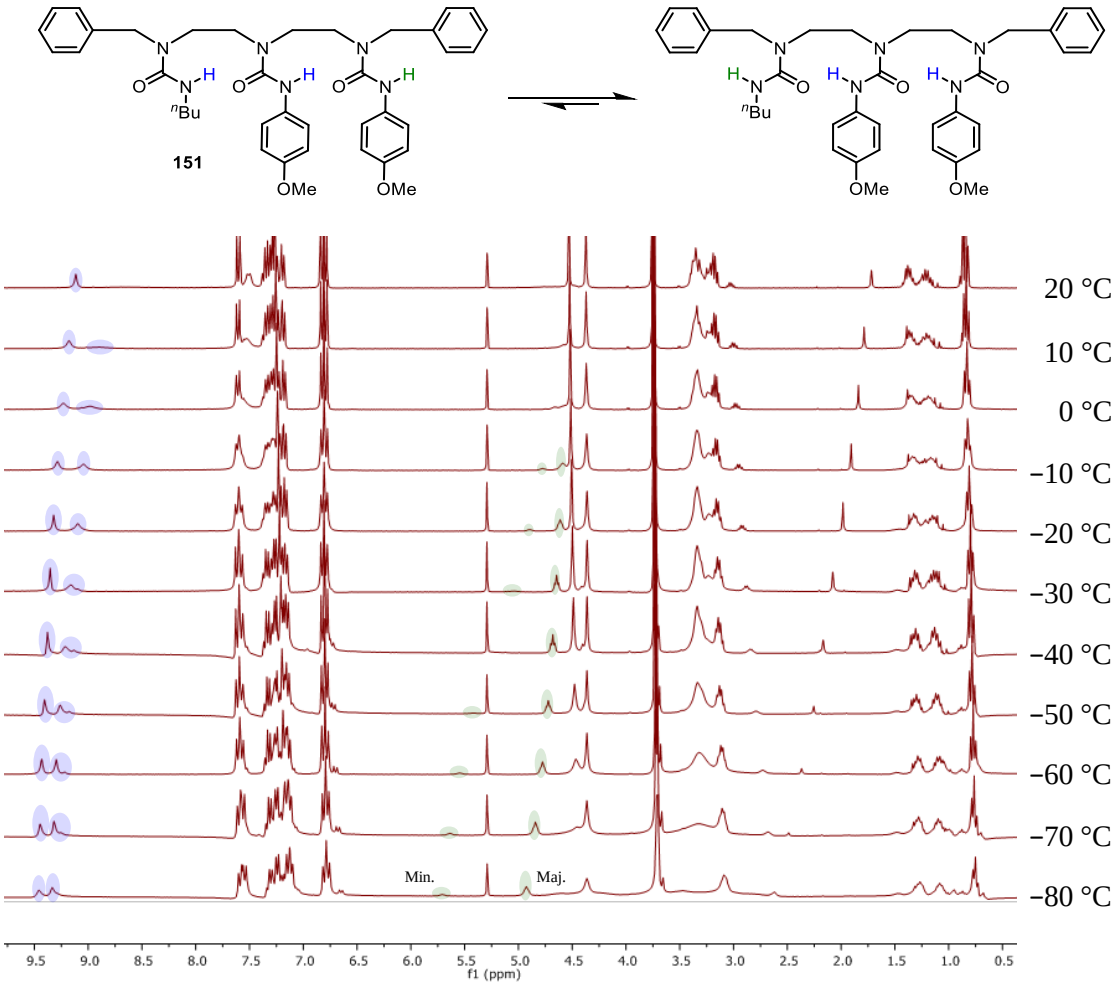

Figure 72 – VTNMR of 151 (CD_2Cl_2, 300 MHz, 15 mM).

Triurea **151** displayed signals at 4.37 (alkyl urea benzylic methylene), 4.53 (aryl urea benzylic methylene), 8.65 (peripheral aryl urea ureido proton) and 9.11 ppm (central ureido proton) at 20 °C. Upon cooling, the signal at 4.37 ppm stayed approximately constant until it broadened at −20 °C and decoalesced into two singlets (0.30 H and 1.70 H) at −30 °C. The signal at 4.53 ppm broadened until it could not be observed at −80 °C. The signals at 8.65 (very broad) and 9.11 ppm sharpened and shifted downfield with decreasing temperature. At −10 °C, signals

appeared at 4.59 (0.85 H) and 4.77 ppm (0.15 H), which sharpened and shifted downfield upon further decreasing the temperature. Another signal appeared at 9.10 ppm (0.15 H) at −30 °C, which shifts downfield with further cooling. These data indicated that **151** exists as two conformations populated in a 85:15 ratio at −60 °C. These conformations are the two directionalities, and the major conformer is the directionality where the *n*-butyl urea is at the N-terminus. This is evidenced by the observable decoalescence of the alkyl urea benzylic methylene into two signals in a 85:15 ratio. At −60 °C, the two conformers are in slow exchange on the NMR timescale, and so three ureido protons can be observed for each. For the major conformer, there is a non-hydrogen bonded alkyl ureido proton (4.78 ppm, 0.85 H), and two aryl ureido protons that are (9.30 and 9.43 ppm, 0.85 H each). For the minor conformer, there is an alkyl ureido proton in hydrogen bonding (5.55 ppm, 0.15 H) and an aryl ureido proton in hydrogen bonding (9.21 ppm, 0.15 H). There should also be a non-hydrogen-bonded peripheral aryl ureido proton around 6.50 ppm but this was not observed, presumably as a result of exchange processes with trace water in the sample.

It was shown by triurea **151** that alkyl ureas can significantly perturb the equilibrium distribution of directionalities in otherwise aryl-substituted oligoureas. Due to the difference in hydrogen-bonding properties of these two types of urea, it was proposed that external HBAs could also significantly change the conformer distribution. To investigate this, triurea **151** was studied by VTNMR using 10% v/v d_6-DMSO as a competitive HBA (Figure 73).

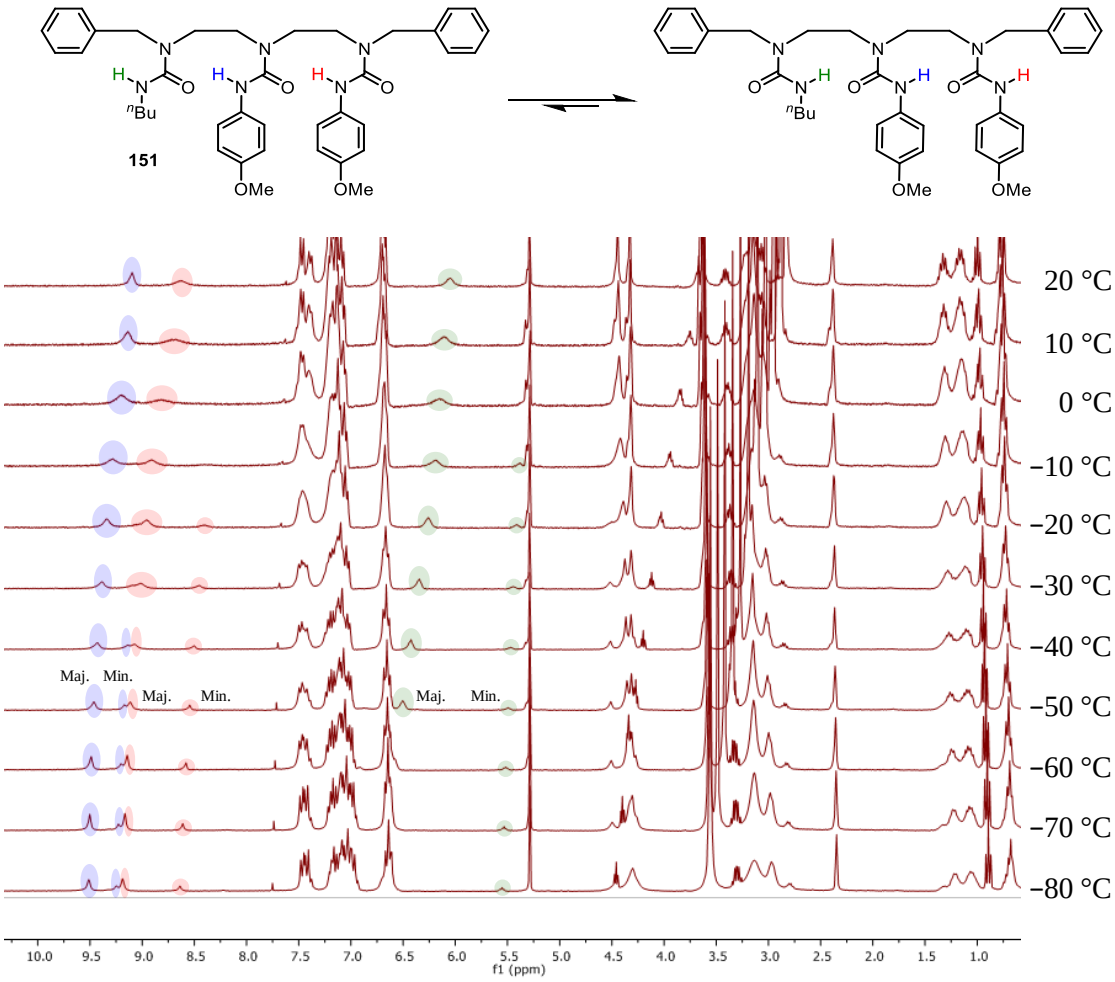

Figure 73 – VTNMR of 151 (10% v/v d_6-DMSO in CD_2Cl_2, 300 MHz, 15 mM).

In triurea **151**, signals were shown at 4.33 (alkyl urea benzylic methylene), 4.44 (aryl urea benzylic methylene), 6.05 (alkyl urea ureido proton), 8.62 (peripheral aryl urea ureido proton) and 9.09 ppm (central ureido proton) at 20 °C. Upon cooling, the signal at 4.33 ppm broadened throughout the experiment. The same was observed for the signal at 4.44 ppm but it also moved upfield. The signals at 6.05, 8.62 and 9.09 ppm shifted downfield with decreasing temperature. Additional signals appeared at 5.38 (0.30 H), 8.38 (0.30 H) and 9.07 ppm (0.30 H) at −10 °C, which sharpened and shifted downfield upon further cooling. These observations can be explained by the population of two conformers in a 70:30 ratio. This was not elucidated by an observable decoalescence of the benzylic methylene signals but could be inferred from the chemical shifts and relative integrations of the ureido protons. The two conformers corresponded to the two directionalities and in each case, d_6-DMSO hydrogen bonded to the exposed ureido proton. At slow exchange, each of the two conformers contain three ureido protons. In one directionality, the *n*-butyl urea acts as an intramolecular HBA, forcing the other two aryl ureido protons into intramolecular hydrogen bonding and leaving its own ureido proton to hydrogen bond to d_6-DMSO. This is shown by the signals at 5.52 (alkyl urea ureido proton, 0.30 H), 8.58 (peripheral

aryl urea ureido proton, 0.30 H) and 9.20 ppm (central ureido proton, 0.30 H) at −60 °C. This also identifies this directionality as the minor conformer. In the other directionality (the major conformer), where the *n*-butyl urea acts as an intramolecular HBD, one of the aryl ureas is in an intramolecular hydrogen bond and the other an intermolecular hydrogen bond with d_6-DMSO. This shows signals at 6.58 (alkyl urea ureido proton, 0.70 H), 9.18 (peripheral aryl urea ureido proton) and 9.49 ppm (central ureido proton) at −60 °C. This is a particularly pertinent result as it shows that triurea **151** can change, and even invert its ratio of directionalities upon introduction of a hydrogen-bond-accepting additive. Crucially, it has also been shown that all-alkyl and alkyl/aryl mixed oligoureas still exhibit uniform directionality, although the differing hydrogen-bonding properties of alkyl and aryl ureas can play a crucial role in hydrogen-bond strength.

Now that it had been shown that the oligourea scaffold was conducive to mixtures of alkyl and aryl ureas, a target fluorescent anion-sensitive foldamer **154** was pursued. DTM **154** was synthesised by reductive alkylation and urea formation on amine **152**, which proceeded in reasonable yield over the two steps (Scheme 45, n = 1, R = ^{n}Bu).

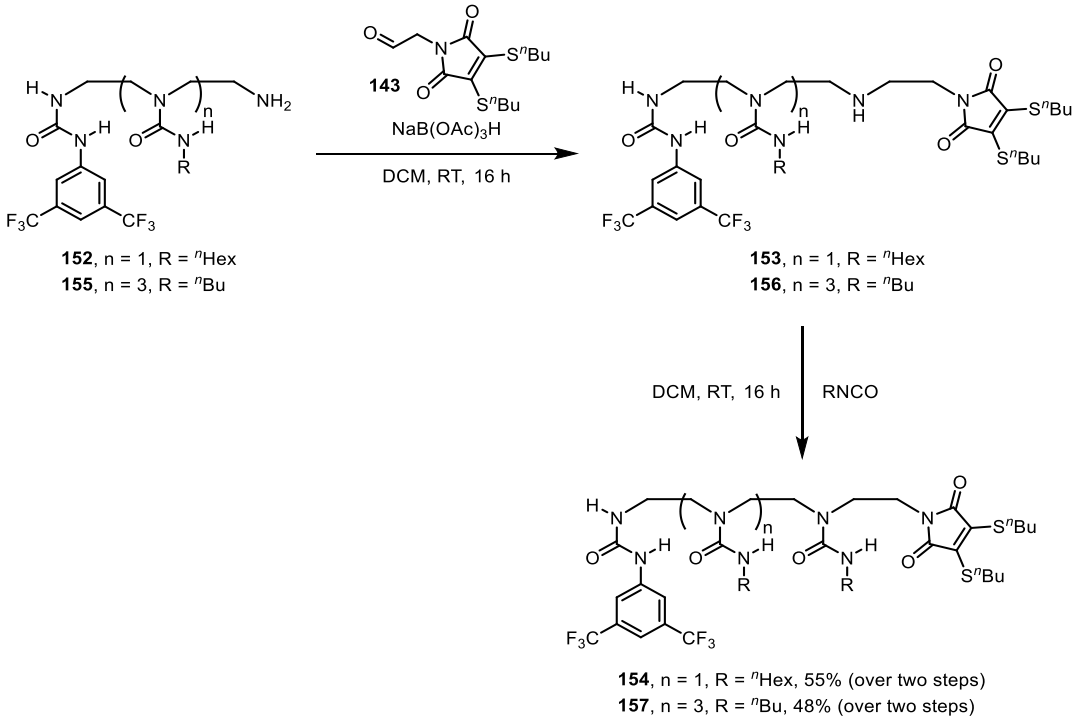

Scheme 45 – Synthesis of 154 and 157.

A 1 mM solution of DTM **154** was then analysed by fluorimetry and various anionic ligands were added (Figure 74). A tetrabutylammonium cation was used in each case to promote solubility in DCM. Solubility was further bolstered by a diphenylphosphate anion in the case of the phosphate (Figure 74c).

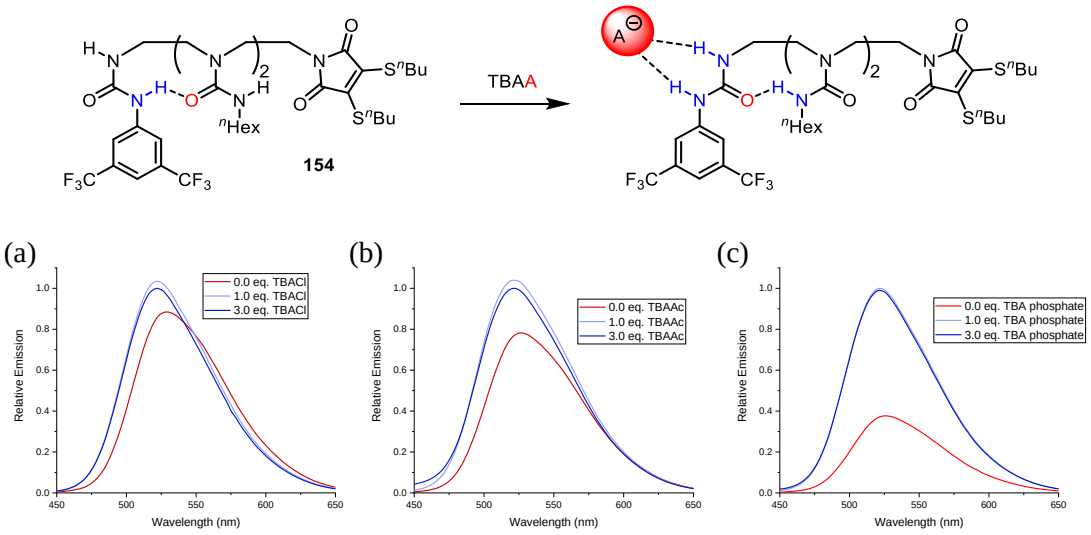

Figure 74 – Emission profiles of 154 after addition of anionic ligands (a) TBACl (b) TBAAc (c) TBA diphenylphosphate (irradiation at 405 nm, ~1 mM).

Before ligand addition, DTM **154** exhibited fluorescence at 529 nm. In each case, one equivalent of the tetrabutylammonium salt resulted in a blueshifting of the nominal wavelength to 522 nm. Further addition of tetrabutylammonium salt resulted in an attenuation of the signal but remained otherwise constant. These results indicated that in each case, the DTM starts in a hydrogen-bonded state, hence its deviation from the non-hydrogen-bonded state emission, 522 nm. The blueshift relative to the non-hydrogen-bonded state is much less than that of DTM **145** ($\Delta\lambda$ = 17 nm vs 7 nm), which is attributed to the fact that the alkyl urea is hydrogen bonding to the DTM. This is a weaker HBD, and so the DTM will form a weaker hydrogen bond with it and be less affected. After addition of one equivalent of tetrabutylammonium salt, the emission profiles centred about 522 nm, indicating that the DTM was no longer hydrogen bonding and that a successful directionality switch had taken place. To ensure switching orthogonality in the different fluorescent switches, DTMs **142** and **145** were exposed to the various tetrabutylammonium salts, resulting in no nominal wavelength shift (see Appendix, section 8.4).

Next, an analogous DTM **157** was synthesised in which the directionality switch was to be transmitted over four ureas. **157** was made in the same manner as amine **154** using amine **155** and *n*-butyl isocyanate (Scheme 45, n = 3, R = ^{n}Hex). TBAAc was then titrated into a 1 mM sample of DTM **157** and analysed by fluorimetry (Figure 75).

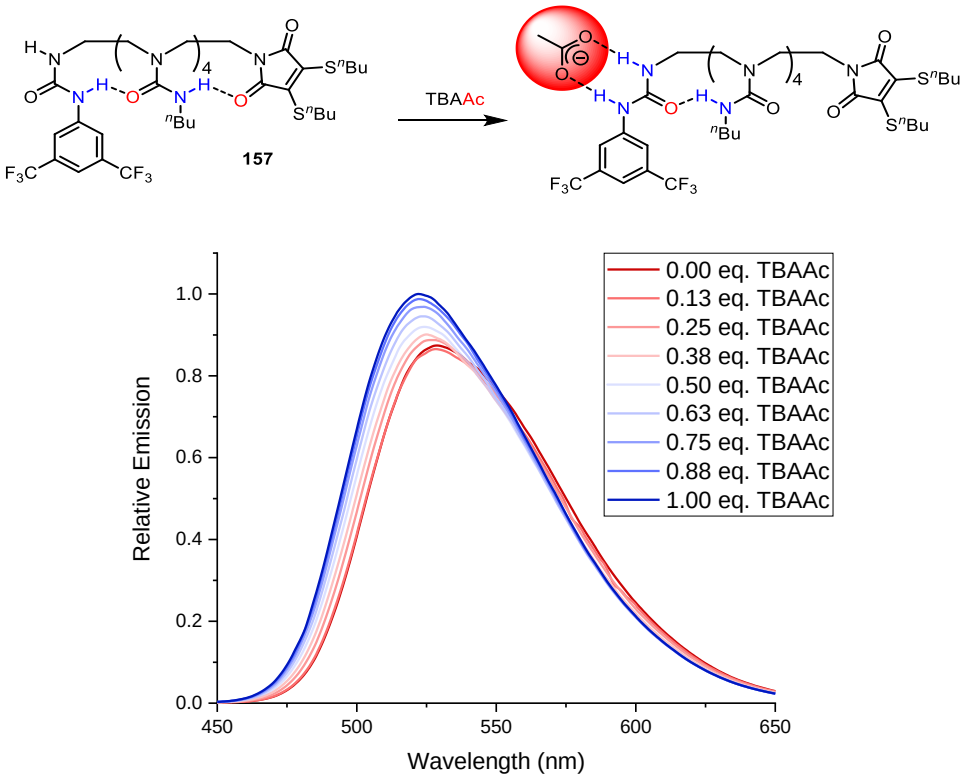

Figure 75 – Titration of TBAAc into 157 (irradiation at 405 nm, ~1 mM).

Before ligand addition, DTM **157** showed a nominal wavelength of 529 nm. Titration of TBAAc into **157** blueshifted the profile accompanied by a hyperchromic shift to arrive at a nominal wavelength of 522 nm at 1.00 equivalents of TBAAc. This experiment also showed that the DTM in **157** was also hydrogen bonding to its proximate urea, but it was switched out of hydrogen bonding upon addition of TBAAc. This was consistent with a directionality switch taking place at the *N*,*N'*-disubstituted urea binding site, which was communicated through four ureas and reported by the DTM.

To further demonstrate switching orthogonality and the efficacy of the DTM in reporting it, DTMs **142**, **145** and **157** were each treated with TFA and TBAAc and the change in their fluorescence was recorded (Table 2). The extent of DTM hydrogen bonding was qualitatively determined by calculating the ratio of the emission at 529 (hydrogen-bonded) to 522 nm (non-hydrogen-bonded) as acid/ligand was added.

Table 2 – Switching orthogonality in ethylene-bridged oligoureas as reported by a DTM.

Function	Acid	Acetate
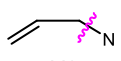 **142**	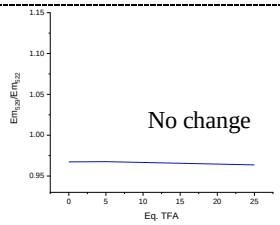	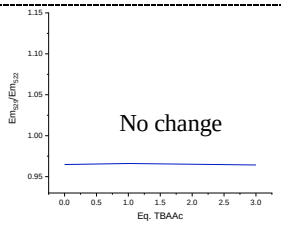
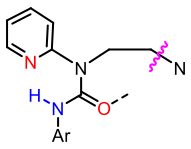 **145**	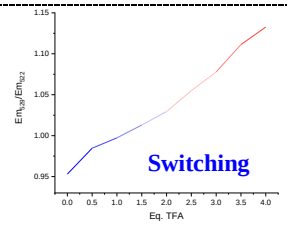	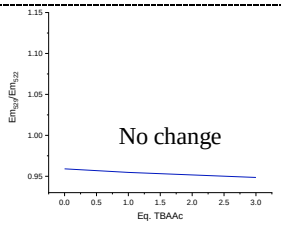
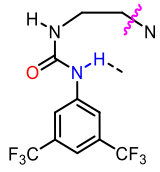 **157**	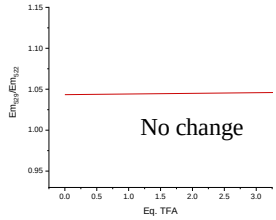	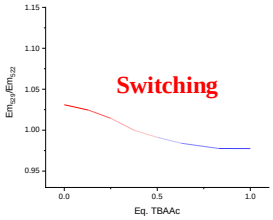

The DTM in **142** did not form hydrogen bonds, which did not change upon addition of TFA or TBAAc. Pyridyl urea **145** responded to TFA by switching the DTM into hydrogen bonding but did not respond to TBAAc. Conversely, *N*,*N'*-disubstituted urea **157** was insensitive to TFA but switched the DTM out of hydrogen bonding upon addition of TBAAc.

Foldamers terminated with a *N*-3,5-bis(trifluoromethyl)phenyl-*N'*-alkyl urea can control directionality in ethylene-bridged oligourea foldamers, which can be reported by a fluorescent DTM at the opposite end of the foldamer. Three different anions (chloride, acetate and diphenylphosphate) were shown to coordinate to the *N*-3,5-bis(trifluoromethyl)phenyl-*N'*-alkyl urea and switch the directionality, which can be detected by a change in fluorescence at millimolar concentrations. This further confirms the robustness of the DTM reporter in detecting local directionality changes and indicates that the strength of the hydrogen bond can be qualitatively inferred from the relative redshift of the DTM emission in the hydrogen-bonded state. The detection of anions such as chloride, acetate and phosphate and subsequent communication over four ureas lends further weight to the versatility of the scaffold. The results discussed here suggest that biological molecules bearing a negative charge can be used to communicate information through the oligourea foldamer and result in a directionality change. This method could be developed further to make the anion-binding site more anion-specific to achieve foldamers sensitive to different biomolecules.

3.9 Inducing a Fault in the Hydrogen-Bonding Network

Thus far, all the compounds studied have the whole length of oligourea in exclusively one hydrogen-bond directionality, even if the two modes are in exchange, and so there has been no observed disruption to the hydrogen-bonding network. Intermolecular hydrogen-bonding additives such as d_6-DMSO and Schreiner's thiourea imparted no observable disruption. When the reporting end of the foldamer is appended with biomimetic functions, it is likely they will contain hydrogen-bonding groups themselves, which could damage hydrogen-bonding fidelity in the scaffold and wither the efficacy of the function it was designed to perform. Hence, it was desirable to know what electronic properties would be necessary to disrupt the 9-membered hydrogen-bonding rings in an intramolecular fashion.

The beginning of this investigation involved synthesising and studying diureas which had directionality-controlling groups on both ends, each vying for control of directionality. If uniform directionality prevailed, this would leave one of the controlling groups unsatisfied. Therefore, the only way to satisfy both directionality-controlling groups would be to induce a fault in the hydrogen-bonding network. The initial substrate chosen was a diurea with terminal succinimides. The disuccinimidyl diurea, **160** (Scheme 46) could either fault in the centre, where the ureas would not hydrogen bond with each other, or next to one of the succinimide groups, where one succinimide would not hydrogen bond. This structure was contrived such that fault induction in the centre would cause the diurea to fault symmetrically, but if it occurred next to one of the succinimides, it would do so unsymmetrically. These forms would be identifiable by ^{1}H NMR and so VTNMR could be used to detect a fault and the degree to which it was present.

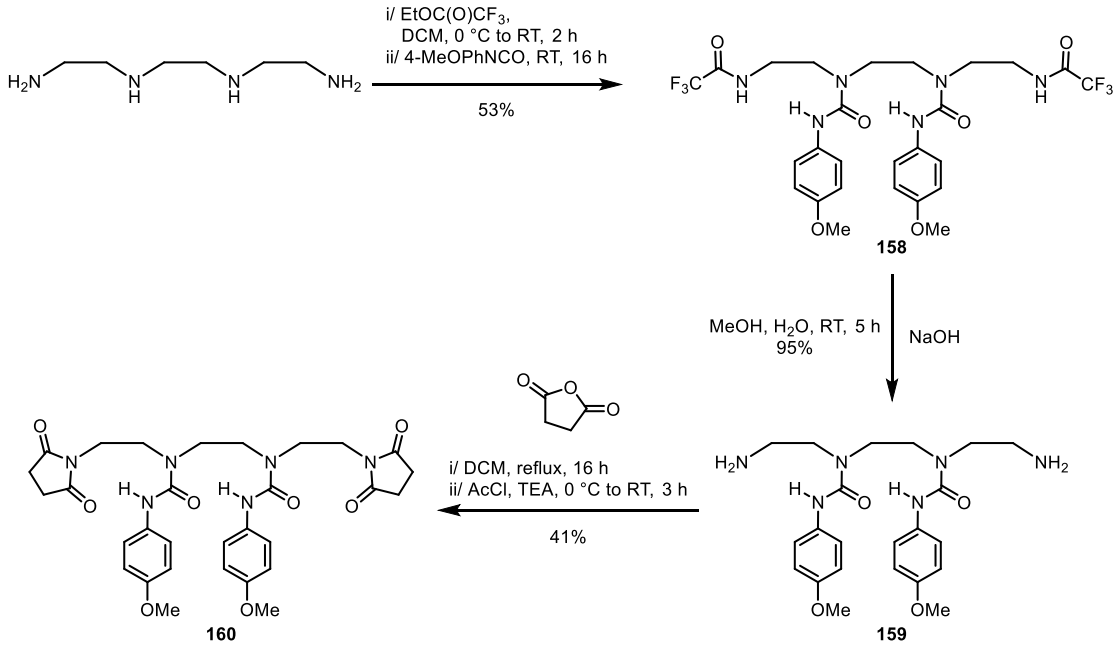

Scheme 46 – Synthesis of 160.

Disuccinimide **160** was synthesised from triethylenetetramine by trifluoroacetamide protection and urea formation to give bis(trifluoroacetamide) **158** in moderate yield. The trifluoroacetamides were hydrolysed, and the corresponding amines were reacted with succinic anhydride followed by acetyl chloride to give disuccinimide **160** in reasonable yield over two steps. Disuccinimide **160** was then studied using VTNMR (Figure 76).

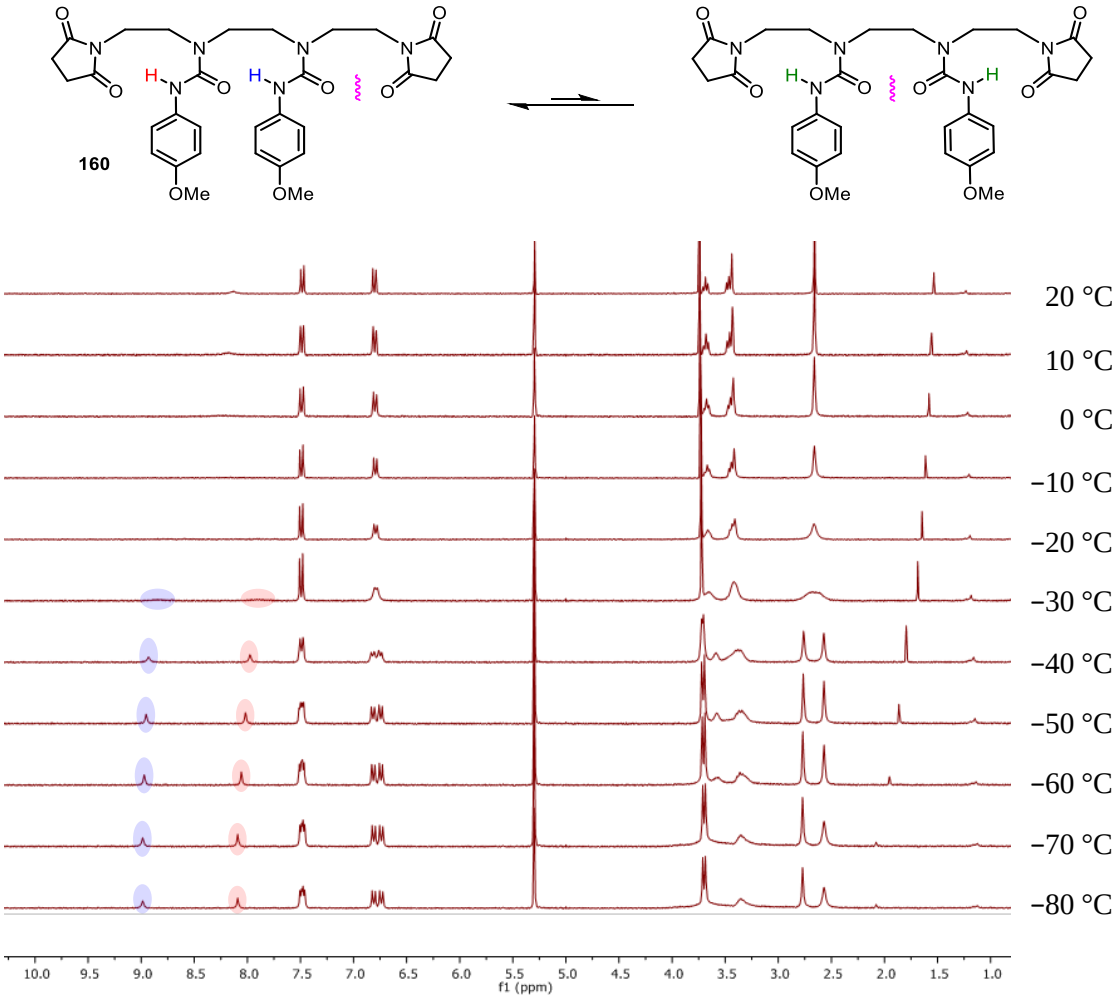

Figure 76 – VTNMR of 160 (CD_2Cl_2, 300 MHz, 16 mM).

Disuccinimide **160** displayed signals at 2.66 (succinimidyl methylenes) and 8.13 ppm (ureido protons) at 20 °C. Upon cooling, the signal at 2.66 ppm broadened and decoalesced into two equal singlets at −40 °C, where one of the singlets sharpened upon further decreasing the temperature and the other broadened. The signal at 8.13 ppm broadened with decreasing temperature and decoalesced into two equal singlets at −30 °C, which shifted downfield with further cooling. These results indicated the presence of one populated conformer, where no fault in hydrogen bonding between the ureas had been induced. This was concluded by the decoalescence, as at slow exchange, one of the succinimides is in hydrogen bonding and the other one is not. At slow exchange, two ureido proton resonances are observed, one corresponding to a ureido proton hydrogen bonding to a succinimide (8.06 ppm at −60 °C) and a ureido proton hydrogen bonding to the other urea (8.97 ppm at −60 °C). It can be concluded from this that succinimides are not strong enough HBAs to disturb the inter-urea hydrogen bonding to any observable degree. This is consistent with the observation in pyridyl urea **145** that the DTM does not strongly oppose the conformational preference induced by the pyridine.

To impart a fault in inter-urea hydrogen bonds, compounds with increased hydrogen-bond-accepting power were proposed. In tetraurea **161** (Figure 77), the succinimides were replaced with tetrasubstituted ureas, which are expected to be of similar hydrogen-bond-accepting power to the trisubstituted ureas. Bis(pyridine) **162** has the tetrasubstituted ureas of **161** replaced with 2-pyridyl groups, which is expected to be of greater hydrogen-bond-accepting power than the trisubstituted ureas.

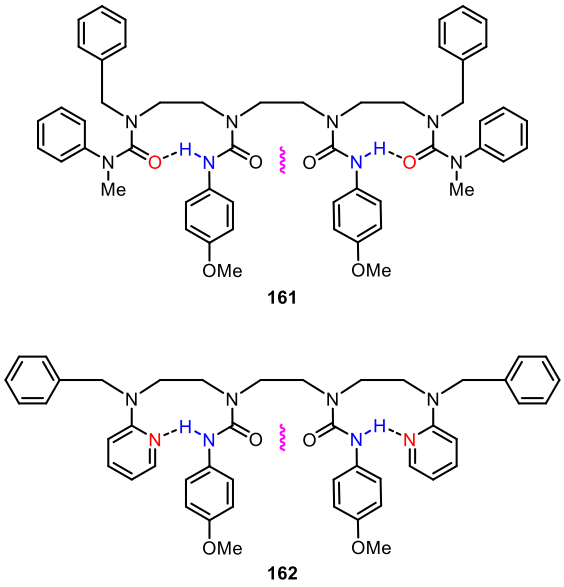

Figure 77 – Fault-inducing substrates, 161 and 162.

An initial investigation into the synthesis of **161** and **162** involved the derivatisation of diamine **159** (Scheme 47).

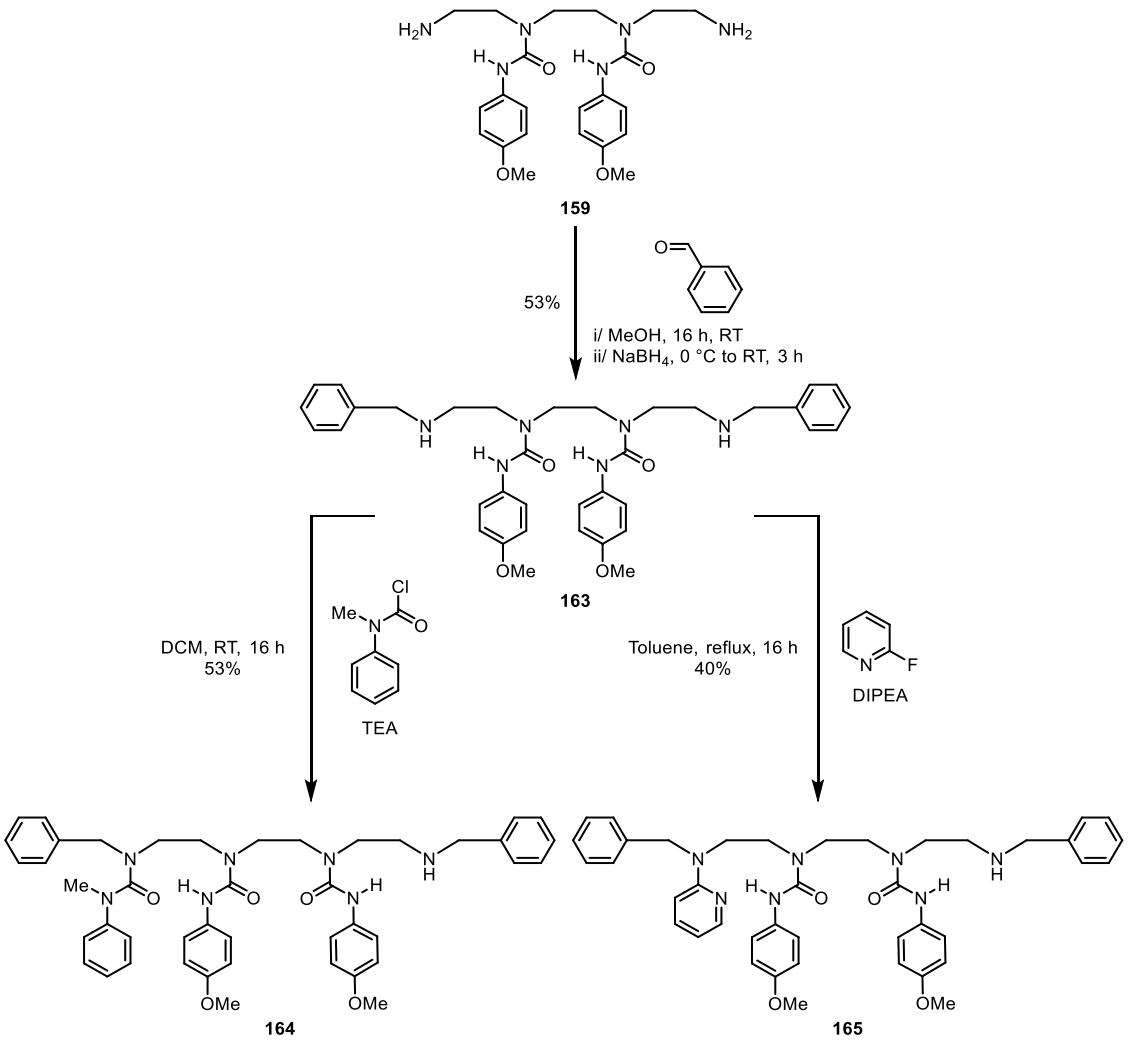

Scheme 47 – Attempted syntheses of fault-inducing substrates.

Dibenzylation of diamine **159** proceeded in moderate yield to give diamine, **163**, which was then reacted with *N*-methyl-*N*-phenylcarbamoyl chloride. This afforded none of the desired substrate, **161**. Instead, the monosubstituted triurea **164** was isolated in 53% yield. It was speculated that upon formation of the first urea, the resultant tetrasubstituted urea and the remaining secondary amine competed for directional control. The secondary amine is a stronger HBA than the tetrasubstituted urea, so the amine formed a strong hydrogen bond with the adjacent urea, inhibiting its nucleophilicity and stopping the reaction. Repeating the reaction in refluxing DCE saw no further conversion of the triurea. Similar effects were observed when attempting twofold S_NAr on **163** with 2-fluoropyridine, where monosubstitution proceeded in 40% yield, giving **165** with no conversion to the desired disubstituted product. To combat this issue, the ureas were attached after the directionality-controlling groups had been formed, such that the amines would not form hydrogen bonds and would therefore be more nucleophilic (Scheme 48).

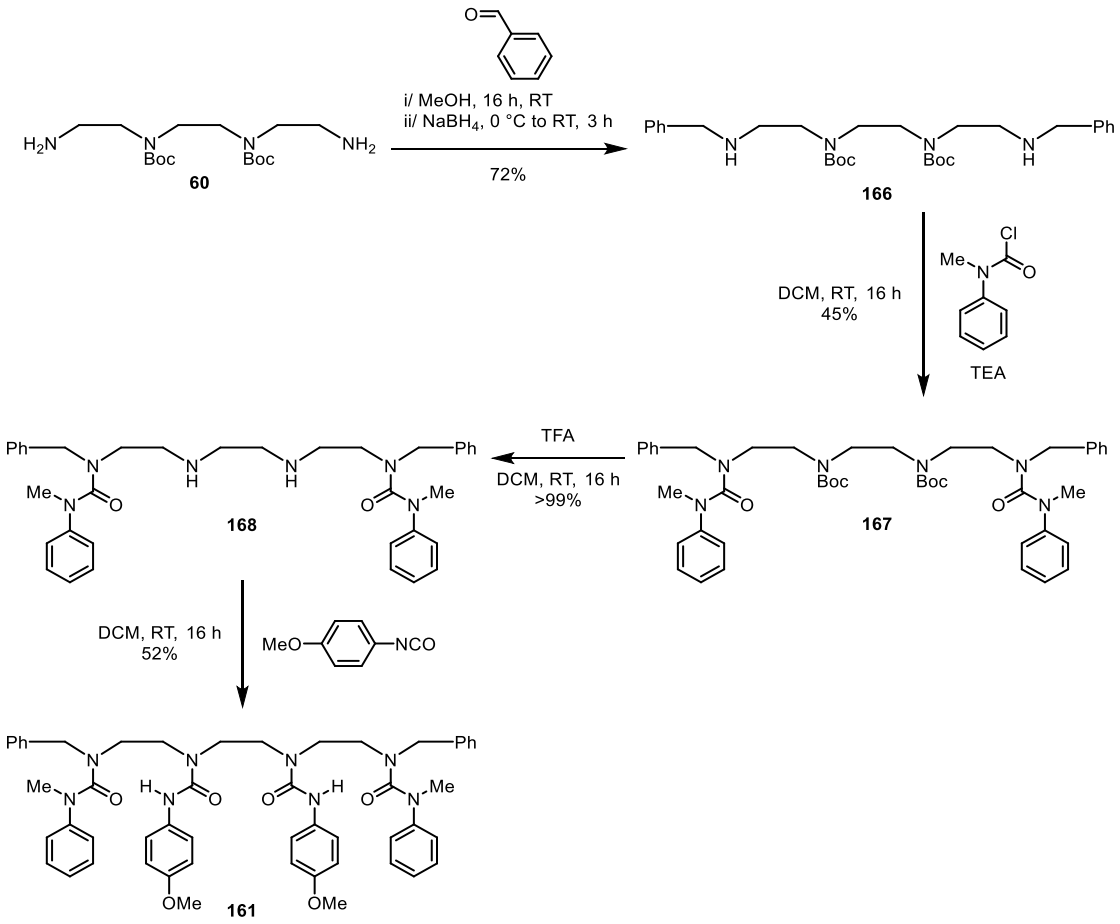

Scheme 48 – Synthesis of 161.

Diamine **60** was dibenzylated by reductive alkylation with benzaldehyde to give **166**, which proceeded in good yield. The tetrasubstituted ureas were then attached by reaction with *N*-methyl-*N*-phenylcarbamoyl chloride, which gave the desired disubstituted product, **167** in good yield. Subsequent removal of the Boc groups with TFA and carboxamidation of the resultant amines gave the target tetraurea **161** in good yield over two steps. **161** was then studied by VTNMR (Figure 78).

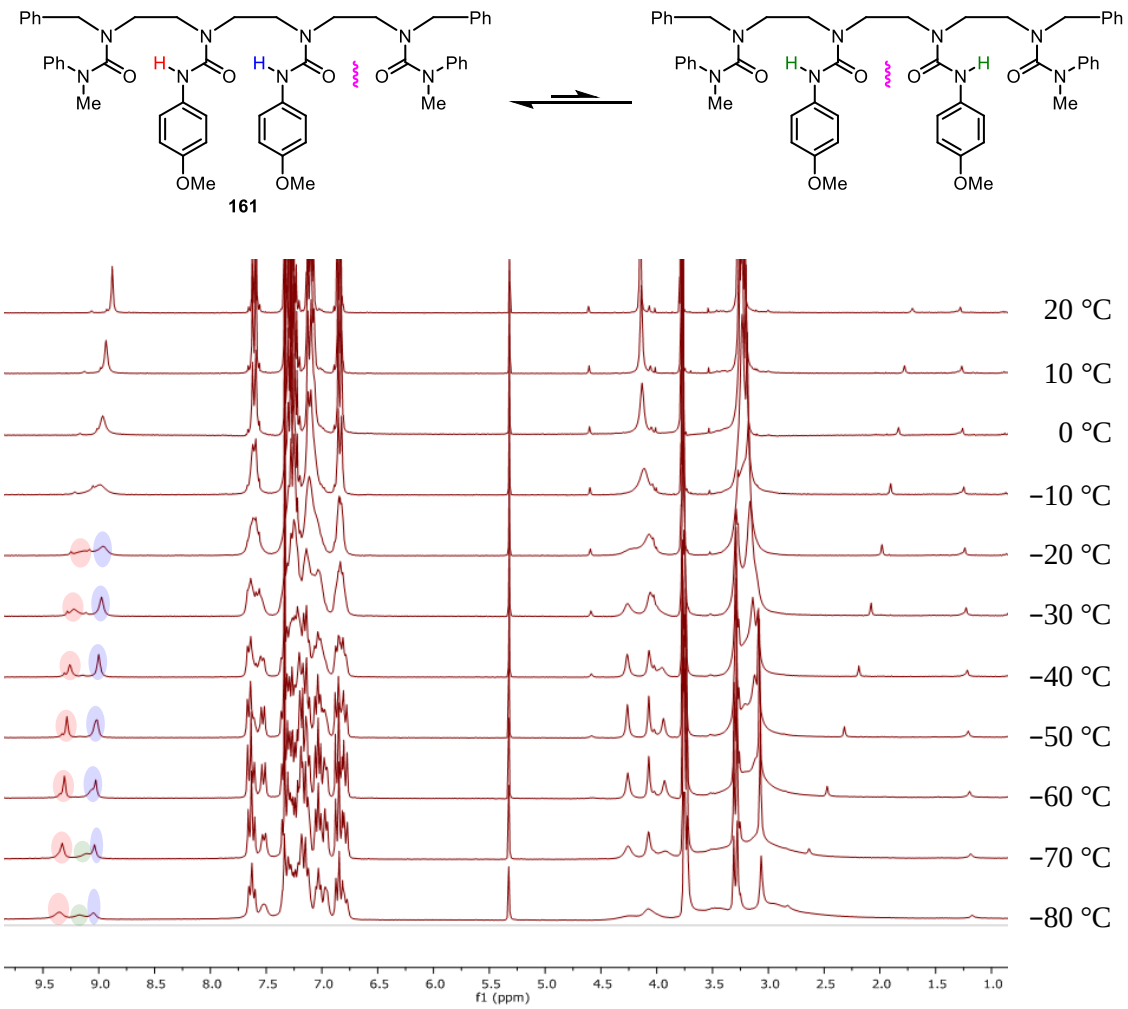

Figure 78 – VTNMR of 161 (CD_2Cl_2, 300 MHz, 11 mM).

Tetraurea **161** displayed signals at 4.15 (benzylic methylenes) and 8.87 ppm (ureido protons) at 20 °C. Upon cooling, the signal at 4.15 ppm broadened and decoalesced into three singlets in the ratio 37:37:26 at −20 °C. These singlets sharpened with decreasing temperature until they broadened again at −70 °C. The signal at 8.87 ppm broadened and shifted downfield with decreasing temperature until it decoalesced into three singlets in the ratio 37:26:37 at −20 °C. These singlets then sharpened and shifted downfield upon further cooling. These experiments showed that **161** exists as two conformations populated in a 74:26 ratio. The major conformer has two chemical environments for benzylic methylenes as shown by the singlets of equal integration, and the minor has only one chemical environment. The same applies to the ureido protons. This indicated that the major conformer is that where the tetrasubstituted ureas do not cause a fault in hydrogen bonding in the centre. However, the minor conformer is the one in which a fault has been induced in the centre as shown by its solitary benzylic methylene and ureido proton signal. These results indicated that some degree of fault induction can take place if the terminal HBAs are of comparable hydrogen-bond-accepting power to the trisubstituted ureas.

Focus then returned to synthesising the fault-inducing substrate, bis(pyridine) **162**. Twofold S_NAr was attempted with diamine **166** (Scheme 48) and 2-fluoropyridine by heating to reflux in toluene and *N*,*N*-diisopropylethylamine (DIPEA) but unfortunately, no reaction occurred, which was attributed to the steric encumbrance about the amines. The same result occurred when Buchwald-Hartwig coupling with 2-bromopyridine was attempted. Due to the difficulty associated with the installation of the pyridines, an alternate route was sought.

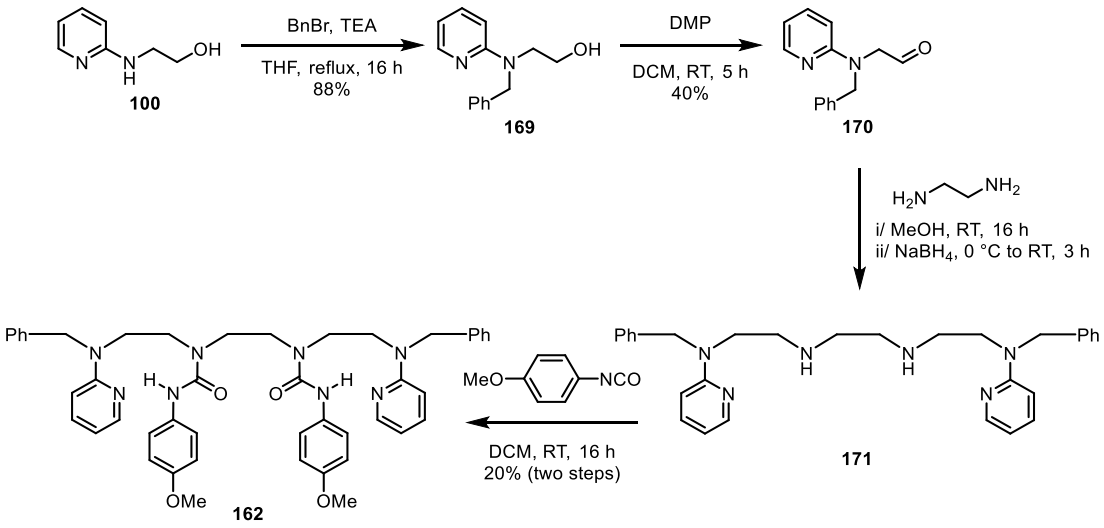

Scheme 49 – Synthesis of 162.

To avoid the steric encumbrance issues concerning the S_NAr and Buchwald-Hartwig coupling in the synthesis of bis(pyridine) **162**, the pyridine moiety was installed first. Previously synthesised amine **100** underwent benzylation at the secondary amine, which proceeded in good yield to give **169**. Oxidation using DMP was then carried out which gave aldehyde **170** in moderate yield. Ethylenediamine then underwent twofold reductive alkylation with two equivalents of aldehyde **170**, which occurred in poor yield as the major product was the single reductive alkylation product. This is explicable by formation of an imidazolidine by cyclisation of the second amine onto the imine formed after the first amine had undergone condensation with **170**. This would inhibit second condensation reaction, promoting single reduction to the monosubstituted product. Despite this, the crude mixture was reacted with 4-methoxyphenyl isocyanate, giving the desired diurea **162**, albeit in poor yield. **162** was then studied by VTNMR (Figure 79).

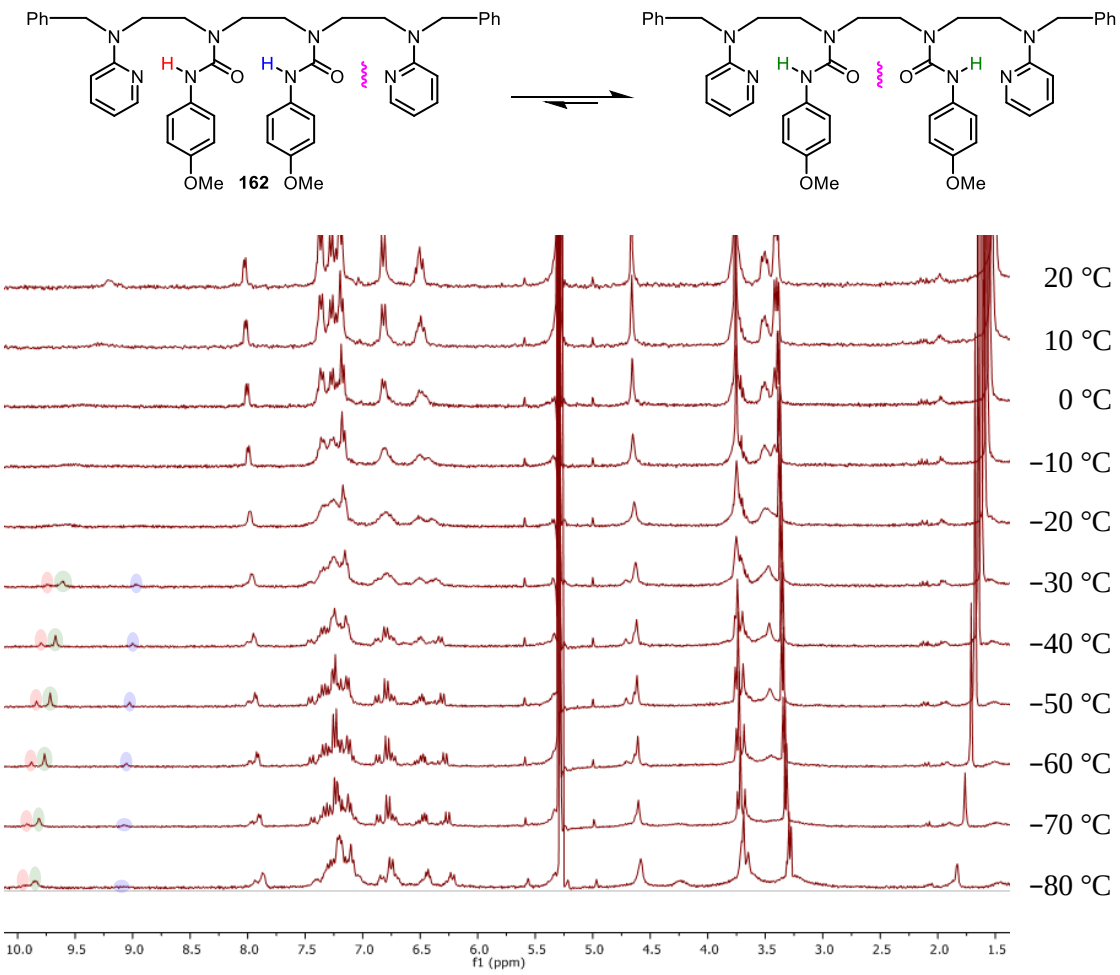

Figure 79 – VTNMR of 162 (CD_2Cl_2, 300 MHz, 12 mM).

In bis(pyridine) **162**, signals were displayed at 4.66 (benzylic methylenes) and 9.20 ppm (ureido protons) at 20 °C. Upon cooling, the signal at 4.66 ppm broadened and decoalesced into three singlets of ratio 20:20:60 at −30 °C. These singlets then sharpened upon further decreasing the temperature and broadened again at −70 °C. The signal at 9.20 ppm broadened and shifted downfield with decreasing temperature until it decoalesced into three singlets of ratio 20:60:20 at −30 °C. This showed that **162** exists as two conformations that are in slow exchange below −30 °C in a 40:60 ratio. The major conformer is that where the pyridines have induced a fault in the inter-urea hydrogen bonding, and the minor conformer is that where they have not. This shows that upon introducing a more powerful HBA to the termini of the diurea, more of the fault-induced conformer is populated.

As a 2-aminopyridine was not a powerful enough HBA to induce a complete fault in inter-urea hydrogen bonding, more stable hydrogen-bonding rings had to be used to effect the desired fault. It was speculated that due to the greater strength of all-sp^2 6-membered versus 9-membered hydrogen-bonding rings, a pyridine in a 6-membered hydrogen-bonding ring with a urea could form a sufficiently strong hydrogen bond so as to induce a complete fault in the

hydrogen-bonding network.[21] Bis(pyridine) **173** was synthesised as a new hydrogen-bond-disrupting substrate (Scheme 50).

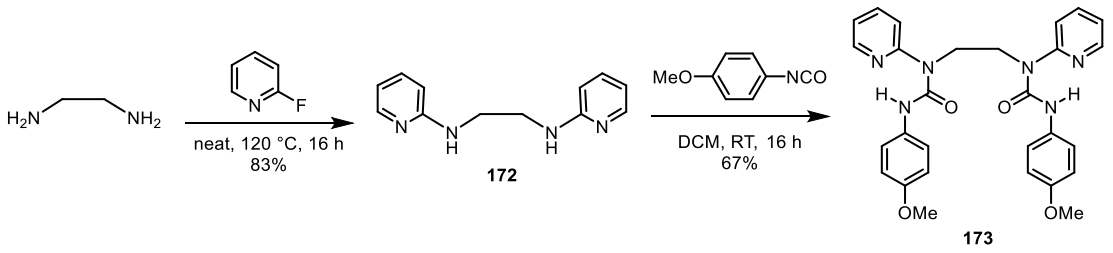

Scheme 50 – Synthesis of 173.

Diurea **173** was synthesised by twofold S_NAr with ethylenediamine with 2-fluoropyridine, giving bis(pyridine) **172**, followed by twofold carboxamidation using 4-methoxyphenyl isocyanate, giving the desired diurea **173** in good yield. Diurea **173** was then studied by VTNMR (Figure 80).

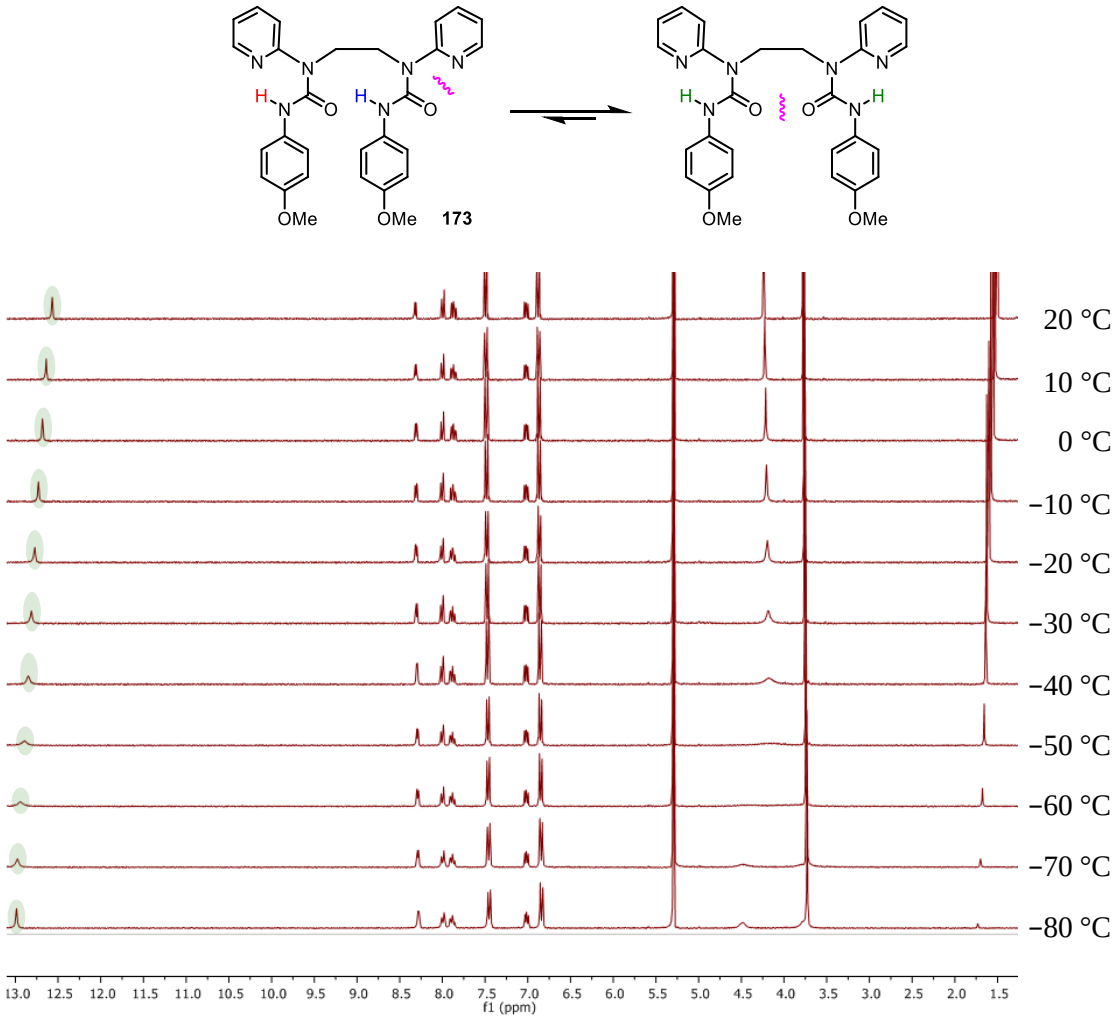

Figure 80 – VTNMR of 173 (CD_2Cl_2, 300 MHz, 18 mM).

Bis(pyridine) **173** showed signals at 4.23 (methylenes) and 12.57 ppm (ureido protons) at 20 °C. Upon cooling, the signal at 4.23 ppm stayed approximately constant until it broadened at −20 °C and decoalesced into two equal singlets at −70 °C. The signal at 12.57 ppm shifted downfield with decreasing temperature before broadening at −40 °C and sharpening at −70 °C. The remainder of the signals stayed the same throughout the experiment. It was deduced from these data that **173** exists as one conformation, where there is a complete fault in inter-urea hydrogen bonding due to the single chemical environment of the pyridines and ureido protons. Interestingly, the methylenes decoalesced into two equal signals corresponding to two protons each. It was inferred from this that at very low temperatures, **173** adopts a C_2-symmetric and therefore chiral conformation that racemises on the NMR timescale above −40 °C.

As this conformation is C_2-symmetric, the carbon atoms of the methylenes should be chemically identical at slow exchange. This hypothesis was validated by comparison of the low-temperature (−60 °C) ^{13}C NMR spectra of diureas **43** and **173** (Figure 81).

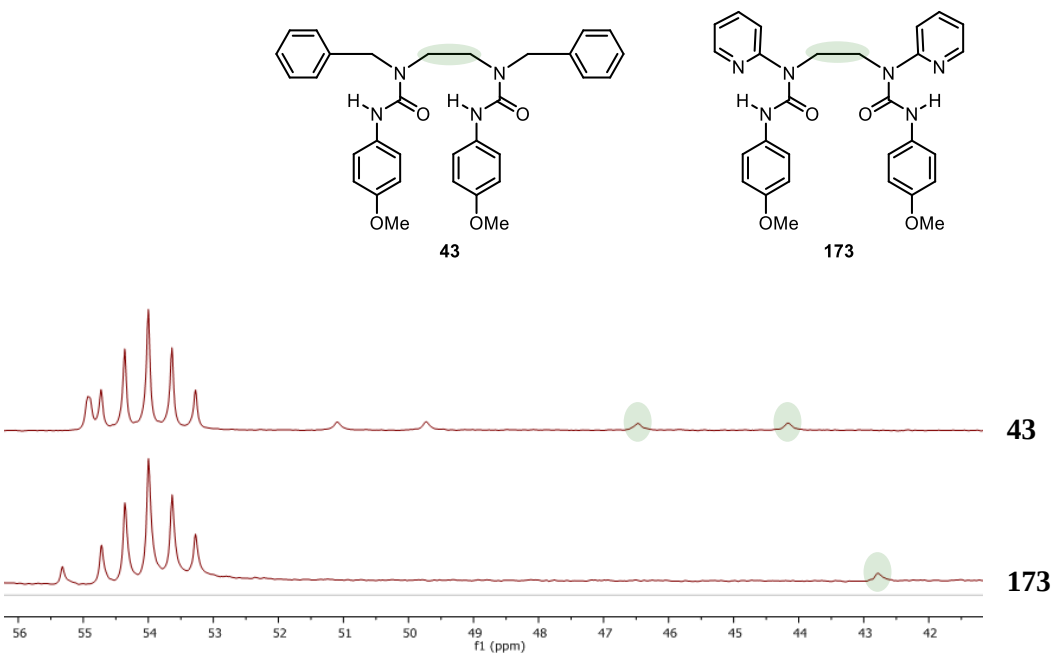

Figure 81 – ^{13}C NMR spectra of 43 and 173 at −60 °C (40.0-56.0 ppm region, CD_2Cl_2, 300 MHz).

At −60 °C, diurea **173** exhibited one signal corresponding to its methylenes, whereas diurea **43**, an analogous diurea without a fault in hydrogen bonding, exhibited two. This experiment corroborated the supposition that **173** exists as one chiral conformation, where a complete fault has been induced in the inter-urea hydrogen bonding. This result is also commensurate with studies on pyridyl ureas **97** and **145**, which have shown that pyridines in 6-membered hydrogen-bonding rings with ureas can completely control the directionality of that urea.

Now that complete faults had been induced in diureas, it was desirable to extend the oligourea to deduce whether multiple faults are possible and if a fault preferentially lies between certain residues in an oligourea foldamer. With this, triurea **174** was synthesised by twofold S_NAr of diethylenetriamine with 2-fluoropyridine and subsequent threefold carboxamidation using 4-methoxyphenyl isocyanate.

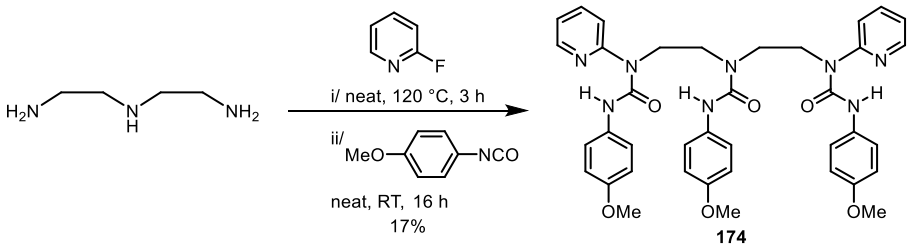

Scheme 51 – Synthesis of 174.

Triurea **174** was then studied by VTNMR (Figure 82).

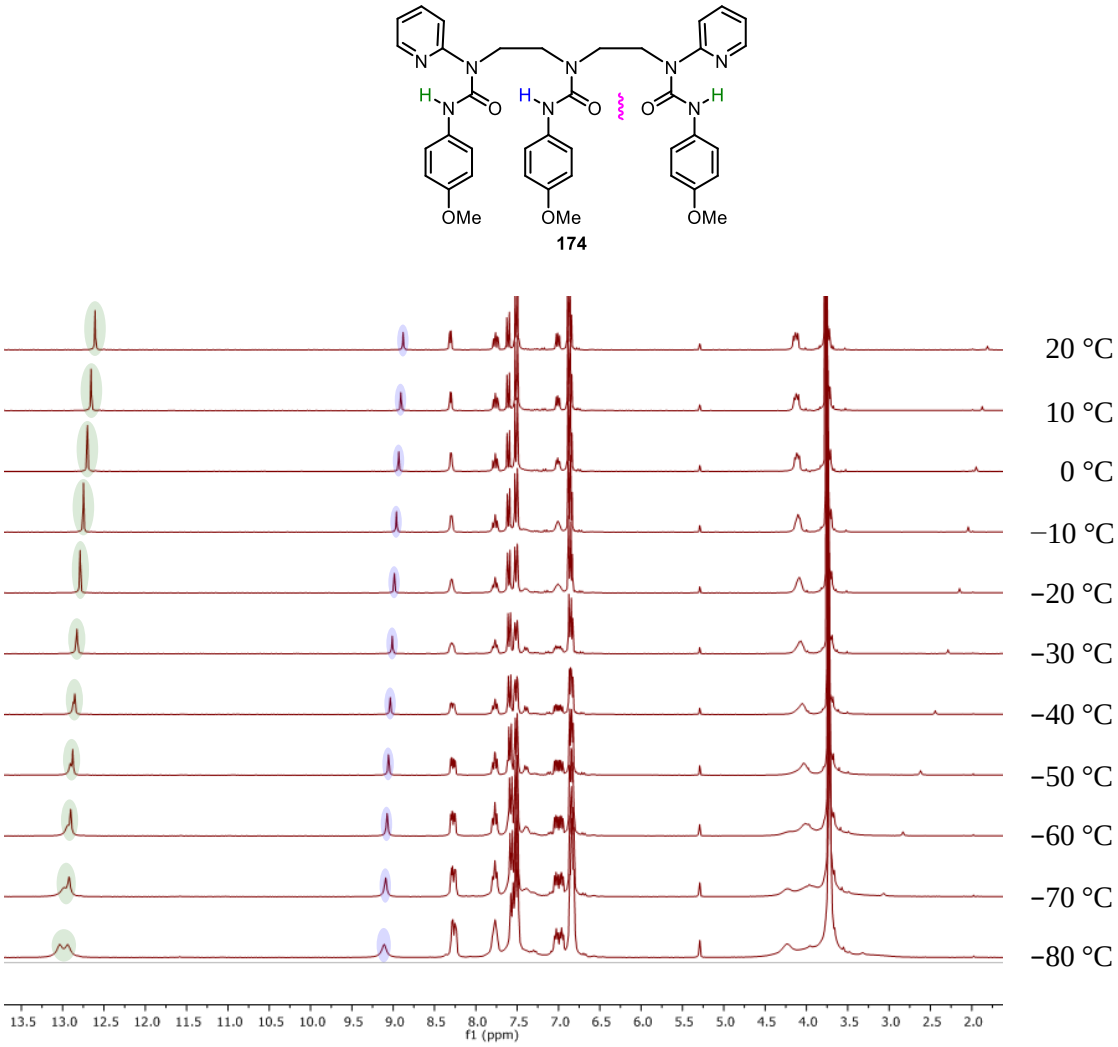

Figure 82 – VTNMR of 174 (CD_2Cl_2, 300 MHz, 14 mM).

Triurea **174** showed signals at 4.13 (pyridyl urea α methylenes), 8.88 (central ureido proton) and 12.61 ppm (pyridyl urea ureido protons) at 20 °C. Upon cooling, the signal at 4.13 ppm broadened and decoalesced into two equal multiplets at −60 °C. The signal at 8.88 ppm shifted downfield with decreasing temperature, before broadening at −60 °C. The signal at 12.61 ppm shifted downfield and broadened with decreasing temperature and decoalesced into two equal singlets at −40 °C. These data showed that **174** exists as one populated conformer, where a hydrogen-bonding fault has occurred between one of the pyridyl ureas and the central urea. The directionalities of the central urea are in slow exchange below −40 °C. This is evidenced by the decoalescence of the pyridyl urea α methylenes and pyridyl urea ureido protons in equal ratio, whilst the central ureido proton stayed the same throughout. This experiment showed that pyridines control the directionality of the ureas adjacent to them, effectively making the whole of the pyridyl ureas new HBAs, which hydrogen bond to the central urea. The directionality of the central urea interconverts by changing the pyridyl urea that it hydrogen bonds to.

To summarise, the hydrogen-bonding network in ethylene-bridged oligoureas is robust to intramolecular electronic effects. The ability of a group to induce a fault in directionality correlates with its hydrogen-bond-accepting ability relative to the central ureas. Succinimides, being weaker HBAs than ureas, fail to induce a fault in the network. Tetrasubstituted ureas and pyridines in 9-membered hydrogen-bonding rings, being of similar hydrogen-bond-accepting capacity to trisubstituted ureas, can induce a partial fault in directionality. If pyridines are involved in more stable hydrogen-bonding rings, complete fault induction can take place. This evidence suggests that only the formation of a very strong hydrogen-bonding alternative is sufficient to induce a fault in directionality. This promises that with judicious care over the hydrogen-bonding rings and functions at the ends of these foldamers, hydrogen-bonding fidelity can be maintained throughout the structure, conferring robust informational communication and great tolerance of chemical function.

4.0 Cyclochirality

There are four well-established types of chirality, each of which is prominent either in nature and/or in synthetic chemistry – central, axial, helical and planar chirality (Figure 83).[105,106] Other forms of chirality exist but will not be discussed here.[107] Central chirality is ubiquitous in natural systems and control of it is vital in all cases where orientation in three-dimensional space is involved, such as in the selective binding of substrates in the active sites of enzymes and in the correct folding of DNA. Other forms of chirality are a result of non-covalent interactions. For example, axial chirality is very important in the function of ligands for asymmetric catalysis in organometallic chemistry. Axial chirality arises when the rotation of a specific single bond is inhibited by steric interactions. In the chiral ligand BINAP, the biaryl bond cannot rotate due to steric interactions between the naphthyl groups, meaning that two different enantiomers of the phosphine can be isolated.

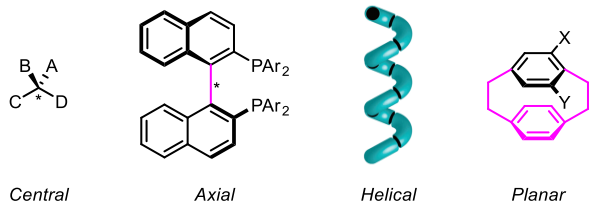

Figure 83 – Types of chirality.

Conversely, helical chirality arises either because the barrier to screw-sense inversion of a helix is too great due to steric encumbrance, or because intramolecular hydrogen bonding is too strong for rapid racemisation.[26] Planar chirality typically arises from restricted movement of groups from one side of a planar moiety to the other. As previously discussed, hydrogen-bonding networks can be used to perform a plethora of useful functions in both natural and synthetic contexts. A pertinent natural example is the cyclic arrangement of guanine tetrads in G-quadruplexes. Telomeric DNA, which is rich in guanine, allow for guanines to aggregate by Hoogsteen base-pairing and alkali metal cation binding. This confers stability to single-stranded chromosomes and prevents them from being incorrectly processed and damaging the cell.[108] The directionality of the G-quadruplex is dictated by the central and therefore helical chirality in the telomeric DNA.

The ubiquity of central chirality in biological systems means that there are no known natural examples where chirality is derived solely from the strength of a cyclic hydrogen-bonding array. However, numerous synthetic examples have been reported, a simple example of which is the campestarenes (Figure 84).

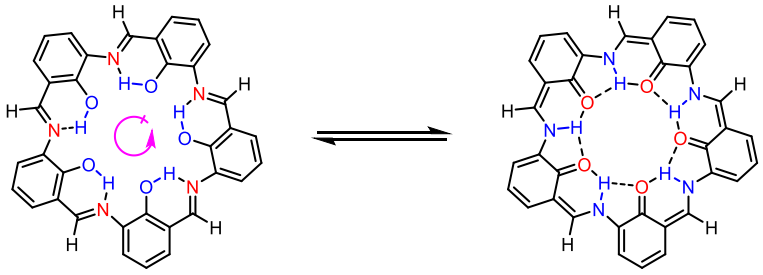

Figure 84 – Campestarenes and their tautomeric behaviour.

Campestarenes are highly symmetrical Schiff-base macrocycles with interesting tautomeric behaviour. They are formed from the polycondensation of 2-amino-6-formylphenols to form the corresponding macrocyclic polyimine.[109] This polymerisation occurs spontaneously, therefore precursors are required to synthesise these structures with selectivity. As shown by MacLachlan and co-workers, in the case of 2-nitro-6-formylphenols, reduction of a nitro group to acquire the amine resulted in exclusive formation of the C_{5h} campestarene (Figure 84).[109] The campestarene could exist in two different tautomeric forms, a keto-enamine form and an enol-imine form. In different solvents, the energy difference between the two tautomeric forms differs greatly, allowing solvent-dependent modulation of the equilibrium. Crucially, ^{1}H NMR, computational and X-ray crystallographic evidence suggested that the phenolic protons are in identical chemical environments and in very strong hydrogen bonding. To satisfy this criterion, in the enol-imine form, all of the hydroxyl groups have to be aligned in either a clockwise or anticlockwise fashion. This means that if these structures were not degenerate from the horizontal plane of symmetry, they would be enantiomers of each other by virtue of their cyclic hydrogen-bonding array alone.

Aida and co-workers used a cyclic hydrogen-bonding network to slow the bowl-to-bowl inversion of corannulenes as a means of accessing the corannulene family's unique properties and functions (Figure 85). The group functionalised the corannulene with both enantiopure and achiral amide-appended thioalkyl residues.[110]

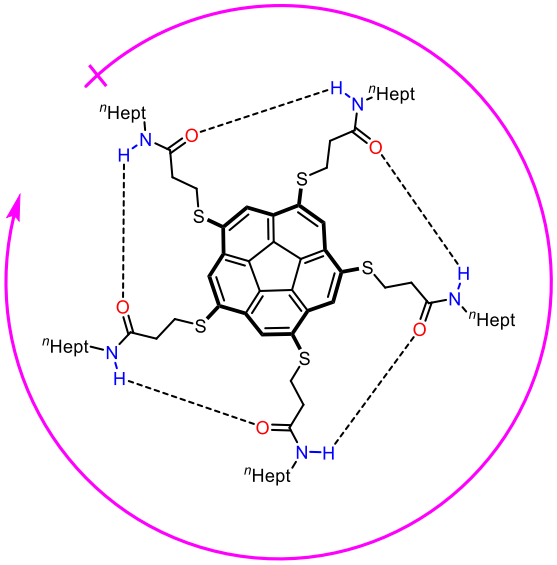

Figure 85 – Amide-appended thioalkyl-substituted C_5-symmetrical corannulenes.

Serendipitously, the hydrogen-bonding network gave rise to some unexpected chiroptical properties. When achiral side chains were used on the corannulene, all of the amides hydrogen bonded in an intramolecular fashion to form a cyclic hydrogen-bonding array. Due to the helical chirality of the corannulene, which arose from its bowl shape and substitution pattern, the two hydrogen-bond directionalities were diastereomeric, and therefore one was favoured over the other. As desired, the strength of the cyclic hydrogen-bonding array slowed down the bowl-to-bowl inversion of the corannulene significantly. The corannulene was then examined in enantiomerically pure (*R*)-limonene as a chiral solvent. Due to the chiral environment the (*R*)-limonene imposed on the molecule, a clear Cotton effect was observed in the absorbance range of the corannulene motif. The presence of the chiral solvent induced global directionality of the amides in the cyclic hydrogen-bonding array, which was communicated to the corannulene. The same effect was observed upon introduction of chiral residues on the corannulene. Analogues were synthesised with (*R*) and (*S*)-2,6-dimethyloctane residues. Studies of these in an achiral solvent, methylcyclohexane resulted in opposite Cotton effects. This indicated that the chiral residues induced preferential directionality in the cyclic hydrogen-bonding array. This effect was further exemplified by addition of ethanol to the mixture. The ethanol disrupted the cyclic hydrogen-bonding array by competitive hydrogen-bonding interactions, which increased the rate of bowl-to-bowl inversion, and thus no Cotton effect was observed. This supported the notion that the cyclic hydrogen-bonding array was responsible for the corannulene's chiroptical properties. Whilst these examples showed that cyclic hydrogen-bonding arrays can give rise to interesting properties and useful functions, they did not exploit the function that the directionality of the hydrogen bonds could provide.

4.1 Cyclochirality in Cyclic Ethylene-Bridged Oligoureas

Macrocyclic oligoethylenediamines and their derivatives have found widespread use in coordination and medicinal chemistry. Much like the crown ethers, they can be used to accommodate a variety of metal cations and can sometimes exhibit selectivity between them depending on their cavity size.[111] Due to their enhanced basicity in comparison to crown ethers, they and their ammonium salts also make for useful cation and anion hosts, respectively.[112] Their rich coordination chemistry makes them interesting targets for biomimetic esterases, β-cyclodextrin hosts and other supramolecular devices.[113–115] Due to the rich dynamic behaviour discovered in oligoureas derived from acyclic oligoethylenediamines, it was interesting to see if the properties translated to their cyclic analogues, where a cyclic hydrogen-bonding array could form.

As an initial investigation into this, 1,4,7-triazacyclononane (TACN) was reacted with 4-methoxyphenyl isocyanate to give the corresponding triurea **175** in reasonable yield. **175** was then studied by ^{1}H NMR (Figure 86).

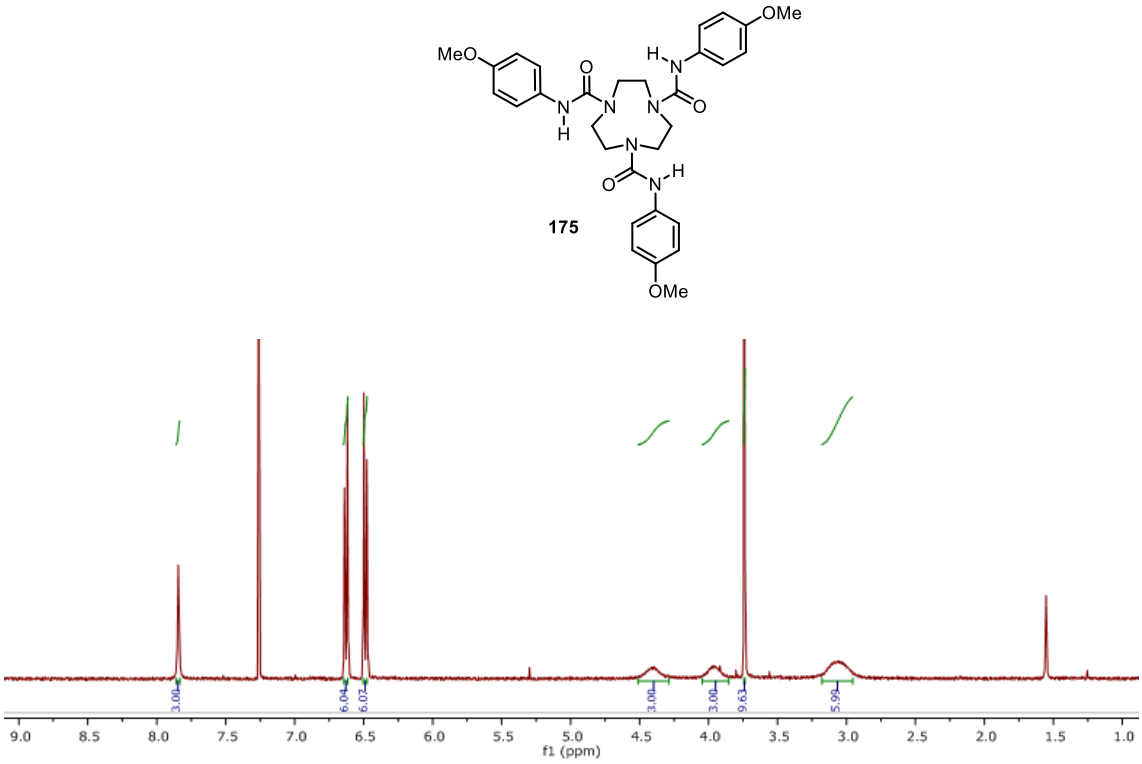

Figure 86 – ^{1}H NMR of 175 ($CDCl_3$, 500 MHz).

At 25 °C, triurea **175** showed signals at 3.06 (alkyl methines, 6 H), 3.95 (alkyl methines, 3 H), 4.40 (alkyl methines, 3 H) and 7.84 ppm (ureido protons, 3 H). This spectrum showed that diastereotopicity has been revealed in the ethylene bridges, consistent with C_3-symmetry, as four

broad signals can be observed (two of them overlapping, 3.06 ppm) in the alkyl region. These signals were attributed to four different methine environments in the ethylene bridges, and three identical ethylene bridges. There is one signal corresponding to the ureido protons (7.84 ppm), further validating the C_3-symmetry, and suggesting that the ureido protons are each in hydrogen bonding. It is proposed that the diastereotopicity arises because each of the ureas orient themselves into a bowl shape in order to hydrogen bond in a cyclic manner. **175** was then recrystallised from $CHCl_3/Et_2O$ and studied by X-ray crystallography (Figure 87).

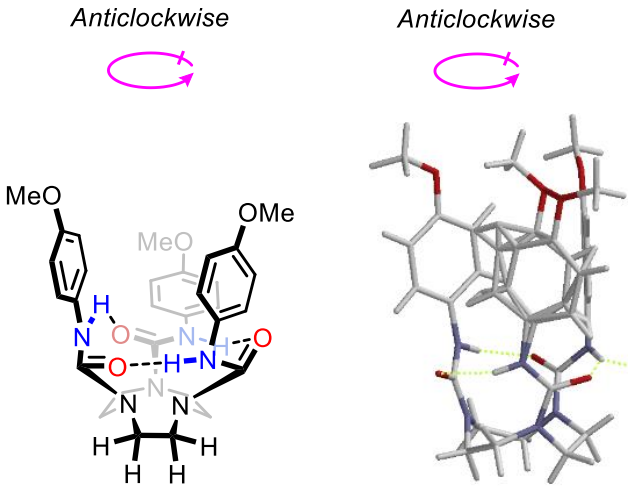

Figure 87 – Depiction and X-ray crystal structure of 175.

The X-ray crystal structure of triurea **175** corroborates the supposition that the ureas hydrogen bond with each other by forming a bowl-like structure. This contradicted simulations carried out by Charbonnier which suggested TACN-derived triureas orient one ureido carbonyl into the cavity so the other two ureido protons can hydrogen bond to it.[113] A similar conformation is adopted in $CDCl_3$ solution, rationalising the observed diastereotopicity by ^{1}H NMR. This conformation is chiral due to the cyclic hydrogen-bonding array alone, representing an interesting opportunity for enantiospecific host-guest chemistry or enantioselective catalysis. In order to have any applicability in these areas, the cyclic hydrogen-bonding network must racemise at a rate slower than the timescale of chiral separation, and of the desired chiral function. To ascertain this, **175** was studied by VTNMR (Figure 88). d_8-Toluene was selected as the solvent due to its inability to hydrogen bond and its high boiling point relative to the analytical temperatures.

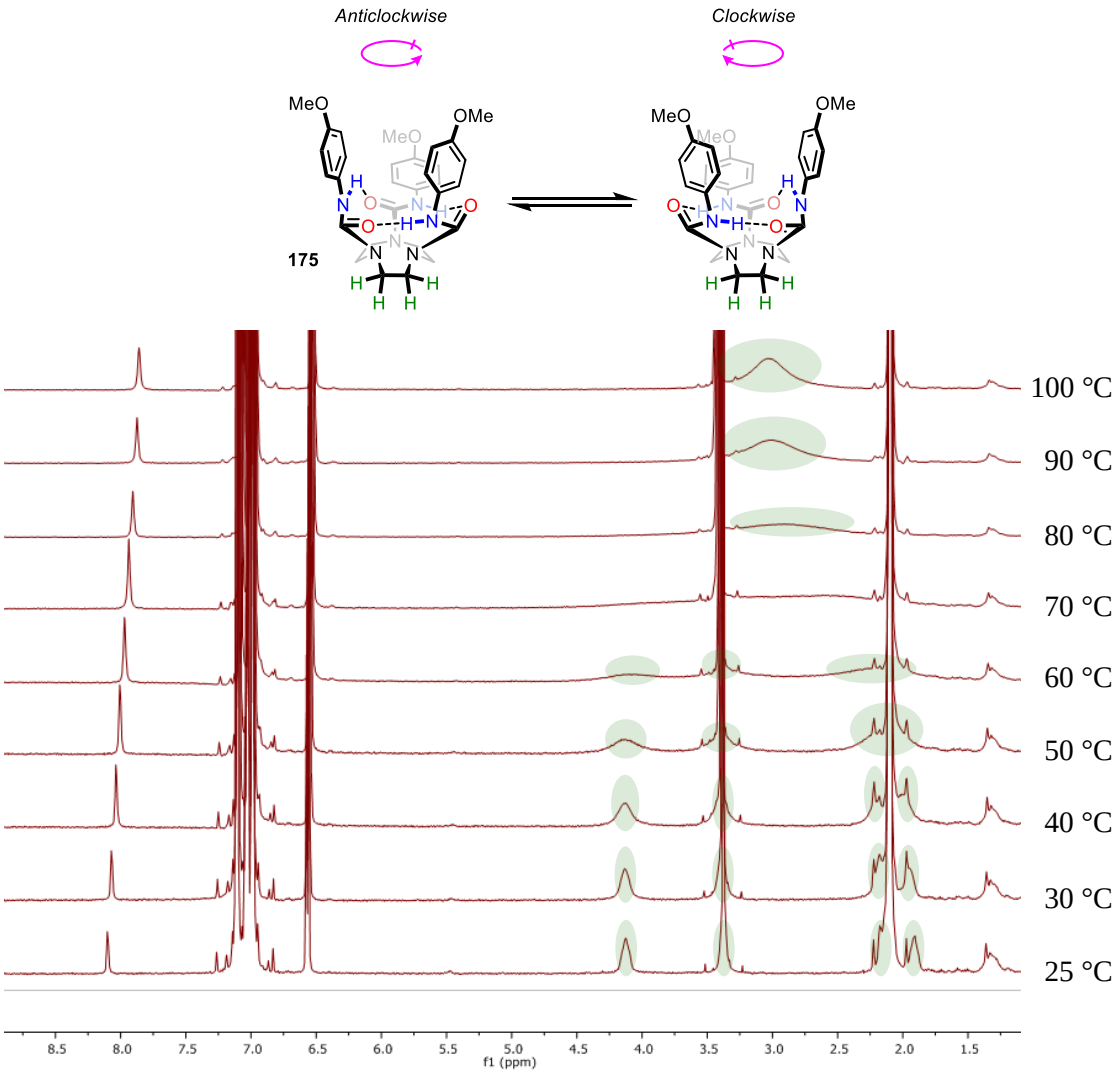

Figure 88 – VTNMR of 175 (d_8-toluene, 500 MHz, 17 mM).

At 25 °C, triurea **175** showed signals at 1.90 (alkyl methines, 3 H), 2.09 (alkyl methines, 3 H, obscured by $C_6D_5CD_2H$), 3.39 (alkyl methines, 3 H, obscured by methoxy groups), 4.12 (alkyl methines, 3 H) and 8.10 ppm (ureido protons). Upon heating, the signals at 1.90, 2.09, 3.39 and 4.12 ppm all broadened until they could not be observed at 70 °C. These signals then coalesced into one singlet (12 H) at 80 °C, which sharpened with increasing temperature. The signal at 8.10 ppm shifted upfield with increasing temperature. These data showed that the enantiotopic conformers were in slow exchange on the NMR timescale at 25 °C. This racemisation rate increased with temperature until it was in fast exchange at temperatures above 80 °C. The ureido protons signal also moved upfield with temperature as hydrogen bonding gets weaker at higher temperature.

Triurea **175** was then subjected to Eyring analysis (under the assumption that each of the alkyl methines exchange with each other at the same rate), unveiling $\Delta G^{\ddagger}_{298\,K}$ (d_8-toluene) = 65.3 kJ mol^{-1} and $t_{1/2}$ = 17 ms. Unfortunately, this racemisation rate is too fast to allow chiral separation

in toluene, so other solvents were screened. The same approximate coalescence temperatures were reached in $CDCl_3$ and d_6-benzene, but it was suspected that the hydrogen-bonding network could be strengthened in polar or hydrogen-bonding solvents. To investigate this, CD_3OH was titrated into a solution of **175** in $CDCl_3$ (Figure 89).

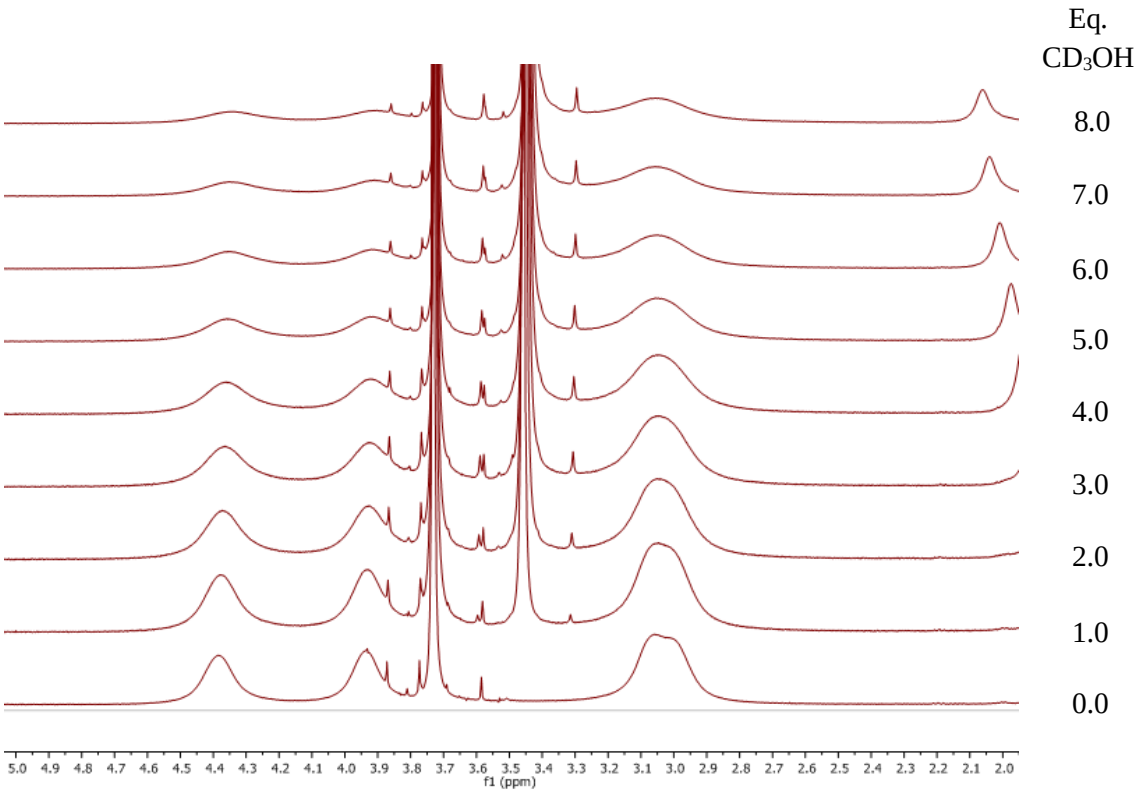

Figure 89 – Titration of CD_3OH into 175 (2.00-5.00 ppm region, $CDCl_3$, 500 MHz).

The signals at 3.06 (alkyl methines, 6 H), 3.95 (alkyl methines, 3 H) and 4.40 ppm (alkyl methines, 3 H) all broadened upon addition of CD_3OH, indicating that, in the presence of CD_3OH, triurea **175** was brought closer to the fast exchange region. This showed that addition of hydrogen-bonding solvents damaged the cyclic hydrogen-bonding network, lowering $\Delta G^{\ddagger}$. This was further corroborated as solutions of **175** in d_6-DMSO and 50% v/v $CDCl_3$/d_4-methanol displayed only one signal corresponding to alkyl methines at 25 °C, showing that it was already in fast exchange. Subsequent efforts focused on derivatisation of the arenes of **175** in attempts to raise $\Delta G^{\ddagger}$ (Scheme 52).

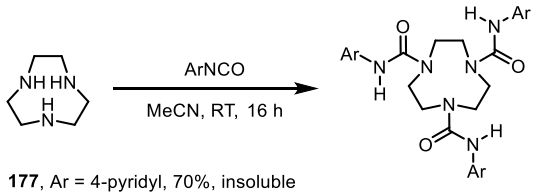

177, Ar = 4-pyridyl, 70%, insoluble
178, Ar = 4-trifluoromethylphenyl, 56%, insoluble
179, Ar = 4-cyanophenyl, 33%, insoluble
180, Ar = 4-chlorophenyl, 45%
181, Ar = 4-ethyl benzoate, 80%.

Scheme 52 – Derivatisation of 175.

TACN was reacted with a variety of aryl isocyanates to liberate the corresponding triureas in variable yields. 4-Pyridyl isocyanate is unstable and so triurea **177** was made from 4-pyridyl phenyl carbamate, **176** in good yield. Unfortunately, **177** (4-pyridyl), **178** (4-trifluoromethylphenyl) and **179** (4-cyanophenyl) were all insoluble in the desired non-hydrogen-bonding solvents, but dissolved in d_6-DMSO where the ureas did not adopt a cyclochiral conformation at 25 °C. However, **180** (4-chlorophenyl) and **181** (4-ethyl benzoate) were soluble in $CDCl_3$ and d_8-toluene, which allowed them to be studied by VTNMR and Eyring analysis (see Appendix, section 8.2). These analyses corresponded to $\Delta G^{\ddagger}_{298\ K}$ (d_8-toluene) = 63.2 kJ mol^{-1} for **180** and $\Delta G^{\ddagger}_{298\ K}$ (d_8-toluene) = 62.7 kJ mol^{-1} for **181**, indicating that alternate substitution on the arenes did not give rise to a significant change to $\Delta G^{\ddagger}$. Additionally, previous work by Clayden and co-workers has shown that alkyl triureas have much lower $\Delta G^{\ddagger}$ values (49.5 kJ mol^{-1} for ethyl ureas), and are very sensitive to degree of substitution.* In order to deduce what could be done to raise $\Delta G^{\ddagger}$, the rate-determining step to racemisation had to be determined, so the correct parameters could be altered for racemisation inhibition (Scheme 53).

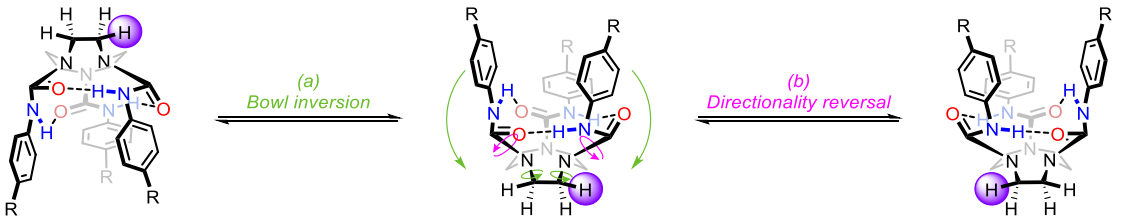

Scheme 53 – Postulated mechanisms of racemisation of TACN-derived triureas.

Two mechanisms that result in racemisation are possible – (a) bowl inversion, where each of the ureas move onto the other side of the TACN with a concomitant bowl inversion of the TACN, and (b) directionality reversal, where each of the ureas undergoes a 180° C–N bond rotation, analogously to the acyclic oligoureas. These mechanisms bifurcate with the alkyl methines they exchange with. If directionality reversal was the rate-determining racemisation

* Work performed by BSc student Elliot Seward.

mechanism, then the alkyl methines would exchange with vicinal methines; if it were bowl inversion, then the alkyl methines would exchange with geminal methines.

Initially, the mechanistic elucidation was attempted by using variable-mixing time NOE experiments. The ureido protons were irradiated, and the time that passed before the spectrum was recorded was altered. If a proton is irradiated, it can exhibit an NOE correlation if another proton is proximate to it. However, if that proximate proton is exchanging with another in a dynamic process, then an NOE can be observed after it has exchanged, even if it is no longer proximate to the irradiated proton. The extent of this phenomenon depends on how long the NOE signal is built relative to the speed of the dynamic process. If the dynamic process is slow, the NOE correlation is shown between the irradiated proton and the proximate proton before the proximate proton can exchange and so one correlation is observed. If the dynamic process is fast, the proton is irradiated, and the proximate proton equilibrates before the spectrum is recorded, so NOEs are observed with each proton in exchange, even if they are not proximate to the irradiated proton. This experiment could potentially prove whether the bowl inversion mechanism operates. The half-life of triurea **175** at 25 °C is 28 ms, theoretically meaning that if the ureido protons are irradiated, they will only exhibit an NOE with the methines on top of the bowl if the spectrum was taken immediately. If the spectrum was recorded after 28 ms, then half of the methines on top of the bowl would have equilibrated, generating a 3:1 ratio of signals corresponding to methines on top and bottom of the bowl (if bowl inversion is the rate-determining mechanism). Unfortunately, the spectrum cannot be taken at this time as insufficient time has passed to allow spin relaxation to take place to generate a signal. NOEs were recorded after 50 ms (≈ two half-lives) of mixing time but unfortunately, equal NOEs were observed with all alkyl methines. The same was observed when the NOEs were recorded at 0 °C. This result meant that racemisation occurs too quickly for mechanistic elucidation by NOE studies, so another method will have to be used.

Next, it was envisaged that mechanically locking the ureas together would prohibit both mechanisms and increase $\Delta G^{\ddagger}$. This was attempted by linking the ureas through an alkyl linker derived from trimethylolethane (Scheme 54).

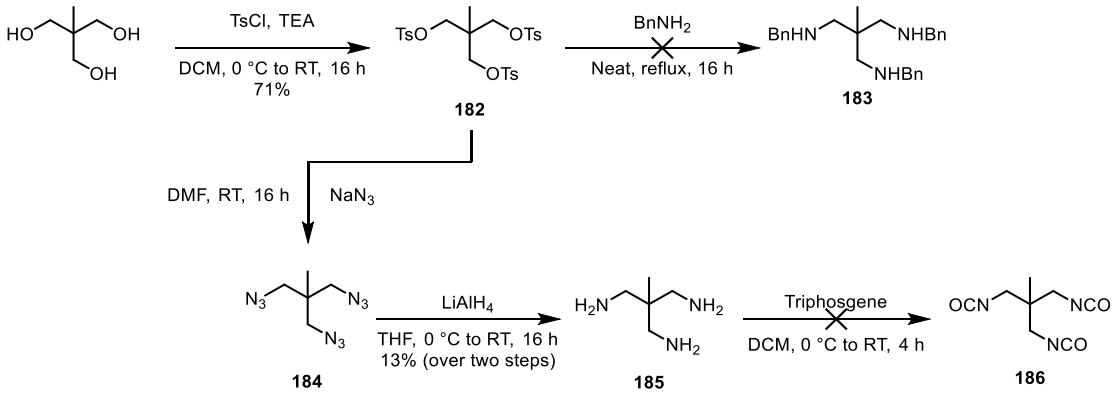

Scheme 54 – Synthesis of 186.

Trimethylolethane underwent a threefold tosylation to give tritosylate **182** in good yield. **182** was then to undergo a threefold S_N2 with benzylamine, but unfortunately, no conversion of **182** occurred. Instead, threefold S_N2 was performed with sodium azide to give **184**, which was hydrogenated to the corresponding triamine in reasonable yield over two steps. Next, triamine **185** was to form the tris(isocyanate) by reaction with triphosgene, but unfortunately, after formation of the first isocyanate, the other two amines cyclised to form the corresponding triazabicyclo[2.2.2]octanol. It was suspected that the same would occur if aryl carbamates were used instead of isocyanates, so a different strategy was sought.

To prevent cyclisation of the other amines, a tris(isocyanate) scaffold used by Davis and co-workers was prepared (Scheme 55).[31]

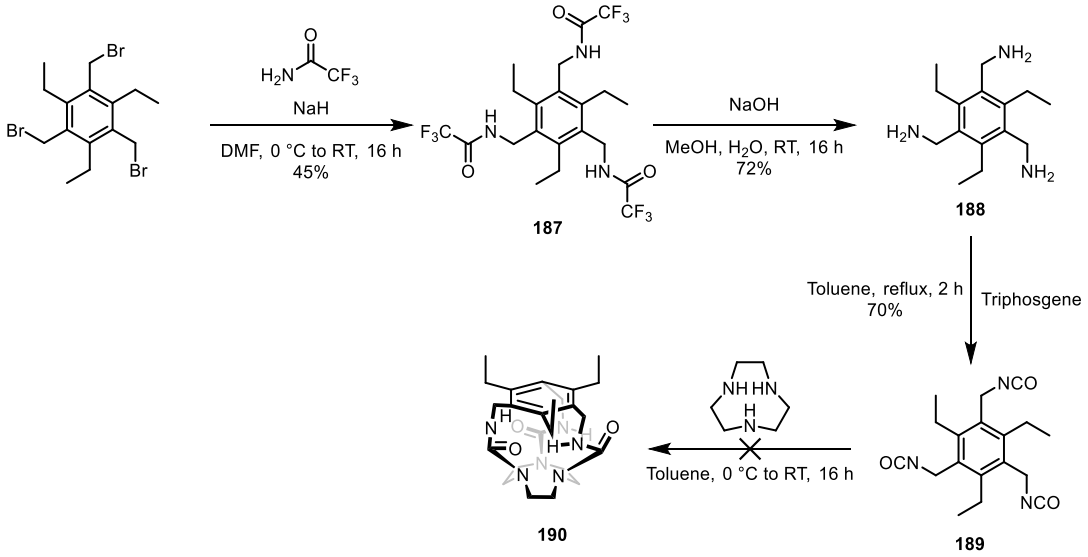

Scheme 55 – Synthesis of 190.

Threefold S_N2 of 1,3,5-tris(bromomethyl)-2,4,6-triethylbenzene with trifluoroacetamide and NaH gave tris(trifluoroacetamide) **187** in good yield. The trifluoroacetamides were then

hydrolysed and the tris(isocyanate) was formed using triphosgene in excellent yield over two steps. TACN was added slowly to triisocyanate **189** at high dilution in an attempt to make triurea **190**, but unfortunately an insoluble precipitate formed which could not be characterised by mass spectrometry.*

A preliminary attempt was made to synthesise a tris(guanidine) analogue of **175** (Scheme 56), where it was hoped that modification of the amphoteric functional group would result in a new family of cyclochiral TACN derivatives. Additionally, it was foreseen that protonation of one of the guanidines could be stabilised by proton transfer to the other two guanidines, effectively stabilising positive charge over nine nitrogen atoms. This could potentially render the tris(guanidine) a very powerful organic superbase, which could have chiral influence through appropriate substitution.

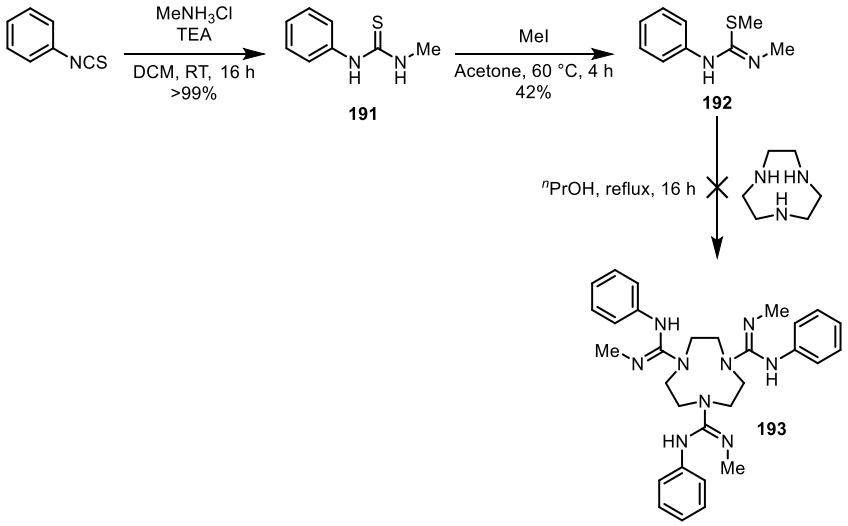

Scheme 56 – Synthesis of 193.

Phenyl isothiocyanate was treated with methylammonium chloride and base to make *N*-methyl-*N'*-phenyl thiourea quantitatively. Thiourea **191** was then reacted with methyl iodide to attain the methyl isothiourea, **192** in poor yield. **192** was then to act as an electrophilic source of guanidine by displacement of methanethiol. Unfortunately, heating an excess of **192** with TACN converted none of the isothiourea. Heating to 150 °C in a sealed tube under microwave irradiation saw decomposition of the isothiourea. Future work on the synthesis of tris(guanidines) will involve seeking alternate conditions or electrophilic sources of guanidine to effect the desired trisubstitution.

Next, cyclochirality was researched in the analogous tetramine, 1,4,7,10-tetraazacyclododecane (cyclen). Cyclen was reacted with 4-methoxyphenyl isocyanate to give the

* Work performed by Giulia Marsico.

desired tetraurea, **194** in good yield. Unfortunately, no diastereotopicity was observed in **194** in $CDCl_3$ or d_6-benzene. The same feature was observed in analogous alkyl tetraureas.* It was suspected that the cyclododecane was unable to adopt a conformation where the ureas hydrogen bond to each other in a cyclochiral fashion. It has been reported that alcohols can be used to form intermolecular bridging hydrogen bonds between the ureas in cyclen-derived tetraureas in the solid state.[112] It was hoped that this could be used to induce cyclochirality, so CD_3OH was titrated into a sample of tetraurea **194** in $CDCl_3$. Unfortunately, this gave no change in **194**, so a new scheme was envisaged where alcohols could be used to make bridging hydrogen bonds in an intramolecular manner (Scheme 57).

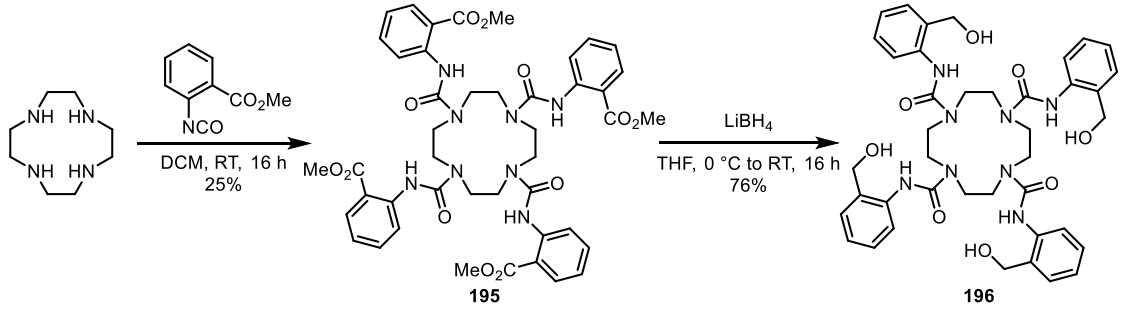

Scheme 57 – Synthesis of 196.

Cyclen was reacted with methyl 2-isocyanatobenzoate to give the corresponding tetraurea **195** in poor yield. The ethyl esters of **195** were then reduced to alcohols using $LiBH_4$, yielding tetrol, **196** in good yield. Unfortunately, **196** was insoluble in $CDCl_3$, d_6-benzene and $CDCl_3/CD_3OH$ mixtures. It was soluble in d_6-DMSO but this displayed no chiral conformation.

Mechanical locking of the cyclen-derived tetraureas was then attempted by making a calix[4]arene, where the arenes were linked together by bridging methylenes (Scheme 58).

* Work performed by BSc student Elliot Seward.

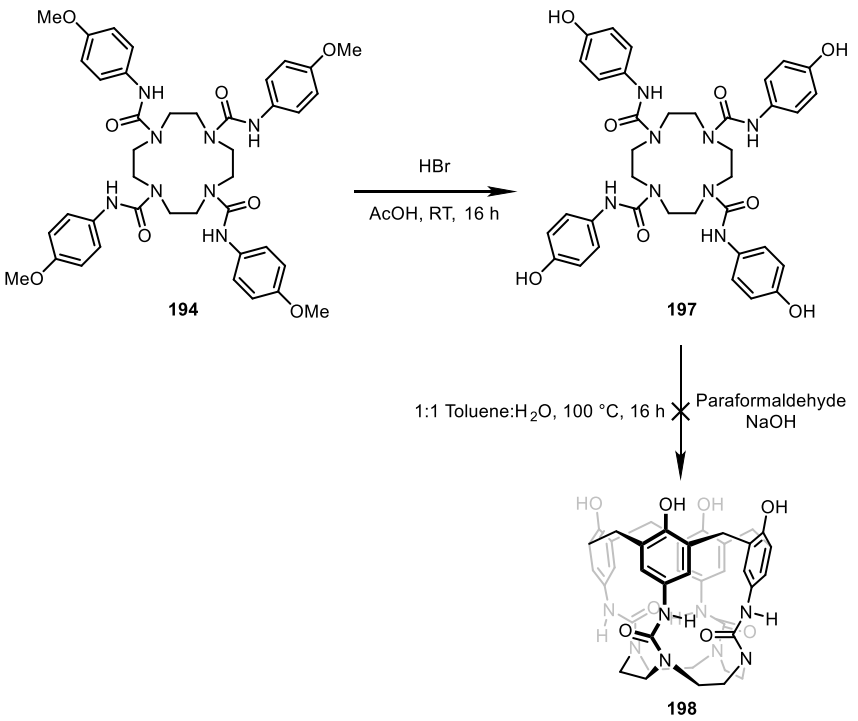

Scheme 58 – Synthesis of 198.

Calixarene synthesis is normally achieved by iterative electrophilic aromatic substitutions on aldehydes followed by condensation of water.[116] Therefore, it was proposed that calix[4]arene, **198** could be made from the corresponding tetrol, **197**. Attempts at fourfold demethylation of **194** using BBr_3 saw decomposition of **194**, presumably by reaction at the ureas. Instead, **194** was demethylated using HBr in AcOH, resulting in precipitation of several products which unfortunately could not be separated due to their lack of solubility. However, phenolic resonances were observed by ^{1}H NMR, so the crude material was heated in toluene/H_2O in an attempt to make the calix[4]arene. Unfortunately, this gave only insoluble products which could not be characterised by ^{1}H NMR or mass spectrometry. It was assumed that polymerisation had occurred instead.

Finally, cyclochirality was preliminarily investigated in the hexamine, 1,4,7,10,13,16-hexaazacyclooctadecane (hexacyclen) by reacting it with an excess of 4-methoxyphenyl isocyanate, giving hexaurea, **199** in excellent yield (Scheme 59).

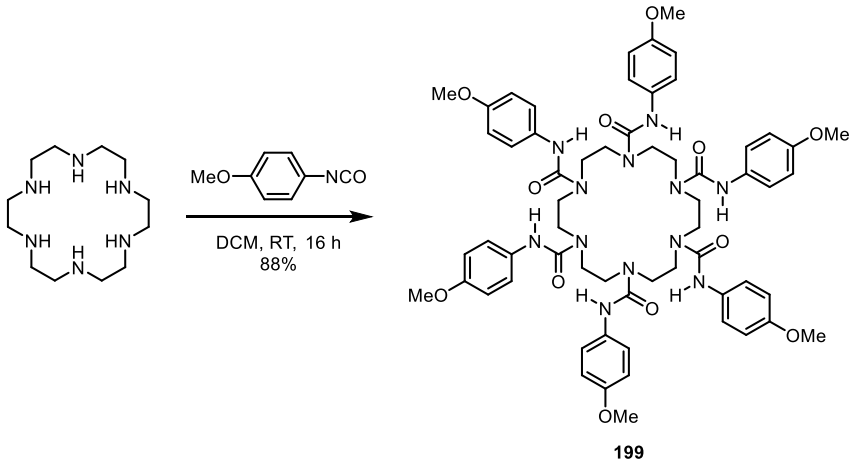

Scheme 59 – Synthesis of 199.

Hexaurea **199** was then studied by ^{1}H NMR (Figure 90).

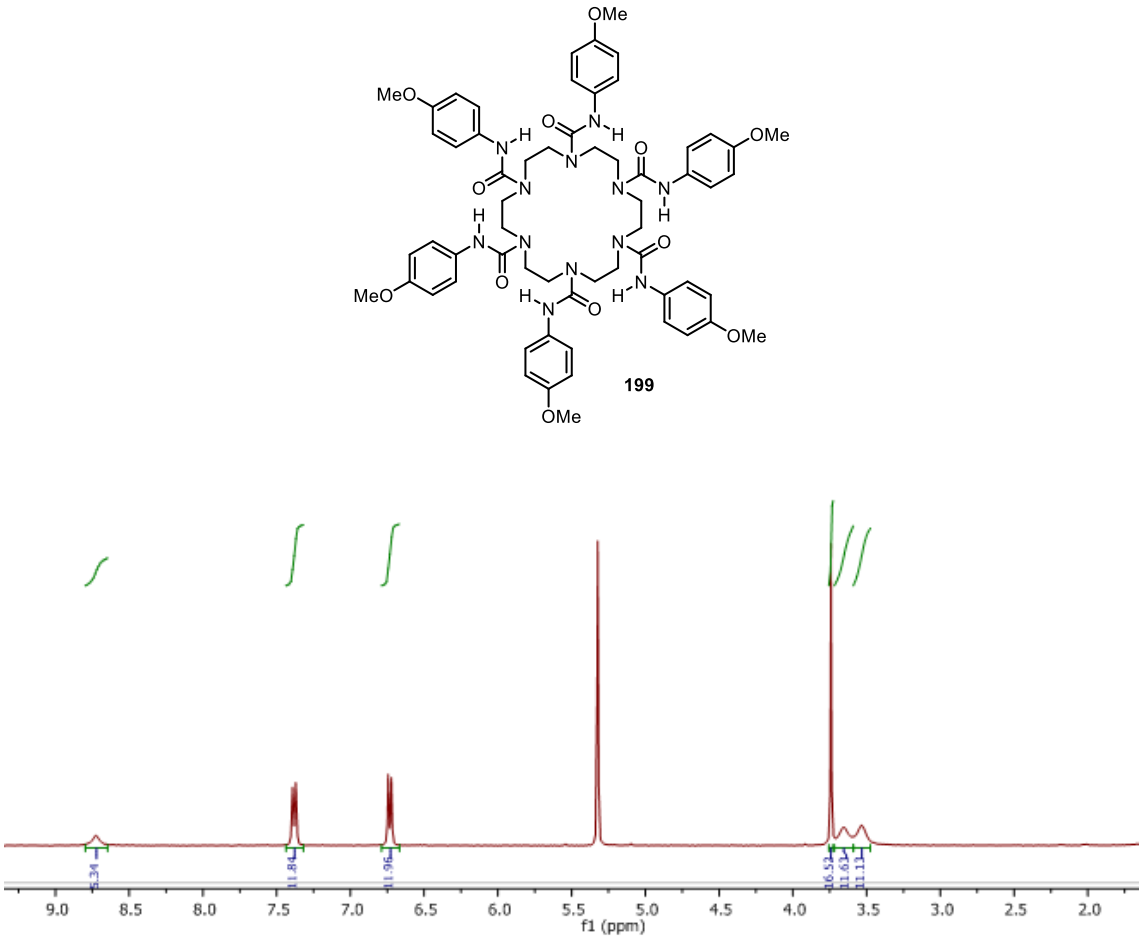

Figure 90 – ^{1}H NMR of 199 (CD_2Cl_2, 400 MHz).

Hexaurea **199** showed signals at 3.53 (alkyl methines, 12 H), 3.66 (alkyl methines, 12 H) and 8.72 ppm (ureido protons, 6 H). This spectrum showed that diastereotopicity had been revealed in the ethylene bridges, giving rise to two equal signals. It also indicated that each of the six ureas were in the same chemical environment, and that the ureido protons were in hydrogen bonding. The diastereotopicity gave rise to two signals as opposed to the four in triurea **175**. Interestingly, hexaurea **199** could exist as one continuous cyclic hydrogen-bonding network (C_6-symmetry), or as two separate three-urea cyclic hydrogen-bonding networks (Figure 91). The ^{13}C NMR and HSQC data indicates one environment for all of the methylenes, as opposed to two in triurea **175**.

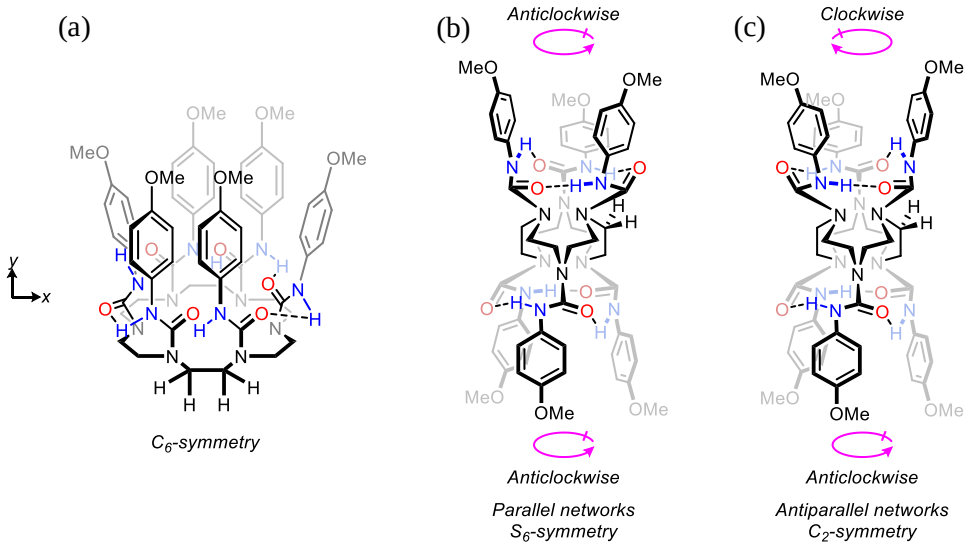

Figure 91 – Possible conformations of 199.

Interestingly, in the proposed conformations (Figure 91, b and c), there are two sources of chirality, meaning that diastereomeric conformers could form of parallel and antiparallel hydrogen-bonding network alignments. In the parallel form, **199** is S_6-symmetrical (rotational axis is the *y* axis), and in the antiparallel form, **199** is C_2-symmetrical (rotational axis is the *x* axis). For all of the methylene carbons to be the same, directionality reversal must be fast on the NMR timescale, revealing bowl-inversion to be the mechanism of methine interconversion in these structures. Alkyl hexaureas did not exhibit this conformational phenomenon at 25 °C.[*]

To summarise, a novel class of cyclochiral compounds derived from TACN have been discovered. These compounds are chiral due to the directionality of the hydrogen bonds in the cyclic hydrogen-bonding network and could be exploited as such. In order to access chiral function, the TACN-derived triureas were modified to raise the racemisation barrier and make it feasible to isolate enantioenriched triureas. Unfortunately, differing substitution on the arene saw

[*] Work performed by BSc student Elliot Seward.

no appreciable change in barrier, and efforts to mechanically lock the ureas together were unfruitful. This conformational phenomenon was not observed in the analogous tetraurea but was alluded to in the hexaurea. Future work in this area will involve mechanistic elucidation of the racemisation of the TACN-derived triureas, and the result of this will be considered when making future analogues with greater barriers. When this informs new targets, the racemisation barriers will be ascertained and, if they are great enough, the triureas will be enantioenriched and applied in enantiospecific host-guest chemistry and asymmetric catalysis. The conformation of the hexaurea will be investigated further, and it is hoped that the same desirable functions can be applied to this scaffold as well.

4.2 Cyclochirality in 2,2,5,5-Tetracarboxamidopyrrolidinyl Amino Acids

Chirality in cyclic systems was first alluded to by Frisch and Wasserman, where they discuss the 'enantiomorphism' in Möbius strips and asymmetric catenanes.[117] This was refined by Vögtle and co-workers through their work on the topological chirality of asymmetric rotaxanes.[118,119] Since then, the term 'cyclochiral' has been used extensively to describe the unidirectional orientation of hydrogen bonds in resorcinarenes.[120–123] Here, the unidirectionality of the hydrogen bonds derives from the helical chirality of the resorcinarene.

Kawabata and co-workers have published seminal work on hydrogen-bonding catalysts that allow site-specific functionalisation of prochiral molecules.[124] The 4-pyrrolidinopyridine (PPY) synthesised by the group was made to serve the same function, but it was discovered that it was in fact the first example of a compound that was chiral solely due to its cyclic hydrogen-bonding array (Figure 92).[125]

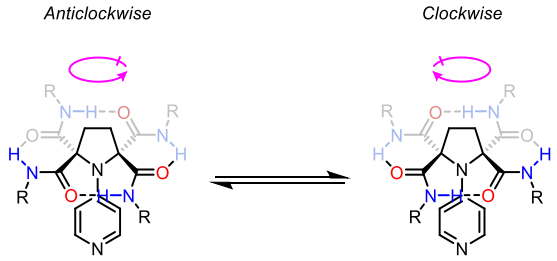

Figure 92 – Kawabata's cyclochiral 4-pyrrolidinopyridines.

In this structure, the four amides on the pyrrolidine ring laid approximately coplanar to form a series of alternating 6- and 8-membered hydrogen-bonding rings in a cyclic hydrogen-bonding array. The hydrogen bonds formed between the amides were so strong that two different sets of ^{1}H NMR signals corresponding to the amido protons were observed at room temperature. Thus, the compound was chiral by virtue of the strength and orientation of its hydrogen-bonding array. Heating the compound caused the signals corresponding to the amide protons to coalesce into one signal. Subsequent line shape and Eyring plot analysis indicated that the racemisation barrier, $\Delta G^{\ddagger}_{298\,K}$ of the compound was 84 kJ mol^{-1} where R = Ph. This high $\Delta G^{\ddagger}_{298\,K}$ corresponded to a half-life of over a week in hexane solution. Additionally, the enantiomers of the PPY could be separated by preparative chiral HPLC at 0 °C.

PPYs with a wide variety of amide substituents were synthesised, all showing similarly large $\Delta G^{\ddagger}_{298\,K}$, with a maximum of 100 kJ mol^{-1} when R = dicyclohexylmethyl. The amides were then synthesised with chiral substituents so that the conformers with opposite hydrogen-bond directionalities would be diastereomeric. The chiral group introduced was an (*R*)-1-(1-naphthyl)ethyl group and in this case, the compound was present as a 73:27 mixture of

diastereomers. The pyridine of the PPY was then protonated using HCl, which interestingly resulted in an inversion of the equilibrium to 32:68. This cyclochiral PPY found use as a chiral nucleophilic catalyst found use in an acylative kinetic resolution of a chiral secondary alcohol. With a 10 mol% loading of the PPY, enantioselective acylation occurred with 59% e.e. and no racemisation of the catalyst.

The following research was undertaken as part of a 3-month Young Researcher International Internship at the Institute for Chemical Research, Kyoto, Japan from September – December 2017.

It was interesting to know whether this specific cyclochiral scaffold could lend itself to types of organocatalysis other than acylative kinetic resolution. The Iwasa group have previously shown that BINAP-derived catalysts with primary amine functions can be used in the asymmetric fluorination of aldehydes, furnishing trisubstituted aldehydes in high yield and enantioselectivity (Scheme 60).[126] Asymmetric fluorination to give quaternary stereocentres is a highly desirable transformation due to the prevalence of quaternary fluorides in pharmaceuticals and due to their capacity for further synthetic elaboration.

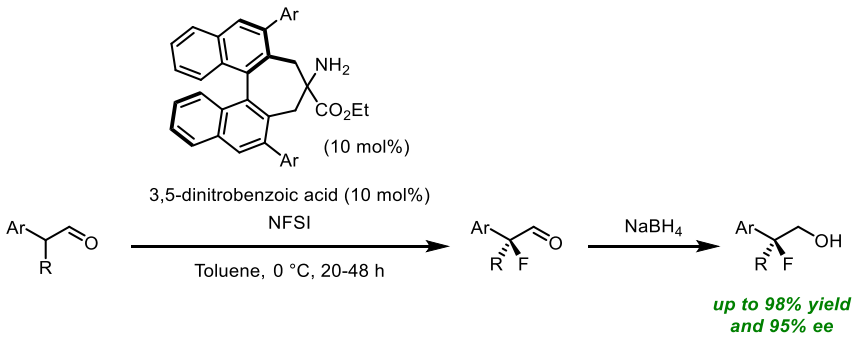

Scheme 60 – Asymmetric fluorination of aldehydes to give quaternary fluorides.

It was speculated that the cyclochiral pyrrolidine derivative of phenylalanine could be used to elicit a similar transformation (Scheme 61).

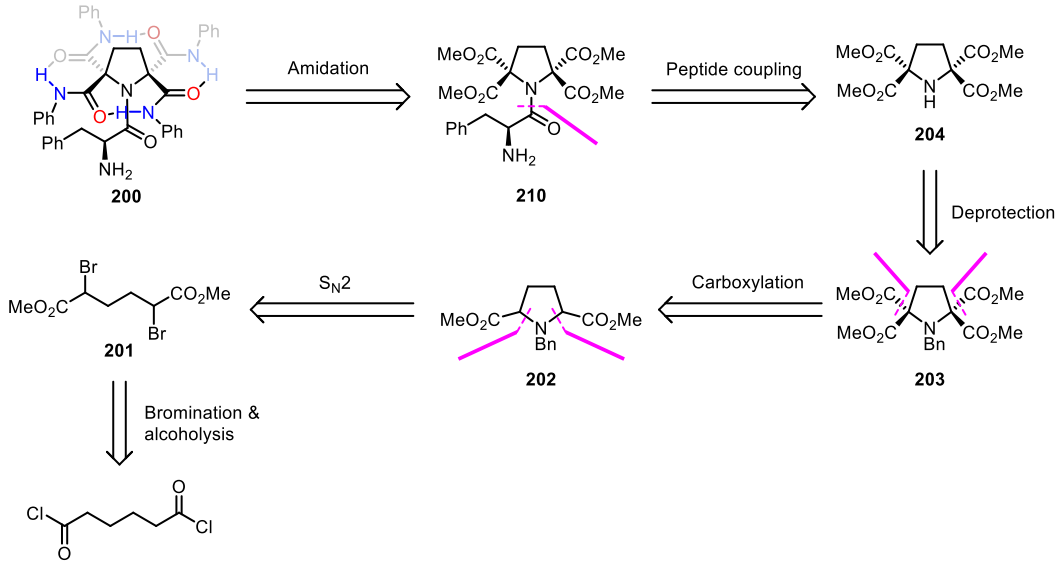

Scheme 61 – Retrosynthetic analysis of 200.

Target primary amine catalyst **200** was to be made by a method similar to what is typically used for the synthesis of PPYs in the Kawabata group.[124] The tetramide was to be formed by tetraamidation of the corresponding tetraester, **210** which could be made by peptide coupling between phenylalanine and the secondary pyrrolidine, **204**. **204** would be revealed by deprotection of *N*-benzylpyrrolidine, **203**, which was to be made by dicarboxylation of **202**. S_N2 and cyclisation of benzylamine would afford **202** from bis(bromo)diester, **201**, which would be made by dibromination and methanolysis of adipoyl chloride.

Firstly, adipoyl chloride underwent dibromination and subsequent methanolysis to yield the corresponding bis(bromo)diester **201**, as a mixture of *cis* and *trans* diastereomers in good yield (Scheme 62). Benzylamine was then used in a twofold S_N2 reaction to yield *cis*- and *trans*-*N*-benzylpyrrolidines in a 1:1.2 ratio. The diastereomers were then separated, and dicarboxylation of **202** to give the tetraester was attempted.

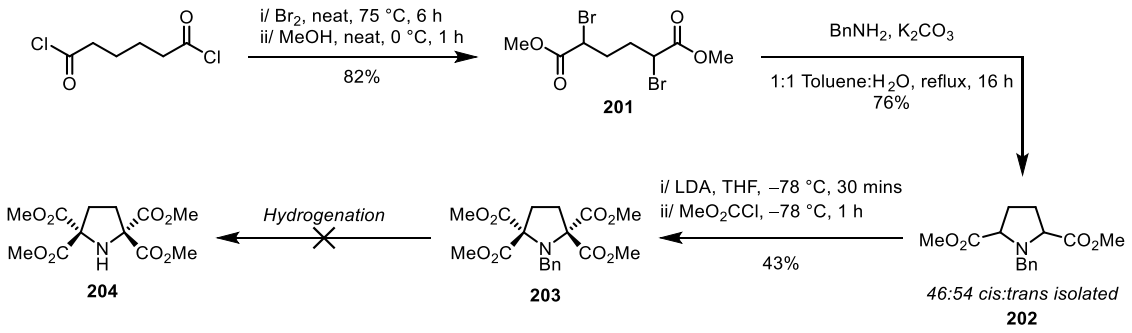

Scheme 62 – Attempted synthesis of 204.

Initially, dicarboxylation of the pyrrolidine was attempted with potassium bis(trimethylsilyl)amide (KHMDS) and methyl cyanoformate. Unfortunately, this yielded only the triester, and so it was speculated that KHMDS was basic enough to deprotonate the pyrrolidine once, but not twice. The reaction was attempted again using lithium diisopropylamide (LDA) as the base, which gave the desired tetraester in 20% yield. The reaction was repeated using methyl chloroformate as the source of methyl ester and the yield was improved to 43%. Initial attempts to hydrogenolyse the benzyl group of the resultant *N*-benzyltetracarboxypyrrolidine, **203** using hydrogen with Pd/C gave no conversion of the starting material. More forcing reductions were attempted, such as using $Pd(OH)_2$ in AcOH and Pd/C in MeOH at 5 bar pressure of hydrogen but these also proved unsuccessful. It was speculated that the bond to undergo cleavage may be too sterically encumbered by the proximate esters to be reduced. In order to circumvent this problem, an alternative route was proposed (Scheme 63).

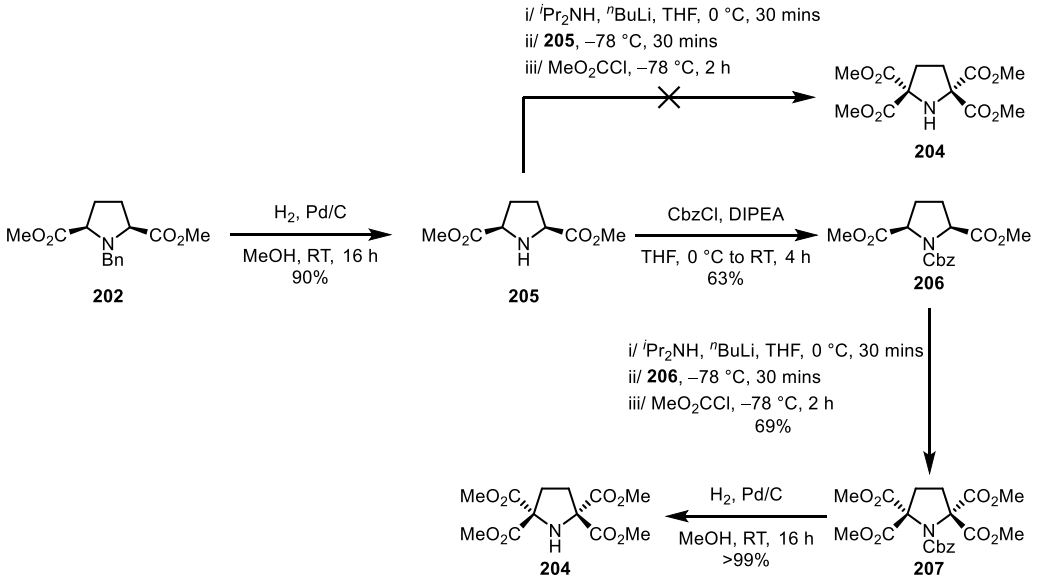

Scheme 63 – Synthesis of 204.

N-benzylpyrrolidine **202** was hydrogenated to give the corresponding secondary amine, and dicarboxylation was attempted, but unfortunately only carbamate formation at the pyrrolidinyl nitrogen was observed. From this, it was deduced that the pyrrolidinyl nitrogen needed to be protected with something other than a benzyl group. A Cbz group was used instead, so that the bond to be cleaved would be more remote from the steric bulk, allowing reduction to proceed.

Pyrrolidine **205** was protected with CbzCl to give carbamate, **206**. **206** then underwent dicarboxylation to give the corresponding tetraester in good yield,. Gratifyingly, the Cbz group could be cleaved using hydrogen and Pd/C, liberating the desired deprotected pyrrolidine, **204** in quantitative yield.

Initial attempts to couple pyrrolidine **204** were performed in DCM using phenylalanine, HOBt/EDC and *N*-methylmorpholine (NMM) as base. Unfortunately, this gave no conversion, presumably due to poor solubility of the phenylalanine. The reaction was attempted again with the more soluble *N*-Boc-phenylalanine, but no reaction occurred, even under more forcing coupling conditions using HATU. It was speculated that this lack of reactivity could be attributed to steric bulk about the pyrrolidinyl nitrogen. It was hypothesised that steric encumbrance about the pyrrolidinyl nitrogen could be mitigated by preforming the cyclic hydrogen-bonding network as the amides should lie approximately coplanar in order to hydrogen bond, instead of protruding towards the pyrrolidinyl nitrogen (Scheme 64). Additionally, this route would avoid the use of strong base after coupling to the amino acid, thereby lowering epimerisation risk.

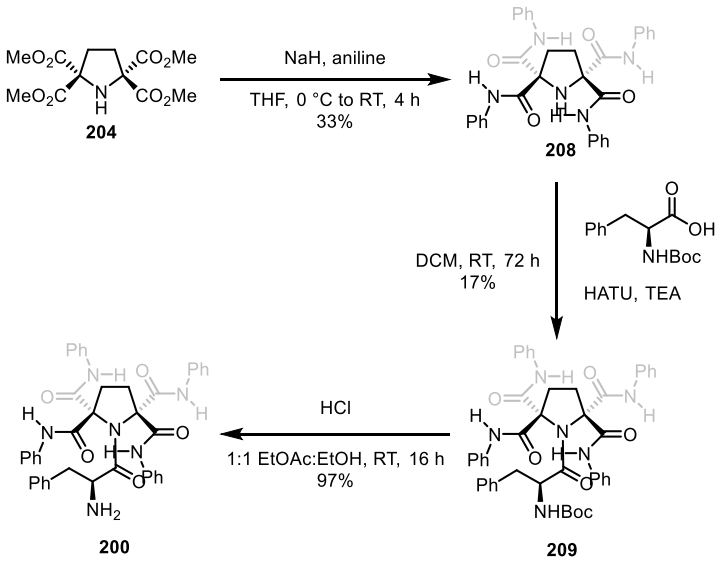

Scheme 64 – Synthesis of 200.

Tetraamidation of tetraester **204** was achieved in poor yield by treatment with sodium hydride and aniline. Use of *N*-Boc-phenylalanine, HOBt, EDC and NMM gave no conversion of **208** to the desired peptide, but fortunately, treatment with HATU and TEA afforded the desired product, **209** in 17% yield. The Boc group was cleaved with HCl in EtOAc to give the target primary amine catalyst, **200** in excellent yield. **200** was then studied by ^{1}H NMR (Figure 93).

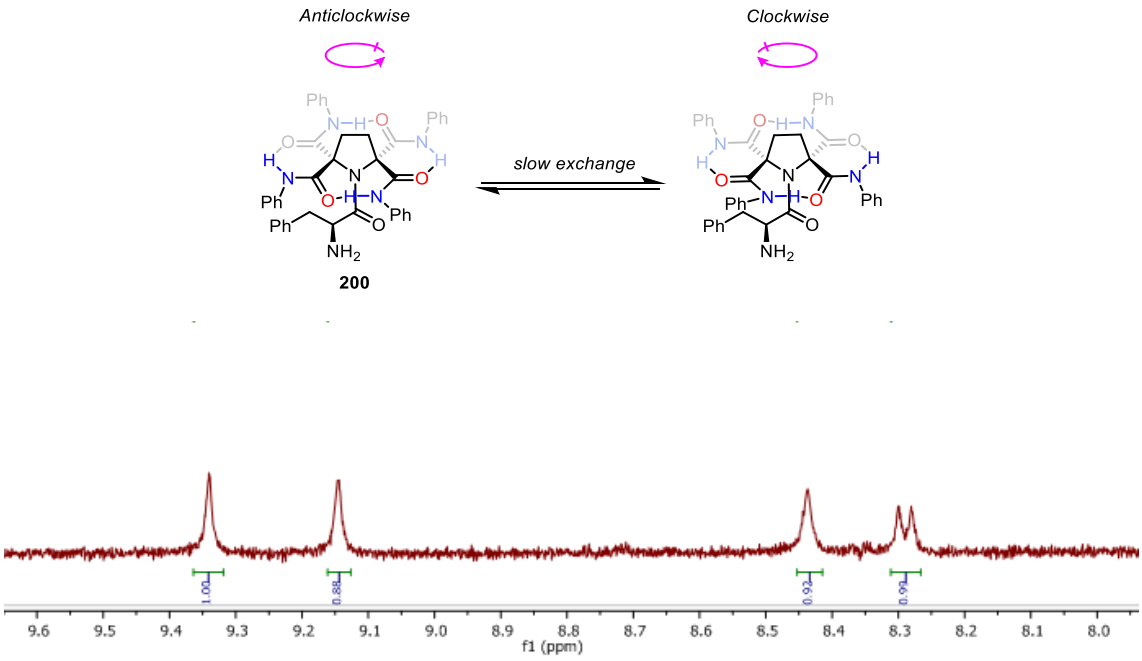

Figure 93 – ^{1}H NMR of 200 in ($CDCl_3$, 300 MHz).

Tetramide **200** showed signals at 8.28 (amido proton, 0.5 H), 8.30 (amido proton, 0.5 H), 8.44 (amido proton, 1 H), 9.15 (amido proton, 1 H) and 9.34 ppm (amido proton, 1 H). The spectrum showed eight different signals corresponding to the amido protons. Three pairs of these amido proton signals came at the same chemical shift, but one pair (8.28 and 8.30 ppm) displayed observable anisochronicity. This phenomenon can be explained through consideration of the different exchange processes active in the molecule (Figure 94).

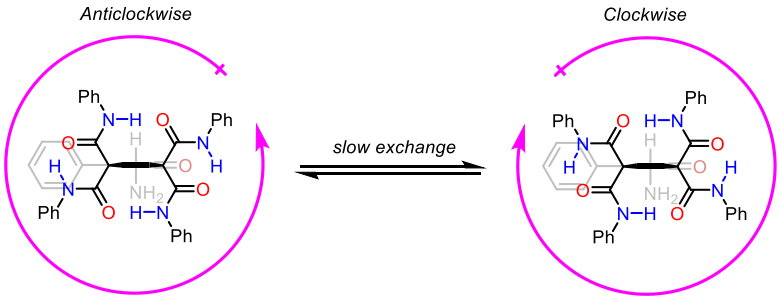

Figure 94 – Dynamic processes in 200 (viewing the top of the pyrrolidine).

The cyclic hydrogen-bonding network is exchanging between its two directionalities slowly on the NMR timescale at 20 °C. This means that the amido protons in adjacent amides are chemically different as one pair of them are in 6-membered hydrogen-bonding rings, and the other in 8-membered hydrogen-bonding rings. Also, the peptide bond is rotameric, meaning that at 20 °C, one of the amido protons in a 6-membered ring is proximate to an amido carbonyl, and the other is proximate to the amino acid residue. Finally, due to the chiral centre in the amino acid, one of the amido protons in an 8-membered hydrogen-bonding ring is adjacent to an amine, and

the other adjacent to a methine, making them also chemically inequivalent. Each of the four amido protons in **200** are chemically distinct from each other due to the chiral centre in the amino acid and the rotameric peptide bond. Each of these four different amido protons corresponded to two different signals in the ^{1}H NMR spectrum because the cyclic hydrogen-bonding network gives rise to two diastereomeric conformers that are in slow exchange on the NMR timescale. The diastereomeric conformers appeared to be present in a 50:50 ratio. Finally, **200** was studied by VTNMR (Figure 95).

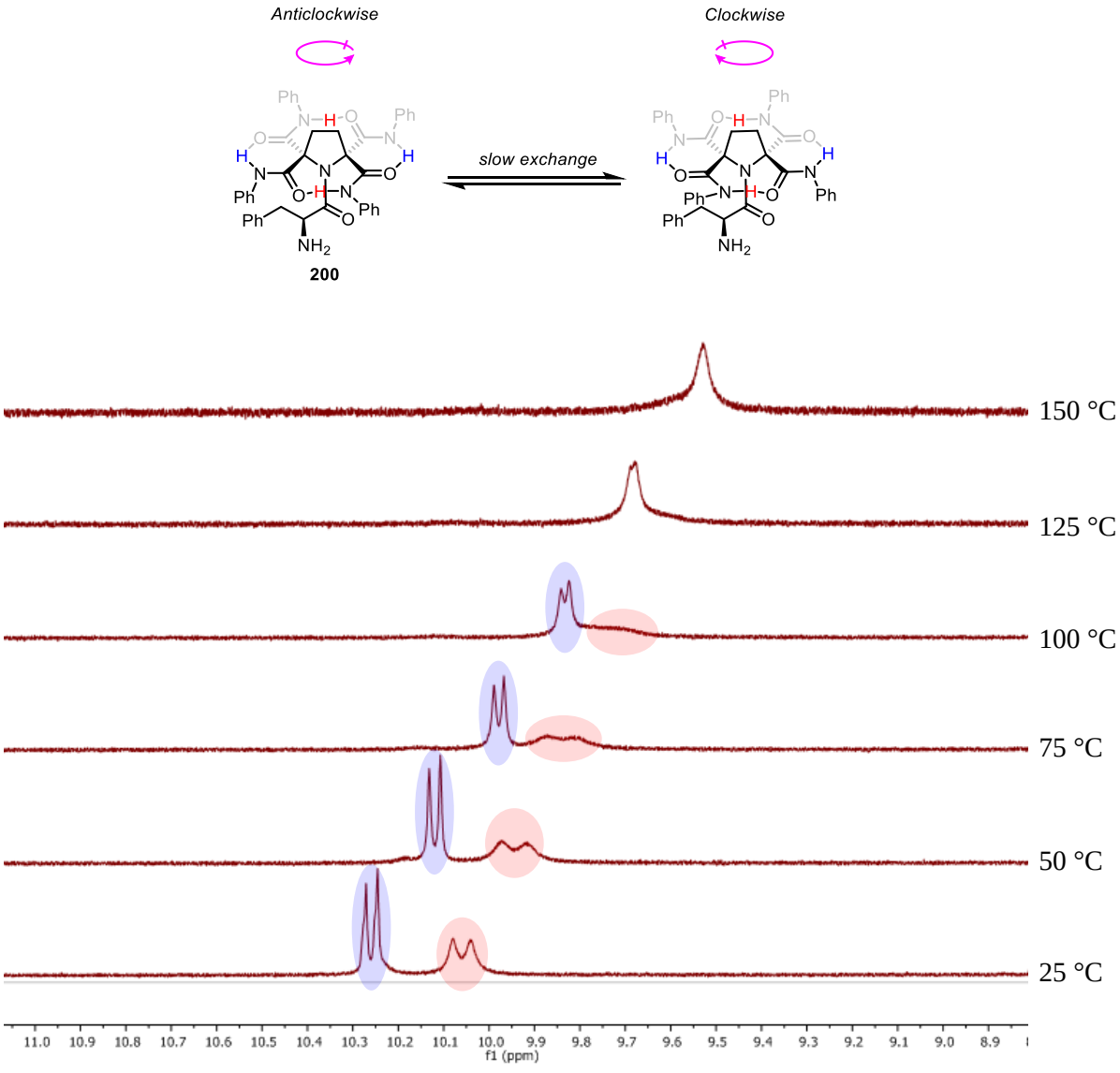

Figure 95 – VTNMR of 200 (600 MHz in d_6-DMSO, 14 mM).

At 25 °C, signals were observed at 10.04 (amido proton, 1 H), 10.08 (amido proton, 1 H), 10.25 (amido proton, 1 H) and 10.27 ppm (amido proton, 1 H). Upon heating, each of the signals moved significantly upfield and broadened. At 100 °C, the signals at 9.74 ppm coalesced, and upon further heating to 150 °C, the signals at 9.53 ppm coalesced. These data indicated that

tetramide **200** exists as two diastereomeric conformations that are in slow exchange at 25 °C in d_6-DMSO, and enter fast exchange between 125 and 150 °C. Interestingly, each of the amido proton signals occurred much more downfield than they did in $CDCl_3$, indicating that the d_6-DMSO can hydrogen bond to the amido protons when they are phenyl amides. This experiment also showed that the incorporation of an amino acid was not detrimental to the robustness of the cyclic hydrogen-bonding network, implying its potential utility in asymmetric catalysis. **200** was then trialled in the organocatalytic asymmetric fluorination of 2-phenylpropionaldehyde using *N*-fluorobenzenesulfonimide (NFSI) (Table 3).

Table 3 – Attempted asymmetric fluorination of 2-phenylpropionaldehyde.

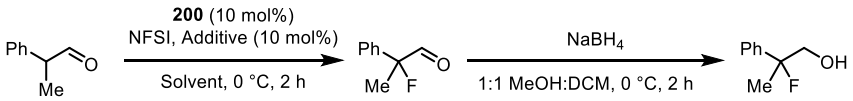

Entry	Solvent	Additive	Yield
1	THF	None	NR
2	Toluene	None	NR
3	Toluene	3,5-dinitrobenzoic acid	Trace conversion

For entries 1 and 2, where no additive was employed, only non-fluorinated, reduced substrate was isolated. However, when 3,5-dinitrobenzoic acid was added, a trace amount of an alternative compound was isolated in trace amounts, but its structure could not be elucidated. In other examples of asymmetric fluorination, much longer reaction times were required, which could explain the initial lack of conversion.[126]

To conclude, the desired cyclochiral amino acid was successfully synthesised and its dynamics investigated in different solvents and by VTNMR. These studies showed that the cyclic hydrogen-bonding network can be appended with peptide bonds and primary amine functions and still exhibit cyclochirality. Preliminary investigations into the use of the amino acid derivative in asymmetric catalysis were performed, but this proved unfruitful. However, it is hoped that further investigation may show the utility of cyclochiral amino acids in organocatalysis. Once this has been demonstrated, the ability of the cyclic hydrogen-bonding network alone to effect asymmetric reaction will be probed using an analogous pyrrolidine derived from achiral glycine.

5.0 Conclusion

In conclusion, ethylene-bridged oligoureas, a novel class of foldamers with the exotic property of reversible hydrogen-bond directionality, have been extensively investigated. These foldamers are conformationally mobile, yet each of the ureas in the foldamer adopts the same orientation to form hydrogen bonds, resulting in conformational homogeneity. This directional ubiquity was found to be thermodynamically insensitive to the presence of hydrogen-bonding cosolvents and additives and is highly tolerant of intramolecular hydrogen-bonding functions. Strong HBDs and HBAs were used to induce directionality in the urea adjacent to it, which was then propagated throughout the foldamer up to six ureas, without any evidence of communication decay.

Basic and acidic functions were appended to the foldamers, bestowing directional switchability to the foldamers (Figure 96). These foldamers responded to external stimuli, such as pH change and the presence of anions or hydrogen-bond-accepting additives by communicating these stimuli as binary information through the oligourea scaffold. The information was reliably reported by use of a fluorescent spectroscopic reporter, which was sensitive to intramolecular hydrogen bonding at millimolar concentrations. Preliminary investigations have also shown that directional switching may be possible in a temporally selective manner using light.

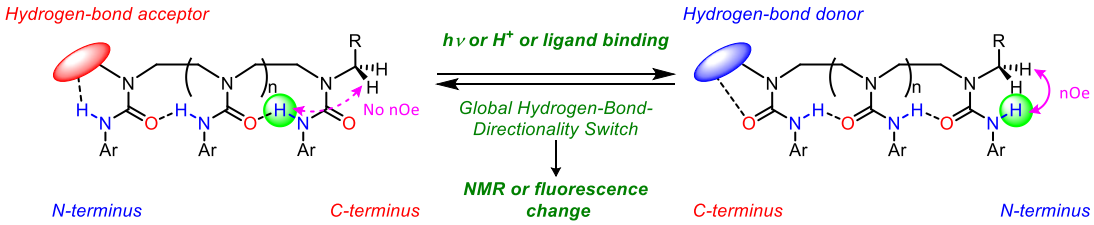

Figure 96 – Ethylene-bridged oligoureas in informational communication.

This novel family of foldamers represents a significant simplification of how biological systems store, communicate and process information. Nature uses hydrogen-bond directionality as a conduit to reliably communicate information in different states, which results in a plethora of specific functions. If ethylene-bridged oligoureas can be used to replicate this phenomenon reliably and without erosion of efficacy, they could be used to perform biomimetic and novel functions. Then, if appended with the appropriate functionality for highly specific binding, they would be able to be delivered where required and undertake those functions in a nanomechanical or biomedical setting.

Ethylene-bridged oligoureas can also be made cyclic. These cyclic triureas adopt a chiral conformation due to hydrogen-bonding interactions, bestowing the property of cyclochirality to them (Figure 97). Several derivatives of the cyclochiral scaffold were synthesised and were revealed to have racemisation barriers of 62-65 kJ mol^{-1}. Whilst this renders the scaffold amenable to dynamic enantioenrichment, it was desirable to raise this barrier so enantioenriched oligoureas could be used for asymmetric organocatalysis or enantiospecific host-guest chemistry. Unfortunately, derivatisation of the scaffold precluded the isolation of stable enantiomers.

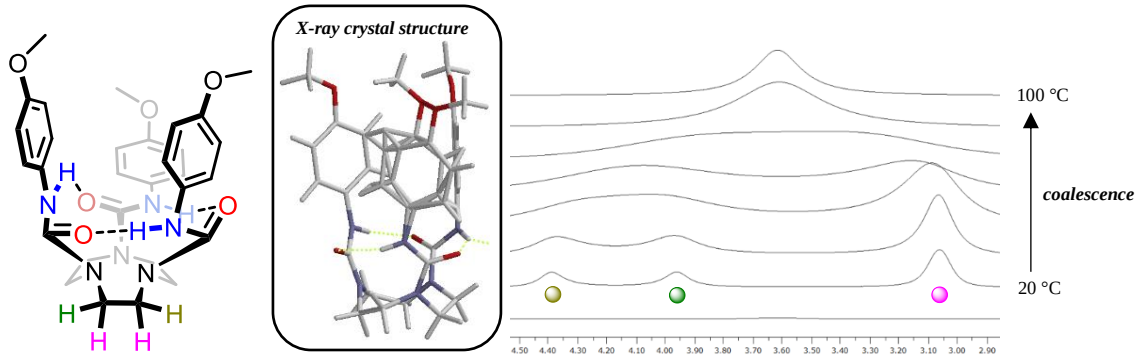

Figure 97 – Cyclochirality in tris(ureido)triazacyclononanes.

The mechanism of racemisation is to inform the appropriate functionalisation that would augment the racemisation barrier. Preliminary investigations have been made and compounds that could elucidate the mechanism have been proposed. Finally, this conformational phenomenon was absent in the analogous tetraurea, but was alluded to by an initial study on the hexaurea.

6.0 Future Work

Research in this project has shown the robustness of ethylene-bridged oligoureas through the efficacy of its communication and the ease of its informational input. However, there has not yet been investigation into functions that could be attained. In principle, there is a vast space to be explored from the selective introduction of a strong HBD or HBA remote from its informational source. Preliminary investigations into this will involve the activation/deactivation of a catalyst or reactive substrate, and selective ion binding (Figure 98).

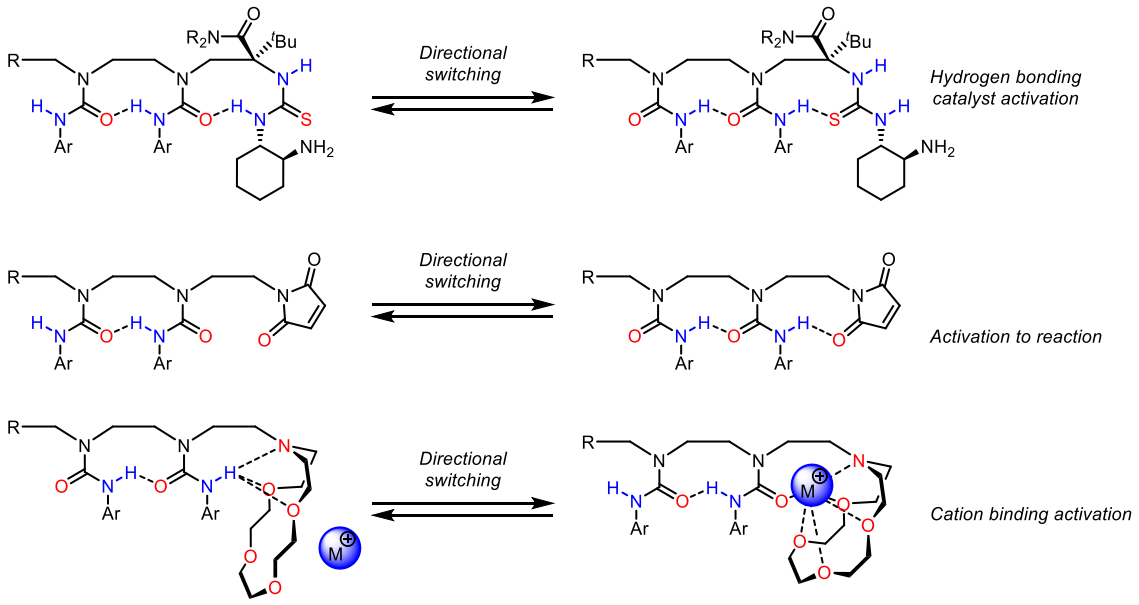

Figure 98 – Chemical functions to be explored in ethylene-bridged oligoureas.

Liberation of a thiourea HBD could reveal a *N,N'*-disubstituted thiourea organocatalyst, which are known to catalyse a wide range of synthetically useful reactions in an enantioselective manner. Reporting *N,N'*-disubstituted thioureas have not been investigated at this point, so initial work here would involve making directionality-controlled molecules that could switch between both directionalities of the reporting thiourea. *N,N'*-disubstituted thioureas and alkyl thioureas are much stronger HBAs than aryl trisubstituted thioureas, so it is hoped that the directionality where the thiourea acts as an HBA could be selected and then used for hydrogen-bonding catalysis by judicious use of the directional controller.

Fluorimetry studies using DTM reporters and fault induction studies using succinimides have already shown that imides can be used to terminate the foldamers, without disrupting the hydrogen-bonding fidelity. This could be exploited by selecting a urea HBD to hydrogen bond to an imide, activating it to reactions such as Diels-Alder cycloadditions or Michael additions. This could also be performed stereoselectively by appendage of chiral groups on the neighbouring

ethylene bridge. Finally, selection of a urea HBD could fill the binding site of a pendent cryptand, where subsequent switching to a urea HBA could open the cryptand and allow cation binding to occur. More exotic function could involve the design of a nanometre-range cargo transporter (Figure 99).

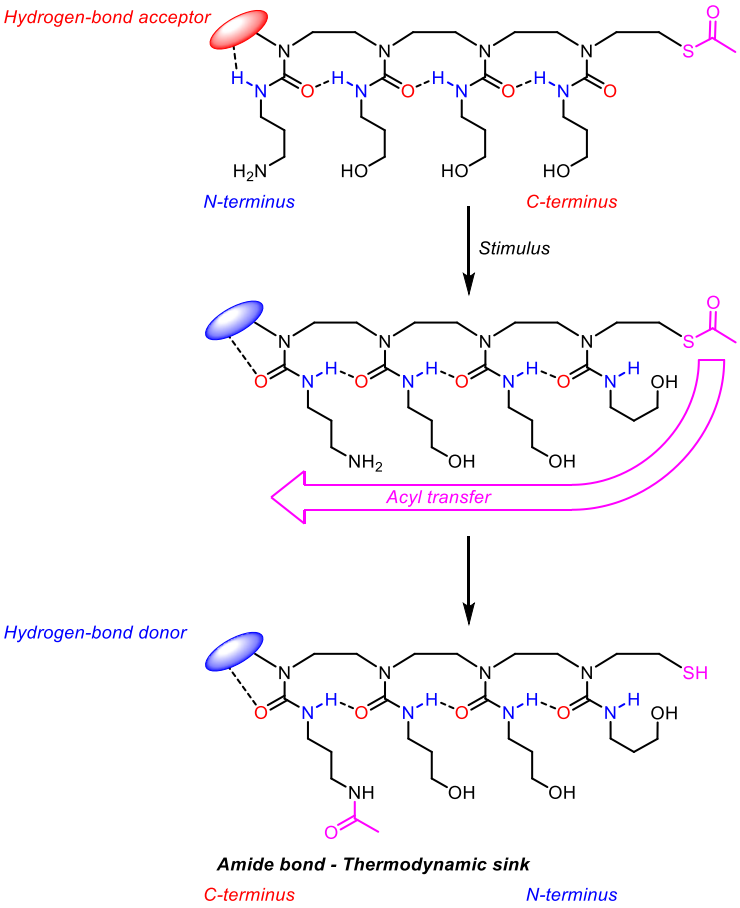

Figure 99 – Proposed nanometre-range cargo transporter.

In one imposed directionality, the hydroxypropyl ureas are too far away from the thioester to be acylated by it. Upon directional switching, the hydroxypropyl group is brought closer to the thioester, allowing acyl transfer to occur. The acyl group is then transferred stepwise between the different alcohols in a random fashion until eventually it is irreversibly captured by the aminopropyl urea. This forms an amide bond, which acts as a thermodynamic sink, and is also kinetically stable to the alcohol, making it the end destination for the acyl group.

Upon furnishing the foldamers with desirable function, analogous molecules that can communicate and perform function over greater distances can be made using the established methodology. This methodology could be extended to larger fragments to access foldamers that can communicate information over even greater distances. Other switching stimuli could be investigated, such as redox/electrochemical manipulations of a quinone HBA / hydroquinone

HBD. Finally, future work will involve derivatisation of the ureido arenes to confer water- and membrane-solubility to the oligoureas. This will bestow greater applicability to the scaffold as appropriate physiological conditions could be simulated, ultimately resulting in transmembrane communication and cellular function.

It would be desirable to synthesise and study oligoureas analogous to bis(pyridine) **174** with more ureas in the centre, where the 2-pyridyl ureas will compete to hydrogen bond to the central ureas (Figure 100).

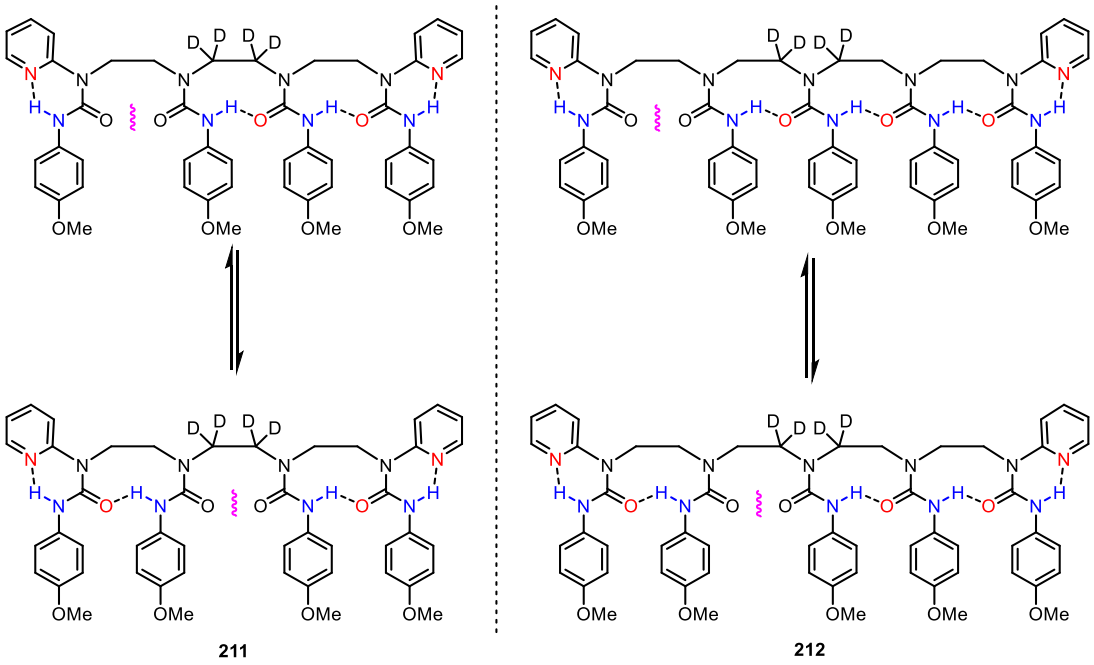

Figure 100 – Dynamics of bis(2-pyridyl urea) oligoureas, 211 and 212.

It is suspected that much like tetraurea **161** and bis(pyridine) **162**, the 2-pyridyl ureas in bis(pyridine) **171** will induce some degree of hydrogen-bonding fault in the centre of the oligourea. ^{2}D VTNMR will reveal the ratio of the conformers in this case. It is envisaged that isotopic labelling and analysis by ^{2}D NMR are necessary due to the congestion of signals in the relevant region. As the directionality-controlling groups are the same in triurea **211** and tetraurea **212**, the ratio of conformers should be the same, unless introduction of another urea to the foldamer results in a change of hydrogen-bond strength. This experiment would serve to determine the presence and degree of hydrogen-bond cooperativity in ethylene-bridged oligoureas. Finally, hexaurea **213** would be of sufficient length to permit the presence of three different faults (Figure 101). Analysis of this would reveal the preference or lack thereof for hydrogen-bonding faults to be closer or farther from the source of directional control. It is suspected that identification of the two unsymmetrical conformers by would be very challenging,

but determination of the conformer ratio would be pertinent to the investigation into multiple possible faults and hydrogen-bond cooperativity.

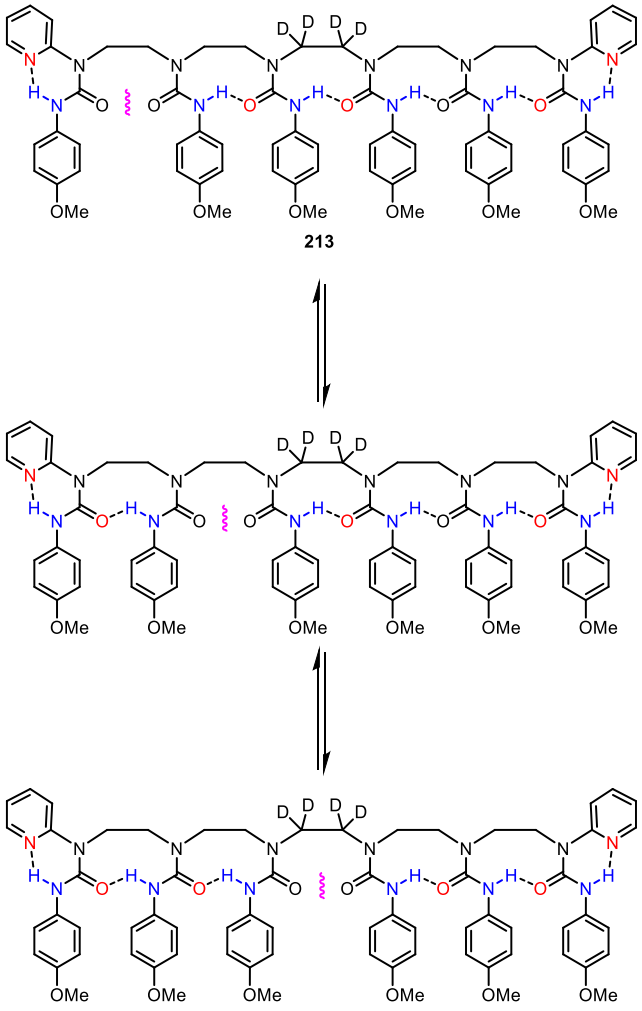

Figure 101 – Dynamics of 213.

Cockroft and co-workers investigated the use of rotameric formamides for the quantification of hydrogen-bond cooperativity.[29] Whilst experiments in this project have indicated a lack of hydrogen-bond cooperativity in ethylene-bridged oligoureas from a kinetic standpoint, these formamides could be used to give evidence for hydrogen-bond cooperativity using thermodynamic parameters (Figure 102) in addition to bis(pyridines) **211-213**.

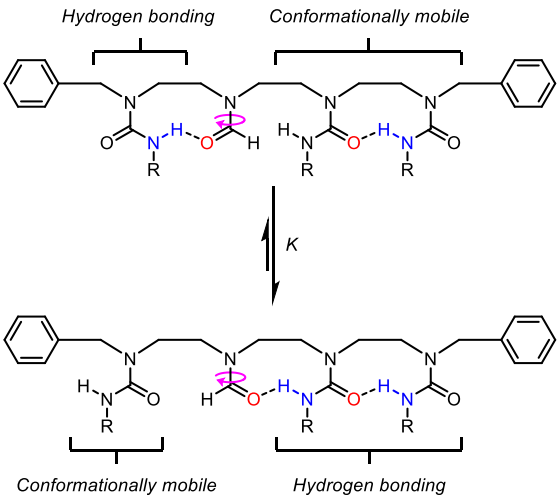

Figure 102 – Hydrogen-bond cooperativity balances for ethylene-bridged oligoureas.

The formamide can hydrogen bond to two different ureas. These two ureas are identical, except one of them is hydrogen bonding to another urea, isolating the thermodynamic connotations of hydrogen-bond cooperativity in these structures. *K* can be easily deduced by NMR and converted to a value for $\Delta G^{\ddagger}$, which will correspond to the energy gain from hydrogen-bond cooperativity. An analogous compound can be made with one urea on one side and three ureas on the other, and this could also be used to quantify the effects of upon further urea extension. This is also not limited to investigating hydrogen-bond cooperativity – this tool could be used to pit different HBDs with different ring sizes against each other, and the observed *K* can be used to measure relative hydrogen-bond-donating power.

In the area of cyclochirality, the racemisation mechanism of TACN-derived triureas could be elucidated by appropriate substitution on the TACN (Figure 103).

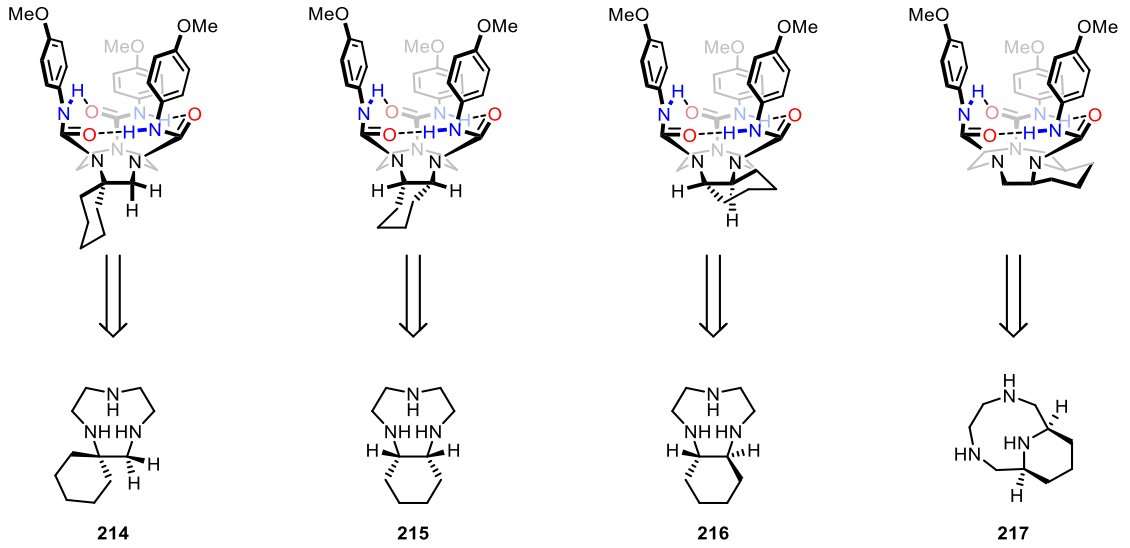

Figure 103 – Substrates for mechanistic elucidation of TACN-derived triurea racemisation.

Spirocycle **214** has a spirocyclic cyclohexane on one of the ethylene bridges of the TACN. This allows isolation of two of the vicinal methines, where they will equilibrate as normal if the bowl inversion is the rate-determining mechanism. Similarly, bicycle **215** bears a *cis*-fused cyclohexane on one of the ethylene bridges, isolating two of the vicinal methines and allowing equilibration as normal if directionality reversal is the operating mechanism. It is assumed that cyclohexane ring-flipping will occur quickly relative to racemisation, allowing facile analysis. Bicycle **216** has a *trans*-fused cyclohexane, where only the operation of both mechanisms would allow interconversion of the methines, meaning that the barrier to racemisation would match that of spirocycle **214** or bicycle **215** depending on which mechanism was rate-determining. It is noteworthy that (a) bowl inversion is associated with a cyclohexane ring flip into a 1,2-diaxial relationship of the ureas, which may be rate-limiting and (b) the chirality of the *trans*-fused cyclohexane may give rise to diastereomeric cyclic hydrogen-bonding networks. Finally, bicycle **217** has a *cis*-fused piperidine (Figure 103, diequatorial conformation depicted), where linking across one of the ureas will block bowl inversion of that urea and therefore force directionality reversal to operate. If $\Delta G^{\ddagger}$ significantly decreases in this case, bowl inversion is the rate-determining mechanism in the parent monocyclic triureas.

Mechanistic elucidation will inform methods to raise the barrier and allow isolation of enantioenriched cyclochiral compounds. Those compounds will then be trialled in asymmetric organocatalysis and enantiospecific host-guest chemistry. The same will apply to the hexacyclen-derived hexaureas, which will have different properties as the size of the cavitand will be different.

At this point, the only cyclochiral compounds isolated racemise quickly. This renders them a chiral cavitand that can potentially undergo dynamic enantioenrichment (Figure 104).

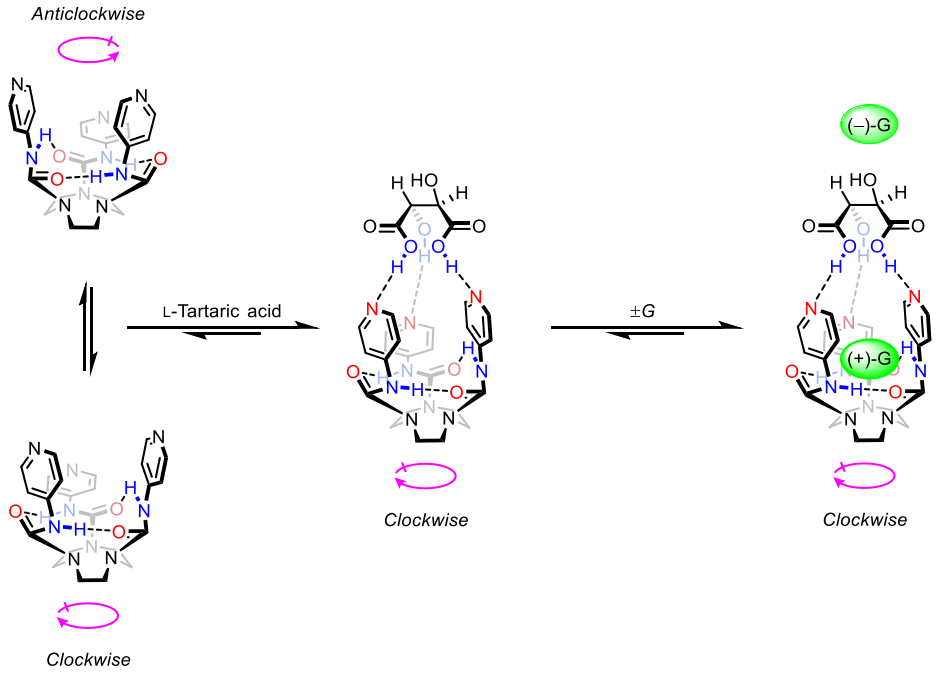

Figure 104 – Dynamic enantioenrichment of TACN-derived triureas.

For example, if the cavitand was appended with basic pyridines, a chiral acid, such as L-tartaric acid, could bind to it and permit a dynamic enantioenrichment of the cyclic hydrogen-bonding network. This makes the cavitand chiral with a fixed directionality, where one enantiomer of a desired guest could be captured, while the other would be enantioenriched and uncomplexed in the solution. This allows dynamic enantioenrichment of a racemic guest which doesn't interact with the original chiral input (the acid) but is of the correct size and geometry to interact with the racemic cavitand.

7.0 Experimental

7.1 General Information

Where specified, procedures were performed using dried solvents and reagents under an atmosphere of nitrogen with glassware dried by flame-drying. Air and moisture-sensitive liquids/solutions were transferred to reaction vessels by syringe under an atmosphere of nitrogen. Anhydrous DCM, THF, MeCN, Et_2O and toluene were dried using an anhydrous Engineering Grubbs-type solvent system. All other solvents and reagents were purchased from commercial suppliers and were used without further purification unless otherwise specified. Agitation was achieved using Teflon coated stirrer bars by magnetic induction. All thin layer chromatography (TLC) experiments were conducted on pre-coated plastic plates (Macherey-Nagel polygram SIL G/UV_{254}) and visualised using ultraviolet light (254 nm) or staining. TLC eluents are reported in solvent:solvent v/v ratios. Irradiation was achieved using Thorlabs mounted high-power LEDs of the appropriate wavelength, mounted onto a Thorlabs LED driver DC4100. Flash chromatography was performed manually using Sigma Aldrich silica gel 60 (40-63 mM) or on an automated Biotage Isolera™ Spektra Four using gradient elution on pre-packed silica gel Biotage® SNAP Ultra or ZIP Sphere columns. All melting point experiments were performed using a Stuart SMP10 Melting Point Apparatus upon recrystallisation from the specified solvent(s). All low-temperature VTNMR experiments were conducted using a JEOL ECS 300 spectrometer (300 MHz) or a Bruker AVANCE III HD 500 MHz NMR Spectrometer with 5 mm DCH ^{13}C–^{1}H/D Cryo Probe (500 MHz). All high-temperature VTNMR experiments were conducted using a Varian VNMRS 500 MHz Direct Drive Spectrometer with Agilent OneNMR probe (500 MHz). All room temperature NMR experiments were conducted using a Bruker Nano 400 Spectrometer (400 MHz) or a Bruker AVANCE III HD 500 MHz NMR Spectrometer with 5 mm DCH ^{13}C–^{1}H/D Cryo Probe (500 MHz), with chemical shifts reported (δ in ppm) relative to the specified deuterated solvent. All ^{19}F NMR spectra are referenced relative to an internal standard (α,α,α-trifluorotoluene). All NMR characterisation experiments were performed at 25 °C and 1 atm unless otherwise specified. Multiplicity is reported as follows – s = singlet, d = doublet, t = triplet, q = quartet. All spin-spin coupling constants (J) are reported in hertz (Hz) to the nearest 0.1 Hz. When signal congestion precludes analysis of multiplicity, they are reported as m = multiplets. Signals of rotameric species are denoted as 'rot.'. All reported signals in ^{13}C NMR spectra are singlets unless otherwise specified. High resolution mass spectrometry experiments (HR-MS) were performed on a Bruker micrOTOF Spectrometer using electrospray ionisation, positive ion mode or a Bruker Ultraflex using MALDI with only molecular ion ($[M+H]^+$ or $[M+Na]^+$) peaks being reported. Fourier transform infrared spectroscopy (FTIR) experiments

were performed using a PerkinElmer Spectrum Two FTIR Spectrometer. All absorbances are reported in cm^{-1}. Fluorescence spectra were recorded using a PerkinElmer LS45 fluorimeter in a Marco Fluorescence Quartz Cuvette. Recrystallisation for X-ray crystallography was achieved by slow evaporation of a precipitant into a solution containing the desired compound. Analysis was performed using a Bruker Apex II Goniometer.

7.2 General Procedures

General procedure A – Palladium-catalysed hydrogenative reductive amination

Under a dry, inert atmosphere, a round-bottomed flask was charged with a solution of amine (1.00 equiv., 0.10 M) in anhydrous MeOH. To this solution was added aldehyde (1.08 equiv.) and palladium on carbon (10% wt., 10 mol%). The flask was equipped with a three-way tap with a hydrogen-filled balloon attached. The flask was evacuated and refilled with nitrogen three times, then evacuated and refilled with hydrogen. The black suspension was left to stir for 16 h. The black suspension was filtered through celite and washed with MeOH. The filtrate was then concentrated *in vacuo* to give the crude secondary amine.

General procedure B1 – (Thio)urea formation by (thio)carboxamidation of amines using iso(thio)cyanates.

Under a dry, inert atmosphere, a solution of secondary amine (1.00 equiv., 0.10 M) in anhydrous DCM was cooled to 0 °C. To this solution was added iso(thio)cyanate (1.50 equiv. per amine) dropwise/over three portions. The resulting solution was stirred for 16 h and concentrated *in vacuo* to give the crude (thio)urea.

General procedure B2 – Urea formation by carboxamidation of amines using carbamoyl chlorides or phenyl carbamates.

Under a dry, inert atmosphere, a solution of secondary amine (1.00 equiv., 0.10 M) in anhydrous DCM was cooled to 0 °C. To this solution was added carbamoyl chloride or phenyl carbamate (1.50 equiv. per amine) dropwise/over three portions. Triethylamine (1.50 equiv. per amine) was added and the resulting solution warmed to room temperature and stirred for 16 h. The solution was concentrated *in vacuo* to give the crude urea.

General procedure C – Boc-deprotection of amines using TFA

Under a dry, inert atmosphere, TFA (20% v/v) was added dropwise to a solution of Boc-protected amine (1.00 equiv., 0.10 M) in anhydrous DCM (80% v/v). The solution was stirred for 16 h and concentrated *in vacuo*. The crude product was diluted with saturated aqueous $NaHCO_3$ and the aqueous phase was extracted with DCM three times. The combined organic extracts were washed with brine, dried ($MgSO_4$), filtered and concentrated *in vacuo* to give the crude amine.

General procedure D – Michael addition of amines with acrylonitrile

Under a dry, inert atmosphere, a solution of amine (1.00 equiv., 0.10 M) in anhydrous MeOH was prepared. To this solution was added acrylonitrile (1.50 equiv.) in one portion. The solution was stirred for 16 h and concentrated *in vacuo* to give the title nitrile.

General procedure E – Reductive amination by one-pot condensation/$NaBH_4$ reduction

Under a dry, inert atmosphere, aldehyde (1.50 equiv. per amine) was added to a solution of primary amine (1.00 equiv., 0.10 M) in anhydrous MeOH. The resulting solution was stirred for 16 h. The solution was cooled to 0 °C and sodium borohydride (3.00 equiv. per amine) was added in one portion. The resulting white suspension was warmed to room temperature, stirred for 3 h and concentrated *in vacuo*. The residue was then diluted with MeOH and concentrated *in vacuo*. The crude product was diluted with deionised water and the aqueous solution was extracted with DCM three times. The combined organic extracts were washed with brine, dried ($MgSO_4$), filtered and concentrated *in vacuo* to give the crude secondary amine.

General procedure F – Chemoselective Boc-protection of secondary amines by trifluoroacetylation, carboxylation and hydrolysis.

Under a dry, inert atmosphere, a solution of amine (1.00 equiv, 1.60 M) in anhydrous DCM was cooled to 0 °C. To the solution was added ethyl trifluoroacetate (1.10 equiv.) dropwise over 30 minutes and the resultant solution was stirred for 30 minutes. The solution was warmed to room temperature and stirred for a further hour. The solution was then diluted with anhydrous DCM (10 mL $mmol^{-1}$) and cooled to 0 °C. A solution of di-*tert*-butyl dicarbonate (1.20 equiv. per amine, 2.00 M) in anhydrous DCM was added over three portions followed by anhydrous TEA (1.00 equiv. per amine) in one portion. The resulting solution was stirred for 16 h and diluted with saturated aqueous $NaHCO_3$. The organic phase was washed with deionised water, dried ($MgSO_4$), filtered and concentrated *in vacuo*. The crude yellow oil (0.20 M) was dissolved in methanol and a solution of aqueous NaOH (7.30 equiv., 4.20 M) was added. The resulting colourless solution was stirred for 5 h and concentrated *in vacuo*. The crude product was dissolved in deionised water and the aqueous phase was extracted with DCM four times. The combined organic extracts were dried ($MgSO_4$), filtered and concentrated *in vacuo* to give the title carbamate.

General procedure G – Oxidation of primary alcohols using DMP

To a solution of alcohol (1.00 equiv, 0.10 M) in DCM was added DMP (1.20 equiv.) at 0 °C. The resulting white suspension was stirred for 16 h at room temperature. Saturated aqueous $NaHCO_3$ and saturated aqueous $Na_2S_2O_3$ were added and the mixture was stirred for 30 minutes. The organic phase was washed with saturated aqueous $NaHCO_3$, dried ($MgSO_4$), filtered and concentrated *in vacuo* to yield the title aldehyde.

General procedure H – Hydrolysis of trifluoroacetamides

To a solution of trifluoroacetamide (1.00 equiv., 0.10 M) was added a solution of aqueous NaOH (7.30 equiv., 4.20 M). The resulting colourless solution was stirred for 5 h and concentrated *in vacuo*. The crude product was dissolved in deionised water and the aqueous phase was extracted with DCM three times. The combined organic extracts were washed with brine, dried ($MgSO_4$), filtered and concentrated *in vacuo* to give the crude primary amine.

General procedure I – Succinimidation of amines by *in situ* activation with acetyl chloride

Under a dry inert, atmosphere, succinic anhydride (1.00 equiv. per amine) was added in one portion to a solution of amine (1.00 equiv., 0.10 M) in anhydrous DCM. TEA (1.00 equiv. per amine) was added and the solution was heated to reflux for 16 h. The solution was cooled to 0 °C and acetyl chloride (2.00 equiv. per amine) was added dropwise and the solution was stirred at room temperature for a further 3 h. The resulting solution was concentrated *in vacuo* and the crude product was diluted in saturated aqueous $NaHCO_3$. The aqueous solution was extracted with DCM three times and the combined organic extracts were washed with brine, dried ($MgSO_4$), filtered and concentrated *in vacuo* to give the crude succinimide.

General procedure J – One-pot trifluoroacetylation/carboxamidation of oligoethylenediamines

Under a dry, inert atmosphere, a solution of amine (1.00 equiv, 1.60 M) in anhydrous DCM was cooled to 0 °C. Ethyl trifluoroacetate (1.10 equiv. per primary amine) was added dropwise over 30 minutes and the resulting solution was stirred for 30 minutes at 0 °C. The resulting solution was warmed to room temperature and stirred for a further hour. The solution was diluted with DCM (10 mL $mmol^{-1}$) cooled to 0 °C. To this solution was added isocyanate (1.50 equiv. per secondary amine) and the resulting solution was stirred for 16 h to give the crude urea.

General procedure K – Boc-protection of amines

To a solution of amine (1.00 equiv. 0.25 M) in DCM was added a solution of aqueous NaOH (1.00 M, 4 mL $mmol^{-1}$). The mixture was cooled to 0 °C and a solution of di-*tert*-butyl dicarbonate (1.00 equiv., 0.25 M) in DCM was added over three portions. The resulting mixture was stirred for 16 h and the aqueous phase was extracted with DCM three times. The combined organic extracts were washed with deionised water twice, dried ($MgSO_4$), filtered and concentrated *in vacuo* to give the crude carbamate.

General procedure L – Swern oxidation of primary alcohols

Under a dry, inert atmosphere, a solution of anhydrous DMSO (3.00 equiv, 0.40 M) in anhydrous DCM was cooled to −78 °C. To this solution was added a solution of oxalyl chloride (1.50 equiv., 2.00 M) in anhydrous DCM dropwise. The resulting solution was stirred for 20 minutes, and a solution of alcohol (1.00 equiv., 0.80 M) in anhydrous DCM was added dropwise. The resulting solution was stirred for 2 h at −78 °C and anhydrous TEA (9.00 equiv.) was added dropwise to give a white suspension. The suspension was warmed to 0 °C and stirred for 30 minutes. The reaction was quenched with aqueous citric acid (10% w/w., 10 mL $mmol^{-1}$). The mixture was stirred for 15 minutes at 0 °C and warmed to room temperature. The aqueous phase was then extracted with DCM three times, and the combined organic extracts washed with aqueous citric acid (10% w/w), deionised water, saturated aqueous Na_2CO_3 and brine. The combined organic extracts were then dried ($MgSO_4$), filtered and concentrated *in vacuo* to give the crude aldehyde.

General Procedure M – Pyridylation of amines by nucleophilic aromatic substitution

Under a dry, inert atmosphere, 2-fluoropyridine (1.00 equiv.) was added to amine (10.00 equiv.) and the resulting solution was heated to 120 °C and stirred for 16 h. The solution was cooled to room temperature, diluted with EtOAc and washed with deionised water three times. The organic phase was washed with brine, dried ($MgSO_4$), filtered and concentrated *in vacuo* to give the title *N*-(2-pyridyl)-amine.

General procedure N – Johnson-Lemieux oxidation of *N*-allyl carbamates/maleimides

Under an inert atmosphere, a solution of allyl carbamate/maleimide (1.00 equiv., 0.10 M) in dioxane:water (3:1) was prepared. To this solution was added sodium periodate (4.00 equiv.), 2,6-lutidine (2.00 equiv.) and osmium tetroxide (4% wt. in water, 10 mol%). The solution was stirred for 4 h and quenched with saturated aqueous $Na_2S_2O_3$. After stirring for 30 minutes, the solution was diluted with EtOAc and the organic phase was washed with saturated aqueous $Na_2S_2O_3$ and brine. The organic phase was dried ($MgSO_4$), filtered and concentrated *in vacuo* to give the crude aldehyde.

General procedure O – Fischer indole reaction to make 3*H*-indoles

Under a dry, inert atmosphere, a solution of arylhydrazine hydrochloride (1.00 equiv, 1.00 M) in AcOH was prepared. To this solution was added ketone (1.20 equiv.) and the solution was heated to 100 °C and stirred for 3 h. The solution was cooled to room temperature and filtered. The filtrate was then diluted in DCM and poured onto deionised water. The organic phase was then washed with brine, dried ($MgSO_4$), filtered and concentrated *in vacuo* to give the title 3*H*-indole.

General procedure P – 3-Sulfonylpropylation of 3*H*-indoles by S_N2 reaction with 1,3-propanesultone

Under a dry, inert atmosphere, a solution of 3*H*-indole (1.00 equiv., 0.50 M) in anhydrous 1,2-DCB was prepared. To this solution was added 1,3-propanesultone (1.10 equiv.) and the solution was heated to 120 °C and stirred for 16 h. The solution was cooled to room temperature and recrystallised from cold Et_2O. The brown suspension was filtered and the residue was washed with Et_2O and air-dried to give the title indolium sulfonate.

General procedure Q – Pseudo-aldol condensation of 3*H*-indoles with salicylaldehydes

Under a dry, inert atmosphere, a solution of indolium sulfonate (1.00 equiv., 0.10 M) in anhydrous EtOH was prepared. To this solution was added salicylaldehyde (1.10 equiv.) and the solution was heated to reflux and stirred for 16 h. The solution was cooled to room temperature and concentrated *in vacuo* to give the crude styrene.

General procedure R – Reductive amination with 2-maleimidoacetaldehydes and subsequent carboxamidation with isocyanates

Under a dry, inert atmosphere, a solution of primary amine (1.00 equiv., 0.10 M) in anhydrous DCM was prepared. To this solution was added aldehyde (1.10 equiv.) and $NaB(OAc)_3H$ (1.50 equiv.) in one portion. The resulting solution was stirred at room temperature for 16 h. The solution was quenched with saturated aqueous $NaHCO_3$ and the aqueous phase was extracted with DCM three times. The combined organic phases were washed with brine, dried ($MgSO_4$), filtered and concentrated *in vacuo* to give the crude secondary amine. Under a dry, inert atmosphere, the crude product (1.00 equiv. 0.10 M) was then dissolved in anhydrous DCM and cooled to 0 °C. To this solution was added isocyanate (2.00 equiv.) and the resulting solution was stirred for 16 h. The solution was concentrated *in vacuo* to give the crude urea.

General procedure S – Hydrogenative cleavage of benzyl groups

Under a dry, inert atmosphere, a round-bottomed flask was charged with a solution of benzyl-protected compound (1.00 equiv., 0.10 M) in anhydrous MeOH. To this solution was added palladium on carbon (10% wt., 10 mol%). The flask was equipped with a three-way tap with a hydrogen-filled balloon attached. The flask was evacuated and refilled with nitrogen three times, then evacuated and refilled with hydrogen. The black suspension was left to stir for 16 h. The black suspension was filtered through celite and washed with MeOH. The filtrate was the concentrated *in vacuo* to yield the title secondary amine.

7.3 Experimental Procedures

1-Phenyl-7-(*tert*-butoxycarbonyl)-1,4,7-triazaheptane, 28

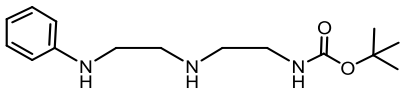

Synthesised according to literature procedure A using *N*-phenylethylenediamine (0.50 mL, 3.80 mmol) and *N*-Boc-2-aminoacetaldehyde (653 mg, 4.10 mmol). The title carbamate was isolated as a colourless oil (727 mg, 2.62 mmol, 69%). **TLC** – R_f = 0.31 (SiO_2, 90:10:1 EtOAc:MeOH:TEA).). **^{1}H NMR** (400 MHz, $CDCl_3$) δ_H 1.45 (s, 9H, C(C*H*$_3$)$_3$), 2.75 (t, J = 5.9, NC*H*$_2$), 2.89 (t, J = 6.0, 2H, NC*H*$_2$), 3.22 (q, J = 5.4, 2H, NC*H*$_2$), 6.64 (d, J = 8.5, 2H, 2 x Ar*H*), 6.71 (tt, J = 1.0, 7.3, Ar*H*), 7.18 (dd, J = 7.3, 8.5, 2H, 2 x Ar*H*). Spectroscopic data matched that previously reported.[79]

1-Phenyl-1,4-bis(4-methoxyanilinylcarbonyl)-7-(*tert*-butoxycarbonyl)-1,4,7-triazanonane, 29

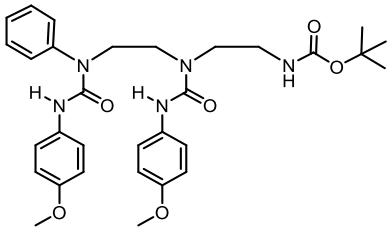

Synthesised according to general procedure B1 using **28** (626 mg, 2.24 mmol) and 4-methoxyphenyl isocyanate (0.87 mL, 6.72 mmol). The crude product was purified by column chromatography (12-100% EtOAc:PE) to yield the title diurea as a foamy white solid (686 mg, 1.19 mmol, 53%). **M.P.** 80-81 °C ($CHCl_3$). **TLC** – R_f = 0.19 (SiO_2, 50:50 EtOAc:PE). **^{1}H NMR** (400 MHz, $CDCl_3$) δ_H 1.40 (s, 9H, C(C*H*$_3$)$_3$), 3.26 (q, J = 5.7, NC*H*$_2$), 3.44 (t, J = 6.1, 2H, NC*H*$_2$), 3.65 (t, J = 5.7, 2H, NC*H*$_2$), 3.77 (s, 3H, OC*H*$_3$), 3.78 (s, 3H, OC*H*$_3$), 3.82 (t, J = 6.1, 2H, NC*H*$_2$), 5.14 (t, J = 5.7, 1H, N*H*), 6.15 (s, 1H, N*H*), 6.81 (d, J = 8.9, 2H, 2 x Ar*H*), 6.83 (d, J = 8.9, 2H, 2 x Ar*H*), 7.19 (d, J = 8.9, 2H, 2 x Ar*H*), 7.31 (d, J = 7.6, 2H, 2 x Ar*H*), 7.41 (t, J = 7.6, 1H, Ar*H*), 7.50 (t, J = 7.6, 2H, Ar*H*), 7.55 (d, J = 8.9, 2H, Ar*H*), 8.67 (s, 1H, N*H*). **^{13}C NMR** (101 MHz, $CDCl_3$) δ_C 28.6 (C(*C*H$_3$)$_3$), 40.2 (N*C*H$_2$), 46.5 (N*C*H$_2$), 47.3 (N*C*H$_2$), 49.6 (N*C*H$_2$), 55.6 (2 x O*C*H$_3$), 79.5 (*C*(CH$_3$)$_3$), 114.0-114.2 (4 x Ar*C*), 121.5-121.8 (4 x Ar*C*), 128.1 (2 x Ar*C*), 128.7 (Ar*C*), 130.9 (2 x Ar*C*), 131.4 (Ar*C*), 133.5 (Ar*C*), 141.8 (Ar*C*), 155.3-155.5 (2 x Ar*C*), 156.0 (*C*O), 156.6 (2 x *C*O). **HR-MS** (ESI, positive ion mode) – *m/z* for $[C_{31}H_{39}N_5O_6+H]^+$ = 578.2979. Found 578.2954. **FTIR** (neat) – 3423, 3321, 2973, 2935, 1652, 1594.

1-Phenyl-1,4-bis(4-methoxyanilinylcarbonyl)-1,4,7-triazaheptane, 30

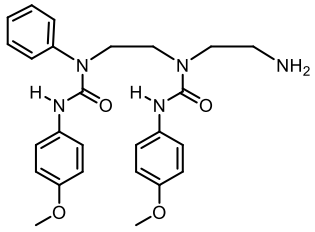

Synthesised according to general procedure C using **29** (200 mg, 0.34 mmol). The title amine was isolated as a foamy white solid (141 mg, 0.30 mmol, 87%). **M.P.** 123-124 °C (DCM). **TLC** – R_f = 0.10 (SiO_2, 90:10 EtOAc:PE). **^{1}H NMR** (500 MHz, $CDCl_3$) δ_H 2.91 (t, J = 5.6, 2H, NC*H*$_2$), 3.41 (t, J = 5.6, 2H, NC*H*$_2$), 3.63 (t, J = 7.2, 2H, NC*H*$_2$), 3.76 (s, 3H, OC*H*$_3$), 3.77 (s, 3H, OC*H*$_3$), 3.86 (t, J = 7.2, 2H, NC*H*$_2$), 6.28 (s, 1H, N*H*), 6.79 (d, J = 9.0, 2H, 2 x Ar*H*), 6.81 (d, J = 9.0, 2H, 2 x Ar*H*), 7.20 (d, J = 9.0, 2H, 2 x Ar*H*), 7.33 (t, J = 8.2, 2H, 2 x Ar*H*), 7.38 (tt, J = 7.4, 1.2, 1H, Ar*H*), 7.42 (d, J = 9.0, 2H, 2 x Ar*H*), 7.48 (t, J = 8.2, 2H, 2 x Ar*H*), 9.23 (s, 1H, N*H*). **^{13}C NMR** (126 MHz, $CDCl_3$) δ_C 41.5 (N*C*H$_2$), 46.6 (N*C*H$_2$), 49.0 (N*C*H$_2$), 51.5 (N*C*H$_2$), 55.5 (2 x O*C*H$_3$), 113.9-114.0 (4 x Ar*C*), 121.1-121.8 (4 x Ar*C*), 128.0-128.2 (3 x Ar*C*), 130.5 (2 x Ar*C*), 131.4 (Ar*C*), 133.5 (Ar*C*), 141.8 (Ar*C*), 155.1-155.4 (2 x Ar*C*), 157.0 (2 x *C*O). **HR-MS** (ESI, positive ion mode) – *m/z* for $[C_{26}H_{31}N_5O_4+H]^+$ = 478.2454. Found 478.2446. **FTIR** (neat) – 3677, 3432, 2985, 2902, 1654.

1-Phenyl-1,4-bis(4-methoxyanilinylcarbonyl)-7-cyanoethyl-1,4,7-triazaheptane, 31

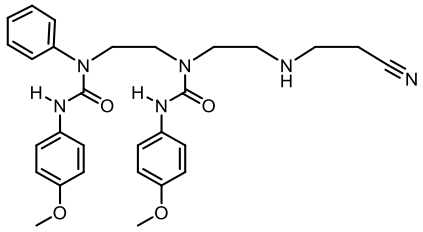

Synthesised according to general procedure D using **30** (141 mg, 0.30 mmol). The title nitrile was isolated as a foamy white solid (157 mg, 0.28 mmol, 94%). **M.P.** 197-198 °C ($CHCl_3$). **TLC** – R_f = 0.11 (SiO_2, 1:99 MeOH:DCM). **^{1}H NMR** (400 MHz, $CDCl_3$) δ_H 2.45 (t, J = 6.6, 2H, NC*H*$_2$), 2.84 (t, J = 6.0, 2H, NC*H*$_2$), 2.93 (t, J = 6.6, 2H, NC*H*$_2$), 3.44 (t, J = 6.0, 2H, NC*H*$_2$), 3.65 (t, J = 7.2, 2H, NC*H*$_2$), 3.77 (s, 3H, OC*H*$_3$), 3.77 (s, 3H, OC*H*$_3$) 3.86 (t, J = 7.2, 2H, NC*H*$_2$), 6.16 (s, 1H, N*H*), 6.80 (d, J = 9.0, 2H, 2 x Ar*H*), 6.82 (d, J = 9.0, 2H, 2 x Ar*H*), 7.18 (d, J = 9.0, 2H, NC*H*$_2$), 7.34 (d, J = 7.4, 2H, 2 x Ar*H*), 7.41 (tt, J = 7.4, 1.2, 1H, Ar*H*), 7.47 (d, J = 9.0, 2H, 2 x Ar*H*), 7.50 (t, J = 7.4, 2H, 2 x Ar*H*), 8.75 (s, 1H, N*H*). **^{13}C NMR** (101 MHz, $CDCl_3$) δ_C 18.9 (N*C*H$_2$), 45.3 (N*C*H$_2$), 46.9 (N*C*H$_2$), 48.6 (N*C*H$_2$), 48.9 (N*C*H$_2$), 49.6 (N*C*H$_2$) , 55.6 (2 x O*C*H$_3$), 114.1 (2 x Ar*C*), 114.2 (2 x Ar*C*) 118.7 (*C*≡N), 121.4 (2 x Ar*C*), 122.0 (2 x Ar*C*), 128.2 (2 x Ar*C*), 128.6 (2 x Ar*C*), 130.8 (Ar*C*) 131.4 (2 x Ar*C*), 133.5 (Ar*C*), 141.8 (Ar*C*), 155.3-155.5 (2 x Ar*C*), 156.1 (*C*O), 156.7 (*C*O). **HR-MS** (ESI, positive ion mode) – *m/z* for $[C_{29}H_{34}N_6O_4+Na]^+$ = 553.2539. Found 553.2546. **FTIR** (neat) – 3433, 3316, 2917, 2253, 1660.

1-Phenyl-1,4,7-tris(4-methoxyanilinylcarbonyl)-7-cyanoethyl-1,4,7-triazaheptane, 32

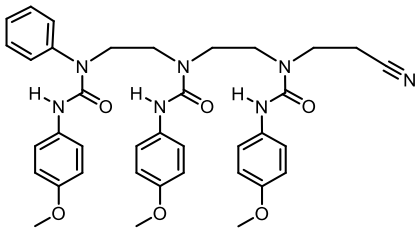

Synthesised according to general procedure B1 using **31** (78 mg, 0.14 mmol) and 4-methoxyphenyl isocyanate (0.03 mL, 0.22 mmol). The crude product was purified by column chromatography (12-100% EtOAc:PE) to yield the title diurea as a foamy white solid (54 mg, 0.08 mmol, 60%). **M.P.** 190-191 °C ($CHCl_3$). **TLC** – R_f = 0.18 (SiO_2, 1:99 MeOH:DCM). **^{1}H NMR** (500 MHz, $CDCl_3$) δ_H 2.67 (t, J = 6.1, 2H, NC*H*$_2$), 3.52 (t, J = 5.4, 2H, NC*H*$_2$), 3.58 (t, J = 6.1, 2H, NC*H*$_2$), 3.61 (t, J = 6.4, 2H, NC*H*$_2$), 3.71 (t, J = 6.4, 2H, NC*H*$_2$), 3.74 (s, OC*H*$_3$), 3.78 (s, OC*H*$_3$), 3.78 (s, OC*H*$_3$), 3.84 (t, J = 5.4, NC*H*$_2$), 6.11 (s, 1H, N*H*), 6.74 (d, J = 9.1, 2H, 2 x Ar*H*), 6.81 (d, J = 9.1, 2H, 2 x Ar*H*), 6.84 (d, J = 9.1, 2H, 2 x Ar*H*), 7.15 (d, J = 9.1, 2H, 2 x Ar*H*), 7.18 (d, J = 9.1, 2H, 2 x Ar*H*), 7.31 (d, J = 7.1, 2H, 2 x Ar*H*), 7.46 (tt, J = 7.8, 1.2, 1H, Ar*H*), 7.47 (d, J = 9.1, 2H, 2 x Ar*H*), 7.54 (t, J = 7.1, 2H, 2 x Ar*H*), 8.15 (s, 1H, N*H*), 8.68 (s, 1H, N*H*). **^{13}C NMR** (126 MHz, $CDCl_3$) δ_C 17.8 (N*C*H$_2$), 46.0 (N*C*H$_2$), 47.3 (N*C*H$_2$), 47.7 (N*C*H$_2$), 48.4 (N*C*H$_2$), 50.1 (N*C*H$_2$), 55.6 (3 x O*C*H$_3$), 114.0-114.1 (6 x Ar*C*), 119.3 (*C*≡N), 121.1 (2 x Ar*C*), 121.8 (2 x Ar*C*), 123.2 (2 x Ar*C*), 127.8 (2 x Ar*C*), 128.1 (Ar*C*), 128.8 (2 x Ar*C*), 130.9 (3 x Ar*C*), 141.6 (Ar*C*), 155.0-155.3 (3 x Ar*C*), 156.1-156.5 (3 x *C*O). **HR-MS** (ESI, positive ion mode) – *m/z* for $[C_{37}H_{41}N_7O_6+Na]^+$ = 702.3016. Found 702.3040. **FTIR** (neat) – 3345, 2974, 2964, 2234, 1652.

1-Ethyl-7-(*tert*-butoxycarbonyl)-1,4,7-triazaheptane, 33

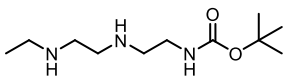

Synthesised according to general procedure A using *N*-ethylethylenediamine (0.60 mL, 5.67 mmol) and *N*-Boc-2-aminoacetaldehyde (910 mg, 6.12 mmol). The title carbamate was isolated as a colourless oil (879 mg, 3.80 mmol, 67%). **TLC** – R_f = 0.23 (SiO_2, 10:90:1 MeOH:DCM:NH_4OH). **^{1}H NMR** (400 MHz, $CDCl_3$) δ_H 1.23 (t, J = 6.5, 3H, C*H*$_3$), 1.44 (s, 9H, C(C*H*$_3$)$_3$), 2.76 (t, J = 5.4, 2H, NC*H*$_2$), 2.91 (t, J = 6.3, 2H, NC*H*$_2$), 3.00 (t, J = 6.3, 2H, NC*H*$_2$), 3.23 (C^{2}H$_2$, 2H, m), 3.71 (q, J = 5.4, 2H, NC*H*$_2$), 5.45 (t, J = 5.4, 1H, N*H*). **^{13}C NMR** (101 MHz, $CDCl_3$) δ_C 18.4 (*C*H$_3$), 28.5 (C(*C*H$_3$), 40.1 (N*C*H$_2$), 46.0 (N*C*H$_2$), 47.1 (N*C*H$_2$), 49.1 (N*C*H$_2$), 58.4 (N*C*H$_2$), 81.4 (*C*(CH$_3$)$_3$), 156.9 (*C*O). **HR-MS** (ESI, positive ion mode) – *m/z* for $[C_{11}H_{25}N_3O_2+H]^+$ = 232.2025 . Found 232.2019. **FTIR** (neat) – 3352, 2963, 1694.

1-Ethyl-1,4-bis(anilinylcarbonyl)-7-(*tert*-butoxycarbonyl)-1,4,7-triazaheptane, 34

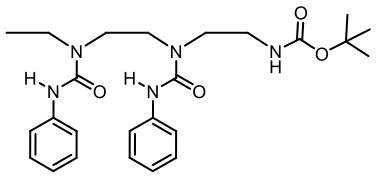

Synthesised according to general procedure B1 using **33** (100 mg, 0.43 mmol) and phenyl isocyanate (0.14 mL, 1.30 mmol). The crude product was purified by column chromatography (18-100% EtOAc:PE) to yield the title diurea as a foamy white solid (137 mg, 0.29 mmol, 68%). **M.P.** 130-131 °C ($CHCl_3$). **TLC** – R_f = 0.19 (SiO_2, 75:25 EtOAc:PE). **^{1}H NMR** (500 MHz, $CDCl_3$) δ_H 1.22 (t, J = 7.1, 3H, C*H*$_3$), 1.48 (s, 9H, C(C*H*$_3$)$_3$), 3.25 (q, J = 7.0, 2H, NC*H*$_2$), 3.42 (q, J = 7.1, 2H, NC*H*$_2$), 3.43-3.50 (m, 6H, 3 x NC*H*$_2$), 5.28 (t, J = 7.0), 7.02 (t, J = 7.3, 1H, Ar*H*), 7.04 (t, J = 7.3, 1H, Ar*H*), 7.29 (t, J = 7.9, 2H, 2 x Ar*H*), 7.31 (t, J = 7.9, 2H, 2 x Ar*H*), 7.62 (d, J = 7.9, 2H, 2 x Ar*H*), 7.70 (d, J = 7.9, 2H, 2 x Ar*H*), 8.68 (s, 1H, N*H*). **^{13}C NMR** (126 MHz, $CDCl_3$) δ_C 14.2 (*C*H$_3$), 28.4 (C(*C*H$_3$)$_3$), 40.2 (N*C*H$_2$), 43.0 (N*C*H$_2$), 46.0 (N*C*H$_2$), 47.8 (N*C*H$_2$), 47.8 (N*C*H$_2$), 80.3 (*C*(CH$_3$)$_3$), 119.6 (2 x Ar*C*), 119.8 (2 x Ar*C*), 122.5 (Ar*C*), 122.6 (Ar*C*), 128.7 (4 x Ar*C*), 139.9 (2 x Ar*C*), 155.6 (*C*O), 156.2 (*C*O), 157.1 (*C*O). **HR-MS** (ESI, positive ion mode) – *m/z* for $[C_{25}H_{35}N_5O_4+Na]^+$ = 492.2587. Found 492.2588. **FTIR** (neat) – 3311, 3137, 2983, 1710, 1664.

1-Ethyl-1,4-bis(anilinylcarbonyl)-1,4,7-triazaheptane, 35

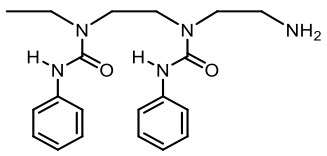

Synthesised according to general procedure C using **34** (500 mg, 1.06 mmol). The title amine was isolated as a foamy white solid (388 mg, 1.05 mmol, 99%). **M.P.** 137-138 °C ($CHCl_3$). **TLC** – R_f = 0.07 (SiO_2, 90:10 EtOAc:PE). **^{1}H NMR** (500 MHz, $CDCl_3$) δ_H 1.20 (t, J = 7.1, 3H, C*H*$_3$), 1.70 (s, 2H, N*H*$_2$), 3.00 (t, J = 4.6, 2H, NC*H*$_2$), 3.40-3.48 (m, 6H, 3 x NC*H*$_2$), 3.52 (t, J = 7.3, 2H, NC*H*$_2$), 6.94 (tt, J = 7.3, 1.2, 1H, Ar*H*), 7.02 (tt, J = 7.3, 1.2, 1H, Ar*H*), 7.24 (t, J =7.8, 2H, 2 x Ar*H*), 7.27 (t, J =7.8, 2H, 2 x Ar*H*), 7.42 (d, J = 8.1, 2H, 2 x Ar*H*), 7.64 (d, J = 8.1, 2H, 2 x Ar*H*), 8.34 (s, 1H, N*H*), 10.22 (s, 1H, N*H*). **^{13}C NMR** (126 MHz, $CDCl_3$) δ_C 14.1 (*C*H$_3$), 41.7 (N*C*H$_2$), 42.6 (N*C*H$_2$), 45.1 (N*C*H$_2$), 48.1 (N*C*H$_2$), 52.9 (N*C*H$_2$), 118.9 (2 x Ar*C*), 119.6 (2 x Ar*C*), 122.2 (Ar*C*), 122.3 (Ar*C*), 128.6 (2 x Ar*C*), 128.8 (2 x Ar*C*), 140.0 (2 x Ar*C*), 155.5 (*C*O), 158.3 (*C*O). **HR-MS** (ESI, positive ion mode) – *m/z* for $[C_{20}H_{27}N_5O_2+Na]^+$ = 392.2062. Found 392.2081. **FTIR** (neat) – 3306, 2999, 2971, 1641.

1-Ethyl-1,4-bis(anilinylcarbonyl)-7-cyanoethyl-1,4,7-triazaheptane, 36

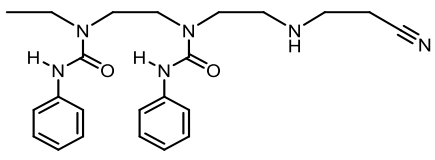

Synthesised according to general procedure D using **35** (300 mg, 0.81 mmol). The title nitrile was isolated as a foamy white solid (317 mg, 0.75 mmol, 93%). **M.P.** 152-

153 °C ($CHCl_3$). **TLC** – R_f = 0.26 (SiO_2, 5:95 MeOH:DCM). **^{1}H NMR** (400 MHz, $CDCl_3$) δ_H 1.15 (t, J = 7.2, 3H, C*H*$_3$), 2.04 (s, 1H, N*H*), 2.38 (t, J = 6.6, 2H, NC*H*$_2$), 2.75 (t, J = 6.6, 2H, NC*H*$_2$), 2.84 (t, J = 6.6, 2H, NC*H*$_2$), 3.32-3.48 (m, 8H, 4 x NC*H*$_2$), 6.98 (t, J = 7.5, Ar*H*), 7.01 (t, J = 7.5, Ar*H*), 7.24 (t, J = 7.6, 2H, 2 x Ar*H*), 7.28 (t, J = 7.6, 2H, 2 x Ar*H*), 7.44 (d, J = 8.0, 2 x Ar*H*), 7.58 (d, J = 8.0, 2 x Ar*H*), 8.23 (s, 1H, N*H*), 9.33 (s, 1H, N*H*). **^{13}C NMR** (101 MHz, $CDCl_3$) δ_C 14.1 (*C*H$_3$), 18.4 (N*C*H$_2$), 42.7 (N*C*H$_2$), 45.3 (2 x N*C*H$_2$), 47.9 (N*C*H$_2$), 48.9 (N*C*H$_2$), 50.4 (N*C*H$_2$), 118.5 (*C*≡N), 119.3 (2 x Ar*C*), 119.8 (2 x Ar*C*), 122.5 (Ar*C*), 122.6 (Ar*C*), 128.7 (2 x Ar*C*), 128.8 (2 xAr*C*), 139.7 (Ar*C*), 140.0 (Ar*C*), 157.0 (*C*O), 157.5 (*C*O). **HR-MS** (ESI, positive ion mode) – *m/z* for $[C_{23}H_{30}N_6O_2+Na]^+$ = 445.2328. Found 445.2294. **FTIR** (neat) – 3341, 2975, 2944, 2230, 1662.

1-Ethyl-1,4,7-tris(anilinylcarbonyl)-7-cyanoethyl-1,4,7-triazaheptane, 37

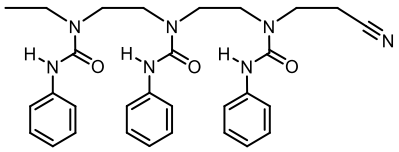

Synthesised according to general procedure B1 using **36** (130 mg, 0.31 mmol) and phenyl isocyanate (0.05 mL, 0.46 mmol). The crude product was purified by column chromatography (1-2% MeOH:DCM) to yield the title triurea as a white solid (135 mg, 0.25 mmol, 80%). **M.P.** 118-119 °C ($CHCl_3$). **TLC** – R_f = 0.26 (SiO_2, 5:95 MeOH:DCM). **^{1}H NMR** (400 MHz, $CDCl_3$) δ_H 1.32 (t, J = 7.1, 3H, C*H*$_3$), 2.74 (t, J = 5.9, 2H, NC*H*$_2$), 3.41 (q, J = 7.1, 2H, NC*H*$_2$), 3.50 (t, J = 6.1, 2H, NC*H*$_2$), 3.55-3.64 (m, 6H, 3 x NC*H*$_2$), 3.68 (t, J = 5.9, 2H, NC*H*$_2$), 6.41 (s, 1H, N*H*), 7.02 (tt, J = 7.5, 1.2, 1H, Ar*H*), 7.03 (tt, J = 7.4, 1.2, 1H, Ar*H*), 7.11 (tt, J = 7.4, 1.2, 1H, Ar*H*), 7.29 (t, J = 7.8, 4H, 4 x Ar*H*), 7.34 (t, J = 8.1, 2H, 2 x Ar*H*), 7.44 (d, J = 7.8, 2H, 2 x Ar*H*), 7.73 (d, J = 8.1, 4H, 4 x Ar*H*), 9.07 (s, 1H, N*H*), 9.14 (s, 1H, N*H*). **^{13}C NMR** (101 MHz, $CDCl_3$) δ_C 14.4 (*C*H$_3$), 18.2 (N*C*H$_2$), 44.4 (N*C*H$_2$), 46.2 (N*C*H$_2$), 47.5 (2 x N*C*H$_2$), 48.0 (N*C*H$_2$), 49.0 (N*C*H$_2$), 119.4 (*C*≡N), 119.4 (2 x Ar*C*), 119.7 (2 x Ar*C*), 120.0 (2 x Ar*C*), 122.6 (Ar*C*), 122.7 (Ar*C*), 123.7 (Ar*C*), 128.7 (2 x Ar*C*), 128.7 (2 x Ar*C*), 129.0 (2 x Ar*C*), 138.2 (Ar*C*), 139.8 (Ar*C*), 139.9 (Ar*C*), 155.4 (*C*O), 155.6 (*C*O), 156.4 (*C*O). **HR-MS** (ESI, positive ion mode) – *m/z* for $[C_{30}H_{35}N_7O_5+Na]^+$ = 564.2699. Found 564.2705. **FTIR** (neat) – 3310, 2957, 2254, 1652.

1-Ethyl-1,4-bis(4-methoxyanilinylcarbonyl)-7-(*tert*-butoxycarbonyl)-1,4,7-triazanonane, 38

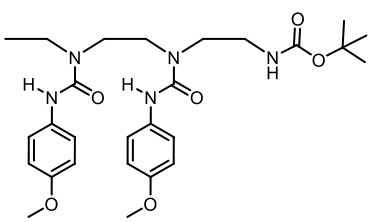

Synthesised according to general procedure B1 using **33** (100 mg, 0.43 mmol) and 4-methoxyphenyl isocyanate (0.17 mL, 1.30 mmol). The crude product was purified by column chromatography (25-100% EtOAc:PE) to yield the title diurea as a foamy white solid (122 mg, 0.25 mmol, 57%). **M.P.** 158-159 °C ($CHCl_3$). **TLC** – R_f = 0.31 (SiO_2, 90:10 EtOAc:PE). **^{1}H NMR** (400 MHz, $CDCl_3$) δ_H 1.15 (t, J = 7.1, 3H, C*H*$_3$), 1.43 (s, 9H, C(C*H*$_3$)$_3$), 3.15 (t, J = 6.5, 2H, NC*H*$_2$), 3.36-3.45 (m, 8H, 4 x

NC*H*$_2$), 3.78 (s, 3H, OC*H*$_3$), 3.79 (s, 3H, OC*H*$_3$), 5.35 (s, 1H, N*H*), 6.82 (d, J = 9.1, 2H, 2 x Ar*H*), 6.84 (d, J = 9.1, 2H, 2 x Ar*H*), 7.4 (d, J = 9.1, 2H, 2 x Ar*H*), 7.54 (d, J = 9.1, 2H, 2 x Ar*H*), 8.51 (s, 1H, N*H*). **^{13}C NMR** (101 MHz, $CDCl_3$) δ_C 14.1 (*C*H$_3$), 28.2 (C(*C*H$_3$)$_3$), 40.1 (N*C*H$_2$), 43.0 (N*C*H$_2$), 45.9 (N*C*H$_2$), 47.8 (N*C*H$_2$), 47.9 (N*C*H$_2$), 55.5 (2 x O*C*H$_3$), 80.1 (*C*(CH$_3$)$_3$), 114.0 (4 x Ar*C*), 121.3 (2 x Ar*C*), 121.8 (2 x Ar*C*), 133.0 (Ar*C*), 133.1 (Ar*C*), 155.3 (Ar*C*), 155.3 (Ar*C*), 155.9 (*C*O) 156.4 (*C*O), 157.1 (*C*O). **HR-MS** (ESI, positive ion mode) – *m/z* for $[C_{27}H_{39}N_5O_6+Na]^+$ = 552.2798. Found 552.2777. **FTIR** (neat) – 3311, 2917, 1645, 1628.

1-Ethyl-1,4-bis(4-methoxyanilinylcarbonyl)-1,4,7-triazanonane, 39

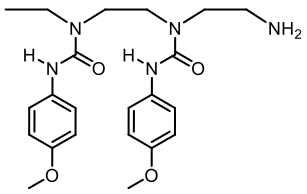

Synthesised according to general procedure C using **38** (100 mg, 0.22 mmol). The title amine was isolated as a foamy white solid (76 mg, 0.21 mmol, 96%). **M.P.** 162-163 °C ($CHCl_3$). **TLC** – R_f = 0.03 (SiO_2, 90:10 EtOAc:PE). **^{1}H NMR** (400 MHz, $CDCl_3$) δ_H 1.14 (t, J = 7.2, 3H, C*H*$_3$), 1.78 (s, 2H, N*H*$_2$), 2.89 (t, J = 4.2, 2H, NC*H*$_2$), 3.34-3.44 (m, 8H, 4 x NC*H*$_2$), 3.74 (s, 3H, OC*H*$_3$), 3.75 (s, 3H, OC*H*$_3$), 6.75 (d, J = 9.0, 2H, x Ar*H*), 6.77 (d, J = 9.0, 2H, x Ar*H*), 7.31 (d, J = 9.0, 2H, Ar*H*), 7.50 (d, J = 9.0, 2H, Ar*H*), 8.29 (s, 1H, N*H*), 10.0 (s, 1H, N*H*). **^{13}C NMR** (101 MHz, $CDCl_3$) δ_C 14.2 (*C*H$_3$), 41.7 (N*C*H$_2$), 42.7 (N*C*H$_2$), 44.8 (N*C*H$_2$), 48.1 (N*C*H$_2$), 52.8 (N*C*H$_2$), 55.5 (O*C*H$_3$), 55.6 (O*C*H$_3$), 113.9 (2 x Ar*C*), 114.0 (2 x Ar*C*), 120.8 (2 x Ar*C*), 121.5 (2 x Ar*C*), 133.3 (Ar*C*), 133.5 (Ar*C*), 155.1 (2 x Ar*C*), 155.9 (*C*O), 158.4 (*C*O). **HR-MS** (ESI, positive ion mode) – *m/z* for $[C_{22}H_{31}N_5O_4+H]^+$ = 430.2454. Found 430.2451. **FTIR** (neat) – 3444, 3354, 2966, 2902, 1671.

1-Ethyl-1,4-bis(4-methoxyanilinylcarbonyl)-7-benzyl-1,4,7-triazanonane, 40

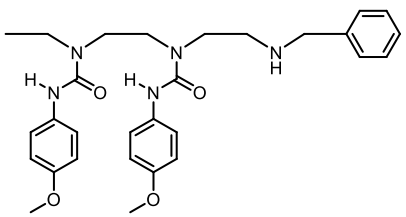

Synthesised according to general procedure E using **39** (396 mg, 0.94 mmol) and benzaldehyde (0.15 mL, 1.41 mmol). The crude product was purified by column chromatography (2-10% MeOH:DCM) to yield the title amine as a white solid (249 mg, 0.48 mmol, 51%). **M.P** – 132-133 °C ($CHCl_3$). **TLC** – R_f = 0.30 (SiO_2, 5:95 MeOH:DCM). **^{1}H NMR** (400 MHz, $CDCl_3$) δ_H 1.14 (t, J = 7.0, 3H, C*H*$_3$), 2.07 (s, 1H, N*H*), 2.85 (t, J = 4.3, NC*H*$_2$), 3.33-3.45 (m, 8H, 4 x NC*H*$_2$), 3.75 (s, 3H, OC*H*$_3$), 3.76 (s, 3H, OC*H*$_3$), 3.81 (s, 2H, C*H*$_2$Ar), 6.76 (d, J = 8.5, 2H, 2 x Ar*H*), 6.79 (d, J = 8.5, 2H, 2 x Ar*H*), 7.18 (d, J = 8.5, 2H, 2 x Ar*H*), 7.23-7.33 (m, 5H, 5 x Ar*H*), 7.51 (d, J = 8.5, 2H, 2 x Ar*H*), 8.27 (s, 1H, N*H*), 9.91 (s, 1H, N*H*). **^{13}C NMR** (101 MHz, $CDCl_3$) δ_C 14.1 (*C*H$_3$), 42.6 (N*C*H$_2$), 45.1 (N*C*H$_2$), 48.2 (N*C*H$_2$), 49.4 (N*C*H$_2$), 50.7 (N*C*H$_2$), 54.2 (*C*H$_2$Ar), 55.5 (O*C*H$_3$), 55.5 (O*C*H$_3$),

113.9 (2 x Ar*C*), 113.9 (2 x Ar*C*), 120.9 (2 x Ar*C*), 121.3 (2 x Ar*C*), 127.5 (2 x Ar*C*), 128.3 (2 x Ar*C*), 128.7 (Ar*C*), 133.1 (Ar*C*), 133.5 (Ar*C*), 138.9 (Ar*C*), 155.0 (2 x Ar*C*), 155.7 (*C*O), 158.2 (*C*O). **HR-MS** (ESI, positive ion mode) – *m/z* for $[C_{29}H_{37}N_5O_4+H]^+$ = 520.2924. Found 520.2893. **FTIR** (neat) – 3337, 3322, 2993, 2912, 1654.

1-Ethyl-1,4,7-tris(4-methoxyanilinylcarbonyl)-7-benzyl-1,4,7-triazanonane, 41

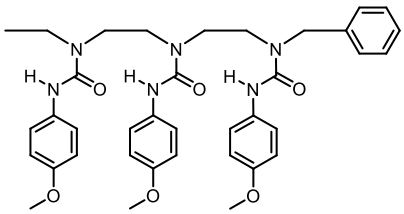

Synthesised according to general procedure B1 using **40** (120 mg, 0.23 mmol) and 4-methoxyphenyl isocyanate (0.04 mL, 0.35 mmol). The crude product was purified by column chromatography (1-2% MeOH:DCM) to yield the title triurea as a foamy white solid (112 mg, 0.17 mmol, 73%). **M.P.** 110-111 °C ($CHCl_3$). **TLC** – R_f = 0.15 (SiO_2, 1:99 MeOH:DCM). **^{1}H NMR** (500 MHz, $CDCl_3$) δ_H 1.16 (t, J = 7.1, 3H, C*H*$_3$), 3.30 (q, J = 7.1, 2H, NC*H*$_2$), 3.29-3.41 (m, 6H, 3 x NC*H*$_2$), 3.49 (t, J = 7.4, 2H, NC*H*$_2$), 3.76 (s, 3H, OC*H*$_3$), 3.77 (s, 3H, OC*H*$_3$), 3.77 (s, 3H, OC*H*$_3$), 4.58 (s, 2H, C*H*$_2$Ar), 6.79-6.83 (m, 6H, 6 x Ar*H*), 7.27-7.33 (m, 4H, 4 x Ar*H*), 7.34-7.39 (m, 5H, 5 x Ar*H*), 7.57 (d, J = 9.0, 2H, 2 x Ar*H*), 8.89 (s, 1H, N*H*). **^{13}C NMR** (126 MHz, $CDCl_3$) δ_C 14.3 (*C*H$_3$), 43.7 (NCH$_2$), 46.7 (NCH$_2$), 47.9 (3 x NCH$_2$), 51.9 (*C*H$_2$Ar), 55.6 (3 x OCH$_3$), 113.9 (2 x Ar*C*), 113.9 (2 x Ar*C*), 114.0 (2 x Ar*C*), 121.2 (2 x Ar*C*), 121.8 (2 x Ar*C*), 122.0 (2 x Ar*C*), 127.2 (2 x Ar*C*), 127.9 (Ar*C*), 129.0 (2 x Ar*C*), 133.3 (3 x Ar*C*), 137.8 (Ar*C*), 155.3 (*C*O), 155.6 (3 x Ar*C*), 156.0 (*C*O), 156.5 (*C*O). **HR-MS** (ESI, positive ion mode) – *m/z* for $[C_{37}H_{44}N_6O_6+H]^+$ = 669.3401. Found 669.3424. **FTIR** (neat) – 3312, 2978, 2923, 1650.

1,1-Dibenzyl-3-(4-methoxyphenyl)urea, 42

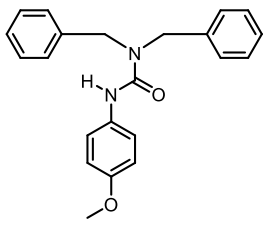

Synthesised according to general procedure B1 using *N*,*N*-dibenzylamine (198 mg, 1.00 mmol) and 4-methoxyphenyl isocyanate (0.10 mL, 0.75 mmol). The crude product was diluted with aqueous HCl (1.00 M) and extracted with DCM (3 x 10 mL). The combined organic extracts were dried ($MgSO_4$), filtered and concentrated *in vacuo* to yield the title amine as a white solid (296 mg, 1.00 mmol, >99%). **M.P.** 179-180 °C ($CHCl_3$). **TLC** – R_f = 0.23 (SiO_2, 1:99 MeOH:DCM). **^{1}H NMR** (400 MHz, $CDCl_3$) δ_H 3.66 (s, 3H, OC*H*$_3$), 4.50 (s, 4H, 2 x C*H*$_2$Ar), 6.17 (s, 1H, N*H*), 6.69 (d, J = 9.0, 2H, 2 x Ar*H*), 7.03 (d, J = 9.0, 2H, 2 x Ar*H*), 7.19-7.31 (m, 10H, 10 x Ar*H*). **^{13}C NMR** (101 MHz, $CDCl_3$) δ_C 50.8 (2 x *C*H$_2$Ar), 55.6 (OCH$_3$), 114.2 (2 x Ar*C*), 122.3 (2 x Ar*C*), 127.5 (4 x Ar*C*), 127.8 (2 x Ar*C*), 129.0 (4 x Ar*C*), 132.1 (2 x

Ar*C*), 137.4 (Ar*C*), 156.0 (Ar*C*), 156.5 (*C*O). **HR-MS** (ESI, positive ion mode) – *m/z* for $[C_{22}H_{22}N_2O_2+H]^+$ = 347.1760. Found 347.1727. **FTIR** (neat) – 3431, 2988, 2901, 1653.

1,4-Dibenzyl-1,4-bis(4-methoxyanilinylcarbonyl)-1,4-diazabutane, 43

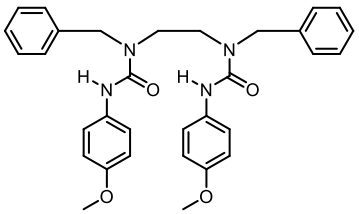

Synthesised according to general procedure B1 using *N*,*N'*-dibenzylethylenediamine (100 mg, 0.42 mmol) and 4-methoxyphenyl isocyanate (0.16 mL, 1.25 mmol). The crude product was purified by column chromatography (25-100% EtOAc:PE) to yield the title diurea as a foamy white solid (152 mg, 0.28 mmol, 67%). **M.P.** 136-137 °C ($CHCl_3$). **TLC** – R_f = 0.23 (SiO_2, 5:95 MeOH:DCM). **^{1}H NMR** (400 MHz, $CDCl_3$) δ_H 3.36 (s, 4H, 2 x NC*H*$_2$), 3.76 (s, 6H, 2 x OC*H*$_3$), 4.45 (s, 4H, 2 x C*H*$_2$Ar), 6.80 (d, J = 9.0, 4H, 4 x Ar*H*), 7.19 (d, J = 9.0, 4H, 4 x Ar*H*, 7.29-7.39 (m, 10H, 10 x Ar*H*), 7.61 (s, 2H, 2 x N*H*). **^{13}C NMR** (101 MHz, $CDCl_3$) δ_C 46.7 (2 x *C*H$_2$), 51.9 (2 x *C*H$_2$Ar), 55.5 (2 x O*C*H$_3$), 114.0 (4 x Ar*C*), 121.9 (4 x Ar*C*), 127.3 (4 x Ar*C*), 127.8 (4 x Ar*C*), 129.0 (2 x Ar*C*), 132.2 (2 x Ar*C*), 137.5 (2 x Ar*C*), 155.5 (2 x Ar*C*), 156.4 (2 x *C*O). **HR-MS** (ESI, positive ion mode) – *m/z* for $[C_{32}H_{34}N_4O_4+Na]^+$ = 561.2478. Found 561.2467. **FTIR** (neat) – 3291, 2945, 2901, 1638.

1,7-Dibenzyl-1,4,7-triazaheptane, 44

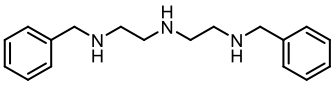

Synthesised according to general procedure E using diethylenetriamine (0.21 mL, 1.94 mmol) and benzaldehyde (0.39 mL, 3.88 mmol). The title triamine was isolated as a white solid (330 mg, 1.18 mmol, 61%). **TLC** – R_f = 0.09 (SiO_2, 90:10 EtOAc:PE). **^{1}H NMR** (400 MHz, $CDCl_3$) δ_H 2.72-2.74 (m, 8H, 4 x NC*H*$_2$), 3.79 (s, 4H, 2 x C*H*$_2$Ar), 7.22-7.33 (m, 10H, 10 x Ar*H*). Spectroscopic data matched that previously reported.[127]

1,7-Dibenzyl-1,4,7-tris(4-methoxyanilinylcarbonyl)-1,4,7-triazaheptane, 45

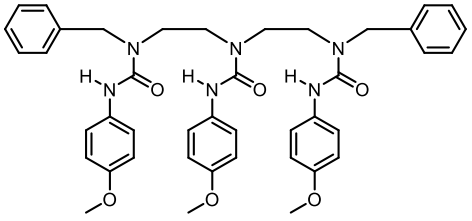

Synthesised according to general procedure B1 using **44** (300 mg, 1.06 mmol) and 4-methoxyphenyl isocyanate (0.41 mL, 3.18 mmol). The crude product was purified by column chromatography (25-100% EtOAc:PE) to yield the title triurea as a white solid (418 mg, 0.57 mmol, 54%). **M.P.** 146-147 °C ($CHCl_3$). **TLC** – R_f = 0.20 (SiO_2, 90:10 EtOAc:PE).

^{1}H NMR (500 MHz, $CDCl_3$) δ_H 3.34 (t, J = 7.4, 4H, 2 x NC*H*$_2$), 3.48 (t, J = 7.4, 4H, 2 x NC*H*$_2$), 3.79 (s, 6H, 2 x OC*H*$_3$), 3.81 (s, 3H, OC*H*$_3$), 4.57 (s, 4H, 2 x C*H*$_2$Ar), 6.83 (d, J = 9.0, 4H, 4 x Ar*H*), 6.85 (d, J = 9.0, 2H, 2 x Ar*H*), 7.29 (d, J = 9.0, 4H, 4 x Ar*H*), 7.32-7.44 (m, 10H, 10 x Ar*H*), 7.59 (d, J = 9.0, 2H, 2 x Ar*H*), 8.84 (s, 1H, N*H*). **^{13}C NMR** (126 MHz, $CDCl_3$) δ_C 47.8 (2 x N*C*H$_2$), 47.8 (2 x N*C*H$_2$), 52.4 (2 x *C*H$_2$Ar), 55.6 (2 x O*C*H$_3$), 55.6 (O*C*H$_3$), 114.0 (2 x Ar*C*), 114.1 (4 x Ar*C*), 121.2 (2 x Ar*C*), 121.8 (4 x Ar*C*), 127.1 (4 x Ar*C*), 127.2 (2 x Ar*C*), 129.2 (4 x Ar*C*), 133.1 (2 x Ar*C*), 133.1 (Ar*C*), 155.4 (2 x Ar*C*), 155.4 (Ar*C*), 156.5 (2 x *C*O), 156.5 (*C*O). **HR-MS** (ESI, positive ion mode) – *m/z* for $[C_{42}H_{46}N_6O_6+Na]^+$ = 753.3377. Found 753.3362. **FTIR** (neat) – 3334, 2992, 2948, 1650, 1624.

1,10-Dibenzyl-1,4,7,10-tetrakis(4-methoxyanilinylcarbonyl)-1,4,7,10-tetraazadecane, 46

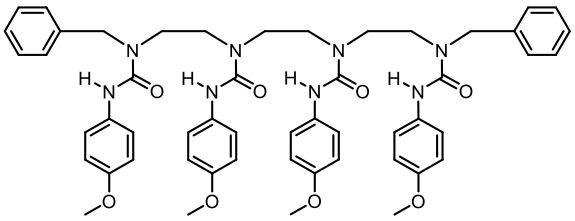

Under a dry, inert atmosphere, a solution of triethylenetetramine (0.31 mL, 2.05 mmol, 1.00 equiv., 0.10 M) in anhydrous MeOH (20 mL) was prepared. To this solution was added benzaldehyde (0.42 mL, 4.10 mmol, 2.00 equiv.) and the resulting colourless solution was stirred for 16 h. The solution was cooled to 0 °C and $NaBH_4$ (388 mg, 10.26 mmol, 6.00 equiv.) was added in one portion. The resulting white suspension was warmed to room temperature, stirred for 3 h and concentrated *in vacuo*. The residue was diluted with MeOH and concentrated *in vacuo*. The crude product was diluted with deionised water (20 mL) and the aqueous solution extracted with DCM (3 x 20 mL). The combined organic extracts were washed with brine, dried ($MgSO_4$), filtered and concentrated *in vacuo* to give the crude secondary amine. Under a dry, inert atmosphere, the crude brown oil (1.00 equiv., 0.10 M) was dissolved in anhydrous DCM (20 mL) and cooled to 0 °C. To the solution was added 4-methoxyphenyl isocyanate (1.30 mL, 12.30 mmol, 3.00 equiv.) dropwise. The resulting solution was stirred for 16 h and concentrated *in vacuo*. The crude product was purified by column chromatography (1-2% MeOH:DCM) to yield the title tetraurea as a white solid (312 mg, 0.34 mmol, 16%). **M.P.** 158-159 °C (DCM). **TLC** – R_f = 0.21 (SiO_2, 1:99 MeOH:DCM). **^{1}H NMR** (400 MHz, $CDCl_3$) δ_H 3.32 (s, 4H, 2 x NC*H*$_2$), 3.39-3.43 (m, 4H, 2 x NC*H*$_2$), 3.48 (t, J = 7.5, 4H, 2 x NC*H*$_2$), 3.76 (s, 6H, 2 x OC*H*$_3$), 3.78 (s, 6H, 2 x OC*H*$_3$), 6.80 (d, J = 9.1, 4H, 4 x Ar*H*), 6.82 (d, J = 9.1, 4H, 4 x Ar*H*), 7.27 (d, J = 9.1, 4H, 4 X Ar*H*), 7.29-7.40 (m, 10H, 10 x Ar*H*), 7.59 (d, J = 9.1, 4H, 4 x Ar*H*), 8.33 (s, 2H, 2 x N*H*), 8.93 (s, 2H, 2 x N*H*). **^{13}C NMR** (101 MHz, $CDCl_3$) δ_C 47.7 (6 x N*C*H$_2$), 52.2 (2 x *C*H$_2$Ar), 55.5 (2 x O*C*H$_3$), 55.5 (2 x O*C*H$_3$), 113.9 (4 x Ar*C*), 114.0 (4 x Ar*C*), 121.1 (4 x Ar*C*), 121.9 (4 x Ar*C*), 126.8 (4 x Ar*C*), 127.9 (2 x Ar*C*), 129.1 (4 x Ar*C*), 133.1 (4 x Ar*C*), 155.2 (4 x Ar*C*), 156.4 (4 x *C*O). **HR-MS** (ESI, positive ion

mode) – *m/z* for $[C_{52}H_{58}N_8O_8+Na]^+$ = 945.4275. Found 945.4233. **FTIR** (neat) – 3330, 2992, 2948, 1643, 1604.

1,4-Diethyl-1,4-bis(4-methoxyanilinylcarbonyl)-1,4-diazabutane, 47

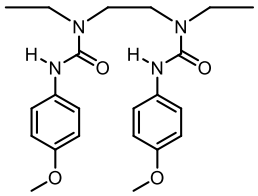

Synthesised according to general procedure B1 using *N,N'*-diethylethylenediamine (100 mg, 0.86 mmol) and 4-methoxyphenyl isocyanate (0.33 mL, 2.58 mmol). The crude product was purified by column chromatography (25-100% EtOAc:PE) to yield the title diurea as a foamy white solid (294 mg, 0.71 mmol, 82%). **M.P.** 219-220 °C ($CHCl_3$). **TLC** – R_f = 0.40 (SiO_2, 90:10 EtOAc:PE). **^{1}H NMR** (400 MHz, $CDCl_3$) δ_H 1.23 (t, J = 7.1, 6H, 2 x C*H*$_3$), 3.40 (q, J = 7.1, 4H, 2 x C*H*$_2$), 3.47 (s, 4H, 2 x C*H*$_2$), 3.78 (s, 6H, 2 x OC*H*$_3$), 6.82 (d, J = 9.0, 4H, 4 x Ar*H*), 7.31 (s, 2H, 2 x N*H*), 7.41 (d, J = 9.0, 4H, 4 x Ar*H*). **^{13}C NMR** (101 MHz, $CDCl_3$) δ_C 14.4 (2 x *C*H$_3$), 43.5 (2 x NCH$_2$CH$_3$), 46.7 (2 x *C*H$_2$), 55.7 (2 x OCH$_3$), 114.1 (4 x Ar*C*), 121.9 (4 x Ar*C*), 132.7 (2 x Ar*C*), 155.7 (2 x Ar*C*), 155.9 (2 x *C*O). **HR-MS** (ESI, positive ion mode) – *m/z* for $[C_{22}H_{30}N_4O_4+Na]^+$ = 437.2165. Found 437.2143. **FTIR** (neat) – 3280, 2984, 2919, 1629.

1,7-Diethyl-1,4-bis(4-methoxyanilinylcarbonyl)-1,4,7-triazanonane, 48

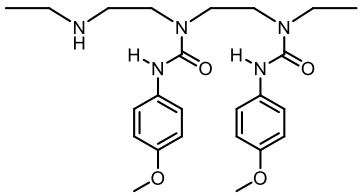

Synthesised according to general procedure E using **39** (216 mg, 0.50 mmol) and acetaldehyde (0.04 mL, 0.75 mmol). The crude product was purified by column chromatography (2-10% MeOH:DCM) to yield the title amine as a white solid (114 mg, 0.25 mmol, 50%). **M.P.** 115-116 °C (DCM). **TLC** – R_f = 0.26 (SiO_2, 5:95 MeOH:DCM). **^{1}H NMR** (400 MHz, $CDCl_3$) δ_H 1.15 (t, J = 7.3, 3H, C*H*$_3$), 1.24 (t, J = 7.1, 3H, C*H*$_3$), 2.67 (q, J = 7.1, 2H, NC*H*$_2$), 2.81 (t, J = 7.0, 2H, NC*H*$_2$), 3.35 (q, J = 7.3, 2H, NC*H*$_2$), 3.41 (t, J = 7.5, 2H, NC*H*$_2$), 3.46 (t, J = 7.5, 2H, NC*H*$_2$), 3.52 (t, J = 7.0, 2H, NC*H*$_2$), 3.77 (s, 3H, OC*H*$_3$), 3.78 (s, 3H, OC*H*$_3$), 6.80 (d, J = 8.9, 2H, 2 x Ar*H*), 6.81 (d, J = 8.9, 2H, 2 x Ar*H*), 7.20 (d, J = 8.9, 2H, 2 x Ar*H*), 7.46 (d, J = 8.9, 2H, 2 x Ar*H*), 8.13 (s, 1H, N*H*), 9.24 (s, 1H, N*H*). **^{13}C NMR** (101 MHz, $CDCl_3$) δ_C 14.9 (*C*H$_3$), 15.7 (*C*H$_3$), 44.0 (NCH$_2$), 45.2 (NCH$_2$), 46.0 (NCH$_2$), 46.1 (NCH$_2$), 47.5 (NCH$_2$), 48.0 (NCH$_2$), 55.5 (OCH$_3$), 55.5 (OCH$_3$), 114.0 (2 x Ar*C*), 114.1 (2 x Ar*C*), 121.4 (2 x Ar*C*), 121.6 (2 x Ar*C*), 132.4 (2 x Ar*C*), 155.4 (2 x Ar*C*), 156.0 (2 x *C*O). **HR-MS** (ESI, positive ion mode) – *m/z* for $[C_{24}H_{35}N_5O_4+Na]^+$ = 480.2587. Found 480.2567. **FTIR** (neat) – 3345, 2941, 1620.

1,7-Diethyl-1,4-bis(4-methoxyanilinylcarbonyl)-7-(4-nitroanilinylthiocarbonyl)-1,4,7-triazaheptane, 49

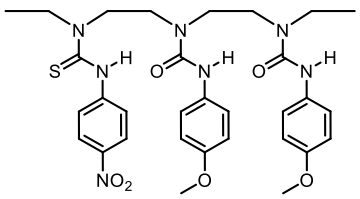

Synthesised according to general procedure B1 using **48** (100 mg, 0.22 mmol) and 4-nitrophenyl isothiocyanate (59 mg, 0.33 mmol). The crude product was purified by column chromatography (1-10% MeOH:DCM) to yield the title thiourea as a yellow solid (145 mg, 0.22 mmol, >99%). **M.P.** 164-165 °C (DCM). **TLC** – R_f = 0.48 (SiO_2, 5:95 MeOH:DCM). **^{1}H NMR** (400 MHz, $CDCl_3$) δ_H 1.31 (t, J = 7.5, 3H, C*H*$_3$), 1.33 (t, J = 7.2, 3H, C*H*$_3$), 3.39 (q, J = 7.2, 2H, NC*H*$_2$), 3.47-3.49 (m, 2H, NC*H*$_2$), 3.50-3.57 (m, 4H, 2 x NC*H*$_2$), 3.74-3.77 (m, 2H, NC*H*$_2$), 3.79, (s, 3H, OC*H*$_3$), 3.80 (s, 3H, OC*H*$_3$), 3.97 (q, J = 7.5, 2H, NC*H*$_2$), 6.34 (s, 1H, N*H*), 6.81 (d, J = 9.0, 2H, 2 x Ar*H*), 6.86 (d, J = 8.9, 2H, 2 x Ar*H*), 7.30 (d, J = 8.9, 2H, 2 x Ar*H*), 7.50 (d, J = 9.0, 2H, 2 x Ar*H*), 7.94 (d, J = 9.1, 2H, 2 x Ar*H*), 8.15 (d, J = 9.1, 2H, 2 x Ar*H*), 9.04 (s, 1H, N*H*), 10.16 (s, 1H, N*H*). **^{13}C NMR** (101 MHz, $CDCl_3$) δ_C 12.8 (*C*H$_3$), 14.5 (*C*H$_3$), 44.4 (NCH$_2$), 47.9 (5 x N*C*H$_2$), 55.7 (2 x O*C*H$_3$), 114.1 (2 x Ar*C*), 114.3 (2 x Ar*C*), 121.3 (2 x Ar*C*), 122.5 (2 x Ar*C*), 122.8 (2 x Ar*C*), 122.9 (2 x Ar*C*), 131.0 (Ar*C*), 132.5 (Ar*C*), 143.0 (Ar*C*), 147.1 (Ar*C*), 155.7 (2 x Ar*C*), 156.0 (*C*O), 156.2 (*C*O), 182.1 (*C*S). **HR-MS** (ESI, positive ion mode) – *m/z* for $[C_{31}H_{39}N_7O_6S+Na]^+$ = 660.2580. Found 660.2559. **FTIR** (neat) – 3676, 3278, 2934, 1646, 1512.

***tert*-Butyl-(2-aminoethyl)(2-hydroxyethyl)carbamate, 52**

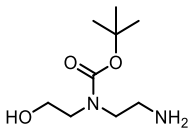

Synthesised according to general procedure F using *N*-(2-hydroxyethyl)-ethylenediamine (2.43 mL, 24.00 mmol). The title carbamate was isolated as a colourless oil (4.66 g, 22.80 mmol, 95%). **TLC** – R_f = 0.54 (SiO_2, 10:90:1 MeOH:DCM:NH_4OH). **^{1}H NMR** (400 MHz, $CDCl_3$) δ_H 1.41 (s, 9H, C(C*H*$_3$)$_3$), 2.89-2.98 (m, 2H, NC*H*$_2$), 3.07-3.14 (m, 2H, NC*H*$_2$), 3.24-3.40 (m, 4H, 2 x NC*H*$_2$), 3.67-3.71 (m, 2H, OC*H*$_2$). Spectroscopic data matched that previously reported.[89]

***tert*-Butyl (2-(phthalimidyl)ethyl)(2-hydroxyethyl)carbamate, 53**

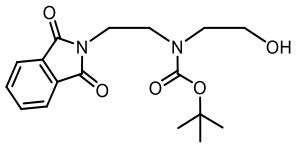

Under a dry, inert atmosphere, phthalic anhydride (218 mg, 1.47 mmol, 1.00 equiv.) was added to a solution of **52** (300 mg, 1.47 mmol, 1.00 equiv., 0.10 M) in anhydrous toluene (15 mL). The solution was heated to reflux for 16 h and concentrated *in vacuo*. The crude brown oil was purified by column chromatography (1-2% MeOH:DCM) to yield the title phthalimide as a white solid (447 mg, 1.34 mmol, 91%). **M.P.** 95-96 °C ($CHCl_3$). **TLC** – R_f = 0.61 (SiO_2, 5:95 MeOH:DCM). **^{1}H NMR** (400

MHz, $CDCl_3$) δ_H 1.16 (s, 9H, C(C*H*$_3$)$_3$), 3.36-3.39 (m, 2H, NC*H*$_2$), 3.52-3.57 (m, 2H, NC*H*$_2$), 3.73-3.77 (m, 2H, NC*H*$_2$), 3.85-3.90 (m, 2H, NC*H*$_2$), 7.69 (d, J = 7.4, 2H, 2 x Ar*H*), 7.79 (d, J = 7.4, 2H, 2 x Ar*H*). **^{13}C NMR** (101 MHz, $CDCl_3$) δ_C 28.0 (C(*C*H$_3$)$_3$), 36.6 (N*C*H$_2$, rot.), 37.4 (N*C*H$_2$, rot.), 47.3 (N*C*H$_2$, rot.), 47.5 (N*C*H$_2$, rot.), 51.5 (N*C*H$_2$, rot.), 52.7 (N*C*H$_2$, rot.), 61.1 (O*C*H$_2$, rot.), 61.6 (O*C*H$_2$, rot.), 79.9 (*C*(CH$_3$)$_3$, rot.), 80.4 (*C*(CH$_3$)$_3$, rot.), 123.2 (2 x Ar*C*, rot.), 123.3 (2 x Ar*C*, rot.), 132.0 (2 x Ar*C*, rot.), 132.2 (2 x Ar*C*, rot.), 133.7 (2 x Ar*C*, rot.), 134.1 (2 x Ar*C*, rot.), 156.0 (*C*O, rot.), 156.5 (*C*O, rot.), 168.3 (*C*O, rot.) 168.9 (*C*O, rot.). **HR-MS** (ESI, positive ion mode) – *m/z* for $[C_{17}H_{22}N_2O_5+Na]^+$ = 357.1426. Found 357.1424. **FTIR** (neat) – 3473, 2970, 1710, 1676.

***tert*-Butyl (2-(phthalimidyl)ethyl)(2-oxoethyl)carbamate, 54**

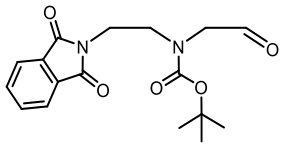

Synthesised according to general procedure G using **53** (160 mg, 0.48 mmol). The crude product was purified by column chromatography (1-2% MeOH:DCM) to yield the title aldehyde as a colourless oil (111 mg, 0.34 mmol, 70%). **TLC** – R_f = 0.18 (SiO_2, 1:99 MeOH:DCM). **^{1}H NMR** (400 MHz, $CDCl_3$) δ_H 1.20 (s, 9H, C(C*H*$_3$), rot.), 1.23 (s, 9H, C(C*H*$_3$), rot.), 3.56 (t, J = 5.8, NC*H*$_2$, rot.), 3.60 (t, J = 5.8, NC*H*$_2$, rot.), 3.79-3.85 (m, 2H, NC*H*$_2$), 3.87 (s, 2H, NC*H*$_2$, rot.), 4.00 (s, 2H, NC*H*$_2$, rot.), 7.70-7.76 (m, 2H, 2 x Ar*H*), 7.80-7.85 (m, 2H, 2 x Ar*H*), 9.56 (s, 1H, C*H*O). **^{13}C NMR** (101 MHz, $CDCl_3$) δ_C 27.9 (C(*C*H$_3$)$_3$, rot.), 28.0 (C(*C*H$_3$)$_3$, rot.), 35.8 (N*C*H$_2$, rot.), 36.1 (N*C*H$_2$, rot.)), 46.6 (N*C*H$_2$, rot.), 46.7 (N*C*H$_2$, rot.), 57.0 (O*C*H$_2$, rot.), 57.7 (O*C*H$_2$, rot.), 81.0 (*C*(CH$_3$)$_3$, rot.), 81.1 (*C*(CH$_3$)$_3$, rot.), 123.2 (2 x Ar*C*, rot.), 123.3 (2 x Ar*C*, rot.), 132.0 (2 x Ar*C*, rot.), 132.1 (2 x Ar*C*, rot.), 133.9 (2 x Ar*C*, rot.), 134.1 (2 x Ar*C*, rot.), 155.1 (*C*O, rot.), 155.4 (*C*O, rot.), 168.0 (*C*O, rot.), 168.3 (*C*O, rot.), 198.4 (*C*HO, rot.), 199.0 (*C*HO, rot.). **HR-MS** (ESI, positive ion mode) – *m/z* for $[C_{17}H_{26}N_2O_5+Na]^+$ = 355.1270. Found 355.1261. **FTIR** (neat) – 2988, 1773, 1706, 1616.

***tert*-Butyl (*N*-2-aminoethyl- *N*-benzyl)carbamate, 56**

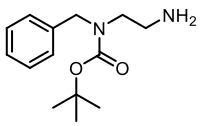

Synthesised according to general procedure F using *N*-benzylethylenediamine (1.00 mL, 6.66 mmol). The title carbamate was isolated as a colourless oil (1.64 g, 6.54 mmol, 98%). **TLC** – R_f = 0.10 (SiO_2, 5:95:1 MeOH:DCM:TEA). **^{1}H NMR** (400 MHz, $CDCl_3$) δ_H 1.42 (s, 9H, C(C*H*$_3$)$_3$), 2.92-2.96 (m, 2H, NC*H*$_2$), 3.18-3.25 (m, 2H, NC*H*$_2$), 4.34 (s, 2H, C*H*$_2$Ar), 7.23-7.30 (m, 5H, 5 x Ar*H*). Spectroscopic data matched that previously reported.[128]

***tert*-Butyl (2-(benzylamino)ethyl)(2-hydroxyethyl)carbamate, 57**

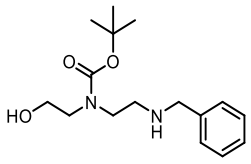

Synthesised according to general procedure E using **52** (2.40 g, 11.80 mmol) and benzaldehyde (1.80 mL, 17.70 mmol). The crude product was purified by column chromatography (1-2% MeOH:DCM) to yield the title amine as a colourless oil (3.04 g, 10.42 mmol, 88%). **TLC** – R_f = 0.43 (SiO_2, 1:99 MeOH:DCM). **^{1}H NMR** (400 MHz, $CDCl_3$) δ_H 1.47 (s, 9H, C(C*H*$_3$)$_3$), 2.90 (t, J = 5.0, 2H, NC*H*$_2$, rot.), 2.94 (t, J = 5.0, 2H, NC*H*$_2$, rot.), 3.41-3.43 (m, 4H, 2 x NC*H*$_2$), 3.75-3.79 (m, 2H, NC*H*$_2$), 3.79-3.84 (m, 2H, OC*H*$_2$), 7.26-7.38 (m, 5H, 5 x Ar*H*). **^{13}C NMR** (101 MHz, $CDCl_3$) δ_C 28.5 (C(*C*H$_3$)$_3$), 47.8 (N*C*H$_2$, rot.), 48.2 (N*C*H$_2$, rot.), 49.1 (N*C*H$_2$, rot.), 49.7 (N*C*H$_2$, rot.), 53.2 (N*C*H$_2$, rot.), 53.8 (N*C*H$_2$, rot.), 62.1 (O*C*H$_2$, rot.), 62.2 (O*C*H$_2$, rot.), 80.0 (*C*(CH$_3$)$_3$), 127.4 (2 x Ar*C*), 128.4 (Ar*C*), 128.7 (2 x Ar*C*), 139.0 (Ar*C*), 156.0 (*C*O). **HR-MS** (ESI, positive ion mode) – *m/z* for $[C_{16}H_{26}N_2O_3+H]^+$ = 295.2022. Found 295.2009. **FTIR** (neat) – 3461, 3305, 2990, 1678.

***tert*-Butyl (2-(1-benzyl-3-(4-nitrophenyl)thioureido)ethyl)(2-hydroxyethyl)carbamate, 58**

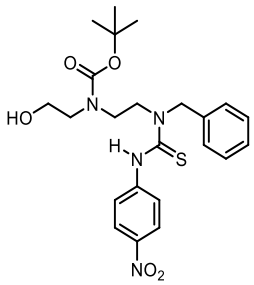

Synthesised according to general procedure B using **57** (1.23 g, 4.19 mmol) and 4-nitrophenyl isothiocyanate (1.13 g, 6.29 mmol). The crude product was purified by column chromatography (2-20% EtOAc:PE) to yield the title diurea as a yellow oil (1.63 g, 3.43 mmol, 82%). **TLC** – R_f = 0.59 (SiO_2, 90:10 EtOAc:PE). **^{1}H NMR** (400 MHz, $CDCl_3$) δ_H 1.44 (s, 9H, C(C*H*$_3$)$_3$), 3.24-3.30 (m, 4H, 2 x NC*H*$_2$), 3.61-3.64 (m, 2H, OC*H*$_2$), 3.71-3.76 (m, 2H, NC*H*$_2$), 5.27 (s, 2H, C*H*$_2$Ar), 7.29-7.37 (m, 5H, 5 x Ar*H*), 8.00 (d, J = 8.7, 2H, 2 x Ar*H*), 8.18 (d, J = 8.7, 2H, 2 x Ar*H*), 10.04 (s, 1H, N*H*). **^{13}C NMR** (101 MHz, $CDCl_3$) δ_C 28.5 (C(*C*H$_3$)$_3$), 46.9 (N*C*H$_2$), 47.4 (N*C*H$_2$), 51.4 (N*C*H$_2$), 56.2 (*C*H$_2$Ar), 61.7 (O*C*H$_2$), 81.9 (*C*(CH$_3$)$_3$), 123.6 (2 x Ar*C*), 123.9 (2 x Ar*C*), 127.9 (Ar*C*), 127.9 (2 x Ar*C*), 128.8 (2 x Ar*C*), 136.6 (Ar*C*), 136.9 (Ar*C*), 147.1 (Ar*C*), 156.7 (*C*O), 181.1 (*C*S). **HR-MS** (ESI, positive ion mode) – *m/z* for $[C_{23}H_{30}N_4O_5S+Na]^+$ = 497.1835. Found 497.1825. **FTIR** (neat) – 3267, 3088, 2940, 1660, 1595, 1510.

4,7-Bis(*tert*-butoxycarbonyl)-1,4,7,10-tetraazadecane, 60

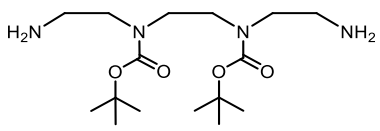

Synthesised according to general procedure F using triethylenetetramine (2.6 mL, 17.10 mmol). The title carbamate as a colourless oil (4.1 g, 11.89 mmol, 67%). **TLC** – R_f = 0.04 (SiO_2, 5:95:1 MeOH:DCM:NH_4OH). **^{1}H NMR** (400 MHz, $CDCl_3$) δ_H 1.41 (s, 18H, 2

x C(CH_3)$_3$), 2.78 (t, J = 6.2, 4H, 2 x NCH_2), 3.18-3.32 (m, 8H, 4 x NCH_2). Spectroscopic data matched that previously reported.[129]

1-(Naphthalen-1-ylmethyl)-4,7-bis(*tert*-butoxycarbonyl)-1,4,7,10-tetraazadecane, 61

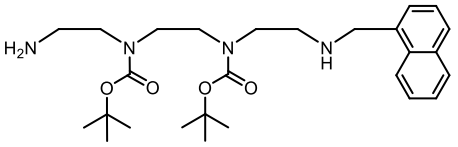

Synthesised according to general procedure E using **60** (4.20 g, 12.10 mmol) and 1-naphthaldehyde (1.68 mL, 12.10 mmol, 1.00 equiv.). The crude product was purified by column chromatography (1-10% MeOH:DCM, 1% NH_4OH) to yield the title amine as a foamy white solid (2.90 g, 6.0 mmol, 50%). **M.P.** 42-43 °C ($CHCl_3$). **TLC** – R_f = 0.09 (SiO_2, 5:95:1 MeOH:DCM:NH_4OH). **^{1}H NMR** (400 MHz, $CDCl_3$) δ_H 1.43 (s, 9H, C(CH_3)$_3$), 1.45 (s, 9H, C(CH_3)$_3$), 2.78 (t, J = 6.2, 2H, NCH_2), 2.88 (t, J = 6.2, 2H, NCH_2), 3.17-3.46 (m, 8H, 4 x NCH_2), 4.24 (s, 2H, CH_2Ar), 7.37-7.53 (m, 4H, 4 x Ar*H*), 7.75 (d, J = 8.1, 1H, Ar*H*), 7.84 (d, J = 7.5, 1H, Ar*H*), 8.11-8.14 (m, 1H, Ar*H*). **^{13}C NMR** (101 MHz, $CDCl_3$) δ_C 28.5 (2 x C(*C*H$_3$)$_3$), 40.6 (N*C*H$_2$, rot.), 40.9 (N*C*H$_2$, rot.), 45.7 (N*C*H$_2$), 46.0 (N*C*H$_2$), 47.7 (N*C*H$_2$), 48.4 (N*C*H$_2$), 51.2 (*C*H$_2$Ar), 51.6 (N*C*H$_2$), 79.5 (*C*(CH$_3$)$_3$), 79.9 (*C*(CH$_3$)$_3$), 123.8 (Ar*C*), 125.3 (Ar*C*), 125.6 (Ar*C*), 126.0 (2 x Ar*C*), 127.7 (Ar*C*), 128.6 (Ar*C*), 131.8 (Ar*C*), 133.9 (Ar*C*), 135.9 (Ar*C*), 155.4 (*C*O), 155.7 (*C*O). **HR-MS** (ESI, positive ion mode) – *m/z* for [$C_{27}H_{43}N_4O_4$+H]$^+$ = 487.3284. Found 487.3279. **FTIR** (neat) – 3401, 2946, 1687.

1-(Naphthalen-1-ylmethyl)-1,4,7-tris(*tert*-butoxycarbonyl)-1,4,7,10-tetraazadecane, 62

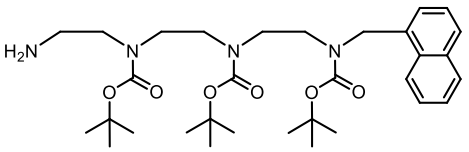

Synthesised according to general procedure F using **61** (2.3 g, 4.70 mmol). The title carbamate was isolated as a foamy white solid (2.3 g, 3.90 mmol, 82%). **M.P.** 56-57 °C ($CHCl_3$). **TLC** – R_f = 0.30 (SiO_2, 5:95 MeOH:DCM). **^{1}H NMR** (400 MHz, $CDCl_3$) δ_H 1.28-1.50 (m, 27H, 3 x C(CH_3)$_3$), 3.05-3.39 (m, 12H, 6 x NCH_2), 4.90 (s, 2H, CH_2Ar), 7.21-7.47 (m, 4H, 4 x Ar*H*), 7.69-7.74 (m, 1H, Ar*H*), 7.78-7.83 (m, 1H, Ar*H*), 8.00-8.02 (m, 1H, Ar*H*). **^{13}C NMR** (101 MHz, $CDCl_3$) δ_C 28.4 (3 x C(*C*H$_3$)$_3$), 39.5 (N*C*H$_2$), 43.5 (N*C*H$_2$), 44.7 (N*C*H$_2$), 45.2 (N*C*H$_2$), 45.4 (N*C*H$_2$), 47.8 (N*C*H$_2$), 53.1 (*C*H$_2$Ar), 79.7 (*C*(CH$_3$)$_3$), 79.9 (*C*(CH$_3$)$_3$), 80.1 (*C*(CH$_3$)$_3$), 125.3 (Ar*C*), 125.8 (Ar*C*), 126.8 (Ar*C*), 128.1 (Ar*C*), 128.9 (Ar*C*), 131.2 (Ar*C*), 132.0 (Ar*C*), 133.2 (Ar*C*), 133.4 (Ar*C*), 133.8 (Ar*C*), 155.2 (*C*O), 155.4 (*C*O), 156.0 (*C*O). **HR-MS** (ESI, positive ion mode) – *m/z* for [$C_{32}H_{50}N_4O_6$+H]$^+$ = 587.3809. Found 587.3795. **FTIR** (neat) – 2947, 2912, 1690.

1-(Naphthalen-1-ylmethyl)-1,4,7-tris(4-methoxyanilinylcarbonyl)-10-trifluoroacetyl-1,4,7,10-tetraazadecane, 65

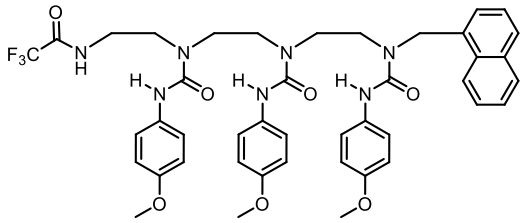

Under a dry, inert atmosphere, a solution of **61** (1.5 g, 5.4 mmol, 1.00 equiv, 1.00 M) in anhydrous DCM (5.4 mL) was cooled to 0 °C. Ethyl trifluoroacetate (0.70 mL, 5.9 mmol, 1.10 equiv.) was added dropwise over 30 minutes and the resulting solution was stirred for 30 minutes. The solution was warmed to room temperature and stirred for a further hour. The solution was then diluted with saturated aqueous $NaHCO_3$ (50 mL) and DCM (50 mL). The organic phase was washed with deionised water, dried ($MgSO_4$), filtered and concentrated *in vacuo* to give the crude trifluoroacetamide. Under a dry, inert atmosphere, the crude product was dissolved in anhydrous DCM (43 mL) and TFA (11 mL) was added dropwise. The resulting solution was stirred for 16 h and concentrated *in vacuo*. The crude product was diluted with saturated aqueous $NaHCO_3$ (100 mL) and extracted with DCM (3 x 50 mL). The combined organic extracts were dried ($MgSO_4$), filtered and concentrated *in vacuo* to give the crude triamine. Under a dry, inert atmosphere, the residue was dissolved in anhydrous DCM (55 mL) and cooled to 0 °C. Anhydrous TEA (6.7 mL, 48.6 mmol, 9.00 equiv.) was added in one portion and 4-methoxyphenyl isocyanate (3.2 mL, 24.3 mmol, 4.50 equiv.) was added dropwise to give a colourless solution. The solution was stirred for 16 h then concentrated *in vacuo* and purified by column chromatography (1-10% MeOH:DCM) to yield the title triurea as a foamy white solid (403 mg, 0.5 mmol, 9%). **M.P.** 140-141 °C ($CHCl_3$). **TLC** – R_f = 0.19 (SiO_2, 5:95 MeOH:DCM). **^{1}H NMR** (400 MHz, $CDCl_3$) δ_H 2.89-3.57 (m, 12H, 6 x NC*H*$_2$), 3.70 (s, 3H, OC*H*$_3$), 3.71 (s, 3H, OC*H*$_3$), 3.74 (s, 3H, OC*H*$_3$), 5.04 (s, 2H, C*H*$_2$Ar), 5.75 (s, 1H, N*H*), 6.66-6.86 (m, 6H, 6 x Ar*H*), 7.03 (d, J = 9.0, 2H, 2 x Ar*H*), 7.35-7.60 (m, 8H, 8 x Ar*H*), 7.76 (d, J = 7.7, 1H, Ar*H*), 7.81 (d, J = 7.7, 1H, Ar*H*), 8.00 (d, J = 7.7, 1H, Ar*H*), 8.57 (s, 1H, N*H*), 8.88 (s, 1H, N*H*). **^{13}C NMR** (101 MHz, $CDCl_3$) δ_C 39.7 (N*C*H$_2$), 45.8 (N*C*H$_2$), 46.3 (N*C*H$_2$), 47.5 (N*C*H$_2$), 47.8 (N*C*H$_2$), 48.4 (N*C*H$_2$), 49.7 (*C*H$_2$Ar), 55.5 (3 x O*C*H$_3$), 114.1 (2 x Ar*C*), 114.2 (2 x Ar*C*), 114.4 (2 x Ar*C*), 117.6 (q, J = 287.2, *C*F$_3$), 121.3 (2 x Ar*C*), 121.7 (2 x Ar*C*), 122.3 (2 x Ar*C*), 125.4 (Ar*C*), 126.3 (Ar*C*), 126.8 (Ar*C*), 128.3 (Ar*C*), 128.6 (Ar*C*), 128.9 (Ar*C*), 129.3 (Ar*C*), 131.3 (Ar*C*), 132.7 (Ar*C*), 132.9 (Ar*C*), 133.1 (Ar*C*), 133.2 (Ar*C*), 133.9 (Ar*C*), 155.3 (Ar*C*), 155.4 (Ar*C*), 155.6 (Ar*C*), 156.2 (q, J = 36.2, *C*O), 156.7 (*C*O), 157.0 (*C*O). **^{19}F NMR** (377 MHz, $CDCl_3$) δ_F −72.3 (C*F*$_3$). **HR-MS** (MALDI) – *m/z* for $[C_{43}H_{46}F_3N_7O_7+Na]^+$ = 852.3309. Found 852.3288. **FTIR** (neat) – 3309, 2976, 2923, 1648.

1-(Naphthalen-1-ylmethyl)-1,4,7-tris(4-methoxyanilinylcarbonyl)-1,4,7,10-tetraazadecane, 66

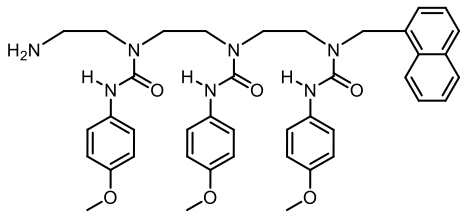

Synthesised according to general procedure H using **65** (400 mg, 0.49 mmol). The title amine was isolated as a foamy white solid (342 mg, 0.47 mmol, 95%). **M.P.** 133-134 °C ($CHCl_3$). **TLC** – R_f = 0.30 (SiO_2, 5:95 MeOH:DCM). **^{1}H NMR** (400 MHz, $CDCl_3$) δ_H 1.88 (s, 2H, N*H*$_2$), 2.80 (t, J = 7.0, 2H, NC*H*$_2$), 3.01-3.26 (m, 8H, 4 x NC*H*$_2$), 3.45 (t, J = 6.3, 2H, NC*H*$_2$), 3.70 (s, 3H, OC*H*$_3$), 3.73 (s, 3H, OC*H*$_3$), 3.75 (s, 3H, OC*H*$_3$), 5.05 (s, 2H, C*H*$_2$Ar), 5.97 (s, 1H, N*H*), 6.75 (d, J = 8.9, 2H, 2 x Ar*H*), 6.77 (d, J = 8.9, 2H, 2 x Ar*H*), 6.80 (d, J = 8.9, 2H, 2 x Ar*H*), 7.03 (d, J = 8.9, 2H, 2 x Ar*H*), 7.34-7.47 (m, 4H, 4 x Ar*H*), 7.50 (d, J = 8.9, 2H, 2 x Ar*H*), 7.59 (d, J = 8.9, 2H, 2 x Ar*H*), 7.75 (d, J = 7.6, 1H, Ar*H*), 7.80 (d, J = 7.6, 1H, Ar*H*), 8.00 (d, J = 7.6, 1H, Ar*H*), 8.67 (s, 1H, N*H*), 9.01 (s, 1H, N*H*). **^{13}C NMR** (101 MHz, $CDCl_3$) δ_C 39.3 (N*C*H$_2$), 46.9 (N*C*H$_2$), 47.3 (N*C*H$_2$), 47.0 (N*C*H$_2$), 48.1 (N*C*H$_2$), 49.2 (N*C*H$_2$), 49.3 (*C*H$_2$Ar), 55.4 (O*C*H$_3$), 55.5 (O*C*H$_3$), 55.5 (O*C*H$_3$), 113.9 (2 x Ar*C*), 113.9 (2 x Ar*C*), 114.0 (2 x Ar*C*), 121.1 (2 x Ar*C*), 121.5 (2 x Ar*C*), 121.6 (2 x Ar*C*), 125.4 (Ar*C*), 125.5 (Ar*C*), 126.2 (Ar*C*), 126.7 (Ar*C*), 128.3 (Ar*C*), 128.4 (Ar*C*), 128.8 (Ar*C*), 131.2 (Ar*C*), 131.6 (Ar*C*), 131.8 (Ar*C*), 132.9 (Ar*C*), 133.1 (Ar*C*), 133.8 (Ar*C*), 155.2 (Ar*C*), 155.3 (Ar*C*), 155.6 (Ar*C*), 156.6 (*C*O), 156.6 (*C*O), 157.4 (*C*O). **HR-MS** (ESI, positive ion mode) – *m/z* for $[C_{41}H_{47}N_7O_6+H]^+$ = 734.3666. Found 734.3659. **FTIR** (neat) – 3307, 3000, 2948, 1647.

1,10-Bis(naphthalen-1-ylmethyl)-1,4,7-tris(4-methoxyanilinylcarbonyl)-1,4,7,10-tetraazadecane, 67

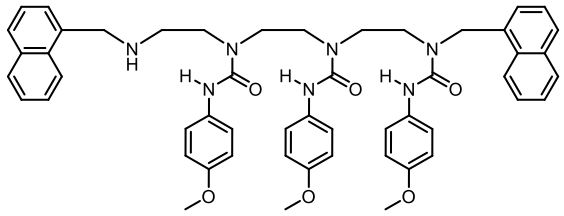

Synthesised according to general procedure E using **66** (175 mg, 0.24 mmol) and 1-naphthaldehyde (0.05 mL, 0.36 mmol). The crude product was purified by column chromatography (2-10% MeOH:DCM) to give the title amine as a foamy white solid (132 mg, 0.15 mmol, 63%). **M.P.** 149-150 °C ($CHCl_3$). **TLC** – R_f = 0.44 (SiO_2, 5:95 MeOH:DCM). **^{1}H NMR** (400 MHz, $CDCl_3$) δ_H 2.90 (t, J = 4.6, 2H, NC*H*$_{2)}$, 2.94-2.98 (m, 2H, NC*H*$_2$), 3.08-3.17 (m, 4H, 2 x NC*H*$_2$), 3.26-3.29 (m, 2H, NC*H*$_2$), 3.45 (t, J = 7.6, 2H, NC*H*$_2$), 3.74 (s, 3H, OC*H*$_3$), 3.76 (s, 3H, OC*H*$_3$), 3.77 (s, 3H, OC*H*$_3$), 4.28 (s, 2H, C*H*$_2$Ar), 5.10 (s, 2H, C*H*$_2$Ar), 6.64 (d, J = 9.0, 2H, 2 x Ar*H*), 6.77 (d, J = 9.0, 2H, 2 x Ar*H*), 6.83 (d, J = 9.0, 2H, 2 x Ar*H*), 6.91 (d, J = 8.0, 2H, 2 x Ar*H*), 7.36-7.60 (m, 8H, 8 x Ar*H*), 7.77-7.83 (m, 2H, 2 x Ar*H*), 7.86-7.89 (m, 2H, 2 x Ar*H*), 8.00 (d, J = 8.0, 1H, Ar*H*), 8.13 (d, J = 8.0, 1H, Ar*H*), 8.48 (s, 1H, N*H*), 8.71 (s, 1H, N*H*), 9.59

(s, 1H, N*H*). **^{13}C NMR** (101 MHz, $CDCl_3$) δ_C 45.4 (N*C*H_2), 46.8 (N*C*H_2), 46.9 (N*C*H_2), 47.8 (N*C*H_2), 49.7 (N*C*H_2), 51.1 (N*C*H_2), 51.8 (*C*H_2Ar), 53.3 (*C*H_2Ar), 55.5 (3 x O*C*H_3), 113.8 (2 x Ar*C*), 113.9 (2 x Ar*C*), 114.0 (2 x Ar*C*), 120.9 (2 x Ar*C*), 121.0 (2 x Ar*C*), 121.5 (2 x Ar*C*), 123.1 (Ar*C*), 123.7 (Ar*C*), 125.3 (Ar*C*), 125.4 (Ar*C*), 126.0 (Ar*C*), 126.2 (Ar*C*), 126.6 (Ar*C*), 126.7 (Ar*C*), 128.4 (Ar*C*), 128.5 (Ar*C*), 128.6 (Ar*C*), 129.0 (Ar*C*), 131.5 (Ar*C*), 131.7 (Ar*C*), 132.6 (Ar*C*), 132.8 (Ar*C*), 133.1 (Ar*C*), 133.8 (Ar*C*), 134.0 (Ar*C*), 134.3 (Ar*C*), 155.1 (Ar*C*), 155.3 (Ar*C*), 156.0 (Ar*C*), 156.1 (*C*O), 156.4 (*C*O), 158.2 (*C*O). **HR-MS** (ESI, positive ion mode) – *m/z* for $[C_{52}H_{55}N_7O_6+Na]^+$ = 896.4112. Found 896.4092. **FTIR** (neat) – 3312, 2965, 2902, 1637.

1,10-Bis(naphthalen-1-ylmethyl)-1,4,7-tris(4-methoxyanilinylcarbonyl)-10-(4-nitroanilinylthiocarbonyl)-1,4,7,10-tetraazadecane, 68

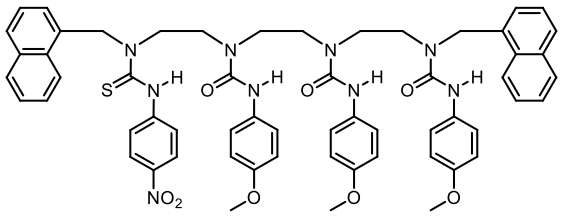

Synthesised according to general procedure B1 using **67** (100 mg, 0.11 mmol) and 4-nitrophenyl isothiocyanate (31 mg, 0.17 mmol). The crude product was purified by column chromatography (1-2% MeOH:DCM) to yield the title thiourea as a yellow solid (116 mg, 0.11 mmol, >99%). **M.P.** 174-175 °C (DCM). **TLC** – R_f = 0.32 (SiO_2, 1:99 MeOH:DCM). **^{1}H NMR** (500 MHz, $CDCl_3$) δ_H 2.89-3.71 (m, 12H, 2 x NCH_2), 3.79 (s, 3H, OCH_3), 3.79 (s, 3H, OCH_3), 3.81 (s, 3H, OCH_3), 5.04 (s, 2H, CH_2Ar), 5.67 (s, 2H, CH_2Ar), 6.38 (s, 1H, N*H*), 6.83 (d, J = 9.0, 2H, 2 x Ar*H*), 6.83 (d, J = 9.0, 2H, 2 x Ar*H*), 6.86 (d, J = 9.0, 2H, 2 x Ar*H*), 7.17-7.48 (m, 8H, 8 x Ar*H*), 7.51 (d, J = 9.0, 2H, 2 x Ar*H*), 7.60 (d, J = 9.0, 2H, 2 x Ar*H*), 7.64-8.18 (m, 12H, 12 x Ar*H*), 8.96 (s, 2H, 2 x N*H*), 10.44 (s, 1H, N*H*). **^{13}C NMR** (126 MHz, $CDCl_3$) δ_C 47.0-47.9 (4 x N*C*H_2), 48.6 (N*C*H_2), 48.9 (N*C*H_2), 51.1 (*C*H_2Ar), 54.1 (*C*H_2Ar), 55.5 (3 x O*C*H_3), 113.9 (2 x Ar*C*), 113.9 (2 x Ar*C*), 114.0 (2 x Ar*C*), 121.0 (6 x Ar*C*), 122.4 (Ar*C*), 123.2 (Ar*C*), 123.4 (Ar*C*), 123.8 (Ar*C*), 124.0 (Ar*C*), 125.3 (Ar*C*), 125.6 (Ar*C*), 126.4 (Ar*C*), 126.7 (Ar*C*), 127.0 (2 x Ar*C*), 127.2 (2 x Ar*C*), 128.5 (Ar*C*), 128.6 (Ar*C*), 128.8 (Ar*C*), 129.1 (Ar*C*), 129.3 (Ar*C*), 130.6 (Ar*C*), 131.0 (Ar*C*), 131.5 (Ar*C*), 132.6 (Ar*C*), 132.8 (Ar*C*), 133.7 (Ar*C*), 134.0 (Ar*C*), 143.7 (Ar*C*), 147.0 (Ar*C*), 155.4 (Ar*C*), 155.5 (Ar*C*), 155.5 (Ar*C*), 156.4 (*C*O), 156.5 (*C*O), 156.9 (*C*O), 180.1 (*C*S). **HR-MS** (ESI, positive ion mode) – *m/z* for $[C_{59}H_{59}N_9O_8S+Na]^+$ = 1076.4105. Found 1076.4112. **FTIR** (neat) – 3698, 3304, 2996, 2901, 1651.

1-(Naphthalen-1-ylmethyl)-1,4,7-tris(4-methoxyanilinylcarbonyl)-7-(succinimidylethyl)-1,4,7-triazaheptane, 69

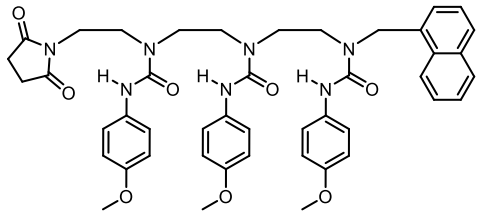

Synthesised according to general procedure I using **66** (75 mg, 0.10 mmol). The crude product was purified by column chromatography (1-10% MeOH:DCM) to give the title succinimide as a foamy white solid (67 mg, 0.08 mmol, 80%). **M.P.** 152-153 °C ($CHCl_3$). **TLC** – R_f = 0.50 (SiO_2, 5:95 MeOH:DCM). **^{1}H NMR** (500 MHz, $CDCl_3$) δ_H 2.74 (s, 4H, 2 x C(O)CH_2), 3.14-3.19 (m, 2H, NCH_2), 3.24-3.29 (m, 4H, 2 x NCH_2), 3.39 (t, J = 6.4, 2H, NCH_2), 3.53 (t, J = 7.3, 2H, NCH_2), 3.68 (t, J = 7.0, 2H, NCH_2), 3.80-3.81 (m, 9H, 3 x OCH_3), 5.13 (s, 2H, CH_2Ar), 6.82-6.86 (m, 6H, 6 x Ar*H*), 7.47-7.63 (m, 10H, 10 x Ar*H*), 7.90 (d, J = 8.3, 1H, Ar*H*), 7.95 (d, J = 8.0, 1H, Ar*H*), 8.11-8.13 (m, 1H, Ar*H*), 8.69 (s, 1H, N*H*). **^{13}C NMR** (126 MHz, $CDCl_3$) δ_C 28.2 (2 x C(O)*C*H_2), 37.0 (N*C*H_2), 45.2 (N*C*H_2), 47.1 (N*C*H_2), 47.3 (N*C*H_2), 47.7 (N*C*H_2), 47.8 (N*C*H_2), 49.4 (*C*H_2Ar), 55.5 (O*C*H_3), 55.5 (O*C*H_3), 55.5 (O*C*H_3), 113.9 (2 x Ar*C*), 113.9 (2 x Ar*C*), 114.0 (2 x Ar*C*), 121.0 (2 x Ar*C*), 121.1 (2 x Ar*C*), 121.7 (2 x Ar*C*), 125.4 (2 x Ar*C*), 126.3 (2 x Ar*C*), 126.9 (3 x Ar*C*), 128.6 (Ar*C*), 128.8 (Ar*C*), 128.9 (Ar*C*), 133.0 (Ar*C*), 133.1 (Ar*C*), 133.9 (Ar*C*), 155.2 (Ar*C*), 155.5 (Ar*C*), 155.5 (Ar*C*), 155.8 (*C*O), 156.2 (*C*O), 156.3 (*C*O), 177.6 (2 x *C*O). **HR-MS** (ESI, positive ion mode) – *m/z* for $[C_{45}H_{49}N_7O_8+Na]^+$ = 838.3540. Found 838.3533. **FTIR** (neat) – 3322, 2997, 2908, 1699, 1651.

***N*-(4-Methoxyphenyl)-*N*-methylcarbamoyl chloride, 70**

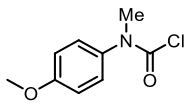

Under a dry, inert atmosphere, a solution of triphosgene (500 mg, 1.68 mmol, 0.46 equiv.) in anhydrous DCM (5 mL) was cooled to 0 °C. To this solution was added anhydrous pyridine (0.30 mL, 3.66 mmol, 1.00 equiv.) dropwise and the solution was stirred for 5 minutes. 4-methoxy-*N*-methylaniline (502 mg, 3.66 mmol, 1.00 equiv., 0.70 M) was added, the solution was warmed to room temperature and stirred for 1 h. Aqueous HCl (1 M, 10 mL) was added and the aqueous phase extracted with DCM (3 x 5 mL). The combined organic extracts were washed with saturated aqueous $NaHCO_3$, dried ($MgSO_4$), filtered and concentrated *in vacuo*. The crude mixture was purified by column chromatography (50% EtOAc:PE) to give the title carbamoyl chloride as a yellow oil (731 mg, 3.66 mmol, >99%). **TLC** – R_f = 0.63 (SiO_2, 50:50 EtOAc:PE). **^{1}H NMR** (400 MHz, $CDCl_3$) δ_H 3.33 (s, 3H, NCH_3), 3.81 (s, 3H, OCH_3), 6.91 (d, J = 8.8, 2 x Ar*H*), 7.14 (d, J = 8.8, 2 x Ar*H*). Spectroscopic data matched that previously reported.[130]

1,10-Bis(naphthalen-1-ylmethyl)-1,4,7-tris(4-methoxyanilinylcarbonyl)-10-((*N*-methyl-4-methoxyanilinyl)carbonyl)-1,4,7,10-tetraazadecane, 71

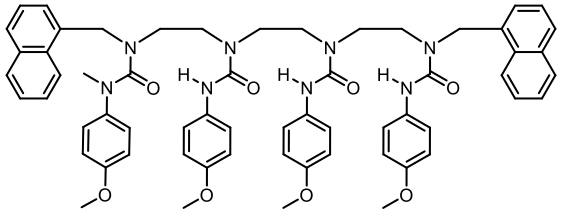

Synthesised according to general procedure B2 using **67** (30 mg, 0.03 mmol) and **70** (10 mg, 0.05 mmol). The crude product was purified by column chromatography (1-2% MeOH:DCM) to yield the title tetraurea as a white solid (27 mg, 0.03 mmol, 88%). **M.P.** 153-154 °C ($CHCl_3$). **TLC** – R_f = 0.14 (SiO_2, 1:99 MeOH:DCM). **^{1}H NMR** (500 MHz, CD_2Cl_2) δ_H 2.86-2.96 (m, 4H, 2 x NC*H*$_2$), 3.05 (NC*H*$_2$), 3.27-3.30 (m, 4H, 2 x NC*H*$_2$), 3.36 (t, J = 7.0, 2H, NC*H*$_2$), 3.66 (s, 3H, NC*H*$_3$), 3.76 (s, 3H, OC*H*$_3$), 3.78 (s, 3H, OC*H*$_3$), 3.78 (s, 3H, OC*H*$_3$), 4.50 (s, 2H, C*H*$_2$Ar), 5.08 (s, 2H, C*H*$_2$Ar), 6.71 (d, J = 8.9, 2H, 2 x Ar*H*), 6.79 (d, J = 9.0, 2H, 2 x Ar*H*), 6.85 (d, J = 9.0, 2H, 2 x Ar*H*), 6.86 (d, J = 9.0, 2H, 2 x Ar*H*), 7.05 (d, J = 8.9, 2H, 2 x Ar*H*), 7.12 (d, J = 6.7, 1H, Ar*H*), 7.27 (t, J = 7.5, 1H, Ar*H*), 7.36-7.73 (m, 13H, 13 x Ar*H*), 7.79 (d, J = 8.0, 1H, Ar*H*), 7.83 (d, J = 8.0, 1H, Ar*H*), 8.15 (d, J = 8.0, 1H, Ar*H*), 8.73 (s, 1H, N*H*), 8.85 (s, 1H, N*H*). 9.09 (s, 1H, N*H*). **^{13}C NMR** (126 MHz, CD_2Cl_2) δ_C 40.9 (N*C*H$_3$), 44.9 (N*C*H$_2$), 47.0 (N*C*H$_2$), 47.1 (N*C*H$_2$), 47.4 (N*C*H$_2$), 47.8 (N*C*H$_2$), 48.5 (N*C*H$_2$), 48.7 (*C*H$_2$Ar), 51.9 (*C*H$_2$Ar), 55.4 (4 x O*C*H$_3$), 113.7 (2 x Ar*C*), 113.7 (2 x Ar*C*), 113.8 (2 x Ar*C*), 114.8 (2 x Ar*C*), 121.0 (2 x Ar*C*), 121.1 (2 x Ar*C*), 122.5 (2 x Ar*C*), 123.5 (2 x Ar*C*), 125.0 (Ar*C*), 125.2 (Ar*C*), 125.3 (Ar*C*), 125.8 (Ar*C*), 126.0 (Ar*C*), 126.1 (Ar*C*), 126.4 (Ar*C*), 126.5 (Ar*C*), 126.7 (Ar*C*), 128.0 (Ar*C*), 128.4 (Ar*C*), 128.3 (Ar*C*), 128.5 (Ar*C*), 128.6 (Ar*C*), 128.9 (Ar*C*), 131.1 (Ar*C*), 131.6 (Ar*C*), 132.3 (Ar*C*), 133.2 (Ar*C*), 133.3 (Ar*C*), 133.6 (Ar*C*), 133.8 (Ar*C*), 138.9 (Ar*C*), 155.0 (Ar*C*), 155.1 (Ar*C*), 155.3 (Ar*C*), 156.4 (*C*O), 156.5 (*C*O), 157.4 (*C*O), 162.8 (*C*O). **HR-MS** (ESI, positive ion mode) – *m/z* for $[C_{61}H_{64}N_8O_8+Na]^+$ = 1059.4745. Found 1059.4725. **FTIR** (neat) – 3315, 2990, 2905, 1652, 1609.

4,7,10,13-Tetrakis(*tert*-butoxycarbonyl)-1,4,7,10,13,16-hexaazahexadecane, 72

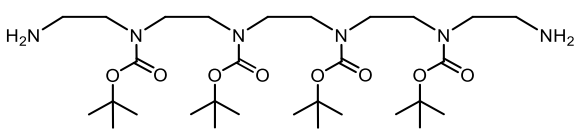

Synthesised according to general procedure F using pentaethylenehexamine (3.16 mL, 12.91 mmol). The title tetracarbamate was isolated as a pale yellow oil (6.53 g, 10.33 mmol, 80%). **TLC** – R_f = 0.10 (SiO_2, 5:95:1 MeOH:DCM:NH_4OH). **^{1}H NMR** (400 MHz, $CDCl_3$) δ_H 1.39-1.44 (m, 36H, 4 x C(C*H*$_3$)$_3$), 2.39 (s, 4H, 2 x N*H*$_2$), 2.71-2.82 (m, 4H, 2 x NC*H*$_2$), 3.15-3.40 (m, 16, 8 x NC*H*$_2$). **^{13}C NMR** (101 MHz, $CDCl_3$) δ_C 28.4-28.6 (2 x C(*C*H$_3$)$_3$), 40.9 (2 x N*C*H$_2$), 45.5-50.5 (8 x N*C*H$_2$), 79.5-80.0 (4 x *C*(CH$_3$)$_3$), 155.1-155.9 (4 x *C*O). **HR-MS** (ESI, positive ion mode) – *m/z* for $[C_{30}H_{60}N_6O_8+H]^+$ = 633.4551. Found 633.4551. **FTIR** (neat) – 2977, 1680.

1-(Naphthalen-1-ylmethyl)-4,7,10,13-tetrakis(*tert*-butoxycarbonyl)-1,4,7,10,13,16-hexaazahexadecane, **73**

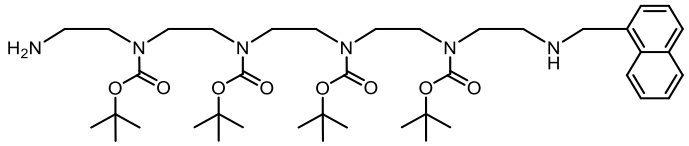

Synthesised according to general procedure E using **72** (3.00 g, 4.74 mmol) and 1-naphthaldehyde (0.66 mL, 4.74 mmol). The crude product was purified by column chromatography (1-10% MeOH:DCM, 1% NH_4OH) to yield the title amine as a foamy white solid (1.83 g, 2.37 mmol, 50%). **M.P.** 80-81 °C ($CHCl_3$). **TLC** – R_f = 0.20 (SiO_2, 5:95:1 MeOH:DCM:NH_4OH). **^{1}H NMR** (400 MHz, $CDCl_3$) δ_H 1.40-1.48 (m, 36H, 4 x C(C*H*$_3$)$_3$), 2.76-2.94 (m, 4H, 2 x NC*H*$_2$), 3.17-3.45 (m, 16H, 8 x NC*H*$_2$), 4.25 (s, 2H, C*H*$_2$Ar), 7.37-7.54 (m, 4H, 4 x Ar*H*), 7.76 (d, J = 7.8, 1H, Ar*H*), 7.85 (d, J = 7.8, 1H, Ar*H*), 8.11 (d, J = 7.8, 1H, Ar*H*). **^{13}C NMR** (101 MHz, $CDCl_3$) δ_C 28.5-28.7 (4 x C(*C*H$_3$)$_3$), 40.8-41.0 (2 x N*C*H$_2$), 45.6-48.3 (8 x N*C*H$_2$), 51.7 (*C*H$_2$Ar), 79.6-80.0 (4 x *C*(CH$_3$)$_3$), 123.8 (Ar*C*), 125.5 (Ar*C*), 125.8 (Ar*C*), 126.5 (Ar*C*), 126.6 (Ar*C*), 127.8 (Ar*C*), 128.8 (Ar*C*), 131.4 (Ar*C*), 131.9 (Ar*C*), 136.0 (Ar*C*), 155.0 (*C*O), 155.5 (*C*O), 155.7 (*C*O), 156.2 (*C*O). **HR-MS** (ESI, positive ion mode) – *m/z* for $[C_{41}H_{68}N_6O_8+H]^+$ = 773.5177. Found 773.5145. **FTIR** (neat) – 3398, 2973, 2931, 1683.

1-(Naphthalen-1-ylmethyl)-16-trifluoroacetyl-1,4,7,10,13,16-hexaazahexadecane, **74**

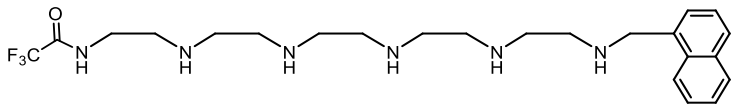

Under a dry, inert atmosphere, a solution of **73** (1.00 g, 1.29 mmol, 1.00 equiv. 1.60 M) in anhydrous DCM (0.8 mL) was cooled to 0 °C. Ethyl trifluoroacetate (0.17 mL, 1.42 mmol, 1.10 equiv.) was added dropwise over 30 minutes and the resulting solution was stirred for 30 minutes at 0 °C. The solution was then warmed to room temperature and stirred for a further hour. The solution was then diluted with anhydrous DCM (10 mL) and TFA (2 mL) was added dropwise. The solution was stirred for 16 h and concentrated *in vacuo*. The crude product was diluted with saturated aqueous $NaHCO_3$ and then extracted with DCM (3 x 25 mL). The combined organic extracts were washed with brine, dried ($MgSO_4$), filtered and concentrated *in vacuo* to give the title pentamine as a colourless oil (369 mg, 0.77 mmol, 61%). **TLC** – R_f = 0.04 (SiO_2, 10:90:1 MeOH:DCM:NH_4OH). **^{1}H NMR** (400 MHz, $CDCl_3$) δ_H 2.86-3.01 (m, 18H, 9 x NC*H*$_2$), 3.42 (NC*H*$_2$), 7.29-7.46 (m, 4H, 4 x Ar*H*), 7.70 (d, J = 8.0, 1H, Ar*H*), 7.86 (d, J = 8.0, 1H, Ar*H*), 8.14 (d, J = 8.0, 1H, Ar*H*). **^{13}C NMR** (101 MHz, $CDCl_3$) δ_C 43.2 (N*C*H$_2$), 44.6-46.8 (9 x N*C*H$_2$), 52.3 (*C*H$_2$Ar), 115.9 (q, J = 288.1, *C*F$_3$), 123.8 (Ar*C*), 125.5 (Ar*C*), 125.8 (Ar*C*), 126.5 (Ar*C*), 126.6 (Ar*C*), 127.8 (Ar*C*), 128.8 (Ar*C*), 131.4 (Ar*C*), 131.9 (Ar*C*), 136.0 (Ar*C*), 157.0 (q, J = 36.5, *C*O).

^{19}F NMR (377 MHz, $CDCl_3$) δ_F −74.3 (C*F*$_3$). **HR-MS** (ESI, positive ion mode) – *m/z* for $[C_{24}H_{35}F_3N_6O+Na]^+$ = 491.2722. Found 491.2701. **FTIR** (neat) – 3410, 2991, 2950, 1650.

1,16-Bis(trifluoroacetyl)-4,7,10,13-tetrakis(4-methoxyanilinylcarbonyl)-1,4,7,10,13,16-hexaazahexadecane, 76

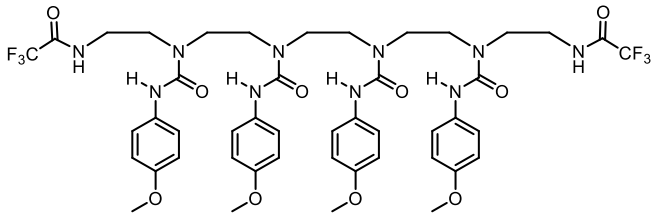

Synthesised according to general procedure J using pentaethylenehexamine (2.11 mL, 8.61 mmol) and 4-methoxyphenyl isocyanate (6.70 mL, 51.70 mmol). After 16 h, a white precipitate formed and was filtered. The residue was washed with DCM (3 x 10 mL) and air-dried to afford the title tetraurea as a white solid (1.76 g, 1.72 mmol, 20%). **M.P.** 228-229 °C (DCM). **TLC** – R_f = 0.31 (5:95 MeOH:DCM). **^{1}H NMR** (400 MHz, $(CD_3)_2SO$) δ_H 3.33 (s, 4H, 2 x NC*H*$_2$), 3.35-3.53 (m, 16H, 8 x NC*H*$_2$), 3.70 (s, 6H, 2 x OC*H*$_3$), 3.72 (s, 6H, 2 x OC*H*$_3$), 6.82 (d, J = 9.1, 4H, 4 x Ar*H*), 6.83 (d, J = 9.1, 4H, 4 x Ar*H*), 7.37 (d, J = 9.1, 4H, 4 x Ar*H*), 7.43 (d, J = 9.1, 4H, 4 x Ar*H*), 8.37 (s, 2H, 2 x N*H*), 8.77 (s, 2H, 2 x N*H*), 9.49 (t, J = 5.7, 2H, 2 x N*H*). **^{13}C NMR** (101 MHz, $(CD_3)_2SO$) δ_C 38.3 (2 x NCH$_2$), 45.9 (2 x NCH$_2$), 46.1 (2 x NCH$_2$), 46.5 (2 x NCH$_2$), 46.6 (2 x NCH$_2$), 55.1 (2 x OCH$_3$), 55.1 (2 x OCH$_3$), 113.4 (4 x Ar*C*), 113.5 (4 x Ar*C*), 115.8 (q, J = 288.6, 2 x *C*F$_3$), 121.6 (4 x Ar*C*), 121.8 (4 x Ar*C*), 132.9 (2 x Ar*C*), 133.1 (2 x Ar*C*), 154.3 (2 x Ar*C*), 154.7 (2 x Ar*C*), 155.6 (*C*O), 155.9 (*C*O), 156.9 (q, J = 35.9, 2 x *C*O),. **^{19}F NMR** (377 MHz, $(CD_3)_2SO$) δ_F −74.5 (2 x C*F*$_3$). **HR-MS** (MALDI) – *m/z* for $[C_{46}H_{54}F_6N_{10}O_{10}+Na]^+$ = 1043.3826. Found 1043.3795. **FTIR** (neat) – 3444, 3240, 2947, 1661, 1640, 1622.

4,7,10,13-Tetrakis(4-methoxyanilinylcarbonyl)-1,4,7,10,13,16-hexaazahexadecane, 77

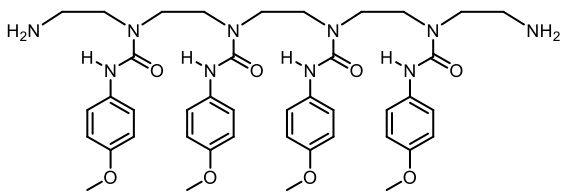

Synthesised according to general procedure H using **76** (3.00 g, 2.94 mmol). After 5 h, a white precipitate formed and was filtered. The residue was washed with MeOH (3 x 10 mL) and air-dried to afford the title diamine as a white solid (2.32 g, 2.79 mmol, 95%). **M.P.** 144-145 °C (DCM). **TLC** – R_f = 0.05 (5:95:1 MeOH:DCM:TEA). **^{1}H NMR** (400 MHz, $(CD_3)_2SO$) δ_H 2.71 (t, J = 5.6, 4H, 2 x NC*H*$_2$), 3.29-3.50 (m, 16H, 8 x NC*H*$_2$), 3.69 (s, 6H, 2 x OC*H*$_3$), 3.71 (s, 6H, 2 x OC*H*$_3$), 6.82 (d, J = 9.0, 4H, 4 x Ar*H*), 6.83 (d, J = 9.0, 4H, 4 x Ar*H*), 7.35 (d, J = 9.0, 4H, 4 x Ar*H*), 7.48 (d, J = 9.0, 4H, 4 x Ar*H*), 8.57 (s, 2H, 2 x N*H*), 9.98 (s, 2H, 2 x N*H*). **^{13}C NMR**

(101 MHz, $(CD_3)_2SO$) δ_C 41.5 (2 x N*C*H_2), 46.7 (2 x N*C*H_2), 46.9 (2 x N*C*H_2), 47.1 (2 x N*C*H_2), 48.4 (2 x N*C*H_2), 55.5 (2 x O*C*H_3), 55.6 (2 x O*C*H_3), 114.0 (4 x Ar*C*), 114.2 (4 x Ar*C*), 120.0 (8 x Ar*C*), 134.0 (2 x Ar*C*), 134.1 (2 x Ar*C*), 154.0 (2 x Ar*C*), 154.3 (2 x Ar*C*), 154.8 (2 x *C*O), 155.0 (2 x *C*O). **HR-MS** (MALDI) – *m/z* for $[C_{42}H_{56}N_{10}O_8+Na]^+$ = 851.4180. Found 851.5194. **FTIR** (neat) – 3276, 2980, 2961, 1643, 1621.

1,13-Bis(trifluoroacetyl)-4,7,10-tris(4-methoxyanilinylcarbonyl)-1,4,7,10,13-pentaazatridecane, 79

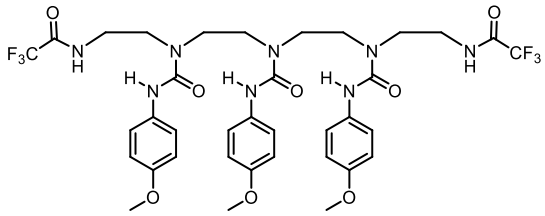

Synthesised according to general procedure J using tetraethylenepentamine (2.51 mL, 13.20 mmol) and 4-methoxyphenyl isocyanate (6.84 mL, 52.80 mmol). After 16 h, a white precipitate formed and was filtered. The residue was washed with DCM (3 x 10 mL) and air-dried to afford the title triurea as a white solid (2.74 g, 3.32 mmol, 25%). **M.P.** 177-178 °C (DCM). **TLC** – R_f = 0.26 (5:95 MeOH:DCM). **^{1}H NMR** (400 MHz, $(CD_3)_2SO$) δ_H 3.36-3.54 (m, 16H, 8 x NC*H*$_2$), 3.71 (s, 6H, 2 x OC*H*$_3$), 3.72 (3H, s, OC*H*$_3$), 6.83 (d, J = 9.0, 4H, 4 x Ar*H*), 6.85 (d, J = 9.0, 2H, 2 x Ar*H*), 7.38 (d, J = 9.0, 4H, 4 x Ar*H*), 7.44 (d, J = 9.0, 2H, 2 x Ar*H*), 8.47 (s, 2H, 2 x N*H*), 8.81 (s, 1H, N*H*), 9.50 (t, J = 5.7, 2H, 2 x N*H*). **^{13}C NMR** (101 MHz, $(CD_3)_2SO$) δ_C 38.3 (2 x N*C*H_2), 46.5 (2 x N*C*H_2), 46.7 (2 x N*C*H_2), 47.0 (2 x N*C*H_2), 55.1 (2 x O*C*H_3), 55.2 (O*C*H_3), 113.5 (4 x Ar*C*), 113.6 (2 x Ar*C*), 116.3 (q, J = 290.7, 2 x *C*F_3), 121.4 (2 x Ar*C*), 121.8 (4 x Ar*C*), 133.2 (2 x Ar*C*), 133.3 (Ar*C*), 154.7 (2 x *C*O), 155.6 (Ar*C*), 155.9 (q, J = 35.6, 2 x *C*O). **^{19}F NMR** (377 MHz, $(CD_3)_2SO$) δ_F −74.5 (2 x C*F*$_3$). **HR-MS** (MALDI) – *m/z* for $[C_{36}H_{42}F_6N_8O_8+Na]^+$ = 851.2927. Found 851.2888. **FTIR** (neat) – 3296, 2976, 2945, 1719, 1645.

4,7,10-Tris(4-methoxyanilinylcarbonyl)-1,4,7,10,13-pentaazatridecane, 80

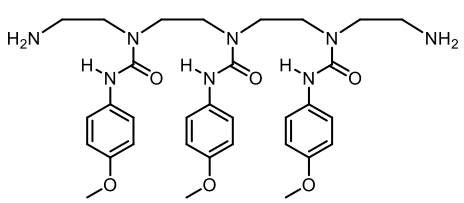

Synthesised according to general procedure H using **79** (4.30 g, 5.19 mmol). After 5 h, a white precipitate formed and was filtered. The residue was washed with MeOH (3 x 10 mL) and air-dried to afford the title diamine as a white solid (3.11 g, 4.88 mmol, 94%). **M.P.** 163-164 °C (DCM). **TLC** – R_f = 0.05 (5:95:1 MeOH:DCM:TEA). **^{1}H NMR** (400 MHz, $(CD_3)_2SO$) δ_H 2.78 (t, J = 5.7, 4H, 2 x N*C*H_2), 3.37 (t, J = 6.0, 4H, 2 x NC*H*$_2$), 3.42 (t, J = 6.6, 4H, 2 x NC*H*$_2$), 3.48 (t, J = 6.6, 4H, 2 x NC*H*$_2$), 3.70 (s, 6H, 2 x OC*H*$_3$), 3.71 (s, 3H, OC*H*$_3$), 6.83 (d, J = 9.0, 4H, 4 x Ar*H*), 6.85 (d, J = 9.0, 2H,

2 x Ar*H*), 7.37 (d, J = 9.0, 4H, 4 x Ar*H*), 7.49 (d, J = 9.0, 2H, 2 x Ar*H*), 8.98 (s, 1H, N*H*), 9.51 (s, 2H, 2 x N*H*). **^{13}C NMR** (101 MHz, $(CD_3)_2SO$) δ_C 40.8 (2 x N*C*H_2), 46.3 (2 x N*C*H_2), 46.8 (2 x N*C*H_2), 47.0 (2 x N*C*H_2), 55.6 (2 x O*C*H_3), 55.7 (O*C*H_3), 114.1 (4 x Ar*C*), 114.1 (2 x Ar*C*), 121.1 (2 x Ar*C*), 121.2 (4 x Ar*C*), 134.0 (Ar*C*), 134.1 (2 x Ar*C*), 154.8 (2 x *C*O), 154.9 (2 x Ar*C*), 156.1 (Ar*C*), 157.0 (*C*O). **HR-MS** (MALDI) – *m/z* for $[C_{32}H_{44}N_8O_6+Na]^+$ = 659.3282. Found 659.3329. **FTIR** (neat) – 3237, 2987, 2930, 1647.

tert-Butyl benzyl(2-hydroxyethyl)carbamate, 81

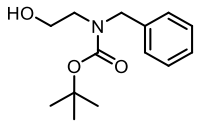

Synthesised according to general procedure K using *N*-benzylethanolamine (3.55 mL, 25.00 mmol). The crude product was purified by column chromatography (10-30% EtOAc:PE) to give the title carbamate as a colourless oil (5.72 g, 22.80 mmol, 91%). **^{1}H NMR** (400 MHz, $CDCl_3$) δ_H 1.41 (s, 9H, C(CH_3)$_3$), 3.13-3.16 (m, 2H, NCH_2), 3.60-3.65 (m, 2H, OCH_2), 4.40-4.45 (m, 2H, CH_2Ar), 7.28-7.35 (m, 5H, 5 x Ar*H*). **TLC** – R_f = 0.05 (10:90 EtOAc:PE). Spectroscopic data matched that previously reported.[131]

tert-Butyl benzyl(2-oxoethyl)carbamate, 82

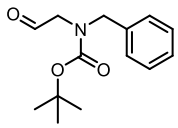

Synthesised according to general procedure L using **81** (1.0 g, 3.98 mmol). The crude product was purified by column chromatography (10-20% EtOAc:PE) to give the title aldehyde as a colourless oil (982 mg, 3.94 mmol, 99%). **^{1}H NMR** (400 MHz, $CDCl_3$) δ_H 1.42 (s, 9H, C(CH_3)$_3$), 4.12-4.16 (m, 2H, NCH_2), 4.60 (s, 2H, CH_2Ar), 7.28-7.35 (m, 5H, 5 x Ar*H*), 9.69-9.73 (m, 1H, C*H*O). **TLC** – R_f = 0.13 (10:90 EtOAc:PE). Spectroscopic data matched that previously reported.[131]

1-Benzyl-1-(*tert*-butoxycarbonyl)-7,10,13-tris(4-methoxyanilinylcarbonyl)-1,4,7,10,13,16-hexaazahexadecane, 83

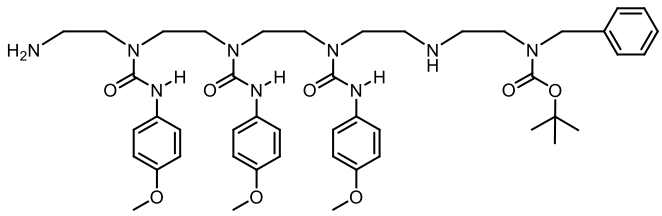

Synthesised according to general procedure E using **80** (200 mg, 0.31 mmol) and **82** (86 mg, 0.35 mmol). The crude product was purified by column chromatography (1-10% MeOH:DCM, 1% TEA) to give the title amine as a foamy white solid (122 mg, 0.14 mmol, 45%). **M.P.** 150-151 °C ($CHCl_3$). **TLC** – R_f = 0.38 (10:90:1 MeOH:DCM:TEA). **^{1}H NMR** (400 MHz, $CDCl_3$) δ_H 1.45 (s, 9H, C(CH_3)$_3$), 2.70-2.83 (m, 4H, 2 x NCH_2), 2.96 (t, J = 4.9, NCH_2), 3.26-3.57

(m, 14H, 7 x NCH_2), 3.76 (s, 3H, OCH_3), 3.76 (s, 3H, OCH_3), 3.77 (s, 3H, OCH_3), 4.41 (s, 2H, CH_2Ar), 6.79 (d, J = 9.1, 2H, 2 x Ar*H*), 6.80 (d, J = 9.1, 2H, 2 x Ar*H*), 6.82 (d, J = 9.1, 2H, 2 x Ar*H*), 7.18 (d, J = 9.1, 2H, 2 x Ar*H*), 7.27-7.37 (m, 7H, 7 x Ar*H*), 7.57 (d, J = 9.1, 2H, 2 x Ar*H*), 8.96 (s, 1H, N*H*), 9.73 (s, 1H, N*H*), 9.83 (s, 1H, N*H*). **^{13}C NMR** (101 MHz, $CDCl_3$) δ_C 28.5 (C(*C*H_3)$_3$), 46.1 (7 x N*C*H_2), 46.4 (N*C*H_2), 47.2 (N*C*H_2), 48.1 (*C*H_2Ar), 49.6 (N*C*H_2), 55.6 (3 x O*C*H_3), 80.4 (*C*(CH_3)$_3$), 113.8-114.3 (6 x Ar*C*), 120.0-121.4 (6 x Ar*C*), 127.3 (2 x Ar*C*), 127.5 (Ar*C*), 128.6 (2 x Ar*C*), 133.3-133.7 (3 x Ar*C*), 138.3 (Ar*C*), 155.1 (3 x Ar*C*), 156.0 (3 x *C*O), 156.4 (*C*O). **HR-MS** (ESI, positive ion mode) – *m/z* for $[C_{46}H_{63}N_9O_8+H]^+$ = 870.4878. Found 870.4899. **FTIR** (neat) – 3290, 2994, 2934, 1649.

1-Benzyl-7,10,13-tris(4-methoxyanilinylcarbonyl)-16-trifluoroacetyl-1,4,7,10,13,16-hexaazahexadecane, 84

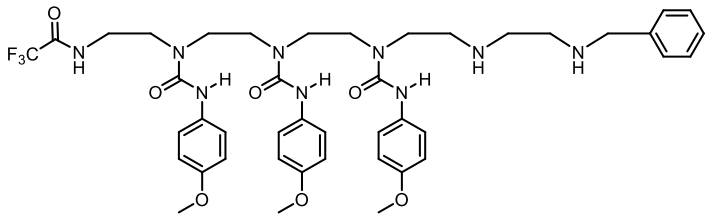

Under a dry, inert atmosphere, a solution of **83** (700 mg, 0.80 mmol, 1.00 equiv., 1.0 M) in anhydrous DCM (0.8 mL) was cooled to 0 °C. Ethyl trifluoroacetate (0.11 mL, 0.88 mmol, 1.10 equiv.) was added dropwise over 30 minutes and the resulting solution was stirred for 30 minutes at 0 °C. The solution was then warmed to room temperature and stirred for a further hour. The solution was then diluted with anhydrous DCM (6 mL) and TFA (2 mL) was added dropwise. The solution was stirred for 16 h and concentrated *in vacuo*. The crude product was diluted with saturated aqueous $NaHCO_3$ and then extracted with DCM (3 x 25 mL). The combined organic extracts were dried ($MgSO_4$), filtered and concentrated *in vacuo* to give the title amine as a foamy white solid (540 mg, 0.62 mmol, 78%). **M.P.** 156-157 °C ($CHCl_3$). **TLC** – R_f = 0.21 (5:95:1 MeOH:DCM:TEA). **^{1}H NMR** (400 MHz, $CDCl_3$) δ_H 2.69-2.85 (m, 8H, 4 x NCH_2), 3.32-3.55 (m, 14H, CH_2Ar, 6 x NCH_2), 3.74 (s, 3H, OCH_3), 3.76 (s, 6H, 2 x OCH_3), 6.74-6.84 (m, 6H, 6 x Ar*H*), 7.21-7.32 (m, 5H, 5 x Ar*H*), 7.52 (d, J = 8.9, 2H, 2 x Ar*H*), 7.59 (d, J = 8.9, 2H, 2 x Ar*H*), 7.60 (d, J = 8.9, 2H, 2 x Ar*H*), 8.82 (s, 1H, N*H*), 9.00 (s, 1H, N*H*), 9.13 (s, 1H, N*H*). **^{13}C NMR** (101 MHz, $CDCl_3$) δ_C 46.4 (N*C*H_2), 47.1 (N*C*H_2), 48.3 (N*C*H_2), 48.4 (N*C*H_2), 48.4 (N*C*H_2), 48.5 (N*C*H_2), 49.2 (*C*H_2Ar), 49.6 (N*C*H_2), 49.7 (N*C*H_2), 50.0 (N*C*H_2), 50.1 (N*C*H_2), 55.5 (3 x O*C*H_3), 113.9 (2 x Ar*C*), 114.0 (2 x Ar*C*), 114.0 (2 x Ar*C*), 115.9 (q, J = 287.8, *C*F_3), 120.9 (2 x Ar*C*), 121.1 (2 x Ar*C*), 121.5 (2 x Ar*C*), 127.1 (Ar*C*), 128.0 (2 x Ar*C*), 128.5 (2 x Ar*C*), 132.9-133.6 (3 x Ar*C*), 140.1 (Ar*C*), 155.0 (Ar*C*), 155.2 (Ar*C*), 155.3 (Ar*C*), 155.3 (*C*O), 155.5 (*C*O), 156.4 (q, J = 36.4, *C*O), 156.6 (*C*O). **^{19}F NMR** (377 MHz, $CDCl_3$) δ_F −74.3 (C*F*$_3$). **HR-MS** (ESI, positive ion mode) – *m/z* for $[C_{43}H_{54}F_3N_9O_7+Na]^+$ = 888.3996. Found 888.3981. **FTIR** (neat) – 3324, 2990, 2945, 1647.

1-Benzyl-1,4,7,10,13-pentakis(4-methoxyanilinylcarbonyl)-16-trifluoroacetyl-1,4,7,10,13,16-hexaazahexadecane, 85

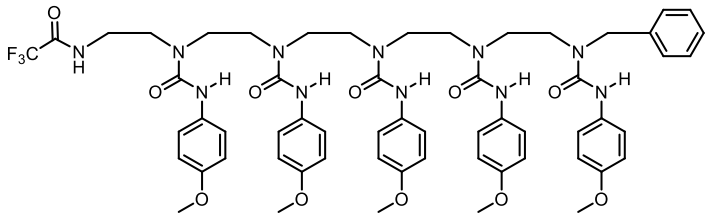

Synthesised according to general procedure B1 using **84** (1.0 g, 1.15 mmol) and 4-methoxyphenyl isocyanate (0.45 mL, 3.46 mmol). The crude product was purified by column chromatography (2-10% MeOH:DCM) to give the title pentaurea as a foamy white solid (503 mg, 0.43 mmol, 38%). **M.P.** 186-187 °C (DCM/Et_2O). **TLC** – R_f = 0.25 (5:95 MeOH:DCM). **^{1}H NMR** (400 MHz, $CDCl_3$) δ_H 3.32-3.64 (m, 20H, 10 x NCH_2), 3.71-3.81 (m, 15H, 5 x OCH_3), 4.49 (s, 2H, CH_2Ar), 5.88 (s, 1H, N*H*), 6.78-6.85 (m, 10H, 10 x Ar*H*), 7.07 (d, J = 9.0, 2H, 2 x Ar*H*), 7.20 (d, J = 9.0, 2H, 2 x Ar*H*), 7.26-7.36 (m, 5H, 5 x Ar*H*), 7.49 (d, J = 9.0, 2H, 2 x Ar*H*), 7.56 (d, J = 9.0, 2H, 2 x Ar*H*), 7.57 (d, J = 9.0, 2H, 2 x Ar*H*), 8.34 (s, 1H, N*H*), 8.87-9.18 (m, 5H, 5 x N*H*). **^{13}C NMR** (101 MHz, $CDCl_3$) δ_C 47.0-48.0 (10 x N*C*H_2), 48.2 (*C*H_2Ar), 55.5-55.6 (5 x O*C*H_3), 114.0 (6 x Ar*C*), 114.1 (2 x Ar*C*), 114.2 (2 x Ar*C*), 116.5 (q, J = 284.9, *C*F_3), 121.1-121.3 (10 x Ar*C*), 126.6 (2 x Ar*C*), 127.9 (Ar*C*), 129.1 (2 x Ar*C*), 132.8 (Ar*C*), 132.9 (Ar*C*), 133.0 (3 x Ar*C*), 140.6 (Ar*C*), 155.3 (4 x Ar*C*), 155.9 (Ar*C*), 156.6 (4 x *C*O), 156.7 (q, J = 36.1, *C*O), 157.3 (*C*O). **^{19}F NMR** (377 MHz, $CDCl_3$) δ_F −74.9 (C*F*$_3$). **HR-MS** (MALDI) – *m/z* for $[C_{59}H_{68}F_3N_{11}O_{11}+Na]^+$ = 1186.4950. Found 1186.4893. **FTIR** (neat) – 3320, 2924, 2898, 1648.

1-Benzyl-1,4,7,10,13-pentakis(4-methoxyanilinylcarbonyl)-1,4,7,10,13,16-hexaazahexadecane, 86

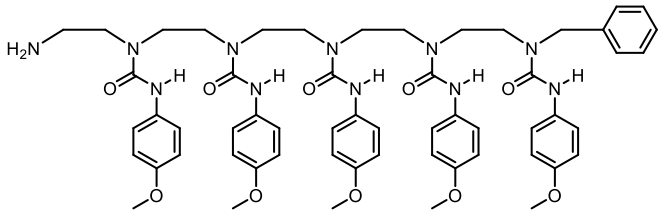

Synthesised according to general procedure H using **85** (450 mg, 0.39 mmol). The title amine was isolated as a foamy white solid (340 mg, 0.32 mmol, 82%). **M.P.** 150-151 °C (DCM/Et_2O). **TLC** – R_f = 0.18 (8:92 MeOH:DCM). **^{1}H NMR** (500 MHz, $CDCl_3$) δ_H 2.97 (t, J = 4.0, 2H, NCH_2), 3.35-3.63 (m, 18H, 9 x NCH_2), 3.79-3.82 (m, 15H, 5 x OCH_3), 4.63 (s, 2H, CH_2Ar), 6.80-6.88 (m, 10H, 10 x Ar*H*), 7.26-7.36 (m, 9H, 9 x Ar*H*), 7.60 (d, J = 8.8, 2H, 2 x Ar*H*), 7.63 (d, J = 8.8, 4H, 4 x Ar*H*), 8.97 (s, 1H, N*H*), 9.08-9.13 (m, 3H, 3 x N*H*), 10.1 (s, 1H, N*H*). **^{13}C NMR** (126 MHz, $CDCl_3$) δ_C 42.1 (N*C*H_2), 46.8-48.6 (9 x N*C*H_2), 51.0 (*C*H_2Ar), 55.5-55.6 (5 x O*C*H_3), 113.9 (6 x Ar*C*), 114.0 (2 x Ar*C*), 114.1 (2 x Ar*C*), 120.6 (2 x Ar*C*), 121.1 (6 x Ar*C*), 121.7 (2 x Ar*C*), 126.9 (2 x Ar*C*), 127.7 (Ar*C*), 129.0 (2 x Ar*C*), 133.2-133.5 (5 x Ar*C*),

140.0 (Ar*C*), 155.2 (5 x Ar*C*), 156.7 (5 x *C*O). **HR-MS** (ESI, positive ion mode) – *m/z* for $[C_{57}H_{69}N_{11}O_{10}+Na]^+$ = 1090.5127. Found 1090.5095. **FTIR** (neat) – 3315, 3031, 2950, 1640.

1,19-Dibenzyl-1,4,7,10,13-pentakis(4-methoxyanilinylcarbonyl)-19-(*tert*-butoxycarbonyl)-1,4,7,10,13,16,19-heptaazanonadecane, 87

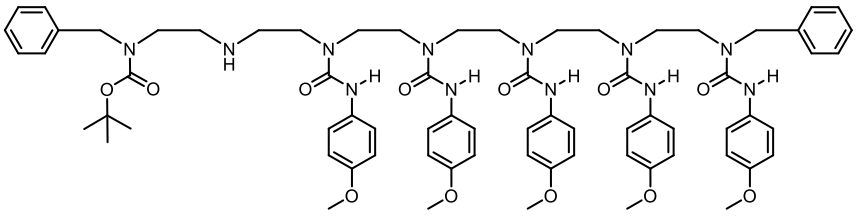

Synthesised according to general procedure E using **86** (340 mg, 0.32 mmol) and **82** (159 mg, 0.64 mmol). The crude product was purified by column chromatography (2-10% MeOH:DCM) to give the title amine as a foamy white solid (233 mg, 0.18 mmol, 56%). **M.P.** 155-156 °C (DCM/Et_2O). **TLC** – R_f = 0.33 (8:92 MeOH:DCM). **^{1}H NMR** (400 MHz, $CDCl_3$) δ_H 1.46 (s, 9H, C(C*H*$_3$)$_3$), 1.91 (s, 1H, N*H*), 2.71-2.79 (m, 4H, 2 x NC*H*$_2$), 3.24-3.58 (m, 20H, 10 x NC*H*$_2$), 3.74-3.79 (m, 15H, 5 x OC*H*$_3$), 4.40 (s, 2H, C*H*$_2$Ar), 4.58 (s, 2H, C*H*$_2$Ar), 6.77-6.87 (m, 10H, 10 x Ar*H*), 7.15 (d, J = 9.0, 2H, 2 x Ar*H*), 7.25-7.39 (m, 14H, 14 x Ar*H*), 7.53-7.68 (m, 6H, 6 x Ar*H*), 8.98-9.15 (m, 4H, 4 x N*H*), 9.91 (s, 1H, N*H*). **^{13}C NMR** (101 MHz, $CDCl_3$) δ_C 28.5 (*C*(CH$_3$)$_3$), 42.4 (NCH$_2$), 43.2 (N*C*H$_2$), 46.4-49.0 (10 x N*C*H$_2$), 50.2 (*C*H$_2$Ar), 51.3 (*C*H$_2$Ar), 55.4-55.6 (5 x O*C*H$_3$), 80.1 (*C*(CH$_3$)$_3$), 113.8-114.1 (10 x Ar*C*), 121.0-121.3 (10 x Ar*C*), 126.9-128.8 (10 x Ar*C*), 132.8-133.9 (5 x Ar*C*), 140.2 (Ar*C*), 140.8 (Ar*C*), 155.1-155.4 (5 x Ar*C*) 156.0-156.5 (6 x *C*O). **HR-MS** (ESI, positive ion mode) – *m/z* for $[C_{71}H_{88}N_{12}O_{12}+H]^+$ = 1301.6723. Found 1301.6700. **FTIR** (neat) – 3287, 2933, 1650.

1,19-Dibenzyl-1,4,7,10,13,16-hexakis(4-methoxyanilinylcarbonyl)-19-(*tert*-butoxycarbonyl)-1,4,7,10,13,16,19-heptaazanonadecane, 88

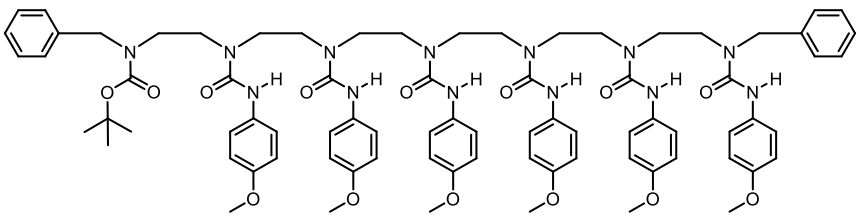

Synthesised according to general procedure B1 using **87** (135 mg, 0.10 mmol) and 4-methoxphenyl isocyanate (0.02 mL, 0.16 mmol). The crude product was purified by column chromatography (2-10% MeOH:DCM) to give the title hexaurea as a foamy white solid (130 mg, 0.09 mmol, 90%). **M.P.** 190-191 °C (DCM/Et_2O). **TLC** – R_f = 0.23 (3:97 MeOH:DCM). **^{1}H NMR** (400 MHz, $CDCl_3$) δ_H 1.50 (s, 9H, C(C*H*$_3$)$_3$), 3.28-3.60 (m, 24H, 12 x NC*H*$_2$), 3.74-3.81

(m, 18H, 6 x OC*H*$_3$), 4.41 (s, 2H, C*H*$_2$Ar), 4.57 (s, 2H, C*H*$_2$Ar), 6.76-6.87 (m, 12H, 12 x Ar*H*), 7.19 (d, J = 9.0, 2H, 2 x Ar*H*), 7.28-7.41 (m, 10H, 10 x Ar*H*), 7.57-7.65 (m, 10H, 10 x Ar*H*), 8.83 (s, 1H, N*H*), 8.97 (s, 1H, N*H*), 9.02 (s, 1H, N*H*), 9.13 (s, 1H, N*H*), 9.17 (s, 1H, N*H*). **^{13}C NMR** (101 MHz, $CDCl_3$) δ_C 28.5 (C(*C*H$_3$)$_3$), 45.8-49.0 (12 x N*C*H$_2$), 50.2-51.5 (2 x *C*H$_2$Ar), 55.5-55.6 (6 x O*C*H$_3$), 80.0 (*C*(CH$_3$)$_3$), 113.7-114.1 (12 x Ar*C*), 120.7-121.7 (12 x Ar*C*), 127.4-128.8 (10 x Ar*C*), 132.8-133.6 (6 x Ar*C*), 139.9-140.6 (2 x Ar*C*), 155.0-155.4 (6 x Ar*C*), 156.7-157.1 (7 x *C*O). **HR-MS** (MALDI) – *m/z* for $[C_{79}H_{95}N_{13}O_{14}+Na]^+$ = 1472.7019. Found 1472.6984. **FTIR** (neat) – 3321, 2924, 2853, 1713.

1,19-Dibenzyl-1,4,7,10,13,16-hexakis(4-methoxyanilinylcarbonyl)-1,4,7,10,13,16,19-heptaazanonadecane, 89

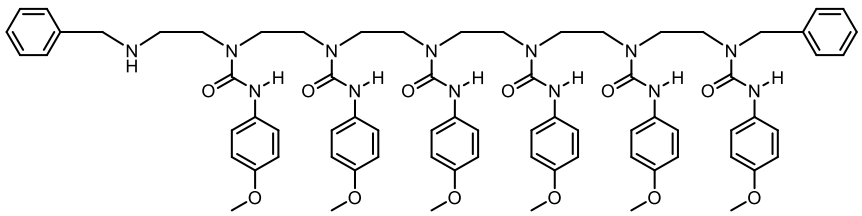

Synthesised according to general procedure C using **88** (130 mg, 0.09 mmol). The title amine was isolated as a foamy white solid (101 mg, 0.07 mmol, 83%). **M.P.** 204-205 °C (DCM/Et$_2$O). **TLC** – R_f = 0.13 (3:97 MeOH:DCM). **^{1}H NMR** (400 MHz, $CDCl_3$) δ_H 2.87 (s, 2H, NC*H*$_2$), 3.30-3.62 (m, 22H, 11 x NC*H*$_2$), 3.75-3.78 (m, 18H, 6 x OC*H*$_3$), 3.82 (s, 2H, C*H*$_2$Ar), 4.57 (C*H*$_2$Ar), 6.74-6.86 (m, 12H, 12 x Ar*H*), 7.22 (d, J = 9.0, 2H, 2 x Ar*H*), 7.28-7.41 (m, 12H, 12 x Ar*H*), 7.55-7.64 (m, 8H, 8 x Ar*H*), 8.95 (s, 1H, N*H*), 9.06 (s, 1H, N*H*), 9.08 (s, 1H, N*H*), 9.15 (s, 1H, N*H*), 10.04 (s, 1H, N*H*). **^{13}C NMR** (101 MHz, $CDCl_3$) δ_C 47.0-49.2 (12 x N*C*H$_2$), 51.0-52.2 (2 x *C*H$_2$Ar), 55.6-55.7 (6 x O*C*H$_3$), 113.8-114.3 (12 x Ar*C*), 121.1-122.6 (12 x Ar*C*), 127.6-129.0 (10 x Ar*C*), 133.0-133.8 (6 x Ar*C*), 140.3-140.6 (2 x Ar*C*), 155.2-156.8 (6 x *C*O, 6 x Ar*C*). **HR-MS** (ESI, positive ion mode) – *m/z* for $[C_{74}H_{87}N_{13}O_{12}+Na]^+$ = 1372.6495. Found 1372.6494. **FTIR** (neat) – 3338, 2950, 1645.

1,19-Dibenzyl-1,4,7,10,13,16-hexakis(4-methoxyanilinylcarbonyl)-19-(4-nitroanilinylthiocarbonyl)-1,4,7,10,13,16,19-heptaazanonadecane, 90

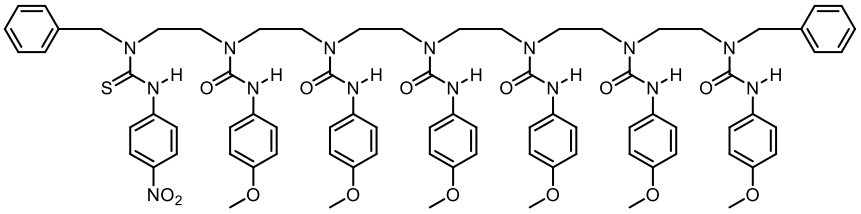

Synthesised according to general procedure B1 using **89** (40 mg, 0.03 mmol) and 4-nitrophenyl isothiocyanate (8 mg, 0.04 mmol). The crude product was purified by column chromatography (2-10% MeOH:DCM) to give the title thiourea as a yellow solid (46 mg, 0.03 mmol, >99%). **M.P.** 159-160 °C (DCM/Et_2O). **TLC** – R_f = 0.28 (3:97 MeOH:DCM). **^{1}H NMR** (500 MHz, CD_2Cl_2) δ_H 3.38-3.68 (m, 24H, 12 x NCH_2), 3.76-3.85 (m, 18H, 6 x OCH_3), 4.61 (s, 2H, CH_2Ar), 5.32 (s, 2H, CH_2Ar), 6.31 (s, 1H, N*H*), 6.84-6.93 (m, 12H, 12 x Ar*H*), 7.17-7.67 (m, 22H, 22 x Ar*H*), 8.06 (d, J = 9.0, 2H, 2 x Ar*H*), 8.19 (d, J = 8.8, 2H, 2 x Ar*H*), 9.03 (s, 1H, N*H*), 9.17 (s, 1H, N*H*), 9.19 (s, 1H, N*H*), 9.23 (s, 1H, N*H*), 9.29 (s, 1H, N*H*), 10.48 (s, 1H, N*H*). **^{13}C NMR** (126 MHz, CD_2Cl_2) δ_C 47.3-49.0 (12 x N*C*H_2), 53.3 (*C*H_2Ar), 55.9-56.2 (6 x O*C*H_3), 56.8 (*C*H_2Ar), 114.3-114.7 (12 x Ar*C*), 121.6-121.9 (12 x Ar*C*), 123.0 (2 x Ar*C*), 124.4 (2 x Ar*C*), 126.6-130.2 (10 x Ar*C*), 133.4-134.0 (6 x Ar*C*), 138.9-139.3 (2 x Ar*C*), 143.7 (Ar*C*), 147.4 (Ar*C*), 155.4-155.8 (6 x Ar*C*), 156.7-157.2 (6 x *C*O), 182.3 (*C*S). **HR-MS** (MALDI) – *m/z* for $[C_{81}H_{91}N_{15}O_{14}S+Na]^+$ = 1552.6488. Found 1552.6491. **FTIR** (neat) – 3675, 3345, 2971, 2914, 1648, 1606, 1551.

1,19-Dibenzyl-1,4,7,10,13,16-hexakis(4-methoxyanilinylcarbonyl)-19-((*N*-methyl-4-methoxyanilinyl)carbonyl)-1,4,7,10,13,16,19-heptaazanonadecane, 91

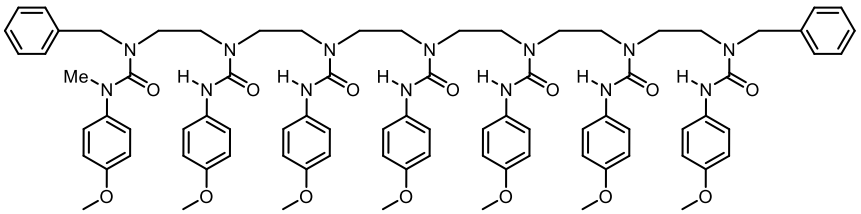

Synthesised according to general procedure B2 using **89** (40 mg, 0.03 mmol) and **70** (9 mg, 0.04 mmol). The crude product was purified by column chromatography (2-10% MeOH:DCM) to give the title heptaurea as a foamy white solid (37 mg, 0.02 mmol, 80%). **M.P.** 170-171 °C (DCM/Et_2O). **TLC** – R_f = 0.15 (3:97 MeOH:DCM). **^{1}H NMR** (500 MHz, CD_2Cl_2) δ_H 3.30-3.60 (m, 12H, 6 x NCH_2), 3.76 (s, 3H, NCH_3), 3.80-3.84 (m, 18H, 6 x OCH_3), 4.07 (s, 2H, CH_2Ar), 4.59 (s, 2H, CH_2Ar), 6.77-6.89 (m, 14H, 14 x Ar*H*), 6.95 (d, J = 7.0, 2H, 2 x Ar*H*), 7.02 (d, J = 8.8, 2H, 2 x Ar*H*), 7.17-7.40 (m, 10H, 10 x Ar*H*), 7.56-7.67 (m, 10H, 10 x Ar*H*), 8.99-9.23 (m, 6H, 6 x N*H*). **^{13}C NMR** (126 MHz, CD_2Cl_2) δ_C 40.4 (N*C*H_3), 46.3-49.1 (12 x N*C*H_2), 53.0

(CH_2Ar), 53.8 (CH_2Ar), 55.3-55.5 (7 x OCH_3), 113.7-114.1 (14 x Ar*C*), 121.0-121.5 (14 x Ar*C*), 126.2-128.7 (10 x Ar*C*), 133.2-133.6 (6 x Ar*C*), 137.7 (Ar*C*), 138.6-139.2 (2 x Ar*C*), 155.2-155.7 (7 x Ar*C*), 156.5-157.0 (6 x *C*O), 163.1 (*C*O). **HR-MS** (MALDI) – *m/z* for $[C_{83}H_{96}N_{14}O_{14}+Na]^+$ = 1535.7128. Found 1535.7096. **FTIR** (neat) – 3349, 2968, 2931, 1649.

N-(2-Pyridyl)ethylenediamine, 92

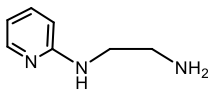

Synthesised according to general procedure M using freshly distilled ethylenediamine (23.40 mL, 350.00 mmol) and 2-fluoropyridine (3.00 mL, 35.00 mmol). The title *N*-(2-pyridyl)-amine was isolated as a colourless oil (2.70 g, 19.40 mmol, 83%). **TLC** – R_f = 0.05 (SiO_2, 10:90:1 MeOH:DCM:TEA). **^{1}H NMR** (400 MHz, $CDCl_3$) δ_H 2.80 (t, J = 6.0, 2H, NCH_2), 3.18 (q, J = 6.0, 2H, NCH_2), 6.40 (d, J = 8.3, 1H, Ar*H*), 6.58 (t, J = 6.0, 1H, Ar*H*), 7.41 (t, J = 7.6, 1H, Ar*H*), 8.04 (d, J = 4.9, 1H, Ar*H*). Spectroscopic data matched that previously reported.[132]

1-(2-Pyridyl)-7-(*tert*-butoxycarbonyl)-1,4,7-triazaheptane, 93

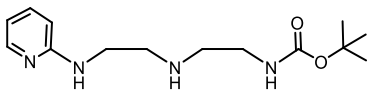

Synthesised according to general procedure A using **92** (490 mg, 3.57 mmol) and *N*-Boc-2-aminoacetaldehyde (614 mg, 3.86 mmol). The title carbamate was isolated as a white solid (370 mg, 1.32 mmol, 37%). **M.P.** 72-73 °C ($CHCl_3$). **TLC** – R_f = 0.09 (SiO_2, 5:95 MeOH:DCM). **^{1}H NMR** (400 MHz, $CDCl_3$) δ_H 1.44 (s, 9H, C(CH_3)$_3$), 2.76 (t, J = 5.8, 2H, NCH_2), 2.88 (t, J = 5.8, 2H, NCH_2), 3.22 (q, J = 5.8, 2H, NCH_2), 3.34 (q, J = 5.8, 2H, NCH_2), 4.85 (s, 1H, N*H*), 4.92 (s, 1H, N*H*), 6.41 (d, J = 8.5, 1H, Ar*H*), 6.56 (t, J = 6.0, 1H, Ar*H*), 7.40 (t, J = 7.6, 1H, Ar*H*), 8.08 (d, J = 4.9, 1H, Ar*H*). **^{13}C NMR** (101 MHz, $CDCl_3$) δ_C 28.6 (C(*C*H_3)$_3$), 40.5 (N*C*H_2), 41.9 (N*C*H_2), 48.7 (N*C*H_2), 49.1 (N*C*H_2), 79.2 (*C*(CH$_3$)$_3$), 107.4 (Ar*C*), 113.0 (Ar*C*), 137.5 (Ar*C*), 148.3 (Ar*C*), 156.5 (*C*O), 158.5 (Ar*C*). **HR-MS** (ESI, positive ion mode) – *m/z* for $[C_{14}H_{26}N_4O+Na]^+$ = 303.1797. Found 303.1807. **FTIR** (neat) – 3356, 2991, 2894, 1695.

1-(2-Pyridyl)-1,4-bis(4-methoxyanilinylcarbonyl)-7-(*tert*-butoxycarbonyl)-1,4,7-triazaheptane, 94

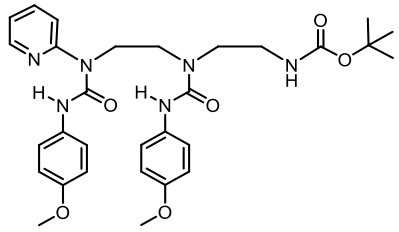

Synthesised according to general procedure B1 using **93** (163 mg, 0.58 mmol) and 4-methoxyphenyl isocyanate (0.23 mL, 1.74 mmol). The crude product was purified by column chromatography (12-100% EtOAc:PE) to yield the title diurea as a foamy white solid (114 mg, 0.20 mmol, 34%). **M.P.** 119-120 °C ($CHCl_3$). **TLC** – R_f = 0.48 (SiO_2, 5:95 MeOH:DCM). **^{1}H NMR** (500 MHz, CD_2Cl_2) δ_H 1.44 (s, 9H, C(C*H*$_3$)$_3$), 3.32 (q, J = 6.3, 2H, NC*H*$_2$), 3.54 (t, J = 6.6, 2H, NC*H*$_2$), 3.64 (t, J = 6.6, 2H, NC*H*$_2$), 3.78-3.79 (m, 6H, 2 x OC*H*$_3$), 4.10 (t, J = 6.3, 2H, NC*H*$_2$), 5.31 (t, J = 5.3, 1H, N*H*), 6.86 (d, J = 9.0, 2H, 2 x Ar*H*), 6.89 (d, J = 9.0, 2H, 2 x Ar*H*), 7.04 (dd, J = 5.1, 7.2, 1H, Ar*H*), 7.42 (s, 1H, Ar*H*), 7.50 (d, J = 9.0, 2H, 2 x Ar*H*), 7.56 (d, J = 9.0, 2H, 2 x Ar*H*), 7.82 (ddd, J = 8.0, 7.5, 1.9, 1H, Ar*H*), 8.34 (dd, J = 4.9, 1.5, 1H, Ar*H*), 8.68 (s, 1H, N*H*), 12.48 (s, 1H, N*H*). **^{13}C NMR** (126 MHz, CD_2Cl_2) δ_C 28.7 (C(*C*H$_3$)$_3$), 41.0 (N*C*H$_2$), 45.2 (N*C*H$_2$), 46.7 (N*C*H$_2$), 48.3 (N*C*H$_2$), 56.0 (2 x O*C*H$_3$), 80.0 (*C*(CH$_3$)$_3$), 113.0 (Ar*C*), 114.3-114.5 (4 x Ar*C*), 118.4 (Ar*C*), 121.8 (2 x Ar*C*), 122.6 (2 x Ar*C*), 132.5 (Ar*C*), 134.1 (Ar*C*), 140.0 (Ar*C*), 146.4 (Ar*C*), 154.9 (Ar*C*), 155.8 (Ar*C*), 155.9 (*C*O), 156.5 (*C*O), 156.8 (*C*O). **HR-MS** (ESI, positive ion mode) – *m/z* for $[C_{30}H_{38}N_6O_6+H]^+$ = 579.2931. Found 579.2895. **FTIR** (neat) – 3497, 2990, 2943, 1694, 1660.

1-(2-Pyridyl)-1,4-bis(4-methoxyanilinylcarbonyl)-1,4,7-triazaheptane, 95

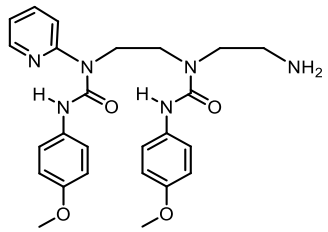

Synthesised according to general procedure C using **94** (200 mg, 0.34 mmol). The title amine was isolated as a foamy white solid (163 mg, 0.34 mmol, >99%). **M.P.** 139-140 °C ($CHCl_3$). **TLC** – R_f = 0.09 (SiO_2, 90:10 EtOAc:PE). **^{1}H NMR** (400 MHz, $CDCl_3$) δ_H 3.00 (t, J = 4.9, 2H, NC*H*$_2$), 3.51 (t, J = 4.9, 2H, NC*H*$_2$), 3.61 (t, J = 7.2, 2H, NC*H*$_2$), 3.77 (s, 3H, OC*H*$_3$), 3.79 (s, 3H, OC*H*$_3$), 4.17 (t, J = 7.2, 2H, NC*H*$_2$), 6.84 (d, J = 8.9, 2H, 2 x Ar*H*), 6.88 (d, J = 8.9, 2H, 2 x Ar*H*), 6.98 (dd, J = 5.0, 6.8, 1H, Ar*H*), 7.35 (d, J = 8.9, 2H, NC*H*$_2$), 7.45 (d, J = 8.9, 2H, NC*H*$_2$), 7.67 (d, J = 7.7, 1H, Ar*H*), 7.78 (ddd, J = 1.8, 5.8, 7.7, 1H, Ar*H*), 8.28 (d, J = 5.0, 1H, Ar*H*), 9.75 (s, 1H, N*H*), 12.61 (s, 1H, N*H*). **^{13}C NMR** (101 MHz, $CDCl_3$) δ_C 41.8 (N*C*H$_2$), 43.6 (N*C*H$_2$), 46.1 (N*C*H$_2$), 52.1 (N*C*H$_2$), 55.5 (2 x O*C*H$_3$), 112.7 (Ar*C*), 114.1 (4 x Ar*C*), 117.5 (Ar*C*), 121.3 (2 x Ar*C*), 122.5 (2 x Ar*C*), 131.9 (Ar*C*), 133.4 (Ar*C*), 139.6 (Ar*C*), 145.3 (Ar*C*), 154.4 (*C*O), 155.1 (Ar*C*), 155.4 (Ar*C*), 158.0 (Ar*C*). **HR-MS** (ESI, positive ion mode) – *m/z* for $[C_{25}H_{30}N_6O_4+H]^+$ = 479.2407. Found 479.2380. **FTIR** (neat) – 3329, 3130, 2992, 2947, 1659.

1-(2-Pyridyl)-1,4-bis(4-methoxyanilinylcarbonyl)-7-benzyl-1,4,7-triazaheptane, 96

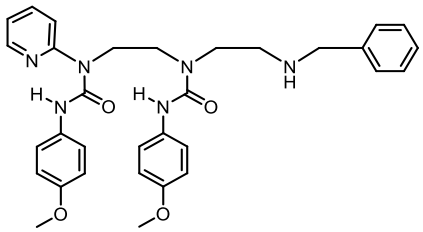

Synthesised according to general procedure E using **95** (140 mg, 0.29 mmol) and benzaldehyde (0.05 mL, 0.44 mmol). The crude product was purified by column chromatography (3-10% MeOH:DCM) to yield the title triamine as a foamy white solid (87 mg, 0.15 mmol, 53%). **M.P.** 142-143 °C ($CHCl_3$). **TLC** – R_f = 0.48 (SiO_2, 10:90 MeOH:DCM). **^{1}H NMR** (500 MHz, $CDCl_3$) δ_H 2.03 (s, 1H, N*H*), 2.95 (t, J = 4.9, 2H, NCH_2), 3.56 (t, J = 4.9, 2H, NCH_2), 3.60 (t, J = 8.2, 2H, NCH_2), 3.78 (s, 3H, OCH_3), 3.80 (s, 3H, OCH_3), 3.84 (s, 2H, CH_2Ar), 4.15 (t, J = 8.2, 2H, NCH_2), 6.80 (d, J = 9.0, 2H, 2 x Ar*H*), 6.88 (d, J = 9.0, 2H, 2 x Ar*H*), 6.98 (dd, J = 5.0, 7.2, 1H, Ar*H*), 7.22 (d, J = 9.0 2H, 2 x Ar*H*), 7.25-7.34 (m, 5H, 5 x Ar*H*), 7.46 (d, J = 9.0, 2H, 2 x Ar*H*), 7.66-7.70 (m, 1H, Ar*H*), 7.74 (ddd, J = 1.8, 7.4, 8.6, 1H, Ar*H*), 8.27 (d, J = 5.0, 1H, Ar*H*), 9.70 (s, 1H, N*H*), 12.61 (s, 1H, N*H*). **^{13}C NMR** (126 MHz, $CDCl_3$) δ_C 43.5 (N*C*H_2), 46.2 (N*C*H_2), 49.6 (N*C*H_2), 50.0 (N*C*H_2), 54.3 (*C*H_2Ar), 55.5 (2 x O*C*H_3), 112.8 (Ar*C*), 114.0 (2 x Ar*C*), 114.1 (2 x Ar*C*) 117.4 (Ar*C*), 121.5 (2 x Ar*C*), 122.4 (2 x Ar*C*), 127.5 (Ar*C*), 128.3 (2 x Ar*C*), 128.7 (2 x Ar*C*), 132.0 (Ar*C*), 133.3 (Ar*C*), 138.9 (Ar*C*), 139.6 (Ar*C*), 145.3 (Ar*C*), 154.3 (Ar*C*), 155.1 (Ar*C*), 155.4 (*C*O), 155.9 (Ar*C*), 158.0 (*C*O). **HR-MS** (ESI, positive ion mode) – *m/z* for $[C_{32}H_{36}N_6O_4+H]^+$ = 569.2876. Found 569.2875. **FTIR** (neat) – 3326, 2993, 2950, 1652.

1-(2-Pyridyl)-1,4,7-tris(4-methoxyanilinylcarbonyl)-7-benzyl-1,4,7-triazaheptane, 97

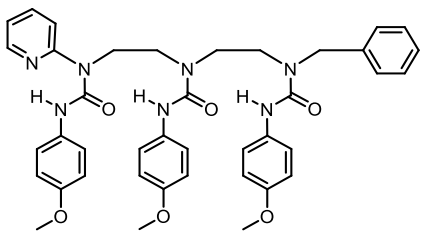

Synthesised according to general procedure B using **96** (62 mg, 0.11 mmol) and 4-methoxyphenyl isocyanate (0.02 mL, 0.17 mmol) dropwise. The crude product was purified by column chromatography (1-2% MeOH:DCM) to yield the title triurea as a foamy white solid (47 mg, 0.07 mmol, 60%). **M.P.** 200-201 °C (DCM). **TLC** – R_f = 0.26 (SiO_2, 1:99 MeOH:DCM). **^{1}H NMR** (500 MHz, $CDCl_3$) δ_H 3.32-3.37 (m, 2H, NCH_2), 3.51 (t, J = 8.0, 2H, NCH_2), 3.54 (t, J = 8.2, 2H, NCH_2), 3.76 (s, 3H, OCH_3), 3.78 (s, 3H, OCH_3), 3.79 (s, 3H, OCH_3), 3.98 (t, J = 8.0, 2H, NCH_2), 4.63 (s, 2H, CH_2Ar), 6.82 (d, J = 9.0, 2H, 2 x Ar*H*), 6.86 (d, J = 9.0, 2H, 2 x Ar*H*), 6.88 (d, J = 9.0, 2H, 2 x Ar*H*), 7.08 (dd, J = 5.0, 7.2, 1H, Ar*H*), 7.30-7.40 (m, 6H, 6 x Ar*H*), 7.48 (d, J = 9.0, 2H, 2 x Ar*H*), 7.51-7.53 (m, 2H, 2 x Ar*H*), 7.61 (d, J = 9.0, 2H, 2 x Ar*H*), 7.82 (ddd, J = 1.9, 7.4, 8.7, 1H, Ar*H*), 8.36 (dd, J = 1.6, 5.0, 1H, Ar*H*), 8.95 (s, 1H, N*H*), 12.34 (s, 1H, N*H*). **^{13}C NMR** (126 MHz, $CDCl_3$) δ_C 45.2 (N*C*H_2), 47.0 (2 x N*C*H_2), 48.5 (N*C*H_2), 51.2 (*C*H_2Ar), 55.4 (3 x O*C*H_3), 112.0 (Ar*C*), 113.7 (2 x Ar*C*), 113.8 (2 x Ar*C*), 114.0 (2 x Ar*C*), 118.1 (Ar*C*), 121.1 (2 x Ar*C*), 121.3 (2 x Ar*C*), 122.0 (2 x Ar*C*), 127.3 (Ar*C*), 127.6 (2 x Ar*C*), 128.7 (2 x Ar*C*), 131.7

(Ar*C*), 133.4 (2 x Ar*C*), 139.5 (2 x Ar*C*), 146.1 (Ar*C*), 154.4 (*C*O), 155.1 (Ar*C*), 155.2 (Ar*C*), 155.3 (Ar*C*), 156.0 (*C*O), 156.3 (*C*O). **HR-MS** (ESI, positive ion mode) – *m/z* for $[C_{40}H_{43}N_7O_6+H]^+$ = 718.3353. Found 718.3348. **FTIR** (neat) – 3307, 3185, 3051, 2981, 2875, 1660, 1607.

1-Phenyl-1,4-bis(4-methoxyanilinylcarbonyl)-7-benzyl-1,4,7-triazaheptane, 98

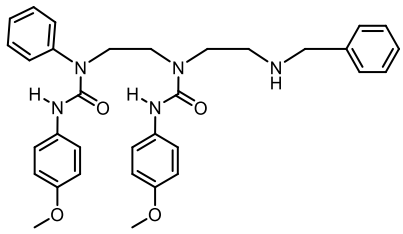

Synthesised according to general procedure E using **30** (300 mg, 0.63 mmol) and benzaldehyde (0.13 mL, 1.26 mmol). The crude product was purified using column chromatography (1-5% MeOH:DCM, 1% TEA) to yield the title amine as a foamy white solid (285 mg, 0.50 mmol, 80%). **M.P.** 187-188 °C ($CHCl_3$). **TLC** – R_f = 0.08 (SiO_2, 1:99 MeOH:DCM). **^{1}H NMR** (400 MHz, $CDCl_3$) δ_H 2.88 (t, J = 5.5, 2H, NC*H*$_2$), 3.48 (t, J = 5.5, 2H, NC*H*$_2$), 3.62 (t, J = 6.9, 2H, NC*H*$_2$), 3.76 (s, 3H, OC*H*$_3$), 3.77 (s, 3H, OC*H*$_3$), 3.81 (s, 2H, C*H*$_2$Ar), 3.85 (t, J = 6.9, 2H, NC*H*$_2$), 6.30 (s, 1H, N*H*), 6.78 (d, J = 9.0, 2H, 2 x Ar*H*), 6.79 (d, J = 9.0, 2H, 2 x Ar*H*), 7.20 (d, J = 9.0, 2H, 2 x Ar*H*), 7.26-7.39 (m, 10H, 10 x Ar*H*), 7.46 (d, J = 9.0, 2H, 2 x Ar*H*), 9.26 (s, 1H, N*H*). **^{13}C NMR** (101 MHz, $CDCl_3$) δ_C 46.8 (N*C*H$_2$), 48.9-49.3 (3 x N*C*H$_2$), 54.1 (*C*H$_2$Ar), 55.5 (2 x O*C*H$_3$), 113.9 (2 x Ar*C*), 114.1 (2 x Ar*C*), 121.2 (2 x Ar*C*), 121.8 (2 x Ar*C*), 127.0 (Ar*C*), 127.2 (2 x Ar*C*), 128.0 (2 x Ar*C*), 128.2 (Ar*C*), 128.3 (2 x Ar*C*), 128.5 (2 x Ar*C*), 131.5 (Ar*C*), 133.5 (Ar*C*), 141.9 (Ar*C*), 150.3 (Ar*C*), 155.0 (Ar*C*), 155.2 (Ar*C*), 155.9 (*C*O), 156.4 (*C*O). **HR-MS** (ESI, positive ion mode) – *m/z* for $[C_{33}H_{37}N_5O_4+H]^+$ = 568.2924. Found 569.2897. **FTIR** (neat) – 3410, 2933, 2833, 1651.

1-Phenyl-1,4,7-tris(4-methoxyanilinylcarbonyl)-7-benzyl-1,4,7-triazaheptane, 99

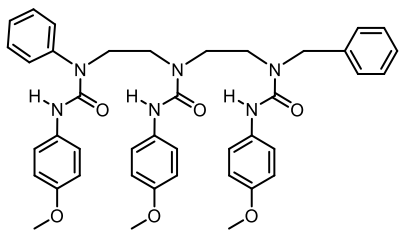

Synthesised according to general procedure D using **98** (100 mg, 0.18 mmol) and 4-methoxyphenyl isocyanate (0.03 mL, 0.26 mmol). The crude product was purified using column chromatography (2-10% MeOH:DCM) to give the title triurea as a foamy white solid (65 mg, 0.09 mmol, 50%). **M.P.** 146-147 °C ($CHCl_3$). **TLC** – R_f = 0.43 (SiO_2, 5:95 MeOH:DCM). **^{1}H NMR** (400 MHz, $CDCl_3$) δ_H 3.15 (t, J = 7.0, 2H, NC*H*$_2$), 3.35 (t, J = 7.0, 2H, NC*H*$_2$), 3.48 (t, J = 7.0, 2H, NC*H*$_2$), 3.64 (t, J = 7.0, 2H, NC*H*$_2$), 3.78 (s, 3H, OC*H*$_3$), 3.78 (s, 3H, OC*H*$_3$), 3.80 (s, 3H, OC*H*$_3$), 4.60 (s, 2H, C*H*$_2$Ar), 6.14 (s, 1H, N*H*), 6.73 (d, J = 9.1, 2H, 2 x Ar*H*), 6.74 (d, J = 9.1, 2H, 2 x Ar*H*), 6.75 (d, J = 9.1, 2H, 2 x Ar*H*), 7.10 (d, J = 9.1, 2H, 2 x Ar*H*), 7.20-7.36 (m, 10H, 10 x Ar*H*), 7.43 (d,

J = 9.1, 2H, 2 x Ar*H*), 7.48 (d, J = 9.1, 2H, 2 x Ar*H*), 8.33 (s, 1H, N*H*), 8.72 (s, 1H, N*H*). **^{13}C NMR** (101 MHz, $CDCl_3$) δ_C 45.5 (N*C*H_2), 47.3 (N*C*H_2), 47.8 (N*C*H_2), 49.9 (N*C*H_2), 51.0 (*C*H_2Ar), 55.5 (3 x O*C*H_3), 113.9 (2 x Ar*C*), 113.9 (2 x Ar*C*), 114.1 (2 x Ar*C*), 121.2 (2 x Ar*C*), 121.4 (2 x Ar*C*), 121.9 (2 x Ar*C*), 127.4-128.7 (10 x Ar*C*), 130.7 (Ar*C*), 131.0 (Ar*C*), 133.0 (Ar*C*), 138.7 (Ar*C*), 141.7 (Ar*C*), 155.2 (Ar*C*), 155.3 (Ar*C*), 155.5 (Ar*C*), 156.1 (*C*O), 156.2 (*C*O), 156.4 (*C*O). **HR-MS** (ESI, positive ion mode) – *m/z* for $[C_{41}H_{44}N_6O_6+H]^+$ = 717.3401. Found 717.3391. **FTIR** (neat) – 3398, 2952, 1651.

2-(Pyridin-2-ylamino)ethan-1-ol, 100

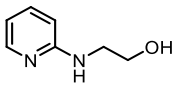

Synthesised according to general procedure M using ethanolamine (29.8 mL, 0.49 mol) and 2-fluoropyridine (4.20 mL, 49.10 mmol). The title *N*-(2-pyridyl)-amine was isolated as a white solid (5.23 g, 37.30 mmol, 76%)**. TLC** – R_f = 0.12 (SiO_2, 5:95 MeOH:DCM). **^{1}H NMR** (400 MHz, $CDCl_3$) δ_H 3.44 (q, J = 5.5, 2H, NCH_2), 3.74 (t, J = 4.6, 2H, OCH_2), 4.79 (s, 1H, O*H*), 6.38 (dt, J = 0.9, 8.4, 1H, Ar*H*), 6.51 (ddd, J = 0.9, 5.2, 7.1, 1H, Ar*H*), 7.33 (ddd, J = 1.1, 7.1, 8.9, 1H, Ar*H*), 7.96 (ddd, J = 0.9, 1.7, 5.2, 1H, Ar*H*). Spectroscopic data matched that previously reported.[133]

***tert*-Butyl (2-hydroxyethyl)(pyridin-2-yl)carbamate, 101**

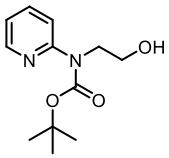

Synthesised according to general procedure K using **100** (2.40 g, 17.37 mmol). The crude product was then purified by column chromatography (2-10% MeOH:DCM) to yield the title carbamate as a colourless oil (3.02 g, 12.68 mmol, 73%). **TLC** – R_f = 0.34 (SiO_2, 5:95 MeOH:DCM). **^{1}H NMR** (400 MHz, $CDCl_3$) δ_H 1.48 (s, 9H, C(CH_3)$_3$), 3.64 (q, J = 5.5, 2H, NCH_2), 4.26 (t, J = 5.1, 2H, OCH_2), 4.73 (s, 1H, O*H*), 6.40 (d, J = 8.3, 1H, Ar*H*), 6.57 (t, J = 5.6, 1H, Ar*H*), 7.39 (t, J = 7.9, 1H, Ar*H*), 8.08 (d, J = 4.5, 1H, Ar*H*). Spectroscopic data matched that previously reported.[133]

1-(2-Pyridyl)-4-(*tert*-butoxycarbonyl)-4-hydroxyethyl-1,4-diazabutane, 103

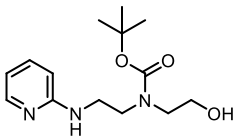

Under a dry, inert atmosphere, 2-fluoropyridine (0.42 mL, 4.90 mmol, 1.00 equiv.) was added to a solution of **52** (1.0 g, 4.90 mmol, 1.00 equiv., 0.10 M) in anhydrous toluene (49 mL). DIPEA (1.71 mL, 9.80 mmol, 2.00 equiv.) was added and the solution was refluxed for 16 h. Upon cooling to room temperature, the solution was concentrated *in vacuo*. The crude product was diluted with deionised water (50 mL) and extracted with DCM three times. The combined organic extracts were dried ($MgSO_4$), filtered

and concentrated *in vacuo*. The crude product was purified by column chromatography (5% MeOH:DCM) to give the title amine as a colourless oil (875 mg, 3.09 mmol, 63%). **TLC** – R_f = 0.32 (5:95 MeOH:DCM). **^{1}H NMR** (400 MHz, $CDCl_3$) δ_H 1.24 (s, 9H, C(C*H*$_3$)$_3$), 3.38-3.54 (m, 6H, 3 x NC*H*$_2$), 3.92-4.04 (m, 2H, NC*H*$_2$), 4.75 (s, 1H, O*H*), 6.40 (dd, J = 4.5, 8.2, 1H, Ar*H*), 6.48 (dd, J = 0.9, 7.3, 1H, Ar*H*), 7.27 (t, J = 7.0, 1H, Ar*H*), 8.02 (d, J = 4.5, 1H, Ar*H*). **^{13}C NMR** (101 MHz, $CDCl_3$) δ_C 28.6 (C(*C*H$_3$)$_3$), 46.7 (N*C*H$_2$), 48.0 (N*C*H$_2$), 51.3 (N*C*H$_2$), 64.4 (O*C*H$_2$), 80.5 (*C*(CH$_3$)$_3$), 110.3 (Ar*C*), 115.5 (Ar*C*), 138.1 (Ar*C*), 148.1 (Ar*C*), 151.0 (Ar*C*), 155.6 (*C*O). **HR-MS** (ESI, positive ion mode) – *m/z* for [$C_{14}H_{23}N_3O_3$+Na]$^+$ = 304.1637. Found 304.1592. **FTIR** (neat) – 3360, 2955, 1691.

1-(2-Pyridyl)-1,4-bis(*tert*-butoxycarbonyl)-4-hydroxyethyl-1,4-diazabutane, 104

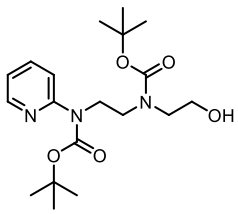

Synthesised according to general procedure K using **43** (1.54 g, 5.47 mmol). The crude product was purified by column chromatography (20-40% EtOAc:PE) to give the title carbamate as a colourless oil (1.65 g, 4.32 mmol, 79%). **TLC** – R_f = 0.10 (20:80 EtOAc:PE). **^{1}H NMR** (400 MHz, $CDCl_3$) δ_H 1.34-1.42 (m, 18H, 2 x C(C*H*$_3$)$_3$), 3.35-3.46 (m, 6H, 3 x NC*H*$_2$), 4.06-4.16 (m, 2H, OC*H*$_2$), 4.64 (s, 1H, O*H*, rot.), 4.96 (s, 1H, O*H*, rot.), 6.34 (d, J = 8.3, 1H, Ar*H*), 6.46-6.48 (m, 1H, Ar*H*), 7.30 (t, J = 7.3, 1H, Ar*H*), 8.00 (d, J = 4.5, 1H, Ar*H*). **^{13}C NMR** (101 MHz, $CDCl_3$) δ_C 27.8 (C(*C*H$_3$)$_3$), 28.4 (C(*C*H$_3$)$_3$), 46.9 (N*C*H$_2$), 47.6 (N*C*H$_2$), 60.3 (N*C*H$_2$), 64.9 (O*C*H$_2$), 80.3 (*C*(CH$_3$)$_3$), 82.2 (*C*(CH$_3$)$_3$), 112.8 (Ar*C*), 120.9 (Ar*C*), 137.1 (Ar*C*), 148.1 (Ar*C*), 153.3 (Ar*C*), 154.4 (*C*O), 154.6 (*C*O). **HR-MS** (ESI, positive ion mode) – *m/z* for [$C_{19}H_{31}N_3O_5$+H]$^+$ = 382.2342. Found 382.2354. **FTIR** (neat) – 3385, 2949, 1741, 1689.

1-(2-Pyridyl)-1,4-bis(*tert*-butoxycarbonyl)-4-oxoethyl-1,4-diazabutane, 105

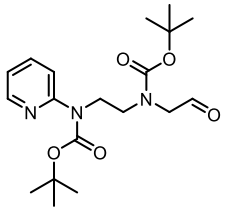

Synthesised according to general procedure L using **104** (500 mg, 1.31 mmol). The crude product was purified by column chromatography (25% EtOAc:PE) to give the title aldehyde as a colourless oil (383 mg, 1.00 mmol, 77%). **TLC** – R_f = 0.30 (25:75 EtOAc:PE). **^{1}H NMR** (400 MHz, $CDCl_3$) δ_H 1.38 (s, 9H, C(C*H*$_3$)$_3$), 1.39 (s, 9H, C(C*H*$_3$)$_3$), 3.34-3.59 (m, 4H, 2 x NC*H*$_2$), 4.07-4.15 (m, 2H, NC*H*$_2$), 6.27 (d, J = 8.8, 1H, Ar*H*), 6.47-6.49 (m, 1H, Ar*H*), 7.13 (dd, J = 1.6, 7.2, 1H, Ar*H*, rot.), 7.23 (d, J = 7.2, 1H, Ar*H*, rot.), 7.90-7.93 (m, 1H, Ar*H*, rot.), 7.96-7.98 (m, 1H, Ar*H*, rot.), 9.48 (s, 1H, C*H*O, rot.), 9.48 (s, 1H, C*H*O, rot.). **^{13}C NMR** (101 MHz, $CDCl_3$) δ_C 27.7 (C(*C*H$_3$)$_3$), 28.3 (C(*C*H$_3$)$_3$), 47.0 (N*C*H$_2$, rot.), 47.2 (N*C*H$_2$, rot.), 47.6 (N*C*H$_2$, rot.), 47.7 (N*C*H$_2$, rot.), 58.3 (N*C*H$_2$, rot.), 58.8 (N*C*H$_2$, rot.), 79.6 (*C*(CH$_3$)$_3$, rot.), 80.1 (*C*(CH$_3$)$_3$, rot.), 81.0

($C(CH_3)_3$, rot.), 82.1 ($C(CH_3)_3$, rot.), 111.7 (Ar*C*, rot.), 112.4 (Ar*C*, rot.), 115.3 (Ar*C*, rot.), 115.8 (Ar*C*, rot.), 136.7 (Ar*C*, rot.), 137.6 (Ar*C*, rot.), 146.0 (Ar*C*, rot.), 146.9 (Ar*C*, rot.), 153.3 (Ar*C*), 156.3 (*C*O), 156.6 (*C*O), 198.5 (*C*HO, rot.), 198.6 (*C*HO, rot.). **HR-MS** (ESI, positive ion mode) – *m/z* for $[C_{19}H_{29}N_3O_5+Na]^+$ = 402.2005. Found 402.1984. **FTIR** (neat) – 2963, 2922, 1719, 1678.

1-Benzyl-1-(4-methoxyanilinylcarbonyl)-4-trifluoroacetyl-1,4-diazabutane, 106

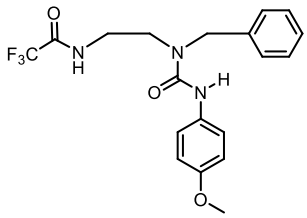

Synthesised according to general procedure K using *N*-benzylethylenediamine (1.00 g, 6.66 mmol) and 4-methoxyphenyl isocyanate (1.29 mL, 9.99 mmol). The crude product was purified by column chromatography (1-10% MeOH:DCM, 1% NH_4OH) to yield the title amine as a colourless oil (2.63 g, 6.66 mmol, >99%). **TLC** – R_f = 0.56 (SiO_2, 5:95 MeOH:DCM). **^{1}H NMR** (400 MHz, $CDCl_3$) δ_H 3.45 (q, J = 5.5, 2H, NCH_2), 3.65 (t, J = 5.5, 2H, NCH_2), 3.74 (s, 3H, OCH_3), 4.54 (s, 2H, CH_2Ar), 6.47 (t, J = 5.5, 1H, N*H*), 6.78 (d, J = 8.8, 2H, 2 x Ar*H*), 7.09 (d, J = 8.8, 2H, 2 x Ar*H*), 7.26 (d, J = 8.5, 2H, 2 x Ar*H*), 7.34 (t, J = 7.5, 1H, Ar*H*), 7.40 (t, J = 8.0, 2H, 2 x Ar*H*), 8.39 (s, 1H, N*H*). **^{13}C NMR** (101 MHz, $CDCl_3$) δ_C 40.3 (N*C*H$_2$), 46.4 (N*C*H$_2$), 51.6 (*C*H$_2$Ar), 55.6 (O*C*H$_3$), 114.2 (2 x Ar*C*), 115.7 (q, J = 286.4, *C*F$_3$), 122.7 (2 x Ar*C*), 126.5 (2 x Ar*C*), 128.4 (Ar*C*), 129.6 (2 x Ar*C*), 131.3 (Ar*C*), 136.1 (Ar*C*), 156.3 (Ar*C*), 157.7 (*C*O), 158.1 (q, J = 37.3, *C*O). **^{19}F NMR** (377 MHz, $CDCl_3$) δ_F −76.4 (C*F*$_3$). **HR-MS** (ESI, positive ion mode) – *m/z* for $[C_{19}H_{20}F_3N_3O_3+Na]^+$ = 418.1354. Found 418.1380. **FTIR** (neat) – 3243, 2980, 1661, 1640.

1-Benzyl-1-(4-methoxyanilinylcarbonyl)-1,4-diazabutane, 107

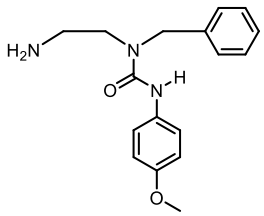

Synthesised according to general procedure H using **106** (1.00 g, 4.74 mmol). The title amine was isolated as a colourless oil (1.13 g, 3.79 mmol, 80%). **TLC** – R_f = 0.23 (SiO_2, 5:95:1 MeOH:DCM:NH_4OH). **^{1}H NMR** (400 MHz, $CDCl_3$) δ_H 2.76 (t, J = 4.9, 2H, NCH_2), 3.31 (t, J = 4.9, 2H, NCH_2), 3.71 (OCH_3), 4.50 (s, 2H, CH_2Ar), 6.76 (d, J = 8.9, 2H, 2 x Ar*H*), 7.21-7.28 (m, 7H, 7 x Ar*H*), 9.39 (s, 1H, N*H*). **^{13}C NMR** (101 MHz, $CDCl_3$) δ_C 40.9 (N*C*H$_2$), 50.6 (N*C*H$_2$), 51.0 (*C*H$_2$Ar), 55.6 (O*C*H$_3$), 114.1 (2 x Ar*C*), 121.1 (2 x Ar*C*), 127.3 (Ar*C*), 127.8 (2 x Ar*C*), 128.6 (2 x Ar*C*), 133.4 (Ar*C*), 138.4 (Ar*C*), 155.1 (Ar*C*), 158.0 (*C*O). **HR-MS** (ESI, positive ion mode) – *m/z* for $[C_{17}H_{21}N_3O_3+Na]^+$ = 322.1531. Found 322.1547. **FTIR** (neat) – 3402, 2959, 2940, 1637.

1-(2-Pyridyl)-4-hydroxyethyl-1,4-diazabutane, 109

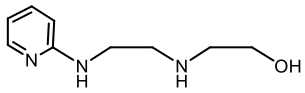

Synthesised according to general procedure M using *N*-(2-hydroxyethyl)ethylenediamine (37.6 mL, 0.37 mol) and 2-fluoropyridine (3.2 mL, 37.2 mmol). The title *N*-(2-pyridyl)-amine was isolated as a colourless oil (6.7 g, 0.26 mmol, 70%). **TLC** – R_f = 0.10 (SiO_2, 10:90:1 MeOH:DCM:NH_4OH). **^{1}H NMR** (400 MHz, $CDCl_3$) δ_H 2.71 (t, J = 6.1, 2H, NC*H*$_2$), 2.90 (t, J = 5.5, 2H, NC*H*$_2$), 3.20 (t, J = 6.1, 2H, NC*H*$_2$), 3.48 (t, J = 5.5, 2H, OC*H*$_2$), 4.98 (s, 1H, O*H*), 6.38 (dd, J = 4.8, 8.0, 1H, Ar*H*), 6.50 (dd, J = 1.2, 7.2, 1H, Ar*H*), 7.21 (t, J = 7.2, 1H, Ar*H*), 7.98 (d, J = 4.8, 1H, Ar*H*). **^{13}C NMR** (101 MHz, $CDCl_3$) δ_C 47.5 (N*C*H$_2$), 48.6 (N*C*H$_2$), 50.1 (N*C*H$_2$), 60.9 (O*C*H$_2$), 111.0 (Ar*C*), 115.2 (Ar*C*), 139.6 (Ar*C*), 149.1 (Ar*C*), 150.3 (Ar*C*), 156.1 (*C*O). **HR-MS** (ESI, positive ion mode) – *m/z* for $[C_9H_{16}N_3O+Na]^+$ = 182.1293. Found 182.1304. **FTIR** (neat) – 3412, 3230, 2973, 2920.

1-(2-Pyridyl)-1,4-bis(4-methoxyanilinylcarbonyl)-4-hydroxyethyl-1,4-diazabutane, 110

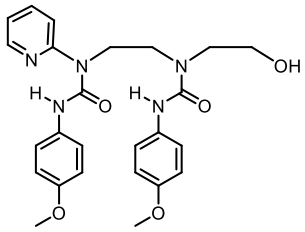

Synthesised according to general procedure B using **109** (518 mg, 1.08 mmol) and 4-methoxyphenyl isocyanate (0.42 mL, 3.24 mmol). The title diurea was isolated as a white solid (259 mg, 0.54 mmol, 45%). **TLC** – R_f = 0.27 (SiO_2, 5:95 MeOH:DCM). **^{1}H NMR** (400 MHz, $CDCl_3$) δ_H 3.51-3.62 (m, 4H, 2 x NC*H*$_2$), 3.69 (t, J = 6.1, 2H, NC*H*$_2$), 3.77 (s, 3H, OC*H*$_3$), 3.78 (s, 3H, OC*H*$_3$), 4.32 (t, J = 6.0, 2H, OC*H*$_2$), 4.98 (s, 1H, O*H*), 6.82 (d, J = 8.9, 2H, 2 x Ar*H*), 6.85 (d, J = 8.9, 2H, 2 x Ar*H*), 6.98 (dd, J = 5.1, 7.0, 1H, Ar*H*), 7.34 (d, J = 8.9, 2H, NC*H*$_2$), 7.39 (d, J = 8.9, 2H, NC*H*$_2$), 7.67 (d, J = 7.5, 1H, Ar*H*), 7.78 (ddd, J = 1.8, 5.1, 7.5, 1H, Ar*H*), 8.28 (d, J = 5.1, 1H, Ar*H*), 9.14 (s, 1H, N*H*), 12.54 (s, 1H, N*H*). **^{13}C NMR** (101 MHz, $CDCl_3$) δ_C 40.7 (N*C*H$_2$), 46.6 (N*C*H$_2$), 47.7 (N*C*H$_2$), 55.5 (2 x O*C*H$_3$), 63.2 (O*C*H$_2$), 109.6 (Ar*C*), 113.9 (2 x Ar*C*), 114.2 (2 x Ar*C*), 120.8 (2 x Ar*C*), 122.2 (2 x Ar*C*), 123.8 (Ar*C*), 131.0 (Ar*C*), 132.8 (Ar*C*), 137.6 (Ar*C*), 147.4 (Ar*C*), 154.1 (*C*O), 156.0 (Ar*C*), 156.8 (Ar*C*), 158.0 (*C*O). **HR-MS** (ESI, positive ion mode) – *m/z* for $[C_{25}H_{29}N_5O_5+Na]^+$ = 502.2066. Found 502.2093. **FTIR** (neat) – 3487, 3309, 2933, 1641.

***N*-(2-Pyridyl)-2-chloroethylamine, 112**

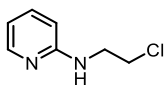

Under a dry, inert atmosphere, a solution of **100** (138 mg, 1.00 mmol, 1.00 equiv., 0.10 M) in anhydrous DCM (10 mL) was prepared and cooled to 0 °C. To this solution was added thionyl chloride (0.09 mL, 1.20 mmol, 1.20 equiv.) and the solution was warmed to room temperature. The solution was stirred for 30 minutes, heated to reflux and stirred for a further 3 h. Upon cooling, the solution was concentrated *in vacuo*. The residue was diluted

with DCM (5 mL) and the resulting solution was concentrated *in vacuo*. The residue was diluted with aqueous NaOH (10 mL, 2.00 M) and extracted with DCM (3 x 10 mL). The combined organic extracts were washed with brine, dried ($MgSO_4$), filtered and concentrated *in vacuo* to yield the desired chloride as a pale-green solid (96 mg, 0.61 mmol, 61%). **M.P.** decomp. >110 °C (EtOAc). **TLC** – R_f = 0.12 (SiO_2, EtOAc). **^{1}H NMR** (400 MHz, $CDCl_3$) δ_H 4.09 (t, J = 9.7, 2H, NC*H*$_2$), 4.84 (t, J = 9.7, 2H, NC*H*$_2$), 6.75 (t, J = 6.8, 1H, Ar*H*), 7.37 (d, J = 8.8, 1H, Ar*H*), 7.71 (ddd, J = 1.2, 7.0, 8.6, 1H, Ar*H*), 8.09 (d, J = 8.8, 1H, Ar*H*). **^{13}C NMR** (101 MHz, $CDCl_3$) δ_C 43.2 (N*C*H$_2$), 50.9 (N*C*H$_2$), 110.1 (Ar*C*), 112.9 (Ar*C*), 135.6 (Ar*C*), 143.4 (Ar*C*), 151.1 (Ar*C*). **HR-MS** (ESI, positive ion mode) – *m/z* for $[C_7H_9N_2Cl+H]^+$ = 157.0533. Found 157.0568. **FTIR** (neat) – 3190, 2980, 2939.

N-(2-Pyridyl)allylamine, 114

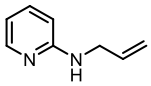

Under a dry, inert atmosphere, a solution of 2-aminopyridine (1.0 g, 10.60 mmol, 1.00 equiv., 0.17 M) in THF (35 mL) was prepared. To this solution was added a solution of potassium *tert*-butoxide in THF (15.9 mL, 1.00 M, 15.90 mmol, 1.50 equiv.). The solution was stirred for 1 h at room temperature and a solution of allyl bromide (1.10 mL, 12.70 mmol, 1.20 equiv.) in THF (10 mL) was added in one portion to give a brown solution. The solution was stirred for 2 h at room temperature and then diluted with deionised water (100 mL). The THF was removed *in vacuo* and the aqueous phase was extracted with EtOAc (2 x 25 mL). The combined organic extracts were washed with brine, dried ($MgSO_4$), filtered and concentrated *in vacuo*. The crude product was purified by column chromatography (20-100% EtOAc:PE) to give the title amine as a white solid (711 mg, 5.30 mmol, 50%). **TLC** – R_f = 0.15 (SiO_2, 20:80 EtOAc:PE). **^{1}H NMR** (400 MHz, $CDCl_3$) δ_H 4.10 (d, J = 5.5, 2H, NC*H*$_2$), 5.05 (dd, J = 1.5, 10.8, 1H, C=C*H*), 5.18 (dd, J = 1.5, 16.0, 1H, C=C*H*), 5.98 (ddd, J = 5.5, 10.8, 16.1, 1H, C=C*H*), 6.78 (t, J = 6.6, 1H, Ar*H*), 7.41 (d, J = 8.6, 1H, Ar*H*), 7.75 (ddd, J = 1.3, 7.1, 8.6, 1H, Ar*H*), 8.13 (d, J = 8.6, 1H, Ar*H*). Spectroscopic data matched that previously reported.[133]

N-(2-Pyridyl)(*tert*-butoxycarbonyl)allylamine, 115

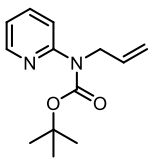

Under a dry, inert atmosphere, to a solution of **114** (536 mg, 4.00 mmol, 1.00 equiv. 0.10 M) in DCM (20 mL) was added 4-(dimethylamino)pyridine (49 mg, 0.40 mmol, 0.10 equiv.). The solution was cooled to 0 °C and a solution of Boc_2O (959 mg, 4.40 mmol, 1.10 equiv.) in DCM (20 mL) was added in one portion. The solution was stirred for 16 h and then diluted with saturated $NaHCO_3$ (100 mL). The aqueous phase was extracted with DCM (3 x 50 mL) and the combined organic extracts were dried

($MgSO_4$), filtered ad concentrated *in vacuo*. The crude product was purified by column chromatography (25-100% DCM:PE) to give the title carbamate as a colourless oil (703 mg, 3.00 mmol, 75%). **TLC** – R_f = 0.20 (SiO_2, 25:75 DCM:PE). **^{1}H NMR** (400 MHz, $CDCl_3$) δ_H 1.49 (s, 9H, C(C*H*$_3$)$_3$), 4.54 (d, J = 5.4, 2H, NC*H*$_2$), 5.07 (dd, J = 1.5, 10.2, 1H, C=C*H*), 5.13 (dd, J = 1.5, 17.2, 1H, C=C*H*), 5.94 (ddd, J = 5.6, 10.2, 16.4, 1H, C=C*H*), 6.98 (t, J = 5.1, 1H, Ar*H*), 7.57-7.65 (m, 2H, 2 x Ar*H*), 8.35 (d, J = 5.0, 1H, Ar*H*). Spectroscopic data matched that previously reported.[133]

_N_-(2-Pyridyl)(*tert*-butoxycarbonyl)-2-oxoethylamine, 102

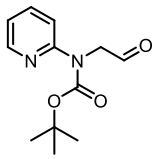

Synthesised according to general procedure N using **115** (250 mg, 1.07 mmol). The crude product was then purified by column chromatography (20-100% EtOAc) to give the title aldehyde as a colourless oil (253 mg, 1.07 mmol, >99%). **TLC** – R_f = 0.36 (SiO_2, 50:50 EtOAc:PE). **^{1}H NMR** (400 MHz, $CDCl_3$) δ_H 1.51 (s, 9H, C(C*H*$_3$)$_3$), 4.64 (NC*H*$_2$), 6.99 (dd, J = 4.0, 7.3, 1H, Ar*H*), 7.64 (t, J = 7.7, 1H, Ar*H*), 7.86 (d, J = 8.5, 1H, Ar*H*), 8.27 (d, J = 4.0, 1H, Ar*H*), 9.65 (s, 1H, C*H*O). **^{13}C NMR** (101 MHz, $CDCl_3$) δ_C 28.3 (C(*C*H$_3$)$_3$), 55.8 (N*C*H$_2$), 82.6 (*C*(CH$_3$)$_3$), 118.1 (Ar*C*), 119.6 (Ar*C*), 137.4 (Ar*C*), 147.2 (Ar*C*), 153.6 (*C*O), 197.9 (*C*HO). **HR-MS** (ESI, positive ion mode) – *m/z* for $[C_{12}H_{16}N_2O_3+H]^+$ = 237.1239. Found 237.1224. **FTIR** (neat) – 2978, 2931, 1716, 1590.

1-Benzyl-1,4,7,10,13-pentakis(4-methoxyanilinylcarbonyl)-19-(2-pyridyl)-19-(*tert*-butoxycarbonyl)-1,4,7,10,13,16,19-heptaazanonadecane, 116

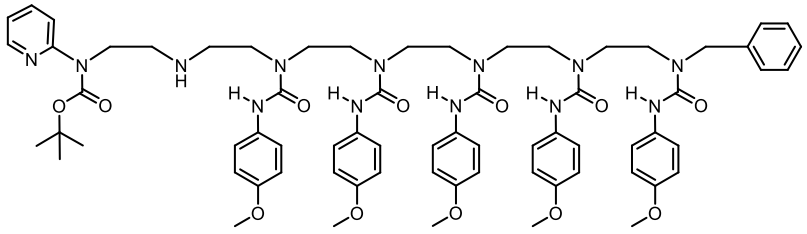

Synthesised according to general procedure E using **86** (250 mg, 0.23 mmol) and **102** (111 mg, 0.47 mmol, 2.00 equiv.). The crude product was purified by column chromatography (2-10% MeOH:DCM) to give the title amine as a foamy white solid (150 mg, 0.12 mmol, 51%). **M.P.** 201-202 °C (DCM/Et_2O). **TLC** – R_f = 0.18 (SiO_2, 5:95 MeOH:DCM). **^{1}H NMR** (500 MHz, $CDCl_3$) δ_H 1.49 (s, 9H, C(C*H*$_3$)$_3$), 2.87-2.90 (m, 2H, NC*H*$_2$), 3.01 (t, J = 5.6, 2H, NC*H*$_2$), 3.33-3.59 (m, 20H, 10 x NC*H*$_2$), 3.75-3.79 (m, 15H, 5 x OC*H*$_3$), 4.01 (t, J = 5.8, 2H, NC*H*$_2$), 4.60 (s, 2H, C*H*$_2$Ar), 6.77-6.85 (m, 10H, 10 x Ar*H*), 6.99 (ddd, J = 1.3, 4.9, 7.2, 1H, Ar*H*), 7.27-7.41 (m, 9H, 9 x Ar*H*), 7.54 (d, J = 8.2, 1H, Ar*H*), 7.59-7.64 (m, 8H, 8 x Ar*H*), 8.29 (dd, J = 1.3, 4.9, 1H, Ar*H*), 8.97 (s, 1H, N*H*), 9.14 (s, 1H, N*H*). 9.18 (s, 1H, N*H*), 10.35 (s, 1H, N*H*). **^{13}C NMR** (126 MHz, $CDCl_3$) δ_C 28.4 (C(*C*H$_3$)$_3$), 46.6-

50.0 (12 x N*C*H$_2$), 51.2 (*C*H$_2$Ar), 55.5 (5 x O*C*H$_3$), 81.8 (*C*(CH$_3$)$_3$), 113.9-114.3 (10 x Ar*C*), 119.8 (Ar*C*), 120.2 (Ar*C*), 120.9-122.0 (10 x Ar*C*), 127.0-129.3 (5 x Ar*C*), 133.1-133.6 (5 x Ar*C*), 137.4 (Ar*C*), 147.7 (Ar*C*), 153.9 (Ar*C*), 154.6 (Ar*C*), 155.2 (3 x Ar*C*), 156.6 (5 x C*O*), 158.6 (*C*O). **HR-MS** (ESI, positive ion mode) – *m/z* for [$C_{69}H_{85}N_{13}O_{12}$+H]$^+$ = 1288.6519. Found 1288.6500. **FTIR** (neat) – 3134, 3090, 2932, 1678, 1620.

1-Benzyl-1,4,7,10,13-pentakis(4-methoxyanilinylcarbonyl)-19-(2-pyridyl)-1,4,7,10,13,16,19-heptaazanonadecane, 117

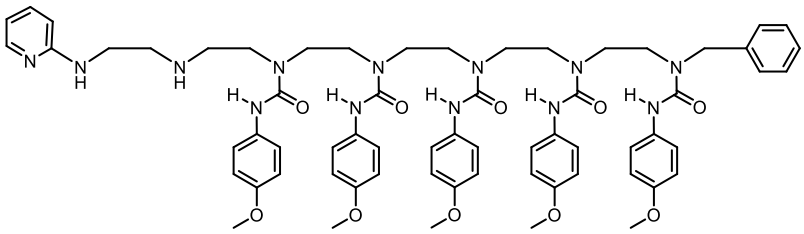

Synthesised according to general procedure C using **116** (150 mg, 0.12 mmol). The title diamine was isolated as a foamy white solid (120 mg, 0.10 mmol, 84%). **M.P.** 222-223 °C (DCM/Et$_2$O). **TLC** – R_f = 0.15 (SiO$_2$, MeOH:DCM 10:90). **^{1}H NMR** (500 MHz, CDCl$_3$) δ_H 2.82-2.85 (m, 2H, NC*H*$_2$), 2.87 (t, J = 5.4, 2H, NC*H*$_2$), 3.31-3.59 (m, 18H, 9 x NC*H*$_2$), 3.75-3.81 (m, 15H, 5 x OC*H*$_3$), 4.60 (s, 2H, C*H*$_2$Ar), 4.76 (s, 1H, N*H*), 6.28 (d, J = 8.0, 1H, Ar*H*), 6.56 (t, J = 5.8, 1H, Ar*H*), 6.79-6.88 (m, 10H, 10 x Ar*H*), 7.29-7.39 (m, 9H, 9 x Ar*H*), 7.60-7.70 (m, 7H, 7 x Ar*H*), 8.02-8.05 (m, 1H, Ar*H*), 8.99-9.13 (m, 4H, 4 x N*H*), 10.10 (s, 1H, N*H*). **^{13}C NMR** (126 MHz, CDCl$_3$) δ_C 41.2 (N*C*H$_2$), 41.3 (N*C*H$_2$), 46.9-48.6 (10 x N*C*H$_2$), 50.0 (*C*H$_2$Ar), 55.4-55.6 (5 x O*C*H$_3$), 113.3-114.3 (10 x Ar*C*), 120.9-122.0 (10 x Ar*C*), 126.6-129.3 (5 x Ar*C*), 133.0-133.5 (5 x Ar*C*), 137.4 (Ar*C*), 147.7 (Ar*C*), 155.1-155.3 (5 x Ar*C*), 156.5 (4 x C*O*), 158.5 (*C*O). **HR-MS** (MALDI, positive ion mode) – *m/z* for [$C_{64}H_{78}N_{13}O_{10}$+H]$^+$ = 1188.5995. Found 1188.5989. **FTIR** (neat) – 3281, 3134, 3074, 2933, 1645.

***N*-(2-Pyridyl)(4-methoxyanilinylcarbonyl)allylamine, 119**

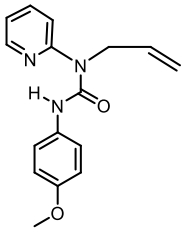

Synthesised according to general procedure B using **114** (1.00 g, 7.45 mmol) and 4-methoxyphenyl isocyanate (1.49 mL, 11.18 mmol). The crude product was purified by column chromatography (1-10% MeOH:DCM) to yield the title urea as a colourless oil (1.31 g, 4.62 mmol, 62%). **TLC** – R_f = 0.18 (SiO$_2$, 20:80 EtOAc:PE). **^{1}H NMR** (400 MHz, CDCl$_3$) δ_H 3.80 (s, 3H, OC*H*$_3$), 4.65 (dt, J = 1.8, 4.7, 2H, NC*H*$_2$), 5.21-5.23 (m, 1H, C=C*H*), 5.24 (dd, J = 1.2, 10.6, 1H, C=C*H*), 5.99 (ddt, J = 4.7, 10.6, 17.2, 1H, C=C*H*), 6.87 (d, J = 9.0, 2H, 2 x Ar*H*), 6.98 (ddd, J = 0.6, 5.0, 7.3, 1H, Ar*H*), 7.05 (d, J = 8.7, 1H, Ar*H*), 7.49 (d, J = 9.0, 2H, 2 x Ar*H*), 7.69 (ddd, J = 2.0, 7.3, 8.7, 1H,

Ar*H*), 8.32 (dd, J = 2.0, 5.0, 1H, Ar*H*), 12.64 (s, 1H, N*H*). **^{13}C NMR** (101 MHz, $CDCl_3$) δ_C 47.8 (N*C*H_2), 55.6 (O*C*H_3), 112.7 (Ar*C*), 114.2 (2 x Ar*C*), 116.2 (Ar*C*), 117.4 (C=*C*H), 122.1 (2 x Ar*C*), 132.5 (Ar*C*), 133.4 (C=*C*H), 138.9 (Ar*C*), 145.7 (Ar*C*), 153.8 (Ar*C*), 155.6 (Ar*C*), 155.8 (*C*O). **HR-MS** (ESI, positive ion mode) – *m/z* for $[C_{16}H_{17}N_3O_2+Na]^+$ = 306.1218. Found 306.1203. **FTIR** (neat) – 3464, 2983, 2941, 1663, 1629.

3,3-Dibutyl-5-hexyl-2-methyl-3*H*-indole, 125

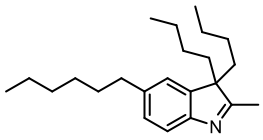

Synthesised according to general procedure O using (4-hexylphenyl)hydrazine hydrochloride (500 mg, 2.18 mmol) and 3-butyl-heptan-2-one (447 mg, 2.62 mmol). The crude product was purified by column chromatography (10% EtOAc:PE) to give the title 3*H*-indole as a brown oil (490 mg, 1.50 mmol, 69%). **TLC** – R_f = 0.23 (10:90 EtOAc:PE). **^{1}H NMR** (400 MHz, $CDCl_3$) δ_H 0.73 (t, J = 7.4, 6H, 2 x C*H*$_3$), 0.87 (t, J = 7.1, 3H, C*H*$_3$), 1.12-1.15 (m, 4H, 2 x C*H*$_2$), 1.27-1.33 (m, 6H, 3 x C*H*$_2$), 1.59-1.64 (m, 2H, C*H*$_2$), 1.66-1.74 (m, 4H, 2 x C*H*$_2$), 1.80-1.89 (m, 4H, 2 x C*H*$_2$), 2.18 (s, 3H, C*H*$_3$), 2.64 (t, J = 7.8, 2H, C*H*$_2$Ar), 6.97 (d, J = 1.2, 1H, Ar*H*), 7.09 (dd, J = 1.2, 7.8, 1H, Ar*H*), 7.39 (d, J = 7.8, 1H, Ar*H*). **^{13}C NMR** (101 MHz, $CDCl_3$) δ_C 13.9 (2 x *C*H$_3$), 14.2 (*C*H$_3$), 16.2 (*C*H$_3$), 22.8 (*C*H$_2$), 23.0 (2 x *C*H$_2$), 25.9 (2 x *C*H$_2$), 29.0 (*C*H$_2$), 31.9 (*C*H$_2$), 31.9 (*C*H$_2$), 36.1 (2 x *C*H$_2$), 36.9 (*C*H$_2$Ar), 62.5 (*C*$_{quat.}$), 119.2 (Ar*C*), 121.9 (Ar*C*), 127.5 (Ar*C*), 139.8 (Ar*C*), 142.5 (Ar*C*), 153.5 (Ar*C*), 185.6 (*C*=N). **HR-MS** (ESI, positive ion mode) – *m/z* for $[C_{23}H_{37}N+Na]^+$ = 350.2824. Found 350.2799. **FTIR** (neat) – 2993, 2970, 2941, 1679.

3-(3,3-Dibutyl-5-hexyl-2-methyl-3*H*-indolium)propane-1-sulfonate, 126

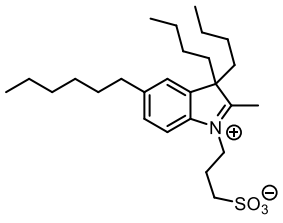

Synthesised according to general procedure P using **125** (490 mg, 1.43 mmol) and 1,3-propanesultone (0.14 mL, 1.58 mmol). The crude product was purified by column chromatography (25% EtOAc:PE) to give the title indolium sulfonate as a brown oil (213 mg, 0.45 mmol, 29%). **TLC** – R_f = 0.15 (25:75 EtOAc:PE). **^{1}H NMR** (400 MHz, $CDCl_3$) δ_H 0.74 (t, J = 7.2, 6H, 2 x C*H*$_3$), 0.86 (t, J = 7.0, 3H, C*H*$_3$), 1.15-1.18 (m, 4H, 2 x C*H*$_2$), 1.22-1.32 (m, 10H, 5 x C*H*$_2$), 1.60-1.64 (m, 2H, C*H*$_2$), 1.97-2.10 (m, 4H, 2 x C*H*$_2$), 2.33-2.37 (m, 2H, C*H*$_2$), 2.72 (t, J = 7.3, 2H, C*H*$_2$Ar), 2.96 (s, 3H, C*H*$_3$), 3.11-3.15 (m, 2H, SC*H*$_2$), 5.07-5.10 (m, 2H, NC*H*$_2$), 7.20 (s, 1H, Ar*H*), 7.41 (d, J = 7.6, 1H, Ar*H*), 7.94 (d, J = 7.6, 1H, Ar*H*). **^{13}C NMR** (101 MHz, $CDCl_3$) δ_C 13.6 (2 x *C*H$_3$), 14.1 (*C*H$_3$), 14.8 (*C*H$_3$), 22.6 (2 x *C*H$_2$), 22.7 (*C*H$_2$), 25.2 (*C*H$_2$), 25.9 (2 x *C*H$_2$), 28.8 (*C*H$_2$), 31.0 (S*C*H$_2$), 31.4 (*C*H$_2$), 31.7 (*C*H$_2$), 36.0 (*C*H$_2$Ar), 37.4 (2 x *C*H$_2$), 47.6 (*C*$_{quat.}$), 63.3 (N*C*H$_2$), 116.0 (Ar*C*), 123.1 (Ar*C*), 130.3 (Ar*C*), 138.7 (Ar*C*), 140.5

(Ar*C*), 145.9 (Ar*C*), 194.3 (*C*=N). **HR-MS** (ESI, positive ion mode) – *m/z* for $[C_{26}H_{43}NO_3S+Na]^+$ = 472.2861. Found 472.2899. **FTIR** (neat) – 2981, 2967, 1613.

(*E*)-3-(3,3-Dibutyl-5-hexyl-2-(2-hydroxystyryl)-3*H*-indolium)propane-1-sulfonate, 127

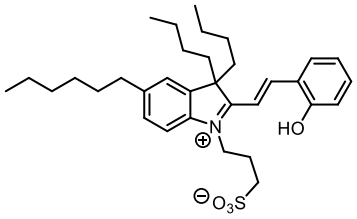

Synthesised according to general procedure Q using **126** (150 mg, 0.33 mmol) and salicylaldehyde (0.04 mL, 0.36 mmol). The crude product was purified by column chromatography (1-5% MeOH:DCM) to give a brown solid, which was recrystallised from $CHCl_3/Et_2O$ to give the title merocyanine as a brown solid (129 mg, 0.22 mmol, 62%). **M.P.** 184-185 °C ($CHCl_3/Et_2O$). **TLC** – R_f = 0.20 (5:95 MeOH:DCM). **^{1}H NMR** (400 MHz, $CDCl_3$) δ_H 0.68 (t, J = 7.3, 6H, 2 x C*H*$_3$), 0.88 (t, J = 6.8, 3H, C*H*$_3$), 1.09-1.13 (m, 4H, 2 x C*H*$_2$), 1.23-1.34 (m, 5 x C*H*$_2$), 1.62-1.66 (m, 2H, C*H*$_2$), 2.26-2.33 (m, 4H, 2 x C*H*$_2$), 2.44-2.47 (m, 2H, C*H*$_2$), 2.73 (t, J = 7.5, 2H, C*H*$_2$Ar), 3.20 (t, J = 5.8, 2H, SC*H*$_2$), 4.89 (t, J = 7.7, 2H, NC*H*$_2$), 6.85 (t, J = 7.5, 1H, Ar*H*), 7.20 (s, 1H, Ar*H*), 7.29 (t, J = 7.6, 1H, Ar*H*), 7.36 (d, J = 8.2, 1H, Ar*H*), 7.43 (d, J = 8.4, 1H, Ar*H*), 7.63 (d, J = 7.6, 1H, Ar*H*), 7.81 (d, J = 8.2, 1H, Ar*H*), 8.22 (d, J = 15.9, 1H, C=C*H*), 8.30 (d, J = 15.9, C=C*H*), 11.32 (s, 1H, O*H*). **^{13}C NMR** (101 MHz, $CDCl_3$) δ_C 13.6 (2 x *C*H$_3$), 14.2 (*C*H$_3$), 22.4-22.8 (3 x *C*H$_2$), 24.8 (*C*H$_2$), 25.9 (2 x *C*H$_2$), 28.8 (*C*H$_2$), 31.5 (*C*H$_2$), 31.8 (*C*H$_2$), 36.1 (*C*H$_2$Ar), 42.0 (2 x *C*H$_2$), 46.2 (N*C*H$_2$), 47.8 (S*C*H$_2$), 61.6 (*C*$_{quat.}$), 112.9 (C=*C*H), 114.8 (Ar*C*), 118.7 (Ar*C*), 120.2 (Ar*C*), 121.3 (Ar*C*), 122.2 (Ar*C*), 130.3 (Ar*C*), 133.1 (Ar*C*), 136.4 (Ar*C*), 140.2 (Ar*C*), 140.5 (Ar*C*), 145.3 (Ar*C*), 152.0 (C=*C*H), 161.8 (Ar*C*), 180.1 (*C*=N). **HR-MS** (ESI, positive ion mode) – *m/z* for $[C_{33}H_{47}NO_4S+Na]^+$ = 576.3123. Found 576.3092. **FTIR** (neat) – 3060, 2958, 1587, 1525.

3,3-Dimethyl-5-hexyl-2-methyl-3*H*-indole, 128

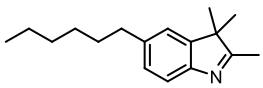

Synthesised according to general procedure O using (4-hexylphenyl)hydrazine hydrochloride (500 mg, 2.18 mmol) and methyl isopropyl ketone (0.28 mL 2.62 mmol). The title 3*H*-indole was isolated as a brown oil (302 mg, 1.24 mmol, 57%). **TLC** – R_f = 0.23 (SiO_2, 50:50 EtOAc:PE). **^{1}H NMR** (400 MHz, $CDCl_3$) δ_H 0.85 (t, J = 5.9, 3H, C*H*$_3$), 1.25-1.33 (m, 6H, 3 x C*H*$_2$), 1.59 (tt, J = 7.0, 7.5, 2H, C*H*$_2$), 2.06 (s, 3H, C*H*$_3$), 2.24 (s, 6H, 2 x C*H*$_3$), 2.60 (t, J = 7.6, 2H, C*H*$_2$Ar), 7.05 (s, 1H, Ar*H*), 7.07 (d, J = 7.8, 1H, Ar*H*), 7.41 (d, J = 7.8, 1H, Ar*H*). **^{13}C NMR** (101 MHz, $CDCl_3$) δ_C 14.1 (2 x *C*H$_3$), 15.1 (*C*H$_3$), 22.5 (*C*H$_3$), 23.1 (*C*H$_2$), 29.0 (*C*H$_2$), 31.7 (*C*H$_2$), 31.9 (*C*H$_2$), 36.0 (*C*H$_2$Ar), 53.3 (*C*$_{quat.}$), 119.3 (Ar*C*), 121.5 (Ar*C*), 127.5 (Ar*C*), 140.3 (Ar*C*), 145.5 (Ar*C*), 151.1 (Ar*C*), 174.9 (Ar*C*), 187.4

(*C*=N). **HR-MS** (ESI, positive ion mode) – *m/z* for $[C_{17}H_{25}N+Na]^+$ = 266.1885. Found 266.1904. **FTIR** (neat) – 2987, 2947, 1666.

3-(3,3-Dimethyl-5-hexyl-2-methyl-3*H*-indolium)propane-1-sulfonate, 129

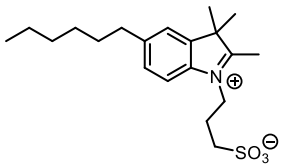

Synthesised according to general procedure P using **128** (304 mg, 1.24 mmol) and 1,3-propanesultone (0.12 mL, 1.37 mmol). The title indolium sulfonate was isolated as a brown gum (340 mg, 0.93 mmol, 75%). **TLC** – R_f = 0.30 (SiO_2, 50:50 EtOAc:PE). **^{1}H NMR** (400 MHz, $CDCl_3$) δ_H 0.85 (t, J = 6.9, 3H, C*H*$_3$), 1.26-1.31 (m, 6H, 3 x C*H*$_2$), 1.52 (s, 6H, 2 x C*H*$_3$), 2.34 (tt, J = 5.9, 6.9, 2H, C*H*$_2$), 2.64 (t, J = 7.7, 2H, C*H*$_2$), 2.95 (s, 3H, C*H*$_3$), 2.97 (t, J = 6.3, SC*H*$_2$), 4.89 (t, J = 7.9, 2H, NC*H*$_2$), 7.22 (d, J = 1.3, 1H, Ar*H*), 7.29 (dd, J = 1.3, 8.3, 1H, Ar*H*), 7.79 (d, J = 8.3, 1H, Ar*H*). **^{13}C NMR** (101 MHz, $CDCl_3$) δ_C 14.6 (*C*H$_3$), 15.8 (*C*H$_3$), 22.9 (*C*H$_2$), 24.6 (*C*H$_2$), 28.4 (*C*H$_2$), 32.0 (*C*H$_2$), 33.7 (*C*H$_2$), 35.4 (S*C*H$_2$), 38.2 (*C*H$_2$Ar), 40.6 (2 x *C*H$_3$), 62.1 (N*C*H$_2$), 116.5 (Ar*C*), 123.7 (Ar*C*), 131.0 (Ar*C*), 139.3 (Ar*C*), 141.0 (Ar*C*), 146.7 (Ar*C*), 190.5 (*C*=N). **HR-MS** (ESI, positive ion mode) – *m/z* for $[C_{20}H_{31}NO_3S+Na]^+$ = 388.1922. Found 388.1946. **FTIR** (neat) – 2983, 2914.

(*E*)-3-(3,3-Dimethyl-5-hexyl-2-(2-hydroxystyryl)-3*H*-indolium)propane-1-sulfonate, 130

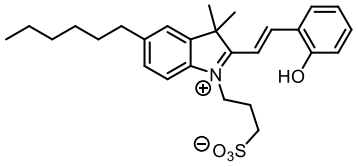

Synthesised according to general procedure Q using **129** (100 mg, 0.36 mmol) and salicylaldehyde (0.04 mL, 0.39 mmol). The crude product was purified by column chromatography (1-5% MeOH:DCM) to give a brown solid, which was recrystallised from $CHCl_3$/Et_2O to give the title merocyanine as a brown gum (68 mg, 0.14 mmol, 40%). **TLC** – R_f = 0.41 (SiO_2, 25:75 acetone:DCM). **^{1}H NMR** (400 MHz, $CDCl_3$) δ_H 0.88 (t, J = 6.7, 3H, C*H*$_3$), 1.25-1.35 (m, 8H, 4 x C*H*$_2$), 1.57-1.61 (m, 2H, C*H*$_2$), 1.68 (s, 6H, 2 x C*H*$_3$), 2.67 (t, J = 7.6, 2H, C*H*$_2$Ar), 3.14-3.16 (m, 2H, SC*H*$_2$), 4.84-4.89 (m, 2H, NC*H*$_2$), 6.70 (t, J = 7.5, 1H, Ar*H*), 7.12 (t, J = 7.5, 1H, Ar*H*), 7.24 (s, 1H, Ar*H*), 7.28 (d, J = 8.0, 1H, Ar*H*), 7.51 (d, J = 5.7, 1H, Ar*H*), 7.53 (d, J = 5.7, 1H, Ar*H*), 7.81 (d, J = 8.0, 1H, Ar*H*), 7.89 (d, J = 15.8, 1H, C=C*H*), 8.34 (d, J = 15.8, C=C*H*), 10.96 (s, 1H, O*H*). **^{13}C NMR** (101 MHz, $CDCl_3$) δ_C 11.2 (*C*H$_3$), 14.0 (2 x *C*H$_3$), 22.5 (*C*H$_2$), 27.5 (*C*H$_2$), 28.9 (*C*H$_2$), 30.4 (*C*H$_2$), 31.5 (*C*H$_2$), 36.0 (*C*H$_2$Ar), 38.7 (S*C*H$_2$), 51.7 (N*C*H$_2$), 68.2 ($C_{quat.}$), 110.8 (C=*C*H), 114.6 (Ar*C*), 117.9 (Ar*C*), 120.1 (Ar*C*), 121.3 (Ar*C*), 122.2 (Ar*C*), 129.8 (Ar*C*), 132.4 (Ar*C*), 138.7 (Ar*C*), 141.6 (Ar*C*), 143.0 (Ar*C*), 145.1 (Ar*C*), 160.1 (C=*C*H), 167.8 (Ar*C*), 181.0 (*C*=N). **HR-MS** (ESI, positive ion mode) – *m/z* for $[C_{27}H_{35}NO_4S+Na]^+$ = 492.2184. Found 492.2196. **FTIR** (neat) – 2991, 2981, 1605, 1570.

1,3,3-Trimethyl-2-methyleneindoline, 131

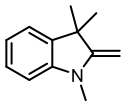

Under a dry, inert atmosphere, a solution of 2,3,3-trimethylindolenine (2.00 g, 12.56 mmol, 1.00 equiv., 0.50 M) in anhydrous MeCN (25 mL) was prepared. To this solution was added methyl iodide (1.95 mL, 31.40 mmol, 2.50 equiv.) and the solution was heated to reflux and stirred for 16 h. The resulting brown solution was cooled to room temperature and concentrated *in vacuo*. The residue was triturated with Et_2O and filtered. The residue was then washed with Et_2O (2 x 25 mL) and dried *in vacuo*. The residue was added to aqueous KOH (25 mL, 1.00 M) and stirred for 30 minutes. The aqueous phase was extracted with Et_2O (3 x 25 mL) and the combined organic extracts were washed with brine, dried ($MgSO_4$), filtered and concentrated *in vacuo* to give the title indoline as a brown oil (2.11 g, 12.12 mmol, 97%). **TLC** – R_f = 0.23 (SiO_2, 50:50 DCM:PE). **^{1}H NMR** (400 MHz, $CDCl_3$) δ_H 1.15 (s, 6H, 2 x C*H*$_3$), 3.02 (s, 3H, NC*H*$_3$), 3.78 (s, 2H, C=C*H*$_2$), 6.36 (d, J = 7.1, 1H, Ar*H*), 6.74 (t, J = 7.8, 1H, Ar*H*), 7.05 (t, J = 7.0, 1H, Ar*H*), 7.33 (d, J = 7.8, 1H, Ar*H*). Spectroscopic data matched that previously reported.[134]

1',3',3'-Trimethylspiro[chromene-2,2'-indoline], 132

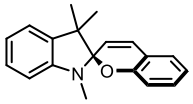

Synthesised according to general procedure Q using **131** (2.00 g, 11.54 mmol) and salicylaldehyde (1.57 mL, 14.73 mmol). The crude product was purified by column chromatography (10% DCM:PE) to yield the title spiropyran as a red solid (2.88 g, 10.39 mmol, 90%). **TLC** – R_f = 0.12 (SiO_2, 50:50 DCM:PE). **^{1}H NMR** (400 MHz, $CDCl_3$) δ_H 1.13 (s, 3H, C*H*$_3$), 1.26 (s, 3H, C*H*$_3$), 2.70 (s, 3H, NC*H*$_3$), 5.75 (d, J = 10.2, 1H, C=C*H*), 6.55 (d, J = 8.1, 1H, Ar*H*), 6.59 (d, J = 8.1, 1H, Ar*H*), 6.81 (dt, J = 0.9, 7.4, 1H, Ar*H*), 6.84 (dt, J = 1.1, 7.4, 1H, Ar*H*), 6.94 (d, J = 10.2, 1H, C=C*H*), 7.07-7.13 (m, 3H, 3 x Ar*H*), 7.16 (dt, J = 1.3, 7.7, 1H, Ar*H*). Spectroscopic data matched that previously reported.[96]

1',3',3'-Trimethyl-6-nitro-spiro[chromene-2,2'-indoline], 133

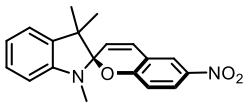

Synthesised according to general procedure Q using **131** (250 mg, 1.44 mmol) and 5-nitrosalicylaldehyde (301 mg, 1.80 mmol). The crude product was purified by column chromatography (10-20% EtOAc:PE) to yield the title spiropyran as a red solid (292 mg, 0.91 mmol, 63%). **TLC** – R_f = 0.47 (SiO_2, 20:80 EtOAc:PE). **^{1}H NMR** (400 MHz, $CDCl_3$) δ_H 1.12 (s, 3H, C*H*$_3$), 1.23 (s, 3H, C*H*$_3$), 2.67 (s, 3H, NC*H*$_3$), 5.79 (d, J = 10.3, 1H, C=C*H*), 6.49 (d, J = 7.8, 1H, Ar*H*), 6.70 (dt, J = 0.6, 8.4, 1H, Ar*H*), 6.82 (td, J = 0.9, 7.5, 1H, Ar*H*), 6.85 (d, J = 10.3, 1H C=C*H*), 7.02 (dd, J = 1.2, 7.3, 1H, Ar*H*),

7.14 (td, J = 1.3, 7.8, 1H, Ar*H*), 7.92-7.96 (m, 2H, 2 x Ar*H*). Spectroscopic data matched that previously reported.[96]

***N*-Phenylmaleamic acid, 134**

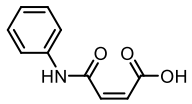

To a solution of maleic anhydride (1.00 g, 10.20 mmol, 1.00 equiv., 0.20 M) in toluene (50 mL) was added aniline (0.93 mL, 10.20 mmol, 1.00 equiv.) dropwise. The solution was stirred for 5 minutes and a white solid precipitated out of solution. The suspension was filtered and the residue was washed with toluene (2 x 25 mL) and dried *in vacuo* to yield the title amic acid as a white solid (1.95 g, 10.20 mmol, >99%). **TLC** – R_f = 0.28 (SiO_2, 10:90 MeOH:DCM). **^{1}H NMR** (400 MHz, $CDCl_3$) δ_H 6.61 (d, J = 11.0, 1H, C=C*H*), 6.93 (d, J = 11.0, 1H, C=C*H*), 7.10 (t, J = 8.0, 1H, Ar*H*), 7.29 (t, J = 6.9, 2H, 2 x Ar*H*), 7.40 (d, J = 7.5, 2H, 2 x Ar*H*), 9.57 (s, 1H, N*H*), 10.31 (s, 1H, O*H*). Spectroscopic data matched that previously reported.[135]

***N*-2-(Benzylamino)(4-methoxyanilinylcarbonyl)ethyl-*N*'-phenylmaleamide, 135**

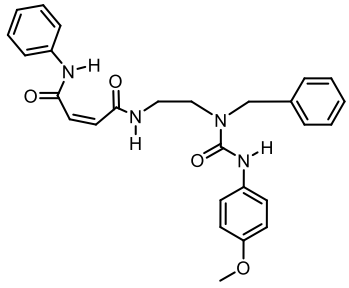

Under a dry, inert atmosphere, a solution of **107** (300 mg, 1.00 mmol, 1.00 equiv., 0.10 M) in anhydrous DMF (10 mL) was prepared. To this solution was added **134** (191 mg, 1.00 mmol, 1.00 equiv.), HBTU (531 mg, 1.40 mmol, 1.40 equiv.) and DIPEA (0.24 mL, 1.40 mmol, 1.40 equiv.) and the resulting solution was stirred for 1 h. The solution was diluted with EtOAc (25 mL) and washed with aqueous LiCl (5% w/w, 3 x 25 mL), saturated aqueous $KHSO_4$ (25 mL) and brine (25 mL). The organic phase was dried ($MgSO_4$), filtered and concentrated *in vacuo* to yield the title maleamide as a white solid (246 mg, 0.52 mmol, 52%). **TLC** – R_f = 0.41 (SiO_2, 5:95 MeOH:DCM). **^{1}H NMR** (400 MHz, $CDCl_3$) δ_H 3.29 (q, J = 6.2, 2H, NCH_2), 3.42 (t, J = 6.2, 2H, NCH_2), 3.72 (s, 3H, OCH_3), 4.54 (s, 2H, CH_2Ar), 6.02 (d, J = 13.3, 1H, C=C*H*), 6.14 (d, J = 13.3, 1H, C=C*H*), 6.75 (d, J = 8.9, 2H, 2 x Ar*H*), 7.08 (t, J = 7.1, 1H, Ar*H*), 7.21-7.34 (m, 9H, 9 x Ar*H*), 7.51 (d, J = 8.9, 2H, 2 x Ar*H*), 7.89 (s, 1H, N*H*), 9.16 (t, J = 6.2, 1H, N*H*), 11.40 (s, 1H, N*H*). **^{13}C NMR** (101 MHz, $CDCl_3$) δ_C 39.4 (N*C*H_2), 45.7 (N*C*H_2), 51.3 (*C*H_2Ar), 55.6 (*C*H_2Ar), 114.2 (2 x Ar*C*), 120.6 (2 x Ar*C*), 123.3 (2 x Ar*C*), 127.3 (2 x Ar*C*), 127.9 (Ar*C*), 128.1 (Ar*C*), 129.0 (2 x Ar*C*), 129.0 (2 x Ar*C*), 131.1 (Ar*C*), 132.0 (Ar*C*), 134.3 (C=*C*H), 135.4 (C=*C*H), 137.8 (Ar*C*), 156.2 (Ar*C*), 157.0 (*C*O), 162.9 (*C*O), 166.7 (*C*O). **HR-MS** (ESI, positive ion mode) – *m/z* for $[C_{27}H_{28}N_4O_4+Na]^+$ = 495.2008. Found 495.2034. **FTIR** (neat) – 3321, 3256, 3193, 2998, 2942, 1662, 1638.

1-(2-Pyridyl)- 1,4-bis(4-methoxyanilinylcarbonyl)-7-(pyren-1-ylmethyl)-1,4,7-triazaheptane, 136

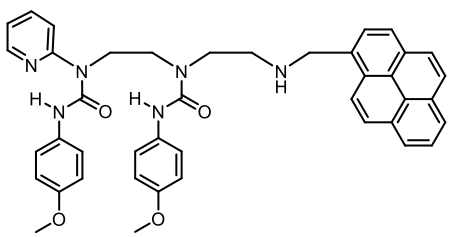

Synthesised according to general procedure E using **95** (350 mg, 0.73 mmol) and 1-pyrenecarboxaldehyde (253 mg, 1.10 mmol) in an anhydrous MeOH:anhydrous DCM mixture (7 mL, 1 :1). The crude product was purified by column chromatography (1-10% MeOH:DCM) to yield the title amine as a pale-yellow solid (278 mg, 0.40 mmol, 55%). **M.P.** 167-168 °C (DCM/Et_2O). **TLC** – R_f = 0.15 (SiO_2, 5:95 MeOH:DCM). **^{1}H NMR** (400 MHz, $CDCl_3$) δ_H 3.05 (t, J = 4.8, 2H, NC*H*$_2$), 3.48-3.56 (m, 4H, 2 x NC*H*$_2$), 3.58 (s, 3H, OC*H*$_3$), 3.72 (s, 3H, OC*H*$_3$), 4.04 (t, J = 7.7, 2H, NC*H*$_2$), 4.47 (s, 2H, C*H*$_2$Ar), 6.80 (d, J = 9.0, 2H, 2 x Ar*H*), 6.81 (d, J = 9.0, 2H, 2 x Ar*H*), 6.88-6.89 (m, 1H, Ar*H*), 7.00-7.03 (m, 1H, Ar*H*), 7.38 (d, J = 9.0, 2H, 2 x Ar*H*), 7.44 (d, J = 9.0, 2H, 2 x Ar*H*), 7.84-8.14 (m, 11H, 11 x Ar*H*), 8.22 (d, J = 9.2, 1H, Ar*H*), 9.35 (s, 1H, N*H*), 12.50 (s, 1H, N*H*). **^{13}C NMR** (101 MHz, $CDCl_3$) δ_C 46.3 (N*C*H$_2$), 50.2 (2 x N*C*H$_2$), 52.3 (N*C*H$_2$), 55.4 (*C*H$_2$Ar), 55.6 (O*C*H$_3$), 113.7 (2 x Ar*C*), 114.1 (2 x Ar*C*), 117.3 (Ar*C*), 121.4 (2 x Ar*C*), 122.4 (2 x Ar*C*), 122.8 (Ar*C*), 124.8 (2 x Ar*C*), 124.8 (Ar*C*), 125.2 (2 x Ar*C*), 125.3 (Ar*C*), 126.0 (Ar*C*), 127.4 (4 x Ar*C*), 128.2 (Ar*C*), 129.1 (Ar*C*), 130.8 (Ar*C*), 131.0 (Ar*C*), 131.3 (Ar*C*), 132.0 (Ar*C*), 133.1 (Ar*C*), 139.4 (Ar*C*), 145.2 (Ar*C*), 154.3 (Ar*C*), 155.0 (Ar*C*), 155.3 (*C*O), 155.9 (*C*O). **HR-MS** (ESI, positive ion mode) – *m/z* for $[C_{42}H_{40}N_6O_4+Na]^+$ = 715.3009. Found 715.3029. **FTIR** (neat) – 3421, 3278, 2957, 2891, 1670.

1-(2-Pyridyl)-1,4,7-tris(4-methoxyanilinylcarbonyl)-7-(pyren-1-ylmethyl)-1,4,7-triazaheptane, 137

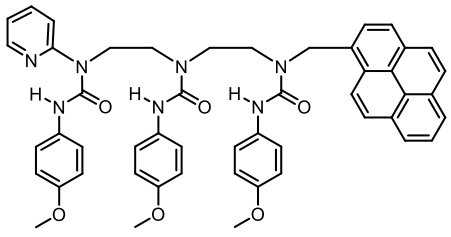

Synthesised according to general procedure B1 using **136** (75 mg, 0.10 mmol) and 4-methoxyphenyl isocyanate (0.02 mL, 0.16 mmol). The crude product was purified by column chromatography (1-10% MeOH:DCM) to yield the title triurea as a white solid (36 mg, 0.04 mmol, 43%). **M.P.** 220-221 °C (DCM). **TLC** – R_f = 0.38 (SiO_2, 5:95 MeOH:DCM). **^{1}H NMR** (400 MHz, $CDCl_3$) δ_H 3.46-3.68 (m, 6H, 3 x NC*H*$_2$), 3.78 (s, 3H, OC*H*$_3$), 3.79 (s, 3H, OC*H*$_3$), 3.79 (s, 3H, OC*H*$_3$), 4.02 (t, J = 6.7, 2H, NC*H*$_2$), 6.85 (d, J = 8.8, 2H, 2 x Ar*H*), 6.85 (d, J = 8.8, 2H, 2 x Ar*H*), 6.85 (d, J = 8.8, 2H, 2 x Ar*H*), 7.00 (dd, J = 5.1, 7.3, 1H, Ar*H*), 7.40 (d, J = 8.8, 2H, 2 x Ar*H*), 7.51 (t, J = 7.7, 1H, Ar*H*), 7.58 (d, J = 8.8, 2H, 2 x Ar*H*), 7.62 (d, J = 8.8, 2H, 2 x Ar*H*), 7.94-8.20 (m, 9H, 9 x Ar*H*), 8.26 (dd, J = 1.9, 5.1, 1H, Ar*H*), 8.34 (d, J = 9.2, 1H, Ar*H*), 8.76 (s, 1H, N*H*), 12.31 (s, 1H, N*H*). **^{13}C NMR** (101 MHz, $CDCl_3$) δ_C 44.9 (N*C*H$_2$), 46.8 (N*C*H$_2$),

48.5 (N*C*H$_2$), 49.3 (N*C*H$_2$), 55.5 (*C*H$_2$Ar), 55.6 (3 x O*C*H$_3$), 114.0 (2 x Ar*C*), 114.0 (2 x Ar*C*), 114.1 (2 x Ar*C*), 117.9 (Ar*C*), 121.1 (2 x Ar*C*), 121.5 (2 x Ar*C*), 122.1 (2 x Ar*C*), 123.0 (Ar*C*), 124.4 (Ar*C*), 124.7 (Ar*C*), 125.0 (Ar*C*), 125.5 (Ar*C*), 125.6 (2 x Ar*C*), 126.3 (Ar*C*), 127.2 (Ar*C*), 127.7 (Ar*C*), 128.5 (Ar*C*), 129.0 (Ar*C*), 129.4 (Ar*C*), 130.8 (Ar*C*), 131.1 (Ar*C*), 131.2 (Ar*C*), 131.4 (Ar*C*), 131.5 (Ar*C*), 133.1 (Ar*C*), 133.4 (Ar*C*), 139.4 (Ar*C*), 145.9 (Ar*C*), 154.2 (Ar*C*), 154.8 (Ar*C*), 155.3 (Ar*C*), 155.3 (Ar*C*), 156.0 (*C*O), 156.1 (*C*O), 156.1 (*C*O). **HR-MS** (ESI, positive ion mode) – *m/z* for $[C_{50}H_{47}N_7O_6+Na]^+$ = 864.3486. Found 864.3495. **FTIR** (neat) – 3336, 2948, 2922, 1652.

Pyren-1-ylmethyl isocyanate, 138

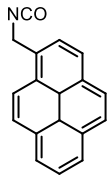

Under a dry, inert atmosphere, 1-pyrenylmethylammonium chloride (250 mg, 0.94 mmol, 1.00 equiv., 0.50 M) was suspended in anhydrous DCM (2 mL). Pyridine (0.08 mL, 0.94 mmol, 1.00 equiv.) was added and the resulting solution was stirred for 10 minutes. The solution was cooled to 0 °C and a solution of triphosgene (128 mg, 0.43 mmol, 0.46 equiv., 1.00 M) in anhydrous DCM (0.5 mL) was added. The solution was warmed to room temperature and stirred for 1 h, after which time the solution was diluted with Et$_2$O (10 mL). A white precipitate formed, and the suspension was filtered. The filtrate was then concentrated *in vacuo* to give the title isocyanate as a white solid (202 mg, 0.78 mmol, 83%). **TLC** – R_f = 0.70 (SiO_2, 50:50 Et$_2$O:PE). **^{1}H NMR** (400 MHz, $CDCl_3$) δ_H 5.24 (s, 2H, C*H*$_2$Ar), 8.21-8.43 (m, 9H, 9 x Ar*H*). Spectroscopic data matched that previously reported.[136]

1-(2-Pyridyl)- 1,4-bis(4-methoxyanilinylcarbonyl)-7-(pyren-1-ylmethyl)-7-(pyren-1-ylmethylaminocarbonyl)-1,4,7-triazaheptane, 139

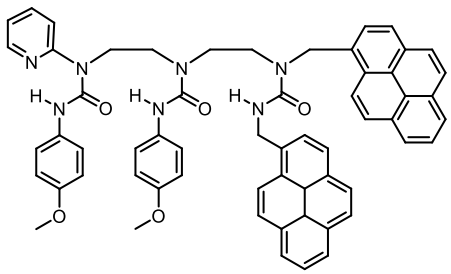

Synthesised according to general procedure B1 using **136** (75 mg, 0.10 mmol) and **138** (39 mg, 0.15 mmol). The crude product was purified by column chromatography (1-10% MeOH:DCM) to yield the title amine as a yellow solid (74 mg, 0.08 mmol, 78%). **M.P.** decomp. >250 °C (DCM). **TLC** – R_f = 0.51 (SiO_2, 5:95 MeOH:DCM). **^{1}H NMR** (400 MHz, $CDCl_3$) δ_H 3.15-3.65 (m, 6H, 3 x NC*H*$_2$), 3.75 (s, 3H, OC*H*$_3$), 3.77 (s, 3H, OC*H*$_3$), 5.12 (s, 2H, C*H*$_2$Ar), 5.17 (s, 2H, C*H*$_2$Ar), 6.74 (d, J = 8.9, 2H, 2 x Ar*H*), 6.81 (d, J = 9.0, 2H, 2 x Ar*H*), 6.93 (dd, J = 5.1, 7.4, 1H, Ar*H*), 7.28 (d, J = 9.0, 2H, 2 x Ar*H*), 7.38 (d, J = 8.9, 2H, 2 x Ar*H*), 7.63-8.18 (m, 19H, 19 x Ar*H*), 8.21 (dd, J = 1.9, 5.0, 1H, Ar*H*), 8.61 (d, J = 4.2, 1H, Ar*H*), 8.68 (s, 1H, N*H*), 12.35 (s, 1H, N*H*). **^{13}C NMR** (101 MHz, $CDCl_3$) δ_C

43.3 (NCH_2), 46.6 (NCH_2), 48.0 (NCH_2), 49.6 (NCH_2), 53.1 (CH_2Ar), 55.4 (CH_2Ar), 55.5 (2 x OCH_3), 113.9 (2 x Ar*C*), 114.0 (2 x Ar*C*), 117.7 (Ar*C*), 121.1 (2 x Ar*C*), 123.8 (2 x Ar*C*), 124.4-131.3 (32 x Ar*C*), 131.6 (Ar*C*), 133.2 (Ar*C*), 136.1 (Ar*C*), 139.3 (Ar*C*), 145.6 (Ar*C*), 149.7 (Ar*C*), 154.1 (Ar*C*), 155.9 (Ar*C*), 156.0 (*C*O), 156.1 (*C*O), 158.3 (*C*O). **HR-MS** (ESI, positive ion mode) – *m/z* for $[C_{60}H_{53}N_7O_5+Na]^+$ = 974.4006. Found 974.4039. **FTIR** (neat) – 3299, 2950, 1638.

Dibromomaleic anhydride, 140

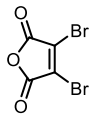

Under a dry, inert atmosphere, bromine (1.57 mL, 30.6 mmol, 2.00 equiv.) was added to maleic anhydride (1.5 g, 15.3 mmol, 1.00 equiv.) in a 20 mL microwave vial. To this solution was added aluminium trichloride (300 mg, 2.3 mmol, 0.15 equiv.). The vial was sealed and heated to 160 °C for 20 h behind a blast shield. The suspension was cooled to room temperature and carefully opened to air. The suspension was diluted with EtOAc (25 mL) and filtered. The residue was washed with EtOAc (10 mL) and the filtrate was concentrated *in vacuo* to give the desired anhydride as a white solid (2.7 g, 10.7 mmol, 70%). **TLC** – R_f = 0.75 (SiO_2, 1:99 MeOH:DCM). **^{13}C NMR** (101 MHz, $CDCl_3$) δ_C 128.1 (2 x *C*=CBr), 161.0 (2 x *C*O). Spectroscopic data matched that previously reported.[137]

Allyl dibromomaleimide, 141

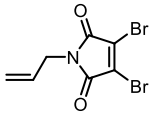

Under a dry, inert atmosphere, allylamine (0.72 mL, 9.58 mmol, 1.00 equiv., 0.10 M) was added to a solution of **140** (2.45 g, 9.58 mmol, 1.00 equiv.) in AcOH (96 mL). The solution was heated to reflux and stirred for 5 h, after which time the AcOH was removed by distillation. The crude product was purified by column chromatography (5-20% EtOAc:PE) to give the title maleimide as a white solid (2.51 g, 8.51 mmol, 89%). **M.P.** 96-97 °C (DCM). **TLC** – R_f = 0.65 (SiO_2, 20:80 EtOAc:PE). **^{1}H NMR** (400 MHz, $CDCl_3$) δ_H 4.20 (dt, J = 1.4, 5.9, 2H, NCH_2), 5.20-5.28 (m, 2H, C=CH_2), 5.79 (ddt, J = 5.9, 10.2, 17.0, 1H, C=C*H*). **^{13}C NMR** (101 MHz, $CDCl_3$) δ_C 41.8 (CH_2), 119.1 (C=CH_2), 129.5 (2 x C=*C*Br), 130.6 (C=*C*H), 163.6 (2 x *C*O). **HR-MS** (ESI, positive ion mode) – *m/z* for $[C_7H_6Br_2NO_2+H]^+$ = 293.8765. Found 293.8760. **FTIR** (neat) – 2932, 1783, 1713.

Allyl di(*n*-butylmercapto)maleimide, 142

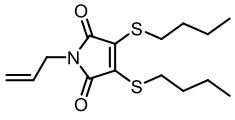

Under a dry, inert atmosphere, triethylamine (0.99 mL, 7.12 mmol, 2.10 equiv.) was added dropwise to a solution of **141** (1.0 g, 3.39 mmol, 1.00 equiv., 0.10 M) in anhydrous Et_2O (34 mL). To this solution was added 1-

butanethiol (0.76 mL, 7.12 mmol, 2.10 equiv.) dropwise and a yellow precipitate formed. The suspension was stirred at room temperature for 16 h. The suspension was then concentrated *in vacuo* and the crude product was purified by column chromatography (5-20% Et_2O:PE) to give the title bis(sulfide) as a yellow oil (814 mg, 2.60 mmol, 77%). **TLC** – R_f = 0.60 (SiO_2, 20:80 Et_2O:PE). **^{1}H NMR** (400 MHz, $CDCl_3$) δ_H 0.92 (t, J = 7.3, 6H, 2 x CH_3), 1.43-1.45 (m, 4H, 2 x CH_2), 1.60-1.63 (m, 4H, 2 x CH_2), 3.29 (t, J = 7.5, 4H, 2 x SCH_2), 4.10 (dd, J = 1.3, 5.7, 2H, NCH_2), 5.14-5.22 (m, 2H, C=CH_2), 5.79 (ddt, J = 5.9, 10.2, 15.9, 1H, C=CH). **^{13}C NMR** (101 MHz, $CDCl_3$) δ_C 13.7 (2 x CH$_3$), 21.7 (2 x CH$_2$), 31.6 (2 x SCH$_2$), 32.6 (2 x CH$_2$), 40.7 (NCH$_2$), 117.8 (C=CH$_2$), 131.7 (C=CH), 135.8 (2 x C=CS), 166.3 (2 x CO). **HR-MS** (ESI, positive ion mode) – *m/z* for $[C_{15}H_{23}NO_2S_2+H]^+$ = 314.1248. Found 314.1231. **FTIR** (neat) – 2958, 2930, 2872, 1764, 1701.

2-Oxoethyl-di(*n*-butylmercapto)maleimide, 143

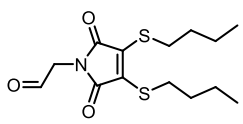

Synthesised according to general procedure N using **142** (250 mg, 0.70 mmol). The crude product was purified by column chromatography (20-100% Et_2O:PE) to give the title aldehyde as a yellow oil (123 mg, 0.39 mmol, 56%). **TLC** – R_f = 0.08 (SiO_2, 20:80 Et_2O:PE). **^{1}H NMR** (500 MHz, $CDCl_3$) δ_H 0.92 (t, J = 7.3, 6H, 2 x CH_3), 1.41-1.44 (m, 4H, 2 x CH_2), 1.62-1.64 (m, 4H, 2 x CH_2), 3.28 (t, J = 7.4, 2 x SCH_2), 4.36 (s, 2H, NCH_2), 9.56 (s, 1H, CHO). **^{13}C NMR** (126 MHz, $CDCl_3$) δ_C 13.5 (2 x CH$_3$), 21.6 (2 x CH$_2$), 31.6 (2 x SCH$_2$), 32.5 (2 x CH$_2$), 47.7 (NCH$_2$), 136.1 (C=CS), 165.8 (2 x CO), 193.6 (CHO). **HR-MS** (ESI, positive ion mode) – *m/z* for $[C_{14}H_{22}NO_3S_2+H]^+$ = 316.1041. Found 316.1016. **FTIR** (neat) – 2957, 2930, 1701.

1-(2-Pyridyl)-4-((di(*n*-butylmercapto)maleimido)ethyl)-1,4,-bis(4-methoxyanilinylcarbonyl)-1,4-diazabutane, 145

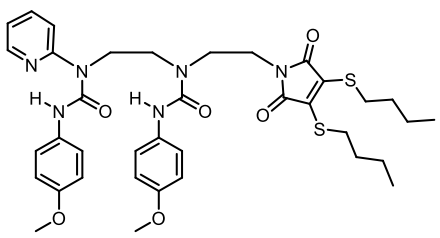

Synthesised according to general procedure R using **92** (43 mg, 0.31 mmol), **143** (72 mg, 0.31 mmol) and 4-methoxyphenyl isocyanate (0.08 mL, 0.62 mmol). The crude product was purified by column chromatography (1-5% MeOH:DCM) to give the title diurea as a yellow solid (30 mg, 0.04 mmol, 13%). **M.P.** 167-168 °C ($CHCl_3$/PE). **TLC** – R_f = 0.13 (SiO_2, 1:99 MeOH:DCM). **^{1}H NMR** (500 MHz, $CDCl_3$) δ_H 0.89 (t, J = 7.4, 6H, 2 x CH_3), 1.40-1.42 (m, 4H, 2 x CH_2), 1.58-1.61 (m, 4H, 2 x CH_2), 3.24 (t, J = 7.5, 4H, 2 x SCH_2), 3.62-3.67 (m, 4H, 2 x NCH_2), 3.78 (t, J = 6.4, 2H, NCH_2), 3.79 (s, 3H, OCH_3), 3.81 (s, 3H, OCH_3), 4.11 (t, J = 7.8, 2H,

NCH_2), 6.84 (d, J = 8.8, 2H, 2 x Ar*H*), 6.89 (d, J = 8.8, 2H, 2 x Ar*H*), 7.04 (dd, J = 5.0, 7.3, 1H, Ar*H*), 7.33 (d, J = 8.4, 1H, Ar*H*), 7.48 (d, J = 8.8, 2H, 2 x Ar*H*), 7.53 (d, J = 8.8, 2H, 2 x Ar*H*), 7.81 (ddd, J = 1.7, 7.3, 8.4, 1H, Ar*H*), 8.28 (s, 1H, N*H*), 8.33 (d, J = 5.0, 1H, Ar*H*), 12.43 (s, 1H, N*H*). **^{13}C NMR** (126 MHz, $CDCl_3$) δ_C 13.7 (2 x *C*H_3), 21.8 (2 x *C*H_2), 31.8 (2 x S*C*H_2), 32.5 (2 x *C*H_2), 37.2 (N*C*H_2), 44.7 (N*C*H_2), 46.0 (N*C*H_2), 46.3 (N*C*H_2), 55.7 (2 x O*C*H_3), 112.3 (Ar*C*), 114.1 (2 x Ar*C*), 114.3 (2 x Ar*C*), 118.0 (Ar*C*), 121.6 (2 x Ar*C*), 122.4 (2 x Ar*C*), 131.9 (Ar*C*), 133.2 (Ar*C*), 136.3 (2 x C=*C*S), 139.7 (Ar*C*), 146.0 (Ar*C*), 154.4 (*C*O), 155.4 (*C*O), 155.5 (Ar*C*), 155.8 (Ar*C*), 156.1 (Ar*C*), 166.9 (2 x *C*O). **HR-MS** (ESI, positive ion mode) – *m/z* for $[C_{37}H_{46}N_6O_6S_2+H]^+$ = 735.2998. Found 735.2994. **FTIR** (neat) – 3281, 2991, 1739, 1671.

1,7-Dibenzyl-1,4,7-tris(butylaminocarbonyl)-1,4,7-triazaheptane, 146

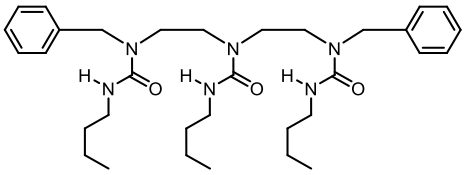

Synthesised according to general procedure B1 using **44** (30 mg, 0.10 mmol) and *n*-butyl isocyanate (0.06 mL, 0.45 mmol). The crude product was purified by column chromatography (1-5% MeOH:DCM) to yield the title triurea as a white solid (31 mg, 0.05 mmol, 54%). **M.P.** 111-112 °C ($CHCl_3$). **TLC** – R_f = 0.68 (SiO_2, 90:10 DCM:MeOH). **^{1}H NMR** (400 MHz, $CDCl_3$) δ_H 0.80 (t, J = 7.4, 6H, 2 x C*H*$_3$), 0.85 (t, J = 7.3, 3H, C*H*$_3$), 1.12-1.50 (m, 12H, 6 x C*H*$_2$), 3.04-3.26 (m, 14H, 7 x NC*H*$_2$), 4.34 (s, 4H, 2 x C*H*$_2$Ar), 5.06 (s, 2H, 2 x N*H*), 6.38 (t, J = 5.0, 1H, N*H*), 7.13 (d, J = 7.5, 4H, 4 x Ar*H*), 7.20 (t, J = 7.2, 2H, 2 x Ar*H*), 7.26 (t, J = 7.5, 4H, 4 x Ar*H*). **^{13}C NMR** (101 MHz, $CDCl_3$) δ_C 13.9 (2 x *C*H_3), 14.0 (*C*H_3), 20.1 (2 x *C*H_2), 20.3 (*C*H_2), 32.2 (*C*H_2), 32.3 (2 x *C*H_2), 47.3 (3 x NCH_2), 52.0 (2 x *C*H_2Ar), 127.0 (4 x Ar*C*), 127.7 (2 x Ar*C*), 129.0 (4 x Ar*C*), 138.0 (2 x Ar*C*), 158.7 (2 x *C*O), 158.8 (*C*O). **HR-MS** (ESI, positive ion mode) – *m/z* for $[C_{33}H_{52}N_6O_3+Na]^+$ = 603.3999. Found 603.4012. **FTIR** (neat) – 3326, 2963, 2910, 1640.

1,7-Bis(trifluoroacetyl)-4-(4-methoxyanilinylcarbonyl)-1,4,7-triazaheptane, 147

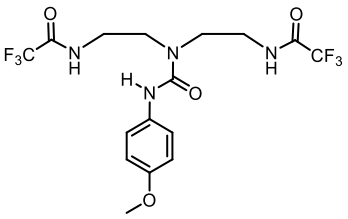

Synthesised according to general procedure J using diethylenetriamine (2.10 mL, 19.4 mmol) and 4-methoxyphenyl isocyanate (3.77 mL, 29.1 mmol). The resulting solution was concentrated *in vacuo* and the residue was recrystallised from DCM:Et_2O. The residue was then washed with Et_2O and air-dried to yield the title urea as a white solid (8.20 g, 18.5 mmol, 95%). **M.P.** 134-135 °C ($CHCl_3$). **TLC** – R_f = 0.25 (SiO_2, 5:95 MeOH:DCM). **^{1}H NMR** (500 MHz, $(CD)_3SO$) δ_H 3.38 (q, J = 5.9, 4H, 2 x NC*H*$_2$), 3.46 (t, J = 5.9, 4H, 2 x NC*H*$_2$), 6.84 (d, J = 8.9, 2H, 2 x Ar*H*), 7.32 (d, J = 8.9, 2H, 2 x Ar*H*), 8.08 (s, 1H, N*H*), 9.50 (t, J = 5.9, 2H, 2 x N*H*). **^{13}C NMR** (126 MHz, $(CD)_3SO$) δ_C 38.1 (2

x N*C*H$_2$), 45.7 (2 x N*C*H$_2$), 55.1 (O*C*H$_3$), 113.5 (2 x Ar*C*), 115.9 (q, J = 287.5, 2 x *C*F$_3$), 122.2 (2 x Ar*C*), 133.1 (Ar*C*), 154.7 (O*C*H$_3$), 155.3 (*C*O), 156.5 (q, J = 37.3, 2 x *C*O). **^{19}F NMR** (377 MHz, $CDCl_3$) δ_F −76.8 (2 x C*F*$_3$). **HR-MS** (ESI, positive ion mode) – *m/z* for $[C_{16}H_{18}F_6N_4O_4+H]^+$ = 445.1310. Found 445.1292. **FTIR** (neat) – 2960, 1731, 1706.

4-(4-Methoxyanilinylcarbonyl)-1,4,7-triazaheptane, 148

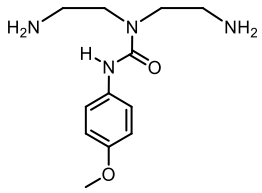

Synthesised according to general procedure H using **147** (2.5 g, 5.63 mmol). The resulting solution was concentrated *in vacuo* and the residue was diluted with deionised water. The aqueous solution was extracted with DCM (3 x 50 mL). The combined organic extracts were washed with brine, dried ($MgSO_4$), filtered and concentrated *in vacuo* to give the title diamine as a colourless oil (450 mg, 1.78 mmol, 32%). **TLC** – R_f = 0.04 (SiO_2, 10:90:1 DCM:MeOH:TEA).**^{1}H NMR** (400 MHz, $CDCl_3$) δ_H 1.49 (s, 4H, 2 x N*H*$_2$), 2.84 (t, J = 5.7, 4H, 2 x NC*H*$_2$), 3.29 (t, J = 5.7, 4H, 2 x NC*H*$_2$), 3.68 (s, 3H, OC*H*$_3$), 6.72 (d, J = 9.0, 2H, 2 x Ar*H*), 7.20 (d, J = 9.0, 2H, 2 x Ar*H*), 9.86 (s, 1H, N*H*). **^{13}C NMR** (101 MHz, $CDCl_3$) δ_C 41.2 (2 x N*C*H$_2$), 51.3 (2 x N*C*H$_2$), 55.5 (O*C*H$_3$), 114.0 (2 x Ar*C*), 120.8 (2 x Ar*C*), 133.8 (Ar*C*), 154.8 (Ar*C*), 158.3 (*C*O). **HR-MS** (ESI, positive ion mode) – *m/z* for $[C_{12}H_{20}N_4O_2+H]^+$ = 253.1665. Found 253.1653. **FTIR** (neat) – 2938, 2838, 1643, 1604.

1,7-Dibenzyl-4-(4-methoxyanilinylcarbonyl)-1,4,7-triazaheptane, 149

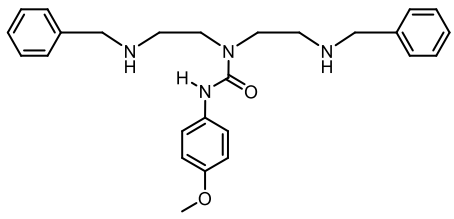

Synthesised according to general procedure E using **148** (380 mg, 1.51 mmol) and benzaldehyde (0.46 mL, 4.52 mmol). The crude product was purified using column chromatography (2-10% MeOH:DCM) to yield the title diamine as a colourless oil (315 mg, 0.73 mmol, 48%). **TLC** – R_f = 0.26 (SiO_2, 10:90 MeOH:DCM). **^{1}H NMR** (400 MHz, $CDCl_3$) δ_H 1.85 (s, 2H, 2 x N*H*), 2.86 (t, J = 5.6, 4H, 2 x NC*H*$_2$), 3.44 (t, J = 5.6, 4H, 2 x NC*H*$_2$), 3.76 (s, 3H, OC*H*$_3$), 3.81 (s, 4H, 2 x C*H*$_2$Ar), 6.76 (d, J = 9.0, 2H, 2 x Ar*H*), 7.14 (d, J = 9.0, 2H, 2 x Ar*H*), 7.26-7.34 (m, 10H, 10 x Ar*H*), 9.70 (s, 1H, N*H*). **^{13}C NMR** (101 MHz, $CDCl_3$) δ_C 48.7 (2 x N*C*H$_2$), 49.2 (2 x N*C*H$_2$), 54.2 (2 x *C*H$_2$Ar), 55.7 (O*C*H$_3$), 114.1 (2 x Ar*C*), 121.1 (2 x Ar*C*), 127.2 (2 x Ar*C*), 128.4 (4 x Ar*C*), 128.7 (4 x Ar*C*), 133.7 (Ar*C*), 139.7 (2 x Ar*C*), 155.0 (Ar*C*), 158.2 (*C*O). **HR-MS** (ESI, positive ion mode) – *m/z* for $[C_{26}H_{32}N_4O_2+H]^+$ = 433.2604. Found 4332.2586. **FTIR** (neat) – 2931, 2835, 1650.

1,7-Dibenzyl-1,4-bis(4-methoxyanilinylcarbonyl)-1,4,7-triazaheptane, 150

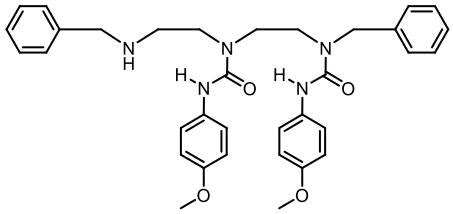

Synthesised according to general procedure B1 using **149** (271 mg, 0.63 mmol) and 4-methoxyphenyl isocyanate (0.08 mL, 0.63 mmol). The crude product was purified using column chromatography (2-10% MeOH:DCM) to yield the title diamine as a foamy white solid (238 mg, 0.41 mmol, 65%). **M.P.** 140-141 °C ($CHCl_3$/PE). **TLC** – R_f = 0.26 (SiO_2, 5:95 MeOH:DCM). **^{1}H NMR** (500 MHz, $CDCl_3$) δ_H 2.82 (t, J = 4.5, 2H, NC*H*$_2$), 3.25 (t, J = 7.8, 2H, NC*H*$_2$), 3.29 (t, J = 4.5, 2H, NC*H*$_2$), 3.47 (d, J = 7.8, 2H, NC*H*$_2$), 3.77 (s, 3H, OC*H*$_3$), 3.77 (s, 3H, OC*H*$_3$), 3.82 (s, 2H, C*H*$_2$Ar), 4.62 (s, 2H, C*H*$_2$Ar), 6.76 (d, J = 8.8, 2H, 2 x Ar*H*), 6.80 (d, J = 9.0, 2H, 2 x Ar*H*), 7.15 (d, J = 9.0, 2H, 2 x Ar*H*), 7.24-7.27 (m, 2H, 2 x Ar*H*), 7.27-7.35 (m, 8H, 8 x Ar*H*), 7.52 (d, J = 8.8, 2H, 2 x Ar*H*), 8.36 (s, 1H, N*H*), 9.81 (s, 1H, N*H*). **^{13}C NMR** (126 MHz, $CDCl_3$) δ_C 45.3 (N*C*H$_2$), 48.0 (N*C*H$_2$), 49.4 (N*C*H$_2$), 51.0 (N*C*H$_2$), 51.1 (*C*H$_2$Ar), 54.4 (*C*H$_2$Ar), 55.7 (2 x O*C*H$_3$), 114.0 (2 x Ar*C*), 114.1 (2 x Ar*C*), 121.0 (2 x Ar*C*), 121.5 (2 x Ar*C*), 127.6 (Ar*C*), 127.7 (Ar*C*), 127.9 (2 x Ar*C*), 128.5 (2 x Ar*C*), 128.8 (2 x Ar*C*), 128.9 (2 x Ar*C*), 133.1 (Ar*C*), 133.5 (Ar*C*), 138.6 (Ar*C*), 138.9 (Ar*C*), 155.3 (2 x Ar*C*), 156.3 (*C*O), 158.3 (*C*O). **HR-MS** (ESI, positive ion mode) – *m/z* for $[C_{34}H_{39}N_5O_4+H]^+$ = 582.3080. Found 582.3101. **FTIR** (neat) – 2968, 2905, 1653, 1648.

1,7-Dibenzyl-1,4-bis(4-methoxyanilinylcarbonyl)-7-butylaminocarbonyl-1,4,7-triazaheptane, 151

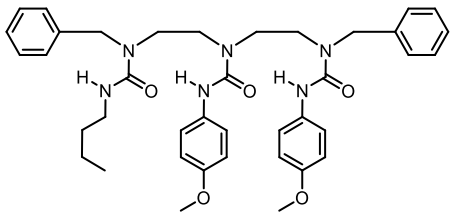

Synthesised according to general procedure B1 using **150** (60 mg, 0.10 mmol) and *n*-butyl isocyanate (0.02 mL, 0.15 mmol). The crude product was purified using column chromatography (2-5% MeOH:DCM) to yield the title triurea as a foamy white solid (38 mg, 0.06 mmol, 56%). **M.P.** 171-172 °C (Et_2O/PE). **TLC** – R_f = 0.45 (SiO_2, EtOAc). **^{1}H NMR** (400 MHz, $CDCl_3$) δ_H 0.85 (t, J = 7.8, 3H, C*H*$_3$), 1.20-1.22 (m, 2H, C*H*$_2$), 1.37-1.40 (m, 2H, C*H*$_2$), 3.16-3.47 (m, 10H, 5 x NC*H*$_2$), 3.76 (s, 3H, OC*H*$_3$), 3.78 (s, 3H, OC*H*$_3$), 4.38 (s, 2H, C*H*$_2$Ar), 4.57 (s, 2H, C*H*$_2$Ar), 6.81 (d, J = 9.0, 2H, 2 x Ar*H*), 6.84 (d, J = 9.0, 2H, 2 x Ar*H*), 7.12 (d, J = 7.5, 2H, 2 x Ar*H*), 7.18-7.33 (m, 10H, 10 x Ar*H*), 7.38 (s, 1H, N*H*), 7.53 (d, J = 8.9, 2H, 2 x Ar*H*), 8.84 (s, 1H, N*H*). **^{13}C NMR** (101 MHz, $CDCl_3$) δ_C 13.9 (*C*H$_3$), 20.0 (*C*H$_2$), 32.2 (*C*H$_2$), 40.7 (N*C*H$_2$), 46.7 (N*C*H$_2$), 47.6 (N*C*H$_2$), 48.4 (N*C*H$_2$), 49.9 (N*C*H$_2$), 51.9 (*C*H$_2$Ar), 52.7 (*C*H$_2$Ar), 55.7 (2 x O*C*H$_3$), 114.0 (4 x Ar*C*), 121.1 (2 x Ar*C*), 121.6 (2 x Ar*C*), 126.6 (2 x Ar*C*), 127.6 (2 x Ar*C*), 128.0 (2 x Ar*C*), 128.9 (2 x Ar*C*), 129.2 (2 x Ar*C*), 133.0 (Ar*C*), 133.4 (Ar*C*), 137.7 (Ar*C*), 138.2 (Ar*C*),

155.3 (Ar*C*), 155.4 (Ar*C*), 156.4 (*C*O), 156.6 (*C*O), 158.9 (*C*O). **HR-MS** (ESI, positive ion mode) – *m/z* for $[C_{39}H_{48}N_6O_5+Na]^+$ = 703.3584. Found 703.3575. **FTIR** (neat) – 2960, 2932, 1644, 1607.

1-(3,5-Bis(trifluoromethyl)anilinylcarbonyl)-4,7-bis(hexylaminocarbonyl)-7-((di(butylmercapto)maleimido)ethyl)-1,4,7-triazaheptane, 154

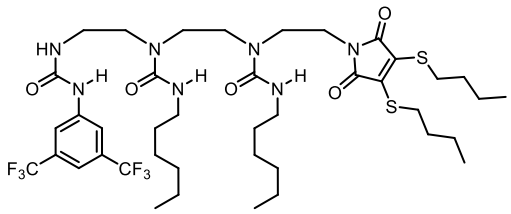

Synthesised according to general procedure R using **152** (160 mg, 0.35 mmol), **143** (89 mg, 0.39 mmol) and *n*-hexyl isocyanate (0.02 mL, 0.08 mmol). The crude product was purified by column chromatography (2-10% MeOH:DCM) to give the title urea as a yellow oil (25 mg, 0.03 mmol, 55%). **TLC** – R_f = 0.50 (SiO_2, 5:95 MeOH:DCM). **^{1}H NMR** (500 MHz, $CDCl_3$) δ_H 0.82 (t, J = 7.2, 3H, C*H*$_3$), 0.87 (t, J = 6.9, 3H, C*H*$_3$), 0.94 (t, J = 7.2, 6H, 2 x C*H*$_3$), 1.15-1.34 (m, 12H, 6 x C*H*$_2$), 1.41-1.56 (m, 8H, 4 x C*H*$_2$), 1.60-1.66 (m, 4H, 2 x C*H*$_2$), 3.14-3.22 (m, 4H, 2 x NC*H*$_2$), 3.27 (t, J = 7.6, 4H, 2 x SC*H*$_2$), 3.31-3.45 (m, 10H, 5 x NC*H*$_2$), 3.65 (t, J = 7.0, 2H, NC*H*$_2$), 5.67 (s, 1H, N*H*), 6.31 (s, 1H, N*H*), 6.84 (s, 1H, N*H*), 7.43 (s, 1H, Ar*H*), 7.98 (s, 2H, 2 x Ar*H*) 8.73 (s, 1H, N*H*). **^{13}C NMR** (126 MHz, $CDCl_3$) δ_C 13.5 (2 x *C*H$_3$), 13.9 (*C*H$_3$), 14.0 (*C*H$_3$), 21.6 (2 x *C*H$_2$), 22.5 (*C*H$_2$), 22.6 (*C*H$_2$). 26.6 (*C*H$_2$), 26.6 (*C*H$_2$), 29.7 (*C*H$_2$), 29.8 (*C*H$_2$), 31.4 (*C*H$_2$), 31.5 (*C*H$_2$), 31.6 (2 x S*C*H$_2$), 32.4 (2 x *C*H$_2$), 36.4 (N*C*H$_2$), 39.1 (N*C*H$_2$), 41.3 (2 x N*C*H$_2$), 45.6 (N*C*H$_2$), 46.5 (N*C*H$_2$), 46.9 (N*C*H$_2$), 48.1 (N*C*H$_2$), 114.8 (Ar*C*), 117.9 (2 x Ar*C*), 123.4 (q, J = 273.4, 2 x *C*F$_3$), 131.9 (q, J = 33.0, 2 x Ar*C*), 135.9 (2 x C=*C*S), 141.6 (Ar*C*), 156.1 (*C*O), 158.3 (*C*O), 159.1 (*C*O), 166.8 (2 x *C*O). **^{19}F NMR** (377 MHz, $CDCl_3$) δ_F −64.3 (2 x C*F*$_3$). **HR-MS** (ESI, positive ion mode) – *m/z* for $[C_{41}H_{68}F_6N_7O_5S_2+Na]^+$ = 934.4134. Found 934.4097. **FTIR** (neat) – 3250, 2997, 1745, 1643.

1-(3,5-Bis(trifluoromethyl)anilinylcarbonyl)-4,7,10,13-tetrakis(butylaminocarbonyl)-13-((di(butylmercapto)maleimido)ethyl)-1,4,7,10,13-pentaazatridecane, 157

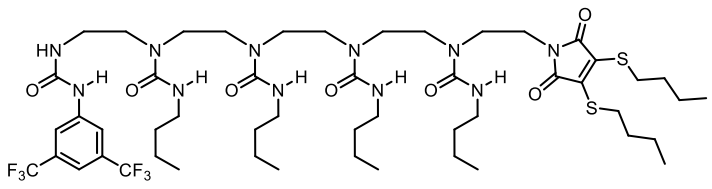

Synthesised according to general procedure R using **155** (45 mg, 0.06 mmol), **143** (15 mg, 0.07 mmol) and *n*-butyl isocyanate (0.06 mL, 0.05 mmol). The crude product was purified by column chromatography (2-10% MeOH:DCM) to give the title urea as a yellow solid (33 mg, 0.03 mmol, 48%). **M.P.** 165-166 °C ($CHCl_3$/PE). **TLC** – R_f = 0.36 (SiO_2, 5:95 MeOH:DCM). **^{1}H NMR** (500 MHz, $CDCl_3$) δ_H 0.93-0.98 (m, 18H, 6 x C*H*$_3$), 1.42-1.67 (m, 24H, 12 x C*H*$_2$), 3.18-3.43 (m, 30H, 13 x NC*H*$_2$, 2 x SC*H*$_2$),

3.65 (t, J = 7.1, 2H, NC*H*$_2$), 6.10 (s, 1H, N*H*), 6.65-6.91 (m, 3H, 3 x N*H*), 7.45 (s, 1H, Ar*H*), 7.99 (s, 2H, 2 x Ar*H*). **^{13}C NMR** (126 MHz, $CDCl_3$) δ_C 13.5-14.3 (6 x *C*H$_3$), 18.8 (*C*H$_2$), 19.4 (*C*H$_2$), 20.2 (*C*H$_2$), 20.4 (*C*H$_2$), 21.7 (*C*H$_2$), 22.3 (2 x *C*H$_2$), 22.6 (2 x *C*H$_3$), 27.7 (*C*H$_2$), 28.9 (*C*H$_2$), 29.1 (*C*H$_2$), 31.6 (2 x S*C*H$_2$), 32.1 (N*C*H$_2$), 32.4 (N*C*H$_2$), 33.7 (N*C*H$_2$), 34.1 (N*C*H$_2$), 36.1 (N*C*H$_2$), 36.4 (N*C*H$_2$), 36.5 (N*C*H$_2$), 40.8 (N*C*H$_2$), 40.8 (N*C*H$_2$), 41.4 (N*C*H$_2$), 46.0 (N*C*H$_2$), 47.3 (N*C*H$_2$), 47.9 (N*C*H$_2$), 49.0 (N*C*H$_2$), 114.8 (Ar*C*), 117.8 (2 x Ar*C*), 123.4 (q, J = 272.2, 2 x *C*F$_3$), 131.9 (q, J = 33.2, 2 x Ar*C*), 136.0 (2 x C=*C*S), 141.5 (Ar*C*), 156.0 (*C*O), 158.1-159.1 (4 x *C*O), 166.9 (2 x *C*O). **^{19}F NMR** (377 MHz, $CDCl_3$) δ_F −64.6 (2 x C*F*$_3$). **HR-MS** (ESI, positive ion mode) – *m/z* for $[C_{51}H_{83}F_6N_{11}O_7S_2+Na]^+$ = 1162.5720. Found 1162.5765. **FTIR** (neat) – 3294, 3211, 2995, 1761, 1633.

1,10-Bis(trifluoroacetyl)-4,7-bis(4-methoxyanilinylcarbonyl)-1,4,7,10-tetraazadecane, 158

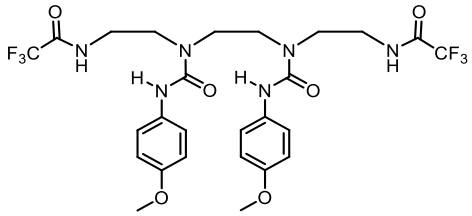

Synthesised according to general procedure J using triethylenetetramine (2.0 mL, 13.7 mmol) and 4-methoxyphenyl isocyanate (4.2 mL, 32.8 mmol). After 16 h, a white precipitate formed and was filtered. The residue was washed with DCM (3 x 10 mL) and air-dried to afford the title diurea as a white solid (4.60 g, 7.23 mmol, 53%). **M.P.** 191-192 °C ($CHCl_3$). **TLC** – R_f = 0.23 (SiO_2, 90:10 EtOAc:PE). **^{1}H NMR** (400 MHz, $(CD_3)_2SO$) δ_H 3.39 (t, J = 6.1, 4H, 2 x NC*H*$_2$), 3.42 (s, 4H, 2 x NC*H*$_2$), 3.50 (t, J = 6.1, 4H, 2 x NC*H*$_2$), 3.72 (s, 6H, 2 x OC*H*$_3$), 6.84 (d, J = 9.2, 4H, 4 x Ar*H*), 7.38 (d, J = 9.2, 4H, 4 x Ar*H*), 8.57 (s, 2H, 2 x N*H*), 9.50 (s, 2H, 2 x N*H*). **^{13}C NMR** (101 MHz, $(CD_3)_2SO$) δ_C 39.0 (2 x N*C*H$_2$), 46.5 (2 x N*C*H$_2$), 46.7 (2 x N*C*H$_2$), 55.6 (2 x O*C*H$_3$), 114.0 (4 x Ar*C*), 116.3 (q, J = 287.1, 2 x *C*F$_3$), 122.1 (4 x Ar*C*), 133.7 (2 x Ar*C*), 155.1 (2 x Ar*C*), 156.2 (2 x *C*O), 157.2 (q, J = 36.1, 2 x *C*O). **^{19}F NMR** (377 MHz, $(CD_3)_2SO$) δ_F −74.4 (2 x C*F*$_3$). **HR-MS** (ESI, positive ion mode) – *m/z* for $[C_{26}H_{30}F_6N_6O_6+H]^+$ = 637.2209. Found 637.2193. **FTIR** (neat) – 3442, 3261, 2969, 1652, 1638.

4,7-Bis(4-methoxyanilinylcarbonyl)-1,4,7,10-tetraazadecane, 159

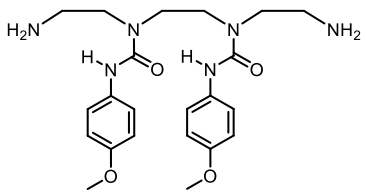

Synthesised according to general procedure H using **158** (4.60 g, 7.23 mmol). After 5 h, a white precipitate formed and was filtered. The residue was washed with MeOH (3 x 10 mL) and air-dried to afford the title diamine as a white solid (3.05 g, 6.87 mmol, 95%). **M.P.** 163-164 °C (DCM). **TLC** – R_f = 0.04 (SiO_2, 5:95 MeOH:DCM). **^{1}H NMR** (400 MHz, $CDCl_3$) δ_H 2.96 (t, J = 5.1, 4H, 2 x NC*H*$_2$), 3.43 (t, J = 5.1, 4H, 2 x NC*H*$_2$), 3.50 (s,

4H, 2 x NCH_2), 3.77 (s, 6H, 2 x OCH_3), 6.81 (d, J = 9.0, 4H, 4 x Ar*H*), 7.36 (d, J = 9.0, 4H, 4 x Ar*H*), 9.62 (s, 2H, 2 x N*H*). **^{13}C NMR** (101 MHz, $CDCl_3$) δ_C 41.7 (2 x N*C*H_2), 46.8 (2 x N*C*H_2), 52.2 (2 x N*C*H_2), 55.5 (2 x O*C*H_3), 114.0 (4 x Ar*C*), 120.9 (4 x Ar*C*), 133.5 (2 x Ar*C*), 155.0 (2 x Ar*C*), 157.7 (2 x *C*O). **HR-MS** (ESI, positive ion mode) – *m/z* for $[C_{22}H_{32}N_6O_4+Na]^+$ = 467.2383. Found 467.2401. **FTIR** (neat) – 3242, 2980, 1650.

1,4-Bis(succinimidylethyl)-1,4-bis(4-methoxyanilinylcarbonyl)-1,4-diazabutane, 160

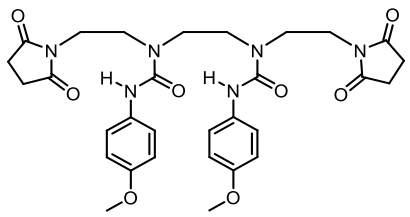

Synthesised according to general procedure I using **159** (200 mg, 0.45 mmol). The crude product was purified by column chromatography (2-10% MeOH:DCM) to give the title disuccinimide as a white solid (112 mg, 0.18 mmol, 41%). **M.P.** 181-182 °C ($CHCl_3$). **TLC** – R_f = 0.10 (SiO_2, 5:95 MeOH:DCM). **^{1}H NMR** (400 MHz, $CDCl_3$) δ_H 2.64 (s, 8H, 4 x C(O)CH_2), 3.41 (s, 4H, 2 x NCH_2), 3.44 (t, J = 6.4, 4H, 2 x NCH_2), 3.66 (t, J = 6.4, 4H, 2 x NCH_2), 3.74 (s, 6H, 2 x OCH_3), 6.79 (d, J = 9.0, 4H, 4 x Ar*H*), 7.46 (d, J = 9.0, 4H, 4 x Ar*H*), 8.04 (s, 2H, 2 x N*H*). **^{13}C NMR** (101 MHz, $CDCl_3$) δ_C 28.3 (4 x C(O)*C*H_2), 37.1 (2 x N*C*H_2), 45.0 (2 x N*C*H_2), 46.5 (2 x N*C*H_2), 55.5 (2 x O*C*H_3), 114.0 (4 x Ar*C*), 121.0 (4 x Ar*C*), 132.9 (2 x Ar*C*), 155.3 (2 x Ar*C*), 155.9 (2 x *C*O), 177.7 (4 x *C*O). **HR-MS** (ESI, positive ion mode) – *m/z* for $[C_{30}H_{36}N_6O_8+Na]^+$ = 631.2492. Found 631.2481. **FTIR** (neat) – 3332, 2988, 2902, 1698, 1644.

1,10-Dibenzyl-4,7-bis(4-methoxyanilinylcarbonyl)-1,4,7,10-tetraazadecane, 163

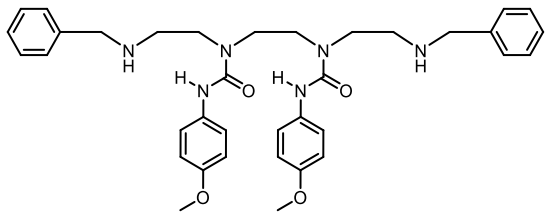

Synthesised according to general procedure E using **159** (500 mg, 1.12 mmol) and benzaldehyde (0.23 mL, 2.25 mmol). The crude product was purified by column chromatography (3-10% MeOH:DCM) to give the title diamine as a white solid (87 mg, 0.15 mmol, 53%). **M.P.** 192-193 °C ($CHCl_3$). **TLC** – R_f = 0.26 (SiO_2, 5:95 MeOH:DCM). **^{1}H NMR** (400 MHz, $CDCl_3$) δ_H 1.92 (s, 2H, 2 x N*H*), 2.85 (t, J = 5.0, 4H, 2 x NCH_2), 3.39 (s, 4H, 2 x NCH_2), 3.45 (t, J = 5.0, 4H, 2 x NCH_2), 3.76 (s, 6H, 2 x OCH_3), 3.81 (s, 4H, 2 x CH_2Ar), 6.77 (d, J = 9.0, 4H, 4 x Ar*H*), 7.23-7.35 (m, 14H, 14 x Ar*H*), 9.62 (s, 2H, 2 x N*H*). **^{13}C NMR** (101 MHz, $CDCl_3$) δ_C 47.0 (2 x N*C*H_2), 49.2 (2 x N*C*H_2), 49.8 (2 x N*C*H_2), 54.2 (2 x *C*H_2Ar), 55.5 (2 x O*C*H_3), 113.9 (4 x Ar*C*), 121.0 (4 x Ar*C*), 127.3 (2 x Ar*C*), 128.3 (4 x Ar*C*), 128.6 (4 x Ar*C*), 133.5 (2 x Ar*C*), 139.3 (2 x Ar*C*), 155.0 (2 x Ar*C*), 157.6 (2 x

*C*O). **HR-MS** (ESI, positive ion mode) – *m/z* for $[C_{36}H_{44}N_6O_4+H]^+$ = 625.3502. Found 625.3500. **FTIR** (neat) – 3306, 2954, 1653.

1,10-Dibenzyl-4,7-bis(*tert*-butoxycarbonyl)-1,4,7,10-tetraazadecane, 166

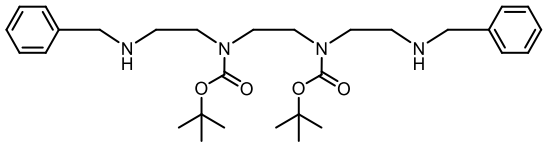

Synthesised according to general procedure E using **60** (2.00 g, 5.8 mmol) and benzaldehyde (1.76 mL, 17.3 mmol). The crude product was purified by column chromatography (3-10% MeOH:DCM) to yield the title diamine as a foamy white solid (2.20 g, 4.15 mmol, 72%). **M.P.** 77-78 °C ($CHCl_3$). **TLC** – R_f = 0.13 (SiO_2, 5:95 MeOH:DCM). **^{1}H NMR** (400 MHz, $CDCl_3$) δ_H 1.38-1.44 (s, 18H, 2 x C(C*H*$_3$)$_3$), 2.34-2.45 (t, J = 4.8, 2H, 2 x N*H*), 2.71-2.78 (q, J = 4.8, 4H, 2 x NC*H*$_2$), 3.22-3.38 (m, 8H, 4 x NC*H*$_2$), 3.75-3.76 (s, 4H, 2 x C*H*$_2$Ar), 7.17-7.29 (m, 10H, 10 x Ar*H*). **^{13}C NMR** (101 MHz, $CDCl_3$) δ_C 28.4 (2 x (C(*C*H$_3$)$_3$), 45.5 (2 x N*C*H$_2$), 47.2 (2 x N*C*H$_2$), 48.0 (2 x N*C*H$_2$), 53.4 (2 x *C*H$_2$Ar), 79.6 (2 x *C*(CH$_3$)$_3$), 126.8 (2 x Ar*C*), 128.0 (4 x Ar*C*), 128.3 (4 x Ar*C*), 140.3 (2 x Ar*C*), 155.6 (2 x *C*O). **HR-MS** (ESI, positive ion mode) – *m/z* for $[C_{30}H_{46}N_4O_4+H]^+$ = 527.3597. Found 527.3575. **FTIR** (neat) – 3361, 2973, 2877, 1674.

1,10-Dibenzyl-1,10-bis(*N*-methylanilinylcarbonyl)-4,7-bis(*tert*-butoxycarbonyl)-1,4,7,10-tetraazadecane, 167

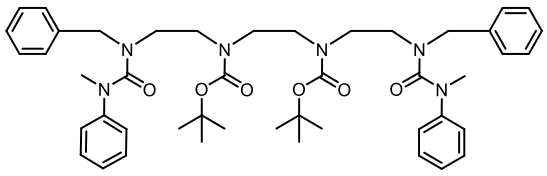

Synthesised according to general procedure B2 using **166** (1.0 g, 1.9 mmol) and *N*-methyl-*N*-phenylcarbamoyl chloride (967 mg, 5.7 mmol). The crude product was purified by column chromatography (2-10% MeOH:DCM) to yield the title diurea as a foamy white solid (678 mg, 0.86 mmol, 45%). **M.P.** 111-112 °C ($CHCl_3$). **TLC** – R_f = 0.26 (SiO_2, 5:95 MeOH:DCM). **^{1}H NMR** (400 MHz, $CDCl_3$) δ_H 1.28-1.38 (m, 18H, 2 x C(C*H*$_3$)$_3$), 2.99-3.14 (m, 18H, 2 x NC*H*$_3$, 6 x NC*H*$_2$), 4.16-4.28 (m, 4H, 2 x C*H*$_2$Ar), 6.96-7.26 (m, 20H, 20 x Ar*H*). **^{13}C NMR** (101 MHz, $CDCl_3$) δ_C 28.5 (2 x C(*C*H$_3$)$_3$), 40.1 (2 x N*C*H$_3$), 44.9-45.6 (6 x N*C*H$_2$), 52.9 (2 x *C*H$_2$Ar), 79.8 (2 x *C*(CH$_3$)$_3$), 124.0-129.6 (20 x Ar*C*), 137.3 (2 x Ar*C*), 146.7 (2 x Ar*C*), 155.0 (2 x *C*O), 162.1 (2 x *C*O). **HR-MS** (MALDI) – *m/z* for $[C_{46}H_{60}N_6O_6+Na]^+$ = 815.4472. Found 815.4499. **FTIR** (neat) – 2973, 2915, 1674.

1,10-Dibenzyl-1,10-bis(*N*-methylanilinylcarbonyl)-1,4,7,10-tetraazadecane, 168

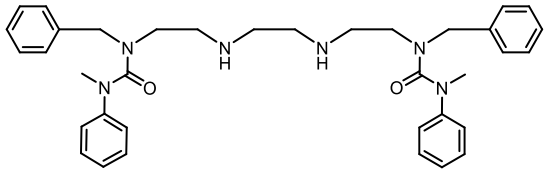

Synthesised according to general procedure C using **167** (400 mg, 0.50 mmol). The title diamine was isolated as a foamy white solid (296 mg, 0.50 mmol, >99%). **M.P.** 99-100 °C ($CHCl_3$). **TLC** – R_f = 0.10 (SiO_2, 50:50 EtOAc:PE). **^{1}H NMR** (400 MHz, $CDCl_3$) δ_H 2.02 (s, 2H, 2 x N*H*), 2.46 (s, 4H, 2 x NCH_2), 2.49 (t, J = 6.6, 4H, 2 x NCH_2), 3.09 (s, 6H, 2 x NCH_3), 3.09 (t, J = 6.6, 4H, 2 x NCH_2), 4.14 (s, 4H, 2 x CH_2Ar), 7.00-7.05 (m, 10H, 10 x Ar*H*), 7.13-7.25 (m, 10H, 10 x Ar*H*). **^{13}C NMR** (101 MHz, $CDCl_3$) δ_C 39.9 (2 x NCH_3), 47.2 (2 x NCH_2), 47.5 (2 x NCH_2), 48.9 (2 x NCH_2), 52.3 (2 x CH_2Ar), 123.9 (4 x Ar*C*), 124.8 (2 x Ar*C*), 127.4 (2 x Ar*C*), 127.7 (4 x Ar*C*), 128.5 (4 x Ar*C*), 129.5 (4 x Ar*C*), 137.9 (2 x Ar*C*), 146.8 (2 x Ar*C*), 162.4 (2 x *C*O). **HR-MS** (ESI, positive ion mode) – *m/z* for $[C_{36}H_{44}N_6O_2+H]^+$ = 593.3604. Found 593.3570. **FTIR** (neat) – 3303, 2928, 1643.

1,10-Dibenzyl-1,10-bis(*N*-methylanilinylcarbonyl)-4,7-bis(4-methoxyanilinylcarbonyl)-1,4,7,10-tetraazadecane, 161

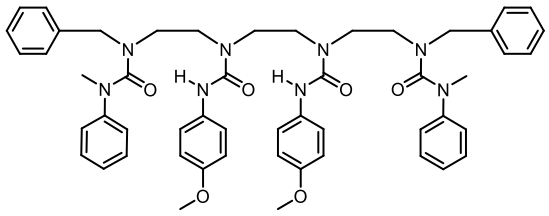

Synthesised according to general procedure B1 using **168** (100 mg, 0.17 mmol) and 4-methoxyphenyl isocyanate (0.07 mL, 0.51 mmol). The crude product was purified by column chromatography (25-100% EtOAc:PE) to give the title tetraurea as a foamy white solid (79 mg, 0.09 mmol, 52%). **M.P.** 138-139 °C ($CHCl_3$). **TLC** – R_f = 0.39 (SiO_2, 50:50 EtOAc:PE). **^{1}H NMR** (400 MHz, $CDCl_3$) δ_H 3.25 (s, 6H, 2 x NCH_3), 3.27-3.36 (m, 12H, 6 x NCH_2), 3.79 (s, 6H, 2 x OCH_3), 4.09 (s, 4H, 2 x CH_2Ar), 6.85 (d, J = 9.0, 4H, 4 x Ar*H*), 7.01-7.14 (m, 10H, 10 x Ar*H*), 7.20-7.33 (m, 10H, 10 x Ar*H*), 7.62 (d, J = 9.0, 4H, 4 x Ar*H*), 8.83 (s, 2H, 2 x N*H*). **^{13}C NMR** (101 MHz, $CDCl_3$) δ_C 40.1 (2 x NCH_3), 46.2 (2 x NCH_2), 47.3 (2 x NCH_2), 47.7 (2 x NCH_2), 53.7 (2 x CH_2Ar), 55.6 (2 x OCH_3), 114.1 (4 x Ar*C*), 121.1 (4 x Ar*C*), 124.2 (4 x Ar*C*), 125.4 (2 x Ar*C*), 127.6 (4 x Ar*C*), 127.6 (2 x Ar*C*), 128.8 (4 x Ar*C*), 129.8 (4 x Ar*C*), 133.7 (2 x Ar*C*), 137.4 (2 x Ar*C*), 146.3 (2 x Ar*C*), 155.2 (2 x Ar*C*), 156.1 (2 x *C*O), 162.5 (2 x *C*O). **HR-MS** (MALDI) – *m/z* for $[C_{52}H_{58}N_8O_6+Na]^+$ = 913.4377. Found 913.4372. **FTIR** (neat) – 3307, 2997, 2893, 1648.

***N*-(2-Pyridyl)(benzyl)ethanolamine, 169**

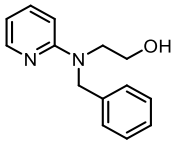

Under a dry, inert atmosphere, benzyl bromide (2.4 mL, 19.9 mmol, 1.10 equiv.) was added to a solution of **100** (2.5 g, 18.1 mmol, 1.00 equiv., 0.50 M) in anhydrous THF (36 mL). The solution was heated to reflux and stirred for 16 h. After cooling to room temperature, the solution was concentrated *in vacuo* and purified by column chromatography (2-10% MeOH:DCM) to yield the title amine as a white solid (4.0 g, 17.5 mmol, 88%). **TLC** – R_f = 0.29 (SiO_2, 5:95 MeOH:DCM). **^{1}H NMR** (400 MHz, $CDCl_3$) δ_H 3.74 (t, J = 4.7, 2H, NC*H*$_2$), 3.79 (t, J = 4.7, 2H, NC*H*$_2$), 4.59 (s, 2H, C*H*$_2$Ar), 5.67 (s, 1H, O*H*), 6.40 (d, J = 8.4, 1H, Ar*H*), 6.52 (ddd, J = 0.6, 5.1, 7.1, 1H, Ar*H*), 7.13-7.16 (m, 2H, 2 x Ar*H*), 7.18-7.21 (m, 1H, Ar*H*), 7.24-7.28 (m, 2H, 2 x Ar*H*), 7.31 (ddd, J = 2.0, 7.1, 8.8, 1H, Ar*H*), 8.01 (dd, J = 1.9, 5.1, 1H, Ar*H*). Spectroscopic data matched that previously reported.[138]

***N*-(2-Pyridyl)(benzyl)aminoacetaldehyde, 170**

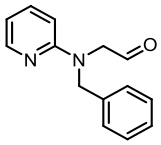

Synthesised according to general procedure G using **169** (650 mg, 2.9 mmol). The crude product was purified by column chromatography (1-2% MeOH:DCM) to yield the title aldehyde as a yellow oil (262 mg, 1.2 mmol, 40%). **TLC** – R_f = 0.60 (SiO_2, 5:95 MeOH:DCM). **^{1}H NMR** (400 MHz, $CDCl_3$) δ_H 4.10 (d, J = 1.5, 2H, NC*H*$_2$), 4.61 (s, 2H, C*H*$_2$Ar), 6.47 (d, J = 8.7, 1H, Ar*H*), 6.53 (ddd, J = 7.1, 5.1, 0.7, 1H, Ar*H*), 7.13-7.26 (m, 5H, 5 x Ar*H*), 7.34 (ddd, J = 8.9, 7.1, 1.9, 1H, Ar*H*), 8.07 (d, J = 5.1, 1H, Ar*H*), 9.40 (s, 1H, C*H*O). **^{13}C NMR** (101 MHz, $CDCl_3$) δ_C 53.6 (N*C*H$_2$), 58.6 (*C*H$_2$Ar), 106.2 (Ar*C*), 113.4 (Ar*C*), 126.9 (2 x Ar*C*), 127.6 (Ar*C*), 128.9 (2 x Ar*C*), 137.3 (Ar*C*), 138.1 (Ar*C*), 147.2 (Ar*C*), 157.6 (Ar*C*), 193.3 (*C*HO). **HR-MS** (ESI, positive ion mode) – *m/z* for $[C_{14}H_{14}N_2O+H]^+$ = 227.1184. Found 227.1178. **FTIR** (neat) – 2990, 2901, 1690.

1,10-Dibenzyl-1,10-bis(2-pyridyl)-4,7-bis(4-methoxyanilinylcarbonyl)-1,4,7,10-tetraazadecane, 162

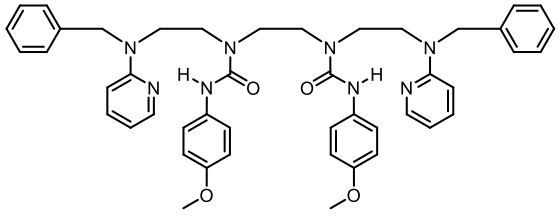

Under a dry, inert atmosphere, to a solution of ethylenediamine (0.03 mL, 0.75 mmol, 1.00 equiv., 0.10 M) in anhydrous MeOH (8 mL) was added **170** (170 mg, 0.75 mmol, 2.00 equiv.). The resulting solution was stirred for 16 h. The solution was then cooled to 0 °C and sodium borohydride (71 mg, 1.88 mmol, 6.00 equiv.) was added in one portion. The resulting white suspension was warmed to room temperature, stirred for 3 h and concentrated *in vacuo*. The residue was diluted in MeOH (10 mL)

and concentrated *in vacuo*. The crude product was diluted with deionised water and the aqueous solution extracted with DCM (3 x 5 mL). The combined organic extracts were washed with brine, dried ($MgSO_4$), filtered and concentrated *in vacuo*. Under a dry, inert atmosphere, the crude product (1.00 equiv. 0.10 M) was dissolved in anhydrous DCM (8 mL), cooled to 0 °C and 4-methoxyphenyl isocyanate (0.29 mL, 2.25 mmol, 3.00 equiv.) was added dropwise. The solution was stirred for 16 h and concentrated *in vacuo*. The crude product was purified by column chromatography (18-100% EtOAc:PE) to yield the title diurea as a white solid (117 mg, 0.15 mmol, 20%). **M.P.** 121-122 °C ($CHCl_3$). **TLC** – R_f = 0.33 (SiO_2, 70:30 EtOAc:PE). **^{1}H NMR** (500 MHz, $CDCl_3$) δ_H 3.51 (s, 4H, 2 x NC*H*$_2$), 3.58 (t, J = 7.5, 4H, 2 x NC*H*$_2$), 3.80 (s, 6H, 2 x OC*H*$_3$), 3.81-3.84 (m, 4H, 2 x NC*H*$_2$), 6.45 (d, J = 8.7, 2H, 2 x Ar*H*), 6.54 (t, J = 6.1, 2H, 2 x Ar*H*), 6.86 (d, J = 9.0, 4H, 4 x Ar*H*), 7.17 (d, J = 9.0, 4H, 4 x Ar*H*), 7.24 (t, J = 7.7, 4H, 4 x Ar*H*), 7.25 (d, J = 7.7, 2H, 2 x Ar*H*), 7.30 (t, J = 7.6, 4H, 4 x Ar*H*), 7.36-7.37 (m, 2H, 2 x Ar*H*), 8.04 (d, J = 5.2, 2H, 2 x Ar*H*), 9.39 (s, 2H, 2 x N*H*). **^{13}C NMR** (126 MHz, $CDCl_3$) δ_C 45.4 (2 x NCH_2), 47.7 (2 x NCH_2), 48.9 (2 x NCH_2), 54.0 (2 x *C*H_2Ar), 55.7 (2 x OCH_3), 107.2 (2 x Ar*C*), 112.6 (2 x Ar*C*), 114.1 (4 x Ar*C*), 124.1 (4 x Ar*C*), 126.4 (4 x Ar*C*), 127.4 (2 x Ar*C*), 129.0 (4 x Ar*C*), 133.2 (2 x Ar*C*), 137.6 (2 x Ar*C*), 138.0 (2 x Ar*C*), 147.8 (2 x Ar*C*), 156.1 (2 x Ar*C*), 157.0 (2 x *C*O), 158.1 (2 x Ar*C*). **HR-MS** (ESI, positive ion mode) – *m/z* for $[C_{46}H_{50}N_8O_4+H]^+$ = 779.4033. Found 779.4023. **FTIR** (neat) – 3299, 2988, 2915, 1655.

1,4-Bis(2-pyridyl)-1,4-diazabutane, 172

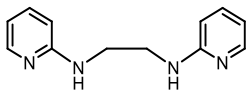

Synthesised according to general procedure M using freshly distilled ethylenediamine (1.56 mL, 23.41 mmol) and 2-fluoropyridine (1.00 mL, 11.73 mmol). The title diamine was isolated as a yellow solid (2.62 g, 19.42 mmol, 83%). **TLC** – R_f = 0.30 (SiO_2, 10:90:1 MeOH:DCM:NH_4OH). **^{1}H NMR** (400 MHz, $CDCl_3$) δ_H 2.94 (s, 4H, 2 x NC*H*$_2$), 6.38 (d, J = 8.2, 2H, 2 x Ar*H*), 6.59 (t, J = 6.0, 2H, 2 x Ar*H*), 7.43 (t, J = 7.6, 2H, 2 x Ar*H*), 8.08 (d, J = 4.9, 2H, 2 x Ar*H*). Spectroscopic data matched that previously reported.[139]

1,4-Bis(2-pyridyl)-1,4-bis(4-methoxyanilinylcarbonyl)-1,4-diazabutane, 173

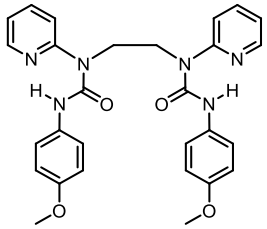

Synthesised according to general procedure B using **172** (50 mg, 0.23 mmol) and 4-methoxyphenyl isocyanate (0.09 mL, 0.70 mmol). The crude product was purified by column chromatography (2-10% MeOH:DCM) to yield the title diurea as a foamy white solid (152 mg, 0.28 mmol, 67%). **M.P.** 215-216 °C (DCM). **TLC** – R_f = 0.44 (SiO_2,

5:95 MeOH:DCM). **^{1}H NMR** (500 MHz, $CDCl_3$) δ_H 3.81 (2 x OC*H*$_3$), 4.27 (2 x NC*H*$_2$), 6.91 (d, J = 9.0, 4H, 4 x Ar*H*), 7.05 (ddd, J = 7.2, 5.0, 0.8, 2H, 2 x Ar*H*), 7.52 (d, J = 9.0, 4H, 4 x Ar*H*), 7.89 (ddd, J = 7.2, 5.0, 0.8, 2H, 2 x Ar*H*), 8.02 (dt, J = 8.6, 0.8, 2H, 2 x Ar*H*), 8.34 (ddd, J = 5.0, 2.0, 0.8, 2H, 2 x Ar*H*), 12.59 (s, 2H, 2 x N*H*). **^{13}C NMR** (126 MHz, CD_2Cl_2) δ_C 43.9 (2 x NCH_2), 56.0 (2 x OCH_3), 113.5 (2 x Ar*C*), 114.5 (4 x Ar*C*), 118.0 (2 x Ar*C*), 123.0 (4 x Ar*C*), 132.8 (2 x Ar*C*), 140.1 (2 x Ar*C*), 146.0 (2 x Ar*C*), 155.0 (2 x Ar*C*), 156.2 (2 x *C*O), 156.5 (2 x Ar*C*). **HR-MS** (ESI, positive ion mode) – *m/z* for $[C_{28}H_{28}N_6O_4+H]^+$ = 513.2250. Found 513.2237. **FTIR** (neat) – 3031, 2992, 2955, 1672.

1,7-Bis(2-pyridyl)-1,4,7-tris(4-methoxyanilinylcarbonyl)-1,4,7-triazaheptane, 174

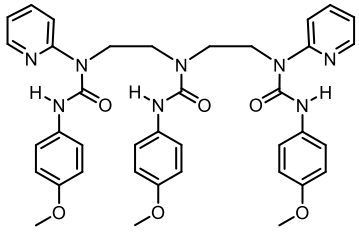

Under a dry, inert atmosphere, a solution of diethylenetriamine (0.28 mL, 2.57 mmol, 1.00 equiv.) and 2-fluoropyridine (4.4 mL, 51.5 mmol, 20.00 equiv.) was prepared. The solution was heated to 120 °C and stirred for 3 h. The solution was cooled to 0 °C and 4-methoxyphenyl isocyanate (2.0 mL, 15.45 mmol, 6.00 equiv.) was added. The solution was warmed to room temperature and stirred for a further 16 h, generating a white solid. The solid was dried *in vacuo* and purified by column chromatography (1-10% MeOH:DCM) to yield the title triurea as a white solid (308 mg, 0.44 mmol, 17%). **M.P.** 266-267 °C (DCM). **TLC** – R_f = 0.55 (SiO_2, 5:95 MeOH:DCM). **^{1}H NMR** (400 MHz, $CDCl_3$) δ_H 3.79 (t, J = 8.1, 4H, 2 x NCH_2), 3.81 (s, 9H, 3 x OCH_3), 4.17 (t, J = 8.1, 4H, 2 x NCH_2), 6.89 (d, J = 9.0, 6H, 6 x Ar*H*), 7.00 (dd, J = 5.4, 6.9, 2H, 2 x Ar*H*), 7.51 (d, J = 9.0, 4H, 4 x Ar*H*), 7.64 (d, J = 9.0, 2H, 2 x Ar*H*), 7.76 (dt, J = 1.6, 7.9, 2H, 2 x Ar*H*), 8.29 (d, J = 4.8, 2H, 2 x Ar*H*), 8.95 (s, 1H, N*H*), 12.68 (s, 2H, 2 x N*H*). **^{13}C NMR** (101 MHz, $CDCl_3$) δ_C 45.1 (2 x N*C*H$_2$), 47.1 (2 x N*C*H$_2$), 55.6 (2 x O*C*H$_3$), 55.6 (O*C*H$_3$), 112.6 (2 x Ar*C*), 114.1 (2 x Ar*C*), 114.2 (4 x Ar*C*), 117.8 (2 x Ar*C*), 121.7 (2 x Ar*C*), 122.2 (4 x Ar*C*), 132.1 (Ar*C*), 133.5 (2 x Ar*C*), 139.8 (2 x Ar*C*), 145.6 (2 x Ar*C*), 154.4 (2 x Ar*C*), 155.4 (Ar*C*), 156.0 (2 x *C*O), 156.3 (*C*O). **HR-MS** (ESI, positive ion mode) – *m/z* for $[C_{38}H_{40}N_8O_6+Na]^+$ = 727.2969. Found 727.2990. **FTIR** (neat) – 3120, 2963, 2910, 1650.

1,4,7-Tris(4-methoxyanilinylcarbonyl)-1,4,7-triazacyclononane, 175

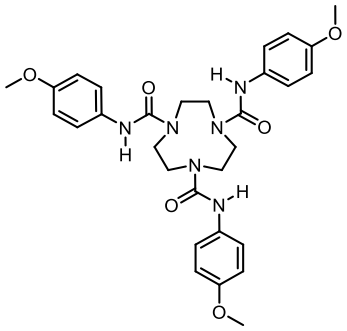

Synthesised according to general procedure B1 using TACN (20 mg, 0.15 mmol) and 4-methoxyphenyl isocyanate (0.03 mL, 0.70 mmol). The crude product was purified by column chromatography (1-10% MeOH:DCM) to yield the title triurea as a foamy white solid (78 mg, 0.14 mmol, 90%). **M.P.** 207-208 °C ($CHCl_3$). **TLC** – R_f = 0.17 (SiO_2, 5:95 MeOH:DCM). **^{1}H NMR** (400 MHz, $CDCl_3$) δ_H 3.04-3.06 (m, 6H, 6 x C*H*^{A}H^B), 3.74 (s, 9H, 3 x OC*H*$_3$), 3.94-3.96 (m, 3H, 3 x CH^A*H*^{B}), 4.40-4.42 (m, 3H, 3 x CH^A*H*^{B}), 6.49 (d, J = 9.0, 6H, 6 x Ar*H*), 6.63 (d, J = 9.0, 6H, 6 x Ar*H*), 7.84 (s, 3H, 3 x N*H*). **^{13}C NMR** (101 MHz, $CDCl_3$) δ_C 45.0 (3 x N*C*H$_2$), 47.0 (3 x N*C*H$_2$), 55.6 (3 x O*C*H$_3$), 113.6 (6 x Ar*C*), 122.7 (6 x Ar*C*), 132.3 (3 x Ar*C*), 155.4 (3 x Ar*C*), 159.0 (3 x *C*O). **HR-MS** (ESI, positive ion mode) – *m/z* for $[C_{30}H_{30}N_6O_6+Na]^+$ = 599.2594. Found 599.2565. **FTIR** (neat) – 3337, 2939, 1641.

Phenyl *N*-(4-pyridyl)carbamate, 176

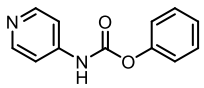

Under a dry, inert atmosphere, a solution of 4-aminopyridine (1.00 g, 10.6 mmol, 1.00 equiv., 0.10 M) in anhydrous DCM (60 mL) was cooled to 0 °C. To this solution was added phenyl chloroformate (1.47 mL, 11.7 mmol, 1.10 equiv.) dropwise followed by anhydrous TEA (2.07 mL, 14.9 mmol, 1.40 equiv.) in one portion. The resulting colourless solution was warmed to room temperature and stirred for 2 h, after which time saturated aqueous $NaHCO_3$ (60 mL) was added slowly. The aqueous phase was extracted with DCM (3 x 50 mL) and the combined organic extracts were dried ($MgSO_4$), filtered and concentrated *in vacuo* to yield the title carbamate as a white solid (1.30 g, 6.0 mmol, 57%). **TLC** – R_f = 0.25 (SiO_2, 1:99 MeOH:DCM). **^{1}H NMR** (400 MHz, $CDCl_3$) δ_H 7.19 (d, J = 8.1, 2H, 2 x Ar*H*), 7.26-7.29 (m, 1H, Ar*H*), 7.39-7.44 (m, 4H, 4 x Ar*H*), 7.99 (s, 1H, N*H*), 8.51 (d, J = 8.1, 2H, 2 x Ar*H*). Spectroscopic data matched that previously reported.[140]

1,4,7-Tris(4-pyridylaminocarbonyl)-1,4,7-triazacyclononane, 177

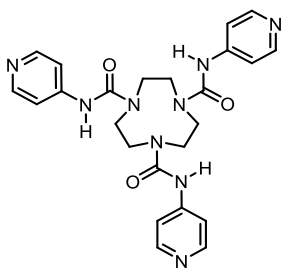

Synthesised according to general procedure B2 using TACN (50 mg, 0.39 mmol) and **176** (373 mg, 1.74 mmol). The title triurea was isolated as a white solid (132 mg, 0.27 mmol, 70%). **M.P.** decomp. >300 °C (MeCN). **TLC** – R_f = 0.08 (SiO_2, 10:90:1 MeOH:DCM:NH_4OH). **^{1}H NMR** (400 MHz, DMSO) δ_H 3.59 (s, 12H, 6 x NC*H*$_2$), 7.38 (d, J = 5.8, 6H, 6 x Ar*H*), 8.21 (d, J = 5.8, 6H, 6 x Ar*H*), 8.67 (s, 3H, 3 x N*H*). **^{13}C**

NMR (101 MHz, DMSO) δ_C 45.7 (6 x N*C*H_2), 114.0 (6 x Ar*C*), 150.0 (6 x Ar*C*), 156.2 (3 x *C*O). **HR-MS** (ESI, positive ion mode) – *m/z* for $[C_{24}H_{27}N_9O_3+Na]^+$ = 512.2135. Found 512.2129. **FTIR** (neat) – 3288, 2976, 2928, 1644.

1,4,7-Tris(4-trifluoromethylanilinylcarbonyl)-1,4,7-triazacyclononane, 178

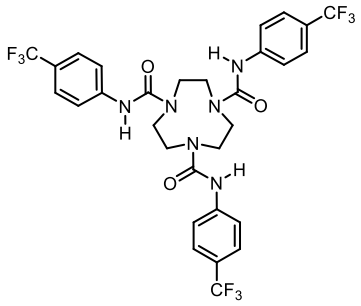

Synthesised according to general procedure B1 using TACN (50 mg, 0.39 mmol) and 4-(trifluoromethyl)-phenyl isocyanate (0.25 mL, 1.74 mmol). The title triurea was isolated as a white solid (132 mg, 0.27 mmol, 56%). **M.P.** decomp. >300 °C (MeCN/DMF). **TLC** – R_f = 0.36 (SiO_2, 10:90 MeOH:DCM). **^{1}H NMR** (500 MHz, 1:1 CD_3OD:CD_2Cl_2) δ_H 3.42 (s, 12H, 6 x N*C*H_2), 6.78 (d, J = 8.3, 6H, 6 x Ar*H*), 7.05 (d, J = 8.3, 6H, 6 x Ar*H*), 8.06 (s, 3H, 3 x N*H*). **^{13}C NMR** (126 MHz, 1:1 CD_3OD:CD_2Cl_2) δ_C 48.0 (6 x N*C*H_2), 118.8 (6 x Ar*C*), 122.4 (q, J = 293.5, 3 x *C*F_3), 124.1 (6 x Ar*C*), 134.1 (q, J = 45.8, 3 x Ar*C*), 141.0 (3 x Ar*C*), 157.6 (3 x Ar*C*). **^{19}F NMR** (377 MHz, 1:1 CD_3OD:CD_2Cl_2) δ_F −62.5 (3 x C*F*$_3$). **HR-MS** (MALDI) – *m/z* for $[C_{30}H_{27}F_9N_6O_3+Na]^+$ = 713.1899. Found 713.1893. **FTIR** (neat) – 3338, 2990, 2907, 1648.

1,4,7-Tris(4-cyanoanilinylcarbonyl)-1,4,7-triazacyclononane, 179

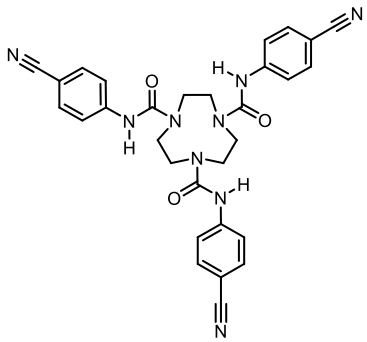

Synthesised according to general procedure B1 using TACN (50 mg, 0.39 mmol) and 4-cyanophenyl isocyanate (251 mg, 1.74 mmol). The title triurea was isolated as a white solid (72 mg, 0.13 mmol, 33%). **M.P.** decomp. >300 °C (MeCN/DMF). **TLC** – R_f = 0.54 (SiO_2, 10:90 MeOH:DCM). **^{1}H NMR** (500 MHz, 1:1 CD_3OD:CD_2Cl_2) δ_H 3.42 (s, 12H, 6 x N*C*H_2), 7.60 (d, J = 7.5, 6H, 6 x Ar*H*), 7.94 (d, J = 7.5, 6H, 6 x Ar*H*), 8.10 (s, 3H, 3 x N*H*). **^{13}C NMR** (126 MHz, 1:1 CD_3OD:CD_2Cl_2) δ_C 47.1 (6 x N*C*H_2), 110.5 (3 x Ar*C*), 118.8 (3 x *C*≡N), 120.8 (6 x Ar*C*), 133.5 (6 x Ar*C*), 142.2 (3 x Ar*C*), 158.0 (3 x Ar*C*). **HR-MS** (ESI, positive ion mode) – *m/z* for $[C_{30}H_{27}F_9N_9O_3+H]^+$ = 562.2315. Found 562.2322. **FTIR** (neat) – 3338, 2982, 2216, 1635.

1,4,7-Tris(4-chloroanilinylcarbonyl)-1,4,7-triazacyclononane, 180

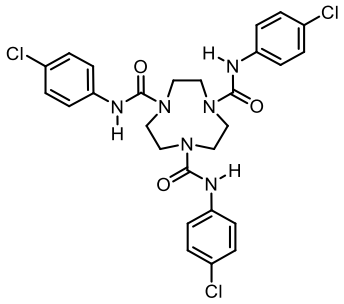

Synthesised according to general procedure B1 using TACN (50 mg, 0.39 mmol) and 4-chlorophenyl isocyanate (267 mg, 1.74 mmol). The title triurea was isolated as a white solid (267 mg, 0.18 mmol, 45%). **M.P.** decomp. >300 °C (MeCN). **TLC** – R_f = 0.36 (SiO_2, 10:90 MeOH:DCM). **^{1}H NMR** (400 MHz, $CDCl_3$) δ_H 3.02-3.04 (m, 3H, 3 x C*H*^{A}H^B), 3.11-3.15 (m, 3H, 3 x C*H*^{A}H^B), 3.89-3.91 (m, 3H, 3 x CH^A*H*^{B}), 4.34-4.37 (m, 3H, 3 x CH^A*H*^{B}), 6.58 (d, J = 8.9, 6H, 6 x Ar*H*), 6.85 (d, J = 8.9, 6H, 6 x Ar*H*), 7.90 (s, 3H, 3 x N*H*). **^{13}C NMR** (101 MHz, $CDCl_3$) δ_C 44.9 (3 x N*C*H$_2$), 46.9 (3 x N*C*H$_2$), 122.3 (6 x Ar*C*), 128.3 (3 x Ar*C*), 128.4 (6 x Ar*C*), 137.4 (3 x Ar*C*), 158.7 (3 x *C*O). **HR-MS** (MALDI) – *m/z* for $[C_{27}H_{27}Cl_3N_6O_3+Na]^+$ = 611.1108. Found 611.1102. **FTIR** (neat) – 3257, 2966, 2934, 1641.

1,4,7-Tris(4-(ethylcarboxy)anilinylcarbonyl)-1,4,7-triazacyclononane, 181

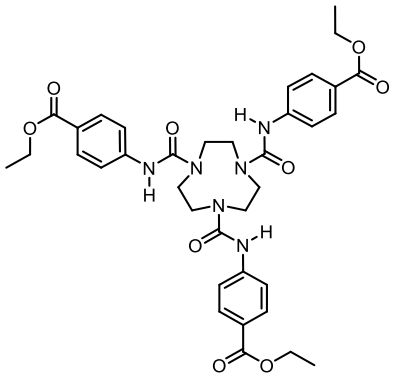

Synthesised according to general procedure B1 using TACN (50 mg, 0.37 mmol) and ethyl 4-isocyanatobenzoate (333 mg, 1.74 mmol). The residue was washed with cold acetonitrile and air-dried to give the title triurea as a white solid (272 mg, 0.30 mmol, 80%). **M.P.** 189-190 °C ($CHCl_3$). **TLC** – R_f = 0.35 (SiO_2, 5:95 MeOH:DCM). **^{1}H NMR** (400 MHz, $CDCl_3$) δ_H 1.37 (t, J = 7.1, 9H, 3 x C*H*$_3$), 3.08-3.15 (m, 6H, 6 x C*H*^{A}H^B), 4.00-4.02 (m, 3H, 3 x CH^A*H*^{B}), 4.32 (q, J = 7.1, 6H, 3 x OC*H*$_2$), 4.44-4.47 (m, 3H, 3 x CH^A*H*^{B}), 6.91 (d, J = 8.9, 6H, 6 x Ar*H*), 7.61 (d, J = 8.9, 6H, 6 x Ar*H*), 8.19 (s, 3H, 3 x N*H*). **^{13}C NMR** (101 MHz, $CDCl_3$) δ_C 14.4 (3 x *C*H$_3$), 44.9 (3 x N*C*H$_2$), 46.9 (3 x N*C*H$_2$), 60.8 (3 x O*C*H$_2$), 119.5 (6 x Ar*C*), 124.9 (3 x Ar*C*), 130.2 (6 x Ar*C*), 143.0 (3 x Ar*C*), 158.3 (3 x *C*O), 166.3 (3 x *C*O). **HR-MS** (ESI, positive ion mode) – *m/z* for $[C_{36}H_{42}N_6O_9+Na]^+$ = 725.2911. Found 725.2901. **FTIR** (neat) – 3326, 2995, 2958, 1714, 1649.

1,3-Ditosyloxy-2-tosyloxymethyl-2-methylpropane, 182

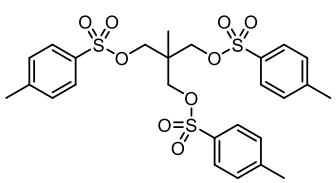

Under a dry, inert atmosphere, a solution of trimethylolethane (2.0 g, 16.7 mmol, 1.00 equiv., 0.28 M) in anhydrous DCM (60 mL) was prepared. The solution was cooled to 0 °C and tosyl chloride (14.3 g, 74.9 mmol, 4.50 equiv.) was added over three portions. Triethylamine (13.9 mL, 100.0 mmol, 6.00 equiv.) was then added and the resulting solution was

warmed to room temperature and stirred for 2 h. The solution was diluted with saturated aqueous $NaHCO_3$ and the aqueous phase was extracted with DCM (3 x 50 mL). The combined organic extracts were washed with brine, dried ($MgSO_4$), filtered and concentrated *in vacuo* to give the title tritosylate as a white solid (6.9 g, 11.8 mmol, 71%). **TLC** – R_f = 0.10 (SiO_2, 20:80 EtOAc:PE). **^{1}H NMR** (400 MHz, $CDCl_3$) δ_H 2.40 (s, 9H, 3 x C*H*$_3$), 3.69 (s, 6H, 3 x OC*H*$_2$), 7.29 (d, J = 8.0, 6H, 6 x Ar*H*), 7.64 (d, J = 8.0, 6H, 6 x Ar*H*). Spectroscopic data matched that previously reported.[141]

1,3-Diazido-2-azidomethyl-2-methylpropane, 184

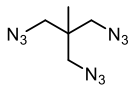

Under a dry, inert atmosphere, a solution of **182** (100 mg, 0.51 mmol, 1.00 equiv., 0.10 M) in anhydrous DMF (5 mL) was prepared. To this solution was added sodium azide (166 mg, 2.55 mmol, 5.00 equiv.) over three portions and the resulting solution was stirred for 16 h behind a blast shield at room temperature. The solution was then poured onto cold water (25 mL) and the aqueous phase was extracted with Et_2O (3 x 5 mL). The combined organic phases were dried ($MgSO_4$), filtered and concentrated to half their volume *in vacuo* to give the crude triazide, which was used without further purification.

1,3-Diamino-2-aminomethyl-2-methylpropane, 185

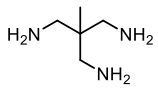

Under a dry, inert atmosphere, a solution of **184** (25 mg, 0.13 mmol, 1.00 equiv., 0.07 M) in anhydrous THF (2 mL) was prepared. The solution was cooled to 0 °C and $LiAlH_4$ (50 mg, 1.30 mmol, 10.00 equiv.) was added in one portion. The suspension was warmed to room temperature and stirred for 16 h. The solution was cooled to 0 °C and aqueous NaOH (2 mL, 1.00 M) was added dropwise. The aqueous phase was then extracted with Et_2O (3 x 5 mL) and the combined organic extracts were washed with brine, dried ($MgSO_4$), filtered and concentrated *in vacuo* to give the title triamine as a colourless oil (7 mg, 0.06 mmol, 50%). **TLC** – R_f = 0.07 (SiO_2, 10:90:1 MeOH:DCM:NH_4OH). **^{1}H NMR** (400 MHz, D_2O) δ_H 1.21 (s, 3H, C*H*$_3$), 3.24 (s, 6H, 3 x NC*H*$_2$). Spectroscopic data matched that previously reported.[141]

1,3,5-Tris(trifluoroacetamidomethyl)-2,4,6-triethylbenzene, 187

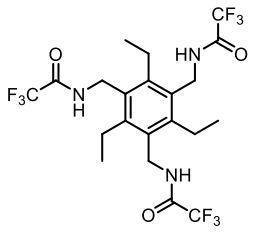

Under a dry, inert atmosphere, a solution of sodium hydride (60% wt. in mineral oil, 1.36 g, 34.14 mmol, 6.00 equiv.) in anhydrous DMF (15 mL) was prepared. The suspension was cooled to 0 °C and a solution of trifluoroacetamide (5.77 g, 51.0 mmol, 9.00 equiv.) in anhydrous DMF (15 mL) was added dropwise. The resulting suspension was warmed to room temperature and stirred for 1 h. To the suspension was added 1,3,5-tris(bromomethyl)-2,4,6-triethylbenzene (2.50 g, 5.69 mmol, 1.00 equiv., 0.19 M) and the suspension was stirred for 16 h. Aqueous HCl (50 mL, 0.50 M) was added and a white precipitate formed. The suspension was filtered and the residue was washed with deionised water (50 mL) and dried *in vacuo* to give the title tris(trifluoroacetamide) as a white solid (1.38 g, 2.56 mmol, 45%). **TLC** – R_f = 0.54 (SiO_2, 5:95 MeOH:DCM). **^{1}H NMR** (400 MHz, $CDCl_3$) δ_H 1.20 (t, J = 5.4, 9H, 3 x C*H*$_3$), 2.90 (q, J = 5.4, 6H, 3 x C*H*$_2$Ar), 4.47 (s, 6H, 3 x C*H*$_2$Ar), 9.20 (s, 3H, 3 x N*H*). Spectroscopic data matched that previously reported.[142]

1,3,5-Tris(aminomethyl)-2,4,6-triethylbenzene, 188

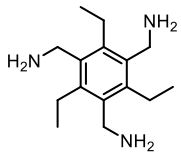

Synthesised according to general procedure H using **187** (1.0 g, 1.86 mmol). The title triamine was isolated as a colourless oil (334 mg, 1.34 mmol, 72%). **TLC** – R_f = 0.16 (SiO_2, 5:95:1 MeOH:DCM:NH_4OH). **^{1}H NMR** (400 MHz, $CDCl_3$) δ_H 1.21 (t, J = 5.1, 9H, 3 x C*H*$_3$), 2.86 (q, J = 5.4, 6H, 3 x C*H*$_2$Ar), 3.43 (s, 6H, 3 x C*H*$_2$Ar) . Spectroscopic data matched that previously reported.[142]

***N*-Methyl-*N*'-phenyl thiourea, 191**

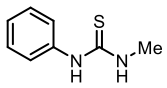

Synthesised according to general procedure B1 using methylammonium chloride (570 mg, 8.45 mmol), triethylamine (1.18 mL, 8.45 equiv.) and phenyl isothiocyanate (1.0 g, 7.68 mmol). The crude product was diluted in Et_2O and filtered. The filtrate was concentrated *in vacuo* to yield the title thiourea as a yellow solid (701 mg, 4.22 mmol, 55%). **TLC** – R_f = 0.23 (SiO_2, 5:95 MeOH:DCM). **^{1}H NMR** (400 MHz, $CDCl_3$) δ_H 3.06 (d, J = 4.6, 3H, NC*H*$_3$), 6.00 (s, 1H, N*H*), 7.15 (d, J = 8.0, 2H, 2 x Ar*H*), 7.23 (tt, J = 1.1, 7.5, 1H, Ar*H*), 7.36 (t, J = 8.0, 2H, 2 x Ar*H*), 7.93 (s, 1H, N*H*). Spectroscopic data matched that previously reported.[143]

_N_-Methyl-_N_'-phenyl-_S_-methyl isothiourea, 192

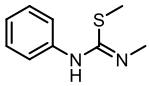

Under a dry, inert atmosphere, a solution of **191** (700 mg, 4.21 mmol, 1.00 equiv., 0.10 M) in anhydrous acetone (42 mL) was prepared. To this solution was added methyl iodide (0.39 mL, 6.32 mmol, 1.50 equiv.) and the resulting solution was heated to 60 °C and stirred for 4 h. The solution was concentrated *in vacuo* and suspended in Et_2O (50 mL). The suspension was filtered and the residue was washed with Et_2O (25 mL). The residue was then dissolved in H_2O:THF mixture (1:1, 25 mL) and basified with aqueous K_2CO_3 (1.00 M) until the solution reached pH = 10. The solution was then extracted with DCM (3 x 25 mL) and the combined organic extracts were washed with brine, dried ($MgSO_4$), filtered and concentrated *in vacuo* to give the title isothiourea as a yellow solid (319 mg, 1.77 mmol, 42%). **TLC** – R_f = 0.40 (SiO_2, 10:90 MeOH:DCM). **^{1}H NMR** (400 MHz, $CDCl_3$) δ_H 0.80 (s, 3H, NC*H*$_3$), 2.40 (s, 3H, SC*H*$_3$), 7.17 (d, J = 7.8, 2H, 2 x Ar*H*), 7.26 (m, 1H, Ar*H*), 7.33 (t, J = 7.8, 2H, 2 x Ar*H*). Spectroscopic data matched that previously reported.[143]

1,4,7,10-Tetrakis(4-methoxyanilinylcarbonyl)-1,4,7,10-tetraazacyclododecane, 194

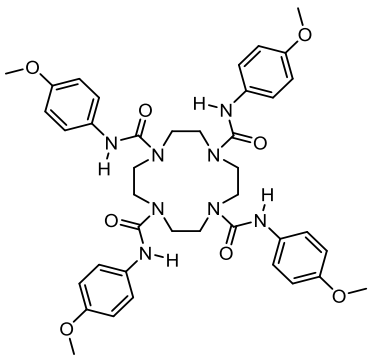

Synthesised according to general procedure B using cyclen (100 mg, 0.58 mmol) and 4-methoxyphenyl isocyanate (0.45 mL, 3.48 mmol). The white suspension was filtered and the residue washed with ice-cold DCM to give the title tetraurea as a white solid (758 mg, 0.99 mmol, 85%). **M.P.** 206-207 °C (DCM). **TLC** – R_f = 0.42 (SiO_2, 10:90 MeOH:DCM). **^{1}H NMR** (400 MHz, $CDCl_3$) δ_H 3.65 (s, 16H, 8 x NC*H*$_2$), 3.75 (s, 12H, 4 x OC*H*$_3$), 6.71 (d, J = 9.1, 8H, 8 x Ar*H*), 7.09 (d, J = 9.1, 8H, 8 x Ar*H*), 7.49 (s, 4H, 4 x N*H*). **^{13}C NMR** (101 MHz, $CDCl_3$) δ_C 49.7 (8 x N*C*H$_2$), 55.6 (4 x O*C*H$_3$), 114.1 (8 x Ar*C*), 122.8 (8 x Ar*C*), 131.6 (4 x Ar*C*), 156.2 (4 x Ar*C*), 158.7 (4 x *C*O). **HR-MS** (ESI, positive ion mode) – *m/z* for $[C_{40}H_{48}N_8O_8+Na]^+$ = 791.3493. Found 791.3494. **FTIR** (neat) – 3514, 1633.

1,4,7,10-Tetrakis(2-(methylcarboxy)anilinylcarbonyl)-1,4,7,10-tetraazacyclododecane, 195

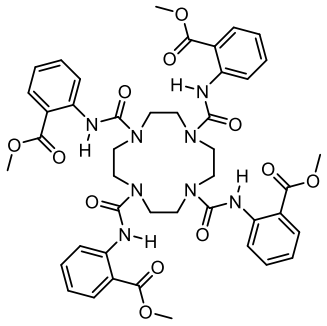

Synthesised according to general procedure B using cyclen (200 mg, 1.16 mmol) and methyl 2-isocyanatobenzoate (1234 mg, 6.97 mmol, 6.00 equiv.) The crude product was triturated with acetone and dried *in vacuo* to give the title tetraurea as a white solid (260 mg, 0.30 mmol, 25%). **M.P.** = 236-237 °C (acetone/PE). **TLC** – R_f = 0.56 (SiO_2, 90:10 EtOAc:PE). **^{1}H NMR** (400 MHz, $CDCl_3$) δ_H 3.51 (s, 12H, 4 x OC*H*$_3$), 3.78 (s, 16H, 8 x NC*H*$_2$), 6.95 (dt, J = 1.1, 7.7, 4H, 4 x Ar*H*), 7.47 (ddd, J = 1.7, 7.2, 8.8, 4H, 4 x Ar*H*), 7.92 (dd, J = 1.7, 8.0, 4H, 4 x Ar*H*), 8.52 (d, J = 8.4, 4H, 4 x Ar*H*), 10.79 (s, 4H, 4 x N*H*). **^{13}C NMR** (101 MHz, $CDCl_3$) δ_C 51.3 (8 x N*C*H$_2$), 56.2 (4 x O*C*H$_3$), 114.5 (4 x Ar*C*), 120.3 (4 x Ar*C*), 121.0 (4 x Ar*C*), 130.6 (4 x Ar*C*), 134.4 (4 x Ar*C*), 143.4 (4 x Ar*C*), 156.6 (4 x *C*O), 169.0 (4 x *C*O). **HR-MS** (ESI, positive ion mode) – *m/z* for $[C_{44}H_{48}N_8O_{12}+Na]^+$ = 903.3289. Found 903.3255. **FTIR** (neat) – 3324, 2967, 2930, 1720, 1642.

1,4,7,10-Tetrakis(2-(hydroxylmethyl)anilinylcarbonyl)-1,4,7,10-tetraazacyclododecane, 196

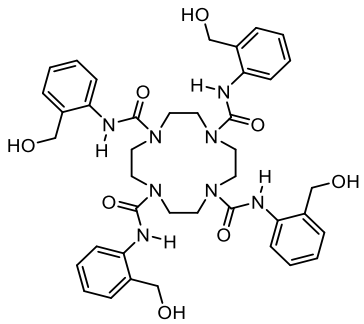

Under a dry, inert atmosphere, a solution of **195** (70 mg, 0.08 mmol, 1.00 equiv., 0.10 M) in anhydrous THF (1 mL) was cooled to 0 °C. To this solution was added $LiBH_4$ (14 mg, 0.63 mmol, 8.00 equiv.) in one portion and the resulting solution was stirred for 16 h at room temperature. The reaction mixture was concentrated *in vacuo* and the crude product diluted with MeOH (1 mL) and saturated aqueous $KHSO_4$ (1 mL). The aqueous phase was extracted with ethyl acetate (3 x 2 mL) and the combined organic extracts were washed with brine, dried ($MgSO_4$), filtered and concentrated *in vacuo* to yield the title tetrol as a white solid (46 mg, 0.06 mmol, 76%). **M.P.** 225-226 °C (THF). **TLC** – R_f = 0.40 (SiO_2, 90:10 EtOAc:PE). **^{1}H NMR** (400 MHz, DMSO) δ_H 3.70 (s, 16H, 8 x NC*H*$_2$), 4.54 (s, 8H, 4 x C*H*$_2$Ar), 5.59 (s, 4H, 4 x O*H*), 7.03 (t, J = 7.7, 4H, 4 x Ar*H*), 7.19 (t, J = 7.7, 4H, 4 x Ar*H*), 7.28 (d, J = 7.4, 4H, 4 x Ar*H*), 7.60 (d, J = 8.0, 4H, 4 x Ar*H*), 8.62 (s, 4H, 4 x N*H*). **^{13}C NMR** (101 MHz, DMSO) δ_C 48.2 (8 x N*C*H$_2$), 61.3 (4 x O*C*H$_2$), 123.2 (4 x Ar*C*), 123.2 (4 x Ar*C*), 127.2 (4 x Ar*C*), 127.5 (4 x Ar*C*), 133.3 (4 x Ar*C*), 137.7 (4 x Ar*C*), 155.8 (4 x *C*O). **HR-MS** (MALDI) – *m/z* for $[C_{40}H_{48}N_8O_8+Na]^+$ = 791.3493. Found 791.3487. **FTIR** (neat) – 3395, 3330, 2988, 2946, 1678.

1,4,7,10,13,16-Hexakis(4-methoxyanilinylcarbonyl)-1,4,7,10,13,16-hexaazacyclooctadecane, 199

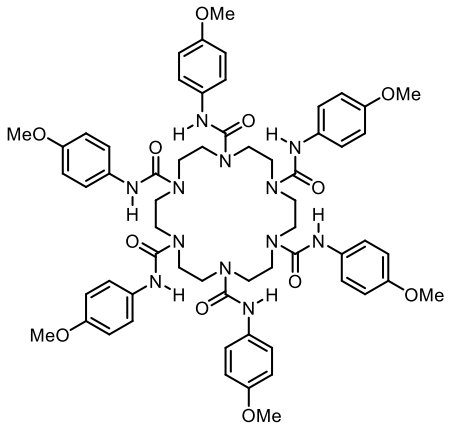

Synthesised according to general procedure B using hexacyclen (100 mg, 0.39 mmol) and 4-methoxyphenyl isocyanate (0.45 mL, 3.48 mmol) dropwise. The white suspension was filtered and the residue washed with ice-cold DCM to give the title hexaurea as a white solid (398 mg, 0.35 mmol, 88%). **M.P.** 238-239 °C (DCM). **TLC** – R_f = 0.51 (SiO_2, 10:90 MeOH:DCM). **^{1}H NMR** (400 MHz, CD_2Cl_2) δ_H 3.53 (s, 12H, 12 x CH^AH^B), 3.66 (s, 12H, 12 x CH^AH^B), 3.74 (s, 18H, 18 x OCH_3), 6.73 (d, J = 9.1, 12H, 12 x Ar*H*), 7.38 (d, J = 9.1, 12H, 12 x Ar*H*), 8.73 (s, 6H, 6 x N*H*). **^{13}C NMR** (101 MHz, $(CD_3)_2SO$) δ_C 46.1 (12 x NCH_2), 55.1 (6 x OCH_3), 113.6 (6 x Ar*C*), 113.9 (6 x Ar*C*), 119.8 (6 x Ar*C*), 121.4 (6 x Ar*C*), 132.1 (3 x Ar*C*), 133.2 (3 x Ar*C*), 154.1 (3 x Ar*C*), 154.7 (3 x Ar*C*), 154.7 (3 x *C*O), 155.6 (3 x *C*O). **HR-MS** (ESI, positive ion mode) – *m/z* for $[C_{60}H_{72}N_{12}O_{12}+Na]^+$ = 1175.5290. Found 1175.5286. **FTIR** (neat) – 3411, 2962, 1653.

Dimethyl 2,5-dibromoadipoate, 201

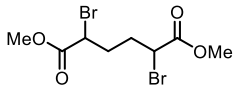

A three-necked round-bottomed flask was appended with a condenser attached to a conical flask charged with aqueous NaOH/$Na_2S_2O_3$ (1.00 M NaOH/15% wt. $Na_2S_2O_3$). Adipoyl chloride (5.0 mL, 34.4 mmol, 1.00 equiv.) was added to the flask and then heated to 75 °C. Bromine (3.5 mL, 68.8 mmol, 2.00 equiv.) was then added over 2 h by use of a dropping funnel and the resulting solution was stirred for a further 4 h. The solution was cooled to 0 °C and anhydrous MeOH (14.0 mL, 344.0 mmol, 10.00 equiv.) was added dropwise. The resulting solution was stirred for 1 h and quenched with aqueous $Na_2S_2O_3$ (250 mL, 1.00 M). The aqueous phase was extracted with Et_2O (3 x 100 mL) and the combined organic extracts were washed with aqueous $Na_2S_2O_3$ (1.00 M), brine, dried (Na_2SO_4), filtered and concentrated *in vacuo* to give the title diester as a colourless oil, some of which crystallised on standing (9.4 g, 28.2 mmol, 82%). **TLC** – R_f = 0.58 (SiO_2, 50:50 EtOAc:PE). **^{1}H NMR** (400 MHz, $CDCl_3$) δ_H 2.06-2.36 (m, 4H, 2 x CH_2), 3.82 (s, 6H, 2 x OCH_3), 4.24-4.30 (m, 2H, 2 x C*H*Br). Spectroscopic data matched that previously reported.[144]

Dimethyl *N*-benzylpyrrolidine-2,5-dicarboxylate, 202

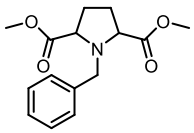

In a round-bottomed flask, a solution of **201** (4.57 g, 13.72 mmol, 1.00 equiv., 0.10 M) in toluene (69 mL) was prepared. To this solution was added deionised water (68 mL), K_2CO_3 (9.51 g, 68.83 mmol, 5.00 equiv.) and freshly distilled benzylamine (2.10 mL, 19.21 mmol, 1.40 equiv.). The mixture was heated to reflux and stirred for 16 h. The mixture was cooled to room temperature and the aqueous phase was extracted with EtOAc (3 x 50 mL). The combined organic extracts were washed with brine, dried ($MgSO_4$), filtered and concentrated *in vacuo*. The crude products were then purified by column chromatography (20-40% EtOAc:PE) to give the desired pyrrolidines, *cis*-**202** (1.33 g, 4.80 mmol, 35%) and *trans*-**202** (1.56 g, 5.63 mmol, 41%) as colourless oils. **TLC** – R_f (*trans*) = 0.16 (SiO_2, 20:80 EtOAc:PE). R_f (*cis*) = 0.25 (SiO_2, 20:80 EtOAc:PE). **^{1}H NMR** (400 MHz, $CDCl_3$) δ_H (*trans*) 1.88-1.95 (m, 2H, 2 x C*H*), 2.26-2.34 (m, 2H, 2 x C*H*), 3.63 (s, 6H, 2 x OCH_3), 3.77 (d, J = 13.4, 1H, CH^AH^{B}Ar), 3.81-3.85 (m, 2H, 2 x C(O)C*H*), 3.95 (d, J = 13.4, 1H, CH^AH^BAr), 7.21-7.32 (m, 5H, 5 x Ar*H*). δ_H (*cis*) 2.04-2.07 (m, 4H, 2 x CH_2), 3.40-3.44 (m, 2H, 2 x C(O)C*H*), 3.57 (s, 6H, 2 x OCH_3), 3.91 (s, 2H, CH_2Ar), 7.25-7.33 (m, 5H, 5 x Ar*H*). Spectroscopic data matched that previously reported.[144]

Tetramethyl *N*-benzylpyrrolidine-2,2,5,5-tetracarboxylate, 203

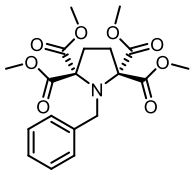

Under a dry, inert atmosphere, a solution of diisopropylamine (4.89 mL, 34.92 mmol, 6.00 equiv.) in anhydrous THF (58 mL) was cooled to 0 °C. To this solution was added ^{n}BuLi (1.60 M in hexane, 17.5 mL, 17.46 mmol, 3.00 equiv.) dropwise and the resulting solution was stirred for 30 minutes. The solution was cooled to −78 °C and **202** (1.61 g, 5.82 mmol, 1.00 equiv., 0.05 M) in anhydrous THF (58 mL) was added dropwise. The solution was stirred for 30 minutes at −78 °C and methyl chloroformate (2.70 mL, 34.92 mmol, 3.00 equiv.) was added dropwise. The solution was then stirred for a further 2 h and quenched with saturated aqueous NH_4Cl (100 mL). The aqueous phase was then extracted with DCM (3 x 50 mL) and the combined organic extracts were washed with brine, dried (Na_2SO_4), filtered and concentrated *in vacuo*. The crude product was then purified by column chromatography (30-60% EtOAc:PE) to give the title tetraester as a white solid (984 mg, 2.50 mmol, 43%). **M.P.** 145-146 °C (DCM). **TLC** – R_f = 0.25 (SiO_2, 50:50 EtOAc:PE). **^{1}H NMR** (400 MHz, $CDCl_3$) δ_H 2.48 (s, 4H, 2 x CH_2), 3.51 (s, 12H, 4 x OCH_3), 3.67 (s, 2H, CH_2Ar), 7.11 (t, J = 7.8, 1H, Ar*H*), 7.22 (t, J = 7.8, 2H, 2 x Ar*H*), 7.30 (d, J = 7.4, 2H, 2 x Ar*H*). **^{13}C NMR** (101 MHz, $CDCl_3$) δ_C 33.3 (2 x *C*H$_2$), 50.3 (*C*H$_2$Ar), 52.4 (4 x O*C*H$_3$), 75.0 (2 x N*C*$_{quat.}$), 126.5 (Ar*C*), 127.8 (2 x Ar*C*), 127.8 (2 x Ar*C*), 139.9 (Ar*C*), 170.5 (4 x *C*O). **HR-MS** (ESI, positive ion mode) – *m/z* for $[C_{19}H_{23}NO_8+H]^+$ = 394.4000. Found 394.4001. **FTIR** (KBr) – 2973, 2891, 1748.

***cis*-Dimethyl pyrrolidine-2,5-dicarboxylate, *cis*-205**

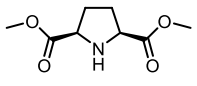

Synthesised according to general procedure S using ***cis*-202** (1.0 g, 3.61 mmol). The title secondary amine was isolated as a colourless oil (608 mg, 3.25 mmol, 90%). **TLC** – R_f = 0.10 (SiO_2, EtOAc). **^{1}H NMR** (400 MHz, $CDCl_3$) δ_H 1.97-2.03 (m, 4H, 2 x CH_2), 3.23-3.29 (m, 2H, 2 x C(O)C*H*), 3.49 (s, 6H, 2 x OCH_3). Spectroscopic data matched that previously reported.[145]

***trans*-Dimethyl pyrrolidine-2,5-dicarboxylate, *trans*-205**

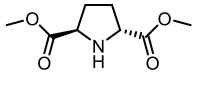

Synthesised according to general procedure S using ***trans*-202** (1.0 g, 3.61 mmol). The title secondary amine was isolated as a colourless oil (608 mg, 3.25 mmol, 90%). **TLC** – R_f = 0.11 (SiO_2, EtOAc). **^{1}H NMR** (400 MHz, $CDCl_3$) δ_H 1.88-1.96 (m, 2H, 2 x C*H*), 2.20-2.29 (m, 2H, 2 x C*H*), 3.60 (s, 6H, 2 x OCH_3), 3.67-3.72 (m, 2H, 2 x C(O)C*H*). Spectroscopic data matched that previously reported.[146]

***cis*-Dimethyl *N*-benzyloxycarbonylpyrrolidine-2,5-dicarboxylate, *cis*-206**

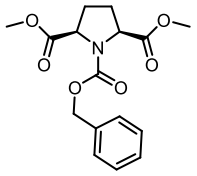

Under a dry, inert atmosphere, a solution of ***cis*-205** (579 mg, 3.09 mmol, 1.00 equiv., 0.10 M) in anhydrous THF (31 mL) was prepared. To this solution was added DIPEA (0.59 mL, 3.40 mmol, 1.10 equiv.) and the solution was cooled to 0 °C. Benzyl chloroformate (0.49 mL, 3.40 mmol, 1.10 equiv.) was added dropwise and the resulting solution was warmed to room temperature and stirred for 4 h. Saturated aqueous $NaHCO_3$ (50 mL) was added and the aqueous phase was extracted with DCM (3 x 25 mL). The combined organic extracts were then washed with brine, dried (Na_2SO_4), filtered and concentrated *in vacuo*. The crude product was then purified by column chromatography (20-40% EtOAc:PE) to give the desired carbamate as a white solid (636 mg, 1.98 mmol, 64%). **TLC** – R_f = 0.16 (SiO_2, 20:80 EtOAc:PE). **^{1}H NMR** (400 MHz, $CDCl_3$) δ_H 2.10-2.15 (m, 4H, 2 x CH_2), 3.67-3.72 (m, 2H, 2 x C(O)C*H*), 3.70 (s, 6H, 2 x OCH_3), 5.02 (s, 2H, CH_2Ar), 7.24-7.33 (m, 5H, 5 x Ar*H*). Spectroscopic data matched that previously reported.[147]

***trans*-Dimethyl *N*-benzyloxycarbonylpyrrolidine-2,5-dicarboxylate, *trans*-206**

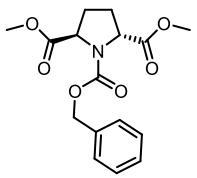

Under a dry, inert atmosphere, a solution of ***trans*-205** (600 mg, 3.21 mmol, 1.00 equiv., 0.10 M) in anhydrous THF (32 mL) was prepared. To this solution was added DIPEA (0.61 mL, 3.53 mmol, 1.10 equiv.) and the solution was cooled to 0 °C. Benzyl chloroformate (0.50 mL, 3.53 mmol, 1.10 equiv.) was

added dropwise and the resulting solution was warmed to room temperature and stirred for 4 h. Saturated aqueous $NaHCO_3$ (50 mL) was added and the aqueous phase was extracted with DCM (3 x 25 mL). The combined organic extracts were then washed with brine, dried (Na_2SO_4), filtered and concentrated *in vacuo*. The crude product was then purified by column chromatography (20-40% EtOAc:PE) to give the desired carbamate as a white solid (712 mg, 2.22 mmol, 69%). **TLC** – R_f = 0.12 (SiO_2, 20:80 EtOAc:PE). **^{1}H NMR** (400 MHz, $CDCl_3$) δ_H 1.90-1.96 (m, 2H, 2 x C*H*), 2.32-2.35 (m, 2H, 2 x C*H*), 3.81 (s, 6H, 2 x OCH_3), 3.81-3.85 (m, 2H, 2 x C(O)C*H*), 5.01 (d, J = 12.4, 1H, CH^AH^{B}Ar), 5.25 (d, J = 12.4, 1H, CH^AH^BAr), 7.21-7.32 (m, 5H, 5 x Ar*H*). Spectroscopic data matched that previously reported.[147]

Tetramethyl *N*-benzyloxycarbonylpyrrolidine-2,2,5,5-tetracarboxylate, 207

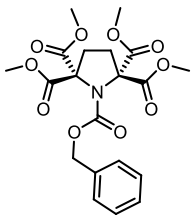

Under a dry, inert atmosphere, a solution of diisopropylamine (1.43 mL, 10.2 mmol, 6.00 equiv.) in anhydrous THF (17 mL) was cooled to 0 °C. To this solution was added ^{n}BuLi (1.60 M in hexane, 3.2 mL, 5.1 mmol, 3.00 equiv.) dropwise and the resulting solution was stirred for 30 minutes. The solution was cooled to −78 °C and **206** (545 mg, 1.70 mmol, 1.00 equiv., 0.05 M) in anhydrous THF (17 mL) was added dropwise. The solution was stirred for 30 minutes at −78 °C and methyl chloroformate (0.79 mL, 10.2 mmol, 6.00 equiv.) was added dropwise. The solution was then stirred for a further 2 h and quenched with saturated aqueous NH_4Cl (50 mL). The aqueous phase was then extracted with DCM (3 x 20 mL) and the combined organic extracts were washed with brine, dried (Na_2SO_4), filtered and concentrated *in vacuo*. The crude product was then purified by column chromatography (2-4% MeOH:DCM to give the title tetraester as a white solid (512 mg, 1.17 mmol, 69%). **M.P.** 180-181 °C (DCM). **TLC** – R_f = 0.17 (SiO_2, 50:50 EtOAc:PE). **^{1}H NMR** (400 MHz, $CDCl_3$) δ_H 2.52 (s, 4H, 2 x CH_2), 3.55 (s, 6H, 2 x OCH_3), 3.83 (s, 6H, 2 x OCH_3), 5.13 (s, 2H, CH_2Ar), 7.27-7.34 (m, 5H, 5 x Ar*H*). **^{13}C NMR** (101 MHz, $CDCl_3$) δ_C 34.4 (*C*H_2), 35.7 (*C*H_2), 53.2 (2 x O*C*H_3), 53.5 (2 x O*C*H_3), 68.4 (*C*H_2Ar), 73.7 (N*C*$_{quat.}$), 74.1 (N*C*$_{quat.}$), 128.4 (Ar*C*), 128.5 (2 x Ar*C*), 128.6 (2 x Ar*C*), 135.7 (Ar*C*), 153.7 (*C*O), 168.8 (2 x *C*O), 168.9 (2 x *C*O). **HR-MS** (ESI, positive ion mode) – *m/z* for $[C_{20}H_{23}NO_{10}+H]^+$ = 438.4090. Found 438.4105. **FTIR** (KBr) – 2962, 2917, 1740, 1662.

Tetramethyl pyrrolidine-2,2,5,5-tetracarboxylate, 204

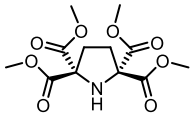

Synthesised according to general procedure S using **207** (354 mg, 0.81 mmol. The title secondary amine was isolated as a white solid (245 mg, 0.81 mmol, >99%). **M.P.** 148-149 °C (MeOH). **TLC** – R_f = 0.12 (SiO_2, 5:95 MeOH:DCM).

^{1}H NMR (400 MHz, $CDCl_3$) δ_H 2.39 (s, 4H, 2 x C*H*$_2$), 3.72 (s, 12H, 4 x OC*H*$_3$). **^{13}C NMR** (101 MHz, $CDCl_3$) δ_C 33.8 (2 x *C*H$_2$), 52.4 (4 x O*C*H$_3$), 70.9 (2 x N*C*$_{quat.}$), 168.1 (4 x *C*O). **HR-MS** (ESI, positive ion mode) – *m/z* for $[C_{12}H_{17}NO_8+H]^+$ = 304.1032. Found 304.1039. **FTIR** (KBr) – 3295, 2976, 2955, 1741.

N^2,*N*'^{2},*N*^{5},*N*'^{5}-Tetraphenyl pyrrolidine-2,2,5,5-tetracarboxamide, 208

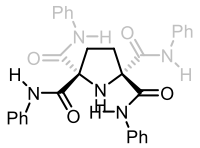

Under a dry, inert atmosphere, NaH (323 mg, 60% in mineral oil, 8.09 mmol, 10.00 equiv.) was washed with hexane (3 x 10 mL). The pure NaH was then suspended in anhydrous THF (20 mL) and cooled to 0 °C. To the suspension was added aniline (1.11 mL, 12.15 mmol, 15.00 equiv.) dropwise and the resulting suspension was stirred for 30 minutes at 0 °C. A solution of **204** (245 mg, 0.81 mmol, 1.00 equiv., 0.02 M) in anhydrous THF (20 mL) was added dropwise. The resulting suspension was warmed to room temperature and stirred for 4 h. The suspension was then quenched with saturated aqueous NH_4Cl (25 mL) and stirred for 15 minutes. The aqueous phase was then extracted with DCM (3 x 25 mL) and the combined organic phases were washed with brine, dried (Na_2SO_4), filtered and concentrated *in vacuo*. The crude product was then purified by column chromatography (2-5% MeOH:DCM) to yield the title tetramide as a white solid (146 mg, 0.27 mmol, 33%). **M.P.** 166-167 °C (DCM). **TLC** – R_f = 0.38 (SiO_2, 5:95 MeOH:DCM). **^{1}H NMR** (400 MHz, $CDCl_3$) δ_H 2.55 (s, 4H, 2 x C*H*$_2$), 7.06 (t, J = 8.1, 4H, 4 x Ar*H*), 7.19 (t, J = 7.7, 8H, 8 x Ar*H*), 7.29 (d, J = 7.7, 8H, 8 x Ar*H*), 11.51 (s, 4H, 4 x N*H*). **^{13}C NMR** (101 MHz, $CDCl_3$) δ_C 38.1 (2 x *C*H$_2$), 75.5 (2 x N*C*$_{quat.}$), 123.5 (8 x Ar*C*), 127.3 (4 x Ar*C*), 128.5 (8 x Ar*C*), 138.3 (4 x Ar*C*), 165.6 (4 x *C*O). **HR-MS** (ESI, positive ion mode) – *m/z* for $[C_{32}H_{29}N_5O_4+H]^+$ = 548.2298. Found 548.2307. **FTIR** (KBr) – 3276, 3199, 2957, 1672.

N^1-(L-(*N*-*tert*-butoxycarbonyl)phenylalaninyl) *N*^{2},*N*'^{2},*N*^{5},*N*'^{5}-Tetraphenylpyrrolidine-2,2,5,5-tetracarboxamide, 209

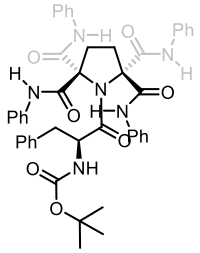

Under a dry, inert atmosphere, a solution of **208** (113 mg, 0.21 mmol, 1.00 equiv., 0.10 M) in anhydrous DMF (2 mL) was prepared. To this solution was added HATU (15 mg, 0.29 mmol, 1.40 equiv.), TEA (0.04 mL, 0.29 mmol, 1.40 equiv.) and Boc-L-phenylalanine (10 mg, 0.29 mmol, 1.40 equiv.). The resulting solution was stirred for 72 h at room temperature and then diluted with aqueous $HKSO_4$ (5 mL, 1.00 M). The aqueous phase was extracted with DCM (3 x 5 mL) and the combined organic phases were washed with aqueous $KHSO_4$ (2 x 5 mL) and brine, dried (Na_2SO_4), filtered and concentrated *in vacuo*. The crude product was then purified

by column chromatography (2-5% MeOH:DCM) to yield the title amide as a white solid (28 mg, 0.04 mmol, 17%). **M.P.** 139-140 °C (DCM). **TLC** – R_f = 0.40 (SiO_2, 5:95 MeOH:DCM). **^{1}H NMR** (400 MHz, $CDCl_3$) δ_H 1.40 (s, 9H, C(C*H*$_3$)$_3$), 2.52 (s, 4H, 2 x C*H*$_2$), 3.08-3.18 (m, 2H, C*H*$_2$Ar), 4.80 (dd, J = 6.2, 9.8, 1H, NC*H*, rot.), 4.87 (dd, J = 6.2, 9.8, 1H, NC*H*, rot.), 6.91 (d, J = 6.8, 2H, 2 x Ar*H*), 6.96 (d, J = 6.1, 1H, Ar*H*), 7.09 (t, J = 7.3, 1H, Ar*H*), 7.15-7.58 (m, 21H, 21 x Ar*H*), 7.92 (s, 1H, N*H*, rot.), 7.93 (s, 1H, N*H*, rot.), 8.18 (s, 1H, N*H*), 8.86 (s, 1H, N*H*), 8.96 (s, 1H, N*H*). **^{13}C NMR** (101 MHz, $CDCl_3$) δ_C 28.4 (C(*C*H$_3$)$_3$), 36.9 (*C*H$_2$), 37.8 (*C*H$_2$), 41.8 (*C*H$_2$Ar), 58.7 (N*C*H), 72.3 (N*C*$_{quat.}$), 74.0 (N*C*$_{quat.}$), 80.2 (*C*(CH$_3$)$_3$), 121.2 (2 x Ar*C*), 121.3 (2 x Ar*C*), 121.8 (2 x Ar*C*), 122.0 (2 x Ar*C*), 125.2 (Ar*C*), 127.6 (2 x Ar*C*), 128.0 (Ar*C*), 128.3 (Ar*C*), 128.4 (Ar*C*), 128.4 (Ar*C*), 128.6 (2 x Ar*C*), 128.8 (2 x Ar*C*), 129.0 (2 x Ar*C*), 129.1 (2 x Ar*C*), 129.1 (2 x Ar*C*), 139.0 (Ar*C*), 139.0 (Ar*C*), 139.4 (Ar*C*), 139.4 (Ar*C*), 140.3 (Ar*C*), 156.5 (*C*O), 168.2 (*C*O), 168.4 (*C*O), 168.5 (*C*O), 168.8 (*C*O), 172.8 (*C*O). **HR-MS** (ESI, positive ion mode) – *m/z* for $[C_{46}H_{46}N_6O_7+Na]^+$ = 817.3326. Found 817.3352. **FTIR** (KBr) – 3271, 3196, 2974, 1662, 1638.

N^1-(L-phenylalaninyl) *N*^{2},*N*'^{2},*N*^{5},*N*'^{5}-Tetraphenylpyrrolidine-2,2,5,5-tetracarboxamide, 200

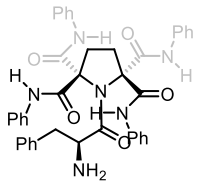

Under a dry, inert atmosphere, a solution of **212** (24 mg, 0.03 mmol, 0.03 M) in anhydrous EtOH (0.5 mL) was prepared. To this solution was added HCl (4.00 M in EtOAc, 0.5 mL) and the resulting solution was stirred for 16 h at room temperature. The solution was concentrated *in vacuo* and the residue was diluted with EtOAc (4 mL). The solution was diluted with saturated aqueous $NaHCO_3$ (4 mL) and the organic phase was washed with saturated aqueous $NaHCO_3$ (4 mL) and brine, dried (Na_2SO_4), filtered and concentrated *in vacuo* to yield the title amine as a white solid (20 mg, 0.03 mmol, 97%). **M.P.** 193-194 °C ($CHCl_3$). **TLC** – R_f = 0.20 (SiO_2, 5:95 MeOH:DCM). **^{1}H NMR** (400 MHz, $CDCl_3$) δ_H 2.56 (s, 4H, 2 x C*H*$_2$), 3.00-3.10 (m, 2H, C*H*$_2$Ar), 4.11 (dd, J = 7.3, 9.2, 1H, NC*H*, rot.), 4.30 (dd, J = 7.3, 9.2, 1H, NC*H*, rot.), 7.01 (d, J = 7.1, 2H, 2 x Ar*H*), 7.06 (d, J = 6.1, 1H, Ar*H*), 7.10 (t, J = 7.0, 1H, Ar*H*), 7.13-7.60 (m, 21H, 21 x Ar*H*), 8.28 (s, 1H, N*H*, rot.), 8.30 (s, 1H, N*H*, rot.), 8.44 (s, 1H, N*H*), 9.15 (s, 1H, N*H*), 9.34 (s, 1H, N*H*). **^{13}C NMR** (101 MHz, $CDCl_3$) δ_C 37.0 (*C*H$_2$), 37.9 (*C*H$_2$), 40.5 (*C*H$_2$Ar), 50.3 (N*C*H), 74.6 (N*C*$_{quat.}$), 75.3 (N*C*$_{quat.}$), 121.4 (2 x Ar*C*), 121.5 (2 x Ar*C*), 122.0 (2 x Ar*C*), 122.0 (2 x Ar*C*), 125.2 (Ar*C*), 127.2 (2 x Ar*C*), 128.1 (Ar*C*), 128.1 (Ar*C*), 128.5 (Ar*C*), 128.6 (Ar*C*), 128.8 (2 x Ar*C*), 129.1 (2 x Ar*C*), 129.4 (2 x Ar*C*), 129.5 (2 x Ar*C*), 129.8 (2 x Ar*C*), 139.1 (Ar*C*), 141.4 (Ar*C*), 141.4 (Ar*C*), 141.9 (Ar*C*), 141.9 (Ar*C*), 166.3 (*C*O), 166.4 (*C*O), 167.2 (*C*O), 167.2 (*C*O), 174.9 (*C*O). **HR-MS** (ESI, positive ion mode) – *m/z* for $[C_{41}H_{38}N_6O_5+H]^+$ = 695.2982. Found 695.2997. **FTIR** (KBr) – 3354, 3219, 3201, 2981, 1659, 1645.

8.0 Appendix

8.1 Miscellaneous NMR Experiments

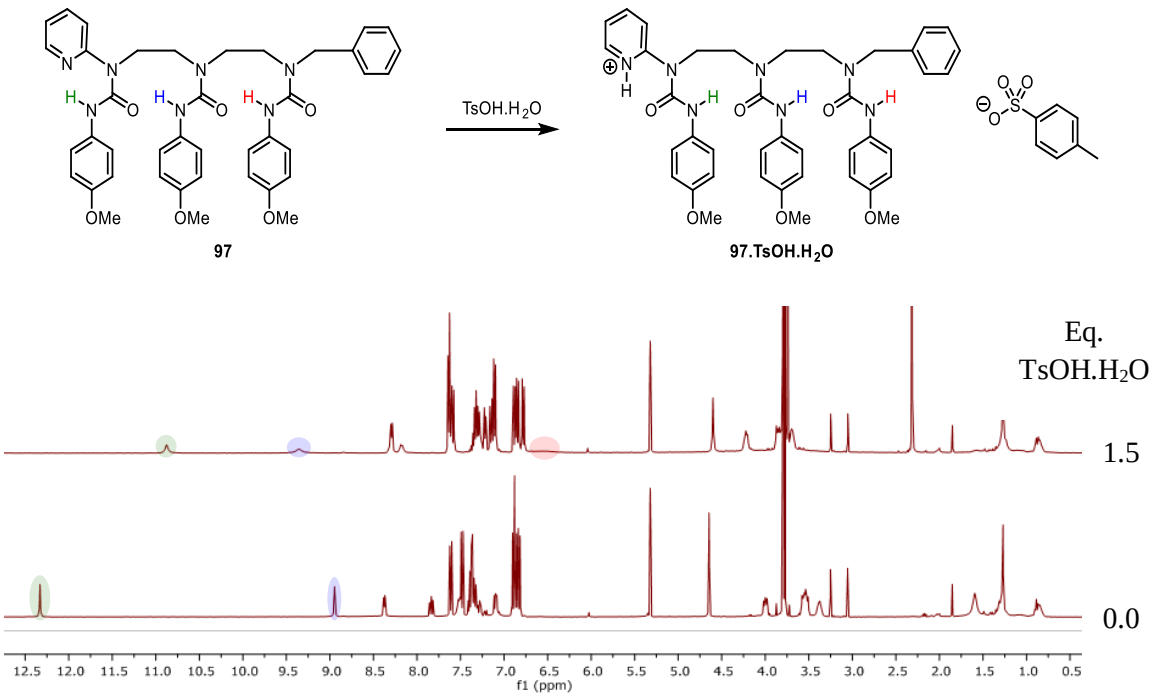

Figure A1 – Addition of TsOH.H$_2$O to 97 (CD$_2$Cl$_2$, 500 MHz).

8.2 VTNMR Experiments

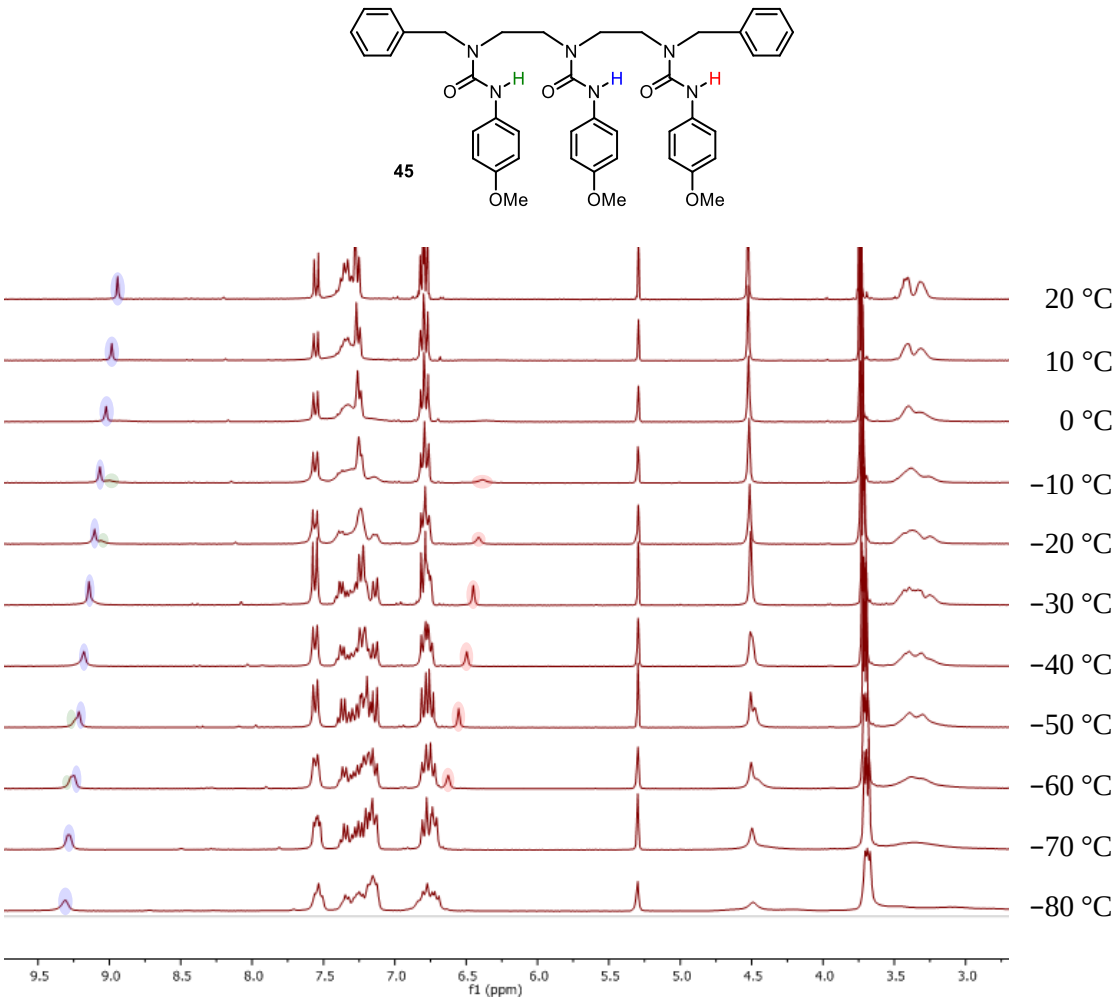

Figure A2 – VTNMR of 45 (CD_2Cl_2, 300 MHz, 14 mM).

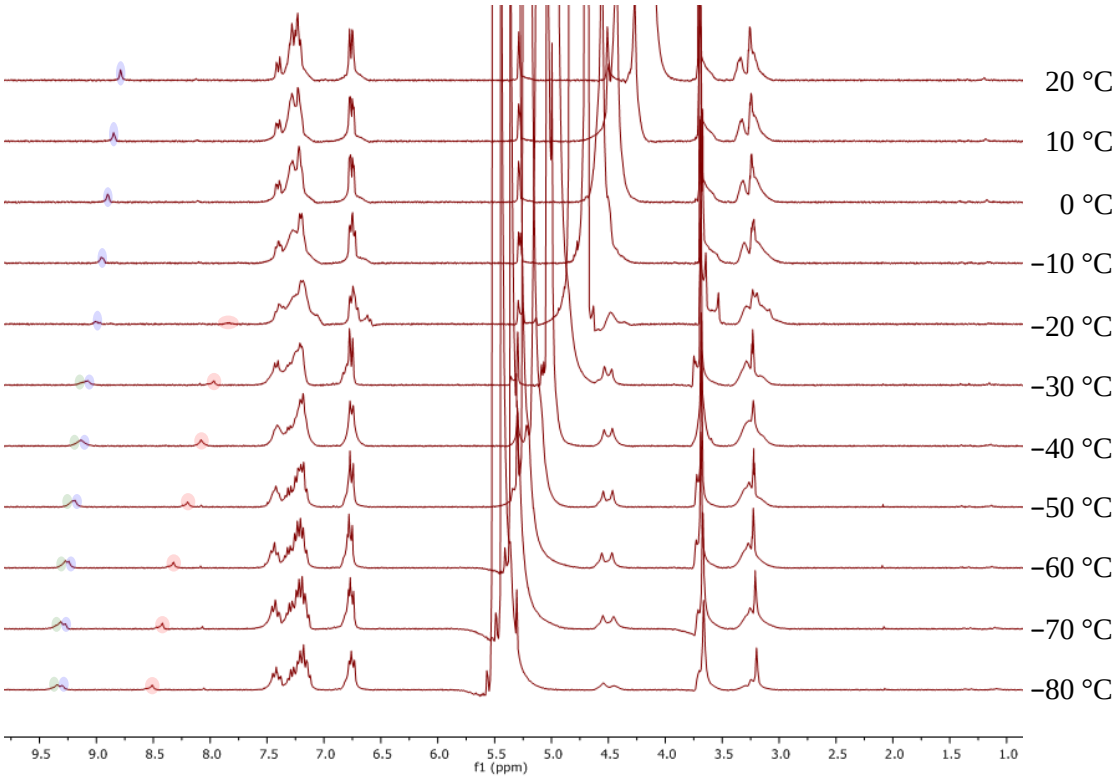

Figure A3 – VTNMR of 45 (40% v/v CD_3OH in CD_2Cl_2, 300 MHz, 14 mM).

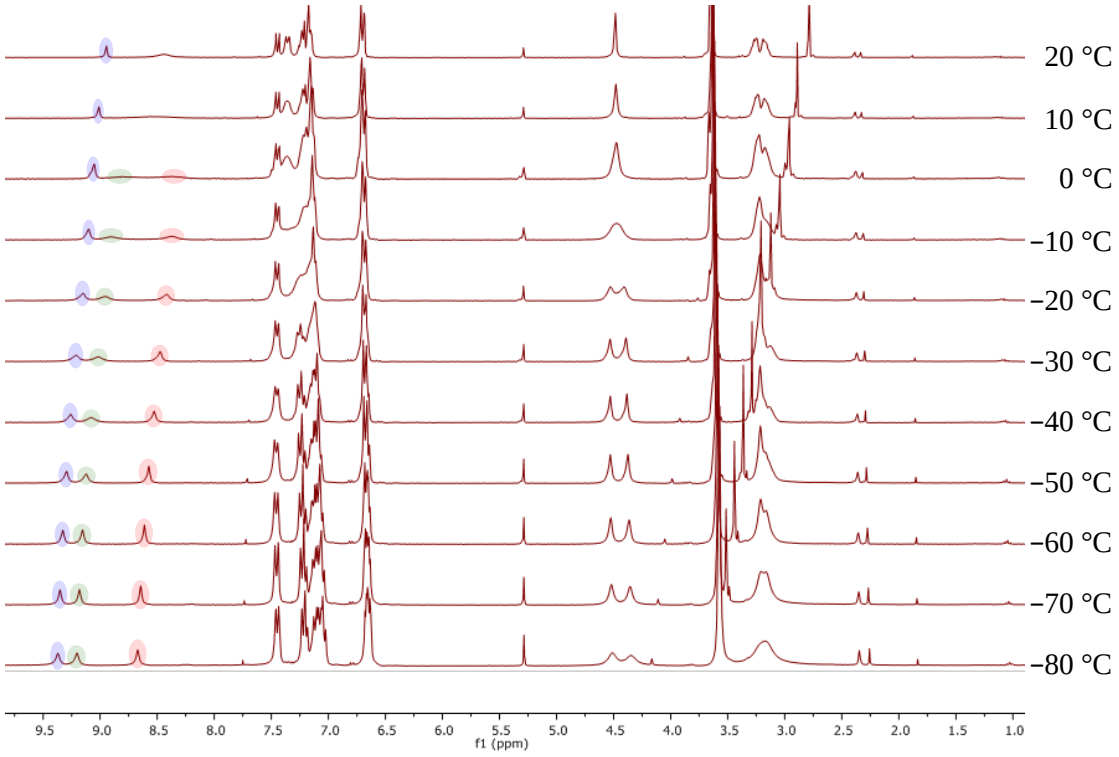

Figure A4 – VTNMR of 45 (10% v/v d_6-DMSO in CD_2Cl_2, 300 MHz, 14 mM).

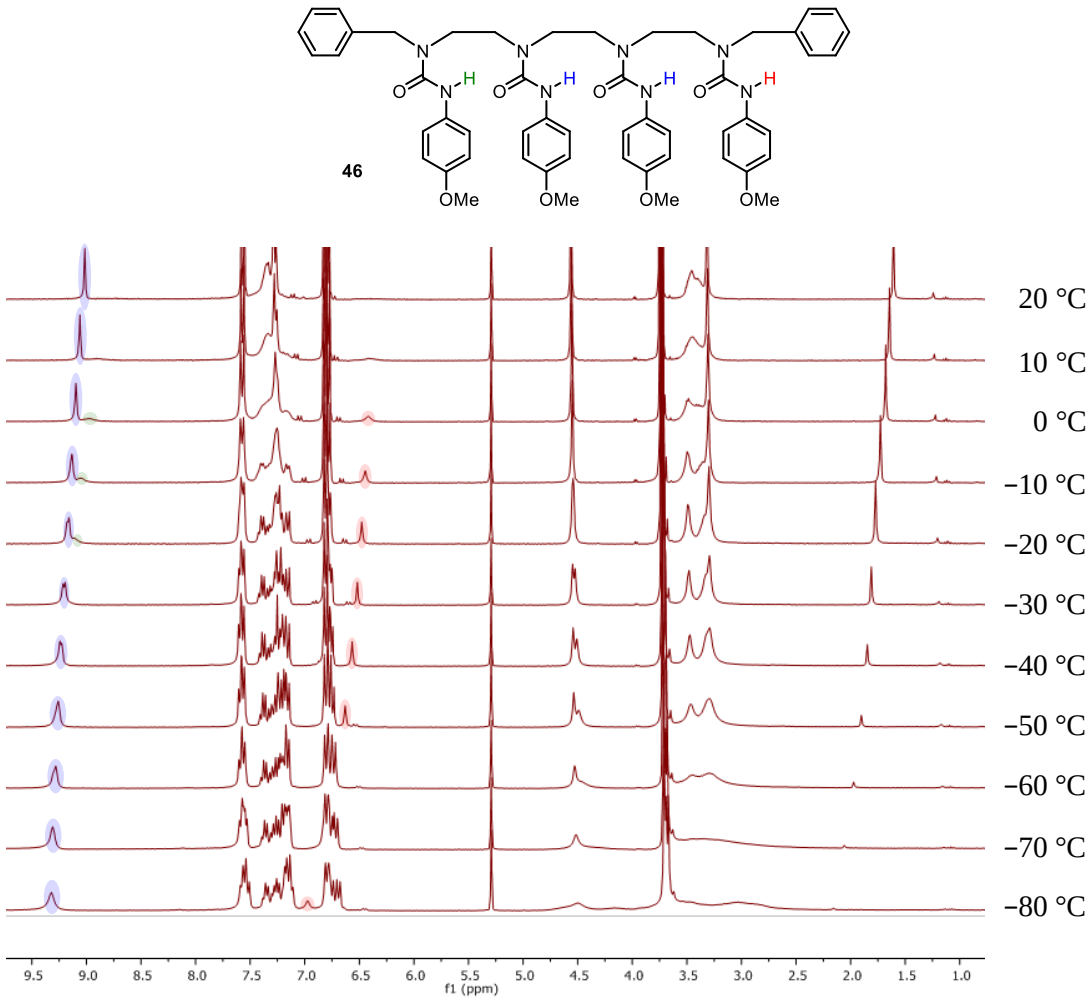

Figure A5 – VTNMR of 46 (CD_2Cl_2, 300 MHz, 11 mM).

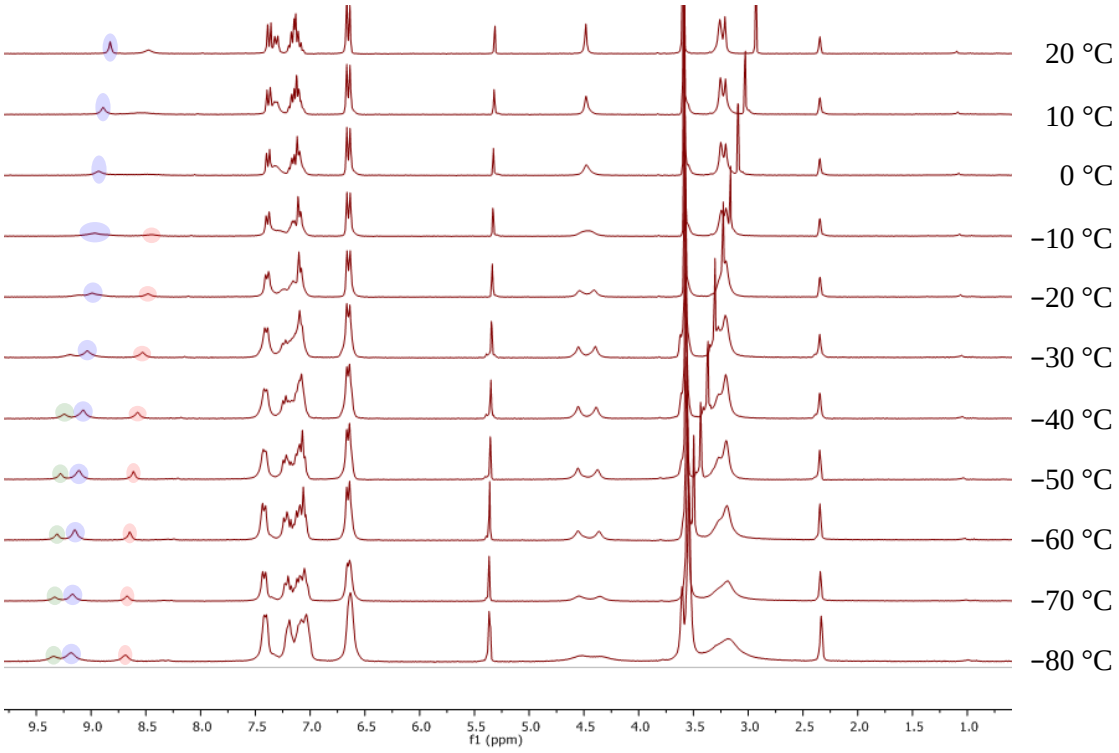

Figure A6 – VTNMR of 46 (10% v/v d_6-DMSO in CD_2Cl_2, 300 MHz, 11 mM).

8.3 Eyring Analyses

All Eyring plots were constructed using rate constants that were attained by line shape fitting of experimental spectra at different temperatures. Spectra were simulated using SpinWorks 4 NMR processing software (available at ftp://davinci.chem.umanitoba.ca/pub/marat/SpinWorks/) with appropriate exchange vectors. For each temperature, the corresponding rate of hydrogen-bond-directionality reversal was estimated using the dynamic NMR simulation module DNMR3. The Eyring-Polanyi equation was rearranged to give an equation of the form y = mx + c such that a plot of *1/T* against *ln(k/T)* gave a straight line of gradient $\frac{-\Delta H^{\ddagger}}{R}$ and intercept $ln\frac{k_B}{h} + \frac{\Delta S^{\ddagger}}{R}$. These data were used with the Gibbs free energy equation to extrapolate $\Delta G^{\ddagger}_{298\ K}$. Examples of the simulation of systems in mutual exchange and non-mutual exchange are shown below.

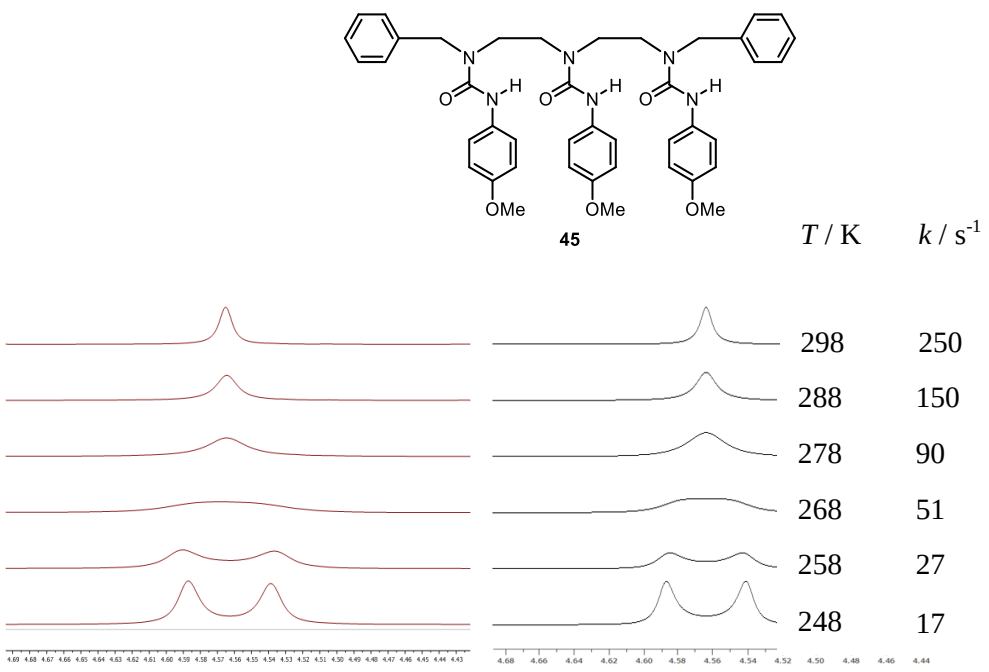

Figure A7 – Experimental (left) and simulated (right) spectra for 45.

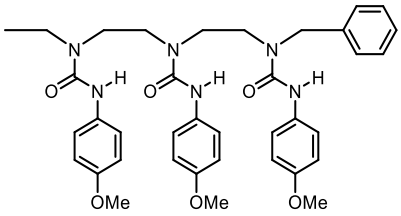

41

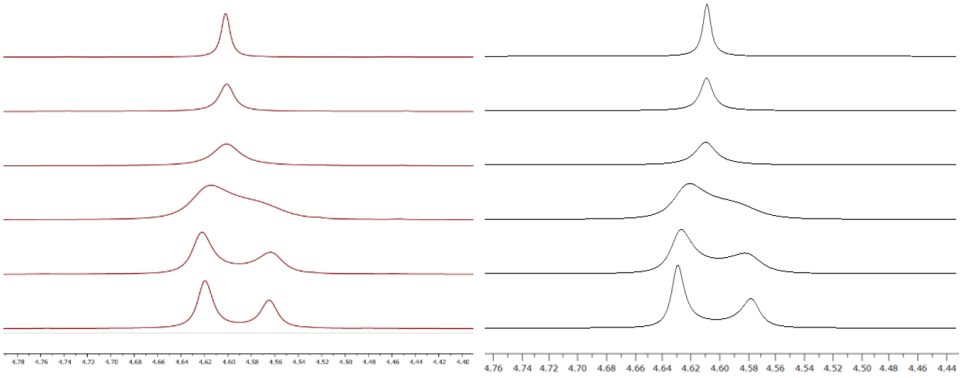

T / K	k / s^{-1}
298	330
288	200
278	120
268	44
258	27
248	15

Figure A8 – Experimental (left) and simulated (right) spectra for 41.

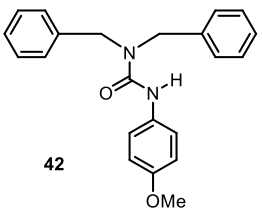

42

$\Delta G^{\ddagger}_{298\ K}$ = 48.9 kJ mol^{-1}

(CD_2Cl_2)

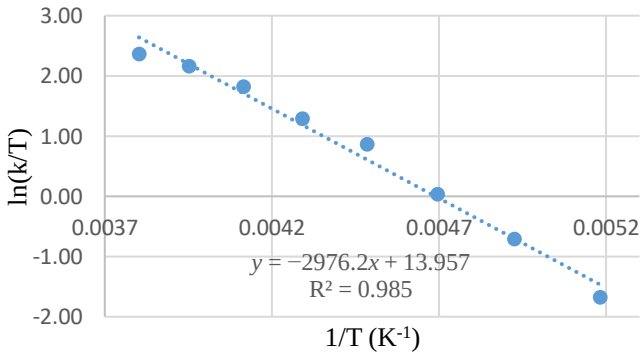

Temperature (K)	Rate Constant, k (s^{-1})	1/T (K^{-1})	ln(k/T)	$\Delta G^{\ddagger}$ (kJ mol^{-1})	$t_{½}$ (s)
193	36	0.0052	-1.6792	40.4763	0.0096
203	100	0.0049	-0.7080	41.2913	0.0035
213	220	0.0047	0.0323	42.1064	0.0016
223	530	0.0045	0.8657	42.9215	0.0007
233	850	0.0043	1.2942	43.7365	0.0004
243	1500	0.0041	1.8202	44.5516	0.0002
253	2200	0.0040	2.1628	45.3667	0.0002
263	2800	0.0038	2.3652	46.1817	0.0001

Figure A9 – Eyring plot for 42.

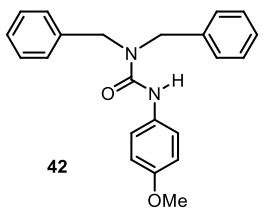

$\Delta G^{\ddagger}_{298\ K}$ = 59.9 kJ mol^{-1}

(40% CD_3OD in CD_2Cl_2)

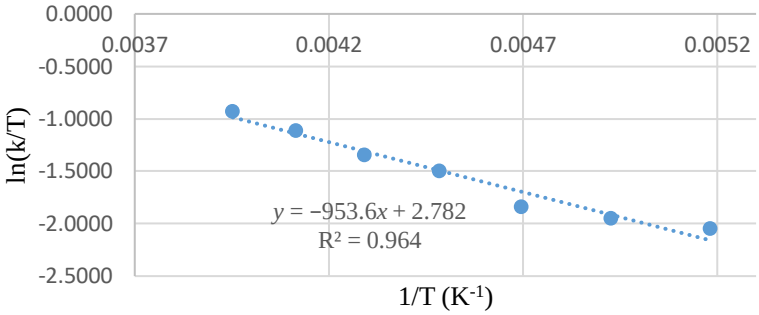

Temperature (K)	Rate Constant, *k* (s^{-1})	1/T (K^{-1})	ln(*k*/T)	$\Delta G^{\ddagger}$ (kJ mol^{-1})	$t_{½}$ (s)
193	25	0.0052	-2.0438	41.5908	0.0139
203	29	0.0049	-1.9459	43.3350	0.0120
213	34	0.0047	-1.8349	45.0791	0.0102
223	50	0.0045	-1.4951	46.8233	0.0069
233	61	0.0043	-1.3402	48.5674	0.0057
243	80	0.0041	-1.1110	50.3116	0.0043
253	100	0.0040	-0.9282	52.0557	0.0035

Figure A10 – Eyring plot for 42 (40% CD_3OH in CD_2Cl_2).

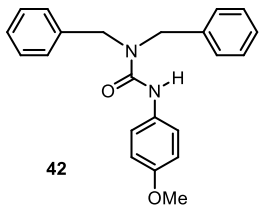

42

$\Delta G^{\ddagger}_{298\ K}$ = 54.5 kJ mol^{-1}

(10% $(CD_3)_2SO$ in CD_2Cl_2)

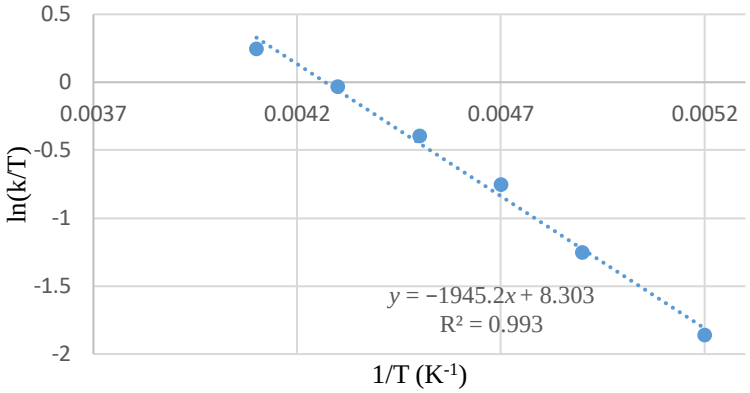

Temperature (K)	Rate Constant, *k* (s^{-1})	1/T (K^{-1})	ln(*k*/T)	$\Delta G^{\ddagger}$ (kJ mol^{-1})	$t_{½}$ (s)
193	30	0.0052	-1.8615	40.9945	0.0116
203	58	0.0049	-1.2528	42.2732	0.0060
213	100	0.0047	-0.7561	43.5518	0.0035
223	150	0.0045	-0.3965	44.8305	0.0023
233	225	0.0043	-0.0349	46.1091	0.0015
243	310	0.0041	0.2435	47.3878	0.0011

Figure A11 – Eyring plot for 42 (10% $(CD_3)_2SO$ in CD_2Cl_2).

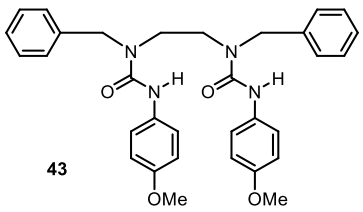

$\Delta G^{\ddagger}_{298\ K} = 59.4$ kJ mol^{-1}

(CD_2Cl_2)

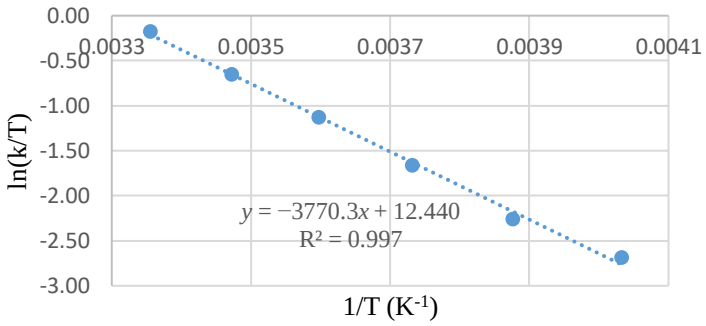

Temperature (K)	Rate Constant, *k* (s^{-1})	1/T (K^{-1})	ln(*k*/T)	$\Delta G^{\ddagger}$ (kJ mol^{-1})	$t_{½}$ (s)
248	17	0.0040	-2.6802	54.6897	0.0204
258	27	0.0039	-2.2571	55.6309	0.0128
268	51	0.0037	-1.6592	56.5721	0.0068
278	90	0.0036	-1.1278	57.5133	0.0039
288	150	0.0035	-0.6523	58.4544	0.0023
298	250	0.0034	-0.1756	59.3956	0.0014

Figure A12 – Eyring plot for 43.

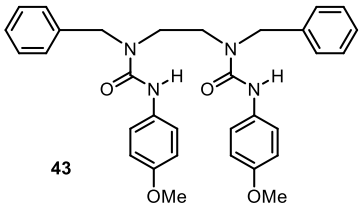

$\Delta G^{\ddagger}_{298\ K}$ = 55.3 kJ mol^{-1}

(40% CD_3OD in CD_2Cl_2)

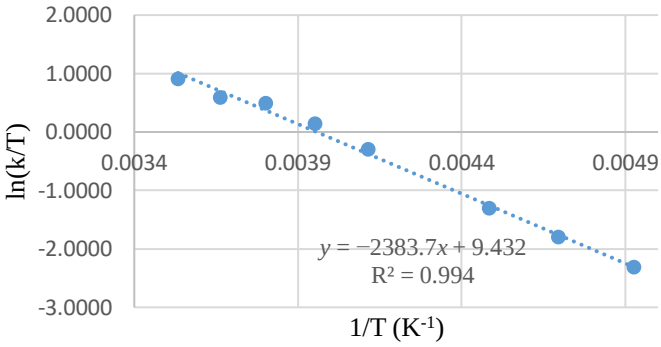

Temperature (K)	Rate Constant, *k* (s^{-1})	1/T (K^{-1})	ln(*k*/T)	$\Delta G^{\ddagger}$ (kJ mol^{-1})	$t_{½}$ (s)
203	20	0.0049	-2.3175	44.0026	0.0173
213	35	0.0047	-1.8059	45.1939	0.0099
223	60	0.0045	-1.3128	46.3852	0.0058
243	180	0.0041	-0.3001	48.7678	0.0019
253	290	0.0040	0.1365	49.9591	0.0012
263	430	0.0038	0.4916	51.1504	0.0008
273	490	0.0037	0.5849	52.3418	0.0007
283	700	0.0035	0.9056	53.5331	0.0005

Figure A13 – Eyring plot for 43 (40% CD_3OH in CD_2Cl_2).

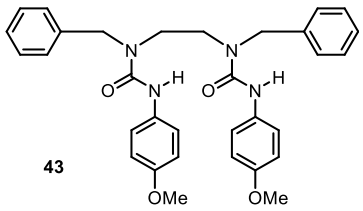

$\Delta G^{\ddagger}_{298\ K}$ = 52.3 kJ mol^{-1}

(10% $(CD_3)_2SO$ in CD_2Cl_2)

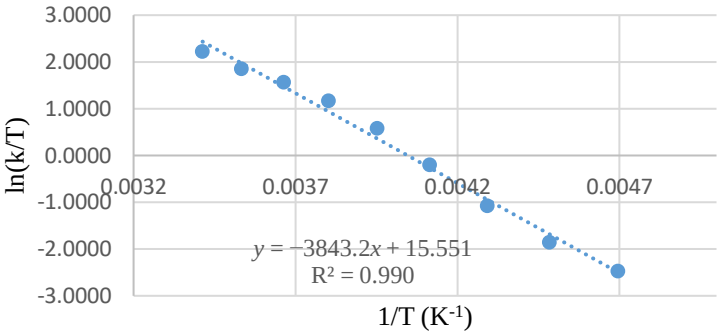

Temperature (K)	Rate Constant, *k* (s^{-1})	1/T (K^{-1})	ln(*k*/T)	$\Delta G^{\ddagger}$ (kJ mol^{-1})	$t_{½}$ (s)
213	18	0.0047	-2.4709	46.4921	0.0193
223	35	0.0045	-1.8518	47.1746	0.0099
233	80	0.0043	-1.0690	47.8572	0.0043
243	200	0.0041	-0.1947	48.5397	0.0017
253	450	0.0040	0.5759	49.2222	0.0008
263	850	0.0038	1.1731	49.9048	0.0004
273	1300	0.0037	1.5606	50.5873	0.0003
283	1800	0.0035	1.8501	51.2698	0.0002

Figure A14 – Eyring plot for 43 (10% $(CD_3)_2SO$ in CD_2Cl_2).

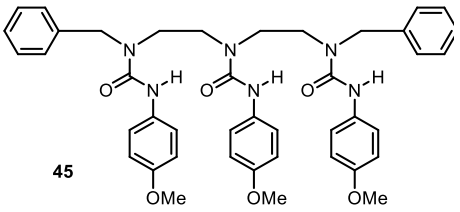

$\Delta G^{\ddagger}_{298\ K}$ = 59.0 kJ mol^{-1}

(CD_2Cl_2)

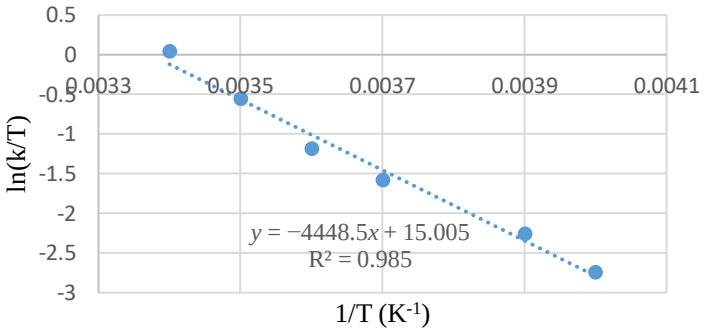

Temperature (K)	Rate Constant, *k* (s^{-1})	1/T (K^{-1})	ln(*k*/T)	$\Delta G^{\ddagger}$ (kJ mol^{-1})	$t_{½}$ (s)
248	16	0.0040	-2.7408	54.8299	0.0217
258	27	0.0039	-2.2571	55.6705	0.0128
268	55	0.0037	-1.5837	56.5110	0.0063
278	85	0.0036	-1.1850	57.3515	0.0041
288	165	0.0035	-0.5570	58.1920	0.0021
298	310	0.0034	0.0395	59.0325	0.0011

Figure A15 – Eyring plot for 45.

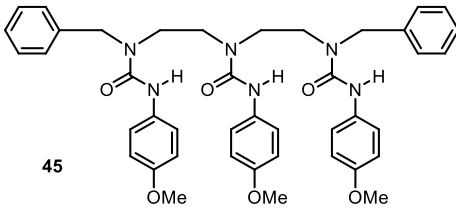

$\Delta G^{\ddagger}_{298\ K}$ = 58.6 kJ mol^{-1}

(40% CD_3OD in CD_2Cl_2)

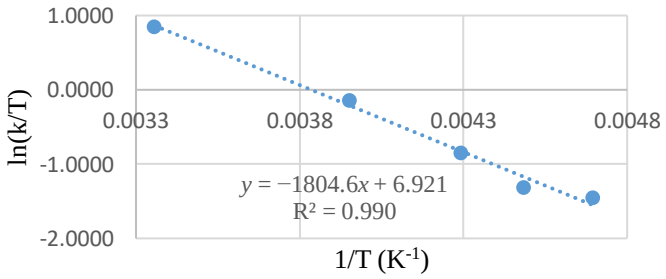

Temperature (K)	Rate Constant, *k* (s^{-1})	1/T (K^{-1})	ln(*k*/T)	$\Delta G^{\ddagger}$ (kJ mol^{-1})	$t_{½}$ (s)
213	50	0.0047	-1.4493	52.4842	0.0069
223	60	0.0045	-1.3128	53.2037	0.0058
233	100	0.0043	-0.8459	53.9233	0.0035
253	220	0.0040	-0.1398	55.3623	0.0016
298	700	0.0034	0.8540	58.6002	0.0005

Figure A16 – Eyring plot for 45 (40% CD_3OH in CD_2Cl_2).

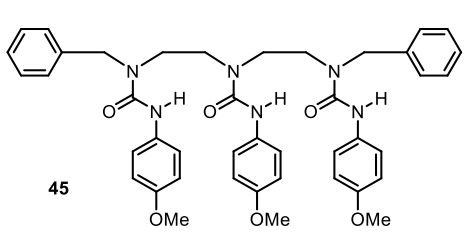

$\Delta G^{\ddagger}_{298\ K}$ = 54.9 kJ mol^{-1}

(10% $(CD_3)_2SO$ in CD_2Cl_2)

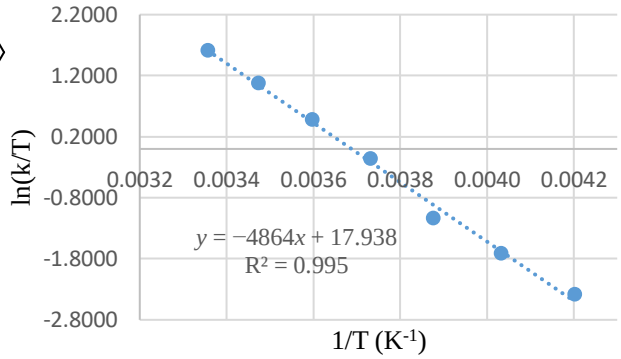

Temperature (K)	Rate Constant, *k* (s^{-1})	1/T (K^{-1})	ln(*k*/T)	$\Delta G^{\ddagger}$ (kJ mol^{-1})	$t_{½}$ (s)
238	22	0.0042	-2.3812	51.9623	0.0158
248	45	0.0040	-1.7068	52.4464	0.0077
258	83	0.0039	-1.1341	52.9305	0.0042
268	230	0.0037	-0.1529	53.4145	0.0015
278	450	0.0036	0.4816	53.8986	0.0008
288	850	0.0035	1.0823	54.3827	0.0004
298	1500	0.0034	1.6161	54.8667	0.0002

Figure A17 – Eyring plot for 45 (10% $(CD_3)_2SO$ in CD_2Cl_2).

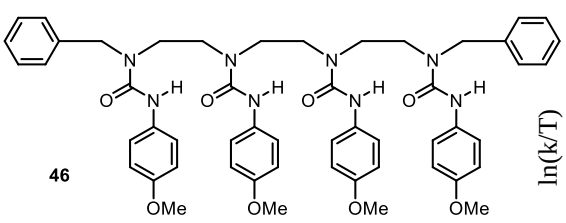

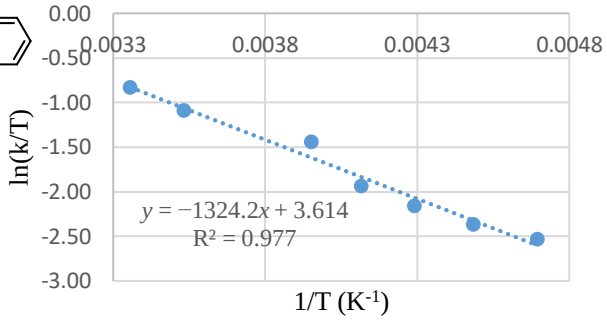

$\Delta G^{\ddagger}_{298\ K}$ = 60.9 kJ mol^{-1}

(CD_2Cl_2)

Temperature (K)	**Rate Constant, *k* (s^{-1})**	**1/T (K^{-1})**	**ln(*k*/T)**	**$\Delta G^{\ddagger}$ (kJ mol^{-1})**	**$t_{½}$ (s)**
213	17	0.0047	-2.5281	46.6874	0.0204
223	21	0.0045	-2.3626	48.3624	0.0165
233	27	0.0043	-2.1552	50.0374	0.0128
243	35	0.0041	-1.9377	51.7124	0.0099
253	60	0.0040	-1.4390	53.3874	0.0058
283	95	0.0035	-1.0916	58.4124	0.0036
298	130	0.0034	-0.8296	60.9249	0.0027

Figure A18 – Eyring plot for 46.

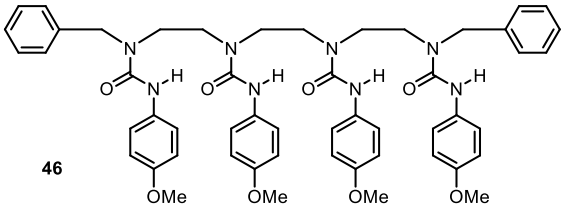

$\Delta G^{\ddagger}_{298\ K}$ = 53.7 kJ mol^{-1}

(10% $(CD_3)_2SO$ in CD_2Cl_2)

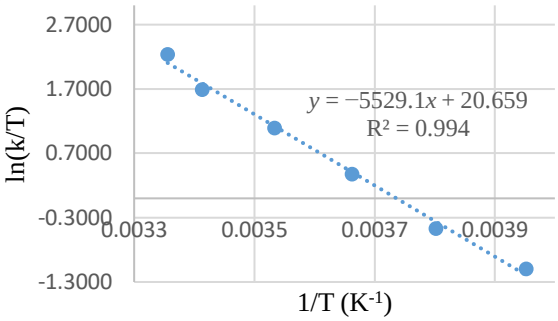

Temperature (K)	Rate Constant, *k* (s^{-1})	1/T (K^{-1})	ln(*k*/T)	$\Delta G^{\ddagger}$ (kJ mol^{-1})	$t_{½}$ (s)
253	85	0.0040	-1.0907	52.4946	0.0041
263	165	0.0038	-0.4662	52.7524	0.0021
273	400	0.0037	0.3820	53.0102	0.0009
283	850	0.0035	1.0998	53.2681	0.0004
293	1600	0.0034	1.6976	53.5259	0.0002
298	2800	0.0034	2.2403	53.6548	0.0001

Figure A19 – Eyring plot for 46 (10% $(CD_3)_2SO$ in CD_2Cl_2).

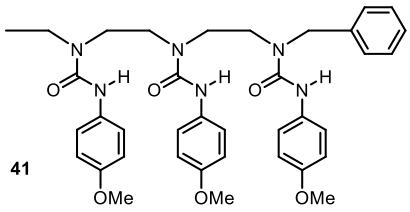

$\Delta G^{\ddagger}_{298\ K}$ = 58.1 kJ mol^{-1} (minor conformer to major conformer)

$\Delta G^{\ddagger}_{298\ K}$ = 59.2 kJ mol^{-1} (major conformer to minor conformer)

(CD_2Cl_2)

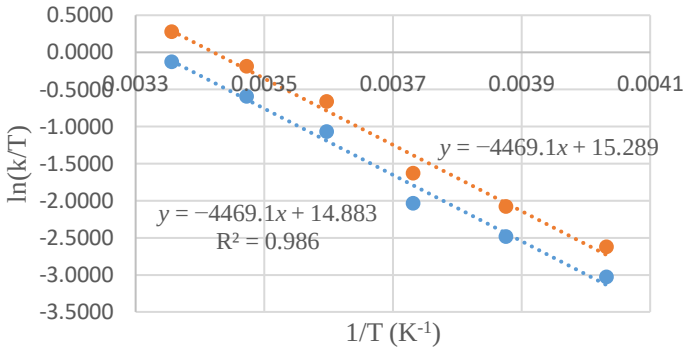

Temperature (K)	Rate Constant, *k* (s^{-1})	1/T (K^{-1})	ln(*k*/T)	$\Delta G^{\ddagger}$ (kJ mol^{-1})	$t_{½}$ (s)
248	18	0.0040	-2.6231	54.6252	0.0193
258	32	0.0039	-2.0748	55.3295	0.0107
268	52	0.0037	-1.6245	56.0338	0.0066
278	144	0.0036	-0.6578	56.7382	0.0024
288	240	0.0035	-0.1823	57.4425	0.0014
298	396	0.0034	0.2843	58.1468	0.0009

Figure A20 – Eyring plot for 41 (minor conformer to major conformer).

Temperature (K)	Rate Constant, *k* (s^{-1})	1/T (K^{-1})	ln(*k*/T)	$\Delta G^{\ddagger}$ (kJ mol^{-1})	$t_{½}$ (s)
248	12	0.0040	-3.0285	55.4624	0.0289
258	22	0.0039	-2.4803	56.2005	0.0160
268	35	0.0037	-2.0299	56.9385	0.0098
278	96	0.0036	-1.0633	57.6766	0.0036
288	160	0.0035	-0.5878	58.4147	0.0022
298	264	0.0034	-0.1211	59.1527	0.0013

Figure A21 – Eyring plot for 41 (major conformer to minor conformer).

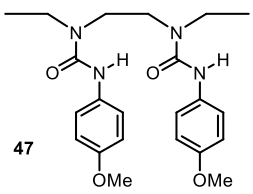

$\Delta G^{\ddagger}_{298\ K}$ = 51.5 kJ mol^{-1}

(CD_2Cl_2)

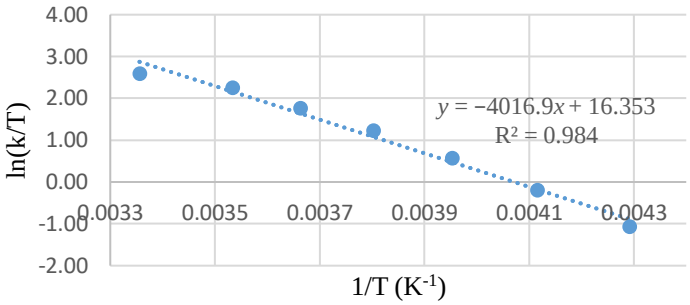

Temperature (K)	Rate Constant, *k* (s^{-1})	1/T (K^{-1})	ln(*k*/T)	$\Delta G^{\ddagger}$ (kJ mol^{-1})	$t_{½}$ (s)
193	55	0.0052	-1.2554	45.5790	0.0063
233	80	0.0043	-1.0690	47.8309	0.0043
243	200	0.0041	-0.1947	48.3939	0.0017
253	450	0.0040	0.5759	48.9569	0.0008
263	900	0.0038	1.2302	49.5198	0.0004
273	1600	0.0037	1.7683	50.0828	0.0002
283	2700	0.0035	2.2556	50.6458	0.0001
298	4000	0.0034	2.5970	51.4902	0.0001

Figure A22 – Eyring plot for 47.

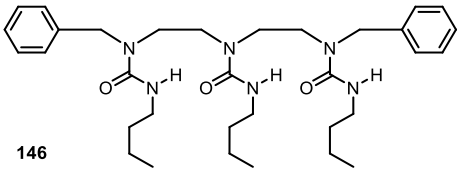

146

$\Delta G^{\ddagger}_{298\ K}$ = 57.9 kJ mol^{-1}

(CD_2Cl_2)

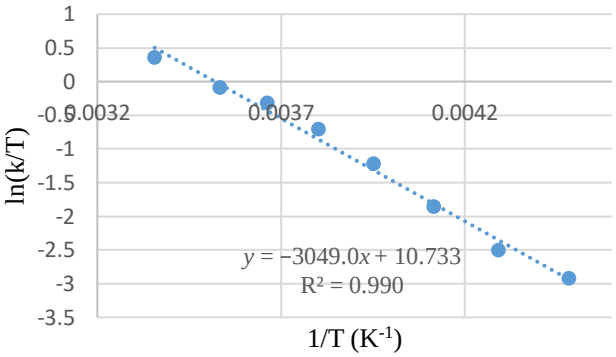

Temperature (K)	Rate Constant, *k* (s^{-1})	1/T (K^{-1})	ln(*k*/T)	$\Delta G^{\ddagger}$ (kJ mol^{-1})	$t_{½}$ (s)
223	12	0.0045	-2.9223	49.3977	0.0289
233	19	0.0043	-2.5066	50.5376	0.0182
243	38	0.0041	-1.8555	51.6775	0.0091
253	75	0.0040	-1.2159	52.8173	0.0046
263	130	0.0038	-0.7046	53.9572	0.0027
273	198	0.0037	-0.3212	55.0970	0.0018
283	260	0.0035	-0.0848	56.2369	0.0013
298	310	0.0034	0.0395	57.9467	0.0011

Figure A23 – Eyring plot for 146.

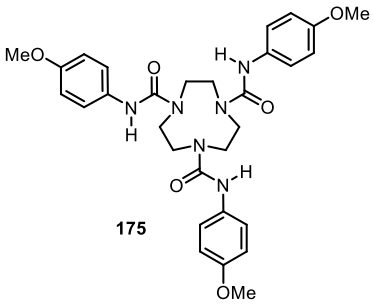

175

$\Delta G^{\ddagger}_{298\ K}$ = 65.3 kJ mol^{-1}

(d_8-Toluene)

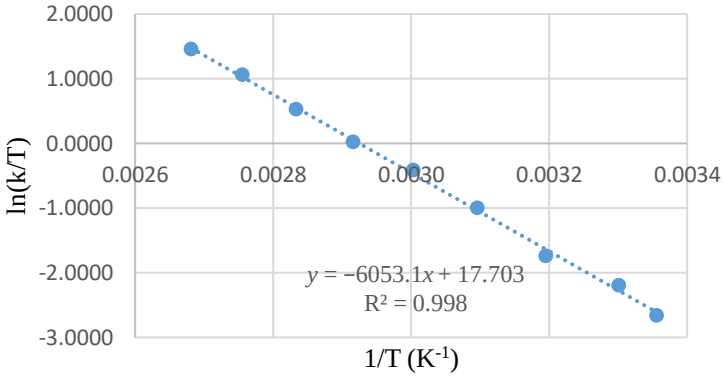

Temperature (K)	Rate Constant, *k* (s^{-1})	1/T (K^{-1})	ln(*k*/T)	$\Delta G^{\ddagger}$ (kJ mol^{-1})	$t_{½}$ (s)
298	21	0.0034	-2.6526	65.3357	0.0165
303	34	0.0033	-2.1874	65.5875	0.0102
313	55	0.0032	-1.7389	66.0911	0.0063
323	120	0.0031	-0.9902	66.5947	0.0029
333	220	0.0030	-0.4145	67.0983	0.0016
343	350	0.0029	0.0202	67.6019	0.0010
353	600	0.0028	0.5305	68.1055	0.0006
363	1050	0.0028	1.0621	68.6091	0.0003
373	1600	0.0027	1.4562	69.1128	0.0002

Figure A24 – Eyring plot for 175.

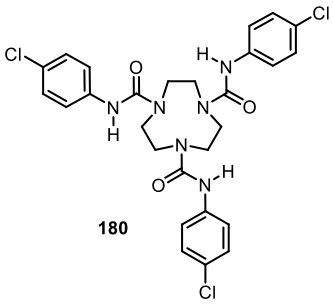

$\Delta G^{\ddagger}_{298\ K}$ = 63.2 kJ mol^{-1}

(CD_2Cl_2)

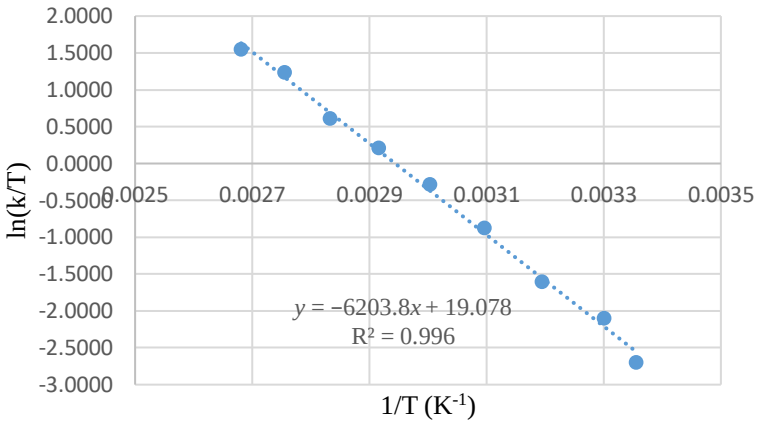

Temperature (K)	Rate Constant, *k* (s^{-1})	1/T (K^{-1})	ln(*k*/T)	$\Delta G^{\ddagger}$ (kJ mol^{-1})	$t_{½}$ (s)
298	20	0.0034	-2.7014	63.1811	0.0173
303	37	0.0033	-2.1028	63.3757	0.0094
313	63	0.0032	-1.6031	63.7650	0.0055
323	135	0.0031	-0.8724	64.1542	0.0026
333	250	0.0030	-0.2867	64.5435	0.0014
343	425	0.0029	0.2144	64.9328	0.0008
353	650	0.0028	0.6105	65.3220	0.0005
363	1250	0.0028	1.2365	65.7113	0.0003
373	1750	0.0027	1.5458	66.1005	0.0002

Figure A25 – Eyring plot for 180.

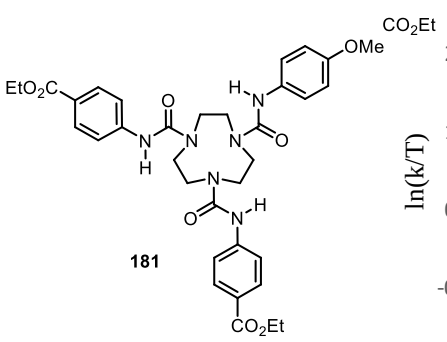

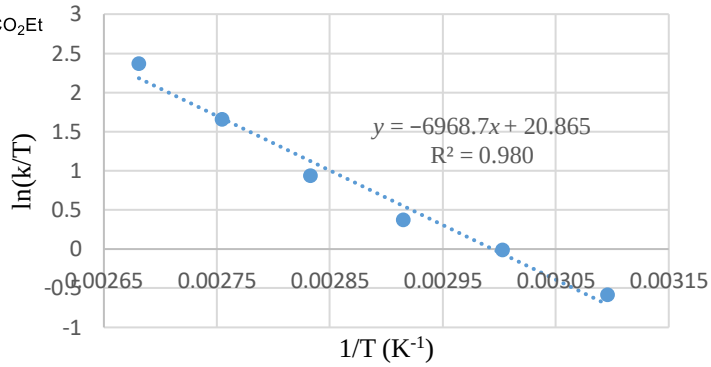

$\Delta G^{\ddagger}_{298\ K} = 62.7$ kJ mol^{-1}

(CD_2Cl_2)

Temperature (K)	Rate Constant, *k* (s^{-1})	1/T (K^{-1})	ln(*k*/T)	$\Delta G^{\ddagger}$ (kJ mol^{-1})	$t_{½}$ (s)
323	180	0.0031	-0.5847	65.7157	0.0019
333	330	0.0030	-0.0090	65.9564	0.0011
343	500	0.0029	0.3769	66.1971	0.0007
353	900	0.0028	0.9359	66.4378	0.0004
363	1900	0.0028	1.6552	66.6785	0.0002
373	4000	0.0027	2.3725	66.9192	0.0001

Figure A26 – Eyring plot for 181.

8.4 NOE Analyses

All 1D NOE studies were conducted on a Bruker AVANCE III HD 500 MHz NMR Spectrometer with 5 mm DCH ^{13}C–$^{1}H/D$ Cryo Probe (500 MHz) at 0 °C in CD_2Cl_2.

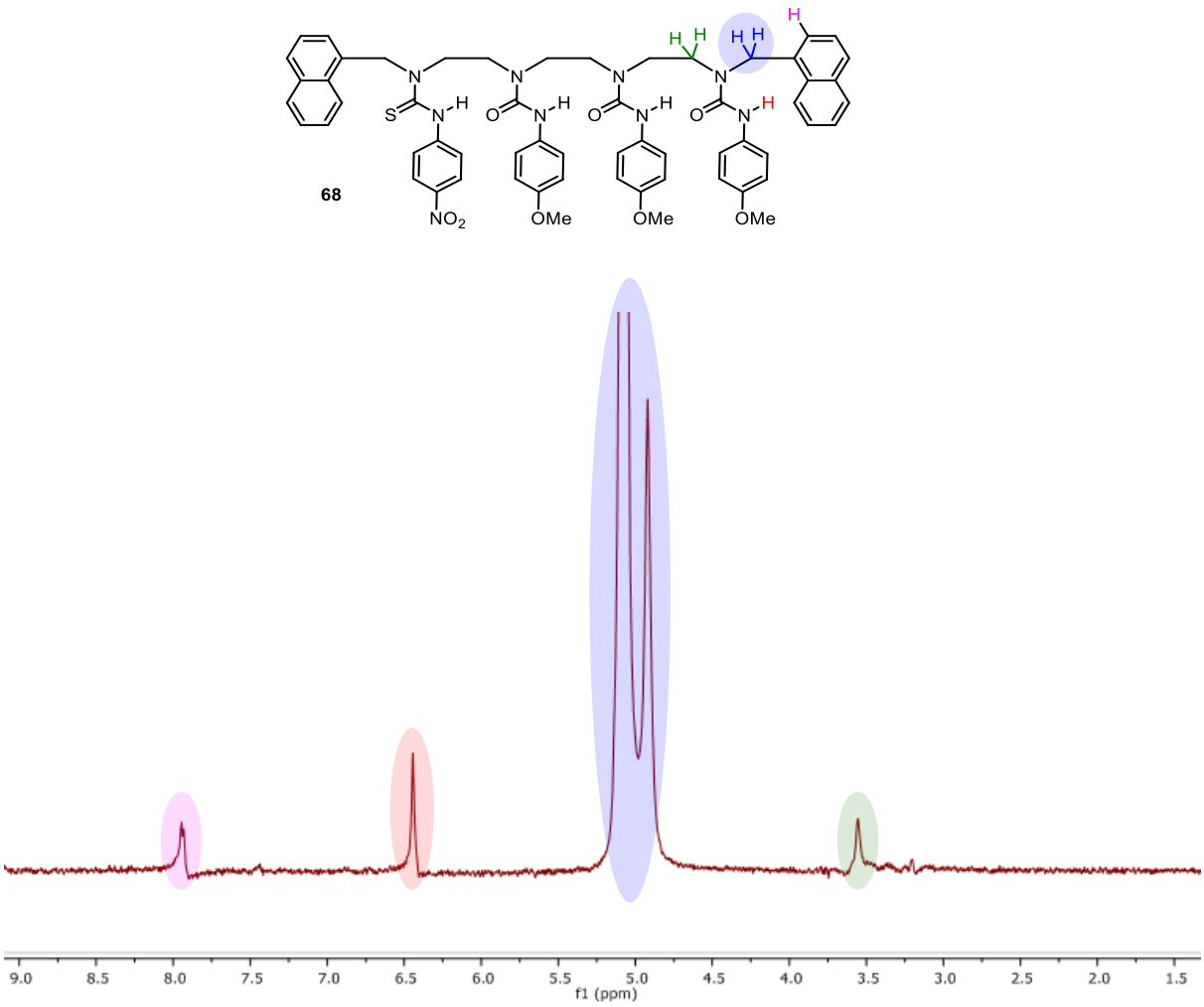

Figure A27 – NOE studies of 68 (irradiation of blue).

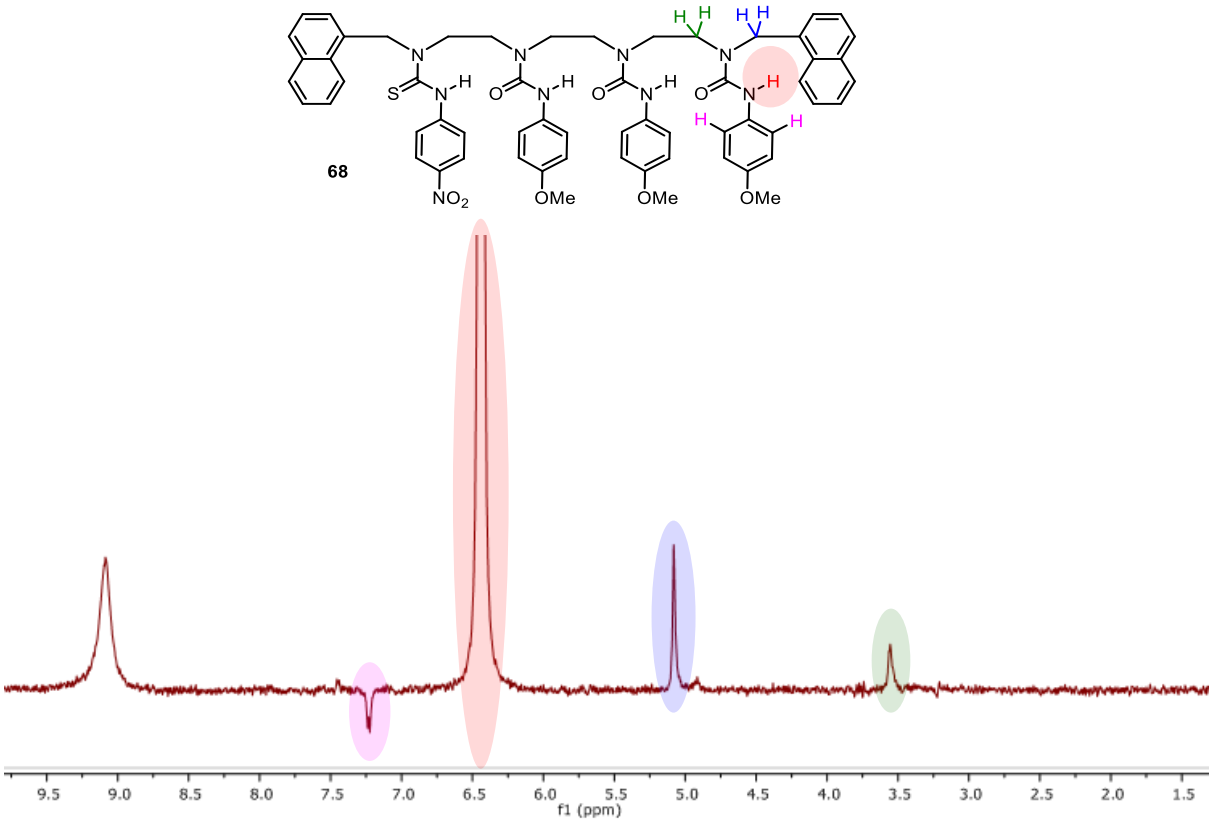

Figure A28 – NOE studies of 68 (irradiation of red).

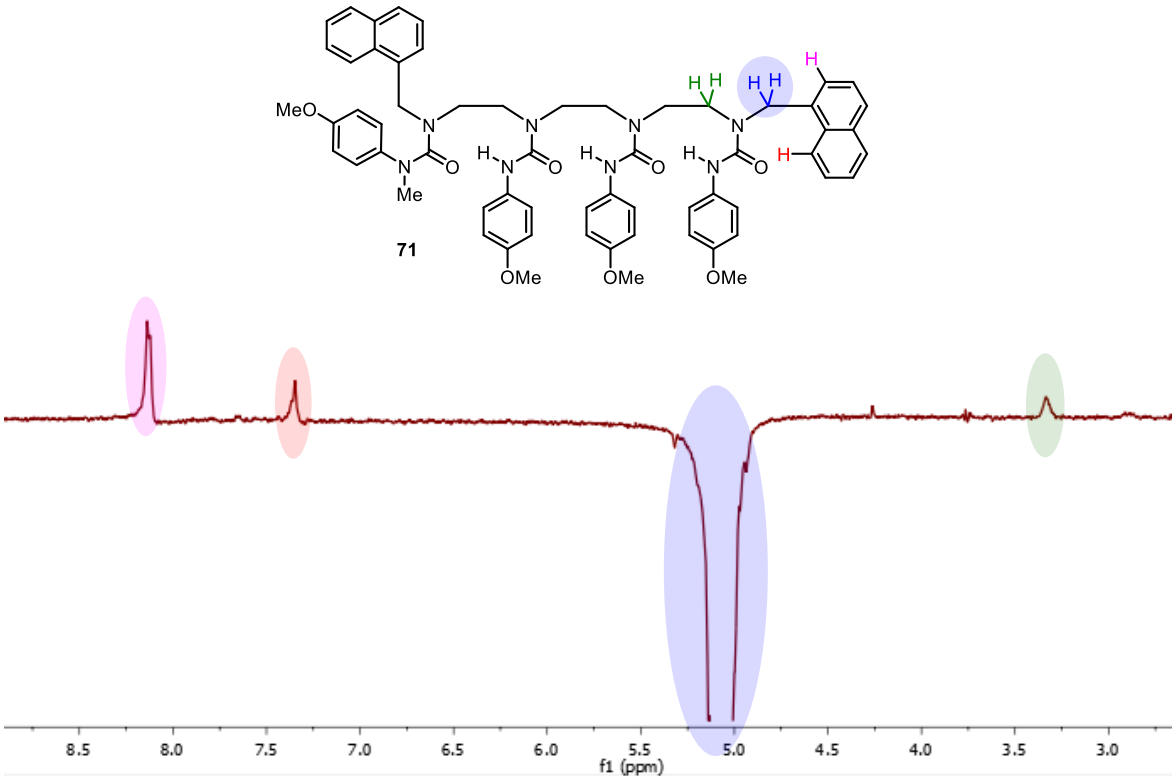

Figure A29 – NOE studies of 71 (irradiation of blue).

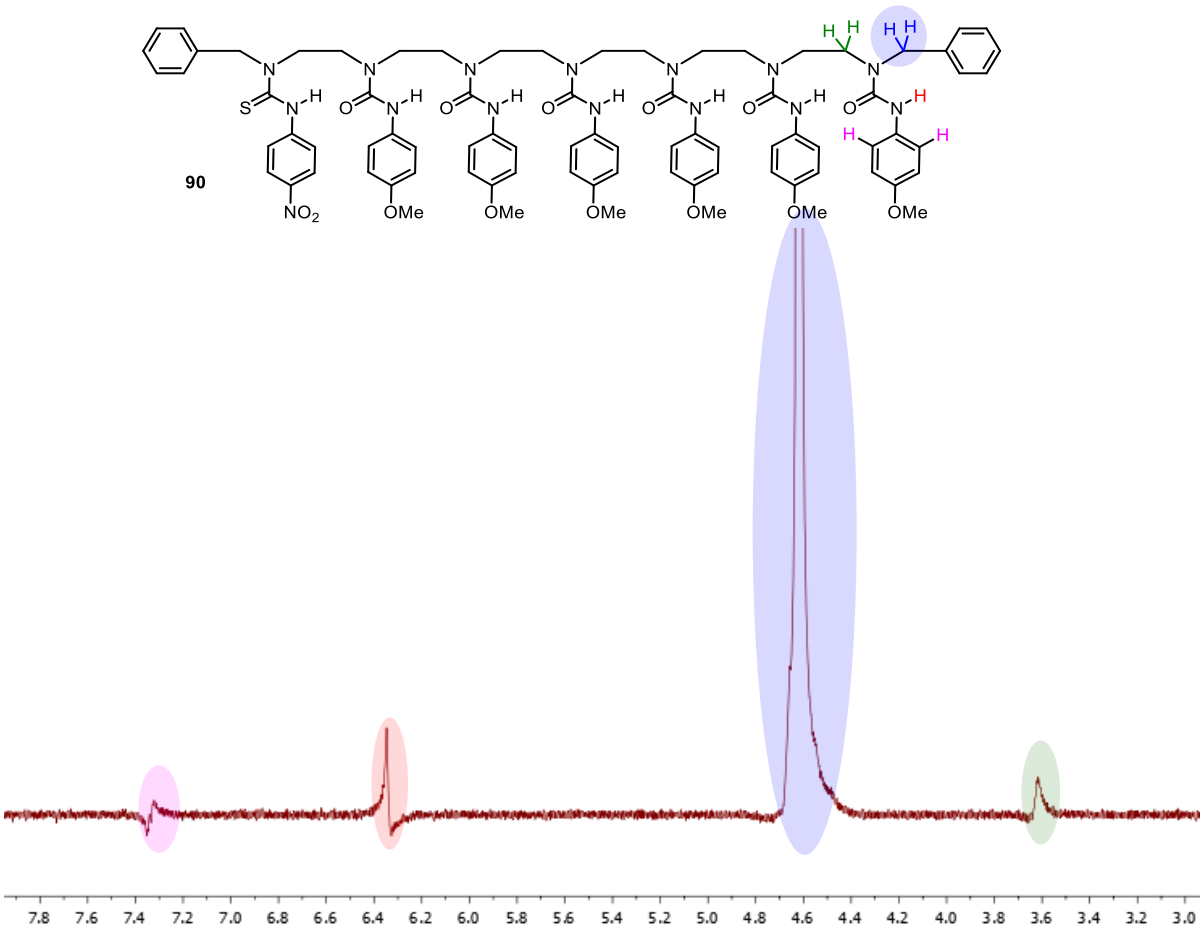

Figure A30 – NOE studies of 90 (irradiation of blue).

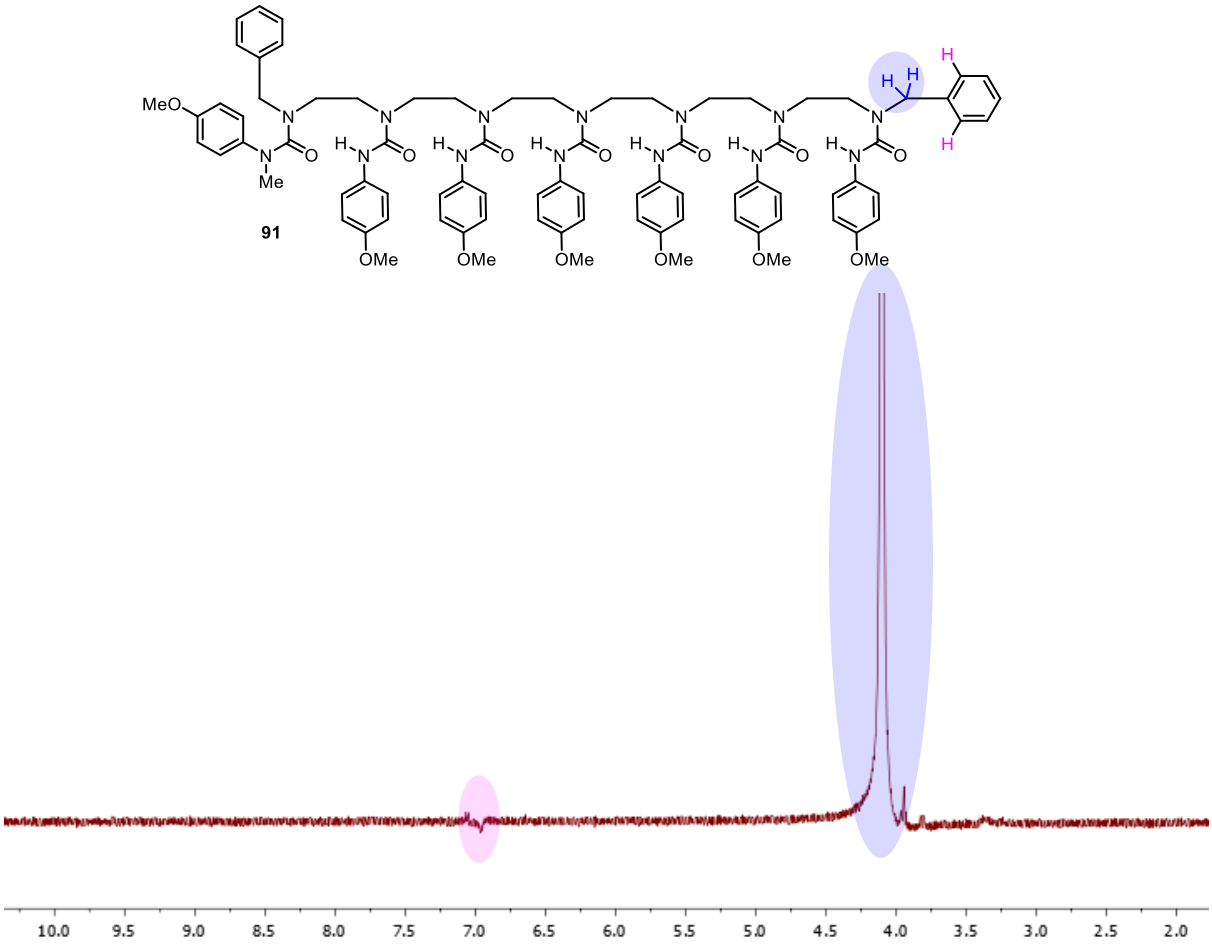

Figure A31 – NOE studies of 91 (irradiation of blue).

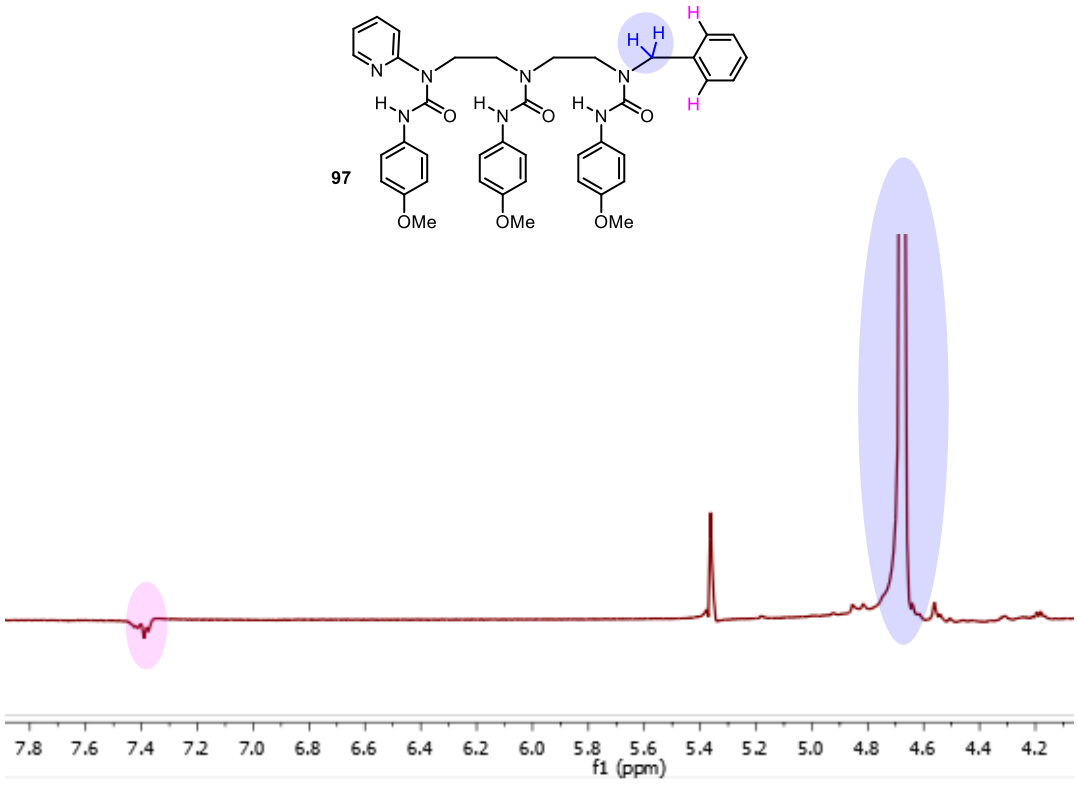

Figure A32 – NOE studies of 97 (irradiation of blue).

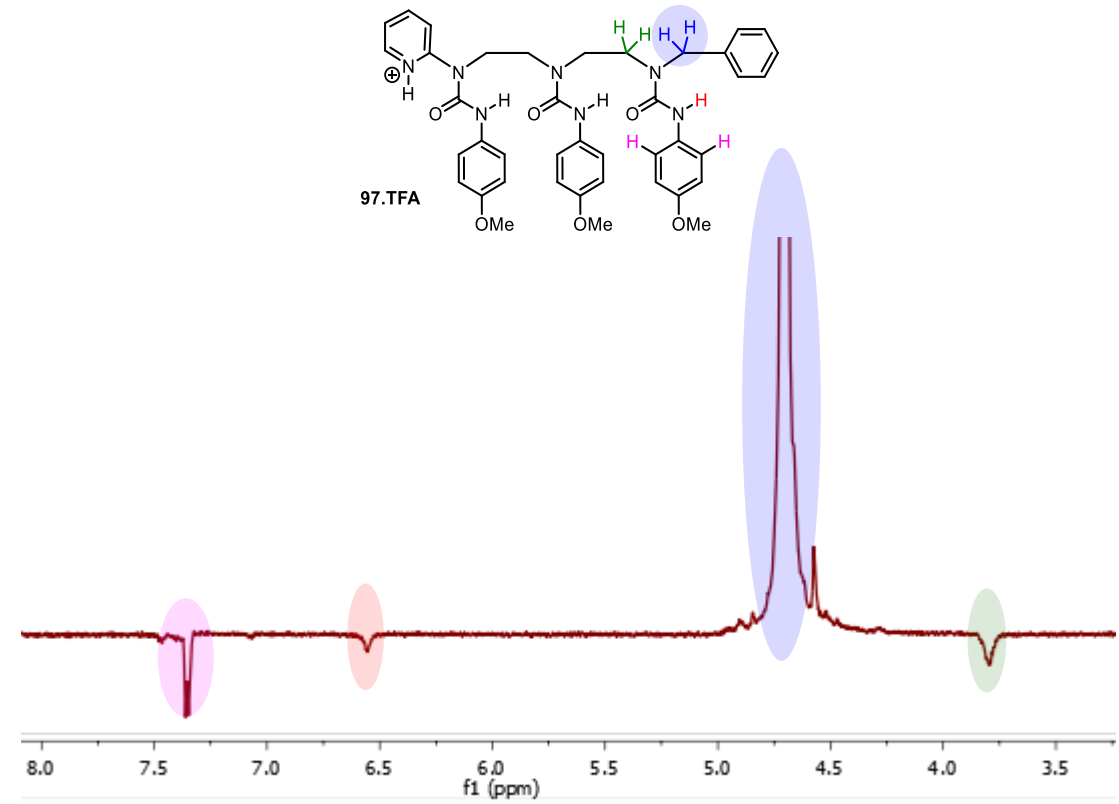

Figure A33 – NOE studies of 97.TFA (irradiation of blue).

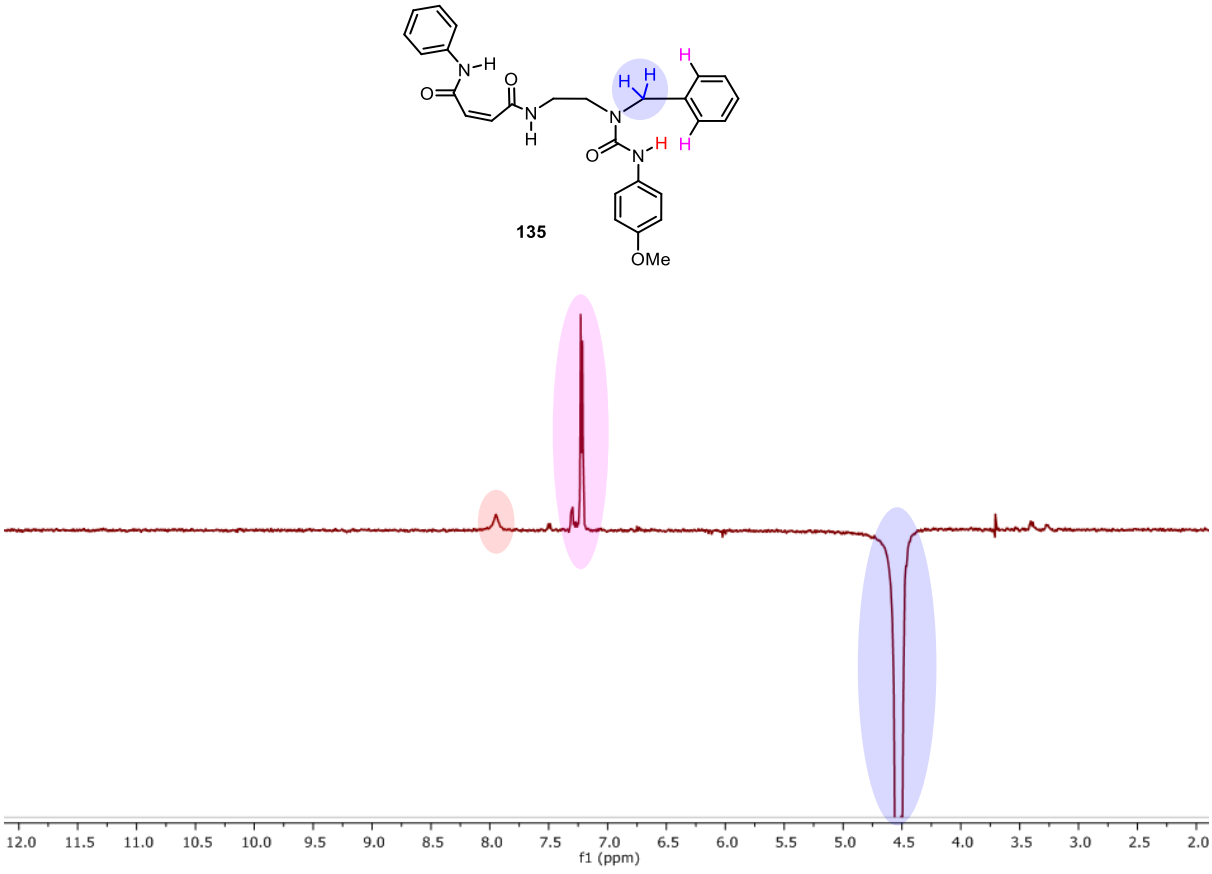

Figure A34 – NOE studies of 135 (irradiation of blue).

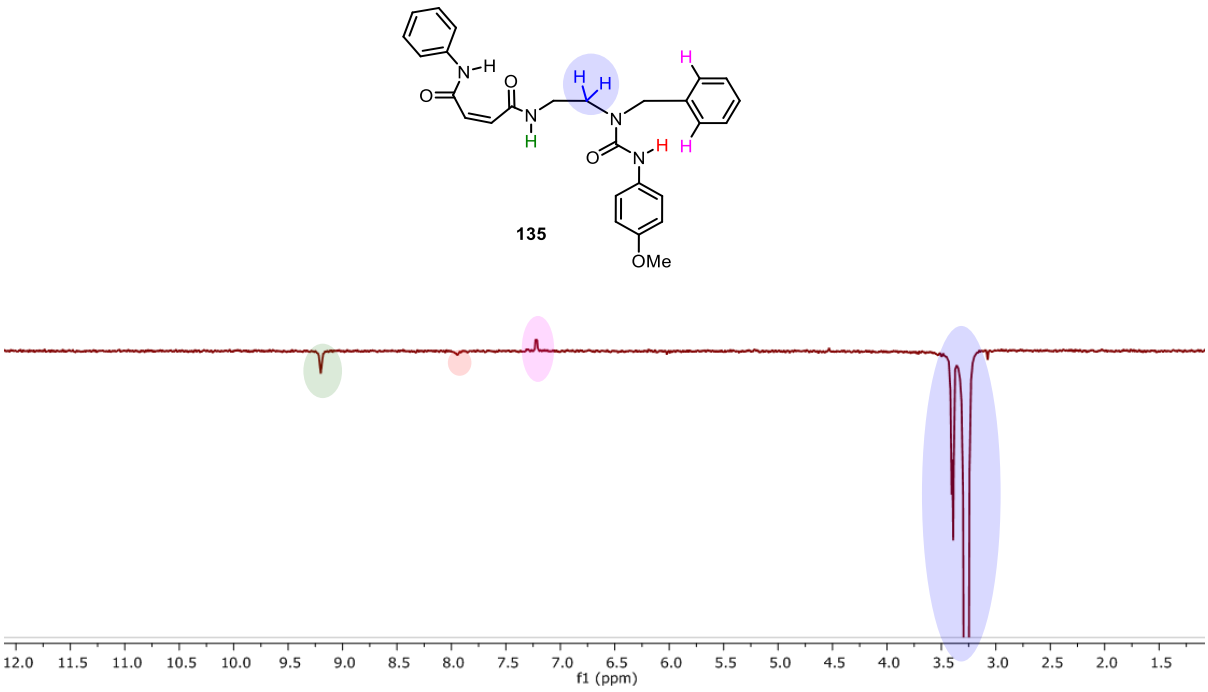

Figure A35 – NOE studies of 135 (irradiation of blue).

8.5 Fluorimetry

Fluorescence spectra were recorded using a PerkinElmer LS45 fluorimeter in a Marco Fluorescence Quartz Cuvette in anhydrous DCM.

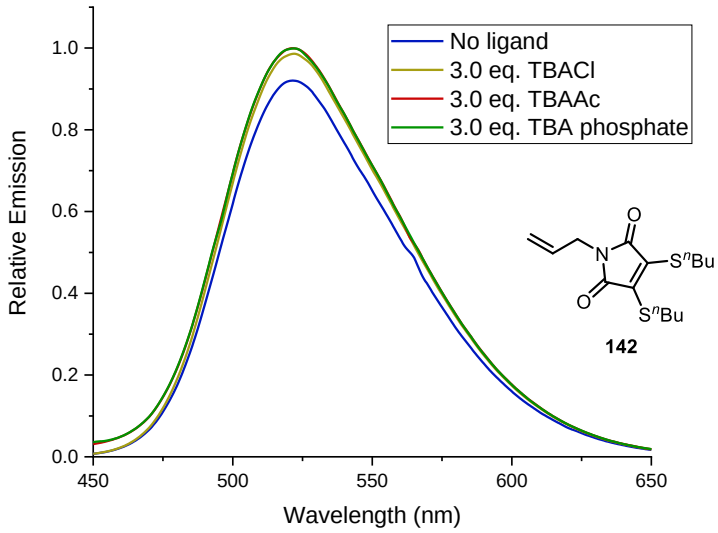

Figure A36 – Emission profile of 142 after addition of anionic ligands (irradiation at 405 nm, ~1 mM).

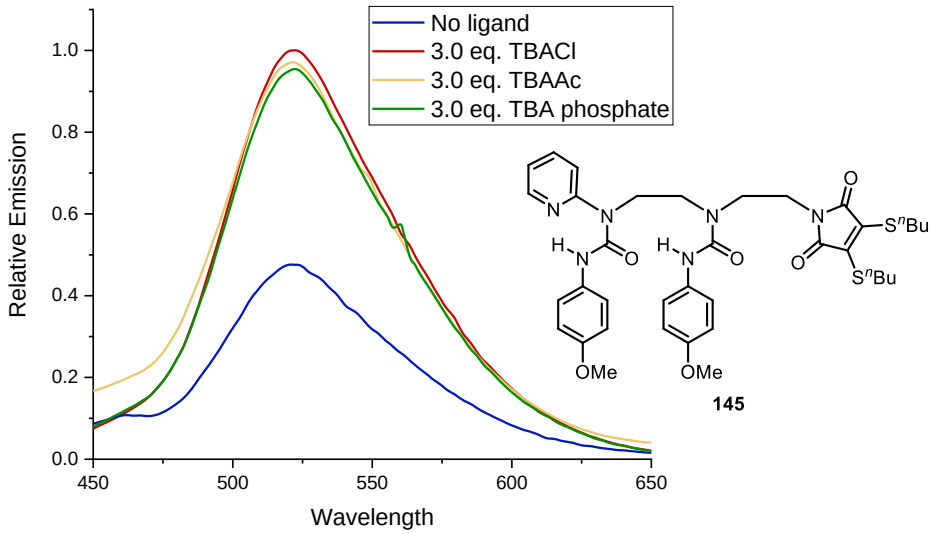

Figure A37 – Emission profile of 145 after addition of anionic ligands (irradiation at 405 nm, ~1 mM).

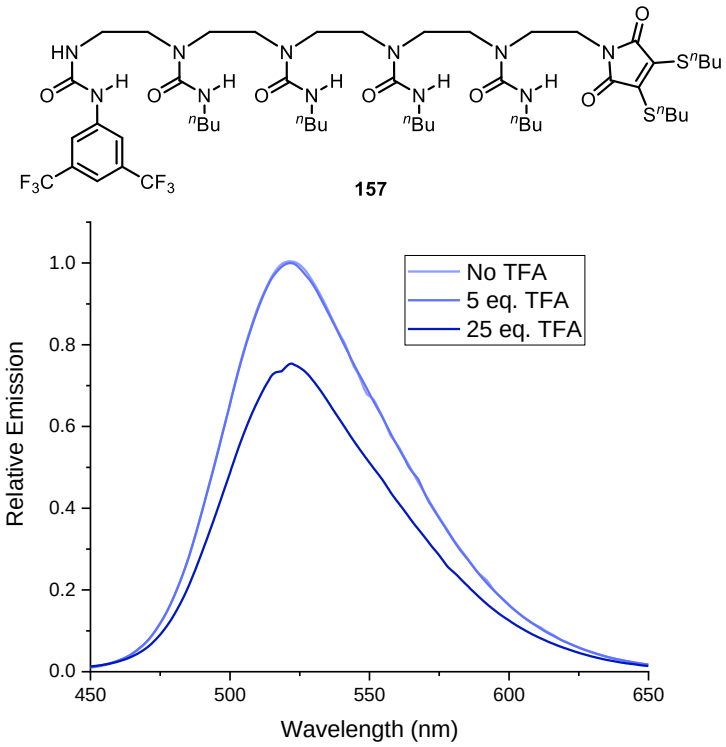

Figure A38 – Emission profile of 157 after addition of TFA (irradiation at 405 nm, ~1 mM).

8.6 X-Ray Crystallographic Data

Recrystallisation for X-ray crystallography was achieved by slow evaporation of a precipitant into a solution containing the desired compound. Analysis was performed using a Bruker Apex II Goniometer.

X-ray data for **175** (recrystallised from $CHCl_3$/PE) –

Bond precision: C-C = 0.0038 A Wavelength=0.71073

Cell: a=12.6236(4) b=14.4638(4) c=34.9564(9)
alpha=90 beta=92.5613(17) gamma=90

Temperature: 100 K

	Calculated	Reported
Volume	6376.2(3)	6376.1(3)
Space group	P 21/c	P 1 21/c 1
Hall group	-P 2ybc	-P 2ybc
Moiety formula	C30 H36 N6 O6 [+ solvent]	C30 H36 N6 O6
Sum formula	C30 H36 N6 O6 [+ solvent]	C30 H36 N6 O6
Mr	576.65	576.65
Dx,g cm-3	1.201	1.201
Z	8	8
Mu (mm-1)	0.085	0.085
F000	2448.0	2448.0
F000'	2449.10	
h,k,lmax	15,18,43	15,18,43
Nref	13032	13032
Tmin,Tmax	0.969,0.984	0.688,0.746
Tmin'	0.961	

Correction method= # Reported T Limits: Tmin=0.688 Tmax=0.746 AbsCorr = MULTI-SCAN

Data completeness= 1.000 Theta(max)= 26.372

R(reflections)= 0.0564(9664) wR2(reflections)= 0.1332(13032)

S = 1.033 Npar= 1099

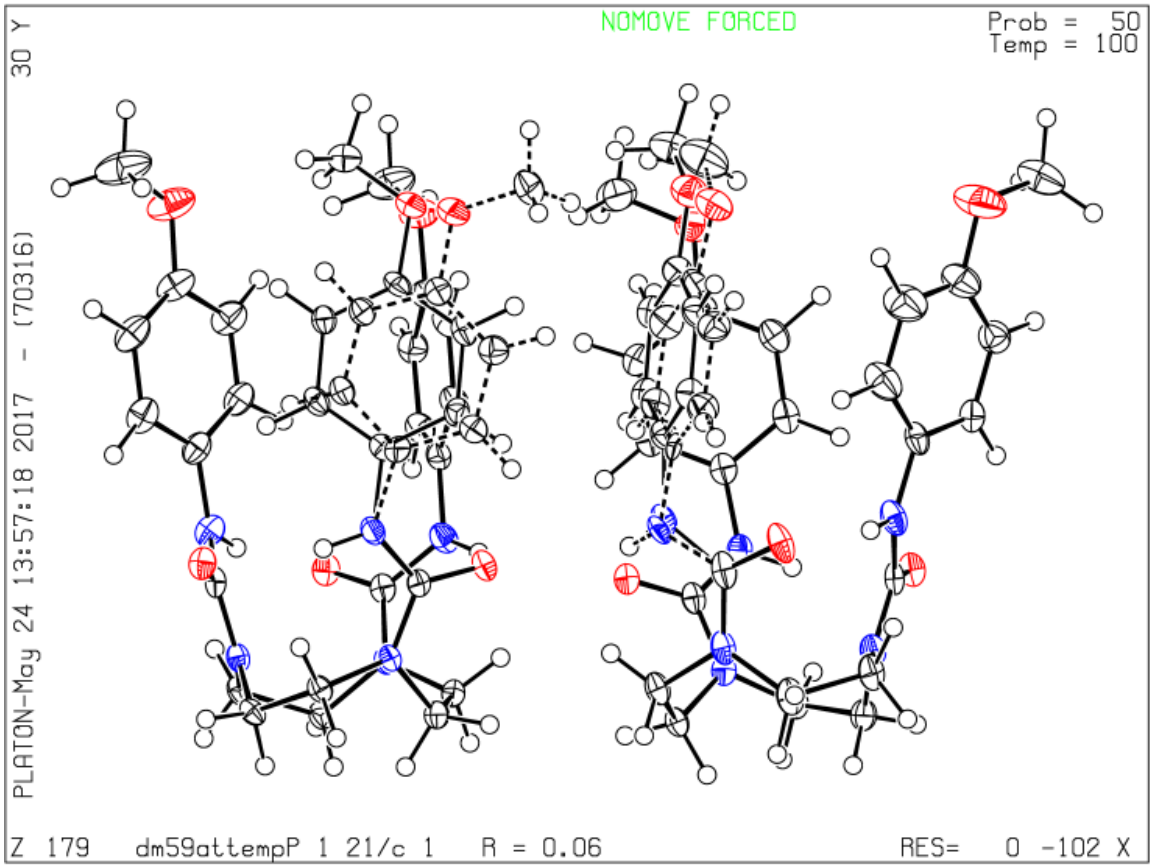
NOMOVE FORCED
Prob = 50
Temp = 100
30 Y
PLATON-May 24 13:57:18 2017 - (70316)
Z 179 dm59attempP 1 21/c 1 R = 0.06
RES= 0 -102 X

9.0 References

(1) Nowick, J. S.; Holmes, D. L.; Mackin, G.; Noronha, G.; Shaka, A. J.; Smith, E. M. *J. Am. Chem. Soc.* **1996**, *118* (11), 2764–2765.

(2) Wechsel, R.; Raftery, J.; Cavagnat, D.; Guichard, G.; Clayden, J. *Angew. Chem. Int. Ed.* **2016**, *55* (33), 9657–9661.

(3) Blake, R. D. *Informational Biopolymers of Genes and Gene Expression*, 1st ed.; University Science Books: Herndon, 2005.

(4) R. E. Hubbard, M. K. H. *Hydrogen Bonds in Proteins: Role and Strength*, 1st ed.; John Wiley & Sons: Chichester, 2001.

(5) Gellman, S. H.; Adams, B. R. *Tetrahedron Lett.* **1989**, *30* (26), 3381–3384.

(6) Emsley, J. *Chem. Soc. Rev.* **1980**, *9* (1), 91–124.

(7) Molcanov, K. *Acta Chim. Slov.* **2008**, *55*, 692–708.

(8) Kollman, P. A. *J. Am. Chem. Soc.* **1972**, *94* (6), 1837–1842.

(9) Cherezov, V.; Rosenbaum, D. M.; Hanson, M. A.; Rasmussen, S. G. F.; Foon, S. T.; Kobilka, T. S.; Choi, H. J.; Kuhn, P.; Weis, W. I.; Kobilka, B. K. *Science* **2007**, *318* (5854), 1258–1265.

(10) Lister, F. G. A.; Le Bailly, B. A. F.; Webb, S. J.; Clayden, J. *Nat. Chem.* **2017**, *9* (5), 420–425.

(11) A. J. F. Griffiths, J. H. Miller, D. T. Suzuki, R. C. Lewontin, W. M. G. *Introduction to Genetic Analysis*, 7th ed.; W. H. Freeman: New York, 2000.

(12) Korkmaz, G.; Holm, M.; Wiens, T.; Sanyal, S. *J. Biol. Chem.* **2014**, *289* (44), 30334–30342.

(13) Lehn, J.-M. *Supramolecular Chemistry: Concepts and Perspectives*, 1st ed.; Wiley-VCH: Weinheim, 1995.

(14) Huggins, M. L. *J. Phys. Chem.* **1936**, *40* (6), 723–731.

(15) Pauling, L. *J. Am. Chem. Soc.* **1931**, *53* (4), 1367–1400.

(16) Linus Pauling. *The Nature of the Chemical Bond*, 3rd ed.; Cornell University Press: New York, 1960.

(17) Van Duijneveldt, F. B.; Murrell, J. N. *J. Chem. Phys.* **1967**, *46* (5), 1759–1767.

(18) A. Kollman, P. *J. Am. Chem. Soc.* **2002**, *94* (6), 1837–1842.

(19) Li, X.-Z.; Walker, B.; Michaelides, A. *Proc. Natl. Acad. Sci.* **2011**, *108* (16), 6369–6373.

(20) Ferro-Costas, D.; Francisco, E.; Pendás, Á. M.; Mosquera, R. A. *Phys. Chem. Chem. Phys.* **2015**, *17* (39), 26059–26071.

(21) A. Hubbard, T.; J. Brown, A.; A. W. Bell, I.; L. Cockroft, S. *J. Am. Chem. Soc.* **2016**, *138* (46), 15114–15117.

(22) Krishnamurthy, V. M.; Semetey, V.; Bracher, P. J.; Shen, N.; Whitesides, G. M. *J. Am. Chem. Soc.* **2007**, *129* (5), 1312–1320.

(23) Sun, H.; Hunter, C. A.; Navarro, C.; Turega, S. *J. Am. Chem. Soc.* **2013**, *135* (35), 13129–13141.

(24) Chekmeneva, E.; Hunter, C. A.; Misuraca, M. C.; Turega, S. M. *Org. Biomol. Chem.* **2012**, *10* (30), 6022–6031.

(25) Nochebuena, J.; Cuautli, C.; Ireta, J. *Phys. Chem. Chem. Phys.* **2017**, *19* (23), 15256–15263.

(26) Byrne, L.; Solà, J.; Boddaert, T.; Marcelli, T.; Adams, R. W.; Morris, G. A.; Clayden, J. *Angew. Chem. Int. Ed.* **2014**, *53* (1), 151–155.

(27) Filot, I. A. W.; Palmans, A. R. A.; Hilbers, P. A. J.; Van Santen, R. A.; Pidko, E. A.; De Greef, T. F. A. *J. Phys. Chem. B* **2010**, *114* (43), 13667–13674.

(28) Simic, V.; Bouteiller, L.; Jalabert, M. *J. Am. Chem. Soc.* **2003**, *125* (43), 13148–13154.

(29) Dominelli-Whiteley, N.; Brown, J. J.; Muchowska, K. B.; Mati, I. K.; Adam, C.; Hubbard, T. A.; Elmi, A.; Brown, A. J.; Bell, I. A. W.; Cockroft, S. L. *Angew. Chem. Int. Ed.* **2017**, *56* (26), 7658–7662.

(30) Doyle, A. G.; Jacobsen, E. N. *Chem. Rev.* **2007**, *107* (12), 5713–5743.

(31) Tromans, R. A.; Carter, T. S.; Chabanne, L.; Crump, M. P.; Li, H.; Matlock, J. V.; Orchard, M. G.; Davis, A. P. *Nat. Chem.* **2019**, *11* (1), 52–56.

(32) Wechsel, R.; Žabka, M.; Ward, J. W.; Clayden, J. *J. Am. Chem. Soc.* **2018**, *140* (10), 3528–3531.

(33) Patel, B. H.; Percivalle, C.; Ritson, D. J.; Duffy, C. D.; Sutherland, J. D. *Nat. Chem.* **2015**, *7* (4), 301–307.

(34) Ritter, S. L.; Hall, R. A. *Nat. Rev. Mol. Cell Biol.* **2009**, *10* (12), 819–830.

(35) Kroeze, W. K.; Sheffler, D. J.; Roth, B. L. *J. Cell Sci.* **2003**, *116* (24), 4867–4869.

(36) Gellman, S. H. *Acc. Chem. Res.* **1998**, *31* (4), 173–180.

(37) Appella, D. H.; Christianson, L. A.; Karle, I. L.; Powell, D. R.; Gellman, S. H. *J. Am. Chem. Soc.* **1996**, *118* (51), 13071–13072.

(38) Horne, W. S.; Boersma, M. D.; Windsor, M. A.; Gellman, S. H. *Angew. Chem. Int. Ed.* **2008**, *47* (15), 2853–2856.

(39) Lee, E. F.; Sadowsky, J. D.; Smith, B. J.; Czabotar, P. E.; Peterson-Kaufman, K. J.; Colman, P. M.; Gellman, S. H.; Fairlie, W. D. *Angew. Chem. Int. Ed.* **2009**, *48* (24), 4318–4322.

(40) Müller, M. M.; Windsor, M. A.; Pomerantz, W. C.; Gellman, S. H.; Hilvert, D. *Angew. Chem. Int. Ed.* **2009**, *48* (5), 922–925.

(41) Sebaoun, L.; Maurizot, V.; Granier, T.; Kauffmann, B.; Huc, I. *J. Am. Chem. Soc.* **2014**, *136*, 2168–2174.

(42) Horeau, M.; Lautrette, G.; Wicher, B.; Blot, V.; Lebreton, J.; Pipelier, M.; Dubreuil, D.; Ferrand, Y.; Huc, I. *Angew. Chem. Int. Ed.* **2017**, *56* (24), 6823–6827.

(43) Lamouroux, A.; Sebaoun, L.; Wicher, B.; Kauffmann, B.; Ferrand, Y.; Maurizot, V.; Huc, I. *J. Am. Chem. Soc.* **2017**, *139* (41), 14668–14675.

(44) Jones, I. M.; Lingard, H.; Hamilton, A. D. *Angew. Chem. Int. Ed.* **2011**, *50* (52), 12569–12571.

(45) Knipe, P. C.; Lingard, H.; Jones, I. M.; Thompson, S.; Hamilton, A. D. *Org. Biomol. Chem.* **2014**, *12* (40), 7937–7941.

(46) Jones, I. M.; Knipe, P. C.; Michaelos, T.; Thompson, S.; Hamilton, A. D. *Molecules* **2014**, *19* (8), 11316–11332.

(47) German, E. A.; Ross, J. E.; Knipe, P. C.; Don, M. F.; Thompson, S.; Hamilton, A. D. *Angew. Chem. Int. Ed.* **2015**, *54* (9), 2649–2652.

(48) Knipe, P. C.; Thompson, S.; Hamilton, A. D. *Chem. Commun.* **2016**, *52* (39), 6521–6524.

(49) Jones, I. M.; Hamilton, A. D. *Angew. Chem. Int. Ed.* **2011**, *50* (20), 4597–4600.

(50) Clayden, J.; Lund, A.; Vallverdú, L.; Helltwell, M. *Nature* **2004**, *431* (7011), 966–971.

(51) Brioche, J.; Pike, S. J.; Tshepelevitsh, S.; Leito, I.; Morris, G. A.; Webb, S. J.; Clayden, J. *J. Am. Chem. Soc.* **2015**, *137* (20), 6680–6691.

(52) Delgado-Bonal, A.; Martín-Torres, J. *Sci. Rep.* **2016**, *6*, 1–5.

(53) Linsenmeier, R. A.; Zhang, H. F. *Prog. Retin. Eye Res.* **2017**, *58*, 115–151.

(54) Ernst, O. P.; Lodowski, D. T.; Elstner, M.; Hegemann, P.; Brown, L. S.; Kandori, H. *Chem. Rev.* **2014**, *114* (1), 126–163.

(55) Yokoyama, Y. *Chem. Rev.* **2000**, *100* (5), 1717–1739.

(56) Habault, D.; Zhang, H.; Zhao, Y. *Chem. Soc. Rev.* **2013**, *42* (17), 7244–7256.

(57) Xiang, J.; Tong, X.; Shi, F.; Yan, Q.; Yu, B.; Zhao, Y. *J. Mater. Chem. B* **2018**, *6* (21), 3531–3540.

(58) Koumura, N.; Geertsema, E. M.; Meetsma, A.; Feringa, B. L. *J. Am. Chem. Soc.* **2000**, *122* (48), 12005–12006.

(59) Colard-Itté, J. R.; Li, Q.; Collin, D.; Mariani, G.; Fuks, G.; Moulin, E.; Buhler, E.; Giuseppone, N. *Nanoscale* **2019**, *11* (12), 5197–5202.

(60) Barrell, M. J.; Campaña, A. G.; Von Delius, M.; Geertsema, E. M.; Leigh, D. A. *Angew. Chem. Int. Ed.* **2011**, *50* (1), 285–290.

(61) Gole, B.; Kauffmann, B.; Maurizot, V.; Huc, I.; Ferrand, Y. *Angew. Chem. Int. Ed.* **2019**, 8147–8151.

(62) Wang, Q.; Frisch, J.; Herder, M.; Hecht, S.; Koch, N. *ChemPhysChem* **2017**, *18* (7), 717.

(63) Ihrig, S. P.; Eisenreich, F.; Hecht, S. *Chem. Commun.* **2019**, *55* (30), 4290–4298.

(64) Gurke, J.; Quick, M.; Ernsting, N. P.; Hecht, S. *Chem. Commun.* **2017**, *53* (13), 2150–2153.

(65) Herder, M.; Pätzel, M.; Grubert, L.; Hecht, S. *Chem. Commun.* **2011**, *47* (1), 460–462.

(66) Zweig, J. E.; Newhouse, T. R. *J. Am. Chem. Soc.* **2017**, *139* (32), 10956–10959.

(67) Mazzier, D.; Crisma, M.; De Poli, M.; Marafon, G.; Peggion, C.; Clayden, J.; Moretto, A. *J. Am. Chem. Soc.* **2016**, *138* (25), 8007–8018.

(68) Poli, M. De; Zawodny, W.; Quinonero, O.; Lorch, M. *Science* **2016**, *352* (6285), 575–580.

(69) Bécart, D.; Diemer, V.; Salaün, A.; Oiarbide, M.; Nelli, Y. R.; Kauffmann, B.; Fischer, L.; Palomo, C.; Guichard, G. *J. Am. Chem. Soc.* **2017**, *139* (36), 12524–12532.

(70) Diemer, V.; Fischer, L.; Kauffmann, B.; Guichard, G. *Chem.—Eur. J.* **2016**, *22* (44), 15549.

(71) Antunes, S.; Corre, J. P.; Mikaty, G.; Douat, C.; Goossens, P. L.; Guichard, G. *Bioorg. Med. Chem.* **2017**, *25* (16), 4245–4252.

(72) Tarai, A.; Baruah, J. B. *ACS Omega* **2017**, *2* (10), 6991–7001.

(73) Nowick, J. S.; Powell, N. A.; Martinez, E. J.; Smith, E. M.; Noronha, G. *J. Org. Chem.* **1992**, *57* (14), 3763–3765.

(74) Yamasaki, R.; Tanatani, A.; Azumaya, I.; Saito, S.; Yamaguchi, K.; Kagechika, H. *Org. Lett.* **2003**, *5* (8), 1265–1267.

(75) Clayden, J.; Hennecke, U.; Vincent, M. A.; Hillier, I. H.; Helliwell, M. *Phys. Chem. Chem. Phys.* **2010**, *12* (45), 15056–15064.

(76) Nowick, J. S.; Holmes, D. L.; Mackin, G.; Noronha, G.; Shaka, A. J.; Smith, E. M. *J. Am. Chem. Soc.* **1996**, *118*, 2764–2765.

(77) Nowick, J. S.; Abdi, M.; Bellamo, K. A.; Love, J. A.; Martinez, E. J.; Noronha, G.; Smith, E. M.; Ziller, J. W. *J. Am. Chem. Soc.* **1995**, *117* (1), 89–99.

(78) Taylor, R.; Kennard, O.; Versichel, W. *J. Am. Chem. Soc.* **1983**, *105* (18), 5761–5766.

(79) Nowick, J. S.; Mahrus, S.; Smith, E. M.; Ziller, J. W. *J. Am. Chem. Soc.* **1996**, *118* (5), 1066–1072.

(80) Junquera, E.; Nowick, J. S. *J. Org. Chem.* **1999**, *64* (7), 2527–2531.

(81) Le Bailly, B. A. F., Controlling Molecular Helicity for Transmembrane Communication. Ph.D. Thesis, University of Manchester, Manchester, 2012.

(82) Nowick, J. S.; Antonovich, V.; Noronha, G.; Ziller, J. W. *J. Org. Chem.* **1995**, *60* (6), 1888–1890.

(83) Goyal, S.; Chattopadhyay, A.; Kasavajhala, K.; Priyakumar, U. D. *J. Am. Chem. Soc.* **2017**, *139* (42), 14931–14946.

(84) Costil, R.; Dale, H. J. A.; Fey, N.; Whitcombe, G.; Matlock, J. V.; Clayden, J. *Angew. Chem. Int. Ed.* **2017**, *56* (41), 12533–12537.

(85) Laidler, K. J.; King, M. C. *J. Phys. Chem.* **1983**, *87* (15), 2657–2664.

(86) Rablen, P. R.; Miller, D. A.; Bullock, V. R.; Hutchinson, P. H.; Gorman, J. A. *J. Am. Chem. Soc.* **1999**, *121* (1), 218–226.

(87) Lippert, K. M.; Hof, K.; Gerbig, D.; Ley, D.; Hausmann, H.; Guenther, S.; Schreiner, P. R. *Eur. J. Org. Chem.* **2012**, *30*, 5919–5927.

(88) Platts, J. A. *Phys. Chem. Chem. Phys.* **2000**, *2* (5), 973–980.

(89) Campaña, A. G.; Leigh, D. A.; Lewandowska, U. *J. Am. Chem. Soc.* **2013**, *135* (23), 8639–8645.

(90) Sedaghat Doost, A.; Akbari, M.; Stevens, C. V.; Setiowati, A. D.; Van der Meeren, P. *Trends Food Sci. Technol.* **2019**, *86*, 16–24.

(91) Li, H. X.; Cheng, M. L.; Wang, H. M.; Yang, X. J.; Ren, Z. G.; Lang, J. P. *Organometallics* **2011**, *30* (2), 208–214.

(92) Morpurgo, M.; Bayer, E. A.; Wilchek, M. *J. Biochem. Biophys. Meth.* **1999**, *38* (1), 17–28.

(93) Matsui, T.; Baba, T.; Kamiya, K.; Shigeta, Y. *Phys. Chem. Chem. Phys.* **2012**, *14* (12), 4181–4187.

(94) Liao, Y. *Acc. Chem. Res.* **2017**, *50* (8), 1956–1964.

(95) Kundu, P. K.; Samanta, D.; Leizrowice, R.; Margulis, B.; Zhao, H.; Börner, M.; Udayabhaskararao, T.; Manna, D.; Klajn, R. *Nat. Chem.* **2015**, *7* (8), 646–652.

(96) Balmond, E. I.; Tautges, B. K.; Faulkner, A. L.; Or, V. W.; Hodur, B. M.; Shaw, J. T.; Louie, A. Y. *J. Org. Chem.* **2016**, *81* (19), 8744–8758.

(97) Kortekaas, L.; Chen, J.; Jacquemin, D.; Browne, W. R. *J. Phys. Chem. B* **2018**, *122* (24), 6423–6430.

(98) Shi, Z.; Peng, P.; Strohecker, D.; Liao, Y. *J. Am. Chem. Soc.* **2011**, *133* (37), 14699–14703.

(99) Li, J.; Yin, X.; Li, B.; Li, X.; Pan, Y.; Li, J.; Guo, Y. *Anal. Chem.* **2019**, *91* (8), 5354–5361.

(100) ter Schiphorst, J.; Melpignano, G. G.; Amirabadi, H. E.; Houben, M. H. J. M.; Bakker, S.; den Toonder, J. M. J.; Schenning, A. P. H. J. *Macromol. Rapid Commun.* **2018**, *39* (1), 1–6.

(101) Majce, V.; Kočevar, M.; Polanc, S. *Tetrahedron Lett.* **2011**, *52* (26), 3287–3290.

(102) Figueira-Duarte, T. M.; Müllen, K. *Chem. Rev.* **2011**, *111* (11), 7260–7314.

(103) Robin, M. P.; Mabire, A. B.; Damborsky, J. C.; Thom, E. S.; Winzer-Serhan, U. H.; Raymond, J. E.; O'Reilly, R. K. *J. Am. Chem. Soc.* **2013**, *135* (25), 9518–9524.

(104) Perutz, M. F. *Br. Med. Bull.* **1976**, *32* (3), 195–208.

(105) Pizzolato, S. F.; Štacko, P.; Kistemaker, J. C. M.; Van Leeuwen, T.; Otten, E.; Feringa, B. L. *J. Am. Chem. Soc.* **2018**, *140* (49), 17278–17289.

(106) Ghasemabadi, P. G.; Yao, T.; Bodwell, G. J. *Chem. Soc. Rev.* **2015**, *44* (18), 6494–6518.

(107) Fielden, S. D. P.; Leigh, D. A.; Woltering, S. L. *Angew. Chem. Int. Ed.* **2017**, *56* (37), 11166–11194.

(108) Shay, J. W.; Wright, W. E. *Nat. Genet.* **2019**, *20* (5), 299–309.

(109) Chen, Z.; Guieu, S.; White, N. G.; Lelj, F.; MacLachlan, M. J. *Chem.—Eur. J.* **2016**, *22* (49), 17657–17672.

(110) Pérez-Victoria, I.; Kemper, S.; Patel, M. K.; Edwards, J.; Errey, J. C.; Primavesi, L. F.; Paul, M.; Claridge, T. D. W.; Davis, B. G.; Kang, J.; et al. *J. Am. Chem. Soc.* **2014**, *136* (30), 200–203.

(111) Austin, C. A.; Chen, Y.; Rodgers, M. T. *Int. J. Mass Spectrom.* **2012**, *332*, 27–34.

(112) König, B.; Pelka, M.; Subat, M.; Dix, I.; Jones, P. G. *Eur. J. Org. Chem.* **2001**, *10*, 1943–1949.

(113) Charbonnier, F.; Marsura, A.; Roussel, K.; Kovács, J.; Pintér, I. *Helv. Chim. Acta* **2001**, *84* (3), 535–551.

(114) Evans, N. H.; Carr, R.; Delbianco, M.; Pal, R.; Yufit, D. S.; Parker, D. *Dalt. Trans.* **2013**, *42* (44), 15610–15616.

(115) Aoki, S.; Kagata, D.; Shiro, M.; Takeda, K.; Kimura, E. *J. Am. Chem. Soc.* **2004**, *126* (41), 13377–13390.

(116) Guérineau, V.; Rollet, M.; Viel, S.; Lepoittevin, B.; Costa, L.; Saint-Aguet, P.; Laurent, R.; Roger, P.; Gigmes, D.; Martini, C.; et al. *Nat. Commun.* **2019**, *10* (1), 1–14.

(117) Frisch, H. L.; Wasserman, E. *J. Am. Chem. Soc.* **1961**, *83* (18), 3789–3795.

(118) Yamamoto, C.; Okamoto, Y.; Schmidt, T.; Jager, R.; Vogtle, F. *J. Am. Chem. Soc.* **1997**, *119* (43), 10547–10548.

(119) Reuter, C.; Schmieder, R.; Vögtle, F. *Pure Appl. Chem.* **2007**, *72* (12), 2233–2241.

(120) Page, P. C. B.; Bygrave, T. R.; Chan, Y.; Heaney, H.; McKee, V. *Eur. J. Org. Chem.* **2011**, No. 16, 3016–3025.

(121) Fraschetti, C.; Letzel, M. C.; Paletta, M.; Mattay, J.; Speranza, M.; Filippi, A.; Aschi, M.; Rozhenko, A. B. *J. Mass Spectrom.* **2012**, *47* (1), 72–78.

(122) Szumna, A. *Org. Biomol. Chem.* **2007**, *5* (9), 1358–1368.

(123) Wzorek, A.; Mattay, J.; Iwanek, W. *Tetrahedron: Asymmetry* **2012**, *23* (3–4), 271–277.

(124) Nobuta, T.; Kawabata, T. *Chem. Commun.* **2017**, *53* (67), 9320–9323.

(125) Mishiro, K.; Furuta, T.; Sasamori, T.; Hayashi, K.; Tokitoh, N.; Futaki, S.; Kawabata, T. *J. Am. Chem. Soc.* **2013**, *135* (37), 13644–13647.

(126) Shibatomi, K.; Kitahara, K.; Okimi, T.; Abe, Y.; Iwasa, S. *Chem. Sci.* **2016**, *7* (2), 1388–1392.

(127) Galaup, C.; Couchet, J. M.; Bedel, S.; Tisnès, P.; Picard, C. *J. Org. Chem.* **2005**, *70* (6), 2274–2284.

(128) Laduron, F.; Tamborowski, V.; Moens, L.; Horváth, A.; De Smaele, D.; Leurs, S. *Org. Process Res. Dev.* **2005**, *9* (1), 102–104.

(129) Srinivasachari, S.; Liu, Y.; Zhang, G.; Prevette, L.; Reineke, T. M. *J. Am. Chem. Soc.* **2006**, *128* (25), 8176–8184.

(130) Nishizawa, A.; Takahira, T.; Yasui, K.; Fujimoto, H.; Iwai, T.; Sawamura, M.; Chatani, N.; Tobisu, M. *J. Am. Chem. Soc.* **2019**, *141* (18), 7261–7265.

(131) Si, C.; Fales, K. R.; Torrado, A.; Frimpong, K.; Kaoudi, T.; Vandeveer, H. G.; Njoroge, F. G. *J. Org. Chem.* **2016**, *81* (10), 4359–4363.

(132) Robinson, A.; Thomas, G. L.; Spandl, R. J.; Welch, M.; Spring, D. R. *Org. Biomol. Chem.* **2008**, *6* (16), 2978–2981.

(133) Blomberg, D.; Brickmann, K.; Kihlberg, J. *Tetrahedron* **2006**, *62* (47), 10937–10944.

(134) Mançois, F.; Pozzo, J. L.; Pan, J.; Adamietz, F.; Rodriguez, V.; Ducasse, L.; Castet, F.; Plaquet, A.; Champagne, B. *Chem.—Eur. J.* **2009**, *15* (11), 2560–2571.

(135) Sánchez, A.; Pedroso, E.; Grandas, A. *Eur. J. Org. Chem.* **2010**, *13*, 2600–2606.

(136) Botterhuis, N. E.; Karthikeyan, S.; Veldman, D.; Meskers, S. C. J.; Sijbesma, R. P. *Chem. Commun.* **2008**, No. 33, 3915–3917.

(137) Castañeda, L.; Maruani, A.; Schumacher, F. F.; Miranda, E.; Chudasama, V.; Chester, K. A.; Baker, J. R.; Smith, M. E. B.; Caddick, S. *Chem. Commun.* **2013**, *49* (74), 8187–8189.

(138) Chmielewski, M. K. *Tetrahedron Lett.* **2012**, *53* (6), 666–669.

(139) Rajesh, Y. B. R. D. *J. Heterocycl. Chem.* **2018**, *55* (2), 486–491.

(140) Hron, R.; Jursic, B. S. *Tetrahedron Lett.* **2014**, *55* (9), 1540–1543.

(141) Akbar, R.; Baral, M.; Kanungo, B. K. *RSC Adv.* **2015**, *5* (21), 16207–16222.

(142) Gavette, J. V.; McGrath, J. M.; Spuches, A. M.; Sargent, A. L.; Allen, W. E. *J. Org. Chem.* **2009**, *74* (10), 3706–3710.

(143) Paesano, N.; Marzocco, S.; Vicidomini, C.; Saturnino, C.; Autore, G.; De Martino, G.; Sbardella, G. *Bioorganic Med. Chem. Lett.* **2005**, *15* (3), 539–543.

(144) Bartuschat, A. L.; Wicht, K.; Heinrich, M. R. *Angew. Chem. Int. Ed.* **2015**, *54* (35), 10294–10298.

(145) Feng, L.; Yang, K. W.; Zhou, L. S.; Xiao, J. M.; Yang, X.; Zhai, L.; Zhang, Y. L.; Crowder, M. W. *Bioorganic Med. Chem. Lett.* **2012**, *22* (16), 5185–5189.

(146) Sunilkumar, G.; Nagamani, D.; Argade, N. P.; Ganesh, K. N. *Synthesis (Stuttg).* **2003**, No. 15, 2304–2306.

(147) Karaki, F.; Kabasawa, Y.; Yanagimoto, T.; Umeda, N.; Firman; Urano, Y.; Nagano, T.; Otani, Y.; Ohwada, T. *Chem.—Eur. J.* **2012**, *18* (4), 1127–1141.